MODIFICATION OF THE PERMEABILITY OF POLYMER LATEX FILMS

by

PAUL A. STEWARD.

A thesis submitted in partial fulfilment of the requirements of
The Nottingham Trent University
for the degree of
Doctor of Philosophy.

1995

A collaborative programme between
The Chemical and Biological Defence Establishment,
(M.o.D.), Porton Down,
and
The Nottingham Trent University.

Dedication.

To

Mum & Dad

Acknowledgments.

I would sincerely like to thank **Dr. John Hearn**, Reader in Surface Chemistry, at The Nottingham Trent University, for his guidance, support and friendship over the time that this project took place. I am also grateful to **Dr. Mike Wilkinson**, Principal Scientific Officer at C.B.D.E., for his support and encouragement.

Without the financial support of the **C.B.D.E.**, this project would never have taken place, and I am also indebted to my parents, **Irene** and **Raymond**, for their support and patronage during the preparation of this Thesis.

Finally, I would like to acknowledge the support and friendship of the **academic and technical staff** of The Nottingham Trent University, especially **Arthur** and **Amanda Richards**, whom provided a third hand when such was required.

Thanks all,
Paul.

Parts of this work have been presented at:

1, Meeting of the Colloid and Interface Science Group, held at School of Chemistry, University of Bristol, 1992;
2, Second meeting of the UK Polymer Colloids Forum, Keele University, 1994;
3, Steward P.A., Hearn J., Wilkinson M.C., Roulstone B.J., Wilson A.J., Studies of Permeation and Morphology in Polymer Latex Films Containing Leachable Additives. Paper presented at the ACS (Division of Polymeric Materials, Science and Engineering) International Symposium on Film Formation, August 20-25, 1995, Chicago USA.

Publications arising from this work:

1, Hearn J., Steward P.A., Chainey M., Roulstone B.J., Wilkinson M.C., *Permeation Through Polymer Latex Films Made From Model Colloids*, in Colloidal Polymer Particles. Eds. J.W. Goodwin & R. Buscall, p137-179, Academic Press, London, (1995).
2, Steward P.A., Hearn J., Wilkinson M.C., *Studies on Permeation Through Polymer Latex Films. I. Films Containing No or only Low Levels of Additives.*, Polymer International, 38, p1-12, (1995).
3, Steward P.A., Hearn J., Wilkinson M.C., *Studies on Permeation Through Polymer Latex Films. II. Permeation Modification by Sucrose Addition.*, Polymer International, 38, p13-22, (1995).
4, Steward P.A., Hearn J., Wilkinson M.C., *Studies on Permeation Through Polymer Latex Films. III. Modification Using Soluble Polymeric Additives.*, Polymer International, 38, p23-32, (1995).
5, Steward P.A., Hearn J., Wilkinson M.C., Roulstone B.J., Wilson A.J., *Studies of Permeation and Morphology in Polymer Latex Films Containing Leachable Additives*. ACS Symposium Series, Film Formation.

The author acknowledges all trademarks and registered trademarks.

Abstract.

Modification of the Permeability of Polymer Latex Films

by

Paul A. Steward.

The modification of the aqueous solute permeability of methacrylic acid ester polymer latex-cast films resulting from the leaching of water soluble additives has been studied. The effects of the additives on the leached films' morphology are investigated with respect to the films' transport properties. The films' permeation properties to both gases and water vapour are also reported.

The solute permeability of surfactant-free, additive-free, homopolymer methacrylate latex films was found to be dependent on the hydrophobicity of the polymer: the longer the alkyl side-chain, the greater the permeability coefficient. In the case of a range of commercial (Eudragit®) latices, the solute permeability was influenced by whether the films contained endogenous surfactant, or required a plasticiser: both of which underwent a degree of leaching.

The loading of the films with water soluble additives could be used to modify their permeability coefficients. Low levels of addition, being difficult to leach, yielded lower permeability coefficients than higher levels of addition which afforded greater porosity more quickly. The mechanism of solute permeant transport changed gradually from a predominantly Fickian solution-diffusion type mechanism in the additive-free film to a mechanism of predominantly convective transport through water filled channels.

Initially, the solute permeability coefficient increased linearly with increasing additive load since low levels of additive did not confer continuous porosity through the full thickness of the film. The increase in permeability was therefore attributed to increased void volume in the film allowing increased polymer chain motion – plasticised by the progressive percolation of water into the film as the additive leached. The inability of such films to transport electrolyte showed that continuous porosity did not exist, and the linear increase in permeability is considered to indicate a gradual thinning of the barrier in the region of a leached channel, upto the point when the pore does span the full film thickness. Porosity was confirmed by the sudden ability of a film to exhibit transport of electrolyte at a certain level of additive addition. The porosity was, however, of an effective diameter similar to that of the solute permeants, and increased little, with increasing additive load, before the film became structurally weakened. The ability to retain porosity following additive leaching was dependent on the polymer either being kept below its glass transition temperature, or kept wet: the process of drying allowing a soft-polymer, porous, film to heal.

The water vapour permeability of additive containing films was little affected by the additive as a result of the film not swelling to the same extent as in liquid water. Water (in filled channels) inhibits diffusion to a lesser extent than does polymer such that whilst the diffusion of a solute permeant may be less impeded if it can remain in water without having to dissolve in polymer, the same is not true for the water vapour (or gas) whose diffusion can be further impeded by the presence of an additive which is less permeable than the polymer.

Access to latex particle functionality was achieved with the use of leachable additives, where it was not possible in the additive-free film.

Contents.

Section 1: Introduction.

Section 2: Experimental.

Section 3: Results and Discussion.

Section 4: Conclusions.

◆

Figure Index.

Chapter 4: Latex Film Formation and Properties p-4:1-

Chapter 5: Diffusion and Permeation in Polymer Films p-5:1-

Chapter 6: Controlled Release Methods and Devices p-6:1-

Chapter 7: Procedures and of Analysis of Results p-7:1-

Chapter 8: Morphology and Permeability of Eudragit® Films p-8:1-

Chapter 10: Sucrose as a Film Additive p-10:1-

Table Index.

Chapter 11: Film Additives Other Than Sucrose p-11:1-

Plate Index.

Chapter 11: Film Additives Other Than Sucrose p-11:1-

Introduction, Chapter 1: Background and Aims.

1.1 Introduction.

The phenomenal growth in the development and use of plastics during the twentieth century has led to an increased need to understand their permeability properties. Their strength, together with lightness, clarity and processability have made them popular for use as packaging materials, encapsulates and for protective coatings.

When using plastics for the aforementioned purposes, the permeability properties of the polymer, or the polymer and any additives used, is of obvious importance. In order to prevent oxygen or water vapour ingress into perishable goods, or carbon dioxide egress from carbonated beverages, multiple layer polymers may be necessary. In barrier coatings, crosslinking and high loadings of inert fillers may be used to prevent water vapour and ionic impurity permeation. Polymers are used in the sustained release of drugs, pesticides, fertilisers and herbicides in order to avoid the cyclical changes in concentration arising from periodic administration. Both monolithic devices and reservoir devices are employed. In the former, the permeant is trapped in the polymer matrix whose permeability controls the release rate. In a reservoir device the permeant, as a solution or suspension, is surrounded by a polymer membrane. If the concentration of permeant within the device is held constant (suspension) then a uniform release rate is maintained.

Enteric coatings exploit the pH sensitivity of the polymer (coating) – being impermeable in the acid environment of the stomach but becoming permeable in the alkaline environment of the intestine. The slow leaching of low molecular weight additives, such as plasticizers and pigments may, however, be undesirable. This is especially the case in food packaging.

Increasingly, membranes are gaining in importance in separation processes, by exploiting selective permeability. Such membranes tend to be very thin films ($\langle$0.1 μm) to give an economic flux, with a porous supporting sub-layer often in the form of a composite asymmetric membrane. Pervaporation, which enables azeotropic mixtures to be separated simply, and at low cost, exploits the differential sorption characteristics of the polymer for one component of the mixture, typically water, which is then removed from the other membrane face by evaporation.

Environmental pressures, and the advantages of safer handling properties and lower toxicity, have led to a greatly increased use of aqueous based coatings. This is at the cost of the greater energy requirements demanded to evaporate water, arising from the higher latent heat of vaporisation compared to more volatile organic solvents, and other disadvantages including poorer film properties, such as a lower gloss finish.

If water soluble polymers are used, then the high solution viscosity limits the rate at which solid film former can be delivered to the substrate, and multiple coating steps may be required. The films formed are likely to show poor resistance on re-exposure to water in the environment, as liquid or its vapour. These disadvantages can be overcome by the use of latices when hydrophobic polymers can be employed and high loadings delivered from the aqueous phase quickly and at lower viscosity.

1.2 Project aims and objectives.

Latex coatings can be applied in a variety of ways including, for example, doctor blades, rollers, or sprays. Rates of delivery of the aqueous phase, in relation to the flow rate and the temperature of a drying air stream, can influence the film morphology, as can the porosity and substrate hydrophilicity. For the current work, consideration was initially given to producing a bench-scale version of a coating apparatus, of the type used in the pharmaceutical industry. However, the large number of process variables, and doubts about the validity of scaling down from pilot plant to laboratory scale led to its rejection.

In order to concentrate on the properties directly attributable to the latex itself, including a reproducible film forming process, a pour-casting technique was preferred, followed by release to yield a free film. The aims of the work were to use the latex films to:

- ✘ give an increased understanding of the mode of transport of solutes, vapours, and gases across the film in order to better control the process of transport (the existing literature on permeant transport through latex films is sparse);
- ✘ study the rate of permeation of probe molecules having a range of solubilities in the polymer phase: in order to identify transport mechanisms by solution-diffusion or through pores;
- ✘ control such permeation by use of leachable additives, and to study the rate of leaching of such additives;
- ✘ test for any asymmetry of permeation arising from differing morphologies on the faces of the film, or from polymer-additive stratifications within the film;
- ✘ study the morphology of films with respect to particle coalescence and to test for aqueous porosity, size exclusion transport, and for permanent porosity developed within the film.

Additives (*i.e.*, water soluble) which were considered included: i, soluble polymers; ii, sucrose; iii, salt; iv, plasticisers; and v, surface active agents. Of these five, i and ii have been studied in detail, and the results are presented in the 'Results and Discussion' section of this thesis. Salt (NaCl) was investigated in less detail, following results showing the effects of its latex destabilising properties on a film's permeability. The addition of plasticiser to certain polymers was found to be a necessity in order to yield a workable free film. However, the level of addition of such an additive, as a means to control a film's transport properties, is limited by the film becoming increasingly tacky and elastic with increasing levels of plasticiser addition (this again limiting the usability of free films prepared from such). The addition of surfactant to a film was overly complicated by the majority of the work being based on commercially available latices which contained endogenous surfactant (see Chapters 6 and 7). Hence, this too was judged as not being a suitable additive.

1.3 Abbreviations.

The following is a list of common abbreviations which occur in the body of the text:

Ø	diameter;
AA	acrylic acid;
AMA	amyl methacrylate (monomer);
BMA	butyl methacrylate (monomer);
C.C.C.	critical coagulation concentration;
C.M.C.	critical micelle concentration;
C.P.V.C.	critical pigment volume concentration;
C_{suc}	level of additive loading in films which causes a break in the trend of the solute permeability coefficient (see Chapter 10);
D.S.C.	differential scanning calorimetry;
E.M.	electron microscope/microscopy/micrograph;
G.P.C.	gel permeation chromatography;
g.p.u.	gas permeability coefficient units (= cm^3 cm s^{-1} cm^{-2} cm.Hg^{-1}) – used in Chapters 8 → 11;
HMA	hexyl methacrylate (monomer);
M.E.K.	methyl ethyl ketone (butan-2-one);
M.F.F.T.	minimum film forming temperature;
N.M.R.	nuclear magnetic resonance (spectroscopy);
PAMA	poly(*n*-amyl methacrylate) (polymer);
PBMA	poly(*n*-butyl methacrylate) (polymer);
P.C.S.	photon correlation spectroscopy;
PHMA	poly(*n*-hexyl methacrylate) (polymer);
P.V.C.	pigment volume concentration;
R.H.	relative humidity;
S.A.N.S.	small angle neuron scattering;
S.E.M.	scanning electron microscope/microscopy/micrograph;
S.I.M.S.	secondary ion mass spectroscopy;
T.E.M.	transmission electron microscope/microscopy/micrograph;
T_g	polymer glass transition temperature
T_m	crystalline melting point.

Introduction, Chapter 2: Preparation and Properties of Polymers and Polymer Colloids.

2.1 Introduction.

The mechanisms of polymerisation reactions can be divided into two main types: **condensation polymerisation**, and **addition polymerisation**. Classifications originally suggested by Carothers in 1929[80], but whose definitions have changed somewhat in the intervening years. The preparation of a polymer latex is usually performed by the process of addition polymerisation and, hence, this chapter concentrates on this mechanism.

2.2 Addition polymerisation.

Polymers prepared from unsaturated monomers are formed by addition reactions across the unsaturated bond, and include poly(vinyl) polymers such as poly(vinyl chloride) and polyethylene (polythene), and also polystyrene and the poly(alkyl acrylates) and poly(alkyl methacrylates). Addition polymerisation occurs by a chain addition process with **initiation** of the active centre (*i.e.*, the site of polymerisation initially on a monomer molecule and henceforth on the growing polymer molecule), **propagation** of the growing molecule (from monomer, to dimer, to trimer......to oligomer......to polymer), and finally **termination** (removal of the active centre) steps.

Typically, the reaction occurs by one of three mechanisms, distinguishable by the way in which the activation of the double bond is carried: free-radical polymerisation; carbonium (cationic) ion; or (anionic) carbanion. (The latter two mechanisms classified under ionic polymerisation.) Many monomers will polymerise by more than one mechanism.

2.2.1 Free-radical polymerisation.

Free radical polymerisations are the most important in regard to the formation of polymer latices. As stated in paragraph 2.2, addition polymerisation occurs by the three steps of initiation, propagation, and termination. In the case of a free-radical polymerisation, the initiation stage concerns the generation of the radicals. A **radical** is an unstable intermediate containing an odd number of electrons and, hence, an unpaired electron. Such an intermediate may be generated by a number of methods, including photolytic decomposition of covalently bonded compounds, dissociation of covalent bonds by high energy gamma radiation, by oxidation-reduction (redox) reactions, or most commonly by thermal decomposition of azo/diazo compounds or peroxides such as potassium peroxydisulphate (persulphate), or benzoyl peroxide.

If I denotes the initiator, and $R\bullet$ the radical, then:

$$\mathrm{I} \xrightarrow{k_d} 2\mathrm{R}\bullet \tag{2.1}$$

where k_d is the initiator decomposition rate constant.

Then, the rate of initiation, R_i, is generally given by:

$$R_i = \left(\frac{d[R\cdot]}{dt}\right)_i = 2fk_d[I] \qquad (2.2)$$

where:

$[R\bullet]$ = radical concentration;
f = represents the fraction of radicals formed;
$[I]$ = initiator concentration.

Propagation occurs by reaction of the radicals with monomer molecules to form monomer radicals. These then further react with monomer molecules such that the chain length is increased:

$$R\bullet + M \xrightarrow{k_i} RM\bullet \qquad (2.3)$$

$$RM\bullet + nM \xrightarrow{k_p} R(M)_nM\bullet \qquad (2.4)$$

where k_i is the initiation rate constant, and k_p is the propagation rate constant.

Termination of the reaction occurs when two radicals react. This may be by one of three mechanisms: combination, disproportionation, or transfer.

Combination: the mutual joining of two radicals:

$$R(M)_mM\bullet + R(M)_nM\bullet \xrightarrow{k_t} R_2(M)_{m+n+2} \qquad (2.5)$$

or:

$$R(M)_nM\bullet + R\bullet \xrightarrow{k_{t,1}} R_2(M)_{n+1} \qquad (2.6)$$

where k_t is the termination rate constant

Disproportionation: in which hydrogen transfer results in the formation of two molecules, one of which has an unsaturated end group:

$$R(M)_mM\bullet + R(M)_nM\bullet \xrightarrow{k_{t,2}} R(M)_mM' + R(M)_nM'' \qquad (2.7)$$

Chain transfer: an atom is transferred between the radical and a different molecule, which is usually capable of continuing the reaction. For example, if the molecule is saturated, the atom must be transferred to the radical:

$$R(M)_mM\bullet + R(M)_n \xrightarrow{k_{t,3}} R(M)_{m+1} + R(M)_{n-1}M\bullet \qquad (2.8)$$

If, however, the molecule is unsaturated (*e.g.*, another monomer molecule) then the atom (*e.g.*, hydrogen) can be transferred either to the molecule or from the molecule:

$$R(M)_nM\bullet + M \xrightarrow{k_{t,4}} R(M)_nM' + M\bullet \qquad (2.9)$$

Termination by chain transfer can lead to branching of the polymer molecule, and also affects the distribution of molecular weights. There is no net loss in the number of radicals available for reaction and so the reaction as a whole is not terminated – only the particular chain from which the radical is transferred.

Bevington [43, 44] *et al.* showed that termination of polystyrene was predominantly by combination, whereas poly(methyl methacrylate) was temperature dependent. Below 333 K, termination was a mixture of disproportionation and combination, whilst above 333 K, termination was entirely by disproportionation.

The rate of termination, R_t, is given by:

$$R_t = -\left(\frac{d[R\cdot]}{dt}\right)_t = 2k_t[R\cdot]^2 \qquad (2.10)$$

2.2.1.1 Retardation and inhibition.

Retardation of a polymerisation reaction occurs when a substance reacts with a radical forming a product that is incapable of adding monomer: the radical so produced being too unreactive to initiate further reactions. The effect of retardation is to reduce the mean lifetime of the radicals, and to reduce their concentration. In the simplest case, retardation acts to reduce the rate of polymerisation. **Inhibition** is very similar to retardation, and occurs when the retarder is very efficient. In the 'idealised' case, inhibition acts to cause a lag at the start of the polymerisation reaction.

It is common for both retardation and inhibition to be seen in the same reaction, with the effect that the length of the polymer chains is reduced compared to the ideal case.

2.3 Polymer colloid polymerisation.

A number of techniques exist which result in the production of a colloidal dispersion of polymer particles. Such dispersions may result from the polymerisation reaction itself, as in an emulsion polymerisation [52, 502], or the polymer, produced in bulk, may be reduced to colloidal dimensions and dispersed to form a pseudo-latex. Polymers prepared by both techniques are the subject of the experimental work in this study.

2.3.1 Free-radical emulsion polymerisation.

Commercially, polymer latices are often prepared by oil-in-water emulsion polymerisation. The reaction involves an oil phase (*i.e.*, the monomer) being partially emulsified in water using a surfactant. (The monomer is typically of low water solubility, *e.g.*, styrene – whose solubility is 0.0271% at 25° C; 0.0382% at 50° C [60] – or the higher molecular weight alkyl methacrylates, etc.) The polymerisation then being initiated by a water soluble initiator – typically an inorganic or organic peroxide – at a temperature greater than the initiator dissociation temperature. Photo or gamma radiation may also be used as initiators, and despite the disadvantage of requiring a gamma source, the method has the advantage of producing a latex uncontaminated by residual initiator fragments (the initial radicals being H• and OH• species [495]), and also not functionalised by the initiator [138] (see Chapter 3).

The result of such a polymerisation is typically a polydisperse latex. However, careful control of the reaction recipe (*e.g.*, initiator type, surfactant type and amount, comonomers, etc.) and polymerisation conditions allow for the particle size distribution to be greatly narrowed leading to monodisperse latices [117, 160, 510] whose size may vary from, typically, 50 → ⟩ 500 nm (but possibly as high as 5 → 10 μm [9, 491]), with controlled (surface) functionality [191, 192, 283, 395, 484, 488] (by the use of a copolymer or selected initiator), and high percentage polymer solids content (up to 60%).

The term emulsion polymerisation is also used, albeit strictly incorrectly, to describe the polymerisation of monomers in systems containing no added surface active agent, and also monomers that are water soluble but whose polymers are insoluble, such as acrylonitrile.

Hofmann and Delbruk [237, 238, 239] patented the results of their work on the polymerisation of monomers in an aqueous suspension just after the turn of the nineteenth century. Their early work on emulsions, stabilised by protective colloids, made no use of initiators, and took some six weeks to react at ambient temperature. In 1927, new patents from America and Germany introduced the use of soaps to aid formation of the emulsion, and initiator to enhance the rate of reaction making production of synthetic latices a viable proposition [119, 328].

The shortage of materials, such as rubber, during the Second World War prompted further work in the area of emulsion polymerisation, and soon afterwards, Harkins produced two papers, first [221] giving the qualitative '*General Theory of Emulsion Polymerisation*' followed, a few years later in 1950, by a more quantitative paper [222], dealing with the emulsion polymerisation of virtually water insoluble monomers in emulsions containing surfactant above its C.M.C. Also at around this time, Smith and Ewart [457] introduced a quantitative treatment of the kinetics of emulsion polymerisation. This paper more than any other has influenced the contemporary literature on emulsion polymerisation kinetics of both surfactant-present *and* surfactant-free systems.

It was in 1946 that Hohenstein and Mark [241] produced a paper on emulsion polymerisation of polystyrene in the absence of surfactant. Although the latices so produced tend to be less stable than those containing surfactant, surfactant-free latices tend to be more easily prepared monodispersed and are thus of considerable academic interest [194, 200, 201, 226] due to their model nature: the properties of surfactant-free latices being more readily characterised without the necessity of removing 'contaminating' surfactant.

2.3.1.1 Mechanism and kinetics of radical-initiated, surfactant-present, emulsion polymerisation.

The vast majority of aqueous emulsion polymerisation reactions are performed in the presence of a surfactant (soap, emulsifier or detergent), above the surfactant's C.M.C. The C.M.C. is that surfactant concentration above which there occurs a great increase in the formation of aggregates (micelles) of surface active agents. These aggregates are arranged such that the surfactant molecules (50 → 100) are oriented with the hydrophobic chains facing inwards, and the hydrophilic heads forming the water-micelle interface. (For a given surfactant, the C.M.C. decreases with increasing hydrophobic chain length. However, the value remains approximately constant above a length of ca C_{18}. This is thought to be due to such carbon chains becoming coiled and, hence, the actual length being less than expected [344]. The methods of manufacture of surfactants often lead to the product having a range of sizes (*i.e.*, number of carbons: due to chain branching) such that the C.M.C. may vary somewhat from batch to batch.) The aforementioned molecular orientation is energetically favourable, whilst still allowing the formation of water-water hydrogen bonds which are prevented by surfactant in solution. The formation of such aggregates was recognised as early as 1913 by McBain [334]. Surfactants used in emulsion polymerisations are typically anionic, but may be cationic [431], zwitterionic (amphoteric [270]), or non-ionic [370]: the latter usually having a lower C.M.C. for a given carbon chain length (*i.e.*, they are more surface active and form micelles more readily than ionic surfactants because there is no charge repulsion to be overcome during aggregation).

Since the work of Harkins [221] and Smith and Ewart [457], a large number of papers have been written on the kinetics of emulsion polymerisation (see review by Vanderhoff [502]). This is partly because the kinetics are not easily defined, despite the simplicity of the fundamental recipe (although it is not uncommon for further components to be added, *e.g.*, more than one surfactant, monomer, or buffer), and partly because no single regime works for all types of monomer. The polymerisation of styrene is particularly well covered, based on Smith and Ewart's regime, but those kinetics apply less favourably to the more water soluble (*e.g.*, vinyl) monomers due to the increased monomer in the aqueous phase [352].

The emulsion polymerisation reaction is normally divided into three intervals [179, 348, 486]:

Interval 1: particle nucleation. This lasts until the total number of polymer particles (number density) becomes constant (typically at ca 5% conversion).

Interval 2: lasts from the end of interval 1 until the monomer no longer exists as a separate phase. During this stage, particle volume increases in direct proportion to the degree of conversion of monomer to polymer.

Interval 3: starts at the end of interval 2, and lasts until the end of the reaction. Interval 3 is probably the least studied by researchers in the field of emulsion polymerisation kinetics.

2.3.1.1.1 Polymerisation interval 1.

Harkins [221] has explained the important role of surfactant in emulsion polymerisation reactions.

Agitation of an oil-soap system, in which the soap is present above its C.M.C., causes the formation of an oil (monomer) in water emulsion, consisting of droplets of oil in the aqueous phase. These droplets may vary over an order of magnitude in size (but are not usually less than 1 μm in diameter, dependent on the degree of agitation). Before the Harkins paper of 1947, it was generally believed that the emulsion droplets themselves were polymerised. However, as pointed out by Harkins, the polymer particles so produced were very much smaller than the droplets forming the emulsion.

Harkins proposed that the emulsion droplets simply acted as reservoirs for the monomer, when it was virtually insoluble in the aqueous phases: the surfactant (and monomer) being in dynamic equilibrium between: i, the emulsion droplets; ii, the aqueous phase; and iii, the surfactant micelles. The monomer was transferred, via diffusion through the aqueous phase, from these storage sites, to soap micelles, typically present at a number density of ca 10^{18} g^{-1} of water. The cores of these micelles, swollen with solubilised monomer, were thus proposed to be the principal sites for the initiation of polymer nuclei: the radicals, generated in the aqueous phase diffusing and having a greater chance of collision (and, hence, absorption), with the micelles, than the monomer droplets (typically present with a number density of ca 10^{12} g^{-1} of water). This is thus termed the **micellar nucleation** theory. As these nuclei grew larger than the micellar core, they appeared in the aqueous phase as exceedingly small particles which attracted monomer from it (the aqueous phase), becoming monomer-swollen polymer particles. (Harkins [221], citing an earlier paper [157], also noted that nucleation could occur in a minor secondary locus, *i.e.*, the water phase, and that this locus became increasingly important as the amount of soap was reduced, becoming the principal loci if no soap was present.) The principal loci of polymer chain growth were thus the monomer-swollen polymer particles (in the aqueous phase), with the polymer stabilised by the adsorption of surfactant from the aqueous phase. Hence, the growth of the particle initially utilises the monomer within the micelle, and henceforth, from the aqueous phase, which swells the growing polymer particle: the monomer lost from the water being replenished by that from the emulsified droplets. Not all micelles would be utilised in the reaction, and those not targeted by a radical would break up with the surfactant being used to stabilise the growing polymer particles. Harkins concluded that the disappearance of the surfactant micelles corresponded to the time after which no new particles were formed.

In view of the fact that particles can be formed at surfactant concentrations below the C.M.C., doubts [416] were cast on the micellar nucleation theory. Harkins' theory of micellar nucleation gave no explanation of how the (typically) anionic initiator ion radical (hydrophilic) entered the hydrophobic interior of the micelle. To do so, it presumably must also overcome the charge repulsion generated as it approached the (typically) anionic micelle (anionic by virtue of the polar functional head groups of the surfactant molecules forming the water-micellar interface). The resolution of this problem also aids the explanation of the emulsion polymerisation of the more water soluble monomers, of surfactant-free emulsion polymerisation, and of emulsion polymerisation where surfactant is present at a concentration below its C.M.C.

Priest [403], Roe [416], and Fitch [161, 163] *et al.* proposed essentially similar mechanisms under which nucleation occurred in the aqueous phase and, hence, favoured the more water soluble monomers. Fitch's **homogeneous nucleation** mechanism proposes that the initiator reacts with the monomer present in the aqueous phase: the reaction propagating the formation of oligomeric material. Beyond the addition of a certain critical number of monomer units (4 → 6), the hydrophobic chain together with the anionic head lead to the oligomer achieving surface active properties which precipitate the oligomer above a critical concentration and/or, in surfactant-present systems, can form micelles with the soap [497] (presumably due to exchange with a surfactant molecule of a micelle, made possible due to the dynamic equilibrium between surfactant in the water and that in the micelle).

Coagulative nucleation extends the theory of homogeneous nucleation stating that the oligomer ('precursor') initially formed by precipitation may be colloidally unstable, in systems below the C.M.C. of the soap, and undergo limited coagulation with other particles until stability is attained[217 - 220]. A quantitative theory of coagulative nucleation was developed by Feeney[153] *et al.* based on the DL[114]VO[516] theory of colloid stability.

Ugelstad and Hansen[486] describes a further mechanism whereby initiation of a polymerisation occurs mainly in the emulsified monomer droplets. This was, however, brought about by preparing a finely divided, stable, emulsion, with low amounts of surfactant, such that the particles were more effective in capturing the radicals produced in the aqueous phase.

The various theories of nucleation (collectively known as the HUFT theory of Hansen and Ugelstad, and Fitch and Tsai – as described above), and current research trends, have recently been reviewed by Hansen[215], showing that homogeneous/limited coagulation mechanisms of nucleation are of obvious importance for the understanding of nucleation in surfactant-free systems, or systems of low surfactant concentration. However, micellar nucleation cannot be ignored: differences in the number of particles are apparent in polymerisation systems when the C.M.C. is encompassed, such that homogeneous and micellar nucleation should both be considered for such systems with high soap concentrations.

The qualitative theory of Harkins was addressed quantitatively by Smith and Ewart who determined limits to the number of particles generated, and derived a recursive formula that described the steady state process of interval 2 of the polymerisation, for the system in which the number of polymerising loci is constant (**steady-state approximation**).

The treatment of interval 1, and the determination of the upper and lower limits to the absolute number of particles generated, *N*, was based on a number of assumptions that in practice may be somewhat erroneous. The upper limit arrives by considering only micellar capture of radicals; the lower limit includes capture by polymer particles as well as by micelles. However, it is generally agreed by most researchers in this field that the true value is within the calculable range, as given by Smith and Ewart:

$$0.37\left(\frac{\rho}{\mu}\right)^{\frac{2}{3}}(a_sS)^{\frac{2}{3}} \leq N = K\left(\frac{\rho}{\mu}\right)^{\frac{2}{3}}(a_sS)^{\frac{2}{3}} \leq 0.53\left(\frac{\rho}{\mu}\right)^{\frac{2}{3}}(a_sS)^{\frac{2}{3}} \qquad (2.11)$$

where:

ρ = rate of formation of radicals per cubic centimetre of aqueous phase;
μ = (constant) rate of increase of volume of a particle;
a_s = interfacial area occupied by a gram of soap (assumed to be the same for on the polymer particles as in the soap micelles);
S = total amount of soap associated with one cubic centimetre of water;
K = a constant in the range: $0.37 \leq K \leq 0.53$.

For the above two limiting cases, the average number of radicals per particle has been calculated. The upper limit, according to Ugelstad and Hansen[486], is approximately equal to unity (100% radical capture efficiency), at the end of interval 1. The lower limit was not determined by Smith and Ewart, but has been determined by Gardon[179], using his own extension to the theory, as 0.67. These values are higher than the value of 0.5 predicted by Smith-Ewart case 2 kinetics for interval 2 (see below), implying a maximum in the emulsion polymerisation rate at the end of interval 1. Ugelstad and Hansen[486] note that such a maximum has not been detected (for styrene polymerisations).

2.3.1.1.2 Polymerisation interval 2.

The equation that describes interval 2 contains variables that describe: the formation rate of radicals; the termination rate in their isolated reaction loci (*i.e.*, the particles) and the water; the rate of polymerisation of a radical in its reaction locus; and the size and number of reaction loci. The Smith and Ewart[457] **recursion equation** is derived from the rate of formation of reaction loci, containing *n* number of radicals, being equal to the rate of disappearance of such loci, such that the number of loci, N_n, is constant:

$$\begin{aligned} N_{n-1}\left(\frac{\rho'}{N}\right)+N_{n+1}k_0a\left(\frac{n+1}{\upsilon}\right)+N_{n+2}k_t\left(\frac{(n+1)(n+2)}{\upsilon}\right) \\ = N_n\left[\frac{\rho'}{N}+k_0a\left(\frac{n}{\upsilon}\right)+k_tn\left(\frac{n-1}{\upsilon}\right)\right] \end{aligned} \tag{2.12}$$

where:

N = number of particles containing n radicals;
ρ' = the overall rate of entrance of radicals into all N loci;
k_0 = rate constant for the rate of transfer of radicals out of locus;
a = interfacial (surface) area through which radical transfer can occur from a locus;
υ = particle volume, such that (υ/n) = radical concentration at some loci;
k_t = radical termination rate constant.

Alternatively, this can be rewritten in the more general form of a differential equation:

$$\begin{aligned} \frac{dN_n}{dt} = \left(N_{n-1}-N_n\right)\frac{\rho'}{\upsilon}+\left[N_{n+1}(n+1)-nN_n\right]\frac{k_0a}{\upsilon} \\ +\left[N_{n+2}(n+2)(n+1)-n(n-1)N_n\right]\frac{k_t}{\upsilon} \end{aligned} \tag{2.13}$$

where n = 0, 1, 2, 3...n. Note that under steady state conditions, the left-hand side of equation 2.13 is equal to zero, such that equation 2.13 simplifies to equation 2.12. The validity of this was questioned by Ugelstad and Hansen[486] and Gardon[179] due to the time variant nature of the particle volume, υ, which in the case of large polymer particles may lead to variation in the average number of radicals per particle, $\bar{n}$, as the volume increases (*i.e.*, Smith and Ewart case 3: see below). Ugelstad answers this explaining that the assumption:

$$\frac{dN_n}{dt} = 0 \tag{2.14}$$

is a valid assumption providing that the rate of attainment of the equilibrium value of $\bar{n}$ for any value of υ is rapid compared to the rate of change of the equilibrium as υ increases, and that this is fulfilled under typical reaction conditions, but dependent on the ratio of the termination rate constant to the propagation rate constant ($k_t : k_p \gg 0.075$ in the worst case). Such an assumption is known as the **quasi-steady-state condition.**

Smith and Ewart solved the recursion equation for just three limiting cases, based upon the average number of radicals per particle, $\bar{n}$:

Case 1: $\bar{n} \ll 1$: the rate of radical entry into the particles is much less than the rate of disappearance of the radicals. Chain transfer of radicals to other particles, usually monomer, has a high probability, and the number of particles containing radicals are relatively few in number.

Case 2: $\bar{n} \approx ½$: there exists a low probability of a radical being transferred from a particle, after entry, and activity only ceases by termination due to the entry of another radical. It is assumed that the particle will grow for 50% of the time: 50% of the radicals entering the particle will 'activate' particle growth, whilst 50% will cause termination. Hence, on average, one half of the total number of particles will be growing at any time during interval 2.

Case 3: $\bar{n} \gg 1$: the particles are large enough to support two or more growing radicals at any one time.

Of the above three cases, 1 and 3 are the two extremes, whilst in practice, case 2 could bias towards either. Experimental evidence suggested that case 2 best fitted the results for emulsion polymerisation of relatively insoluble monomers, notably styrene [456]. It is assumed that the rate of reaction in the particles is equal to the rate of polymerisation, R_p (moles dm^{-3} s^{-1}):

$$R_p = -\frac{d[M]}{dt} = k_p[M]_p[R\cdot] = k_p[M]_p\bar{n}\left(\frac{N}{N_A}\right) \tag{2.15}$$

where:

$[M]$ = Overall monomer concentration;
k_p = radical propagation rate constant;
$[M]_p$ = monomer concentration in the particles;
$[R\bullet]$ = free radical concentration;
N = number of particles per unit volume of the aqueous-phase;
N_A = Avogadro's constant.

(Note that steady state implies that $R_i = R_t$ (as given by equations 2.2 and 2.10) such that:

$$[R\cdot] = \left(\frac{fk_d[I]}{k_t}\right)^{½} \tag{2.16}$$

where:

f = represents fraction of free radicals formed;
k_d = initiator decomposition rate constant;
$[I]$ = initiator concentration;
k_t = termination rate constant.)

Hence, for Smith-Ewart case 2 kinetics, and thus emulsion polymerisation, the rate of polymerisation is given by:

$$R_p = k_p[M]_p\frac{N}{2N_A} \tag{2.17}$$

The mean degree of polymerisation, $\overline{DP}$, (*i.e.*, the average number of monomer units per polymer molecule) is given by:

$$\overline{DP} = k_p[M]_p \frac{N}{\rho N_A} \tag{2.18}$$

Over the last forty-five years, the basic ideas of the theory of Smith and Ewart have resulted in much research as to its applicability, and the theory has been extended to include assumptions originally not considered, or simply dismissed. Stockmayer [467] first determined a **general solution** for the Smith and Ewart recursion equation, with the results (for the values of $\bar{n}$) in the form of a ratio of Bessel functions: a theory later extended by O' Toole [368] to include the rate of radical transfer from a particle relative to the rate of radical termination. Ugelstad [487] *et al.* also calculated a solution to the recursion formula, based on a mass balance of the free radicals in the system. These solutions did still, however, rely on steady-state conditions. Other workers have produced solutions under non-steady-state conditions. Gardon produced a whole series of papers [179 - 184] on the kinetics of intervals 1 and 2 of the emulsion polymerisation reaction, that started with an extension to the Smith and Ewart theory [179] and included a computer-generated general solution under non-steady-state conditions (accounting for radical termination but assuming a negligible rate of radical exit from the polymerisation loci) in the third paper of the series [181]; the results to which verified those of Smith and Ewart, and Stockmayer for case 2 assuming no desorption of radicals. Gilbert [193, 224, 225] *et al.* also investigated the non-steady-state kinetics, using a method involving matrices (analogous to quantum mechanical methods for determining solutions to Schrödinger's wave equation), to produce a result showing good correlation with the results of O' Toole for values of $\bar{n} \leq 0.6$.

2.3.1.1.3 Polymerisation interval 3.

For relatively insoluble monomers, the monomer will be dissolved in the polymer particles, whereas in the case of the more soluble monomers (*e.g.*, vinyl acetate), a significant amount may still be dissolved in the water. In particles containing relatively large amounts of monomer, the particle volume may decrease as the monomer polymerises.

Russell [428] *et al.* considers the termination reaction as occurring in three steps: i, translational diffusion of the radical coils to bring two radicals into close proximity; ii, contact of the radical chain ends by conformational reorientation (segmental diffusion); iii, surmounting the (small) activation energy of termination. Because of the high degree of polymer chain entanglement at high monomer to polymer conversion, the chain segment translational diffusion is decreased such that radicals come into contact by what Russell refers to as "roving head diffusion" (Russell notes that this has previously been referred to as reaction diffusion [438] and residual termination [183]). The termination rate is a function of the ability of the radicals to diffuse in a medium of high viscosity (if the activation energy of termination is small). In bulk polymerisation reactions, as the viscosity of the media increases with increasing conversion of monomer to polymer, the radical termination rate, k_t, decreases, due to the decreased diffusivity of the polymer radicals. The decrease in termination rate may lead to an increase in the rate of polymerisation, and increased molecular weight, due to the increased lifetime of the growing polymer chains. This effect is known as the **Trommsdorff effect** [483] (also called the gel effect, and auto-acceleration). The effect is also important in emulsion polymerisation[1] (in reactions where radical termination is rate limiting {*i.e.*, when radical desorption is rate determining} and where there is some chain flexibility), and Van der Hoff[496] cites a number of authors [40, 566] who have observed the effect in methyl methacrylate, where the effect is particularly strong. Russell [428] suggests that the Trommsdorff effect in emulsion polymerisation arises at high conversions due to a transition from a flexible polymer chain to an increasingly rigid "dangling" chain end and, hence, the gradual increase in reaction rate. Similarly, Howard [223] discusses the applicability of 'compartmentalisation', in which the active centres (radicals) are isolated, and thus decrease the probability of termination by combination, to account for the relatively high rates of reaction in emulsion polymerisations.

2.3.1.2 Surfactant-free emulsion polymerisation.

Latices for use as **model colloids** (*i.e.*, well characterised with respect to end group functionality, ideally spherical, and free of electrolyte/surfactant) were reviewed by Hearn [228] *et al.* in 1981, and the cleaning techniques applied to latices were more recently reviewed by Wilkinson [539]. If surfactant is not added to the latex preparation, then the uncertainty as to its complete removal by cleaning is eliminated. Low molecular weight, and surface active agents, may, however, be generated during the polymerisation process. Goodall [196] *et al.* showed that the surfactant-free process was reproducible for styrene with respect to particle size, but the surface charge characteristics were less certain, being particularly dependent on the cleaning process employed (*e.g.*, dialysis or serum replacement {see Chapter 3}).

In surfactant-free emulsion polymerisation, the monomer is not emulsified prior to initiation and so forms a water immiscible layer that is consumed, as the reaction proceeds, by imbibition to the growing particles. The driving force for the depletion of the bulk monomer phase is the maintenance of saturation solubility in the water phase. Guthrie [211] (following Palit [380] *et al.* and Eliseeva [143] *et al.*) preferred the terminology that describes styrene surfactant-free polymerisation as **A.P.S.** *i.e.*, **A**queous **P**olymerisation of a **S**lightly soluble monomer. (*cf.* **E.P.S.** for **E**mulsion **P**olymerisation). All A.P. systems commence with polymerisation in the aqueous phase, and depending on the solubility of the monomer, S (⟨15 mM), M (⟨290 mM), or V (⟩290 mM), may yield latex, precipitated polymer or solution polymer products. Fitch and Tsai's [163] work on homogeneous nucleation described the nucleation mechanism of methyl methacrylate (**A.P.M.**). However, the presence of a large amount of oligomeric, 1000 molecular weight, material for styrene suggests a micellisation type mechanism might be more appropriate for that particular A.P.S. system. Guthrie calculated that a '**binary flocculation**' process, *i.e.*, aggregation of identically sized particles, best described Goodall's [196] data for the nucleation process. After stabilisation at constant number density, the kinetics followed a linear $C^{2/3}$ versus t (C = percentage conversion, t = polymerisation time) relationship in accord with the Smith-Ewart case III

---

[1] The effect differs in emulsion polymerisation compared to bulk polymerisation. In the former, the reaction rate increases with increasing weight fraction of polymer, whereas in bulk polymerisation there is a large increase in rate over a narrow conversion range [428].

core-shell regime, as proposed by Grancio and Williams [206] (see paragraph 2.3.1.3). That this oversimplified the process was suggested by the bimodal molecular weight distribution indicative of two reaction loci. Although core and shell were the obvious candidates, a further complication in this system was the occurrence of an anomalous particle morphology [196, 197]: despite the final products appearing as complete spheres, a void region existed during growth, whose size tended to be greatest at around 40% (monomer to polymer) conversion, which could be observed in particles viewed by transmission electron microscopy. This void was believed to arise from a region of oligomeric material in which the monomer was preferentially soluble and protected from polymerisation by a local high surface charge density until the later stages of the reaction when other supplies of monomer were exhausted.

Chang and Chen [94] found, for surfactant-free styrene co. 2-methyl-2-propene sulphonate, the same linear $C^{2/3}$ versus t relationship, and bimodal molecular weight distributions. This was attributed to a failure of the monomer concentration to be maintained uniformly in larger particles, the monomer tending to be consumed in the outer layers before reaching the core. The lower monomer concentration in the core yielding higher viscosity, retards termination and leads to higher molecular weights in the core. Thus, the importance of the shell increases with increasing particle size, finally becoming the dominant locus. Chang did not report anomalous particle morphology for their system, presumably reflecting the different nature of the copolymer involved in nucleation.

Elbing *et al.* [141] also found $C^{2/3}$, as a function of reaction time, was linear for surfactant-free acrylonitrile polymerisation. Acrylonitrile, *cf.* other vinyl monomers, is very soluble in water, but insoluble in its polymer.

Roulstone [423] found that for the surfactant-free polymerisation of BMA, Smith-Ewart case III kinetics was obeyed. Particle size could be controlled by changing the ionic strength and initiator concentration of the polymerisation recipe, but instead of a steady particle number density being established, it decreased throughout the reaction. This was ascribed to the particles tending to aggregate throughout the reaction (although the final product was said to be monodisperse, and this was apparent in electron micrographs of films produced from the latices). Rates of reaction were essentially constant. There was, however, some uncertainty as to the kinetics, due to the (high) speed of the reaction, and the particle sizes (measured during the course of the reaction, by P.C.S.) being those of the monomer swollen particles.

2.3.1.3 Core-shell (latex particle growth) theory.

In 1970, Grancio and Williams [206] proposed a model, for compatible systems of monomer and polymer (*i.e.*, when the monomer is soluble in the polymer), for the morphology of a growing polymer particle, based on the hypothesis that polymerisation, causing the growth of the particle, occurred at the particle surface. The particle morphology, during the course of the reaction, thus consisted of a polymer-rich core surrounded by a shell of highly monomer-swollen polymer. (Such a core-shell morphology was already known for incompatible copolymers [506]. See paragraph 2.3.1.4.) Their evidence for this was based on the assumption that styrene polymerisation followed Smith and Ewart case 2 kinetics (such that $\bar{n}$ = ½), and led to the classical equation of rate, for interval 2, taking the form:

$$R_p = k_p[M]_s \bar{n} \frac{N}{N_A} \tag{2.19}$$

where:

$[M]_s$ = concentration of monomer in the shell.

(*Cf.* Equation 2.15)

Williams *et al.* produced a number of research papers (showing both morphological, kinetic and thermodynamic evidence) to authenticate their ideas [278 - 280, 540, 541], and the pros and cons of the core-shell hypothesis have been reviewed by both Gardon [185], concluding that it was unlikely that a concentration gradient would develop in the latex particles, and Vanderhoff[499] who concluded that the model was "reasonable" but that the experimental observations could be explained by other hypotheses.

As stated previously, the larger particle sizes resulting from surfactant-free polymerisation would best be described by Smith and Ewart case III kinetics, which provides a polymerisation rate, during interval 2, given by:

$$R_p = \frac{k_p[M]_p}{N_A}\left(\frac{\rho_A \upsilon_p}{2k_t}\right)^{\frac{1}{2}} \tag{2.20}$$

where:

υ_p = volume of particles per dm^3;

ρ_A = rate of radical absorption.

In terms of the core-shell model, this becomes [486]:

$$R_p = \frac{k_p[M]_s}{N_A}\left(\frac{\rho_A S_p L_s}{2k_{ts}}\right)^{\frac{1}{2}} \tag{2.21}$$

where:

$[M]_s$ = monomer concentration in the shell;

S_p = particle surface area per dm^3;

L_s = shell thickness;

k_{ts} = radical termination rate constant in the shell.

Hearn [229] *et al.* investigated the surfactant-free emulsion polymerisation of styrene in interval 2, and found that the results were best in accord with the theories using a surface polymerisation method for large particles: *i.e.*, Smith and Ewart case III applied to the core-shell model.

The research at Lehigh University involving S.A.N.S. to characterise latex particle structure in latices resulting from equilibrium swelled (monomer-polymer) polymerisations, has been reviewed by Sperling[459] *et al.*, with the author claiming that the results are in agreement with both Williams' [206, 278 - 280, 540, 541] core-shell model and Gardon's [185] uniform (structure-wise) particle: the differences in structure being determined as a result of differences in the ratio, R_g/r (where R_g = chain radius of gyration[1] and r = latex particle radius), or the 'squared dimensional ratio' (*S.D.R.*), *i.e.*, the ratio of the weight average molecular weight to the square of the particle diameter. (Note that R_g/r is comparable to the *S.D.R.* When the *S.D.R.* = 0.1, R_g/r = 0.2.) Citing the work of Linné[321] *et al.* and Yang[546] *et al.*, results showed that as the *S.D.R.* increased (*i.e.*, large particle → small particle) the particles showed a maximum in terms of 'supramolecular' structure when the ratio = 0.1. When the latex systems used in the work of Williams and Gardon were compared (with respect to their *S.D.R.*), it was found that Williams' system was in the regions where structure would have been possible, whereas Gardon's particles were closer to the region of uniform molecular mixing. Following further study at Lehigh, Sperling defined three polymerisation regimes that may occur for equilibrium swelled latices:

- ✗ Large particle radius and/or low molecular weight polymer ⇒ homogeneous particle;
- ✗ $R_g/r \cong 0.1 \rightarrow 0.2$, the particle core forms from the polymer that polymerises first ⇒ core-shell particle structure;
- ✗ High molecular weight and/or small particle size ⇒ homogeneous particle.

The polymerisation reaction is thus discussed by Sperling[459] *et al.*, in terms of initiation occurring in the water phase, followed by capture of the oligomeric radical by the monomer-rich shell of the latex particles (assuming that the reaction is not starved of monomer). The polar end groups were then said to remain on the particle's surface whilst the growing chain propagated into the (initially) monomer rich core – therefore reducing the monomer concentration gradient within the particle to a limiting concentration and (monomer) shell thickness. The monomer rich shell being maintained by an 'entropic repulsive wall' depletion layer effect[2]. If, however, chain transfer were to occur, then the chains need not have ionic end groups, and are not restricted to the particle surface

As a further complication to the core-shell model, Cox[102] *et al.* attributed the formation of anomalous particles (*i.e.*, particles, taken from the polymerisation before complete conversion, which showed a hollow – apparent as regions of low electron density in both scanning and transmission electron micrographs), as observed in surfactant-free styrene polymerisations, to monomer partially surrounded by a polymer shell: the monomer being evaporated by the electron beam during electron microscopy to leave a void.

2.3.1.4 Seeded growth, functionalised and core-shell latex particles.

Production of surface-modified latices by staged addition of monomers in emulsion polymerisation is an important industrial process to control particle properties, improve film forming ability and mechanical properties, and to increase selective reactivity. For model colloid applications it should be possible to control surface charge density at fixed particle size, control particle size at fixed charge density, and to produce model films from hard core-soft shell latices or vice-versa.

---

[1] The radius of gyration is defined[349] as the root-mean-square distance of the component of the polymer chain from the polymer molecule's centre of gravity.

[2] An interfacial 'repulsive wall' is formed when a surface shows a preference for the solvent, compared to the polymer, such that a (polymer) depletion layer is formed[8, 113, 414].

The technique of **seeded polymerisation** (surfactant-present or surfactant-free) involves the use of a pre-prepared latex to act as the seed particles for new growth. In kinetic studies of emulsion polymerisation, this method has the advantage of bypassing the particle nucleation stage: if sufficient number of seed particles are available initially, then no new particles are formed [456]. A disadvantage is that careful control is required in order to prevent the growth of a secondary crop of particles. Seeded polymerisations may be used to prepare abnormally large latex particles [97, 227]. This requires the particle size being increased in successive stages, with the previous stage being used as the seed for the next.

A functional comonomer can be added: i, in the initial monomer charge; ii, semi-continuously; iii, in a seeded growth; iv, by shot-growth, *i.e.*, when the core is allowed to proceed to high percentage conversion before the addition of the second monomer.

In terms of concentrating the second monomer in the surface layers, the seeded-growth and shot-growth techniques offer the best prospects. However, in addition to the complications of secondary nucleation and growth, a concentric shell over-coating morphology cannot be assumed, especially if the seed is more polar than the shell polymer. (Similarly, semi-continuous graft copolymerisations [5] or seeded growth reactions [96] do not necessarily lead to an encapsulation of the core polymer.) *E.g.*, complex confetti shaped particles, '*current bun*' morphologies, interpenetrating polymer networks [340], and incomplete '*raspberry-like*' shells can occur [101, 364]. However, Lee and Rudin [309] describe some methods by which the particle morphology may be controlled. Sakota and Okaya [433] found 60% incorporation of carboxyl group (-COOH) functionality in shot-growth at 80% conversion, rising to 80% incorporation at 95% conversion. Chainey [86, 89] *et al.* compared shot-growth with seeded-growth, finding that the critical number density required to prevent secondary growth was lower, and that the particles were regular in shape and with the shell attachment increased, presumably by interfacial graft copolymer, for the shot growth technique. Greater swelling of core-polymer by monomer was observed for shot-growth, but no direct proof that a core-shell morphology had been attained was provided in this work. Kim [282] produced a range of highly sulphonated polystyrene latices in which the surface charge density and particle size could be independently varied. A sodium styrene sulphonate-styrene shot was employed (the styrene being used to promote oligomer hydrophobicity and enhance attachment), being added at $\rangle$ 90% conversion. The sodium styrene sulphonate to styrene ratio (0.16 : 0.46) was found to be critical in avoiding secondary growth and poly-electrolyte formation. Ruthenium tetroxide staining of the shell was used to confirm a core (dark)-shell (light) morphology.

As stated above, the particle morphology resulting from a staged polymerisation is dependent on the respective hydrophilicity of the core (or seed) and shell monomers. The net interfacial energy is minimised when the shell monomer is more hydrophilic than the core. The polymerisation of a hydrophobic monomer in the presence of a hydrophilic core can result in the hydrophobic monomer (polymer) forming a core inside the initial hydrophilic latex. This was thus termed an "inverted" particle morphology [308]. Rudin [310, 511] *et al.* have used inversion polymerisation techniques to produce a core-shell latex in which the hydrophilic polymer resides at the core. Although apparently thermodynamically unfavourable (in terms of minimising the Gibbs free energy of the system {as discussed by

Lee [310, 311], following Sundberg [473]}), the desired result was achieved by careful selection of reaction recipe, and mode of monomer addition, etc. – to control particle surface polarities and areas and also the thermodynamics and kinetics of the process. (The kinetics of any morphological development are of importance since a thermodynamically stable morphology may not be attained if the change encounters a kinetic barrier.)

2.3.2 Other polymerisation techniques.

The technique of **suspension polymerisation**, like emulsion polymerisation, involves a heterogeneous mixture of a monomer phase dispersed as droplets in an aqueous system: dispersion being by means of a dispersant (water soluble suspending agent, *e.g.*, poly(vinyl alcohol), gelatin, and small amounts of emulsifiers) combined with agitation. Polymerisation leads to a dispersed, solid, polymer phase. The technique differs from emulsion polymerisation in that the initiator is monomer soluble rather than water soluble, and the kinetics of bulk polymerisation are more appropriate. The polymer particles produced by suspension polymerisation are, typically, approximately the same size as the droplets of the dispersed phase, and are thus much larger than the product of emulsion polymerisation reactions, ranging in size from tens of microns up to a few millimetres in diameter [19]. The particle size can be controlled and is dependent on a number of factors such as recipe, agitation rate and reactor design [20]. Commercially, the technique is normally used to prepare hard glassy polymers such as poly(methyl methacrylate) and polystyrene. Softer polymers tend to become sticky and aggregate. Inverse (water in oil) suspension polymerisation is, as its name suggests, the opposite of that described above.

In the process of **Dispersion polymerisation**, the monomer and initiator are dissolved in an organic solvent (or aqueous solvent for water soluble monomer) which is a non-solvent for the polymer (*e.g.* styrene in alcohol), together with a steric stabiliser (*e.g.*, poly(vinyl pyrrolidone)) to form a homogeneous mixture. After nucleation, oligomeric material is precipitated, absorbing stabiliser to form the stable particle nuclei. The polymerisation reaction continues in the particles as they swell with monomer from the continuous phase. Particles produced by dispersion polymerisation may range in size from less than a micron up to ten microns [19]. Almog [9] *et al.* found that the final particle size was dependent on the solvency power of the organic continuous phase, whilst the surfactant concentration affected the dispersity, but not the particle size.

Precipitation polymerisation is similar to the process of dispersion polymerisation with the exception that the particles formed are not swollen by the monomer (or the continuous phase). The reaction is performed without a stabiliser. The locus of polymerisation is the particle's surface, and particles so produced are generally extremely polydisperse, irregular in shape and may be porous. Size ranges produced are similar to those of dispersion polymerisation reaction.

Pseudolatices are colloidal-sized polymer dispersions prepared from, for example, bulk-polymerised water insoluble polymers by mechanical means. The method of preparation, developed in the mid-seventies, allows virtually any water insoluble polymer to turned into a pseudolatex, even natural polymers such as cellulose derivatives. Natural-polymer pseudolatices, when compared to latices prepared by emulsion polymerisation, although not very monodisperse, have the advantages of not containing residual monomer, catalyst or initiator fragments. It is thus easier to prepare a pseudolatex that is readily acceptable (safe) for use as a drug coating: utilising polymers that cannot be prepared directly in the form of a latex. The first such commercial pseudolatex, accepted for drug use, was an ethyl cellulose pseudolatex called 'Aquacoat®', produced by the FMC Corporation[1] of America. This is typically used for controlled release drug encapsulation [14].

2.4 Microparticles and encapsulation.

Polymers and latices are often used to encapsulate, for example: active drug compounds (to protect, contain, and assist in targeting their site of application [127]); as *scratch-and-sniff* type devices; although originally they were developed to encapsulate dye in carbonless copy-paper. In addition to tablet coating, they are used pharmaceutically as what are known collectively as microencapsulants or **microparticles** (also called **microspheres** and **nanoparticles**). The particles find use as encapsulants for controlled release devices (see Chapter 6), and are also suitable, by virtue of the ability to functionalise the surface, for immunological studies [410]. Arshady defines a microsphere as an empty microcapsule, and the various manufacturing techniques for such particles (such as coacervation, suspension and crosslinking, and solvent extraction or evaporation) have been reviewed [16, 17, 18, 19, 127, 481]. In keeping with the trend towards environmentally friendly products, Scranton [441] *et al.* described a method of producing hydrophilic microparticles (poly(hydroxyethyl methacrylate)) from an aqueous salt solution, using the technique of suspension polymerisation and crosslinking: the salt acting to reduce the monomer's aqueous solubility and, hence, form the suspension.

Encapsulation of, for example, a drug requires that the discontinuous phase of the emulsion (which is used to form the particles) is prepared from the agent to be encapsulated, as well as the polymer and perhaps an organic solvent, in the aqueous continuous phase.

In the coatings industry, hollow latex particles, which encapsulate an air void, are of interest due to their forming opaque films (see Chapter 4) which exhibit hiding characteristics making them suitable for use as paints. Interest [244, 292, 297, 361, 362, 363, 365, 505] in such hollow (or multi-hollow) polymer particles has grown since the publication of a European patent [291] in 1981. Their preparation is typically a multistage process whereby a shell polymer is formed around a core which can be hollowed, for example, by neutralisation and drying.

◆

---

[1] FMC Corporation, Food and Pharmaceutical Products Division, Philadelphia, U.S.A.

Introduction, Chapter 3: Latex (and Polymer) Characteristics.

3.1 Introduction.

In most studies of polymers, latices, and polymer films, it is necessary to know at least some characteristics of the polymer being used. These characteristics may vary from the particle size of a latex or the polymer's molecular weight to its surface charge density, and what functional groups constitute that charge.

The aim of this Chapter is to provide an overview of some of the available methods of characterisation used in polymer latex chemistry. A number of the methods are, however, applicable for polymers other than polymer latices.

3.2 Physical properties of polymers.

The physical properties of polymers are generally dependent on their chemical composition. With regard to the film formation work of this study, the most important properties are those that are mechanical and temperature related; defining whether the polymer is glassy or rubbery. (General references: Billmeyer[48] and Brydson[73].)

3.2.1 Polymer crystallisation and the glass transition temperature.

The two extremes of structure (morphology) in which polymers may exist are **amorphous** or **crystalline**. Rarely are polymers truly amorphous, however, and crystalline polymers will normally show amorphous regions, as indicated by X-ray diffraction studies which show both sharp peaks and more diffuse peaks. Below a critical temperature (the **glass transition temperature**, or T_g), amorphous polymers may become glassy due to the movement of the polymer chains' single bonds becoming restricted (*i.e.*, rotation of sigma bonds is restricted but molecular vibration still occurs), and exhibit crystalline features. The polymer is said to be in its **glassy state** below the T_g, and in its **rubbery state** when above the T_g.

Restricted rotation of bonds, possibly due to intramolecular hydrogen bonding, dipole repulsion or steric hindrance can lead to polymer chain tacticity in which the polymer takes the conformation of lowest energy. Ring structures also lead to chain-segment stiffening, as does the presence of double (pi) bonds. Double bonds, however, increase the flexibility of adjacent single bonds such that the net effect on a polymer molecule may be to decrease the T_g.

Crosslinking generally increases chain stiffness, leading to greater crystallinity at a given temperature, whilst for copolymers, the T_g is usually between that of the two homopolymers. In the case of two (or more) mixed polymers of differing T_g, it is normally possible to measure the different values of T_g for each polymer. The presence of a compatible **plasticiser** in a polymer will lower the T_g: the magnitude of the reduction being dependent on the concentration of plasticiser, whilst other additives (*e.g.*, fillers or colourants added to a polymer membrane, etc.) may increase the T_g.

The stiffening effects of polar groups and hydrogen bonding can be offset by the addition of *n*-alkyl groups which increase separation between the active forces. Such separation is important for the lower poly(alkyl methacrylates). However, above poly(*n*-dodecyl methacrylate) the T_g increases due to entanglement of the alkyl groups.

Polymer chain ends have greater freedom to rotate than the mid-sections and, hence, molecular weight is important also. Higher molecular weight polymers generally showing a higher transition temperature. T_g is related to molecular weight by[169]:

$$T_g = T_g^{\infty} - k(\overline{M}_n)^{-1} \tag{3.1}$$

where:

T_g^{∞} = glass transition temperature at infinite molecular weight;
k = positive constant;
$\overline{M}_n$ = number average molecular weight.

Polymer age may also affect the T_g. Okhamafe & York[353] determined an approximate 10 K reduction in the T_g (which was initially 429 K) of hydroxypropyl methylcellulose films stored for one year at 293 K and 37% R.H. Similar films plasticised with polyethylene glycol 400, with an initial T_g of ≈ 356 K, showed no decrease with age. The decrease in T_g of the unplasticised film was thus attributed to the loss of residual solvent from within the crystalline regions of the film: such crystalline regions being virtually absent in the plasticised film. Additives that interacted either physically (by virtue of shape) or chemically to hinder polymer chain motion increased polymer T_g, whilst polar repulsions could possibly lower the T_g due to enhanced chain segment mobility. The T_g may also be considered as being time dependent as a result of polymer chain relaxation[48], as described by a Williams-Landel-Ferry type equation[1]: a plot of T_g versus logarithm[time] being typically linear.

If a polymer is made from a regular series of identical repeating units, and consists of a backbone-chain of limiting flexibility, it is possible for the units to form a crystal lattice of repeating 'unit cells': a **crystalline polymer**. The T_g of a crystalline polymer is less significant than is the case for an amorphous polymer, due to the crystalline uniformity limiting chain mobility of the polymer when in its rubbery state. Polymer crystallinity may be reduced by the presence of side chains, which interrupt the ordered structure. Atactic polymers may be crystalline, however, if the side chains of the asymmetric carbon are of similar size such that the 'shape' of the unit cell is not interrupted.

The **crystalline melting-point**, T_m, of a polymer is typically affected by the same factors that affect the T_g, and for homopolymers, there is an approximately linear relationship between the T_m and the T_g. (The glass transition may occur over a range of temperatures, however, whereas the melting-point is sharply defined.)

---

[1] Originally used to describe polymer viscosity and temperature relationships, but can be used to describe a number of polymer properties which change as a function of temperature, when the change arises as a result of changes in the polymer's viscosity.

Above the T_m, the polymer will be an amorphous and rubbery liquid. On cooling it may either crystallise (if the structure allows) or vitrify. A crystalline polymer can be forced to the glassy state by rapid cooling. However, a polymer with an irregular chain-structure may never be made crystalline. Above the T_g, but below the T_m, a crystalline polymer will contain some amorphous regions where chain segment mobility still occurs. Below the T_g, this mobility is negligible.

Although it is possible to 'grow' single polymer crystals, crystalline polymer structure containing both crystalline and amorphous polymer has been explained in terms of a 'fringed micelle concept.' This proposes that a single polymer chain, being long in length, can contribute to both crystalline and amorphous regions, explaining the structural 'bonding' strength between the two regions. Polymer crystals can show the typical defects seen in true crystals (dislocations, point defects, etc.), which together with the amorphous regions, contribute to the diffuse regions of the X-ray diffraction patterns of polymers.

3.2.1.1 Effect of plasticisers.

The addition of a liquid (or solid) to a polymer that increases polymer chain separation and therefore increases segment mobility, thus, lowering the polymer T_g (and elastic modulus) is said to plasticise the polymer. Plasticisers typically have similar solubility parameters [73] to the polymers that they plasticise, and are generally of high molecular weight ($\rangle$300) to reduce diffusion out of the polymer. If the polymer and plasticiser interact, then the plasticisation effect can be reduced. Interaction may be between polar groups, or by the formation of hydrogen bonds.

3.2.1.2 Determination of the T_g and T_m.

Methods of polymer analysis by thermal means have been reviewed by Holsworth [243]. In addition to the 'simple' determination of the decomposition temperature of a polymer (which could be determined by measuring the change in its weight as a function of increasing temperature, using the technique of **thermogravimetric analysis**), or the glass-rubbery transitions (as determined by **Differential scanning calorimetry** {D.S.C.} and **Differential thermal analysis** {D.T.A.}), etc., thermal methods of analysis can be utilised to characterise, for example, the effectiveness of a crosslinking reaction, or plasticisation by a plasticiser. Ottewill and Saturunathan [370], for example, have used D.S.C. to investigate the adsorption/grafting of additives on to polystyrene latices, prepared with and without surfactant and copolymer and then dialysed.

D.S.C. is used to compare the temperature of a sample against a reference sample-holder, for a predefined time-temperature program. The temperature of the sample and reference is adjusted to remain equal, whilst the *difference* in power for the sample and reference is output such that the integral of the output (which is a plot of temperature versus difference in power), as a function of time, is a measure of the heat transition. Glass transitions and melting-points are indicated by anomalous changes in the specific heat curves for the polymer. D.T.A. measures the temperature difference, ΔT, as a function of temperature, T, between a sample and inert reference substance. A temperature difference is only observed when the sample evolves or absorbs heat (shown as a peak), or undergoes an abrupt change of heat capacity such as at the T_g (shown as a change of gradient in the ΔT versus T curve).

3.2.2 Determination of polymer (latex) structure.

Many techniques exist which yield information on polymer structure, allowing the determination of, for example, polymer chain conformation, to latex particle morphology, or coating morphology. As with 'true' crystals, the structures of crystalline polymers may be probed using diffraction studies, typically using **X-rays** as the probe (due to their wavelength being of the appropriate intermolecular size). Ordered structure, as might be found in a crystalline polymer lattice, causes interference patterns in the scattered or diffracted radiation allowing the determination of the molecular geometry. X-ray crystallographic data can provide information on polymer properties such as chain conformation and chain packing, typically providing information on the repeating units rather than the arrangement of atoms (molecules) within the unit cell. The data so produced is, however, diffuse due to disorder in the crystal structure.

Other spectroscopic techniques discussed in the literature include **Nuclear Magnetic Resonance** (N.M.R.) and **infrared spectroscopy**. Lange[305] *et al.* reported an **infrared** technique to estimate the interfacial layer thickness in core-shell particles, being typically 5 nm and comparing favourably with results from D.S.C., N.M.R. spectroscopy, and S.A.N.S. spectroscopy. N.M.R. spectroscopy is, like X-ray spectroscopy, suitable for the determination of polymer chain structure. Using isotopically labelled polymer components (*e.g.*, ^{13}C or ^{10}F), N.M.R. spectroscopy allows the site of the component (*e.g.*, a functionalised copolymer) to be determined: Pichot[395] used the variation in signal breadth, caused by the restricted movement of bulk polymer compared to that at the interface, to determine whether the labelled component was at the polymer interface or in the bulk polymer.

Electron microscopy is a suitable technique for observing latex particle (and film) morphology. A number of methods exist by which the observation of latex particles by S.E.M./T.E.M. can be enhanced. Bradford and Vanderhoff[64] cite several techniques whereby low T_g particles may be hardened: *e.g.*, bromination[70] of unsaturated bonds or electron irradiation[65] to crosslink polymer chains. Shaffer[447, 448] *et al.* discuss the increased complexity of T.E.M. when core-shell particles are involved, with often more than one technique being required from: osmium tetroxide to crosslink and stain unsaturated polymers; a cold stage for latices too soft at room temperature; negative staining (using phosphotungstic acid) to increase contrast; shadowing to study sag at room temperature (hard shell attempted around a soft core); ultramicrotoming or cryo-ultramicrotoming.

An example of the results available by T.E.M. is the work of Disanayaka[120] *et al.*, who in order to study the internal morphology of latex particles, used a 'freeze-fracture' T.E.M. technique which involved rapidly freezing the sample of latex under liquid nitrogen, to retain its structure, and then fracturing the frozen sample with a cooled knife. Depending on the position of the particles, with respect to the matrix fracture section, the particles may either fracture or be present as a protrusion, or be removed to leave an indentation. Using this technique, Disanayaka observed the particle fracture cross-sections of both aqueous latices and non-aqueous dispersions. The micrographs depicting the surfaces of particles of (surfactant-free polymerised) poly(methyl methacrylate) showed an uneven texture that was attributed to the particles' growth by primary particle coagulation, in agreement with the observations and conclusions by Bassett [36]. The fracture cross-sections of the particles showed a graininess (globules) that was attributed to what were thought to be vestiges of such primary particles, whilst the uniformity of the graininess across the whole of the cross section was thought to be characteristic of the continued growth of the primary particles, within the latex particle, by polymerisation of adsorbed monomer.

Disanayaka [120] found the fracture cross-sections of polystyrene latices to differ from those of PMMA, showing no graininess, but showing radial lines from the particles' centres. These lines were attributed to the surfactant-free particle growth being at the particle surface, in agreement with Hearn [229] *et al.*, but being non-uniform. Such radial lines were also observed in the PMMA prepared in a non-aqueous dispersion, implying similarity in the particle growth mechanisms to that of the aqueous polystyrene, attributed to a similar radial increase in monomer concentration within the particle, from the centre outwards.

Ghebre-Sellassie [187] *et al.* used the high energy of electrons to determine the location of additives within the cross-section of a proposed sustained release formulation. The electrons (〉 30 kV) caused X-ray emissions from the samples, which were detected by an energy dispersive X-ray spectrometer. A plot of the X-ray output intensity of certain elements, as a function of position on the cross-section, providing the required information.

Small angle neutron scattering (S.A.N.S.) has been used to study the structure of polymer latex films. The technique is complex in that it typically requires the radioactive (deuterium) labelling of some component in order to provide a means of scattering contrast. Like light scattering, the technique can provide information on the weight-average polymer molecular weight and the z-average radius of gyration. In addition, the interference patterns so produced, although complex to interpret, can yield information on polymer structure. The technique has found particular application in the study of latex film formation [95, 212, 213, 257, 459, 555, 556], providing information on chain inter-diffusion and particle coalescence (see Chapter 4), and has also been utilised for latex particle sizing, and by the use of a deuterated shell, for the study of core-shell type particles [158, 459].

3.2.3 Determination of polymer molecular weight.

The nature of the distributed molecular-size of polymers determines that their molecular weight is normally quoted as an average value dependent, for example, on the number of particles or their viscosity, etc. A number of **colligative properties** are theoretically suitable for the determination of polymer molecular weight. In practice, however, **osmometry** is the most widely used due to the very small changes that require measuring by the other methods. (*E.g.*, a polymer solution {0.01 g cm^{-3}} with a molecular weight of 20,000 produces a change in the boiling/freezing-point of the order of 0.001° C, and a lowering of the vapour pressure {mm Hg} by a similar order [48].) As suggested by the name, colligative properties yield a **number average molecular weight**, $\overline{M}_n$.

In a polymer solution, light is scattered due to the irregular changes of refractive index, caused by the polymer. Such scattering is described by the equations of Rayleigh, Debye, Gans and Mie. Conventionally, the angular profile of the scattered light can be used to determine the polymer molecular weight by means of the Debye theory [111] and, in the case of large particles, the method of Zimm [565], which allows for multiple scattering from single particles. The result of **light scattering** experiments are a **weight average molecular weight**, $\overline{M}_w$. The ratio of the weight average molecular weight to the number average molecular weight provides a measure of the polydispersity of the system. The methods invariably require that the polymer is in solution.

Many other techniques exist for the determination of polymer molecular weight, such as **chromatography, sedimentation, viscometry**. The latter provides the viscometry average molecular weight, $\overline{M}_\upsilon$. The various equations are summarised below:

$$\overline{M}_n = \frac{\sum N_i M_i}{\sum N_i} \qquad \overline{M}_w = \frac{\sum N_i M_i^2}{\sum N_i M_i} \qquad \overline{M}_\upsilon = \left[\frac{\sum N_i M_i^{i+a}}{\sum N_i M_i}\right] \tag{3.2}$$

where:

N_i = number of molecules of molecular weight M_i, in the i^{th} fraction.
a = constant for a given polymer, solvent and temperature as in the Mark-Houwink equation:

$$[\eta] = KM_r^a \tag{3.3}$$

where:

$[\eta]$ = intrinsic viscosity;
K = constant;
M_r = relative molecular mass, as determined by equations (3.2)

The above techniques generally are secondary methods, requiring a standard for calibration. A further technique is **gel permeation chromatography** (G.P.C.). This has the advantage of providing number *and* weight average molecular weights.

With regard to the study of latices (and latex films), polymer molecular weight data can provide information on the mechanisms of the polymerisation reaction, and may also be of importance with regard to permeability studies. Goodall [196] *et al.* used G.P.C. data showing the presence of low molecular weight oligomeric material to study particle nucleation in surfactant-free styrene polymerisations. Such low molecular weight material was found to be present only in the initial stages of the reaction. This is in contrast to similar studies on BMA, in which low molecular weight material was found for the "duration of the reaction" [423] whilst monomer was still present in the aqueous phase (*i.e.*, even after the attainment of a constant particle number density), implying different mechanisms propagate during the reaction: the nucleation of styrene being completed earlier than the nucleation of BMA.

The formation of a film from a latex (see Chapter 4) requires coalescence of the particles, which itself is dependent on polymer chain interdiffusion. Recently, Yoo [555, 556] *et al.* have studied this interdiffusion, as a function of chain radius of gyration, which is proportional to (polymer molecular weight)^{½}, concluding that film formation is partly controlled by the spatial distribution of chain ends *and* polymer molecular weight, and critically, the ratio of the polymer chains' radii of gyration compared to the latex particle's radius.

3.2.4 Latex particle sizing.

A number of methods exist for the purpose of sizing latex particles, each with its own advantages and disadvantages.

3.2.4.1 Microscopy.

Simple optical transmission/reflectance microscopy is limited in its use for observing colloidal sized particles by its resolution and the need for good contrast between the object and its surroundings (although the latter problem can be overcome to some extent by the technique of '**dark-field**' or '**phase contrast**' microscopy in which light scattered by the object is observed against a dark background allowing particles of ca 10 nm[374] to be observed, *cf.* ⟩ 1 μm for a normal optical microscope).

Electron microscopes utilise wavelengths smaller than those of visible light to resolve greater detail, and fall into one of the two main types: the **scanning electron microscope** (S.E.M.), or the **transmission electron microscope** (T.E.M.). In the S.E.M., the electron beam traverses the sample, which must be coated with a thin conducting film, in a series of parallel tracks. The electron beam may be back-scattered, or interact with the sample to produce secondary electron emission (or X-rays, etc.), which can be detected. Secondary electron emission provides a diffusely illuminated two-dimensional view, whilst back scattered electrons provide a third dimension, giving the sample a shadow as if side illuminated from a point source. The resolution of S.E.M. is less than T.E.M. (ca 5 nm for S.E.M. {greater resolution requires a higher beam energy, which damages the polymer} *cf.* 0.3 nm for T.E.M.[174]) but S.E.M. provides a greater depth of field.

In the technique of T.E.M., the sample is supported by an electron transparent substrate, held on a copper grid. Electrons either pass through the sample or are scattered by it dependent on sample thickness and atomic number (electron density). The image is thus provided by the amount of contrast between regions that scatter to a greater or lesser extent. By vacuum-evaporating a heavy metal (*e.g.*, gold) onto the sample at a known angle, contrast is enhanced, and the image appears to have a third dimension. For samples such as latex films, etc., it is often necessary to prepare a carbon replica of the sample to avoid the specimen becoming deformed in the electron beam.

For the purpose of sizing, the latex (typically at 0.05% [370] solids content) must be totally dried due to the process requiring a vacuum for the electron beam. Further disadvantages are (i) that the sample may become distorted (either by the electron beam itself causing the polymer to flow within a few seconds of illumination, or the particles may become flattened on to the substrate {although methods exist for the sizing of deformed particles[66]}), and (ii) the method is tedious requiring multiple batches of large particle numbers to allow for the statistical deviations in particle size. Davidson and Collins[108] also demonstrate the necessity of latex cleaning before E.M. examination, showing that artefacts resulting from the emulsifier, used in the latex preparation, may appear as a second generation of particles: the cleaned latex providing a clearer micrograph without affecting particle size.

The treatments to latex particles, used to assist in the E.M. process, were discussed in the previous section and whilst some of these treatments are equally useful when E.M. is used for particle sizing, others may adversely affect particle size: *e.g.*, bromination may change the particle diameter [64]. (Bradford and Vanderhoff[64] cite the work of Brown [70] and Wilson [542] *et al.* who claimed an increase in particle diameter of between 9% → 10%.) Whereas bromination only works for unsaturated polymers, Vanzo [515] *et al.* describe a method of polymer hardening whereby styrene (10%) is sorbed into the particles and polymerised by irradiation. The size increase can be calculated from the known amount of added styrene, and the technique only required one thirtieth of the radiation necessary to cause hardening by crosslinking of the polymer chains. A negative staining technique, in which the background to the particles is made electron dense, is described by Scholsky and Fitch [437].

The technique of sizing by T.E.M. is a secondary technique in that it requires a standard against which the particles may be compared. This standard may be in the form of a calibrated grid (*e.g.*, diffraction grating replica), or a monodisperse latex of predetermined size (secondary standard). E.M. is, however, the only sizing technique to permit visual observation of the sample and, hence, particle shape may also be observed.

3.2.4.2 Light scattering.

Ottewill and Shaw [373] used the colours and angular position of scattered light (higher order Tyndall effect)[1] to characterise the particle size of monodisperse polystyrene latices, finding good correlation with the size results of E.M., provided that the latex was monodisperse.

If the latex particles are in the size range 200 → 400 nm, are monodisperse, and there is a difference in refractive index between the particle interior and interface, then particles which form an ordered crystal-like structure (particle crystal structure as opposed to polymer crystal structure) will undergo **Bragg diffraction iridescence** [121]. Such iridescence is also seen in both water swollen [121] and dry films [121, 509], prepared from polymer latices, which retain some of the original structure. Vanderhoff[509] *et al.* note that the colours seen in a latex may differ from those seen in a film prepared from the same latex, due to the different interparticle spacing. Vanderhoff also quotes the colours seen for a given particle size. However, these presumably vary with the angle of observation.

With reference to the scattering of light from latex particles, light scattering theory is dependent upon both the latex particle size and its shape, in addition to the wavelength of the incident light. The simplest theory depicts the particle as a point source of light

---

[1] Due to the particle size of a latex being of a similar order to that of the wavelength of light, latices typically undergo scattering phenomena. This is evident from latices made of clear polymer appearing white when concentrated, or turbid when dilute (**Tyndall effect**).

(particle diameter, $\emptyset \langle \lambda/20$ where λ = wavelength of light) by assuming the amplitudes of the scattered waves are additive. This is described by Rayleigh scattering in which the scattered intensity is proportional to λ^{-4} and, more significantly, proportional to $(\emptyset/2)^6$ [159]. The total amplitude of light scattered from a particle is proportional to its volume and therefore its mass. Such scattering therefore leads to a weight-average particle size [159]. Larger particles ($\emptyset \rangle 0.33\lambda$) cannot be considered as point sources of light as scattering can occur from more than one point on the particle, and interference patterns develop, requiring the use of differing scattering theory such as those of Debye and Gans, or Mie. Van Tent and te Nijenhuis [512, 513, 514] have used light transmission studies (*i.e.*, transmission is dependent on scattering and interference) to study particle size (and packing) during latex film formation.

The advent of lasers and computers led to the development of instruments that use scattering theory to dynamically measure the particle size of latices using the process termed **photon correlation spectroscopy** (P.C.S.). The physics of the process together with some applications (in addition to particle sizing) and the methods of analysis of the resultant data are described in a number of references [e.g., 75, 168, 406, 407, 466].

Advantages of the P.C.S. technique are that it yields an absolute size measurement (rather than a secondary result requiring a calibration standard as does E.M.) and the sample is not distorted as can happen when soft latex samples are deposited on a grid, or under an E.M. beam. A disadvantage of P.C.S. is that it yields a hydrodynamic particle diameter. However, Goossens and Zembrod [203] used this feature to study the latex particle surface: using the increase in particle diameter, caused by raising the pH from 3 → 14, to investigate carboxylated latices. (The increase in hydrodynamic size is a result of surface charge neutralisation and ionisation of the carboxyl groups, leading to greater electrostatic repulsion and, hence, expansion: a feature found when the polymer T_g is sufficiently low to allow chain flexibility and/or chain polarity allows the chain segments to interact and be plasticised by the aqueous phase [245].) Similarly, P.C.S. has been used to study the surface adsorption of macromolecules [281]. Other disadvantages of P.C.S. result from the technique relying on the random diffusion of the particles. Thus, factors that affect the diffusion can lead to spurious results, *e.g.*, sedimentation of large diameter particles.

A newer technique than P.C.S., but still using light scattering theory (Rayleigh-Gans-Debye or Mie theory) is integrated light scattering (I.L.S.). This method is closer to neutron or X-ray scattering experiments than P.C.S. Strawbridge and Hallet [470] showed that it could be combined, using Mie theory, with electron microscopic or P.C.S. data to yield information on particle size and polydispersity. Strawbridge also used the techniques to determine the shell thickness of hollow latex spheres.

3.3 Chemical properties of latices.

The control and characterisation of the surface properties of a latex are often required in order that the properties of the latex are understood for its prospective use: be it the formation of a film, as a coating; or for use as model colloid [265, 503]. Because of the small size of a latex particle, the extremely high surface area to volume ratio means that the particle's properties are very much dictated by the surface properties. The complete characterisation of a latex obviously requires the determination of the surface charge density, and identification of the source of that charge, due to the fact that this plays such an important function in the colloidal properties of a latex and its stability[369, 480].

3.3.1 Surface chemistry.

Factors affecting the surface chemistry of a polymer latex particle include the various items of the polymerisation reaction recipe such as the initiator type, monomer and comonomer functionality, and surfactant type. In surfactant-free polymerisations, the latex surface properties are mainly dependent on the initiator type: Goodwin[202] *et al.* list a number of the common initiators and their possible functional groups. After preparation, the surface chemistry may be changed by the cleaning method employed (see paragraph 3.3.2) or simply from prolonged storage.

The ideal model colloid would contain only one type of charged end group. However, in the case of an aqueous, surfactant-free latex, polymerised, for example, from non-polar styrene monomer using potassium persulphate as the initiator, it is to be expected that the reaction would follow the mechanisms described in Chapter 2, with the typical steps for a free radical reaction of initiation, propagation and termination:

$$S_2O_8^{2-} \longrightarrow 2SO_4^{-}\bullet \qquad (3.4)$$

$$SO_4^{-}\bullet + M \longrightarrow SO_4^{-}M\bullet \qquad (3.5)$$

etc.

The termination step would therefore be expected to lead to the formation of two sulphate end groups per polymer chain (if chain transfer, etc., is neglected), *i.e.*, the initiator is the source of the charged end groups. If chain transfer is included, other end groups (*e.g.*, carboxyl groups) might also be included and, hence, the number of sulphate groups, in practice, is normally less than two[509]. Grancio and Williams'[206] core-shell theory would imply that these end groups reside at the particle surface. However, end groups buried within the particles may also account for the fact that less than two sulphate groups per chain are detected.

In an aqueous environment, hydroxyl radicals[289] are possible which are able to initiate polymerisation, leading to the formation of hydroxyl end groups:

$$SO_4^{-}\bullet + H_2O \longrightarrow HSO_4^{-} + OH\bullet \qquad (3.6)$$

Acidic hydrolysis of sulphate end groups may also lead to the formation the hydroxyl end groups[503], and oxidation of such hydroxyl groups may possibly be the source of the carboxyl end groups sometimes found during the characterisation of persulphate-initiated polymerisations:

$$ROSO_3H + H_2O \longrightarrow ROH + H_2SO_4 \qquad (3.7)$$

$$RCH_2OH \xrightarrow{[O]} RCOOH \qquad (3.8)$$

The hydroxyl radicals may also prove to be a source of oxygen, by the following disproportionation reaction:

$$2OH\bullet \xrightarrow{\quad\quad} H_2O + \tfrac{1}{2}O_2 \qquad (3.9)$$

The oxidising behaviour of persulphate initiator can be eliminated by the use of different initiators such as azo compounds that decompose forming nitrogen rather than oxygen.

Vanderhoff[503] found that allowing a persulphate-initiated latex to age at ambient temperature, with the sulphate groups in the H^+ form, at low pH (as might result from the polymerisation being un-buffered, and due to bisulphate formation), led to the appearance of carboxyl groups, whilst storage at 363 K led to the formation of hydroxyl end groups.

There is, however, uncertainty as to whether such carboxyl groups should be present, and if so, from what source: *e.g.*, chain transfer with buffer, various oxidative side reactions, cleaning method, etc. [228].

Industrial emulsion polymerisations commonly use redox initiation systems containing sulphites or metabisulphites (in addition to the persulphates, etc.) which form sulphonate ($HSO_3\bullet$) radicals and, hence, sulphonate end groups in addition to the sulphate end groups. McCarvill and Fitch[335] prepared a sulphonated polystyrene latex, using a bisulphite/Fe(III) redox system alone, with no persulphate:

$$HSO_3^- + Fe^{3+} \xrightarrow{\quad\quad} Fe^{2+} + \bullet SO_3H \qquad (3.10)$$

The final latex contained only strong acid sulphonic groups, and was thus resistant to the hydrolysis/air oxidation.

In many instances, surface functionality is deliberately introduced by means of the reaction recipe, using a functional monomer[488], or by using techniques such as copolymerisation or 'shot growth' type addition[433]. In his review of polymer colloids, Fitch[159] notes that in order to augment functionality at the particle surface, the co-monomer should be surface-active and insoluble in both the polymer and water. Vijayendran[521] investigated the carboxylation of polystyrene looking at the affect of a number of carboxylated acidic monomers (itaconic acid {IA}, acrylic and methacrylic acid {AA and MAA, respectively}). It was found that the more hydrophobic acid (and hence, the most soluble in the styrene) concentrated at the particle core during the polymerisation, in the order MAA ⟩ AA ⟩ IA, citing the ease of diffusion of the MAA into the styrene as the reason, but also noting the lower reactivity of the IA. From the result of similar experiments investigating the mode of addition of a carboxylated monomer (in industrial type reactors), Hoy[245] discusses how the method of addition (be it in the aqueous feed, the monomer feed, or the initial reactor charge) has little effect on where the carboxyl groups are finally located: *i.e.*, on or near the particle surface.

Typical of the functional monomers are: (meth)acrylic acids, for the introduction of carboxyl groups[433]; styrene sulphonate for the introduction of strong acid groups[283]; and tertiary amines such as, for example, *N*, *N*-dimethylaminoethyl methacrylamide, for the preparation of quaternary ammonium salts[488]. Many of these functional monomers are capable of forming polyelectrolyte and, in addition to becoming part of the latex polymer, will be present in the aqueous phase, or weakly bound to the particle and, hence, labile.

Post polymerisation reactions may also be used to modify the surface functionality. Typical of this is the oxidation of hydroxyl end groups to carboxyl groups – necessary to allow for their detection by titration. However, surface species may also be grafted onto the particles [429]. Pelton [389] has reviewed a number of reactions that are possible on the latex surface.

In addition to their role as steric stabilisers, surfactants and emulsifiers can also contribute to the stabilising surface charge density due to hydrophilic end groups (again typically sulphate groups), which may be either physically or chemically bound to the latex particle's surface. Stone-Masui and Watillon [469] determined that latices prepared in the presence of sodium alkyl sulphate or sulphonate surfactants contained only strong acid groups, after cleaning by ion exchange (see paragraph 3.3.2.3), whereas those latices prepared in the presence of potassium stearate or sodium laurate contained weak acid groups in addition to the strong acid groups. It should be noted that characterisation should be performed immediately after cleaning since it has been shown that the number of strong acid sulphate groups decreases with time [265] due to hydrolysis or oxidation. Fitch and McCarvill [162] also investigated the ability of surfactant to contribute to surface charge, finding sodium dodecyl sulphate and sodium dodecyl sulphonate contributed considerably to the number of chemically bound sulphate and sulphonate groups, respectively. Citing the work of Brace [61], who (using of radioactively labelled surfactant) showed that the heating of a polymer to near its T_g allowed surfactant to desorb, Fitch reasoned that since similar treatment of his latices did not cause surfactant desorption, then it must be chemically bound.

3.3.2 Cleaning of latices.

It has previously been mentioned that the cleaning of a latex, to remove any artefacts, improved the quality of electron micrographs of the latex. E.M. has also been shown to be able to detect physically adsorbed surfactant [64] (which was visible in the micrographs as a diffuse border on normally well resolved particles). Ideally such surfactant should therefore be removed before the particles are sized by E.M.

When trying to characterise the surface functionality/charge of a latex, the removal of surfactant, if present, and/or residual reaction by-products, such as initiator fragments, oxidation products, thermally polymerised polymer, polyelectrolyte, residual monomer, and microbial contamination, etc. [198, 230, 538] becomes even more important. Physically adsorbed surfactant may desorb during or after the characterisation process leading to time variant surface properties. This may be overcome by using a block copolymer to aid the stability of the latex, whilst alternatively, Ottewill [370, 371] *et al.* prepared a latex, albeit non-ionic and showing no surface charge, using a polymeric monomer: methoxy poly(ethylene glycol) methacrylate. Removal of contaminants from a monodisperse latex provides a model colloid [503] stabilised only by chemically bound (as opposed to physically bound) surface groups.

Contamination of an emulsion polymerisation by oxygen is normally to be avoided (by performing the reaction under a nitrogen atmosphere) due to the oxygen inhibiting the polymerisation [226] by the formation of organic peroxides.

Surfactant-free latices are readily attacked by fungal and microbial contaminants that can affect the surface properties of a latex[230, 538]. Sielicki[453] *et al.* determined that certain bacteria were able to metabolise the carbon in styrene; oxidising the styrene monomer to phenylethanol and phenylacetic acid, and also forming oligomeric styrene material.

For the aforementioned reasons, the cleaning of a latex is desirable. However, the methods of cleaning have led to controversy as to whether various latex surface functionalities (in particular, weak acid carboxyl groups) occur as a result of the reaction recipe or the cleaning method itself. Common methods of cleaning a latex have been reviewed by Wilkinson[539], and include steam stripping, dialysis, ion exchange, and serum replacement.

3.3.2.1 Steam stripping. .

The technique of **steam stripping** is widely used for the removal of volatile organic contaminants from latices, such as residual monomer and the possible reaction by-products such as, in the case of styrene, benzaldehyde. Everett[148] *et al.* found, however, that the steam stripping of persulphate-initiated polystyrene latices increased the rate of sulphate surface group **hydrolysis**, compared to the rate at ambient temperature during 'normal' storage, and appeared to expose fresh weak acid groups. A similar loss (53%) of strong acid groups was observed by Hearn[230] *et al.* The rate of hydrolysis, during steam stripping may be reduced by lowering the temperature[195, 198]. The process of steam stripping has also been recommended[195] for the cleaning of latices, suitable for use as model colloids, when prepared by sulphite redox couples, such that no hydrolysable species are present on the latex surface.

3.3.2.2 Dialysis.

The cleaning of latices has conventionally been performed by **dialysis**: utilising the semi-permeability properties of Visking dialysis membranes to remove both dispersed contaminants and those detachable from the surface. The technique requires large volumes of dialysate (latex to doubly distilled water = 1 : 30 [230]) and regular changes to clean water, over the course of a number (3 → 4 [230]) of weeks (during which the latex is liable to attack by microbial agents), until the conductivity of the dialysate equals that of the clean water. It is necessary to thoroughly clean the dialysis tubing to remove polysulphides (preservative) and glycerine (humectant), etc. before use. Because the mechanism of dialysis is diffusion based, the procedure may be speeded up by agitation of the dialysate with respect to the latex. McCarvill and Fitch[335] increased the rate by the use of a dynamic hollow-fibre dialysis.

Vanderhoff[509] *et al.* found that extensively dialysed samples of polystyrene latex showed a very low surface charge. This was originally attributed to the efficiency of dialysis in removing surfactant, but was later found to be a result of the incomplete exchange of Na^+ and K^+ for H^+ ions. It was therefore necessary for the samples to also undergo an ion exchange process [509]. Hearn[230] *et al.* found that the conductivity of the dialysate initially dropped rapidly, but soon reached a plateau level. Many authors report the inefficiency of dialysis for the removal of adsorbed surfactant[503] or monomer[148, 537] in addition to the aforementioned ions. However, Shaw[450] found that 98.89% of ^{14}C-labelled sodium dodecanoate emulsifier, when used in a polystyrene polymerisation at a concentration below its C.M.C., *could* be removed by dialysis. The removal of surfactant, if present above its C.M.C., may prove particularly difficult, due to the micelles being of a size greater than the porosity of the dialysis membrane. Such micelles may stabilise other contaminants, hence, preventing their removal[136]. However, micelles will disband as the concentration of surfactant in the aqueous phase decreases.

A problem observed by a number of researchers, has been the effect of dialysis on the surface charge of a latex. Yates[554] *et al.* found that a latex, prepared surfactant-free, which initially showed only strong acid groups, still showed only strong acid groups after cleaning by centrifugation and washing. However, after dialysis, titration revealed the presence of weak acid groups in addition to strong groups. This was attributed to prolonged exposure of the latex to the cellulosic dialysis tubing under acid conditions, despite the fact that the Visking tubing had been extensively cleaned before use using a number of treatments such as washing in EDTA; an ethanol-water mix; dilute sulphuric acid; or dilute sodium hydroxide, and the fact that the dialysis was performed under a nitrogen atmosphere. The acid groups must have been bound to the particle or they would presumably have been removed by the dialysis, and Yates attributed this to the adsorption of carboxylated polysaccharides formed by the hydrolysis or oxidation of the cellophane tubing.

Hearn[230] *et al.* found small quantities of a weak acid in the water used for boiling (cleaning) a sample of Visking tubing, showing that such groups could be leached from the dialysis tubing to be possibly adsorbed by a latex. Wilkinson[537] *et al.* concentrated and analysed the water finding evidence of low molecular weight species (⟨ 10^3) and glycerine. Wilkinson also investigated the long term effects of exposure of a latex to dialysis tubing, finding an increased concentration of weak acid groups. There was uncertainty, however, as to its origin (*e.g.*, the dialysis tubing; oxidation of residual monomer; or microbial activity, etc.): a similar latex stored in a Pyrex container also showing increased levels of acid (again possibly benzoic acid or low molecular weight oligomer) which was removed by dialysis – indicating that it was unbound.

3.3.2.3 Ion exchange.

The technique for using mixed anion and cation **ion exchange** resins (sulphonate and trimethyl ammonium salt resins of styrene/divinyl benzene, 4% crosslinked {*cf.* more typical 8%} to provide a pore size better suited for adsorption of emulsifier) to clean latices was established by van den Hul and Vanderhoff[492, 493, 509]; the latter who has detailed the process of cleaning and characterisation of a latex using the technique[498]. Using rigorously cleaned resins, ions in the aqueous phase are exchanged for protons and hydroxide ions that in turn leads to the desorption of ions adsorbed onto the latex particles in order to maintain the equilibrium between adsorbed and aqueous phase ions[503]. This process continues until all adsorbed ions have been removed and a constant surface charge is achieved (also indicating that the cleaned resins do not contaminate the latex). Vanderhoff[509] gave quantitative results as to its efficiency in removing surfactant.

Disadvantages of the technique are that it primarily removes only ionic impurities, and the resins require meticulous cleaning before use. This **conditioning of the resins**, as performed by van den Hul and Vanderhoff[492, 493, 509], initially involved washing in hot (358 K) water and methanol until no further discolouration of the washing water, followed by repeated successive washing with hydroxide and acid, and rinsing with hot water, methanol, and cold water, to remove leachable polyelectrolyte, as observed by Shenkel and Kitchener[452]. The resins were finally rinsed with either acid or hydroxide depending on the type of resin, cation or anion exchange, to convert it to the correct form (H^+ or OH^-) and finally rinsed with double distilled water[509]. The anion exchange resin should be stored in the chloride form to prevent decomposition of the hydroxide form, with the formation of amines[335]. It was noted by van den Hul and Vanderhoff[494] that the ability of the resin to be cleaned may be dependent on the particular batch of resin used.

Hearn[230] *et al.* note that the purity checks on the state of cleanliness of the resins is based on the analysis of the wash water (*e.g.*, Vanderhoff[498]), and comments on the fact that the latex may adsorb impurity directly from the resin, and that although removal of adsorbed emulsifier and electrolyte is efficient, the ability to remove solubilised material is an unknown quantity.

McCarvill and Fitch[335] found a loss in the latex polymer solids content due to adsorption of the latex onto the anionic part of the ion exchange resin, presumably as a result of electrostatic attraction. A process that may cause a change in the size distribution of a polydisperse latex[494]. McCarvill also found that the latices were best purified by a combination of dialysis and ion exchange, and that several exchanges using small amounts of resin were preferable to a single large exchange: producing a purer product and preventing coagulation of the latex.

Advantages of the ion exchange cleaning technique are that it is relatively quick, compared to dialysis, and that it can be used to exchange surface group counter ions (*e.g.*, sulphate end group cations such as K^+, Na^+, etc.) for the required form (either protons, in the case of the sulphate groups, or hydroxide ions if required).

3.3.2.4 Serum replacement.

Serum replacement (**solvent exchange** or **microfiltration**) as a technique to clean latices for characterisation was developed by Ahmed *et al.*[6]. The latex is contained in a reservoir over a filter paper[1] of a pore size 30% → 75% of that of the latex particle diameter such that the particles are retained, but not the contaminants. Clean water is fed into the top of the filtration cell to replace that serum lost through the filter paper: the conductivity of the eluent typically being monitored as a test the state of cleanliness of the latex. The serum flux can be controlled by the pressure head of clean water (or by an applied {pure} nitrogen gas pressure, or by a suction pump connected to the filtrate side of the system),

---

[1] *E.g.*, Nucleopore® Corporation: British importer: Sterilen Ltd., Teddington, Middlesex, England, or Millipore® U.K. Ltd., London, England.

however, Ahmed found too high a pressure resulted in blockage of the filter paper[1]. Stirring using a magnetic stirrer helped alleviate the problem of filter blockage, and the build-up of coagulum, but this, in itself, may lead to erosion of the filter paper.

Cleaning by dialysis is reliant upon the diffusion of molecules from the latex, which in the case of large surfactant molecules can be slow such that the concentration gradient near to the latex is quickly diminished. The flux of water through the microfiltration cell prevents the attainment of such a pseudo-equilibrium and, hence, leads to a higher rate of cleaning of the latex. The efficiency of the serum replacement technique has been characterised by Ahmed[6] *et al.*, Wilkinson[536] *et al.* and Chainey[84] in relation to ion exchange and dialysis with each group of researchers concluding that the method is superior in many respects (effectiveness of cleaning, ease of use, etc.) to either dialysis or ion exchange. Wilkinson found that the method completely removes surface active agents (even when present above the C.M.C., due to the micelles being smaller than the pores of the filter paper), residual monomer, low molecular weight reaction by-products, benzaldehyde, etc. However, serum replacement, using clean water, did not remove counterions associated with the particle (*e.g.*, K^+ and Na^+, etc. from the initiator and surfactant) within the electrical double layer, although it would be expected to remove electrolyte from the aqueous phase. Both Ahmed[6] and Chainey[84] overcame this problem by including an acid washing stage, whereby acid replaced water in the reservoir and, hence, caused exchange of the K^+ and Na^+ for H^+, after which, a further clean water stage was used to remove the excess acid.

Practical problems in the process arise from the fragility of the filter papers (particularly the polycarbonate Nucleopore® type, which are liable to wear from the abrasive effect of the stirrer, and attack by acrylate monomers), and blockage of the filter by the latex particles. Selective use of appropriate filter pore-sizes, however, permits the technique to be used to refine, for example, bimodal latex dispersions, and the technique also provides opportunity to concentrate the polymer solids content of the latex, by allowing a shortfall in the amount of serum replaced.

3.3.3 Analysis of latex surface chemistry.

3.3.3.1 Chemical methods of analysis.

Most, if not all, of the aforementioned researchers in paragraphs 3.3.1 and 3.3.2 have characterised the surface chemistry of their latices' functional end groups by means of either **potentiometric or conductometric titrations** in which hydroxyl or hydrogen ions are exchanged for the counter ions of the ionisable functional groups. Because the techniques are only sensitive to charged groups, this has meant, in some instances, that it was necessary to oxidise surface groups (*e.g.*, hydroxyl groups) to the required state[498] (*e.g.*, acid groups), and as described in the previous sections, the presence of contaminants,

---

[1] **Diafiltration**[299] is a dynamic method in which the latex is circulated, under pressure tangentially across a filter paper, with clean water introduced at a rate equal to the filtration rate. The technique is more complex, and offers similar advantages and disadvantages (shear instability and blockage of the plumbing) to the aforementioned method of serum replacement, when compared to dialysis and ion exchange.

whether from the reaction recipe or from the cleaning process, can lead to results that are difficult to interpret.

The **conductometric characterisation** is performed with the latex (typically at 10% polymer solids content) titrated against either acid or base (typically 0.01 mol dm^{-3}), added to the latex by means of a microlitre syringe or autoburette. The latex should be degassed and contained, at constant temperature, under nitrogen, to prevent oxygen or carbon dioxide contamination, and the change in conductivity measured by means of a sensitive dip-type cell. Low percentage polymer solids content (⟨2%) can lead to long equilibrium times. Everett[148] *et al.* found this time could be reduced by performing the titration in the presence of electrolyte (1:1 KBr) which was thought to change the acid-bearing polymer chain "conformation", presumably giving easier access to the end groups.

In the case of both strong acid and base end groups, the measured conductivity initially decreases, as the end groups are neutralised, until the end-point, after which the conductivity increases due to the excess of added acid or base ions. The end-point can be determined by the extrapolation of the ascending and descending lines on a graph of conductance versus volume of titrant. The lines would ideally be linear but are frequently curved, especially as the equivalence-point is approached due to the slow attainment of the equilibrium, (and also due to the type of hydroxide: *e.g.*, in the case $Ba(OH)_2$, the Ba^{2+} is initially exchanged with the H^+ innermost in the latex particle double layer before the outer ions, and these inner ions contribute least to the conductance[498]), making interpretation by extrapolation difficult. Even when the lines are linear, the slope is less than that expected for ions in solution, due to the reduced mobility of the ions in the electrical double layer. The presence of weak acid carboxyl groups in a latex containing both sulphate and carboxyl groups is indicated by the presence of an inflection in the gradient of the ascending leg of the acid neutralisation curve.

The results of a conductometric titration provide information on the total surface charge, and surface charge density, σ, if the latex surface area is known, *e.g.*, from the use of techniques such as gas[450] or soap[331] adsorption experiments, or from calculations as performed, for example, by Tamai[475] *et al.*:

$$\sigma = \frac{Fna\rho}{3W} \tag{3.12}$$

where:

F = Faraday constant;
n = number of moles of, for example, OH^- taken up by particles;
a = latex particle radius;
ρ = latex particle density;
W = total solid content of latex.

The technique is suitable for the determination of strong acid groups (sulphate and sulphonate) and weak acid groups (carboxyl), although the latter can be complex if the percentage solids of the latex is low, or the concentration of carboxyl groups is low due to, for example, atmospheric carbon dioxide adsorbed onto the latex[194] or in the water. (Chainey[87] *et al.*, and Hearn[230] *et al.*, found the problem of carbon dioxide could be minimised by nitrogen purging, and that the effect was negligible in a titration of a latex where the solids content was $>$2%.) The technique is also suitable for the determination of surface basic groups, as might result from a cationic initiator – a procedure first performed by Sakota and Okaya[431]. As has previously been shown for latices prepared with potassium persulphate, the sulphate end groups require converting to the acid form with the exchange of sodium and potassium ions. Sakota's latices were believed to contain both amidino and amino groups, with the groups initially being partially neutralised by hydrogen chloride, and dissociated. It was thus necessary to "unneutralise" the surface groups (*i.e.*, return them to their basic form, *e.g.*: $\text{–C(NH}_2)_2^+\text{Cl}^- \longrightarrow \text{–C(NH)(NH}_2)$) by ion exchange before the titrations could be performed. Sakota's end groups are both weak bases, however, and the titration technique could not differentiate between them.

The presence of more than one type of end group (*e.g.*, strong and weak acid groups) can lead to the titration curve showing more than one change of slope (e.g., in the case of the strong and weak acids, the addition of OH^- will give both a minimum and a change in the ascending slope), one of which may be indistinct if the surface groups are few in number, necessitating the use of a back-titration to aid in the analysis. Uncleaned latex containing electrolyte can show further changes of slope due to the neutralisation of H^+ in the aqueous phase and its replacement by metal ions. Labib and Robertson[300] studied the interpretation of the results for such titrations when weak acid groups were present, concluding that it was important that the addition of titrant was continued until the attainment of the theoretical slope

A problem observed by Egusa and Makuuchi[138], and typical of latex titrations, is a difference in the amount of surface charge observed between the forward and back titrations. In the work of Egusa on carboxylated latices, the amount of surface acid groups detectable in the back titration was greater than in the forward direction. This is ascribed to the excess of added OH^-, after the forward titration, penetrating and finding acid groups in the interior of the latex particles during the period between the two titrations and, hence, resulting in a decreased amount of OH^- for neutralisation during the back titration. A repeat of the forward titration, however, proved identical to the initial forward titration, and this, Egusa explained by way of the particle morphology: during the forward titration, the particle surface is compressed to the core allowing the detection of the surface groups only, whilst during the back titration electrostatic repulsions cause the surface layer to become expanded due to dissociation of the acid groups, allowing access to the particle interior.

Potentiometric titrations are similar to conductometric titrations but rely upon the use of a potentiometric bridge circuit to determine surface charge. The bridge circuit output is calibrated such that it provides the change in pH proportional to the volume, or charge, of titrant added. The shape of the output curve makes the end-point analysis difficult and Vanderhoff[498] recommends the use of conductometric titrations in preference.

In addition to the use of titrations, methods using **dyes** for the detection of polymer chain end groups (*e.g.*, carboxyl[189, 381], hydroxyl[189, 381], and sulphate and sulphonate[189, 190] groups) have also been reported. The polymer is dissolved in organic solution followed by the partitioning[376, 377] or interaction[378, 379] with a suitable dye. By utilising the oxidisable nature of sulphate groups, it is possible to distinguish between a polymer containing only sulphate groups compared to one containing both sulphate *and* sulphonate groups.

3.3.3.2 Instrumental methods of analysis.

The charge surrounding a latex particle in a polar medium such as water consists of bound surface ions plus an outer diffuse region in which the distribution of ions (mainly counter-ions, but also co-ions, such that the colloid is electrically neutral) is determined by electrostatic forces from the bound ions, and thermal motion in the medium. Together this constitutes the **electrical double layer.** Suspended in electrolyte, in an applied electric field, the charged latex particle and its most closely associated ions will move towards the charge opposite to that of the particle. The potential at the shear boundary between this unit and the surrounding medium is termed the **zeta potential** (ζ). A technique suitable for the measurement of this ζ potential is **electrophoresis**[449] (see footnote[1]) and methods include: i, microscope electrophoresis, in which the particles are illuminated, in a horizontal capillary containing an electrode at either end allowing a known voltage to be applied, whilst the movement of the particles is timed and observed through a microscope with an eyepiece graduated for distance; and ii, laser Doppler microelectrophoresis[330]. Laser Doppler microelectrophoresis utilises Young's interference fringes – formed when two laser beams of equal intensity, and constant phase difference, cross. The intensity of the fringes (and their number) is dependent on the angle of crossing. The intensity of light scattered from particles moving through the fringes is dependent on the position of the particles. Calculation of the ζ potential is typically an automated process based on scattered intensity data as a function of time. The former of these two techniques has the disadvantage that larger particles are more easily illuminated than smaller particles and are, hence, more easily seen, possibly leading to unrepresentative results. Laser Doppler microelectrophoresis is advantageous in that a large representative sample of particles (thousands) are observed (*cf.* single particles in the microscope method). Both of the electrophoretic techniques require careful operation to avoid other electrokinetic effects such as the streaming potential (the electric field created by the movement of liquid along a stationary

---

[1] Following the application of the electric field, the latex particles will move at a constant velocity (once the electrolyte solution viscosity is overcome), dependent on: the field strength; the (absolute) permittivity, ε (= $\varepsilon_r\varepsilon_0$); the viscosity, η, of the medium; and the ζ potential. (The direction of the movement being dependent on the sign of the surface charge with respect to the electrodes.) The electrophoretic mobility, U_E, (particle velocity) is related to the particle's ζ potential by the Henry equation for non-conducting particles[449]:

$$U_E = \frac{\varepsilon\zeta f(\kappa a)}{1.5\eta} \tag{3.13}$$

The function f(κa) varies between 1.0 (as in the Hückel equation) to 1.5 (as in the Smoluchowski equation) for small ($\approx$ 0.5) to large ($\approx$ 300) values of κa (= radius of curvature × Debye-Hückel reciprocal {double layer} thickness). The typical latex particle size places it between the two aforementioned values of f(κa). However, conversion tables of mobilities to zeta potentials for various values of κa between 0.01 and 1000 exist[372], which also account for relaxation and retardation by the use of calculations based on the treatment of Wiersema[533, 534] *et al.*

charged surface) or electro-osmosis (the movement of liquid relative to a fixed charged surface). Such effects occur in a typical electrophoresis apparatus due to the charged cell walls and circulation of the liquid in the confined area, and necessitate the measurement being made in the stationary boundary between the electro-osmotic flow and the resultant circulatory flow. In addition to the electrokinetic effects, relaxation and retardation can also lead to erroneous results. Retardation is caused by the counter ions of the double layer undergoing a force, due to the electric field, in the opposite direction to that of the particle. The relaxation time is the time required for the movement of the double layer to reflect that of the particle, and regain its original symmetry: the asymmetric double layer retards the electrophoretic movement of the particle: a process termed relaxation.

Jayasuriya [253] *et al.* described a method using (multinuclear) **N.M.R. spectroscopy** as a means to detect hydroxyl groups. This method is advantageous in that it provides a means of direct measurement of the groups, whereas alternative methods of analysis, such as conductometric titration, involve the oxidation of the hydroxyl groups to carboxyl groups. For polymers possibly containing a mix of surface groups (in particular sulphate and hydroxyl groups), such a method requires the prior determination of the number of sulphate groups as these too would be oxidised together with the hydroxyl groups. Using the N.M.R. technique, Jayasuriya was also able to gain additional information on two types of hydroxyl group within the polymer, since differences in the termination reaction led to oligomer chains of differing molecular weight.

Infra-red spectroscopy can yield information on the presence and type of polymer chain end groups [468], such as carboxyl, sulphate, etc., and has been used in the study of core-shell type copolymers [305]. Zhao [560, 561, 562] *et al.* has used Fourier transform infra-red-attenuated total reflection (F.T.I.R.-A.T.R.), together with X.P.S. and S.I.M.S (see below) to investigate the distribution of surfactants in films formed from polymer latices.

X-ray photoelectron spectroscopy [67] (X.P.S. {or E.S.C.A.}) allows the quantitative analysis of elements on polymer surfaces and also provides information on the chemical bonding within the surface layers. Under ultra-high vacuum, the sample's surface is irradiated with X-rays that interact with inner-shell electrons of the target atoms (with the exception of hydrogen and helium), leading to a spectrum of photo-ionisation energies: the energy of the electrons is characteristic of the atom(s) from where they were emitted and integration of the resultant intensity signal can provide quantitative information.

The technique of **Secondary Ion Mass Spectrometry** [518] (S.I.M.S.) bombards a sample, held under ultra-high vacuum with, for example, noble gas ions or atoms, which penetrate the sample and in doing so lose energy via collisions which may in turn generate a mix of ions and neutral fragments which are lost from the sample surface, and whose charge to mass ratio can be analysed to provide information on the surface species present.

Introduction, Chapter 4: Latex Film Formation and Properties.

4.1 Introduction.

The physical and mechanical properties of thin polymer films are important from both an academic and an industrial point of view. These properties are affected not only by the nature of the polymer, but also by the method of film preparation and conditioning. In many cases, films are obtained from commercial sources, where they are manufactured by processes such as calendering or extrusion. On a smaller scale, films are prepared by solvent-casting or compression moulding. All of these techniques start with the bulk polymer, and are obviously therefore unsuitable for the direct preparation of films from latex dispersions.

4.2 Preparation of polymer (latex) films.

4.2.1 Casting substrates.

Paint and coating technologists have long been interested in the preparation of films from aqueous-based and oil-based formulations. For the coatings technologist, adhesion to (and in the case of waterborne coatings, wetting of) the substrate will be one of the main requirements [349]. Such surfaces, as required for film formation from an academic point of view, are far removed from the typical everyday surfaces that the developed end-coatings will typically be used on. In contrast to commercial polymer coatings, the academic study of films typically requires that they be free of any substrate, and ease of removal of the film from its casting substrate is thus one of the main requirements. Several methods for assisting with this problem have been devised. These include: casting onto photographic paper and removing the film by soaking in warm water to dissolve the gelatin; casting onto aluminium foil followed by amalgamation with mercury; and casting onto silanised plate glass and into P.T.F.E. dishes, in which case the film is removed by gently peeling it from the substrate.

Chainey [84, 90] *et al.* evaluated several film preparation techniques during an investigation of the transmission properties of films formed from surfactant-free polymer latices, including casting onto a mercury surface, onto photographic paper, onto P.T:F.E., into silicone rubber dishes, and onto silanised glass. After extensive trials, all were rejected on the grounds that either the substrate concerned contaminated the film, or that the minimum thickness of film that it was possible to cast was at least an order of magnitude greater than that required. The method of film preparation eventually adopted was developed from the flash coating method used for tablet coating, which is widely used in the pharmaceutical industry. The aim was to form the film so quickly that it could not disjoin, and this was achieved by spraying the latex onto a heated block, coated with P.T.F.E., at temperatures exceeding 393 K. Multiple (20 → 50) passes of the spray gun were employed and the film was allowed to return to room temperature before it was removed from the block, and in some cases was cooled to near the polymer T_g using an appropriate solid-CO_2 slush bath. Spitael and Kinget [462], however, found that sprayed solvent-cast films exhibited a higher degree of porosity than solvent dish-cast films, due to their droplet-like nature, during spraying, which remained apparent in the final film structure.

Roulstone [423] cast PBMA films onto Pyrex glass plates, from which they could be removed by soaking in hot water, or in the case of additive-present films, cast onto nylon plates from which the films could be removed without soaking.

Yaseen and Raju [547] have reviewed the full range of film preparation techniques, finding pros and cons for each depending on the intended application of the film.

4.2.2 Film formation.

The formation of a latex film arises from the coalescence of the individual latex particles – which are normally held apart by stabilising forces (electrostatic and/or steric) resulting from the charged polymer chain end groups or surfactant. These forces (and others, see later) are overcome by the evaporation of the continuous phase (water).

The formation of a continuous film (*i.e.*, transparent and crack-free) is then dependent on the **minimum film formation temperature** (M.F.F.T.) of the polymer, which in turn is dependent on the elastic modulus (resistance to particle deformation), and to a lesser extent, the viscosity of the polymer. If the film is cast above its M.F.F.T., then coalescence of the latex particles can occur. However, if the film is below its M.F.F.T., then a friable discontinuous film or powder compact may form, which is typically opaque due its structured nature and, hence, its ability to diffract light. The more desirable outcome (in the context of this study) of film-formation is something of a compromise since the tendency of the spheres to flow and fuse into a continuous film can, in the extreme, also result in a permanently tacky film that is more suited to adhesive applications [474].

The formation of films at temperatures slightly lower than the M.F.F.T., has been studied by Myers and Schultz [345] using an ultrasonic impedance technique. The results, with respect to the formation of a continuous film, were found to be dependent on the rate of drying and, hence, the rate of relief of stresses within the film. At a temperature within 6 K below the M.F.F.T., and with a drying rate sufficiently slow, a certain amount of creep was able to occur permitting the formation of a film due to the stresses being at a level insufficient to fracture the film. As the rate of drying was increased, the creep mechanism was not fast enough to relieve the stress such that initially the films became crazed, and at the highest drying rates, cracked.

The M.F.F.T., although tending to be close to the T_g of a given polymer, has been reported, for various polymers, to be above *or* below the T_g [135, 256]. Both the M.F.F.T. and T_g are influenced by the same molecular features (*e.g.*, the inclusion of a softer polymer will lower both the T_g and M.F.F.T.). Ellgood [144] showed, for a series of vinylidene chloride (VDC)/ethyl acrylate copolymers, that both the T_g and M.F.F.T. peaked with increasing VDC content, but not at the same composition. Below 55% VDC content, the T_g was found to be greater than the M.F.F.T. A 15 K difference was found between the T_g and M.F.F.T. at the extremes, and different surfactants were also found to alter the M.F.F.T. and its relationship to the T_g of the copolymer. It was noted in Chapter 2 that the staged addition of monomer could lead to unusual particle morphologies. Similarly, the method of feed of a second stage monomer (*e.g.*, seeded growth or blend) can lead to variation in the M.F.F.T. of the resultant latex due to the change in particle morphology [78]. The effect of core-shell morphology on the M.F.F.T. has, however, been found to depend on shell thickness [116]: thin soft shells on hard cores requiring higher drying temperatures than thicker soft shells due to the necessity to deform the core of the former in order to form a film.

Brodnyan and Konan [72] and Kast [269] note that comonomers that impart hydrophilic properties (*e.g.*, methyl and ethyl acrylates, etc.) into a polymer may reduce the M.F.F.T. to below the T_g, in the case of the wet film (as opposed to these properties being measured for the dry polymer) by allowing water to act as a plasticiser. Similarly, surfactant that is compatible with the polymer may also plasticise the polymer, lowering both the T_g and/or the M.F.F.T. [134, 522, 523].

Eckersley and Rudin [135], Jensen and Morgan [256] and Sperry [460] *et al.* found the M.F.F.T. to be related to latex particle size, although this is not always the case [72] (*cf.* the theories of film formation – p-4:6-). Eckersley found the M.F.F.T. to be dependent on latex particle diameter and even in the case of a series of polydisperse copolymer latices, the results suggested that the M.F.F.T. be proportional to the number average particle diameter. However, the increase in M.F.F.T. between a 150 nm latex and 1200 nm latex was only 5 K. Jensen and Morgan [256] found that as the (monodisperse) latex particle size decreased by a factor of seven, the M.F.F.T. was reduced by ca 10 K. Sperry [460] found the time dependent dry M.F.F.T. (*i.e.*, the transition from a cloudy to clear film in a latex pre-dried below its M.F.F.T.) increased with increasing particle size, and concluded that this was due to a simple viscous flow model which accounted for the larger interstitial voids which were present between larger particles and the longer time required for them to be filled (by particle deformation) to give a transparent film.

Following the evaporative drying process (typically by gravimetric methods, although Cansell [77] *et al.* described an alternate method using dielectric measurements), from beginning (*i.e.*, wet latex) to end (*i.e.*, film) leads to a sigmoidal curve, which can be divided into a number of stages for analysis. Vanderhoff [397, 504] *et al.* describe **three stages in the drying process** (see **Figure 4.1**), studying drying with and without the aid of a 'windtunnel' to remove the humidity of the evaporating water. The drying process may be complicated, however, by virtue of it being non-uniform (*i.e.*, different areas of the film may dry at different rates) and, hence, quantitative evaluations of the rate of drying typically involve the use of estimates of the size of, for example, dried areas of film, or the use of averages to give a mean value for the film as a whole. Despite this, attempts have been made to mathematically model the evaporative process [e.g., 402].

Stage I. Water evaporates from the latex surface, concentrating the latex: the rate of evaporation has been determined by a number of workers [105, 451, 504] as being the same as the rate of evaporation from water alone, or of water from a dilute solution of surfactant + electrolyte, *i.e.*, such as that which constitutes the aqueous phase of a latex. This stage is the longest of the three, and lasts until the polymer has reached approximately 60 → 70% volume fraction, Φ, (dependent on the stability of the latex) (*cf.* 74% for close packed spheres) or until the surface area of the latex's liquid-air interface starts to decrease as a result of, for example, disjoining or solid film formation. Initially the particles move with Brownian motion, but this ceases as the electrical double layers undergo significant interaction, once a critical volume of the water has evaporated.

Stage II. This starts from the time at which the particles first come into irreversible contact, and iridescence may be observed on the latex surface. The rate of evaporation per unit area of open wet latex remains constant, but the overall rate of evaporation decreases greatly during this stage. (Reducing the rate of evaporation can lead to a better quality film by allowing the particles more time to pack into an ordered structure before flocculation occurs. Casting at high temperatures gives the particles sufficient energy to overcome their mutual repulsion and the films are formed before the particles are ordered[323].) Particle deformation occurs in soft latices, as the particles start to fill inter-particular capillary channels, driven by interfacial forces (see paragraph 4.2.2.1).

Stage III. This stage starts with the initial formation of a continuous film. The remaining water leaves the film initially via any remaining interparticle channels and by diffusion through the polymer itself, but the rate of evaporation eventually slows to (asymptotically) approach that of diffusion alone. It is during this stage that a soft latex becomes more homogeneous and gains its mechanical properties. The rate of water removal may be decreased by film additives that are impermeable or hydrophilic.

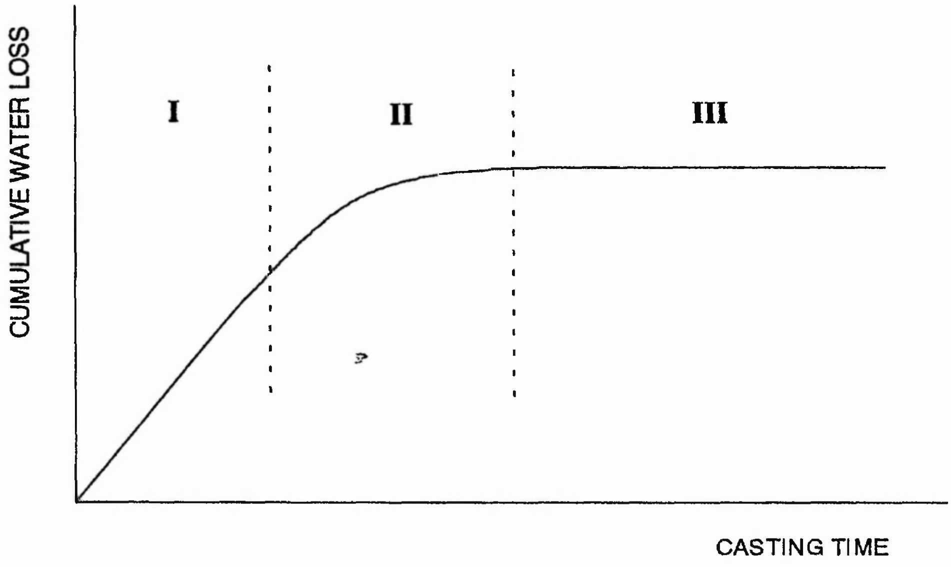

Figure 4.1 Schematic plot of the water loss occurring on latex drying.

Croll[105, 106], however, describes the process of film formation in just two stages as an evaporation front moves into the coating leaving behind a 'dry' layer, containing no continuous water, with ahead of it a transition layer losing water to the dry layer above and supplied with water from the wet latex below. The rapid rate is maintained for as long as wet latex remains at the substrate, then the rate progressively decreases.

Bierwagon[47] considered film formation in relation to the same three regimes as proposed by Vanderhoff, discussing drying in terms of film thickness and latex solids content. *E.g.*, a film of low solids content could dry faster than one of high solids content despite the lower quantity of water to be removed from the latter, which however, reaches the diffusion-controlled stage (*i.e.*, surface closure) sooner, and then loses water more slowly. As the film dries from the surface down, a fixed film area is then subject to contraction in the z-plane, thereby producing stress in the x-y plane. If polymer elasticity is insufficient, then the stress can be overcome by slippage between the coalesced layer and the fluid beneath giving rise to the **'mud-cracked'** surface effect.

Hwa[247] studied the **non-uniformity of film drying** to determine that, as the aqueous phase evaporated, **three distinct regions** could be observed, *e.g.*, a **dry region**, a **wet (latex) region**, and an intermediate **region of flocculated latex** (such that the film as a whole embodied all three periods of Vanderhoff's drying regime). In Hwa's circular films these regions formed concentric bands, and the films dried from the outside inwards. It was noted that these rings differed, dependent on the T_g of the polymer. In the case of a low T_g polymer, the flocculated and dry regions were both continuous, whereas for hard polymers, fine radial cracks were apparent, due to the relief of stresses, and the dry region was more opaque (due to cracks) than the flocculated region. Hwa was able to show that the flocculated region had some mechanical strength (*i.e.*, it was not washed away in a stream of water, as was the wet latex) presumed to result from van der Waals' forces, and that the particles were not close packed (the volume fraction, Φ, was between 0.49 → 0.62) such that the region was porous. The flocculation was found to be dependent, to some extent, on the nature of the surfactant used: easily desorbed soaps were proposed to be squeezed away from the points of particle-particle contact to form micelles in the particle interstices and, hence, aid flocculation, compared to the surfactant-free latices. Surfactant which was not easily desorbed, however, delayed the onset of flocculation to high volume fractions.

The fact that latices of differing stability will flocculate at different particle-particle separations (*i.e.*, at different rates) has been used to advantage by Okubo and He[360] in the preparation of asymmetric films from latex blends. Such films showed side-dependent (*i.e.*, polymer-substrate interface or polymer-air interface) variation in properties such as film tackiness and permeability.

The constant rate (r_c) period of drying was studied by Poehlein[397] *et al.* with respect to latex particle size, using an equation to account for the non-uniform drying. If the three regions described by Hwa[247] are expressed in terms of film areas (*e.g.*, A_I = area of wet latex; A_{III} = area of dry film (the rate of evaporation in this region was assumed to be negligible); and A_{II} = flocculated region area, then:

$$r_c = \frac{1}{A_I + A_{II}} \frac{dW}{dt} \tag{4.1}$$

where:

W = gross film weight;
t = time.

It was shown that the rate, r_c, increased with increasing particle size (although this was not so apparent in still air, and was not predicted by a theoretical equation based on heat transfer theory). Poehlein[397] *et al.* speculated that the rate increase with particle size was a result of the differences in water content in the double layer, or the particle surface area available for surfactant adsorption, although the latter was minimised by attempted adjustment of the surface tension of the latices to a constant value.

Armstrong and Wright[15] noted that the films prepared from latices of a relatively large particle size (750 nm) were of a poorer quality (*i.e.*, poorer corrosion resistance due to greater porosity) than those films prepared from latices of a smaller particle size (105 nm). This was ascribed to the larger particles showing less coalescence, but it was not clear whether the poor quality of the film was the result of differing rates of drying resulting from the differing particles sizes, or simply due to the larger interparticle voids that would be found for the larger sized uncoalesced particles.

4.2.2.1 Particle coalescence and film drying stage II.

Over the years a number of theories regarding the formation of polymer films, from the fusion of latex particle spheres, have been considered. These include:

- ✗ **dry sintering**[118, 170] (see below);
- ✗ **wet sintering**[69] and **capillary theory** (see below);
- ✗ piston-like **compression**[451] arising from the preferentially dried surface layer building in thickness from the top down;
- ✗ And **interparticle cohesion** promoted by surface forces[275].

Dry sintering is driven by the polymer-air surface tension. Dillon[118] *et al.* discuss the coalescence processes in terms of the viscous flow of the polymer. This viscous flow results from the shearing stresses caused by the decrease in the polymer-particle surface area, and the resultant decrease in polymer surface energy, as the film is formed. By appraising values relevant to the typical polymer latex, Dillon considered the forces acting on the interparticle 'holes' (of radius R), as denoted by the Young-Laplace equation:

$$P_i - P_e = \frac{2\gamma}{R} \tag{4.2}$$

where:

P_i = internal pressure (see **Figure 4.2**);
P_e = external pressure;
γ = polymer-air interfacial tension;
R = radius of curvature of the sphere;

and concluded that the pressure acting on the void could not be contained, as a result of the polymer being permeable to the trapped air and water vapour. The extent of coalescence (as determined from the half-angle of coalescence) was then related to an equation developed by Frenkel [170]:

$$\theta^2 = \frac{3\gamma t}{2\pi\eta r} \tag{4.3}$$

where:

θ = angle seen in **Figure 4.2**, *i.e.*, the half-angle of contact;
γ = surface tension;
t = time;
η = polymer viscosity coefficient;
r = particle radius.

Dillon showed that a plot of θ^2 as a function of $1/r$, as measured by electron microscopic observation of shadowed particle pairs, gave the expected linear relationship.

Brown [69] discussed **wet sintering**, driven by the polymer-water interfacial tension, leading to the **deformation of particles**, during drying. He considered the forces acting both for and against the coalescence of the latex particles, with the conclusion that for coalescence to occur, an inequality must exist in which the capillary force, F_C, (resulting from the surface tension of the interstitial water, caused by the formation of small radii of curvature between the particles as the water evaporated) must overcome the forces of resistance to deformation, F_G, of the latex spheres: *i.e.*, $F_C \rangle F_G$. These forces, Brown presumed, were proportional to the relevant pressures, with the area over which they act as the constant of proportionality, and hence: $P_C \rangle P_G$. From Laplace's equation, Brown derived the capillary pressure, P_C for the cylinder of radius R, between three contiguous latex particles (see **Figure 4.2**), in terms of the latex particle radii, r:

$$P_C = \left(\frac{2\gamma_w}{R}\right) = \frac{12.9\gamma_w}{r} \tag{4.4}$$

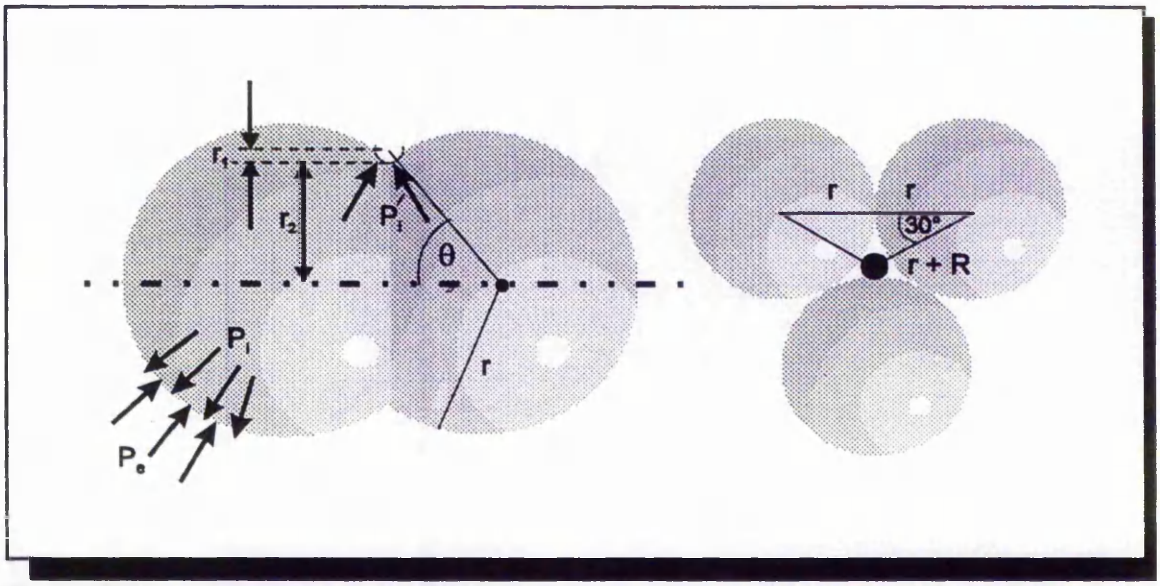

Figure 4.2 A cross-section of sintered latex particles, and a plan view showing the interparticle capillary.

where:

γ_w = polymer-water interfacial surface tension;
Note:

$$\frac{R}{R+r} = \cos 30^\circ \tag{4.5}$$

By treating the particles as elastic bodies, the pressure on the area of contact was also calculated, in terms of the elastic shear modulus, G, of the polymer and, hence, Brown derived an expression for coalescence:

$$G_t < \frac{35\gamma_w}{r} \tag{4.6}$$

where:

G_t = time dependent shear modulus (necessary because the viscoelastic particles are treated as elastic)
r = latex particle radius.

Sheetz [451] later amended Brown's equation for capillary pressure to account for the situation when the contact angle, ϑ, between the polymer and water did not equal zero:

$$P_c = \frac{12.9\gamma_w \cos\vartheta}{r} \tag{4.7}$$

Sheetz also formulated his own theory of latex coalescence. In qualitative terms, as the latex becomes concentrated by evaporation of the water, flocculation occurs as the repulsive forces of the particles are overcome. Particles at the latex-air interface are then subject to the forces of capillarity and therefore coalescence, leading to compaction and deformation of the particles under the surface. Water in the film's interior must then diffuse through the upper layers to escape and this generates a further, vacuum-like, compressive force acting normal to the film's surface. The mechanism is therefore seen to be based on Brown's wet sintering mechanism *and* diffusion. Scheetz analysed the thermodynamics of the system and showed that the source of the energy for the particles' fusion was the heat in the environment – converted for film formation by the evaporation of the water. In evidence for the diffusion being involved in the coalescence mechanism, Sheetz cited the facts that a film containing a water-permeable polymer dried at a rate faster than one that was less water permeable; and that a film in which capillary action was prevented (by means of a thin solvent-cast film) could form a continuous film, whilst the same polymer without the solvent-cast deposit formed a discontinuous film.

Although Dobler [123] *et al.* generally agreed with the mechanism of Scheetz, they believed, from observations of iridescence, that the surface of the latex closes (*i.e.*, complete surface iridescence followed, presumably, by skin formation) long before the particles become close packed in the bulk latex (as they do in Sheetz's theory).

Like Sheetz, Mason [333] also identified a number of erroneous assumptions and points of error in Brown's work. Firstly, in converting his forces (capillary and deformation) to pressures, Brown assumed the same constant of proportionality (an undefined area, A, over which the capillary and contact pressures are exerted) for each, *e.g.*, for equation (4.4):

$$F_C = \frac{12.9\gamma_w A}{r} \tag{4.8}$$

Mason points out that these areas (for F_C and F_G) are not necessarily identical, and repeated the analysis using corrected values for the areas such that the condition Brown quoted in equation (4.6) became:

$$G < \frac{67.6\gamma_w}{r} \tag{4.9}$$

Mason also criticises the fact that Brown assumed that the capillary pressure remained constant whilst the latex particles coalesced, and derived a new equation for the capillary pressure based on the deformation of the spheres. From this, the criterion for film formation moved yet further from Brown's inequality, to give:

$$G < \frac{266\gamma_w}{r} \tag{4.10}$$

It has also been noticed [267, 460] that Brown's work has been criticised for using a polymer modulus which was obtained for the dried polymer, rather than a polymer in an aqueous environment.

Despite Brown's differences with Dillon over the role of the evaporating water phase in latex coalescence mechanisms, both research groups presumed that the forces of coalescence were inversely proportional to the latex particle radii. Vanderhoff[508, & 500, 501] *et al.* indicated that the pressures for coalescence, resulting from the works of Dillon and Brown, were insufficient to cause the coalescence of particles greater than 1 μm in diameter and extended the theories accordingly. These extensions to the theory were again based on determining the forces acting to cause coalescence. Vanderhoff proposed that as the water evaporated, the particle coalescence was initially hindered by repulsion of their stabilising layers. Further evaporation then resulted in particle-particle contact, and the force increased due to (i) the polymer-water interfacial tension, and (ii) the small radii of curvature in the region of coalescence (r_1 and r_2 as seen in **Figure 4.2**). Hence:

$$P_i - P_i' = \gamma_w\left(\frac{1}{r_1} - \frac{1}{r_2} + \frac{2}{r}\right) \tag{4.11}$$

where:

P_i = internal pressure;
P_i' = internal pressure in the region of coalescence;
r = particle radius, and r_1 & r_2 are radii as seen in the diagram;

cf. equation (4.2).

As with the work of Brown [69], Mason [333] criticised Vanderhoff's work for mathematically confusing *force* with *pressure*. However, whereas the error in Brown's model led to the error being less that an order of magnitude, Mason claimed Vanderhoff's error completely invalidated the work.

The aforementioned theories assumed that the latex particles acted as viscous fluids or elastic spheres. Kendall and Padget [275] noted that particles are not truly viscous (as depicted by the Dillon model) from the fact that latex films can show a residual particulate structure, and that they were elastic with a viscous component. Similarly, Kendall reasoned that the fact that a film does not attain its full strength until after the point when all of the water is removed [e.g., 524 - 526] implied modifications were necessary to Brown's model. Accordingly, he introduced a new model based on the theory [259] of adhesion and interfacial surface energy between elastic spheres – again, its applicability is limited by its foundation on elastic spheres. For a hexagonal close packed array of spheres, Padget states that voids are eliminated (*i.e.*, opaque film to clear film) when:

$$\frac{2Er}{\gamma\left(1-\upsilon^2\right)} = \frac{9\pi}{2} \tag{4.12}$$

i.e., for film formation:

$$E < \frac{9\pi\gamma\left(1-\upsilon^2\right)}{4r} \tag{4.13}$$

where:

γ = energy released when two spheres of unit area move into contact;
υ = Poissons ratio[1];
E = Young's modulus – Note that:

$$G = \frac{E}{2(1+\upsilon)} \tag{4.14}$$

The dimensionless ratio on the left of equation (4.12) is described by Kendall [275] as the "crumble number." If this number is high, then coalescence will not occur; if the crumble number is low, then a transparent non-porous film will form. The transition was said to occur at a crumble number of "around ten." Kan [267] indirectly investigated the deforming forces during latex coalescence at the M.F.F.T., by measuring the moduli of water saturated latices. The magnitude of the results showed good agreement with the Kendall theory.

Sperry [460] has investigated the role of water in film formation using M.F.F.T. measurements on latices pre-dried at temperatures below their M.F.F.T. (which shows the M.F.F.T. by a transition from an opaque to a clear film) and also wet latices. In the case of a hydrophobic polymer, the dry M.F.F.T. was virtually identical to the wet M.F.F.T. indicating the presence of water and, hence, capillary forces contributed little to film formation. Plasticisation by water was said to be the cause of hydrophilic polymers yielding wet M.F.F.T.s which were lower than the dry M.F.F.T.s – by up to ca 10 K. The dry M.F.F.T.s decreased linearly with log[*time*] which was attributed to (Williams-Landel-Ferry type) viscoelastic relaxation resulting from van der Waals' attractive forces/polymer-air surface tension and the collapse of interstitial voids.

Lamprecht [304] studied film formation by treating the latex particles as viscoelastic bodies, and included dynamic factors such as creep deformation in relation to the rate of water removal. Eckersley and Rudin [135] indicated a mistake in Lamprecht's calculation, and derived a corrected criterion for film formation assuming viscoelastic spheres:

---

[1] υ = lateral contraction per unit breadth/longitudinal extension per unit length.

$$\frac{1}{J_c(t')} \le \frac{34\gamma_w}{r} \tag{4.15}$$

where:

t' = the time when the two spheres are in closest proximity to one another;
$J_c(t)$ = the polymer's time dependent creep compliance (= time dependent modulus, $G(t)$, in the linear viscoelastic region).

Eckersley went on to develop her own (time-dependent) viscoelastic model of film formation based on the polymer-water interfacial tension forces acting together with the capillary force to cause coalescence. The theoretical results for particle deformation from the model agreed with experimental measurements by S.E.M.

The use of neutron scattering experiments (S.A.N.S.), together with S.E.M./T.E.M. has permitted the 'observation' of latex particle structure during film drying; allowing the three-dimensionally deformed shape of the latex particles to be studied. Joanicot[257] *et al.* and Chevalier[95] *et al.* have studied the particle packing of latices consisting of a soft hydrophobic polystyrene-poly(butyl acrylate) copolymer core, stabilised by a hydrophilic shell (either neutralised poly(acrylic acid) or a monolayer of zwitterionic surfactant). Such a stable configuration allowing the close packing of the particles before coalescence occurs.

By the use of very thin films, the S.A.N.S. scattering patterns, produced by latices as the dispersions concentrated (to approximately 20 → 50%, by evaporation) were studied, and interpreted in terms of each of the monodisperse particles being surrounded by 10 → 12 nearest neighbours, and forming face-centred cubic crystalline-like particle packing. Such ordering of the particles was lost (as shown by the replacement of the scattering pattern by Debye-Scherer rings) either when the dispersion was too dilute (latex volume fraction <20%) or, if salt was present to screen the interparticle electrostatic forces, or when the latex was polydisperse.

It was originally deduced by Lissant[322], when investigating high-internal-phase-ratio emulsions, that above the maximum packing volume available to hard spheres (74%, in a face centre cubic configuration), deformation of a sphere to fill all of the space (whilst keeping the same volume as the original sphere) will give rise to a **rhomboidal dodecahedron**. Joanicot[257] *et al.* showed such polyhedra, by staining the hydrophilic membrane (*i.e.*, particle interfaces – which on particle deformation defined the polyhedra), when a latex had lost most of its water – comparing the structure to that of a foam.

Chevalier[95] *et al.* used the S.A.N.S. evidence to describe particle coalescence. Coalescence was observed to move through the drying surfactant-coated latex in the form of a 'coalescence front' progressing from the periphery of the film inwards: the progress of which could be reversibly halted by stopping the evaporation of the water. At the interface between dry film, and wet latex (in which the packing fraction was <0.74), a phase inversion occurred, from a polymer in water to a water in polymer system. Coalescence was said to only occur if the hydrophilic layer was breached, and this was seen to differ depending whether the hydrophilic layer was the surfactant or the acrylic acid. The films stabilised by poorly adsorbed surfactant formed a continuous matrix of polymer containing hydrophilic domains, whilst those latices stabilised by the polymer retained the foam-like structure: as indicated by a collapse of the diffraction peak in the case of the former, but a peak which could be reinstated by swelling the film with water in the latter case. This work thus differentiated between coalescence, which was defined as the breakup of the hydrophilic layer, and polymer chain interdiffusion, which occurred in a later stage.

4.2.2.2 Particle fusion (film drying stage III), film structure, and aging.

The aforementioned theories of coalescence considered film formation as a process in which, after the intermediate stage, the deformed latex particles were held together by physical forces. This was countered by Voyutskii [524, 525, 526] who, from studies on adherence of rubber coated fabric strips, judged that these forces alone were insufficient to account for the mechanical and physical properties of such a film. Voyutskii discussed film formation from a polymer dispersion in the typical three stages of: evaporation to a concentrated 'solution'; followed by polymer 'globules' coming into close contact, with deformation, due to capillary forces; and then in the final stage, the film gaining its mechanical strength by virtue of the fact that solvated stabiliser molecules migrated to between the polymer globules, as a result of the loss of water, allowing the self-diffusion of polymer chains and leading to an increase in the homogeneity of the polymer. This process of mutual interdiffusion between polymer chain ends is termed **autohesion**, and although not an innovative idea (the mechanism being based on the work of Josewitz and Mark [260]), Voyutskii was the first to apply it to the coalescence of latex particles.

By virtue of an ongoing process, similar to autohesion, Bradford and Vanderhoff studied the changes in structure occurring in a continuous, transparent, film as a function of film age [62]. A styrene-butadiene copolymer film, which was replicated and viewed by T.E.M. within hours of casting, showed the vestiges of the original latex particles. However, over a fourteen-day period, the particle contours on the film surface eventually disappeared, accompanied by the exudation of material from within the film: presumed to be stabiliser (visible as blister-like eruptions), and in some cases, electrolyte (visible as crystallites). Investigation involving a series of non-ionic surfactants showed that it was the long poly(oxyethylene) chained stabiliser which the film exuded, and not the short chained oil-soluble stabiliser. It was concluded that it was additive which was incompatible with the polymer that was secreted. The exuded surfactant was itself observed to change in appearance with time, being initially smooth but later becoming rough. This was attributed to oxidation, which was later shown could cause scission of the poly(oxyethylene) chain thus making it more compatible and, hence, allowing it to diffuse back into the polymer.

Bradford and Vanderhoff went on to study the aging process, which they termed **further gradual coalescence**, in detail [62, 63], and Vanderhoff has discussed the results in a number of reviews of film formation [500, 501]. They showed that it occurred at the film-substrate interface as well as at the film-air interface (albeit at possibly different rates), and also in the film's interior where stabiliser was exuded into "pockets." Porosity due to the leaching of surfactant was reduced if the film was aged before the surfactant was leached. The further gradual coalescence was independent of the casting substrate, with the exception of a mercury substrate which it was proposed induced different stresses into the film when compared to casting on a solid substrate. The proportion of oxygen in the atmosphere also affected the rate of further gradual coalescence – particle contours disappearing rapidly in a high oxygen atmosphere (attributed to oxidative softening of the copolymer) whilst remaining unchanged in a nitrogen atmosphere. Bradford and Vanderhoff also found that reducing the polymer molecular weight (by using a chain transfer agent {*t*-dodecyl mercapton}), increased the rate of further gradual coalescence, and the exudations appeared earlier, whilst an increase in the three-dimensional nature of the polymer (by crosslinking with divinyl benzene), reduced the rate of aging but did not halt it completely.

Bradford and Vanderhoff[63] observed aging in other polymers, including ethyl acrylate-methyl methacrylate copolymer, natural rubber, and vinylidene chloride-vinyl chloride-ethyl acrylate copolymer. Roulstone [424] has observed the disappearance of particle contours within films of surfactant-free PBMA. Bradford and Vanderhoff did not, however, find evidence of aging in poly(vinyl acetate) (P.V.Ac.) films, even after 280 days. This they attributed to the surface hydrolysis of the acetate to poly(vinyl alcohol) (P.V.OH.) which prevented autohesion. The presence of P.V.OH. in such films was later shown by Kast [269] (using osmium tetroxide staining of the hydroxyl groups, and electron microscopy) as a continuous network throughout the film, separating the P.V.Ac. core particles.

Although theories for the interdiffusion of polymer chains at an interface exist [e.g., 288] (and have been shown [555, 556] to be applicable to latex particle film formation), it was the introduction of S.A.N.S. techniques that has, since the mid-1980s, provided a means of investigating the magnitude of the polymer chain interdiffusion and, hence, the reason for a film's strength. Some of this work has recently been reviewed by Sperling [459] *et al.*

Hahn [212, 213] *et al.* used S.A.N.S. experiments on PBMA to show that latex particle coalescence was as a result of the "massive" interdiffusion of polymer from different latex particles. The diffusion coefficients, *D*, during further gradual coalescence at ca 353 K were 10^{-16} cm^2 s^{-1} and demonstrated a thirty-fold increase as a result of a 20 K rise in temperature. A factor of two change in molecular weight changed the diffusion coefficient sixfold. Yoo [555, 556] *et al.* used similar methods to Hahn to investigate the interdiffusion penetration-depth at which the film attained its full tensile strength. Results were found to be dependent on the polymer molecular weight, the spatial distribution and location of chain ends at the polymer-polymer interface, and the ratio of the polymer chains' radii of gyration to the radius of the latex particle.

Linné [320] *et al.* found, also by S.A.N.S., that for small (ca 38 nm Ø) high molecular weight (6×10^6) polystyrene, that the molecules were fourfold constrained in the lattices, and that a retarded non-Fickian diffusion relaxation at 10^{-14} cm^2 s^{-1} occurred by a modified **reptation**[1] model (that accounted for the polymer chains' charged ends {and, hence,

---

[1] The reptation model describes the restricted thermal motion ($\propto t^{1/4}$) of a polymer chain that is entangled in other polymer chains [112]: the 'average' motion effectively being confined to the centre of a tube. The name originally arose from the snake-like movement of polymer chains in concentrated solution.

repulsion}), *cf.* 10^{-16} cm^2 s^{-1} expected for translational diffusion at 443 K. Energy release also occurred during T_g determination with the second run giving a value 6 K lower than the first, and close to the expected value for polystyrene. Linné[320] claimed that polymer chain interdiffusion over 110 Å was sufficient to give a tough coherent film, *i.e.*, diffusion across the particle boundary of 50 → 60 Å; ca 0.15×Ø. The chain end diffusion of high molecular weight (*e.g.*, $> 7.6\times10^4$) polymer may not follow Fickian or reptation models due to polymer chain entanglement[529].

Kim[285] *et al.* studied particle coalescence using "direct mini-emulsified" latex particles, which were claimed to show a narrower molecular weight, and particle size distribution, when compared to conventionally emulsion-polymerised particles, and also contained no ionic chain-end groups. (Particles were prepared by anionic polymerisation to give hydrogen chain ends, which were distributed randomly throughout the particles, as opposed to being predominantly on the particle surface as in conventional ionic chain end groups.) The rates of inter-particle chain-interdiffusion were found to be greater for Kim's particles when compared to conventional latex particles: a feature ascribed to the smaller chain end groups (compared to, for example, sulphate end groups) and the fact that the need to overcome polar repulsions was not required.

The effects on polymer interdiffusion of varying amounts carboxyl chain end groups on the surface of a PBMA latex (prepared to give a PBMA-core, carboxylated-shell morphology) has been investigated by Kim[286] *et al.* using fluorescence direct energy transfer measurements. Whilst not preventing chain interdiffusion, the presence of acid end groups did retard it. Problems of data interpretation arose, however, due to particle surface-composition heterogeneity, and it was presumed that the polymer chains of lowest molecular weight and lowest carboxyl content interdiffused earlier than those of higher molecular weight/carboxyl content: the latter, however, showed increased contribution to the energy transfer at longer annealing times. (Interdiffusion was possibly between miscible phases, *e.g.*, PBMA with PBMA, and PBMA-co-MAA with PBMA-co-MAA.)

Kim[287] also investigated the effects of neutralisation of (carboxyl and sulphate) acid end groups using a range of mono and divalent bases. Like the aforementioned carboxylated polymer, interdiffusion of the neutralised polymer showed an initial quick rate, followed by a longer lasting constant rate period. The presence of an ionomeric shell reduced the rates of interdiffusion further than carboxylation, in the order of $NH_4^+ < Na^+ < Ba^{2+}$. *I.e.*, monovalent ions retard diffusion to a lesser extent than divalent ions. Kim was unable to distinguish the contribution of T_g effects during this work.

Despite their effects on chain interdiffusion, carboxyl groups have been shown to contribute to the viscoelastic cohesive strength of particles in a film due to interfacial crosslinking[412] – via either hydrogen bonding or ionic dipolar interactions when neutralised. (If the neutralising molecule was sufficiently large {*e.g.*, diamino-polyoxyethylene}, then coiled lamella could be formed which had the opposite effect {when compared to neutralised carboxyl groups} of plasticisation and therefore reduced cohesive strength.)

Unsurprisingly, Sperling[459] *et al.* conclude that the rate of coalescence depends on where the polymer chain ends lie with respect to the particle surface, and that films form faster when the ends lie *on* the particle surface. The rate of coalescence of latex particles, as determined by Padget and Moreland[375] using T.E.M. and an A.C. impedance technique, increased with increasing concentration of block copolymer surfactant. This effect was attributed to plasticisation of the (dry) latex polymer by the surfactant. (When wet, the poly(ethylene oxide) groups are hydrated and were relatively incompatible with the polymer, such that the M.F.F.T. was not changed whilst water was still present.) Exudations of the surfactant were only significant at concentrations above surface coverage.

The effect of coalescing aids on the interdiffusion of polymer chains during polymer annealing was also investigated by Winnik[528, 543] *et al.* Organic solvents, typically used as coalescing aids (*e.g.*, glycol derivatives), were found to provide a constant degree of enhancement in inter-diffusion rates (*i.e.*, as a result of plasticisation by the coalescing aid) during annealing, and the effect was described by a modified Williams-Landel-Ferry equation. Deviations from the model (*i.e.*, the degree of enhancement was not constant during the course of annealing) were as a result of evaporation of the coalescing aid from the film, by a Fickian-type process.

Distler and Kanig[121] assumed that latex-cast films would always retain some form of inhomogeneity due to the distribution of stabilising charge (*e.g.*, polymer chain end groups or grafted surfactant). Citing latex particle stability as proof of the particles having an exterior more hydrophilic than their interior, they reasoned that, on deformation of the particles into a film, these surface boundary layers of hydrophilicity would interdiffuse to form an interconnected ‘honeycomb,’ but which would then act to inhibit further interdiffusion by virtue of the incompatibility between the hydrophilic and hydrophobic polymer. In evidence of this, Distler and Kanig point to the fact that a normally transparent film may turn opaque, or even show Bragg diffraction iridescence, when swollen with water: both of which require latex-particulate sized features to cause the necessary difference in refractive index (between the polymer and water) and crystalline structure, respectively, and hence, were testimony of the ability of water to penetrate the hydrophilic honeycomb and expose such features.

The (i) increased water absorbency, (ii) increased difficulty to leach surfactant, and (iii) reduced tendency of a copolymer latex film of vinyl acetate and a vinyl ester of Versatec 10 acid to whiten (swell) in water were attributed, by Aten and Wassenburg[24], to the redistribution of surfactant molecules from the surfaces of the latex particles (where they were sited on latex polymerisation) to a more even distribution throughout the film, following a period of secondary ‘drying’ above the polymer T_g. Such redistribution was ascribed to the increased polymer chain mobility above the polymer T_g, and was not apparent in films annealed below the T_g.

Distler and Kanig also used T.E.M., combined with staining techniques, to observe polyhedra shaped particle boundaries within their films. In a butyl acrylate-acrylonitrile-methylol acrylamide-acrylic acid copolymer, uranyl ions were bound to carboxylic acid groups, to clearly show the particulate network, which was also apparent in similar films [121] contrasted with hydrazine/osmium tetroxide [268]: the 'particles' in the films showing a good degree of correlation of size compared to the original latex size. Such contrast-forming staining techniques also showed the web-like particulate structure in films formed from surfactant-free acrylate latices [121, 122] indicating that such particles have a high degree of surface hydrophilicity (functionality).

Joanicot [258] *et al.* investigated the effect of thermal annealing on the cellular network ("membrane") of hydrophilic particle boundaries, which act to separate the hydrophobic cores of the latex particles in a film: observing the fragmentation of the membranes by the use of S.A.N.S. and T.E.M. Fragmentation of the hydrophilic membrane arose due to the high hydrophilic-hydrophobic interfacial surface area, such that the dispersion was not in a state of lowest free energy. Joanicot discusses the fragmentation of the hydrophilic membrane in comparison with the evolution (droplet maturation) of oil-in-water emulsions. In such an emulsion, the thermal motion of the stabilising surfactant (surrounding the emulsion droplets) can lead to surfactant bridging through the aqueous phase, between droplets, which can in turn allow the oil droplets to combine. For such combination to occur, requires the attainment of a critical thickness of water between the particles. The thickness of membranes between latex particles is thin (ca 2 nm), and their fragmentation is thickness-independent, but requires thermal treatment for the attainment of a threshold beyond which the hydrophilic and hydrophobic parts of the film segregate. Joanicot determined that membrane fragmentation was a function of: i, mobility of the polymer from which the membrane was made (restricted by crosslinking, etc.); ii, the mobility of the particle core (*i.e.*, a function of polymer T_g, etc.); and iii, the anchoring (*i.e.*, due to surface functionality) of the membrane polymers to the core. Once fragmentation had occurred, the hydrophilic polymer was found to form irregular clusters within the hydrophobic polymer. The irregularity was ascribed to the method of cluster formation in which the hydrophilic membranes were said to be 'attached' to cores with a distribution of strengths (*i.e.*, heterogeneous latex particle surface) and, hence, released at differing times: clusters of hydrophilic polymer occurring (in the hydrophobic polymer) at points where the membrane was released initially. This was again compared to the evolution of high internal phase ratio emulsions whereby large droplets capture smaller droplets to yield a distribution of small droplets and much larger ones: 'heterogeneous growth' (*cf.* homogeneous growth: the combination of equally sized smaller droplets to give a monodisperse emulsion which grows continuously).

In the aforementioned work of Joanicot [257] *et al.* and Chevalier [95] *et al.*, it had been shown that latices formed a foam-like structure of rhombic dodecahedra upon coalescence. These actual structures have been observed [424, 527] in latex films of PBMA, by electron microscopy after fracturing under liquid nitrogen. Wang [527] *et al.* noted differences in structure between large and small particles (337 nm and 117 nm, respectively). Whereas the larger particles formed ordered structures, the smaller particles (for which films were formed in the presence of surfactant), underwent random packing. This was also apparent for the larger particles if the film was prepared in the presence of surfactant. Surfactant could be seen in the fracture cross-sections, and this was attributed to it being concentrated in the coalescent front as it moved through the film.

With respect to coalescence and the effect of repulsions between particles due to their surface group functionality, Nicholson and Wasson[349] conclude that coalescence mechanisms may be divided into two groups: (i) those dependent on sintering or capillarity processes, which dominate when there are polar repulsions present; and (ii) those dependent on chain interdiffusion, when there is very little repulsion between particles. Whilst ionogenic groups may lead to polymer chain stiffening, this may be countered during latex film casting by increased water hydration leading to plasticisation.

4.2.2.3 Solvent-casting of a film.

Whilst the formation of films from latices and from polymers in solution may seem to be fundamentally different processes, there are aspects of similarity: *e.g.*, macromolecules in solution behave hydrodynamically as though they are molecular dispersions having solvent-impermeable cores and peripheral solvent-permeable segments[347]; a difference mainly of scale compared with uncharged sterically stabilised latex particles. Whether solvents will necessarily deposit pore-free films of the maximum density and lowest permeability is uncertain. Different outcomes are predicted, depending upon the solvent power, when high concentrations are reached in the later stages of drying. Funke and Zorll[177] suggested, based upon evidence from freeze-dried extracts of films in the gel stage, that good solvents would produce more open, porous structures, and Nicholson and Wassen[349] cite Gould[205] with a similar prediction that compact molecules in the solution will remain compact in the film state. Kesting[276], however, suggests that polymer coils in good solvents will interpenetrate to a more compact structure than in poorer solvents which will favour earlier polymer segment-segment contacts. Spitael and Kinget[461] concluded that the formation of a gel was the most important stage of solvent-cast film formation, and that solvents that did not gel yielded poorer films which exhibited poorer transparency.

Distler and Kanig[121] dissolved freeze-dried samples of poly(ethyl acrylate) and poly(*n*-butyl acrylate) in tetrahydrofuran, diluted to such an extent (0.1%) that the polymer chains were dispersed with no "felting", *i.e.*, the resultant solution was completely homogeneous. In films formed from such solutions, it was found, from analysis by E.M., that there remained a residual particulate structure, with particles of approximately the same size as those of the original latex. This they attributed to sufficient self-crosslinking (*i.e.*, acrylates have a labile tertiary hydrogen[48]) during the polymerisation process to allow the particles to simply swell (*i.e.*, gel) rather than truly dissolve. This hypothesis of crosslinking was tested by repeating the experiment using PBMA, which lacks the ability to self-crosslink: such films cast from tetrahydrofuran showed no sign of residual structure.

The rate of evaporation of solvent from solvent-cast films depends upon (time)$^{1/2}$ as expected for a process controlled, or limited, by diffusion, *i.e.*, Fickian desorption to the surface through a homogeneous solution of increasing concentration[51]. However, the removal of the final traces of solvent from solvent cast films is a problem: attributed to the fact that the polymer may be plasticised by the solvent. Elevated temperature (to assist diffusion of the solvent in the polymer), good vacuum and long drying times are used to overcome the problem, *e.g.*, 323 K at 3 Torr for 96 hrs[517]. The removal of the final traces of solvent can be important with regard to toxicity (in the case of pharmaceutical coatings) and also the permeability properties of solvent-cast coatings. List and Laun[324] found the water vapour permeability of isopropyl alcohol-cast Eudragit® *L* (see Chapter 6) films to be markedly increased by residual solvent. However, the effects of residual solvent were minimised by secondary drying, and the solvent could be almost completely removed in a very short time (8 hrs) if the film was held above its T_g.

4.2.2.3.1 Volatile organic components in aqueous latices.

It is common, for example in the paint industry, to add volatile organic components to latices (*e.g.*, as coalescing aids to lower the elastic modulus and provide temporary plasticisation to promote polymer chain motion and, hence, provide a better film finish). Sullivan [471] investigated the removal of such volatile organic compounds from latices, concluding that the ease of removal was dependent on their molecular size and polarity: the more polar a compound, the more likely it was to partition into the hydrophilic network of the evaporating water (and, hence, find less diffusive resistance), and less residual solvent would remain in the film. Sullivan found that the initial (steady-state) rate of evaporation of water was unaffected by the solvent but may ultimately be slowed if the additive is hygroscopic or interacts with the water, forming hydrogen bonds (*e.g.*, as do ethylene and propylene glycol): in which case the evaporation will not be diffusion-controlled, as is the usual case.

Hansen [216] also discusses the evaporation of various volatile organic components from aqueous latices. Comparing film formation by the evaporation from true solutions (*i.e.*, internal diffusion-controlled {characterised by a concentration gradient across the film thickness, with a concentration of zero at the film surface}) to the system in which the volatile is present as an additive, it was found that, in the latter case, no concentration gradient (of volatile) was apparent in the film implying that the evaporation of the volatiles was controlled at the film surface. As in the work of Sullivan [471], however, the evaporation rate of the aqueous phase was independent of the organic phase.

In the case of diffusion-controlled evaporation, the ratio of the weight of volatiles to polymer can be related to a dimensionless reduced time variable, *T*, given by:

$$T = \frac{Dt}{L^2} \tag{4.16}$$

where:

D = diffusion coefficient;
t = time;
L = film thickness.

Hence, in the case of diffusion-controlled (desorption-controlled) resistance:

$$\frac{W_{volatiles}}{W_{dry\ polymer}} \propto \frac{t}{L^2} \tag{4.17}$$

where:

W = weight of (subscripted) component.

Whereas for surface-controlled resistance:

$$\frac{W_{volatiles}}{W_{dry\ polymer}} \propto \frac{t}{L} \tag{4.18}$$

The effects on polymer chain interdiffusion of small amounts of organic solvents, added to PBMA latices, has been investigated by Juhué and Lang [262]. Results depended on the nature of the solvent's properties (*e.g.*, evaporation time, level of plasticisation) with respect to the polymer. Strong plasticisation was found not to be a desirable feature (to achieve high film strength by enhancing interdiffusion) if the solvent was not easily evaporated, and similarly neither was weak plasticisation and quick evaporation. Desirable properties to enhance film formation were therefore moderate evaporation rate and moderate plasticisation.

4.3 Film morphology.

Roulstone [423] observed that in the case of both solvent-cast and latex-cast films, drying occurred from the upper, open surface, downwards to the substrate. This appeared to result in the solvent-cast film having a higher density skin on the top surface in comparison to the substrate side. Similarly, a difference in appearance between the two surfaces was apparent for latex-cast films, with matt upper surfaces and glossy lower (substrate) faces. Replicas of the two surfaces subjected to the resolution of a T.E.M. showed slippage of the layers of latex particles in the upper surface, presumably arising from mud-cracking.

Monodisperse spherical latices are known to form ordered structures at 0.74 apparent volume fraction when extended diffuse double layers interact, which diffract light and produce opalescence. This behaviour was observed by Roulstone [423] as the model latex-cast films dried, producing 'islands' of iridescence, and may possibly contribute to the surface irregularities. Film asymmetry was also manifest in the permeability towards both water vapour and 4-nitrophenol – which varied according to the film orientation – for both solvent-cast and latex-cast films. When the face towards the donor (permeant containing) compartment was the upper surface, it gave the greater permeability to water vapour, whilst the lower face gave the greater rate of permeability to the 4-nitrophenol. This was explained in terms of desorption being the rate controlling process, and the difference between the permeants arising from their relative affinities for the film: 4-nitrophenol being much more soluble in the film. Opposite trends were found for solvent-cast films in which it was the upper surface that had the greater density, in contrast to the latex-cast films. Abdel-Aziz [1] reported a similar effect for solvent-cast Eudragit® films, although the density was found to vary dependent on the casting solvent used, and the films could be seen, under the S.E.M., to contain pores when cast from acetone containing 5% W/W ethanol [3]. Other researchers [547] have found the polarity of the casting substrate to influence the polarity of the lower surface of a film inducing an asymmetric effect.

Although it is generally assumed that latex particles exhibit sufficient colloidal stability to form a close packed-array of particles prior to coalescence, it has been reported by Okubo [366] *et al.* that, in the case of a surfactant-free latex, a porous, flocculated layer was apparent at the film interfaces. For a latex of only marginal stability, the film-air interface was observed to be porous. Addition of electrolyte to the latex, before casting, further destabilised the latex such that the film-substrate interface was also found to be porous. However, addition of surfactant to increase the latex stability led to a close packed, non-porous structure in agreement with the findings of Isaacs [251].

Both Vanderhoff *et al.* [62, 63] and Chainey [84, 90] *et al.*, but not Roulstone [423], noted changes in the surface of latex films upon aging. Vanderhoff found increased coalescence prior to surfactant exudation to the surface, whilst Chainey found that spray-cast surfaces which appeared rough under the S.E.M. smoothed to the appearance of a solvent-cast film upon aging for one month. Roulstone [424] *et al.*, using a freeze-fracture replication T.E.M. technique (in which the sample is frozen at the temperature of liquid nitrogen and fractured *in-situ*, so as to reduce any thermal effects of the fracture process) showed film structures in PBMA, of close packed spheres deformed into rhombic dodecahedra, with the clarity of the interparticle regions dependent on the temperature of preparation. Only at very high casting temperatures (*i.e.*, 405 K) was there no evidence of particulate structure, such that the film then resembled the appearance of the fracture section of a solvent-cast film. It was suggested, from visual observations and D.S.C. evidence, that PBMA underwent a melting or softening transition in the region of 393 K. Long exposure to temperatures lower than 393 K were not investigated (*e.g.*, 6 hrs at 368 K was the most extreme treatment where particle positions, if not the interparticle boundaries, could still be identified). Wood [545] remarks that whilst polymers are ductile at their T_g they require heating to 40 → 50 K above their T_g to produce a processable 'melt'.

Wang [527 - 529] *et al.* performed similar work to Roulstone [424] *et al.*, investigating the affect of annealing on surfactant-free PBMA films. Results showed a decrease in particle boundaries on annealing at temperatures lower than those investigated by Roulstone. Wang [528, 529] also investigated the degree of chain interdiffusion using fluorescent dyes and direct energy transfer measurements. From this it was concluded that there was extensive polymer interdiffusion: at 363 K for 2 hrs, an interpenetration depth of 6 nm (in particles of 337 nm Ø) was calculated, and this was shown in the fracture cross-sections as a change from fracturing along the interparticle boundaries (in the un-annealed film) to fracturing through the particles. A decrease in the rate of polymer diffusion with annealing time was attributed to polymer polydispersity: low molecular weight polymer dominating diffusion at early times [528] and high molecular weight after long annealing times. List and Kassis [323] attributed the fracture of particles (as opposed to particle boundaries) to the increased strength of the boundary resulting from the interaction of polar groups (situated predominantly on the particles' surfaces).

The existence of porosity in both solvent-cast and latex-cast films has been cited by a number of authors [27, 356]. The structure of a solvent cast film is dependent on the solvent used. Greater enmeshment and density may result from the use of a good solvent (see paragraph 4.2.2.3) compared with a theta[1] solvent. The compacted spherical molecules in the latter somewhat parallel the case of film formation from latices.

Roulstone [423, 424] *et al.* used mercury porosimetry and krypton B.E.T. surface area measurements on both solvent-cast and latex-cast films of PBMA. He attributed the

---

[1] At a given temperature, a polymer molecule (in a theta solvent) is in the theta state and the solution behaves thermodynamically ideal at low concentrations [142]. The theta temperature is defined as the critical miscibility temperature at the limit of the infinite molecular weight.[12]

apparent uptake of mercury at high pressures to the compressibility of both film types, rather than porosity, but, krypton B.E.T. surface areas were greatly in excess (by a factor of ≈ 37 times) of the geometric areas of the films used, and similar values resulted from the two types of film. The excess krypton adsorption could be attributed to microporosity at the low temperature (77 K) of the experiment. Mercury porosimetry, when performed on a harder polymer, did demonstrate the presence of porosity in core-shell (hard polymer core; soft shell) latex films designed to be porous, and also showed its removal when thermal treatment took the film above the T_g of the cores.

Okor [356] cited fracture cross-section S.E.M. evidence for mesoporosity in plasticised solvent-cast Eudragit® films. Roulstone [423, 424] *et al.*, however, using freeze-fracture T.E.M. on solvent-cast, and latex-cast, PBMA films found no evidence of mesoporosity. (I.U.P.A.C.[252] defines pore size according to: **micropores**, ⟨20 Å; **mesopores**, 20 → 500 Å; and **macropores**, ⟩500 Å {where 1 Å = 1×10^{-10} m}.) Nitrogen desorption analysis of the low levels of mesoporosity found to exist in such films is not practically feasible due to the low uptakes involved. Balik [27] *et al.* considered microporosity to be present in his terpolymer (vinyl chloride, butyl acrylate and vinyl acetate) latex films at 40 K above their T_g, but whether this excess carbon dioxide sorption would be better described in terms of free-volume in the rubbery polymer is a matter of semantics. Solvent cast films he considered to be structureless and to furnish a baseline performance for permeability.

4.3.1 Heterogeneous latex films.

In terms of film formation, structure and properties, copolymer films may normally be considered as being effectively homogeneous in nature (assuming that the polymer composition within individual particles is uniform). However, the same is not necessarily true for copolymer films formed from polymers prepared by a shot-growth type mechanism (or any other mechanism intended to give a core-shell type particle), or when one of the comonomers is more hydrophilic in nature such that it may end up forming a (full or partial) 'shell' around the core of the more hydrophobic comonomer. Kast [269] describes such particles as being heterogeneous or composite, and cites the aforementioned work of Distler and Kanig [121], which showed the vestiges of the carboxylated particle boundaries within a film, as being evidence of a heterogeneous network. In similar films of either an acrylic acid-free or acid-containing butylacrylate copolymer, differences in the storage modulus / T_g were cited as experimental confirmation of heterogeneity.

The process of film formation from a heterogeneous particle will be governed [269] by the polymer of lowest T_g, unless that polymer is of low volume fraction (⟨30 → 40%), or surrounded by a shell of high T_g polymer (in which case the polymer may contain voids or will require heating to the M.F.F.T. of the higher T_g polymer). The result is described, with experimental evidence from the polymer's viscoelastic properties, as a multidomain polymer with the high T_g polymer dispersed in a matrix of the lower T_g polymer, although this morphology may be inverted by heating above the T_g of the hard polymer.

Permeation, which may provide useful information on structure, through such heterogeneous latex films has not been widely studied, although the situation in which a solid is dispersed in a continuous polymer phase is not unusual, *e.g.*, pigmented or filled films. Core-shell latex particles in which the core is below its T_g (at the film casting temperature), whilst the shell is soft, may provide the basis for an ideal model filled film since the uniform distribution of the 'filler' core is promoted by its non-deformation and, hence, uniform packing in the latex films. As such, the theoretical treatments of Maxwell[31] (particle interactions neglected), Rayleigh[31] (cubic arrangement of identical spheres), and Higuchi[233] (spheres treated as points, but including particle interaction), for permeability should be applicable.

Peterson[394] has used blends of 28% (volume fraction) of latex polymers, (poly-(styrene), poly(methyl methacrylate), and poly(vinylidene chloride)), in a soft continuous phase of poly(vinyl acetate) latex, and found good agreement with the Higuchi theory for oxygen permeability. Chainey[84, 88] *et al.* studied the helium permeability of flash-cast films formed from hard core-soft shell polymers prepared by a shot growth technique. The latices consisted of particles composed of a poly(styrene) core-PBMA shell, of varying coating thickness. The films aged in the same manner as for free PBMA films, but the extent of the permeability reduction was less, and decreased with decreasing coating thickness. This was attributed to graft copolymer inhibiting further gradual coalescence. When the solvent-cast poly(styrene) permeability value was used for the core, and the aged value for the PBMA at low volume fraction of core, or the initial value at high volume fractions of core, then reasonable agreement with the Higuchi equation was obtained, although experimental results tended to be high. For a PBMA core-poly(ethyl acrylate) shell combination, aging was observed but could not be attributed to shell aging since poly(ethyl acrylate) homopolymer did not age. Unfortunately, for this combination of polymer, the core polymer aged to the same permeability coefficient as the shell polymer, and thus this similarity gave an insensitive test of the Higuchi treatment. Good agreement for core-shell, and copolymers was found but not for blends, and this was attributed to imperfect film structure arising from incompatibility of the components.

Roulstone[423] investigated film aging relative to shell thickness, for 4-nitrophenol permeation through dish-cast PBMA-poly(methyl acrylate) core-shell latex films, and found results conforming with Chainey. As in Chainey's study, there was some agreement with the Higuchi theory, but experimental results were higher than for aged films. Rather better agreement was found when water vapour was the permeant.

4.3.2 Film opacity.

It has been stated previously that non-film-forming latices dry to form an opaque, white, friable powder. Such opacity can be a desirable property of a coating, for example, a paint. Typically, an additive such as TiO_2 is used to achieve the opacity. The opacity results from light being scattered at an interface between substances of different refractive index (*e.g.*, the interface between air and polymer, or air and TiO_2) – dependent on the laws of reflection and refraction[41]. Such scattering and, hence, opacity can therefore also be achieved if a polymer film contains large numbers of voids (*i.e.*, due to the high number of polymer-air boundaries) such as in 'microvoid coatings.' The degree of opacity is dependent on (i) microvoid concentration, (ii) microvoid size and size distribution, and (iii) the aforementioned refractive index ratio. There exist a number of patents for the preparation of such coatings, and the methods have been reviewed by Seiner [445]. By utilising a method of optimising microvoid size using a model system developed by El-Aasser [140] *et al.*, Durbin [133] *et al.* was able to prepare a latex paint containing microvoids, in combination with a small film-forming latex, which used 50% less TiO_2 to yield comparable hiding power without loss of desirable physical properties (*e.g.*, scrub resistance).

An effect similar to that found for microvoid coatings can be achieved through the use of hollow spheres. Such spheres have a large polymer-air interface (requisite for light scattering) as a result of the internal chamber [231].

Film turbidity and light scattering/interference measurements, combined with a knowledge of spherical particle-packing structures in latex films has been used by Van Tent and te Nijenhuis [513, 514] to provide models which allow visible light transmission measurements to be used to characterise the geometrical packing of latex particles during the process of latex film formation.

4.4 Latex film additives.

Polymer latex films may contain a number of additives, ranging from stabilising surfactant (endogenous to the reaction, or post-added) to plasticisers (see Chapter 3) to aid film formation. This is in addition to additives added to enable the film to perform a function: *e.g.*, colourants in latex paints.

Typically, a plasticiser or coalescing aid may be added to ease the deformation of the latex particles (in the manner described in Chapter 3) so that a non-film-forming polymer can become film-forming at a given temperature. The plasticiser may then be required to soften the film or, more frequently, be fugitive to allow the film to harden. In such fugitive plasticisers which partition between the polymer and the aqueous phase, there is a compromise between the necessity of the plasticiser to remain in the latex for sufficient time for it to perform its function, but not to remain so long as to soften the film: a factor dependent on the plasticisers volatility. In addition to its usual role of plasticisation, several authors have added plasticiser to various types of polymer films in an attempt to control the permeability of the film [355], or to provide sustained release pharmaceutical devices as a means of control of the release rate [199,343]. Goodhart [199] *et al.* found that the addition of plasticiser (triethyl citrate or dibutyl sebacate) to Aquacoat® (pseudo-latex) coated drug cores (phenylpropanolamine HCl) changed the flux of the drug such that release rates were inversely proportional to the plasticiser concentration. Addition of plasticiser up to a concentration where it aided coalescence decreased the drug release rate, whilst above a certain level (not stated, but between 24% and 40% W/W) of addition, the solute permeability increased due to the increased solute diffusivity caused by the plasticiser's water solubility. Above the higher loading (40% W/W), an increase in film casting temperature did not effect the rate of drug release, whilst at a loading of 24%, an increase in casting temperature led to reduced release rates.

Hoy [246] provided experimental evidence which accredited the efficiency of various coalescing aids (including a number of acetates and ethoxy alcohols, as used in latex paints) to their degree of partition between the aqueous and polymer phases, and their T_g.

(The ability of the plasticiser to undergo hydrogen bonding had a great effect on the results due to the tendency for the plasticiser to remain in the aqueous phase.) Casting (*i.e.*, painting) on porous substrates was found to aid the removal of plasticiser that partitioned favourably into the aqueous phase, decreasing its efficiency. Additionally, Hoy gave theoretical equations for predicting the action of a coalescing aid on the film's M.F.F.T.

Roulstone [423, 425] *et al.* studied the water vapour permeability of films cast from PBMA surfactant-free latices in the presence of post-polymerisation additives that included surfactants, polymers and inorganic electrolytes. The surfactants had a common C_{12} backbone, but either anionic (sodium dodecyl sulphate, or S.D.S.), cationic (Dodecylethyl-dimethyl-ammonium bromide, or D.E.D.A.B.), or non-ionic (dodecyl tetra-oxyethylene glycol monoether, or $C_{12}E_4$) polar head groups. A minimum in film permeability was found at monolayer coverage of S.D.S., and this was interpreted as a consequence of improved particle packing order due to enhanced charge stabilisation or, more tentatively, as due to surface plasticisation by S.D.S., since somewhat greater coalescence was apparent in freeze-fracture T.E.M. replicas of such films. Below monolayer coverage, permeability decreased with increased S.D.S. concentration, and tended to lower values on film aging. Durbin [132], however, argued that at this level of addition S.D.S. decreased the particle packing order since the increased ionic strength outweighed the effects of increased charge density. At higher S.D.S. concentrations film permeabilities increased, and 'islands' of S.D.S. were visible in micrographs as aggregate defects, with smaller aggregates in the particle interstices. Particle boundaries could be observed and the films did not age to give lower permeabilities.

For the cationic surfactant, at concentrations sufficient to give charge reversal and to maintain stability, a minima in permeability was observed at approximately monolayer coverage. However, permeabilities were higher than for the S.D.S. additions, and higher than for the surfactant-free films. This increased permeability was attributed to the D.E.D.A.B. first forming a salt with the anionic surface groups in the interparticle regions, and then adsorbing tail first onto the surface – with multi-layers forming at higher concentrations. These films, like those with the higher concentration of S.D.S., also did not age to lower permeabilities.

Significantly different behaviour was observed for $C_{12}E_4$, which plasticised the films making them more flexible, but not tacky, and giving increased coalescence. Slightly reduced permeability at surface coverage, but then raised permeabilities at higher concentrations were also observed. Being well coalesced, the films did not age to lower permeabilities. Vanderhoff [500] found compatibility between non-ionic surfactants of this type, and the polymer, with no surface exudations. However, when the ethylene oxide chain length was increased, incompatibility with the polymer did lead to surface exudations. Padget and Moreland [375], using a non-ionic block copolymer surfactant, found increased coalescence at surface coverage, with surface exudation at higher levels of addition.

Atomic Force microscopy was used by Juhué and Lang [261] to measure the peak to valley distances in PBMA films as a function of their concentration of (post-polymerisation added) surfactant (C_9H_{19}–C_6H_6–O–$(CH_2CH_2$–$O)_{25}$–SO_3^- Na^+ or sodium nonylphenolpolyglycolether-sulphate). Surface coverage was again significant, providing a minimum in the peak to valley distance: attributed to a favourable delay in flocculation, due to enhanced particle stability and, hence, the greatest degree of particle close-packing at the film surface. (Below surface coverage by surfactant, particle-particle repulsions are weak and flocculation occurs early during film formation, whilst at high surfactant concentrations, electrostatic repulsions are screened by the large concentration of sodium ions in the latex dispersion – again leading to early flocculation.) Additionally, it was found [263] by using a similar, but non-ionic, surfactant (*i.e.*, the $SO_3^- Na^+$ being replaced by OH) that depletion effects, as well as steric stabilisation (and, in the case of the ionic surfactant, electrostatic repulsion) contributed to the optimal packing of particles during film formation. (Polymer depletion regions {see Juhué [263] for references} occur for colloids in the presence of non-adsorbing polymers. When two particles approach within a distance of less than twice the polymer radius of gyration, exclusion of the polymer from the space between the particles leads to development of an osmotic pressure which flocculates the particles.) The development of micelles at high surfactant concentrations, above surface coverage, contributes to the formation of poor quality films due to depletion flocculation.

Zhao [560, 561, 562] *et al.* used surface analytical techniques including X-ray Photo-electron Spectroscopy (X.P.S.), S.I.M.S., and Fourier Transform Infra-Red-Attenuated Total-internal Reflection (F.T.I.R.-A.T.R.) spectroscopy to show that material that was incompatible with the polymer was exuded to the film surface. They revealed, by F.T.I.R.-A.T.R. spectroscopy, that S.D.S. was exuded from methyl methacrylate-butyl acrylate latex films mostly during drying, but also during further gradual coalescence, to give a concentration gradient which increased towards both interfaces with a higher concentration at the film-air interface than at the film-substrate interface. The same trends were observed, but to a reduced degree, for a more compatible surfactant. Urban and Evanson [489] found surfactant exudation during film formation to be initially dependent on the water flux, but ultimately on the difference in surface tension between the polymer and substrate. It was found that mechanical stretching of the film (as may be encountered during removal from a substrate) affected the distribution of surfactant throughout the film: as the surface area is increased (by stretching), the surface concentration of surfactant is decreased and the resultant increase in surface tension is henceforth reduced by the diffusion of surfactant to the interface. Analogous to the ability of a liquid to wet a solid of higher surface energy; casting the film on a substrate of lower surface tension (*e.g.*, P.T.F.E. {= 18.5 mN m^{-1}}) than the polymer (surface tension typically 25 → 60 mN m^{-1}), prevents the film from wetting the substrate and, hence, surfactant diffuses to the polymer-substrate interface to lower the surface tension.

Roulstone [423, 425] *et al.* used two samples of poly(vinyl pyrrolidone) (P.V.P.) of molecular weights 44,000 and 360,000 at 0.16 g g^{-1} (*cf.*, monolayer coverage 0.1 g g^{-1} and 0.15 g g^{-1} for the two molecular weights, respectively [274]). The P.V.P. was deposited between the particles, which showed good packing but very limited evidence for coalescence and deformation. Limited aging to a lower permeability was observed. List and Kassis [323] suggested that high molecular weight stabilisers immobilised particles in films and inhibited aging. Bondy and Coleman [59] also noted retarded coalescence on film formation

Table 4.1 Possible fates of emulsifier added to polymer films.

FATE OF EMULSIFIER	POLYMER COMPATIBILITY
Migrates and **dissolves** in the polymer.	Compatible
Exudes towards the film surface.	Incompatible
Forms independent **Islets**, possibly corresponding to interstitial voids between particles.	Incompatible
Forms a continuous **network** embedding globules.	Incompatible
Adsorbs at the particle surface.	Incompatible

in the presence of stabilisers. For post added KCl, at below the C.C.C. of PBMA latex, Roulstone found a reduced packing order coupled with an increased permeability, with most of the inorganic material being exuded from the interstices to the surface layers: a tendency that increased on aging.

Pochan[396] found, by measuring the dielectric properties of a PBMA latex film containing a water soluble polymer additive (a carboxylated styrenic terpolymer {25% by weight}), that when cast at ambient temperature, the additive was present in the interparticle interstices forming a continuous network. This morphology was, however, said not to be the equilibrium state, and thermal annealing of the film led to the additive forming isolated domains within the film if the annealing temperature was above the T_g of the additive.

Bindschaedler[49] *et al.* note a broad diversity of works, and conclusions, concerning film additives in the literature with five possible fates for the emulsifier, as shown in **Table 4.1**.

4.4.1 Additives in latex paints: the critical pigment volume concentration.

The **pigment volume concentration** (P.V.C.) (or 'heterogeneous {discontinuous} phase volume concentration' of a 'random composite'[46] embedded in a polymer matrix!) is a measure used in the paint industry to describe the *volumetric* percentage of hiding pigment present (+ extenders), V_P, in the total volume of non-volatile vehicle solids content (polymer matrix), V_B, of a paint:

$$P.V.C. = \frac{V_P}{V_P + V_B} \tag{4.19}$$

In 1949, Asbeck and Van Loo[21] posted an explanation as to why the properties of a coating underwent a dramatic change within a narrow band of the P.V.C. The properties (*e.g.*, gloss, permeability, rust prevention) of a series of oil-based coatings of increasing values of P.V.C., but ground to the same degree of dispersion, showed a sudden break (*e.g.*, the permeability increased sharply; the glossiness {but also blistering} decreased markedly; and the degree of rusting increased markedly) at a value he termed the **critical pigment volume concentration** (C.P.V.C.). Asbeck showed that the C.P.V.C. was dependent not only on the type of pigment, and its degree of dispersion, but also on its physical relationship with the other components of the paint and, hence, the agglomeration[1] of the system: the higher the degree of agglomeration, the lower the C.P.V.C., and noting the fact that systems with high C.P.V.C.s have a smoother texture. From work using different (oil-based) binders, it was reasoned that the degree of colloidal stability imparted to the particles resulted in changes to the packing density, and that this too could influence the C.P.V.C. (in addition to the packing properties resulting from the shape of the particles themselves). Further work allowed the C.P.V.C. to be defined as: 'the point in a pigment-vehicle system at which there is *just* sufficient binder to completely fill the interstices between randomly packed pigment particles after the volatilisation of the thinner, such that it represents the densest degree of packing of the pigment particles commensurate with the degree of dispersion of the system' [22]. The change in properties of the paint at the C.P.V.C. was ascribed to the formation of air voids due to insufficient binder to fill the interstices between the most densely packed particles. Thus, below the C.P.V.C., the pigment packing fraction (Φ_p) is equal to the P.V.C. (see equation (4.19)), whilst above the C.P.V.C., if the total volume of air in the coating is given by V_A, then Φ_p is given by [409]:

$$\Phi_p = \frac{V_P}{V_P + V_B + V_A} \tag{4.20}$$

Various experimental methods of C.P.V.C. determination are mentioned by Anwari [13] *et al.* However, the determination of an accurate method for the calculation of the C.P.V.C. (without preparing a formulation and investigating its properties) has proved elusive. Bierwagon [45] describes a mathematical model based on the ideal random packing of spheres, their size distribution, and adsorbed layer thickness, etc.: the results, however, were described (by Bierwagon) as "good" for alkyd type paints, when compared to experimental results, but only as "fair" in the case of latex paints which was presumed to result from pigment-polymer interactions. Rasenberg and Huisman [409] describe a method which utilises porosity measurements (determined by mercury porosimetry) and the fact that Φ_p remains constant, above the C.P.V.C. (because it represents the highest possible pigment packing density) to determine the value of the C.P.V.C. from a knowledge of the pigment weight fraction (and the values of the densities of pigment and binder). However, this also requires a film be prepared, rather than being a theoretical method.

Citing a previous paper on the use of a polystyrene latex as a filler, Floyd and Holsworth [165] discussed a number of anomalies which may affect the C.P.V.C. The fact that various properties of the film appeared to show differing values for the C.P.V.C., was attributed to the fact that the polystyrene particles were shown to sinter at points of contact (despite it being non-film forming) and, hence, provide the film with some mechanical integrity at values of the P.V.C. above the typical C.P.V.C. Floyd also discussed certain factors that may change the concept of the C.P.V.C.: *e.g.*, **clustering** (*i.e.*, the association of the dispersed phase {pigment particles} as the concentration increases {even at low

---

[1] Defined by Asbeck as in the National Paint Directory (presumably of 1949)) as, "a group of two or more individual pigment particles that are held together so firmly by the force of adhesion that they tend to remain as an intact unit".

volume fractions, *e.g.*, ⟨ 10%} leading to the formation of doublets, triplets, multiplets, etc.: a random process and not the same as flocculation due to colloidal instability) and **percolation** (which commences when the cluster size is sufficient to span the film). Floyd speculated that it was this latter feature which gave rise to the change in the film's permeability properties due to the formation of pathways, and also led to the decrease in film gloss by the introduction of light scattering. At high pigment concentrations, a phase inversion can occur as the primary phase changes from being one that is polymer rich to one that is pigment rich. (This can have important connotations with regard to, for example, the electrolytic properties of a film, *e.g.*, zinc-rich paints for corrosion protection [46], or any type of film requiring a continuous network of additive.)

Although the results of Asbeck's work have been shown to be equally applicable to latex paints, the C.P.V.C. is offset to a lower value by a fixed fractional amount which is termed the binder index[165] of a given latex. Floyd and Holsworth [165] note that air voids are present in *all* latex paints, for *all* values of P.V.C. (and that their concentration increases as the C.P.V.C. is approached) due to the fact that particle deformation is hindered by the pigment. The voids are likened to a second dispersed phase, and can undergo clustering and percolation as their concentration increases with increasing P.V.C. Because the pigment is typically impermeable, it is percolating voids that give the increased permeant flux. The C.P.V.C. of latex paints is thus attributed to a phase inversion from a bi-continuous (polymer-air) system in which the polymer is the primary phase to one in which the primary phase is air.

Typically, a dispersing or wetting agent (surfactant) is added to a paint to prevent agglomeration of the pigment. For a latex (paint), it is not only important that the pigment itself does not destabilise the latex, but also that the pigment does not remove surfactant for its own stabilisation in detriment to the latex. In ensuring this, the C.P.V.C. of a latex paint is usually equal to the ultimate pigment volume concentration (U.C.P.V.C.) [22], *i.e.*, the C.P.V.C. where all the pigment particles are completely separated and act independently, whilst the polymer matrix acts as a continuous fluid [46]. Factors that affect the ability of the pigment particles to act independently (such as clustering and flocculation, etc.) all serve to decrease the C.P.V.C., when compared to a more stable system.

◆

Introduction, Chapter 5: Diffusion and Permeation in Polymer Films.

5.1 Introduction.

The transport properties of a polymer film may be important for a number of reasons. In the packaging industry, the film's barrier properties are of importance, whilst the pharmaceutical industry is interested in the release properties of polymer coatings for active agents (see Chapter 6). Academically, the transport properties are of use as a probe of film structure, and this was referred to in the previous Chapter. The current Chapter aims to discuss the theories of film transport and permeability properties, and their measurement.

There are numerous reviews [85, 99, 103, 104, 115, 167, 463] of the transport properties of polymer films, and the main points are included in this Chapter. The usage of membranes, with respect to their transport properties has been reviewed by Lonsdale [325], and the permeation of ions (and ionic membrane transport) has been reviewed by Lakshminarayanaiah [302], for example.

5.2 Principles of diffusion and permeation.

5.2.1 Fundamental theory of diffusion and permeation.

Transport through polymer membranes may be described in terms of either the generalised Stefan-Maxwell equations, or by the theories of irreversible thermodynamics which analyse the gradients that exist across the membrane, and their resultant fluxes. Generally, however, simplifications of the Stefan-Maxwell equations give adequate descriptions of transport systems [390]: hence, only Fickian diffusion systems will be discussed in this Chapter.

Permeation through non-porous polymer membranes is explained in terms of **solution** of the permeant in the polymer, and **diffusion**.

5.2.1.1 Diffusion.

Diffusion is the mechanism by which components of a mixture are transported around the mixture by means of random molecular (Brownian) motion. Flynn [167] *et al.* cites Berthalot [42] as postulating, at the beginning of the nineteenth century, that the flow of mass by diffusion (*i.e.*, the flux), across a plane, was proportional to the concentration gradient of the diffusant across that plane.

In the mid-1800s, Fick [155, 156] introduced two differential equations that quantified the above statement for the case of transport through thin membranes. **Fick's first law** states that the flux, J, of a component across a membrane of unit area, in a predefined plane, is proportional the concentration differential across that plane, and is expressed by:

$$J = -D\nabla C \tag{5.1}$$

where:

D = **diffusion coefficient**;
C = permeant concentration;
∇ = differential vector operator ('del'), as given by:

$$\nabla = \hat{\imath}\frac{\partial}{\partial x} + \hat{\jmath}\frac{\partial}{\partial y} + \hat{k}\frac{\partial}{\partial z} \tag{5.2}$$

such that, $\nabla C_{(x,\,y,\,z)}$ (gradient C or grad C) is given by:

$$\nabla C = \hat{\imath}\frac{\partial C}{\partial x} + \hat{\jmath}\frac{\partial C}{\partial y} + \hat{k}\frac{\partial C}{\partial z} \tag{5.3}$$

whilst **Fick's second law** states that the rate of change of concentration in a volume element of a membrane, within the diffusional field, is proportional to the rate of change of concentration gradient at that point in the field, and is given as:

$$\nabla.(D\nabla C) = \frac{\partial C}{\partial t} \tag{5.4}$$

where:

t = time;
D = concentration independent diffusion coefficient;
$\nabla.(D\ \nabla C)$ = div (D grad C).

Considering only a single dimension, if the diffusion coefficient, D, is independent of position, x, then Fick's second law may be derived from Fick's first law by considering two parallel planes that are perpendicular to the diffusive flow, at the positions x and $x + \Delta x$[167]. The rate of entry of diffusive mass (M) per unit area into the volume element between x and $x + \Delta x$ is given by:

$$\frac{\partial M}{\partial t} = -D\frac{\partial}{\partial x}\left[C - \frac{\Delta x}{2}\frac{\partial C}{\partial x}\right] \tag{5.5}$$

where C = concentration in the plane mid-way between, and parallel to those at x and $x + \Delta x$.

Similarly, the rate of exit of diffusant is given by:

$$\frac{\partial M'}{\partial t} = -D\frac{\partial}{\partial x}\left[C + \frac{\Delta x}{2}\frac{\partial C}{\partial x}\right] \tag{5.6}$$

The rate of change of diffusant mass is therefore given by:

$$\begin{aligned} \frac{\partial M}{\partial t} - \frac{\partial M'}{\partial t} &= -D\frac{\partial}{\partial x}\left[C - \frac{\Delta x}{2}\frac{\partial C}{\partial x}\right] + D\frac{\partial}{\partial x}\left[C + \frac{\Delta x}{2}\frac{\partial C}{\partial x}\right] \\ &= -D\frac{\partial C}{\partial x} + D\frac{\Delta x}{2}\frac{\partial^2 C}{\partial x^2} + D\frac{\partial C}{\partial x} + D\frac{\Delta x}{2}\frac{\partial^2 C}{\partial x^2} \\ &= D\Delta x\frac{\partial^2 C}{\partial x^2} \end{aligned} \tag{5.7}$$

Equation 5.7 is equivalent to the rate of change of concentration multiplied by the volume of the element. (NB. If the element is of unit area, then the volume = Δx). Hence:

$$\frac{\left[\frac{\partial M}{\partial t} - \frac{\partial M'}{\partial t}\right]}{\Delta x} = \frac{\partial C}{\partial t} = D\,\frac{\partial^2 C}{\partial x^2} \tag{5.8}$$

The application of Fick's laws has been the subject of a number of works [32, 103]. Note that the constant of proportionality, the diffusion coefficient, has dimensions of distance squared divided by time (*e.g.*, cm^2 s^{-1}). Hence, for a membrane of unit thickness, the diffusion coefficient can be considered as a rate of permeant transport.

Fick's second law may be expanded and re-arranged:

$$\left(\hat{\imath}\,\frac{\partial}{\partial x} + \hat{\jmath}\,\frac{\partial}{\partial y} + \hat{k}\,\frac{\partial}{\partial z}\right) D \left(\hat{\imath}\,\frac{\partial C}{\partial x} + \hat{\jmath}\,\frac{\partial C}{\partial y} + \hat{k}\,\frac{\partial C}{\partial z}\right) = \frac{\partial C}{\partial t} \tag{5.9}$$

But:

$$\hat{\imath}.\hat{\jmath} = \hat{\imath}.\hat{k} = \hat{\jmath}.\hat{k} = 0$$

and therefore:

$$\hat{\imath}\,\frac{\partial}{\partial x}\left(D\hat{\imath}\,\frac{\partial C}{\partial x}\right) + \hat{\jmath}\,\frac{\partial}{\partial y}\left(D\hat{\jmath}\,\frac{\partial C}{\partial y}\right) + \hat{k}\,\frac{\partial}{\partial z}\left(D\hat{k}\,\frac{\partial C}{\partial z}\right) = \frac{\partial C}{\partial t} \tag{5.11}$$

Also:

$$\hat{\imath}.\hat{\imath} = \hat{\jmath}.\hat{\jmath} = \hat{k}.\hat{k} = 1$$

and, hence:

$$\frac{\partial}{\partial x}\left(D\,\frac{\partial C}{\partial x}\right) + \frac{\partial}{\partial y}\left(D\,\frac{\partial C}{\partial y}\right) + \frac{\partial}{\partial z}\left(D\,\frac{\partial C}{\partial z}\right) = \frac{\partial C}{\partial t} \tag{5.13}$$

$$\left(D\,\frac{\partial^2 C}{\partial x^2} + \frac{\partial D}{\partial x}\,\frac{\partial C}{\partial x}\right) + \left(D\,\frac{\partial^2 C}{\partial y^2} + \frac{\partial D}{\partial y}\,\frac{\partial C}{\partial y}\right) + \left(D\,\frac{\partial^2 C}{\partial z^2} + \frac{\partial D}{\partial z}\,\frac{\partial C}{\partial z}\right) = \frac{\partial C}{\partial t} \tag{5.14}$$

But:

$$\frac{\partial D}{\partial x} = \frac{\partial D}{\partial C} \bullet \frac{\partial C}{\partial x} \tag{5.15}$$

and therefore:

$$\left(D\,\frac{\partial^2 C}{\partial x^2} + \frac{\partial D}{\partial C}\,\frac{\partial C}{\partial x} \bullet \frac{\partial C}{\partial x}\right) + \left(D\,\frac{\partial^2 C}{\partial y^2} + \frac{\partial D}{\partial C}\,\frac{\partial C}{\partial y} \bullet \frac{\partial C}{\partial y}\right) + \left(D\,\frac{\partial^2 C}{\partial z^2} + \frac{\partial D}{\partial C}\,\frac{\partial C}{\partial z} \bullet \frac{\partial C}{\partial z}\right) = \frac{\partial C}{\partial t} \tag{5.16}$$

i.e.:

$$D\nabla^2 C + \frac{\partial D}{\partial C}(\nabla C.\nabla C) = \frac{\partial C}{\partial t} \tag{5.17}$$

$$D\nabla^2 C + \frac{\partial D}{\partial C}\nabla^2 C = \frac{\partial C}{\partial t} \tag{5.18}$$

In the ideal case, and for simple gases, the diffusion coefficient, D, is independent of concentration, C, film thickness, x, and time, t. (In the non-ideal case, the thermodynamics of irreversible processes show D to be a function of concentration, position, and time.) However, plasticisation of the polymer by the diffusant can lead to concentration dependence. Thus if $D(C)$ is the concentration dependent diffusion coefficient, and the concentration difference across the film is sufficiently small such that $\delta D(C)/\delta t$ is small when compared to $D(C)$, then:

$$D(C)\nabla^2 C = \frac{\partial C}{\partial t} \tag{5.19}$$

where:

$$D(C)\nabla^2 C = D\left[\frac{\partial}{\partial x}\left(\frac{\partial C}{\partial x}\right) + \frac{\partial}{\partial y}\left(\frac{\partial C}{\partial y}\right) + \frac{\partial}{\partial z}\left(\frac{\partial C}{\partial z}\right)\right] \tag{5.20}$$

$$D(C)\nabla^2 C = D\left[\frac{\partial^2 C}{\partial x^2} + \frac{\partial^2 C}{\partial y^2} + \frac{\partial^2 C}{\partial z^2}\right] \tag{5.21}$$

In typical applications of diffusion theory, the membrane/film through which the diffusant is travelling is assumed to be so thin that diffusion occurs only in the direction of film thickness and, hence, the above equation is reduced to:

$$D(C)\frac{\partial^2 C}{\partial x^2} = \frac{\partial C}{\partial t} \tag{5.22}$$

or alternatively[1]:

$$D\frac{\partial^2 C}{\partial x^2} = \frac{\partial C}{\partial t} \tag{5.23}$$

This is the form in which Fick's second law is typically expressed in permeation experiments (*i.e.*, the dependence of D on C, will not usually be known). In situations where Fick's laws are not obeyed (*e.g.*, due to concentration, or position dependence, as a result of permeant-polymer interactions), the diffusion process is described as anomalous [e.g., 7, 485].

Fick derived the laws of diffusion by analogy of permeant diffusion to the equations of heat flow in solids. For example, equation (5.4) is analogous to:

$$\gamma\rho\frac{\partial \theta}{\partial t} = \nabla.(K\nabla\theta) \tag{5.24}$$

where:

γ = specific heat;
ρ = density of medium;
θ = temperature at time t;
K = conductivity of medium.

---

[1] NB. Failure to account for concentration dependence is said to lead to an experimental error of, typically, not greater than a factor of three [307].

The diffusion coefficient, D, may be expressed in Arrhenius form by:

$$D = D_0 \exp - \left[\frac{E_D}{RT} \right] \tag{5.25}$$

where:

E_D = activation energy of diffusion;
R = gas constant;
T = temperature;
D_0 = diffusion coefficient as concentration of diffusant $C \rightarrow 0$.

The **diffusion activation energy** is dependent upon permeant size and level of plasticisation of the polymer (plasticiser can enhance or reduce permeability dependent up on its concentration[385]). For large molecules, E_D can be up to 160 kJ mol^{-1}, *i.e.*, the same order as the activation energy for viscous flow of polymers.

In glassy polymers, D_0 is very dependent on molecular size (Van der Waals' volume). D_0 increases with decreasing T_g. The mechanism for diffusion is the same above or below the T_g, differing only in the frequency of the motion of the polymer segments.

5.2.1.1.1 Experimental determination of diffusion and permeability coefficients.

In determining a diffusion or permeability coefficient, it is necessary to solve Fick's law for the boundary conditions appropriate to the penetrant/membrane system. With respect to the work in this thesis, derivations of permeability coefficients suitable for use with measurements of steady-state permeant transport are given in Appendix A. Such derivations are usually performed considering just the one dimension, *e.g.*, assuming penetrant transport (typically, a gas) in just the x-direction, normal to the plane of the film.

Assuming **steady-state** conditions of diffusion across a membrane element of thickness denoted by x, in which the surfaces of the element are at the points $x = 0$ and $x = x$, respectively, and the concentration at points $x = 0$ and x are maintained at C_1 and C_2, respectively (and diffusion is independent of concentration: the amount of diffusant lost to the membrane is negligible, whilst the membrane instantaneously adjusts to changes in the external conditions), then from the integration of Fick's first law:

$$J \int_{x=0}^{x=x} dx = -D \int_{C=C_1}^{C=C_2} dC \tag{5.26}$$

$$Jx = -D(C_2 - C_1) = D(C_1 - C_2) \tag{5.27}$$

and, hence:

$$J = \frac{D(C_1 - C_2)}{x} \tag{5.28}$$

where:

C_1 - C_2 = concentration gradient between the faces of the film element, *within* the film.

Also:

$$J = \frac{P(C_1' - C_2')}{l} \tag{5.29}$$

where:

P = **permeability coefficient**; &

$C_1' - C_2'$ = concentration gradient *across* the film, in the external phase;

l = total film thickness.

This expression is of greater practical use for not requiring a measurement of the permeant surface concentration. Note that for a gas, the concentration (C) terms may be replaced by pressure (or partial pressure), p, terms since the concentration will be determined by the pressure of gas at the film surface. Equation (5.29) thus becomes:

$$J = \frac{P(p_1 - p_2)}{l} \tag{5.30}$$

This equation results from **Henry's law** being obeyed [417], *i.e.*, the relationship between the permeant concentration in the external phase and the corresponding surface-element concentration is proportional:

$$C = Sp \quad \text{(or, for solutes} \quad C = SC'\text{)} \tag{5.31}$$

where:

S = **solubility coefficient** (*i.e.*, the concentration of permeant in the membrane, divided by the permeant concentration in the phase which is in equilibrium with the membrane [307]).

Hence, from Henry's law and the equations for flux (J), (*e.g.*, equations (5.28) and (5.29)) it is also seen that the permeability, solubility and diffusion coefficients can be related by:

$$P = DS \tag{5.32}$$

Before the steady state diffusive flux is achieved, there is a transient period (see **Figure 5.1**) whilst the permeant partition equilibrium is built-up. This transient region of permeant transport is described by Fick's second law. There is no general solution to this law. However, Daynes [110] provided a solution for Fick's second law, later refined by Barrer [34], for the situation in which the boundary conditions are typical of many experimental situations. It is assumed that:

- ✗ $C = C_1$ at $x = 0$ for all values of time, $t \rangle 0$ (*i.e.*, initial donor concentration is constant throughout);
- ✗ $C = 0$ at $x = l$ for all values of t (*i.e.*, the receiver concentration is always forced to zero);
- ✗ $C = 0$ at $0 \langle x \leq l$ when $t = 0$.

The concentration through any plane in the x-direction, perpendicular to the direction of the flux, assuming a concentration-independent diffusion coefficient is given by[167]:

$$C = C_1 \frac{x}{l} + \frac{2}{\pi} \sum_{n=1}^{\infty} \frac{C_1}{n} \cos(n\pi) \sin\left(\frac{n\pi x}{l}\right) \exp\left[\frac{-n^2\pi^2 Dt}{l^2}\right] \tag{5.33}$$

Evaluation of the cumulative mass of diffusant per unit area (M) transported through the film may be accomplished by[167, 420] (i) finding the derivative as a function of x; calculating the flux (dM/dt), and (ii) integrating the flux between $0 \le t \le t$:

$$M = \frac{DC_1 t}{l} - \frac{lC_1}{6} - \frac{2lC_1}{\pi^2} \sum_{n=1}^{\infty} \frac{(-1)^n}{n^2} \exp\left[\frac{-n^2\pi^2 Dt}{l^2}\right] \tag{5.34}$$

At high values of t (over the steady state region of the curve {see **Figure 5.1**}), the exponential part of the equation tends to zero, such that:

$$M = \frac{DC_1 t}{l} - \frac{C_1 l}{6} = \frac{DC_1}{l}\left(t - \frac{l^2}{6D}\right) \tag{5.35}$$

This is thus the equation of a straight line ($M \propto t$). If the line is extrapolated to $M = 0$, then the intercept on the time axis is the **lag time**, τ. The lag time is related to the diffusion coefficient by equation (5.36):

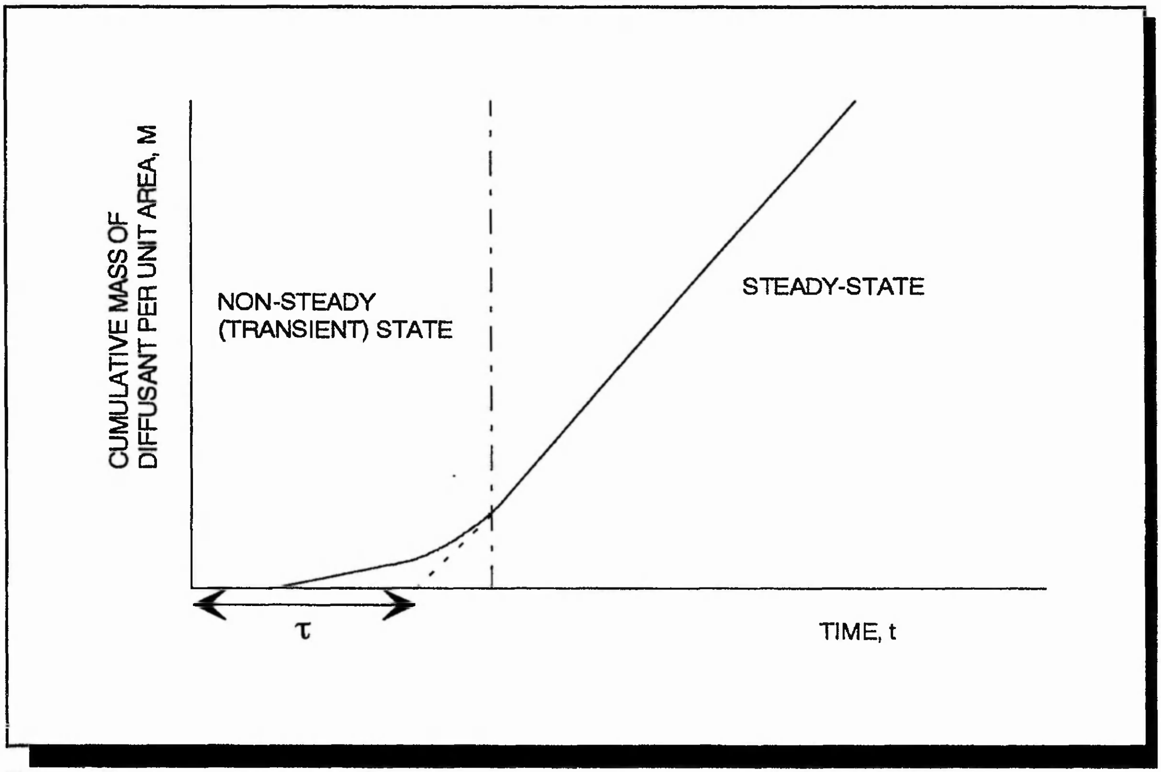

Figure 5.1 Schematic plot of permeant transported through a thin membrane, showing the time lag.

$$\tau = \frac{l^2}{6D} \tag{5.36}$$

The diffusion coefficient, D, can therefore be determined from a permeability experiment without knowledge of the solubility coefficient. The method is best applied to rubbery polymers, being unreliable for glassy polymers, or when the permeant is in solution or is water vapour.

An alternative method is described by Ziegel[563, 564] *et al.*, used in a dynamic system in which gas was permeated through the membrane into a second carrier gas, to a detector. A plot of the flux of permeant gas (*i.e.*, dM_t/dt) versus time, t, (as shown in **Figure 5.2**) was then used: the diffusion coefficient being defined at the half-time ($t_{½}$) to the point at which the steady state flux is achieved by:

$$D = \frac{l^2}{7.199t_{½}} \tag{5.37}$$

However, this obviously requires an accurate knowledge of the time at which the experiment starts.

In the situation where the diffusion coefficient is not independent of concentration (*e.g.*, when the permeant is an organic vapour/solute that swells the membrane, etc.),

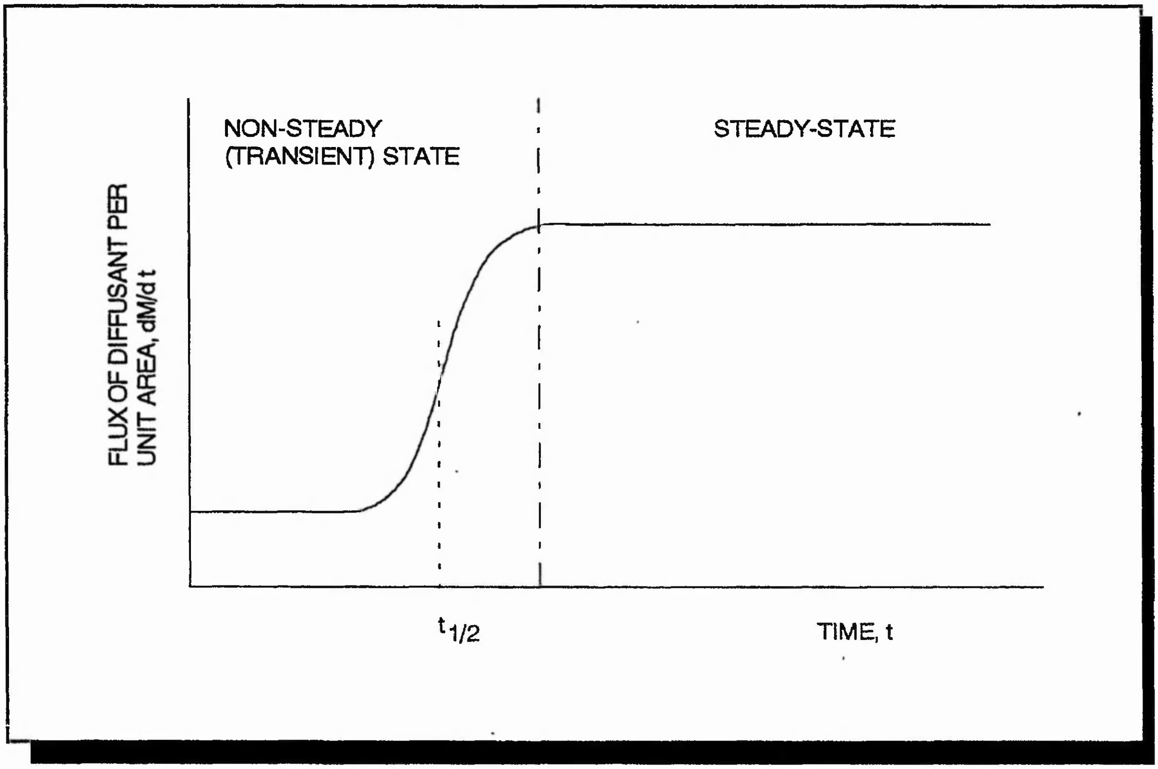

Figure 5.2 Schematic plot of flux, as from Ziegel's gas flow method for the determination of gas diffusion coefficients.

measurement of permeant transport leads to a mean diffusion coefficient, $\overline{D}$, dependent on the magnitude of the effective concentration change:

$$\overline{D} = \frac{1}{C_{eq}} \int_0^{C_{eq}} D(C)\, dc \qquad (5.38)$$

where:

C_{eq} = equilibrium permeant concentration;
$D(C)$ = concentration dependent diffusion coefficient.

In the case of polymers below their T_g, the motion of the polymer chains is slow compared to the movement of the permeant molecules. Thus in addition to concentration dependence, the diffusion coefficient will also be time dependent due to the relationship between polymer chain motion and permeant motion [175].

5.2.1.2 Sorption.

Sorption includes adsorption, absorption, trapping in microvoids and cluster formation, and characterises the initial infiltration of the permeant into the polymer. The nature and magnitude of the sorption is dependent upon the thermodynamics of the permeant-polymer interactions; the distribution of the modes (see following paragraphs) by which the sorption can take place depend upon concentration, temperature, swelling, permeant size and time.

Permeant gases in rubbery polymers have solubilities of less than 0.2% and behave as ideally dilute solutions, showing a linear relationship between sorbed concentration and pressure, and obeying **Henry's Law**, previously defined in the form of an equation by:

$$C = Sp \qquad (5.39)$$

where:

C = sorbed concentration;
p = pressure;
S = **solubility coefficient**.

Specific adsorption of penetrant on sites or into fixed voids in glassy polymers follows the **Langmuir adsorption isotherm**:

$$C_H = \frac{C'_H bp}{1 + bp} \qquad (5.40)$$

where:

C_H = concentration of permeant sorbed by sites or voids;
C'_H = site saturation constant; &
b = site affinity constant: from ratio of rate constants for adsorption and desorption.

Gases in glassy polymers, especially carbon dioxide and $C_1 \rightarrow C_5$ hydrocarbons, and vapours in rubbery polymers with adsorptive fillers show a deviation from Henry's law. The adsorption isotherm can be segregated into two parts: a linear and a non-linear part, explained as being due to an amalgamation of Henry's law and Langmuir type adsorption, respectively, and hence, termed **dual mode sorption** [35, 92, 290, 386, 387, 519]:

$$C_{eq} = Sp + \frac{C'_H bp}{1 + bp} \tag{5.41}$$

where:

C_{eq} = total concentration of sorbed molecules, at low concentration such that Henry's law is obeyed.

When permeant-permeant interactions are stronger than permeant-polymer interactions, this leads to clustering, *e.g.*, water in hydrophilic polymers.

For highly hydrophilic polymers (*e.g.* poly(vinyl alcohol)), B.E.T. type IV isotherms are observed for water adsorption.

The **solubility coefficient**, S, (the ratio of permeant molecules between the fluid phase and the polymer phase) varies with temperature, *T*, according to:

$$S = S_0 \exp\left[\frac{\Delta H_s}{2RT}\right] \tag{5.42}$$

where:

S_0 = solubility coefficient when sorbent concentration $C \rightarrow 0$;
H_s = partial molar heat of solution; &
R = gas constant.

For H_2, N_2 and O_2, ΔH_s is positive, and therefore the solubility coefficient increases with increasing temperature. For more condensible gases, *i.e.* increased molecular size (CO_2, SO_2, NH_3 and hydrocarbons), ΔH_s is negative and solubility decreases with temperature.

The solubility of liquids in polymers normally increases with temperature, dependent upon the nature of any permeant-polymer interactions. These interactions are usually weak in the case of gases, although an increase in permeant molecular size may increase its solubility by virtue of increased condensibility.

Sorption (absorption or desorption) experiments express the magnitude of the penetrant absorbed in, or desorbed from, a given polymer as a function of time. Typically, results are expressed graphically as the amount of penetrant sorbed, M_t, at time *t* per unit volume of dry polymer as a function of time raised to the power *n*, to give a sorption curve. *i.e.*:

$$\frac{M_t}{M_\infty} = kt^n \tag{5.43}$$

where:

M_t = amount of vapour sorbed at time *t*;
M_∞ = equilibrium sorbed quantity;
k = constant indicative of polymer-solvent interaction;
n = number.

The equilibrium sorbed quantity, M_∞, is the limiting value reached when no more penetrant is absorbed/desorbed and the penetrant is at thermal equilibrium with the polymer. A plot of M_t/M_∞ as a function of t^n/l, where l is the film thickness, is termed the reduced sorption isotherm. For example, diffusion into, or out of a slab of thickness, l, is given by:

$$\frac{M_t}{M_\infty} = \frac{4}{\sqrt{\pi}}\left(\frac{Dt}{l^2}\right)^{\frac{1}{2}} \tag{5.44}$$

The sorption isotherm is described as Fickian if, as in the above equation, $n = \frac{1}{2}$, where n is the power required to linearise the isotherm. Fujita [175] lists eight features that denote Fickian type sorption, but states that a sorption curve is typically described as Fickian: when both the absorption and desorption curves are linear over small values of the $t^{1/2}/l$-axis and the absorption curves are linear over at least 60% of the range to M_∞; and when the curves are concave to the $t^{1/2}/l$-axis, following the linear regions. The aforementioned reduced isotherm would also be expected to give a single curve, for films of different thicknesses. The relationship makes no allowance for polymer swelling during the sorption process. However, this is usually negligible for sufficiently dilute penetrant concentrations. In Fickian-type sorption, the rate of diffusion is much less than polymer chain segment mobility.

Non-Fickian sorption results from permeant-polymer interactions or when permeant mobility and polymer chain relaxation rates are similar in magnitude. A plot of M_t/M_∞ as a function of t^n will be non-linear, and values of n will tend to $0.5 < n < 1$ [7].

5.2.1.3 Permeation.

The solubility coefficient, S, is a thermodynamic parameter dependent upon permeant-polymer interactions, and can vary over three orders of magnitude, whilst the diffusion coefficient, D, is a kinetic property dependent upon chain mobility, and can vary over ten orders of magnitude. The permeability coefficient, P, being dependent upon both the parameters S and D, will thus tend to be dominated by the latter. S, P and D all tend to be independent of pressure at a given temperature, but vapours that are good solvents for the polymer show concentration dependence tending to swell and plasticise the polymer and increase the permeability. An increase in permeant size will reduce the diffusion coefficient, D, but this can be offset in its effect on the permeability coefficient, P, by increased solubility, S.

Functional groups in a polymer may increase its cohesive energy density and decrease the permeability coefficient unless the permeant strongly interacts with the functionality such that the solubility coefficient increases: in which case, the permeability coefficient is increased too.

The higher the density of a polymer, the lower will be the diffusion coefficient, and therefore also the permeability coefficient in general. Below the T_g, diffusion in microvoids, in a dense polymer, could be relatively unhindered compared with the possibly sluggish (impeded) mobility above the T_g. Generally, increased rigidity of the polymer backbone leads to lower free volume, and crosslinking decreases the diffusion and permeability coefficients by decreasing polymer chain segment mobility. Crystalline regions act as impermeable barriers and, similarly, inert fillers can decrease the permeability coefficient due to increased tortuosity of the permeation pathway. Fillers which are incompatible with the polymer, however, generate voids at their interfaces and increase the permeability coefficient. For the case of aqueous permeants, then a pore-flow model of diffusion may be more appropriate if the film contains water-filled pores or channels, providing a diffusion pathway of lower resistance than the polymer matrix.

Some of the factors mentioned in this section are discussed in greater detail in the following sections.

5.2.2 Transport models.

The transport of a permeant depends on the nature of the film and the permeant. The three main modes of transport are: solution-diffusion (partition mechanism); porous/ convective flow (sieve mechanism, dependent on permeant size in relation to pore size); and finally, ion exchange.

The permeability of a membrane may be of interest for its barrier properties or, in contrast, membranes may be developed for their porosity[325] for use in separation processes. In such instances the transport properties of the pores are of primary interest. In between these two extremes of a porous membrane and a 'barrier' membrane is a rather grey region where the two come together, complicated by the fact that the permeant (or its solvent) may swell a barrier membrane and either increase or decrease its density (by either introducing, for example, aqueous channels in otherwise non-porous films or 'squeezing out' pore volume).

5.2.2.1 Non-porous polymer films: free-volume model.

Assuming a donor-receiver type system (*i.e.*, on the donor side of the film the initial concentration of permeant = C_I whilst on the receiver side, the concentration of permeant (C_I), then diffusion of the permeant through a non-porous polymer membrane, in the absence of an ion exchange mechanism, is an activated, three-step, process. The permeant must initially **'dissolve'** or partition into the polymer on the donor side, then **diffuse** through the membrane before **desorbing** from the polymer into the receiver side.

The ability of a permeant to diffuse through an amorphous, isotropic polymer, above the T_g of the polymer, is related to the cooperative (thermal) motion of the polymer chains. The diffusion process is therefore probabilistic – dependent on the probability of the formation of a diffusive 'hole,' *i.e.*, the **free-volume** of the film. This free-volume, although part of the bulk of the polymer has no fixed shape/size or location. Several theories of free-volume exist, and have been reviewed by Kumins and Kwei[294]. The polymer chain segmental motion allows the possibility of transient 'holes' that are continually formed and eliminated, and a permeant dissolved in the polymer may 'jump' from one hole to an adjacent hole provided that the hole has sufficient volume to accommodate the diffusant. The activation energy for diffusion has previously been described by equation (5.25). When it is assumed that the diffusional jump length is given by d, and that such a jump occurs every t_d seconds, in a random direction, then the diffusion coefficient (D) is given by[417]:

$$D = \frac{d^2}{6t_d} = \frac{\nu d^2}{6} \tag{5.45}$$

where:

ν = thermal vibrational frequency of the diffusant molecule.

In the case of, for example, diffusion in a liquid or gas, the probability of a permeant making the jump from one equilibrium position to another (of a large enough size to accommodate the permeant molecule) is given by the Boltzmann distribution, with one degree of translational freedom and, hence:

$$D = \frac{\nu d^2}{6} \exp-\left[\frac{E}{RT}\right] \tag{5.46}$$

or, according to the transition state theory[149]:

$$\begin{aligned} D &= K\left(\frac{kT}{h}\right)d^2 \exp-\left[\frac{\Delta G^*}{RT}\right] \\ &= K\left(\frac{kT}{h}\right)d^2 \exp\left[\frac{\Delta S^*}{R}\right]\exp-\left[\frac{\Delta H^*}{RT}\right] \end{aligned} \tag{5.47}$$

where:

K = constant (typically = 1, and neglected);
k = Boltzmann's constant;
h = Plank's constant;
ΔG^* = free energy of activation possessed by the permeant molecules; noting that:

$$\Delta G^* = \Delta H^* - T\Delta S^* \tag{5.48}$$

where:

ΔS^* = entropy of activation;
ΔH^* = heat of activation.

It was previously shown in equation (5.25):

$$D = D_0 \exp-\left[\frac{E_D}{RT}\right] \tag{5.49}$$

However:

$$E_D = \Delta H + RT \tag{5.50}$$

and, hence, by substitution of equation (5.50) into equation (5.21):

$$\begin{aligned} D &= D_0 \exp-\left[\frac{\Delta H}{RT}\right]\exp-\left[\frac{RT}{RT}\right] \\ &= D_0 \exp-\left[\frac{\Delta H}{RT}\right] \times \frac{1}{e} \end{aligned} \tag{5.51}$$

Comparing equation (5.51) to equation (5.47):

$$\frac{D_0}{e}\exp-\left[\frac{\Delta H}{RT}\right] = K\left(\frac{kT}{h}\right)d^2\exp\left[\frac{\Delta S}{R}\right]\exp-\left[\frac{\Delta H}{RT}\right] \tag{5.52}$$

and, therefore:

$$D_0 = eK\left(\frac{kT}{h}\right)d^2\exp\left[\frac{\Delta S}{R}\right] \tag{5.53}$$

The various **free-volume theories for the diffusion of a permeant in a polymer** either attempt to **rationalise a diffusional jump in terms of either** the **activation energy of the formation of a suitably sized hole, *or*** the **availability of a distribution of suitably sized holes.** Generally, the diffusion coefficient, D, is expressed by the following proportionality [552, 553]:

$$D \propto \exp-\left[\frac{V_p}{V_f}\right]\exp-\left[\frac{E}{RT}\right] \tag{5.54}$$

where:

V_p = volume required by the diffusant;
V_f = sample free-volume.

For diffusion in polymers, cooperation of the motion of the polymer chain segments may allow the combination of one or more holes to provide a hole large enough for the diffusing molecule. The activation energy for diffusion will therefore have a number of degrees of freedom [32].

The **activated zone theory** [32, 34] of diffusion gives a generalised equation based upon the energy of the system. It is assumed that the activation energy (E) is shared by the polymer chain segments and the penetrant in a zone of activation as characterised by the number of degrees of freedom (typically 14). The diffusion coefficient is given by:

$$D = \frac{\nu^2 d^2}{2}\sum_{f=1}^{f_{max}} P_f\left\{\left(\frac{E}{RT}\right)^{f-1}\left(\frac{1}{(f-1)!}\right)^{-1}\exp-\left[\frac{E}{RT}\right]\right\} \tag{5.55}$$

where:

ν = thermal vibrational frequency of the diffusant molecule;
P_f = probability that f degrees of freedom will enable a diffusional step;
f_{max} = number of degrees of freedom for which $1/(f-1)!$ is at a maximum.

Fujita's [175] **free-volume theory** satisfactorily describes the diffusion of organic vapours and liquids in 'amorphous' polymers, observing that a molecule can only diffuse if the local free volume exceeds a critical value. The theory is discussed in terms of the polymer free volume (ν_f), the thermodynamic diffusion coefficient (D_T) and permeant mobility (m_p):

$$D_T = RTm_p = RTA_p\exp\left[\frac{B_p}{\nu_f}\right] \tag{5.56}$$

where:

A_p & B_p = factors related to permeant size and shape;
and D_T is related to D (when a = activity of the permeant in the polymer) by:

$$D = D_T \left(\frac{d \ln(a)}{d \ln(v_f)} \right) (1 - v_f) \tag{5.57}$$

In glassy polymers, free volume depends upon sites, or '*holes*', having a distribution of sizes trapped into the polymer during formation. The molecules have a rigid random coil configuration in which atoms, and small groups of atoms, vibrate. On heating, the amplitude of vibration increases until, when above the T_g, segmental motion along the polymer chains can occur and random coils become flexible so that more free volume is available, and the polymer is then rubbery (*i.e.*, free volume increases with temperature).

Fickian diffusion, in terms of penetrant molecular size and membrane free volume, has also been considered by Frisch[173], who found "at least" two classes of diffusion behaviour. Type A behaviour was shown by small penetrant molecules such as helium and isotopes of hydrogen, and also by molecules as large as nitrogen when in elastomers. The behaviour was characterised by (i) low diffusant solubility, and good adherence to Henry's law, (ii) diffusion coefficients independent of diffusant concentration, and (iii) an activation energy of diffusion apparently independent of temperature (and concentration). Type B diffusion behaviour was evident for larger organic diffusants (*e.g.*, benzene), which whilst still being Fickian was characterised by (i) diffusant-polymer solubilities showing a non-linear dependence, (ii) concentration dependent diffusion coefficients, and (iii) diffusional activation energies that were temperature dependent. Frisch concluded that type B behaviour occurred as a result of a failure in the free volume mechanism, *i.e.*, when the minimum void volume required to disperse the diffusant molecules is larger than the average free volume.

5.2.2.2 Porous polymer films.

Many commercial applications require porous membranes which are utilised for their separation properties (*e.g.*, for use in filters, ultrafiltration type devices, or reverse osmosis[1] membranes), or permselectivity, dependent on the 'coarseness' of their porosity[405]. Therefore whilst a knowledge of the transport properties of non-porous membranes (*i.e.*, where transport occurs by solution-diffusion-desorption) is useful for their utilisation as, for example, barriers, an awareness of porous transport mechanisms is also of great importance.

Transport of a permeant through a pore is not activated, in that at no stage is it required that the permeant must partition into the polymer. Other factors must be considered, in addition to 'simple' Fickian molecular diffusion in which the molecular

---

[1] Application of a pressure greater than the osmotic pressure, thus causing solvent flow from the side of high solute concentration to low (in the opposite direction to the usual osmotic flow), is termed reverse osmosis. This and ultrafiltration are similar processes, with the exception that osmosis is negligible when the pressure is removed in an ultrafiltration experiment[277]. The process is termed reverse osmosis when the solute molecular dimensions are within an order of magnitude of those of the solvent, and ultrafiltration if the solute has molecular dimensions greater than ten solvent molecular diameters[418].

motion will be random (Brownian), but may have a net mass 'hydrodynamic' movement resulting from a pressure or the concentration gradient, as described, for example, by Einstein's law[139] of diffusion and, hence, Stokes' law for a spherical body (when the body is much larger than the solvent molecules), etc.:

$$D_\infty = \frac{kT}{f_\infty} = \frac{kT}{6\pi\eta r_H} = \frac{RT}{6\pi\eta r_H N_A} \qquad (5.58)$$

where:

D_∞ = diffusion coefficient in an unbounded solution;
k = constant;
R = gas constant;
T = temperature;
f_∞ = molecular friction coefficient, as described by Stokes' law;
η = viscosity of medium;
r_H = hydrodynamic particle radius (assuming a spherical particle);
N_A = Avogadro's constant.

Pressure driven porous (convective) transport through relatively coarse pores may be described by Knudsen or Poiseuille (etc.) type flow regimes (assuming that the pressure gradient is insufficient to establish turbulent flow). Such regimes typically describe the flow through idealised long (relative to the diameter), straight capillaries of uniform diameter: the Knudsen diffusivity, D_K, of a gas being given by[248]:

$$D_K = \frac{4r}{3}\left(\frac{2RT}{M\pi}\right)^{\frac{1}{2}} \qquad (5.59)$$

where:

r = capillary radius;
M = diffusant molecular weight.

The Knudsen regime describes flow in which the mean free path of the gas molecules is of the same order, or larger than the pore diameter. If the mean free path is much less than the pore diameter or the pressure is higher, then the flow is described by Poiseuille type viscous flow which describes the velocity of flow in terms of the pore radius. The permeability coefficient, P, for Poiseuille-type flow through parallel pores is given by[329]:

$$P = \frac{r^4 N\pi}{8} = \frac{V_f^2}{8N\pi} \qquad (5.60)$$

where:

N = number of independent (cylindrical) pores per unit area;
V_f = fractional void volume available for flow.

Note that the Poiseuille equation was derived to describe incompressible fluid flow, and therefore does not apply to a gas. The volume, V, of fluid flowing through a cylindrical tube is given by the Poiseuille equation as:

$$\frac{dV}{dt} = \frac{\pi(p_F - p_B)r^4}{8\eta l} \qquad (5.61)$$

where p refers to the pressures in the direction of flow (F), and against the direction of flow (B), *i.e.*, the back-pressure. For a gas, however, the volume is pressure dependent. Hence, for a gas whose volume is measured at a pressure of p_0, in a capillary in which the average pressure is given by $(p_F + p_B)/2$, then the Poiseuille equation becomes [341]:

$$\begin{aligned}\frac{dV}{dt} &= \frac{\pi(p_F - p_B)R^4}{8\eta l} \times \frac{p_F + p_B}{2p_0} \\ &= \frac{\pi(p_F^2 - p_B^2)R^4}{16\eta l p_0}\end{aligned} \qquad (5.62)$$

Typically, mathematical models of porous structures relate to idealised cylindrical pores: however, these are rarely found (especially in films from latices, where porous structures are usually the result of the fusion of spheres in which deformation of the particles is incomplete) and the average pore size (as determined, for example, by mercury porosimetry, etc.) is used to model the transport process. A number of equations exist [411] by which pore radius may be determined when Poiseuille flow is assumed, allowing for various factors such as blind pores or pore orientation with respect to the plane of the membrane. Darcy's law is similar Poiseuille's law, but describes very tortuous channels.

Flow through pores is typically greatly affected by a hydrostatic pressure whereas solution-diffusion type transport is not affected significantly. (This is not to be confused with gaseous partial pressure, which being equivalent to concentration in a solute *will* affect permeation in an activated solution-diffusion type mechanism. Similarly, an increase in the permeant vapour pressure may cause an increase in the permeant solubility, therefore increasing the film permeability: Lebovits [307] notes that whilst it is unlikely that a vapour phase will exist in equilibrium with the liquid at high hydrostatic pressures, such a situation can occur if the vapour is a component of a gaseous mixture in which the vapour has a relatively low partial pressure, but the overall gas pressure equals the hydrostatic pressure. Permeant transport may also be affected if the pressure is sufficient to change, for example, the density of the film.) The effects of pressure on porous flow can be used to distinguish between (convective) transport through pores, in contrast to solution-diffusion type transport [172, 478].

In coarse porous membranes, transport by solution-diffusion is negligible compared to the convective transport, and assuming an absence of electrokinetic effects the transport is governed by the hydrostatic pressure, p, difference across the membrane. In terms of irreversible thermodynamics [98]:

$$J_V = L_P(\Delta p - \sigma\Delta\pi_S) \qquad (5.63)$$

$$J_S = C_S(1 - \sigma)J_V + P\Delta\pi_S \qquad (5.64)$$

where:

J_V = net volume flux;

σ = Staverman [337, 465] reflection coefficient[1] (= ratio of $-L_{PD}/L_P$, where L_{PD} = coefficient of osmotic flow when $\Delta p = 0$, such that $J_V = L_{PD}\Delta\pi$);

---

[1] A measure of membrane selectivity: if $\sigma = 1$ then solute is 'reflected'; if $\sigma \langle 1$ then some solute penetrates membrane and is not 'reflected.'

L_p = hydraulic permeability or filtration coefficient (L_p = the velocity of fluid per unit pressure difference);
π = osmotic pressure;
J_S = solute flux;
C_S = mean solute concentration in the membrane;
P = permeability coefficient.

The transport mechanism of fine-porous membranes is typically, however, a combination of activated transport and convective transport, and the convective transport may be further complicated by the shape of the pores and also whether the pores are continuous through the membrane and the route they take. If membrane transport occurs only through the pores in a membrane, then hydrodynamic relationships studied by Anderson and Quinn[11] suggest that if the size ratio of a permeant molecule (assumed to be spherical) to a pore is 0.1, then the diffusivity of the permeant will be ca 0.6 times that of the free, bulk solution, diffusivity. Non-linearity of pores is resolved by a tortuosity factor, τ_l, such that the **effective film thickness** (L) of a porous membrane of actual thickness l, is given by[167]:

$$L = \tau_l \times l \tag{5.65}$$

The total diffusive flux (J_{TOTAL}) given by composite mechanisms is simply additive:

$$J_{TOTAL} = A_{f1}J_1 + A_{f2}J_2 + \cdots\cdots + A_{fn}J_n \tag{5.66}$$

where:

A_f = fractional area over which the flux, J, operates.

Thus the effective diffusion coefficient (D_{eff}) for a film in which transport may occur through solvent filled pores (D_{sol}), but in which the solute may partition into the polymer (such that there is also diffusional transport in the polymer {D_{pol}}) is given by:

$$D_{eff} \propto D_{sol} + D_{pol} \tag{5.67}$$

Diffusion of a solute through solvent filled pores will typically provide less resistance to flow than will diffusion through the polymer as a result of the lower activation energy for the motion of liquid molecules when compared to activation energy for the motion of a polymer chain segment. A complicating factor, however, is the boundary layer resistance[58] at the film's interfaces. The total membrane resistance, R_{TOTAL}, to transport through a film is a function of the membrane resistance, R_m, and the interfacial boundary resistance, R_b:

$$R_{TOTAL} = R_m + 2R_b = \frac{\left(C_{Donor} - C_{Receiver}\right)}{J} \tag{5.68}$$

Note that if the interaction between the membrane and permeant is negligible, and the membrane does not dissolve the permeant, and the permeant is small compared to the pore size, then the total membrane resistance is simply the boundary resistance. This can still result in the diffusion coefficient of a permeant in a pore being less than the free diffusion coefficient of the permeant. Yasuda and Lamaze[551] and Hwang and Tang[249] have determined the boundary layer resistance of polymer membranes by first determining the gas permeability of the membrane (*i.e.*, in a gas-membrane-gas type system) which is unaffected by boundary layers, and then determining the permeability of the same gas, when the gas is dissolved in a liquid (*i.e.*, gas-membrane-liquid, or liquid-membrane-liquid type systems): the difference between the two results providing a measure of the boundary layer resistance.

Other factors may need to be accounted for if the permeant is of a similar molecular radius, r_p, to the radius of the pore, r, such that porous diffusion is hindered by the pore walls [151], etc.

$$A = A_0\left(1 - \frac{r_p}{r}\right) \tag{5.69}$$

where:
A = effective pore area for diffusion;
A_0 = actual pore area;

When a pore diameter is of a comparable size order to the diffusants, the process of molecular sieving [33] may occur. The sieving action may be total, whereby the flux of one species of permeant is prevented, or partial, whereby species diffuse at different velocities. The structure of porous membranes, with respect to their transport properties has been investigated by Pusch and Walch [404, 405]. Fine porous membranes used, for example, for the purification of sea water by the removal of salt, are typically composite membranes consisting of a porous membrane supporting a thin, dense, 'active' (*i.e.*, responsible for the separation) homogeneous film. (Membrane thickness is typically 100 μm, with the active layer ca 0.1 μm.) Homogeneous cellulose acetate has suitable properties, allowing the permeation of water, but not salt, and was used for early hyperfiltration (reverse osmosis) membranes. The flux of water was found to be increased if the cellulose acetate membrane was modified such that only one face consisted of a very thin layer of homogeneous cellulose acetate (the bulk of the membrane being less dense). The technique can be improved further if a film (*e.g.*, poly(ether/urea)) is cast onto a porous substrate (*e.g.*, polysulfone) (*i.e.*, a composite membrane): the porous substrate being coated with a polymer solution, and the thin film being formed *in-situ* by crosslinking [472].

5.2.2.3 Permeation of electrolyte.

Yasuda [552] *et al.* point out that salt will not permeate through most polymer matrices – requiring a diluent for the polymer that must also be a solvent for the salt. For a hydrated polymer membrane, with a volume fraction of diluent denoted by H (units: $g_{water}/g_{hydrated\ polymer}$), the free-volume of the polymer-diluent system is given by:

$$V_f = H_{(v_f, H_2O)} + (1 - H)_{(v_f, polymer)} \tag{5.70}$$

Of this total free-volume, in the polymer matrix, that available for salt permeation is:

$$V_f = H_{(v_f, H_2O)} \tag{5.71}$$

Assuming a linear variation of free volume with the volume fraction of diluent, Yasuda notes that the diffusion coefficient is expected to change exponentially (as shown by equation (5.54)) with changes in the volume fraction of diluent – and the diffusion coefficient of the salt, D_s, (in pure water) in terms of H, is given by:

$$\log(D_s) = \log(D_0) - K\left(\frac{1}{H} - 1\right) \tag{5.72}$$

where:

K = constant;

D_s was determined by measuring the desorption of salt from a film equilibrated in salt solution:

$$D_s = \left[\frac{d\left(\sigma_t/\sigma_\infty\right)}{d\left(t^{0.5}/l\right)}\right]^2 \times \left(\frac{\pi}{16}\right) \tag{5.73}$$

where:

σ_t = conductivity at time t;

σ_∞ = equilibrium conductivity;

l = film thickness.

Hence, a plot of log[D_s] as a function of $1/H$ should be linear if it is assumed that the free volume is directly proportional to the degree of hydration (*i.e.*, D_s increases exponentially with H).

Using this technique, Yasuda [552] *et al.* investigated the diffusion of NaCl through a range of solvent cast hydrophilic membranes and hydrogels, finding linearity of the aforementioned plot over five orders of magnitude of D_s (although in some cases of the highly hydrated films, diffusion coefficients were lower than expected as a result of concentration polarisation at the polymer-sink solution interface). Scatter in the experimental results was also accounted for by the fact that the film tended to compact ("de-swell") on extraction of the NaCl. The mathematical models of Yasuda have been modified by Bo [54] *et al.* to account for salt rejection in highly water-swollen membranes by the inclusion of a coupled salt-water transport coefficient into the solution-diffusion model, as opposed to simply combining both convective (porous) and solution-diffusion flows.

Rather than correlate the permeation of ions through hydrogels in terms of (hydrated) ion size (which was found to be anomalous), Hamilton [214] *et al.* discussed the transport of ions in terms of the water 'structure' (long range tetrahedrally coordinated hydrogen bonds in the bulk water), and the interactions of the ions with this structure. Small ions (Li^+, F^-, H_3O^+, etc.) are described as structure making – electrostatically inducing order to the water, forming a 'long range hydration shell' and, hence, effectively increasing the water viscosity to the permeating ion. In contrast, large monovalent cations (K^+, Cl^-, etc.) are described in terms of being structure breakers and more mobile, but generating only weak electrostatic forces which only affect near-neighbour molecules. It was concluded that anions can have a dramatic effect on cation permeability: diffusion coefficients of the cations showing greater correlation to the hydrodynamic radius of the counteranion, than their own hydrodynamic radius. Results for various ions fitted a spectroscopic trend in 'structure temperature[1]' of the ions, determined by Luck [327], in relation to water binding: the anions playing a dominant role in the trend compared to the cations.

---

[1] Luck defined a temperature at which pure water has the same extinction coefficient, in the region of free or weakly bound OH, as an electrolyte solution.

A membrane containing pores of molecular dimensions may be ion selective as a result of functional polymer chain end groups [293]. *E.g.*, a pore lined with ions will repel co-ions in dilute solution and also electrolyte, in the absence of an electric current subject to conditions of electroneutrality (*i.e.*, Donnan[1] exclusion effect). Such a polymer that is anionic in nature would therefore be described as being cation-selective. The result of such a membrane separating solutions of the same electrolyte, of differing activities is the formation of a membrane potential (E.M.F.). However, counter ions will enter the film if the activities of the ions in solution are greater than those of the fixed ions [405] (hence, reducing the film's degree of permselectivity).

Ionic membranes (ionomers) are often used as cell partitions in electrochemical cells, separating the anode and cathode, often requiring high ionic conductivity, but also selectivity. Typical membranes include sulphonated polystyrene polymers or poly(perfluoro-sulphonic acids): the latter being used as ion exchange polymers due to their ability to swell with water (ca 50% W/W) whilst maintaining their mechanical strength. The transport of protons through ionic membranes has been investigated by Fales [150] *et al.* It is concluded that transport is dependent on the water filled channels of connected 'clusters' of ions within the membrane: the size of which result from the balance of moduli forces and ionic repulsions during film formation. Transport is also dependent on the permeant as a result of the ionic distribution within the clusters.

5.3 Factors affecting polymer film permeability.

5.3.1 Film Structure and the effect of temperature on the polymer.

It has previously been shown (equations (5.25) and (5.42)) that both diffusion and solubility coefficients show an Arrhenius type dependence over small temperature ranges. Similarly, so can the permeability coefficient, P:

$$P = P_0 \exp - \left[\frac{E_P}{RT}\right] \tag{5.74}$$

where:

P_0 = permeability coefficient as given by $D_0 \times S_0$;
E_p = activation energy of permeability;
R = gas constant;
T = temperature.

Above the T_g of the polymer, diffusion is typically Fickian. However, anomalous diffusion may be shown below the T_g. Kumins and Roteman [295] investigated the diffusion coefficients, at different temperatures, of a number of non-condensible gases (*i.e.*, low solubility in the polymer) of various Van der Waals' diameters, ranging from 2.34 Å (hydrogen) up to 3.23 Å (carbon dioxide), and also water vapour (3.48 Å), through a copolymer with T_g's at 303 K and 350 K. Plots of the logarithm of the diffusion coefficient versus reciprocal temperature were found to be linear with the exception of those for CO_2

---

[1] A membrane that is permeable to small, but not large (*e.g.*, macromolecule) electrolyte ions, results in an electrical potential arising from the passage of small ions, attempting to neutralise the larger ions. The concentration of the small co-ions is lower on the side of the large ion, and this is compensated for by an increase in small counter-ion concentration.

and water vapour. the former of these showing a discontinuity in linearity at the higher T_g, whilst the latter showed a discontinuity at the lower T_g. The linearity found for the majority was attributed to the segmental motion, even in the glassy polymer, providing sufficient free volume to allow the permeant to diffuse, such that the increase in free volume above the T_g would have little effect. (Also concluded from the results was the fact that the rise in temperature only increased the rate of polymer segmental motion, rather than increasing the number of holes available for diffusion.) The discontinuities in the lines for CO_2 and water vapour were ascribed to their larger respective molecular sizes in relation to the size of available holes. (An anomalously high diffusion rate for water vapour was explained in terms of the water acting to plasticise the polymer by forming hydrogen bonds with pendent acetate groups, which would otherwise form H-bonds between acetate groups.) Similar results and conclusions were also realised by Stannett and Williams [464] with work on poly(ethyl methacrylate).

Yasuda and Hirotsu [549] report three possible effects, recorded in the literature, of the T_g on the permeability of gases:

✗ no effect on any gas used in the particular study cited;

✗ all gas permeabilities in the study show an anomaly at the T_g;

✗ a limited number of the gases under study show an effect.

Yasuda, however, notes that size alone is not sufficient to explain the results (*e.g.*, the fact that in some instances in the literature, large molecules such as CO_2 or N_2 show no anomaly at the T_g, whilst smaller molecules {Ar} do for the same polymer), and that the relative aspect of the permeant must also be accounted for (*e.g.*, linearity of CO_2). Comparisons of literature values indicated that for a change of slope in the Arrhenius plot to occur, then the diffusion coefficient at the T_g should be below a certain critical nominal value: suggested to be 5×10^{-8} cm^2 s^{-1}.

Such non-Fickian behaviour of transport (or sorption) may result from the **relaxation time** of the polymer. Stresses imposed on the polymer during film formation, or by swelling during the transport process, are relieved (or reach an equilibrium) at a rate dependent on the rates at which changes in polymer structure can occur, and this may be reflected in transport rates. A model founded on a temperature-based transition has been discussed by Frisch [171], using non-equilibrium thermodynamics to explain non-Fickian behaviour.

The effect of polymer **molecular weight** on permeability (of air) has been investigated by Kaminska [266]. Permeability was found to decrease with increasing polymer molecular weight and was also dependent on the polydispersity of the polymer. The results were attributed to an increase in the cohesive energy with increasing molecular weight. Other workers, however, have found molecular weight to have no effect (on sorption): Park [384] stated that it was not surprising that molecular weight had no appreciable effect on sorption (of methylene chloride in polystyrene) due to the fact that the diffusion process (with respect to a single penetrant 'jump') only disturbs one or two units of the polymer chain and, hence, chain length is not significant unless the next segment was a chain end.

Polymers tend towards the lowest free energy state (thermodynamic equilibrium), even when in their glassy form (**polymer aging**). Such aging leads to a decrease in the free volume of the polymer, and will therefore produce a decrease in the permeability of the polymer. Guo [210] *et al.* have derived an equation, based on drug dissolution rates from polymer coated tablets, for the prediction of the permeability of an aging polymer below its T_g, as a function of polymer aging time. The equation is based on the aforementioned equations in Fujita's free volume theory and equations relating the shift in the polymer's creep compliance, as a function of age, to free volume. The resulting equation showing a linear double logarithmic relationship between the polymer's permeability coefficient (P) (or diffusion coefficient) and polymer age (t_a):

$$\frac{d \ln P(T, t_a)}{d \ln t_a} = \text{constant} \qquad (5.75)$$

Film age was also of concern to List and Laun [324], but for reasons of residual solvent content after casting. The water vapour permeability of plasticised isopropyl alcohol-cast Eudragit® *L* (see Chapter 6) was found to decrease (by a factor of three) as a function of film age (three weeks). A secondary 'drying' phase, at higher temperature reduced the amount of residual solvent and meant that the minimum in permeability was achieved in a shorter time. However, only when the secondary drying temperature was greater than the polymer's T_g (348 K) was their significant loss of residual solvent from the film (due to the increased chain segment mobility), in a time of only 8 hrs.

Okor [354, 356] has investigated the effect of the polymer chain end groups on membrane permeability. The aqueous urea permeability was found to increase with increasing film cation content, but not linearly, showing a slow increase at low cation content with a more rapid increase above a certain level (53 moles of cation per mole of polymer chain). The initial slow increase in permeability was attributed to increased film swelling resulting in plasticisation of the polymer by the water. However, in the case of the higher permeabilities, results were attributed to increased porosity and an increase in pore size resulting from the mutual repulsion of the charged end groups: pore size demonstrating good correlation with permeability. It was suggested that during film formation there was a balance between the cohesive and repulsive forces. At low cation content, the cohesive forces outweigh the repulsive forces leading to smaller but more numerous pores, whilst high cation content results in pores of larger diameter.

The effects of plasticiser hydrophilicity have also been investigated by Okor and Anderson [355, 359]. Using comparable films of differing hydrophilicity, containing a constant amount of differing ratios of two similar plasticisers of differing degrees of hydrophilicity, it was found that increasing the fraction of the more hydrophilic plasticiser coupled with a decrease in the less hydrophilic plasticiser increased the urea permeability of the less hydrophilic film. This was related to the leaching of the hydrophilic plasticiser which resulted in enhancement of film porosity. In the more hydrophilic film, urea permeability increased as the more hydrophilic plasticiser fraction was decreased: a result attributed to the potential of the less hydrophilic plasticiser for not leaching to such an extent as the more hydrophilic plasticiser, but promoting film swelling and porosity. It was thus concluded that the permeability was dependent on the hydrophilicity of both the plasticiser and polymer considered together.

5.3.1.1 The effect of polymer crystallinity, crosslinking, and plasticisation.

Crystalline polymers are generally impermeable: Barrer [31] cites Van Amerongen [490] as being one of the first researchers to show that the solubility/diffusivity/permeability was reduced as the crystallinity of a membrane (gutta percha) increased. The effective diffusion coefficient must account for the tortuosity of the path a diffusant must take in avoiding the crystalline regions. The diffusion of a permeant in an amorphous region (of diffusion coefficient = D_a), but near to a crystalline region may also be position dependent as a result of the segmental motion of the polymer being impeded. Hence, Michaels [338, 339] *et al.* proposed a model which included a tortuosity factor, τ_t, and a factor related to the chain immobilisation, β:

$$D_{eff} = \frac{D_a}{\tau_t \beta} \tag{5.76}$$

In films of amorphous polymer containing crystalline regions (or filler), the diffusion coefficient (D_{eff}) is generally given by [417]:

$$D_{eff} = D_a \times \phi_a^m \tag{5.77}$$

where:

ϕ_a = volume fraction of the amorphous regions;
and m is a number typically ≤ 1.

Similarly, the effective solubility, S_{eff}, is typically proportional to ϕ_a:

$$S_{eff} = S_a \times \phi_a \tag{5.78}$$

By virtue of its restrictions on polymer segment mobility, **crosslinking** of a polymer will also decrease the ability of a diffusant to move through such a system (provided that the density of crosslinking is sufficient to affect segment motion). **Plasticisation** has the opposite effect by virtue of the nature of plasticisers in 'loosening' the polymer network.

5.3.1.2 Hydrogels.

Hydrogels are prepared from hydrophilic polymers (*e.g.*, poly(hydroxyalkyl methacrylates). Macroscopically, they appear as homogeneous systems of water and polymer combined into a single phase gel. Kim [284] *et al.* note that the water can be treated as being in one of three states: (i) hydrating hydrophilic polymer surface groups (*i.e.*, bound by hydrogen bonds); (ii) interfacial between the polymer segments; or (iii) 'bulk-like' behaving as 'aqueous solution.' Hydrogels form when a polymer is easily hydrated (swollen), requiring that the interaction between adjacent polymer segments (dimerisation by hydrogen bonding), when in water, be less than the interaction between the polymer and the water [454]. Typically, a crosslinking agent is added to maintain structural integrity. Zentner [558] *et al.* and Kim [284] *et al.* have investigated the permeation of (hydrophobic and hydrophilic) steroids through hydrogel systems, concluding that permeation through the hydrogel without the crosslinking agent (or permeation by a hydrophilic permeant) was predominantly through solvent filled pores (bulk water), whilst in the crosslinked system, permeation resulted from solution-diffusion type transport (and was, hence, subject to changes in functionality of the permeant: *i.e.*, solute permeability through a water swollen polymer will be less dependent on the functionality of the polymer if the solute travels through the water that is swelling the polymer).

5.3.2 Nature of the permeant.

According to the free volume theories of diffusion, in which the cooperative polymer segment motion is required to form a hole for diffusion to occur, it would seem obvious that permeant **molecular size** (and also shape and weight [151]) is important: larger permeant molecules requiring larger holes and, hence, greater segment cooperation with a correspondingly higher activation energy of diffusion. Kumins and Roteman [295] found, in the aforementioned investigation of the effect of polymer T_g on diffusion, that the activation energy for diffusion increased exponentially (*i.e.*, rate of diffusion decreased) with increasing permeant (Van der Waals') diameter, and went on to investigate the relationship between polymer segment mobility (and, hence, free volume) and permeant size [296]. Using equations originally developed by Bueche [37] for diffusant jump frequency, Kumins was able to determine the hole size necessary for diffusion, and the number of polymer segments involved. However, the work assumed a spherical molecule, which in some instances led to over-estimates of hole size. Permeant shape may be important, especially in the case of diffusion through glassy polymers (where the free volume is 'fixed' to a greater extent than rubbery polymers).

Renkin [411] investigated the aqueous transport of a range of diffusants of graded molecular weight (and, hence, radius size) through porous, inert, cellulosic membranes of a range of pore sizes. Restriction to flow (*i.e.*, molecular sieving) agreed with the theories of Pappenheimer [382, 383] *et al.*, fitting the equation:

$$\frac{A}{A_0} = \left(1 - \frac{r_p}{r}\right)^2 \left[1 - 2.104\left(\frac{r_p}{r}\right) + 2.09\left(\frac{r_p}{r}\right)^2 - 0.95\left(\frac{r_p}{r}\right)^5\right] = \frac{D_p}{D} \qquad (5.79)$$

where:

A = effective area of pore opening;
A_0 = cross-sectional area of pore;
r_p = permeant molecular radius;
r = pore radius;
D_p = diffusion coefficient in the pore;
D = free (aqueous) diffusion coefficient.

Values of the aqueous diffusion coefficient, D ($cm^2\ s^{-1}$), and molecular radii, r, have been calculated for a number of diffusants, by Wisniewski and Kim [544] using the following empirical relationships[477, 535]:

$$D = 7.4 \times 10^{-8} \frac{(xM)^{\frac{1}{2}} T}{\eta V^{0.6}} \qquad (5.80)$$

where:

M = solvent molecular weight;

x = association parameter (correction for H-bonding, etc.): $x = 2.6$ for water;
T = temperature /K;
η = solution viscosity /centipoise;
V = molar volume of solute at normal boiling point /cm^3;

and:

$$r_p = \left(\frac{3V}{4\pi N_A} \right)^{\frac{1}{3}} \tag{5.81}$$

where:

N_A = Avogadro's number;
and:

$$\frac{V}{N_A} = \frac{4}{3}\pi r^2 \tag{5.82}$$

In contrast to non-condensible gases, the permeability of liquids and vapours may be affected by interactions (*e.g.*, hydrogen bonding, Van der Waals' forces) of the permeant with the polymer. Polymers with functional groups that are chemically similar to those of a permeant result in large cohesive forces leading to high solubility of the permeant in the polymer. The fact that permeability is a function of solubility, and that polymer swelling results in a 'loosening' of the polymer network and, hence, an increase in the diffusion coefficient, together lead to an increase in the polymer permeability [307]. Yasuda [550, 553] *et al.* found that swelling of a film by water (*i.e.*, hydration of the film) led to a change in the water permeability from a solely solution-diffusion type mechanism to a mechanism in which a hydraulic (convective or non-activated) permeability[1] (*i.e.*, permeability resulting from a pressure gradient see equation 5.63 and 5.64) played a major role, having obvious consequences on the permselectivity[2] of the film. Alternatively, permeant-permeant interactions (in the case where the permeant and polymer are dissimilar) may lead to clustering of the permeant – decreasing the permeant mobility due to the diffusion hole size being required to be large enough to accommodate the cluster. The diffusion coefficient of chloroform into poly(dimethylsiloxane) (non-polar) was seen [53] to be dependent on the chloroform concentration, increasing initially due to plasticisation of the polymer, but decreasing at higher concentrations, which was ascribed to permeant clustering.

The permeability of solutes through polymer films (*i.e.*, a system in which the permeant has an affinity for both the polymer and the external phase, related to the polarity of the various phases and, hence, structure of the permeant) have also been investigated. Serota [446] *et al.* used a series of substituted anilines of increasing side-chain length, finding that the permeability coefficient showed the same trend as that seen for the partition of the anilines between water and hexane.

Whilst increased permeant size may lead to a decrease in the diffusion coefficient, it often leads to an increase in the solubility coefficient. Thus because the permeability

---

[1] Sometimes called a filtration coefficient. Flow is a function of an external pressure gradient (or possibly an osmotic pressure).

[2] A film which can 'sieve' permeant molecules of differing sizes. The sieve coefficient is defined as the ratio of the solute concentration of filtrate to that of the filtrand.

coefficient is the product of the diffusion and solubility coefficients, its variation with permeant size may be minimal in systems with an absence of a porous network.

Permeant size becomes less important as the free volume in the film increases. In a porous film in which the pore diameter is much greater than the permeant size, the effect of the permeant size becomes negligible. In contrast, if a permeant interacts with the polymer, either by physical or chemical interaction, or by sorption into a microvoid, it may become immobilised for a period longer than that required for a diffusion jump. Such an immobilised penetrant molecule does not contribute to the overall permeant flux [417]. (Partial immobilisation results in a concentration dependent diffusion coefficient [463].) Immobilisation may affect the diffusional time lag, but not the steady-state rate of diffusion [387]. In samples where dual mode sorption (*e.g.*, where both Henry's law and Langmuir type sorption occur), then the diffusion process will have contributions from both modes such that the flux, J, is given by:

$$J = -D_S \frac{dC_S}{dx} - D_L \frac{dC_L}{dx} \tag{5.83}$$

where:

D = diffusion coefficient;
C = concentration of permeant;
subscripts S and L refer to Henry's Law and Langmuir modes, respectively.

A model for the diffusion of gases in glassy polymers, undergoing dual mode sorption, has been proposed by Vieth and Sladek [520]

The diffusion of gases and vapours is typically a result of the difference in partial pressure of the permeant on either side of the membrane. This acts as the driving force with the rate of permeation being proportional to the partial pressure difference. If, however, the permeant is also soluble in the membrane, and the rate at which the permeant dissolves in the membrane differs from the rate of change in the partial pressure, then the rate of permeation is a result of the absolute vapour pressure, rather than the pressure differential, and the permeability will deviate from being Fickian in nature.

5.3.3 Heterogeneous films and film additives.

In many commercial applications (*e.g.*, emulsion paints), polymer films contain additives (*e.g.*, fillers, pigment, etc.). Alternatively, films may consist of one polymer dispersed in another, or of laminates of two or more polymers (or even a single polymer with a 'skin' of the same polymer of higher density). Laminates of polymers, in series or in parallel are the two extremes of polymer mixtures. The transport properties of such heterogeneous media have been reviewed by Barrer [31], and have also been discussed by Chainey [85] in his review of transport through polymer films. Compared to homogeneous films, heterogeneous films have the additional complication of their transport properties being functions of diffusant position within the film (as well as, possibly, concentration, temperature, etc.).

In the case of laminates in series, the permeability is independent of the order of the layers of the laminate provided that the permeant does not interact with the polymer. The rate of permeation being expressed by:

$$\frac{1}{r_{Total}} = \frac{1}{r_1} + \frac{1}{r_2} + \ldots\ldots\ldots + \frac{1}{r_n} \qquad (5.84)$$

Rogers qualitatively [419] (and together with Sternberg, quantitatively [421]) discusses the means by which a membrane may show permeability asymmetry using a hypothetical heterogeneous film containing a gradient in the density of crosslinking across the film's thickness. Rogers notes that the rate of transport through the film should be greater when the lightly crosslinked side is exposed to a permeant that solvates the membrane due to the fact that the membrane would swell to a greater extent than if it were the highly crosslinked side that was exposed. In the latter case, the concentration gradient within the membrane would be reduced, when compared to the former case and, hence, the driving force for permeant transport would also be reduced. Rogers then showed experimentally that membrane transport across polymer films with either structural or chemical gradients (prepared by graft copolymerisation) could be directionally dependent.

Exudation of polymer additives that are incompatible with the polymer, such as surfactants, can also lead to an increase in film heterogeneity. The exudation to a film surface leading to a concentration gradient [561], of the additive in relation to the polymer, that decreases with distance from the surface (or in the case of a thin free-film where exudation can presumably occur at the two film faces, to a concentration profile in which the additive concentration is at a minimum at the centre of the film).

A number of studies [e.g., 1, 423] of single-layer free-film permeability have shown surface heterogeneity leading to permeability asymmetry. Such heterogeneity is usually attributed to differences in film density, between the two sides of the film. Abdel-Aziz and Anderson [3] found that the addition of ethanol to a solution of polymer in acetone decreased the solvation of the polymer. Films cast simply from acetone showed a dense surface (polymer-air interface) layer with few pores: increasing amounts of ethanol (5%) led to a surface containing a few large pores, whilst greater amounts of ethanol (10%) reduced the pore size but increased the pore number density, giving pores that passed further into the bulk of the film leading to a high film permeability. Laminated films in which the laminates show surface heterogeneity, (when arranged with the same orientation, *e.g.*, lower face of the second layer against the upper face of the first) give a reduced permeability coefficient when compared to single films of the same thickness [357, 358].

Heterogeneity is often induced into films by penetrant diffusion such that the rates of penetrant transport differ in thick films when compared to thin films of the same material [249, 413]. This is attributed to swelling of the films by, for example, water/water vapour, on the ingoing side of the membrane (*i.e.*, the side where permeant is concentrated).

The addition of an inert filler to a polymer will generally decrease the permeability due to increased tortuosity, τ_l of the permeant's route. Effects on the diffusion lag time (τ) would also be apparent:

$$\tau = \frac{L^2}{6D} = \frac{\tau_l l^2}{6D} \qquad (5.85)$$

(In cases where the permeant is adsorbed onto the filler, this too should be accounted for in the equation [166, 342, 386, 387].) However, a filler that is incompatible with the polymer may result in voids at the polymer-filler interface, hence, leading to an increase in the film's permeability. Such voids result from the inability of the polymer molecules to fill the interstitial spaces between aggregates of filler, and may also affect the spatial arrangement of the polymer segments, resulting in film densities that are less than would be expected from calculations assuming volume additivity [298].

The work of Kwei and Arnheim [298] on filled polymers, and his comparison with the work of Meares [336] on unfilled polymers, showed a 59% reduction in the diffusion coefficient, and a corresponding 56% increase in the activation energy of diffusion[1], of oxygen in poly(vinyl acetate) filled with 12.1% titanium dioxide, compared to the unfilled polymer. Differences in the activation energy of diffusion in the filled polymer, compared to the unfilled polymer, were also apparent in that the filled polymer showed the same activation energy above and below the polymer's T_g, whereas the unfilled polymer showed a *higher* value *above* the T_g. Results of the changes in diffusion activation energy, E_D, were attributed to changes in the internal pressure (p_{int}) of the system:

$$E_D = p_{\text{int}} \times \Delta V \tag{5.86}$$

where:

V = volume of activation (assumed to undergo negligible change in the filled, compared to the unfilled, polymer).

Theories relating films consisting of one polymer dispersed in another are typically based on the theories of capacitance and dielectric permittivity. The results of these theories have been summarised by Chainey [85] using the appropriate mathematical symbolism relating to polymer diffusion.

5.4 Permeation through polymer latex films.

The permeability of latex cast films, when compared to solvent cast films, may be further complicated, in addition to the aforementioned factors affecting the permeability of polymers, due to macro-structure of the films arising from the fusion of the latex particles themselves. The water vapour permeability of latex films prepared from a copolymer of carboxylated styrene-butadiene has been investigated by Richard [413] *et al.* Using labelled water and S.A.N.S., it was shown that sorption and diffusion occurred mainly along the hydrophilic (carboxylated) interparticle boundaries. The time dependent morphology changes that can occur ('further gradual coalescence') can also provide justification for changes in permeability properties.

Chainey [91] *et al.* measured permeability coefficients in films by a dynamic technique in which the penetrant was made to flow over one side of the film, and the permeating gas was swept away and analysed by katharometer. Films of poly(methyl acrylate), poly(ethyl

---

[1] The paper claims that the activation energy of the filled polymer is 56% that of the unfilled polymer, but the figures show this to mean a 56% *increase* rather than the implied decrease.

acrylate), poly(*n*-butyl acrylate), poly(methyl methacrylate), poly(ethyl methacrylate) and poly(*n*-butyl methacrylate) were cast from solution in butanone. Polystyrene films were cast from solution in toluene. The permeabilities to helium were determined at various temperatures and the activation energies of permeation calculated. There was found to be a trend of increasing permeability with decreasing polymer T_g, with activation energies of around 28 kJ mole^{-1}. Comparable latex cast films initially showed much higher permeability coefficients compared to the solvent cast films. However, a major problem arising from the flash casting technique employed, was the inherent irreproducibility in initial permeability coefficient between different films cast from the same latex. A large variation in initial permeabilities was also apparent in films flash cast from solution. However, the lowest values of permeability coefficient recorded were in good agreement with the lowest values obtained from those films dish-cast from solution. It was concluded that the higher permeabilities were due to imperfections in the film. Hence, several films were prepared for each variable examined, and the three lowest concordant results were taken to be correct.

The principal feature of PBMA (the polymer most studied due to its acceptable handling characteristics) latex film permeability was that the permeability coefficient was not constant, but decreased over a period of time. The initial value varied dependent upon the temperature at which the film was cast. Over a period of 320 hrs, however, the permeability dropped to a constant value, which was independent of the casting temperatures (between 393 K and 455 K) but was still more than double the value for the solvent cast film that did not vary over a period of several months. For freshly cast latex films, the activation energies were of the order of 7 → 8 kJ mol^{-1}, rising to 20 kJ mol^{-1} for a film aged 320 hrs. The activation energy for the aging (autohesion) process itself was estimated to be ca 25 kJ mol^{-1} for PBMA. Polymers of lower T_g aged faster, whilst poly(ethyl acrylate) appeared to age fully during casting. The failure in an attempt to discern effects of latex particle size and surface charge density in this study was presumably a result of the high temperatures necessary (all $>$ 393 K) for the flash coating process.

Balik[27] *et al.* found that for a commercial terpolymer (vinyl chloride, butyl acrylate and vinyl acetate) latex film, 30 K above its T_g, the CO_2 sorption isotherm resembled that of a glassy polymer. CO_2 solubility was much greater than that for the solvent cast film of the same polymer. CO_2 solubility and diffusivity decreased with aging time, but did not quite reach the solvent cast value even after 75 days at room temperature. It was suggested that solubility decrease was the dominant cause of reduced permeability upon aging, during which time the polymer density increased, for permeants of low solubility. Roulstone[423] found that for both water vapour transport, and 4-nitrophenol solute permeation, freshly prepared latex films had higher permeabilities than solvent cast films, but then aged to below the solvent cast value. The solubility coefficient, S, for 4-nitrophenol in the solvent cast film was greater than for the latex cast film. Kassis and List[323] also found that solvent cast Eudragit® films were less dense than the corresponding latex films, and that the latter were less permeable to water vapour.

Banker[29] *et al.* showed that water vapour had some affinity for PBMA in solvent cast films since the slope of the permeability coefficient, *P*, versus thickness plots was greater than the -1 (minus one) expected for Fickian behaviour. Roulstone [423] demonstrated Fickian behaviour for *4*-nitrophenol in PBMA solvent cast films and latex cast films, with respect to permeant solution concentration and film thickness, but, there was a negative time lag in that the rate of permeation started high and decreased towards the steady state value. (Senf[442] *et al.* have ascribed the presence of negative time lags in experiments where the permeability was determined spectrophotometrically {*e.g.*, in the work of Serota [446] *et al.*} to contaminants leaching from the film early in the experiment. Serota cites Fujita [176], however, for suggesting that negative time lags result from (i) two simultaneous diffusional flows of different diffusion coefficient, or a convective flow, or (ii) a time dependent diffusion coefficient, or (iii) a structural influence on the film by the permeant, before the attainment of a steady state flux.)

Roulstone [423, 426] prepared PBMA latex films over a range of temperatures (325 → 368 K) and times (3 → 20 hrs). The higher the temperature and the longer the casting time, the lower was the initial (*i.e.*, within 24 hrs of casting) permeability. Each of these films aged to a lower permeability upon storage for one month. Aging was enhanced at elevated temperatures, and slowed at sub-ambient temperature. This phenomenon is usually attributed to autohesion, or further gradual coalescence, but List and Kassis [323] invoked '***relaxation of enthalpy at room temperature***,' in this context, which was said to arise from the gradual removal of free-volume that had been frozen into the glassy state of the polymer after formation at high temperature.

Roulstone [423] found that the activation energies for the permeation of PBMA latex films prepared at a range of temperatures showed increasing values with increased casting temperature, reflecting decreased permeability. The activation energy, E_a, rose to 142 kJ mol^{-1} for a film prepared at 368 K and aged one month at ambient temperature. It can be envisaged that the interparticle boundaries in latex films form a low density network for permeation, and that increased coalescence, and therefore density, in these regions is the reason for the reduced permeation. When the permeants used by Roulstone were a series of structurally related anilines, the permeability increased with increasing molecular volume, paralleling the increase in solute solubility (for films prepared at 353 K for 3 hrs, and aged 1 month) so that a sieve mechanism did not seem appropriate for the interparticle regions.

Introduction, Chapter 6: Controlled Release Methods and Devices.

6.1 Introduction.

An example of the utilisation of latex coatings is by the pharmaceutical industry, in the preparation of drug coatings, and industries where similar technology may be employed in dispersion systems that might previously have relied on the periodic addition of a chemical. These coatings are of relevance to the work carried out in this study, by the fact that the experimental results produced here are based on films, and their additives, that are functionally typical of those used by the pharmaceutical industry: specifically, for protective (of the active agent) barriers and sustained or controlled release type coatings.

The aim of this Chapter is to introduce some of the ideas from the literature for the designs of various (controlled) release methods (based on the mechanisms discussed in Chapter 5), and also to introduce the Eudragit® latices: a commercial range of acrylate/methacrylate copolymers typical of those used by the pharmaceutical industry.

6.2 Polymers and the pharmaceutical industry.

Polymers have gained in importance in the pharmaceutical industry as both drug encapsulants and vehicles of drug carriage: either protecting an active agent during its passage through the body (or in storage by preventing moisture ingress [485]) until its release, or controlling its release. A conventional (*e.g.*, sugar) tablet coating has the disadvantageous side effect of delivering what may be an initially too high and, hence, harmful, dose of active agent (typically, drug is rapidly released from its dosage form, reaching a maximum concentration, which then decays exponentially until the next administration), to regions of the body where the drug may not be at its most effective; when the general aim of any medication is to generate a response in a specific area or organ of the body requiring treatment. These problems can be overcome to some extent by sustained/retarded release, and/or selective delivery of the drug to the targeted organs[*e.g.*, 178, 207, 208, 209, 400, 482]. **Advantages of controlled release** devices thus possibly include: delivery to the required site; delivery at the required rate; fewer applications; reduced dangers of overdose, or side effects; and also economic advantages by virtue of more efficient dosage, at the expense of possibly more complicated fabrication. Much of the relevant literature is very precise in that it either concentrates, for example, on a specific type of polymer offering suitable transport characteristics for an individual permeant, or concentrates on a range of permeants transported through a single polymer type, or concentrates on a unique application. This Chapter considers some of the various techniques.

6.2.1 Drug delivery.

In recent years, there have been numerous developments in polymeric carriers and controlled release systems (some commercially available devices have been described by Lonsdale [325]). A few examples mentioned in the literature include:

- ✗ films with the drug *in* a **polymer matrix**[e.g., 109, 127, 367] (**monolithic devices**);
- ✗ the drug contained *by* the polymer (**reservoir devices**)[e.g., 315];
- ✗ polymeric colloidal particles or **microencapsulates** (**microparticles, microspheres** or **nanoparticles**) in the form of reservoir and matrix devices [e.g., 127, 367];
- ✗ drug contained by a polymer containing a **hydrophilic** and/or **leachable additive** *e.g.*, a second polymer, surfactant or plasticiser, etc. to give a porous device, or a device in which the drug release may be osmotically 'controlled' (both reservoir and matrix devices)[e.g., 164, 343, 434, 559];
- ✗ **enteric coatings** (ionise and dissolve at a suitable pH)[e.g., 343];
- ✗ (soluble) polymers with (covalently) attached **'pendant' drug** molecules[81 → 83, 130, 436];
- ✗ devices where release rate is controlled dynamically: *e.g.*, the **osmotic pump**[479].

More recently, speculation in the literature has centred around the possibility of using the recently discovered large cage-like molecules such as the C_{60} Buckminsterfullerenes[107] ('Buckyballs') (1985[476]), or hyperbranched (starburst) dendrimers[10] (late 1970s). The latter are large, 350,000 molecular weight, uniform, hollow, polymer spheres with a surface area comparable to that of carbon black (1,000 $m^2\,g^{-1}$). Some of these hyperbranched dendrimers are even water soluble.

Ideally, the delivery mechanism should control the rate of release. The ideal release mechanism should be at a constant rate (zero order). However, changing concentration gradients or additive leaching leading to porosity, etc., within the release devices typically mean that the release of the drug varies as a function of time.

Lehmann[315] *et al.* give four advantages of the coating of small drug particles, as opposed to single tablets:

- ✗ coated particles will distribute over the stomach and intestine to give a more uniform release and reduce the effects due to local conditions such as pH;
- ✗ a drug can be coated with different coatings, or thickness of coating, to give the required release profile;
- ✗ disparate active ingredients can be coated individually; and
- ✗ the danger of dosage overdose due to coat faults or, alternatively, incomplete release of drug is reduced.

The size of the dosage form may be controlled by factors such as the potency of the drug, and the amount required (although this may be controlled to some extent by the use of either fillers, to enlarge the formulation, or division of the dose into more than one 'packet' to decrease physical size). Duration of release of the drug is a further factor that must be considered (including the transit time of the dosage form through the body, or to the required site of release) as must the means of administration (*e.g.*, oral or other means, *i.e.*, parenteral).

Polymers used in sustained release coatings are necessarily biocompatible, and ideally biodegradable. The literature gives examples of both naturally occurring polymers such as Aquacoat®[1] (ethylcellulose mechanically spheronised to sub-micron sized, aqueous based, pseudo-latex dispersions), and also synthetic polymers such as the Eudragit®[2] range of poly(acrylate, methacrylate) copolymers. (Comparisons of aqueous versus solvent cast coatings have been made by Hogan[240].)

6.2.1.1 Reservoir devices.

A typical approach to controlled release is to encapsulate or contain the drug entirely (*e.g.*, as a core[*e.g.*, 315]), within a polymer film or coat (*i.e.*, **microcapsules** or spray/pan coated cores). Film coating (with particular reference to polymers and their additives) has been reviewed by Kala[264] *et al.*, whilst microencapsulation has been reviewed by Arshady[16, 17, 18] (see also Chapter 2).

The various factors (discussed in Chapter 5) that can affect the diffusion process may readily be applied to reservoir devices (*e.g.*, the effects of additives, polymer functionality {and, hence, sink-solution pH} porosity, film casting conditions {see Chapter 4}, etc.) and, hence, the choice of polymer must be an important consideration in the development of reservoir devices. Modelling the release characteristics of reservoir devices (and monolithic devices) in which the transport of the drug is by a solution-diffusion mechanism therefore typically involves a solution to Fick's second law (unsteady-state conditions; concentration dependent flux) for the relevant boundary conditions. When the device contains dissolved active agent, the rate of release decreases exponentially with time as the concentration (activity) of the agent (*i.e.*, the driving force for release) within the device decreases (*i.e.*, first order release). If, however, the active agent is in a saturated suspension, then the driving force for release is kept constant (zero order) until the device is no longer saturated[115, 463]. Alternatively the release-rate kinetics may be desorption controlled, and a function of the square root of time (see paragraph 6.2.2).

Transport properties of coated tablets, may be enhanced compared to free-polymer films, due to the enclosed nature of the tablet core (permeant) which may enable the internal build-up of an osmotic pressure which will then act to force the permeant out of the tablet[e.g., 559].

Li and Peck[318] investigated the effect of deionised water on salt containing tablets coated in poly(ethylene glycol) (PEG)-containing silicone elastomer, and also the effects of water on free films. The release of salt from the tablets was found to be a mixture of diffusion through water filled pores, formed by hydration of the coating, and osmotic pumping. KCl transport through films containing just 10% PEG was negligible, despite extensive swelling observed in similar free films, indicating that porosity was necessary for the release of the KCl which then occurred by 'trans-pore diffusion.' Coated salt tablets, shaped as disks, were found to swell in deionised water and change shape to an oblate

---

[1] Aquacoat®, FMC Corporation, Food & Pharmaceutical Products Division, Philadelphia, U.S.A.

[2] Eudragit®, Röhm Pharma, Weiterstadt.

spheroid as a result of the build-up of internal hydrostatic pressure: the change in shape providing a means to measure the 'force' generated. As might be expected, the osmotic force decreased with increasing levels of PEG content. The lower PEG levels allowed water to be imbibed through the hydrated polymer; whilst the porosity resulting from the coating dissolving at higher levels of PEG content (20 → 40%) allowed the pressure to be relieved by the flow of KCl.

Li developed methods and equations, which by monitoring (independently) the release of two different salts (*e.g.*, KCl and NaCl) allowed the calculation of the relative magnitudes that both osmotic pumping and trans-pore diffusion contributed to the release of salt from the tablet. At low PEG levels, osmotic flow was increased to a greater extent than was trans-pore diffusion due to the generation of only a low pore number density: at a loading of 20%, both mechanisms contributed approximately equally to the release. The build-up of hydrostatic pressure, however, decreased the osmotic inflow, and osmotic pumping. At higher loadings of PEG, the hydrated film was more porous and less resistant to outflow of salt. Hence, although the osmotic pumping increased (compared to the lower loading), trans-pore diffusion was the dominant release mechanism. An osmotic release mechanism has also been reported for microcapsules containing a water soluble core [39].

6.2.1.2 Monolithic devices.

Monolithic (matrix) **devices** are possibly the most common of the devices for controlling the release of drugs. This is possibly because they are relatively easy to fabricate, compared to reservoir devices, and there is not the danger of an accidental high dosage that could result from the rupture of the membrane of a reservoir device. In such a device the active agent is present as a dispersion within the polymer matrix, and they are typically formed by the compression of a polymer/drug mixture or by dissolution or melting. The dosage release properties of monolithic devices may be dependent upon the solubility of the drug in the polymer matrix or, in the case of porous matrixes, the solubility in the sink solution within the particle's pore network, and also the tortuosity of the network [455] (to a greater extent than the permeability of the film), dependent on whether the drug is dispersed in the polymer or dissolved in the polymer. For low loadings of drug, (0 → 5% W/V) the drug will be released by a solution-diffusion mechanism (in the absence of pores). At higher loadings (5 → 10% W/V), the release mechanism will be complicated by the presence of cavities formed near the surface of the device as the drug is lost: such cavities fill with fluid from the environment increasing the rate of release of the drug.

It is common to add a plasticiser (*e.g.*, a poly(ethylene glycol)), or surfactant, or adjuvant, to matrix devices (and reservoir devices) as a means to enhance the permeability (although, in contrast, plasticiser may be fugitive, and simply serve to aid film formation [346] and, hence, decrease permeability – a property normally more desirable in polymer paint coatings). It was noted by Donbrow and Friedman [125], that the leaching of PEG acted to increase the permeability of (ethyl cellulose) films linearly as a function of PEG loading by increasing the porosity, however, the films retained their barrier properties, not permitting the transport of electrolyte. It was deduced that the enhancement of their permeability was as a result of the effective decrease in thickness caused by the PEG leaching. This was evinced from plots of the cumulative permeant flux per unit area as a function of time and film reciprocal thickness at a PEG loading of 50% W/W: plots showing a linear relationship between the rate of permeation and reciprocal film thickness, as expected for a (Fickian) solution-diffusion type transport mechanism in a homogeneous membrane. Extrapolation of the linear regions of the graphs to the time axis gave positive intercepts on the time axis: the magnitude of which decreased towards zero with decreasing film thickness. These changing lag times were attributed to the occurrence of two diffusional flows during the early stages of the experiment (the flow of the 'drug' and also the flow of the PEG), and also to the more usual lag time during which the concentration of permeant in the film is building-up. Caffeine, when used as a permeant, showed negative lag times. No explanation of this was forthcoming, but Donbrow noted that caffeine exhibited a low partition coefficient in the system, and that this was also a feature of aniline permeation [446] through polyethylene films which showed a similar negative time lag.

Efentakis[74, 137] *et al.* investigated the effects of added surfactants on (hydrophobic) matrix devices. It was thought that surfactant may increase the drug release rate by three possible mechanisms: (i) increased solubilisation, (ii) improved 'wettability' to the dissolution media, and (iii) pore formation as a result of surfactant leaching. For the system studied (Eudragit® *RL 100* and *RS 100* {see paragraphs 6.4.3 and 6.4.4} plasticised by sorbitol, Flurbiprofen as the drug, and a range of surfactants) it was concluded that improved wetting of the tablet led to only a partial improvement in drug release (implying that the release was diffusion, rather than dissolution, controlled), although the effect was greater for Eudragit® *RS* than Eudragit® *RL*, whilst the greatest influence on release was by those surfactants that were more soluble due to the formation of 'disruptions' in the matrix allowing the dissolution medium access to within the matrix. This is of obvious relevance to a study of latex films which might be suitable for pharmaceutical coatings, due to the ease with which a polymer latex may be prepared with surfactant as opposed to surfactant-free. Differences were found between the two polymers – with only the Eudragit® *RS* showing interactions between the anionic/cationic surfactant and drug. This was ascribed to the differing levels of quaternary ammonium ions on the polymer.

Composite devices consisting of a polymer/drug matrix coated in a polymer containing no drug also exist. Such a device was constructed by Bodmeier and Paeratakul [55] from aqueous Eudragit® latices, and was found to give zero order release by diffusion of the drug from the core through the shell. Laghoueg [301] *et al.* similarly produced a polymer core containing the drug, but coated this with a shell that was eroded by the gastric fluid. The rate of release of the drug was found to be relatively linear (a function of the rate limiting diffusion process through the shell) and inversely proportional to the shell thickness, whereas the release from the core alone was found to decrease with time.

6.2.1.3 Other methods of drug carriage and controlled release.

6.2.1.3.1 Variations on the theme of microspheres.

Kawashima [271] *et al.* have described methods for the preparation of hollow microspheres ('microballoons') with the drug dispersed in the sphere's shell, and also highly porous matrix-type microspheres ('microsponges') [272]. The microsponges were prepared by dissolving the drug and polymer in ethanol. On addition to water, the ethanol diffused from the emulsion droplets to leave a highly porous particle. Variation of the ratios of drug and polymer in the ethanol solution gave control over the porosity of the particle, and the drug release properties were fitted to the Higuchi model (see paragraph 6.2.2.1).

The hollow microspheres were formed by preparing a solution of ethanol/dichloromethane containing the drug and polymer. On pouring into water, this formed an emulsion containing the dispersed polymer/drug/solvent particles, by a coacervation-type process, from which the ethanol (a good solvent for the polymer) rapidly diffused precipitating polymer at the surface of the droplet to give a hard-shelled particle enclosing the drug, dissolved in the dichloromethane. At this point, a gas phase of dichloromethane was generated within the particle which, after diffusing through the shell, was observed to bubble to the surface of the aqueous phase. The hollow sphere, at reduced pressure, then filled with water, which could be removed by a period of drying. (No drug was found in the water.) A suggested use of the microspheres was as floating drug delivery devices for use in the stomach.

6.2.1.3.2 Pendent devices.

Scholsky and Fitch [436] developed a means of attaching a range of drugs such as analgesics and antidepressants, etc., by means of an ester linkage to poly(acrylate) ester latex particles prepared by aqueous emulsion polymerisation. These latices when passed through an ion exchange resin such that the polymer end groups were converted to their strong acid form could 'self-catalyse' the release of the drug by hydrolysis of the ester link.

Chafi[81] *et al.* cite a number of papers where drugs have been attached to polymers, and also where monomers have been synthesised with a pendent drug attached. The research group have also prepared their own dosage forms in which the drug is bound to a biocompatible polymer by a labile chemical bond [81, 83]; *e.g.*, polyanhydrides prepared from a substituted anhydride (itself prepared by reacting an acid chloride with the drug: methacryloyl chloride and the sodium salt of methoxy benzoic acid) were used to form a matrix with a second polymer (Eudragit® *RL*) which released the drug on hydrolysis in gastric fluid. Chafi has also described the use of polymeric Schiff bases suitable for use as carriers of pharmaceutical amines [82].

6.2.1.3.3 Enteric films.

Enteric coatings consist of pH sensitive polymers. Typically the polymers are carboxylated and interact (*i.e.*, swell) very little with water at low pH, whilst at high pH the polymers ionise causing swelling, or dissolving of the polymer. Coatings can therefore be designed to remain intact in the acidic environment of the stomach (protecting either the drug from this environment or the stomach from the drug), but to dissolve in the more alkaline environment of the intestine.

6.2.1.3.4 Osmotically controlled devices.

The osmotic pump is similar to a reservoir device but contains an osmotic agent (*e.g.*, the active agent in salt form) which acts to imbibe water from the surrounding medium via a semi-permeable membrane. Such a device, called the '**elementary osmotic pump**', has been described by Theeuwes [479]. Pressure is generated within the device which forces the active agent out of the device via an orifice (of a size designed to minimise solute diffusion, whilst preventing the build-up of a hydrostatic pressure head which has the effect of decreasing the osmotic pressure and changing the dimensions {volume} of the device). Whilst the internal volume of the device remains constant, and there is an excess of solid (saturated solution) in the device, then the release rate remains constant delivering a volume equal to the volume of solvent uptake.

6.2.1.3.5 Electrically stimulated release devices.

Yuk [557] *et al.* prepared monolithic devices using polyelectrolyte gels which swelled when, for example, an external electrical stimulus was applied, causing a change in pH. The release could be modulated, by the current, giving a pulsatile release profile.

6.2.1.3.6 Hydrogels.

Hydrogels find a use in a number of biomedical applications, in addition to their use in drug matrices (*e.g.*, soft contact lenses, and various 'soft' implants, etc.) [388, 408]. When used as monolithic deices the release profiles follow those described by the equations in paragraph 6.2.2.1 [545].

6.2.2 Drug-release models.

6.2.2.1 Diffusion controlled release; dispersed drugs and porous matrix devices.

Models, widely referred to in the literature, describing the drug release from a homogeneous matrix containing drug dispersed as discrete particles [234], and later revised for a porous polymer matrix [235], have been developed by Higuchi for **diffusion controlled release.** For a system in which the active agent is homogeneously dispersed, and assuming a pseudo-steady state release from a matrix in which the initial concentration of drug (C_d) is greater than the solubility of the drug in the polymer (S_p) by a factor of three to four (*i.e.*, greater than the saturation concentration so that the drug is present as a solid), then the change in the amount of drug released (dM_t) per unit area from a polymer slab, coinciding with a change in thickness of the drug-depleted region of the slab dh, is given by:

$$dM_t = C_d\,dh - \frac{S_P}{2}dh \qquad (6.1)$$

However, in terms of Fick's law:

$$dM_t = \frac{DS_P}{h}dt \qquad (6.2)$$

where:

D = diffusion coefficient of the drug in the polymer;
h = wetted penetration depth at time t.

Therefore, equating equations (6.1) and (6.2):

$$\left(C_d - \frac{S_P}{2}\right)h\,dh = DS_p\,dt \qquad (6.3)$$

and integrating:

$$\left(C_d - \frac{S_p}{2}\right)\frac{h^2}{2} = DS_pt \quad \Rightarrow \quad h = \left(\frac{2DS_pt}{C_d - {}^{S_p}\!/_{2}}\right)^{\frac{1}{2}} \qquad (6.4)$$

By substituting for *h* into the integrated form of equation (6.1), then the amount released over the exposed (to sink solution) area, *A*, of matrix is given by:

$$M_t = A\left(DS_p\left(2C_d - S_p\right)t\right)^{\frac{1}{2}} \tag{6.5}$$

In the situation when the matrix is porous such that granules of drug are connected by capillaries (diffusion through the polymer itself is assumed to be negligible), then an effective diffusion coefficient (D_{eff}) of the drug is assumed, given by:

$$D_{eff} = D_{sol}\frac{\varepsilon}{\tau_l} \tag{6.6}$$

where:

D_{sol} = diffusion coefficient in the surrounding medium (sink solution);
ε = porosity (void) fraction;
τ_l = tortuosity of the pores.

Then, the amount of drug released (M_t) from a porous polymer slab at time *t* is given by:

$$M_t = A\left[D_{eff}S_p\left(2C_d - \varepsilon S_p\right)t\right]^{\frac{1}{2}} \tag{6.7}$$

In terms of the drug's (equilibrium) partition coefficient (*K*) in the polymer, for a film of area *A*, then:

$$M_t = A\left(D_{eff}S_p\left[2C_d - S_p\left(\varepsilon + K(1-\varepsilon)\right)\right]t\right)^{\frac{1}{2}} \tag{6.8}$$

For the above model, Higuchi originally stipulated that the drug must be present at relatively high concentration (3 → 4 times the saturation concentration of the polymer) and was therefore dispersed as discreet particles. The situation where the matrix contained only a low concentration of drug (*i.e.*, drug 'dissolved' in the matrix) was investigated by Fessi[154] *et al.* When $A/\varepsilon \langle S_p$, then Higuchi's model was simplified to:

$$M_t = A\left(D_{eff}t\right)^{\frac{1}{2}} \tag{6.9}$$

6.2.2.2 Dissolution controlled release; first order drug release profiles.

When a film contains a drug, it is generally accepted that the release profile may be modelled using the aforementioned Higuchi model for *diffusion controlled release*. To test this hypothesis, it is usual to investigate the correlation between the amount of drug liberated per unit area, *Q*, ($Q = M_t/A$) as a function of the square root of time.

An alternative model tests for **dissolution controlled release**, and uses a first order rate equation:

$$\log(M_t) = \log(M_\infty) - \frac{kt}{2.303} \tag{6.10}$$

where:

k = rate constant.

This model, which requires correlation between the logarithm of the amount of drug released as a function of time, was developed by Sciarra and Gidwani [439, 440], based on the Noyes-Whitney [351] relationship for determining the rate of solution of a solid:

$$\frac{dC}{dt} = k(C_s - C_t) \tag{6.11}$$

where:

C_s = concentration of saturated solution;
C_t = concentration of the drug in solution at time t.

Although admitting that Sciarra's first order relationship might be applicable in certain circumstances, Donbrow and Friedman [126] were somewhat sceptical as a result of their finding that some results agreed with both the first order release dissolution controlled model *and* the Higuchi diffusion controlled model. More rigorous mathematical testing showed the diffusion controlled model gave better correlation, and a similar treatment performed on Sciarra's results led to a corresponding conclusion. However, this is possibly ascribed to both dissolution and diffusion controlled release mechanisms occurring simultaneously.

In a later paper on the release of a water soluble core, from an ethyl cellulose microcapsule, Benita and Donbrow [39] found osmotic pressure led to pore formation and a dissolution model based on the Hixson-Crowell cube-root law [236] was found to fit the data:

$$W^{\frac{1}{3}} = W_0^{\frac{1}{3}} - kt \tag{6.12}$$

where:

W = amount of drug remaining in microcapsule at time t;
W_0 = initial amount of drug;
k = constant (defined in the paper).

A plot of $W^{1/3}$ versus time, t, showing better correlation than either a first order fit, or a Higuchi-type (square root of time) fit.

6.2.2.3 Osmotic drug release.

A device in which an osmotic pressure may result in the release of drug, may also have a contribution to the release profile by Fickian diffusion. Hence, the following type of equation, in which subscript '*O*' refers to the osmotic component and '*F*' to the Fickian component, has been used by both Zentner [559] *et al.*, and Theeuwes [479] to describe the drug release from such a device:

$$\frac{dm}{dt} = \left(\frac{AS}{l} L_p \sigma \Delta\Pi\right)_O + \left(\frac{PAS}{l}\right)_F \tag{6.13}$$

where:

dm/dt = release rate;
A = surface area of device;
S = solubility of drug core;
l = shell wall thickness;
$L_p\sigma$ = filtration coefficient (or hydraulic permeability) × Staverman reflection coefficient;

Π = osmotic pressure;
P = solute permeability coefficient.

The change in volume (V) due to the osmotic pressure (assuming no hydrostatic pressure) is given by:

$$\frac{dV}{dt} = \frac{A}{l} L_p \sigma \Delta \Pi \qquad (6.14)$$

6.2.2.4 Summary of practices in the literature on controlled release from pharmaceutical devices.

Much of the literature that claims zero order release, or Higuchi ($t^{\frac{1}{2}}$) type release, are in fact only claiming a pseudo zero order (etc.) release: the release eventually showing an exponential decay as, for example, the drug supply is exhausted. This, however, may be insignificant (depending on the time at which the release profile changes), albeit wasteful of the drug, due to the finite time a device may remain in the body.

For the case where the drug is dissolved in the device, various equations exist for the ideal diffusion controlled release (*i.e.*, assuming no lag, and no boundary effects), for various geometries of device, and these have been summarised by Wood [545]. Initially, the release is modelled as a function of the square root of time, but as the drug is exhausted the release decays exponentially, and is also a function of the shape of the device: *e.g.*, the following equations relate to the release from an infinite slab[1]:
Initial release:

$$\frac{M_t}{M_\infty} = 4\left(\frac{Dt}{\pi l^2}\right)^{\frac{1}{2}} \qquad (6.15)$$

where:
M_t = amount release at time, t;
M_∞ = total theoretical amount to be released (*i.e.*, initial drug load in the film);
D = diffusion coefficient;
l = slab thickness.
Final release:

$$\frac{M_t}{M_\infty} = 1 - \frac{8}{\pi^2}\exp\left[\frac{-\pi^2 Dt}{l^2}\right] \qquad (6.16)$$

Other equations exist to account for the shapes of the devices being, for example, spherical or cylindrical, and variations of the above equations are common in the literature, where researchers attempt to account for factors such as, for example, swelling, or the finite size of a device.

Matrix devices containing a programmed drug concentration profile [319] have been shown to allow the release properties to be varied in order to maintain a zero order release profile, at the expense of increased difficulty of fabrication.

---

[1] By defining as infinite, edge effects can be ignored.

Table 6.1 Experimental versus desired results to the Lammas [303] study for a sustained release drug coating.

TIME	REQUIRED	PERCENTAGE RELEASED		
		UNCOATED	5% COAT	10% COAT
2	25 → 50	86	67	45
4	45 → 73	100	82	60
6	60 → 88	100	89	72
12	〉88	100	97	96

6.3 Latex coating for controlled drug release.

Tablet coating is one of the oldest arts employed in the pharmaceutical industry, dating from 1838 (though even earlier than this, the ancient Egyptian Pharaohs used gilded tablets for the supposed aphrodisiac qualities of the gold). Sugar coating was used to mask unpleasant tastes and odours and to protect ingredients from the effects of air and moisture. Some twenty coats of syrups, containing gelatin, acacia gum and bulking agents held in suspension, could be involved in sealing, undercoating, colouring and polishing in sugar coating: a process taking many days to complete. Film coating evolved in the early nineteen fifties, with the preparation of the first commercial non-enteric coating, and was less labour intensive, and less specialist skill was required. Mostly solvent based coating has been used, but environmental acceptability, toxicity, flammability and explosion hazards have promoted interest in water based coatings. Latex can be the preferred choice for such spraying applications, even when water is a potential solvent for the substrate (as might be the case in drug coatings), because of the low viscosity and high loading of the latex (or pseudo latex) formulation [50]. The means of applying a coating to tablets, or beads, has traditionally been to use a rotating pan with drop-wise addition of the coating material. A modern alternative is the use of a fluidised bed with atomizer spray, *e.g.* the Aeromatic[1]. The coating quality of the latter depends upon six interdependent experimental parameters: *i.e.*, air temperature; air speed; height of beads; time of application; atomizer pump speed; and atomizer air pressure, thus giving 6! (*six factorial*) combinations to optimise the process. Also, 1 kg of core material is the minimum charge for this apparatus making it unsuitable for small scale research involving only modest quantities of latices.

In a study by Lammas [303], beads were prepared from an Avicell/Ibuprofen mixture (1:1) which was blended, then extruded and spheronised. Eudragit® *NE 30 D* (see paragraph 6.4.1) with 10% hydroxypropyl methylcellulose (HPMC) gave a sustained release coat. Results compared with the specific requirements as shown in **Table 6.1**.

By coating beads of the above mentioned type with surfactant-free PBMA, Roulstone [423] showed decreased release rates with increasing coating temperature, and

---

[1] Aeromatic Laboratory Model fluidised bed processing unit, type Strea-1, ACM Machinery, Tadley, Hampshire, England.

these rates decreased upon aging at room temperature over four days, and were further reduced, by aging at 333 K for a further two days, to rather similar values. At lower temperatures, the beads appeared (by S.E.M.) to have cracked surfaces, but when heated at 333 K, sufficient polymer flow occurred to heal the cracks. Surface exudations of crystalline material were attributed to Ibuprofen (2-(4-isobutylphenyl)propionic acid, $C_{13}H_{18}O_2$) having been dissolved in the water applied with the latex, and then exuded to the drying surface, which probably explains why immediate release of drug was observed without a time lag.

When a latex was used to coat pellets, Bodmeir and Paeratakul[57] noted that somewhat heterogeneous porous films resulted (depending upon the equipment and the spraying conditions used) which was in contrast to the non-porous surface structure of free films. This poor quality of coatings is a feature much in evidence in the literature, and is possibly a result of coating a water soluble core with an aqueous coating: ideally the water should be evaporated as quickly as possible. However, this too may have detrimental effects on the quality of the coat. It has also been claimed[250] that if the core material is porous, and the coating solvent does not dry immediately, then capillary action will suck the coating into the pore – again reducing the coating quality.

Ghebre-Sellassie[187, 188] *et al.* observed that the porous nature of latex film coated devices resulted in drug diffusion through water-filled pores being the dominant mechanism in dissolution studies, rather than diffusion through the polymer.

6.4 Eudragit® latices.

Röhm Pharma GMBH (Weiterstadt) produce a range of commercially available acrylate latices designed for pharmaceutical coatings. The latices are available as dried powders/granulates, aqueous dispersions, and organic solutions (in isoproponol or isopropanol/acetone). In addition to 'simple' synthetic resin drug coatings[e.g., 316], the research literature describes their utilisation in all types of controlled release systems, *e.g.*, microparticles[e.g., 128], matrix devices[e.g., 74], reservoir devices[e.g., 315], etc.

The Eudragit® products are typically distinguished as to polymer type, and solvent (if any) by a product code based upon the following:

- ✗ *NE* meaning Neutral Ester;
- ✗ *L* meaning 'leichtlöslich' or 'freely soluble' in the case of Eudragit® *L*, or 'leichtdurchlässig' or 'freely permeable' when preceded by an *R*, as in the case of Eudragit® *RL*;
- ✗ *S* meaning 'schwerlöslich' or 'slightly soluble' in the case of Eudragit® *S*, or 'schwerdurchlässig' or 'slightly permeable' in the case of Eudragit® *RS*;
- ✗ *100* meaning powder or granulate (*i.e.*, ≈ 100% polymer solids);
- ✗ *30* or *12.5* declaring the percentage solids content in a dispersion or solution;
- ✗ *D* meaning dispersion.

These codes are thus grouped to indicate the product: *e.g.*, Eudragit® *NE* 30 *D* is thus a neutral ester, aqueous dispersion of 30% dry polymer solids content.

Typical applications and properties of some of the main Eudragit® latices are indicated below as detailed in the Eudragit® product brochure[147].

6.4.1 Eudragit® *NE 30 D.*

A neutral and, hence, pH independent, copolymer consisting of poly(ethyl acrylate, methyl methacrylate) (2:1). Supplied as an aqueous dispersion of 30% polymer solids, with a faint but characteristic odour. The polymer has a mean molecular weight (M.W.) of 800,000, The product is stabilised by iso-nonyl phenyl poly(ethylene glycol) (M.W. 5,000 → 6,000); it does not contain, nor require, a plasticiser[147]. Göpferich and Lee[204] found, using D.S.C., a phase transition at 323 K, which spectroscopic evidence implied was due to the nonyl-phenyl surfactant. Eudragit® *NE* produces clear polymer films, that are water insoluble, but swell and are permeable. Röhm Pharma quote typical applications for Eudragit® *NE 30 D* as being a binding agent, or controlled release coating. This product was previously referred to Eudragit® *E 30 D*, but this should not be confused with the current products entitled Eudragit® *E 100* or *E 12.5* which are cationic copolymers based upon dimethylaminoethyl methacrylate and neutral methacrylic acid esters, supplied as solids or in organic solution. Goodhart[199] *et al.* quote the M.F.F.T. and film softening temperature of *E 30 D* (and thus presumably *NE 30 D*) as being (293 K and 320 K, respectively, whilst Lehmann[313] quotes the M.F.F.T. of Eudragit® *NE* as 278 K. The T_g is given as 265 K[204].

6.4.2 Eudragit® *L 30 D.*

An aqueous dispersion (30% W/W) of an anionic copolymer based on methacrylic acid/ethyl acrylate (*i.e.*, poly(methacrylic acid, ethyl acrylate)). As supplied, the latex has a pH of 2.5. In the most recent product brochure[147], it is stated that the dry polymer contains 0.7% sodium dodecyl sulphate and 2.3% polysorbate 80 as emulsifiers. The ratio of free carboxyl groups to ester groups is 1:1, and the polymer has a mean molecular weight of 250,000. The Eudragit® is supplied plasticiser free, but forms quite brittle films, and the use of a plasticiser is recommended. List and Kassis[323] quote a T_g for the polymer of 302 K,

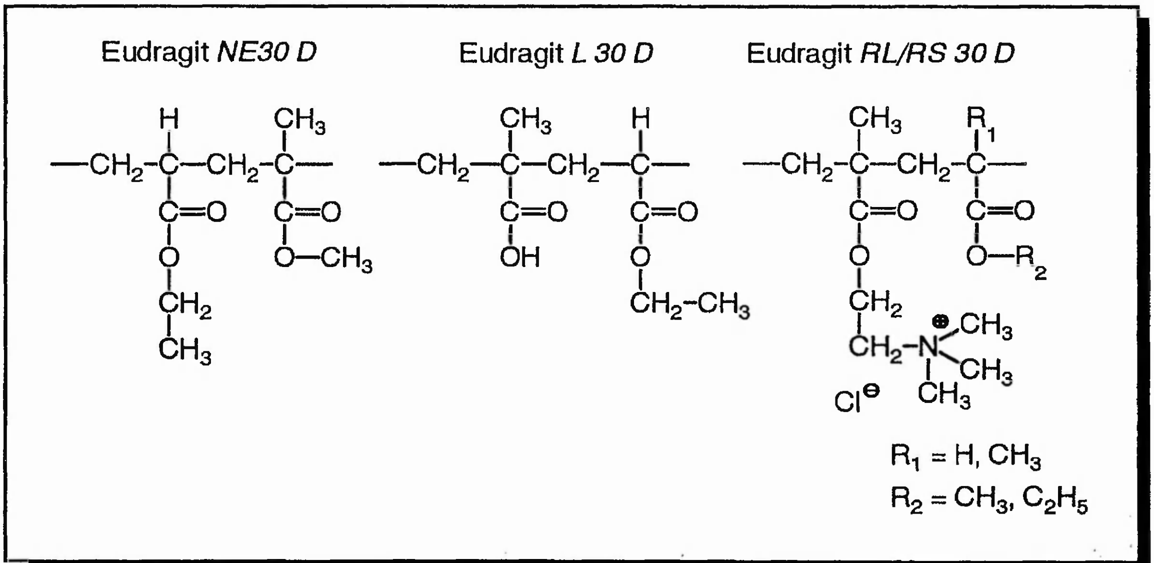

Figure 6.1 Structures of the Eudragit® polymers.

and Lehmann [313] agrees quoting a value 303 K. Eudragit® *L 30 D* has a much stronger, sour, odour than Eudragit® *NE*. Due to the carboxyl groups, Eudragit® *L 30 D* is soluble in neutral to alkaline solution (pH ⟩ 5.5) forming polymeric salts, but is "largely impermeable to water" below pH 5.0. It is thus suitable for the preparation of enteric type dosage forms: being insoluble in gastric fluid of the stomach, but soluble in intestinal fluid [314].

A range of solid (powder/granule) Eudragits® based on a similar copolymer (poly(methacrylic acid, methyl methacrylate)) (M.W. 135,000) are also available: *e.g.*, Eudragit® *L 100* (and also Eudragit® *L 100-55*, which is a re-dispersable spray-dried powder of Eudragit® *L 30 D*, *i.e.*, based on methacrylic acid and ethyl acrylate). Eudragits® *L 12.5 P* and *L 12.5* are organic solutions of the same copolymer as Eudragit® *L 100*. The poly(methacrylic acid, methyl methacrylate) copolymer has a M.F.F.T. of 358 K [313].

6.4.3 Eudragit® *RL 30 D*.

An aqueous dispersion of copolymer based on acrylic and methacrylic acid esters, with a low content of quaternary ammonium salts: poly(ethylacrylate, methyl methacrylate) trimethylammonioethyl methacrylate chloride. The ammonium groups, which are responsible for the permeability of Eudragit® *RL* films, are present as polymeric salts (which virtually totally dissociate at pH 2 to above pH 8, and thus the permeability is pH independent in the physiological pH range). The molar ratio of neutral ester groups to ammonium groups is 20:1, and the polymer has a mean molecular weight of approximately 150,000.

The films formed from Eudragit® *RL* are glossy and are water insoluble. Such films are inert to endogenous digestive fluids: Lehmann [315] *et al.* states that the Eudragit® *RL* (& *RS*) polymer backbone is stable and non-biodegradable, whilst the ester groups are also stable and hydrolysed to ⟨ 1% in the body. Films produced from Eudragit® *RL* are swellable and permeable: the permeability of such dispersions being controllable by the ability of the latex to be mixed with other such Eudragits®. Röhm Pharma state typical uses of Eudragit® *RL* as being readily disintegrating coatings and sustained release (retard) formulations.

Eudragit® *RL 30 D* is a pseudo-latex prepared by emulsification of the (bulk polymerised) polymer in hot water, without the aid of an emulsifying agent [56, 313]. It contains sorbic acid (0.25%) as a preservative, but no emulsifiers or other additives [147]. Lehmann quotes an M.F.F.T. for Eudragits® *RL* and *RS* as between 313 K and 323 K and a T_g of 328 K. The use of a plasticiser is recommended at concentrations of up to ca 20% to improve film handling and reduce the film formation temperature by approximately 20 K. Jenquin [255] *et al.* determined the T_g of the comparable powder mass[1], Eudragit® *RL 100*, as being approximately 328 K.

6.4.4 Eudragit® *RS 30 D*.

This pseudo-latex is similar to Eudragit® *RL 30 D*, but the ratio of ester groups to quaternary ammonium groups is less at 40:1, (*cf.* 20:1 for Eudragit® *RL*). The permeability

---

[1] Eudragit® *RL/RS* powder mass additionally contain talc (0.5%) to promote flow.

of Eudragit® *RS* films is therefore reduced in comparison to Eudragit® *RL* films. Whereas the high permeability of Eudragit® *RL* delays release of the active substance very little, Eudragit® *RS* gives a much greater delay (obviously dependent on film thickness and solubility/size of the active substance). Like Eudragit® *RL*, Eudragit® *RS* also contains 0.25% sorbic acid but no other additives [147].

A range of organic solutions, in isopropanol/acetone, and of polymer solid based on acrylic/methacrylic acid ester and quaternary ammonium groups are also available, suitable for use as sustained release film formers. The T_g of the comparable powder mass, Eudragit® *RS 100* was measured by Jenquin [255] as being approximately 325 K.

6.4.5 Other Eudragits®.

Other Eudragits® include **Eudragit® *S*** and **Eudragit® *E***. Eudragit® *S* is similar to Eudragit® *L*, being based on a copolymer of methacrylic acid/methyl methacrylate. However, the ratio of free carboxyl groups to ester groups is 1:2 (*cf.* 1:1 for Eudragit® *L*) and is consequently of lower permeability, and is soluble at pH $>$ 7 (*cf.* pH $>$ 5.5 for Eudragit® *L*).

Eudragit® *E*. is a cationic copolymer of neutral methacrylic acid esters and di-methylaminoethyl methacrylate suitable for enteric type coatings, forming soluble salts, with acids, up to pH 5. The *E* in the name denotes *'end'* coat. *i.e.*, it is suitable for producing a taste masking final, glossy, coat for oral dosage forms, due to it being insoluble in the saliva of the mouth (weakly alkaline at pH 6 → 7).

◆

Experimental, Chapter 7: Procedures & Analysis of Results.

7.1 Introduction.

This Chapter details the experimental methods and materials used during the course of this study. Where appropriate, **chemical hazard/handling warning** indications are included, marked in the body text with an: ^{H}. Chemical hazard data sources of reference include the BDH[38], and Sigma-Aldrich[317] chemical hazard books.

7.2 Cleaning of glassware.

All glassware was initially cleaned using organic solvent (either toluene^{H} acetone^{H} or butan-2-one^{H}) to remove any grease or traces of polymer. This was followed by drying and finally rinsing with either distilled water, or in the case of the polymerisation vessels, with Fisons analytical grade water[1], until the conductivity of the rinsing solution approximated that of the clean water ($\approx 1.5\ \mu S\ cm^{-1}$, allowing for dissolved CO_2).

The glass substrates used for film casting (see paragraph 7.6.2) were cleaned as above, but with an intermediate stage of soaking in chromic acid^{H}.

7.3 Procedure for surfactant-free emulsion polymerisation.

7.3.1 Materials.

The basic **recipe** for a typical surfactant-free emulsion polymerisation consisted of:

water;
initiator;
buffer to regulate pH;
monomer; and
N_2 gas – to maintain an O_2-free atmosphere.

The water used was supplied by Fisons[1] as the AnalR Grade, (or in the case of the AMA polymerisations was double distilled water, from an all Pyrex glass two-stage still, freshly prepared prior to the polymerisation).

Monomers^{H} used were supplied by, BDH or Polysciences, and included: amyl methacrylate[2]; butyl methacrylate[3]; and hexyl methacrylate[2] (**Figure 7.1**). Acrylic acid[4] (CH_2=CHCOOH) was used to prepare the shell of the core-shell latices.

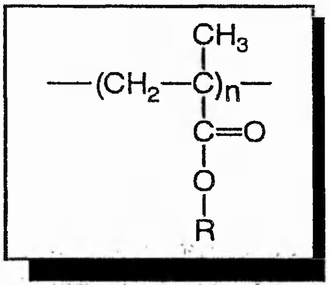

$$-(CH_2-C(CH_3)(C(=O)OR))_n-$$

Figure 7.1 Poly(alkyl methacrylate).
R = C_mH_{2m+1}

---

[1] Fisons PLC, FSA Lab. Supplies, Loughborough, UK.
[2] Polysciences (U.K.) Ltd., Moulton Park, Northampton, UK.
[3] BDH Chemicals Ltd., Poole, Dorset, UK.
[4] Aldrich Chemical Co. Ltd., Gillingham, Dorset, UK.

7.3.2 Determination of monomer solubility.

Most monomers used in aqueous, surfactant-free, emulsion polymerisations are of low water solubility. The solubility of the monomers used in this study was measured by determining the concentration of monomer in a saturated aqueous monomer solution. Analysis for the **total dissolved organic carbon** in the water, was performed by the National Rivers Authority[1]. The test involved the sample's decomposition by oxidation. The sample was injected into a reactor containing acidified ammonium persulphate, and UV-irradiated for 3 → 5 minutes. After being sparged with N_2, the evolved CO_2 was then measured by infra-red spectroscopy.

Preparation of the samples required that the monomer was cleaned of inhibitor (see paragraph 7.3.3.1) and an excess (of monomer) added to water (the water having been previously tested for dissolved organic carbon to provide a controlled 'background' level), and stored, with stirring, for 24 hrs. (All glassware having been cleaned by autoclaving, and with chromic acid^{H}.) At the end of this period, the monomer/water mixture was transferred to a separating funnel and vigorously shaken. After phase separation, an aliquot of the (lower) aqueous layer was removed for analysis.

The results were in the form of total dissolved organic carbon (mg dm^{-3}). It was therefore possible to determine the percentage solubility from the known number of carbon atoms of the monomer in the saturated solution, once the 'background' value of dissolved carbon was accounted for. *E.g.*, for styrene monomer, with eight carbons, if the total carbon is 245 mg dm^{-3}, then the percentage solubility (W/W) is given by:

$$\textit{Percentage Solubility} = \frac{245 \times 10^{-3}}{1000} \times \frac{1}{8} \times 100\% \qquad (7.1)$$

7.3.3 Preparation of materials.

The majority of materials were used as supplied with the exception of the following.

7.3.3.1 Monomers.

The monomers, as supplied, contained an **inhibitor** (quinol^{H} {or hydroquinone}) to prevent polymerisation during transportation and storage.

All monomers (with the exception of AA) were cleaned by repeated **washing with a caustic (1%)/carbonate (25%) solution** (by vigorous shaking, in a separating funnel): the carbonate simply acting to further decrease the monomer solubility in the aqueous solution. The monomer was given a final rinse with Fisons analytical grade water (as used in the polymerisation), which was then run off, and the monomer was left to stand overnight at 278 K such that any remaining water formed a further aqueous layer which was removed. Because of their low water solubilities (see Chapter 9), the monomers were not dried further.

---

[1] N.R.A. Severn Trent Region, Nottingham Laboratory, Nottingham, UK.

BMA monomer and AA were **distilled under reduced pressure** in an O_2-free N_2[1] atmosphere. Liquid $N_2{}^H$ was used as a coolant to condense the distillate, and also in the cold traps used to protect the vacuum pump. The first and last 5% of the distillate were always discarded.

AMA and HMA monomers have too high molecular weights and, hence, boiling points to be easily distilled. Riddle [415] recommends cleaning these higher molecular weight monomers by the aforementioned caustic-washing alone.

7.3.3.2 Testing for monomer contaminants.

Contamination of the monomer by trace amounts of polymer was determined by shaking the monomer with anhydrous methanol^H in the ratio 1:50. The presence of polymer was indicated by the formation of a cloudy precipitate in a period of under 5 min.

The quantity of quinol inhibitor in BMA (the monomer used most often) was determined spectrophotometrically using the following method provided by BDH[2]. The absorbance of a solution of BMA (10%) in methanol^H was measured at 295 nm against a methanol blank in a 1 cm quartz cell. The concentration (parts per million) of quinol^H was then given by:

$$[Quinol] = \frac{Absorbance\ @295\,nm}{0.295} \times 100\,\text{ppm} \tag{7.2}$$

The BDH specification stated that the BMA contained quinol at a concentration of 0.01% (corresponding to 100 ppm). Using the above method, the uncleaned monomer was found to contain an average of 99.5 (±0.2) ppm. After caustic-washing, using four parts of caustic solution to one part of monomer, and distillation, this figure was found to decrease to 2.7 (±1.4) ppm. Washing alone was found to decrease the inhibitor levels to a similar figure, but would not have removed any polymer that may have been present. (NB. Instrument resolution was 0.34 ppm.)

7.3.3.3 Initiator.

Potassium persulphate^H ($K_2S_2O_8$) initiator[2] was recrystallized (typically 24 hrs prior to a polymerisation) from a saturated solution of cold water (Fisons analytical grade). The product was dried in a desiccator, and stored in the dark before use.

7.3.3.4 Polymerisation method.

Polymerisations were performed using either a 0.5 dm^3 or 1 dm^3 four necked (ground-glass jointed) round bottomed flask (in a constant temperature water bath), fitted with a cold water reflux condenser, stirrer and nitrogen bleed. The reaction vessel was initially charged with most of the water to be used (buffered to pH 7 → 8 with potassium hydrogen carbonate); a 50 ml aliquot being held aside to dissolve the initiator. The vessel was continuously stirred, at 250 r.p.m., using a P.T.F.E. paddle-type stirrer mounted

---

[1] O_2-free, "white spot grade" – supplied by BOC Ltd., Brentford. Middlesex, UK.
[2] BDH Chemicals Ltd, Poole, Dorset, UK.

Table 7.1 Typical polymerisation recipes.

RECIPE	BMA MONOMER	HMA OR AMA MONOMERS
MONOMER	45 g	45 g
WATER	450 g	450 g
INITIATOR	0.85 g	0.5 g
BUFFER	0.2 g	0.2 g
TEMPERATURE	323 K	323→353 K

through the central neck of the flask at a height just above (≈ 1 mm) the bottom of the flask (to allow reproducible positioning of the stirrer for each and every reaction). Following addition of the water to the flask, N_2[1] was bubbled through the water, via a narrow bleed inserted into one of the flask's necks, from this point onwards, and the water was allowed to equilibrate for approximately 1 hr. The monomer was then added to the flask, after being outgassed with N_2, via the fourth neck of the flask that was sealed with a ground glass stopper during the course of the reaction, and again the vessel was left to equilibrate for 30 min. The N_2 flow was also reduced at this point, to a level just sufficient to maintain a N_2 atmosphere, in an attempt to reduce monomer evaporation. Finally, the initiator was dissolved in the remainder of the water, outgassed with N_2 for approximately 5 min, and added to the vessel. This point was taken as time zero for the reaction. At this time, the N_2 bleed was exchanged for a shorter one whose end remained above the level of the reactants to prevent it becoming blocked.

Table 7.1 shows typical recipes for the polymerisations. Note: these values are for the 1 dm^3 flask, and that the HMA and AMA reactions were carried out at a number of temperatures.

7.3.3.5 Shot-growth polymerisations.

The **core-shell** type polymers were prepared by the addition of a shot of a second (shell) monomer to a polymerisation already at high percentage conversion of (core) monomer to polymer (*e.g.*, in the region of 90% conversion). The core monomer used was BMA, and the reaction was performed under surfactant-free conditions, with the core monomer recipe as that for BMA shown in **Table 7.1**. The shot used was AA.

The shot of AA (0.9 g) was added at a degree of conversion determined (see paragraph 7.4.1) by monitoring a previous BMA polymerisation reaction of identical recipe. The shot was flushed with N_2 before addition, and its size (mass) was estimated from the ratios of core monomer to shot monomer used by Sakota and Okaya [432] in work on carboxyl groups in carboxylated polystyrene copolymers.

---

[1] O_2-free, "White Spot grade" – BOC Ltd., Brentford, Middlesex, UK.

7.4 Latex particle characterisation.

7.4.1 Determination of percentage conversion/percentage solids.

Percentage conversion of monomer to polymer was determined (via percentage solids calculations) **gravimetrically** by sampling the polymerisation mixture at intervals during the course of the reaction. This was performed to determine the final extent of the polymerisation, and to determine at what time the reaction was completed.

Samples were withdrawn from the reaction vessel by means of a pipette inserted through the auxiliary neck of the flask, allowing the N_2 atmosphere to be maintained by means of the positive pressure supplied from the nitrogen bleed. The stirrer was switched off at approximately 2 min before the sample was extracted to allow phase separation and prevent monomer from being removed from the reaction vessel. The pipette was then inserted under the monomer layer into the aqueous layer to remove the sample.

On removal from the reaction vessel, the samples were sealed in screw top specimen bottles, and were immediately put into an ice bath to quench the reaction. As an alternative method, the reaction in the sample bottles was quenched by adding quinol[1]. Both techniques were found to give the same result, within the limits of experimental uncertainty, and the former method was used in the majority of reactions.

After cooling, a sample was placed into an aluminium dish, of known weight, and weighed (termed *wet weight* in the following equation). The dish (+ sample) was then placed in an oven at 353 K and left until constant weight was achieved, at which time the weight was again recorded (termed *dry weight* in the following equation). The percentage solids of the sample and, hence, the reaction was then given by the following equation:

$$\text{Percentage Solids} = \frac{\text{Dry weight}}{\text{Wet weight} - \text{Dry weight}} \times 100\% \qquad (7.3)$$

From the known initial weight of monomer used in the reaction, the final theoretical weight of polymer, at 100% conversion, can be determined allowing the percentage conversion to be calculated throughout the reaction by sampling at various intervals.

By deliberately doping such a sample with monomer, it was shown that any monomer withdrawn from the reaction as part of the sample would be evaporated off during the oven-drying, rather than polymerising to give a false value of percentage solids. Similarly, residual initiator, and other inorganic, fragments from the reaction recipe were ignored, during this calculation, since they were insignificant compared to the mass of polymer.

7.4.2 Determination of critical coagulation concentration.

The **critical coagulation concentration** (C.C.C.) of the surfactant-free latices was measured (using a method described by Hiemenz[232]) utilising barium chloride, as a measure of their stability. To a series of samples of the latex (500 μl) various ratios of

---

[1] BDH Chemicals Ltd., Poole, Dorset, UK.

electrolyte and water were added (by syringe), such that the total dilution was kept constant whilst different amounts of salt were added. After mixing, the solutions were allowed to stand for 24 hrs, after which time the sample containing the lowest concentration of salt to cause a precipitate was recorded. The procedure was then repeated – adding electrolyte at concentrations between this recorded level and the concentration below it from the previous set of experiments. This allowed the C.C.C. to be encompassed, and it was then calculated from the lowest concentration of electrolyte to cause precipitation.

7.4.3 Determination of latex particle size.

Using samples taken from a polymerisation reaction and quenched as above, particle diameters were determined by **photon correlation spectroscopy** (P.C.S.) in a Malvern[1] Zetasizer 3, fitted with an AZ10, thermostated, sizing cell. Samples were normally measured at an angle of 90° to the incident laser light, however, multi-angle measurements were possible, using the additional Malvern multi-angle data analysis software (Malvern part number 7032MA). This attempts to resolve sample polydispersity (or more importantly to check sample monodispersity).

For many of the latices used in this study, the use of P.C.S. (as opposed to T.E.M.) for particle sizing was a necessity due to the fact that the electron beam of an E.M. was liable to damage particles made of soft (low T_g) polymer. When 'soft' particles are observed under an E.M., the polymer is seen to flow. This results in pictures of such particles being poorly defined and, hence, of little use for sizing purposes.

7.4.3.1 Sample preparation and Zetasizer operation.

Before experimental samples were measured for particle diameter, the P.C.S. apparatus was tested for correct operation (*e.g.*, tested for correct optical alignment, and for contamination of the constant temperature sample-bath water: both of which could lead to possible erroneous results) by measuring the size of a 'standard' latex (Malvern AZ55 electrophoretic standard) of known particle size (*i.e.*, 317 nm).

Samples were prepared by diluting a latex, with Fisons AnalR grade water, until slightly turbid. The Zetasizer 3 displayed an indication, on a sliding scale, of the ideality of sample dilution. Too great a concentration led to false results due to inter-particle back-scatter on the photomultiplier, whilst too dilute a concentration provided insufficient scattering intensity for a measurement to be made. This latter problem, combined with small particle size, was the basis for the inability to size samples taken early in a reaction.

The P.C.S. data is interpreted by the Zetasizer dependent on the initial instrument set-up. The two main methods are the '**cumulants method**' and the '**exponential sampling method**.' Similarly, which of the two light scattering theories is used (Rayleigh {for small particles with respect to the wavelength of light} or Mie {for larger particles}), is also dependent on the initial instrument settings.

---

[1] Malvern Instruments Ltd., Malvern, Worcestershire, UK.

The cumulants method gives only a measure of the '**z-average mean**' particle size and a measure of the sample the polydispersity. (The z-average mean size is a measure of the particles' size, defined by Malvern as "the mean particle size weighted by the amount of light scattered by each size of particle in the sample.") This method is used when the sample distribution width is not known such that an estimated value of one is entered when setting up a measurement. (An estimated value can be set to shorten the experimental time by reducing the range over which analysis is made. A value of one causes the instrument to work over the whole of its range.) The analysis fits the logarithm of the P.C.S. correlation function to a polynomial series:

$$F(t) = A + Bt + Ct^2 + \ldots \text{etc.} \tag{7.4}$$

Where:

$F(t)$ = logarithm of the correlation function.

A – This value divided by 100, gives the % merit (seen during analysis). Typically 30%, but dependent on photomultiplier aperture size; this relates to the signal to noise ratio.

B = initial slope, which gives the z-average mean size.

C – When divided by B^2 gives the value of the polydispersity of the sample ($\langle$ 0.05 indicates good monodispersity).

The z-average mean calculated by this method is always presented no matter which of the two methods of analysis is used.

As stated above, if the sample distribution width is set to one, the instrument defaults to a cumulants fit. This fits a log-normal distribution to the z-average mean and polydispersity such that the intensity weighted distribution produced is always a single Gaussian peak, centred on the modal value, independent of whether the distribution is monodisperse or not. The exponential method of analysis requires the input of an estimated sample size distribution (*e.g.*, as measured using the cumulative method). This is then used to resolve more complex distributions. Least squares analysis is used to determine the mix of chosen sizes that provide the best fit between the experimental data and the correlation function calculated from the mixture. The method iterates the result sixty times, reducing the difference between the experimental and calculated correlation functions.

The chosen sizes form a geometric series, using twenty-four size classes. The computer chooses the mean during initial sample checking. The ratio of the largest size to the smallest size is defined by the sample distribution width. This can either be set manually or left at a value of one such that the machine chooses a suitable value. If too large a width is chosen, some classes will remain empty. If too small a width is chosen, the analysis will be false in that the data will not fit the chosen classes. A symptom of this is a multimodal distribution in a monodisperse sample, and a large increase in the value of the 'fit.' (The fit is the value given by the least squares error of the difference between the experimental and calculated data *i.e.*, a minimum in the fit value indicates the best fit.) Once taken, the experimental data can be re-analysed using a different distribution width. It is thus usual to start with a large distribution width and to reduce the value to give a better resolution. The ideal width distribution leaves just one or two empty classes at either end of the calculated size distribution.

The light scattering theories used, can be either **Rayleigh-Gans-Debye**, or **Mie**. The former is used if no value of particle refractive index is set (*i.e.*, if the value is left at zero), and makes the assumption that the particle refractive index is the same as the liquid refractive index. (This approximation is less valid for turbid latices than for polymer solutions.) Mie theory is used when a value other than zero is set for the particle refractive index. (Mie theory also demands an imaginary refractive index. This is an absorption factor and, as such, is more applicable to blue objects that will absorb the red laser light.)

7.4.4 Determination of polymer molecular weight.

The polymer molecular weights of a number of the surfactant-free polymer latices were determined by both conventional **gel permeation chromatography** (GPC)[1] and by GPC with an additional viscosity detector. GPC is a secondary technique, requiring a calibration standard. The resultant data is therefore only suitable for comparative purposes.

Latices were freeze-dried for supply to R.A.P.R.A., where sample solutions were accurately prepared to an approximate concentration of 2 mg ml^{-1} in tetrahydrofuran (and antioxidant) solvent, with a small amount of *1,2*-dichlorobenzene in the solvent as an internal marker. The solutions were dissolved overnight, and then filtered through a polyamide membrane (0.2 μm pore size) prior to the chromatography.

The chromatography was performed at ambient temperature, using columns of PLgel 2× mixed bed-B, of 30 cm length and packing size 10 μm with viscosity/refractive index (RI) detectors, at a nominal flow rate of 1.0 ml min^{-1}. For the conventional GPC, the viscosity detector was removed to give the RI detector the whole sample concentration. Thus, separate calibrations were used for each method. Samples were run in duplicate, with the same solution being used when both methods were performed. The conventional GPC was calibrated using polystyrene in terms of *log[MW] vs elution volume*, such that results were expressed as the 'polystyrene equivalent' molecular masses. The GPC/Viscosity work, however, is calibrated in terms of *log[MW]* × *intrinsic viscosity vs elution volume* and should provide true molecular mass data provided that the polymer behaves normally in solution.

7.4.5 Conductometric titrations.

Certain PBMA latices (*e.g.*, those shot with AA {paragraph 7.3.3.5}) were characterised with respect to availability of surface charge (*i.e.*, carboxyl groups) by conductometric titration[2]. The latex was first cleaned by serum exchange (paragraph 7.5.2) including an acid washing stage (using hydrochloric acid {0.05 M}) before a known weight of latex solid was titrated against sodium hydroxide[3] in a Pyrex glass beaker. The latex was stirred using a PTFE coated magnetic follower (which was stopped during the course of a measurement). Initially, the latex was outgassed with N_2, to remove any CO_2, and was kept

---

[1] The author acknowledges Dr. S. Holding of the Rubber and Plastics Research Association, R.A.P.R.A. Technology Ltd. (Shawbury, Shrewsbury, Shropshire, UK) who carried out this work.

[2] The author acknowledges M. Ashmore for performing the titrations as part of an undergraduate project.

[3] BDH CVS Ampoule. BDH Chemicals Ltd., Poole, Dorset, UK.

under a blanket of N_2 during the course of the titration. Aliquots of freshly prepared NaOH (initially ca 0.1 M, but dependent on the sensitivity required) were added using a microlitre syringe, and the conductivity determined using a Jenway 4010[1] conductivity meter.

AA-shot PBMA latex films (including sucrose leached films) were also titrated to give comparative results, having been cast to yield a comparable weight of polymer to the aforementioned latices. The method used was similar to that described above but the film was also washed after casting with double distilled water, following an acid washing stage.

7.5 Latex cleaning.

After polymerisation, latices were **steam-stripped** to remove any residual monomer and then cleaned either by **serum exchange**, or by **dialysis** to remove residual ionic contaminants from the polymerisation (*e.g.*, initiator and buffer). The former of these two methods, whilst possibly giving a *cleaner* latex (after appropriate treatment, *e.g.*, acid washing, etc.), was found to be extremely slow. Although not a problem when only small quantities were required, it was not economical for large scale film production. Dialysis on the other hand would yield a suitably cleaned latex (where cleaned is defined as in section 7.5.1), on a larger scale and within a shorter time span.

7.5.1 Dialysis.

PHMA and PAMA latices (250 ml) were dialysed in cleaned (see below) visking tubing placed inside bell-jars containing 5 dm^3 of double distilled water. The water was changed every ca 24 hrs, and its conductivity periodically monitored using a Wayne-Kerr[2] conductivity bridge. The latex was deemed to be sufficiently cleaned when the conductivity of the dialysate was close to the conductivity of the clean water ($\approx 1.0 \rightarrow 1.5\ \mu S\ cm^{-1}$) after allowing for dissolved CO_2.

Dialysis is recognised as not being an ideal cleaning method for the removal of bound cations or emulsifier (the latter due to the slow diffusion times of these relatively large molecules: not applicable to these surfactant-free reactions) due to the protracted times needed to leach impurities from a latex. During this time it is possible for the latex to undergo microbial attack or be contaminated by sulphurous compounds (used as stabiliser) leached from the dialysis tubing[537]. Hence, the dialysis tubing was boiled in several changes of distilled water, before use, for 3 → 4 hrs to remove any additives. During the dialysis procedure the water was vigorously stirred to keep the tubing in motion, to prevent the formation of stationary layers within the dialysis tubing, and aid the diffusion of molecules away from the latex.

7.5.2 Serum exchange.

This method was used for the cleaning of the PBMA latices. As a cleaning technique, the method was tested by Wilkinson[536] *et al.* and was found to be efficient in the removal of reaction by-products, residual monomer, oligomeric material, etc.

---

[1] Supplied by Fisons PLC, FSA Lab. Supplies, Loughborough, UK.
[2] Wayne-Kerr Co. Ltd., Bognor Regis, Sussex, UK.

The all-PTFE microfiltration cell was initially cleaned with organic solvent^H to remove any polymer, followed by rinsing with Fisons AnalR water. The assembled cell was then half filled with Fisons water which was left to run through under atmospheric pressure. The conductivity of the eluent was periodically monitored for conductivity as a test of purity. Once sure that the cell was clean, and also that it did not leak, the cell was half-filled with latex, and a known volume of Fisons water added. The eluted volume was recorded and replaced to prevent the latex drying due to water loss, and again periodically measured for conductivity. The latex was magnetically stirred (using a ridgeless magnetic follower to prevent damage to the filter paper) over a Millipore®[1] cellulosic membrane filter paper (typically 0.3 μm pore size) which was changed daily to prevent (i) blockage, and (ii) loss of the latex via a stirrer-damaged filter paper. Cleaning lasted until the conductivity of the eluted water equalled that of the clean feed-water: taking approximately twenty times the volume of the latex.

7.6 Film preparation.

7.6.1 Materials.

The latices used during the course of this study consisted, in the main, of members of the range of commercial latices called collectively by the name **Eudragit®**, produced by Röhm Pharma GMBH, Weiterstadt, Germany, and imported into Britain by Dumas (U.K.) Ltd.[2] (see Chapter 6). Other latices used included the surfactant-free poly(alkyl methacrylate) latices prepared as part of the study.

7.6.1.1 Film additives.

Additives used (loaded into films to determine their effects on film transport properties) included sucrose, sodium chloride (both supplied by Aldrich[3]), and hydroxypropyl methylcellulose, H.P.M.C. (Celacol® HPM 450 BP, supplied by Courtaulds[4]) (see **Figure 7.2** [401]).

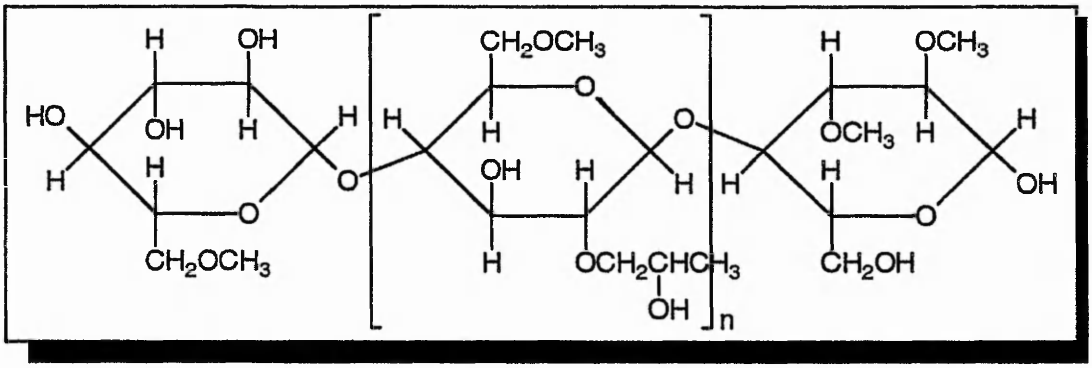

Figure 7.2 Hydroxypropyl methylcellulose.

---

[1] Millipore U.K. Ltd., London, UK.

[2] Dumas (U.K.) Ltd., Tunbridge Wells, Kent, UK. The author gratefully acknowledges Roy Errwood for the free supply of Eudragit® latices.

[3] Aldrich Chemical Co. Ltd., Gillingham, Dorset, UK.

[4] Courtaulds Chemicals, Spondon, Derby, UK.

In addition to the aforementioned additives, mixed latex films were prepared from the soluble (at pH ⟩ 5.5) Eudragit® *L 30 D*, and the water insoluble Eudragit® *NE 30 D*.

Additive loadings were normally expressed as a percentage per gram of Eudragit® latex solid content (*i.e.*, % (g.*NE*)$^{-1}$), or as a ratio of additive to Eudragit® *NE 30 D* solid content. *E.g.*, a 100% (g.*NE*)$^{-1}$ loading is a 1:1 ratio of the additive to polymer, whilst a 50% (g.*NE*)$^{-1}$ loading implies, for example, two parts of *NE 30 D* to one part *L 30 D* and a 150% (g.*NE*)$^{-1}$ ratio implies a two parts of *NE 30 D* to three parts *L 30 D*, etc.

For those films with a T_g above ambient, it was necessary to add a plasticiser in order that the films could be removed from the substrate without fracturing, and in pieces large enough to be used in the required experiments. Such films included those prepared from Eudragit® latices functionalised with either carboxyl (Eudragit® *L*) or quaternary ammonium groups (Eudragits® *RL* and *RS*) (see Chapter 6). In cases where a plasticiser was used to make the film more manageable, it was not considered as an additive in the aforementioned sense, *i.e.*, not used as an attempt to control permeant flux. The plasticiser chosen for use was triacetin (glycerol triacetate $(CH_3CO_2CH_2)_2CH(O_2CCH_3)$, and was supplied by Aldrich[1]). This plasticiser was selected since it is recommended by Röhm Pharma for use with their whole range of Eudragits® (with the exception of Eudragit® *NE 30 D*). The concentrations suggested by Röhm Pharma are in the range of 5 → 25% $W/W_{(\text{polymer solids})}$. For the purpose of this study, the triacetin was always used, when required, at a concentration of 0.15 g g^{-1} of polymer solids content (*e.g.*, 15% (g.*RL*)$^{-1}$). This level of plasticisation was necessary to provide the flexibility for the films' end use as *free-films*.

7.6.1.1.1 Mixing of Eudragit® *NE* and Eudragit® *L*.

The mixing of Eudragits® *NE* and *L* can lead to destabilisation of the polymers due to the differences in pH and electrolyte, and additionally, interactions between the polymer molecules and the stabilising emulsifier systems of the two polymers can cause coagulation [422]. This can be overcome by equalising the differing pH's of the two systems (as described in a Röhm Pharma information sheet [422]). The method varied dependent on whether the Eudragit® *NE* or *L* predominated. When Eudragit® *NE* predominated, hydrochloric acid (1 M) was slowly stirred into the Eudragit® *NE*, in a ratio of approximately 1:300 (W/W) HCl to Eudragit® *NE* until pH 5 was achieved. (The information sheet also recommended the addition of an emulsifier, Tween 80, but this was not used here.) The Eudragit® *L* must also be partially neutralised by the slow addition of sodium hydroxide (1 M), again with stirring, in a ratio of 10:1 (Eudragit® *L* to NaOH) to give pH 5.2 → 5.3. Stirring should be continued for ≈ 10 minutes after addition, at which time the two latices should be slowly mixed, again with stirring. The Eudragit® *NE* + *L* mixture should finally be filtered through glass wool.

Mixing the two latices when Eudragit® *L* predominated was achieved in a similar manner as above, with the exception of not adding the acid to the Eudragit® *NE*. (In this case, the information sheet did not suggest the addition of emulsifier.)

---

[1] Aldrich Chemical Co. Ltd., Gillingham, Dorset, UK.

7.6.2 Film casting.

Films were cast from the range of Eudragit® copolymer latices, and also from the surfactant-free, homopolymer PBMA, PAMA and PHMA latices. Before casting, latices were normally diluted to 5% W/W polymer solids content, and then filtered through glass wool to remove any possibility of coagulum accumulated from storage. Latex films were cast onto substrates of Pyrex glass plates (cleaned as described previously) and contained by cylinders of glass (9.5 cm in diameter and approximately 5 cm in height). These cylinders were sealed against the plates by means of a ground glass bottom rim smeared with high melting point (> 473 K) silicone grease[1]. Other substrates were tested, but found to be disadvantageous: nylon plaques[2] were found to warp at the higher casting temperatures; whilst casting on to a mercury[H] substrate led to small amounts of mercury becoming entrapped in the film, particularly at the film edges. The latex was pipetted onto the substrate to allow a controlled thickness to be cast. This thickness depended on the particular film being prepared, and was chosen as a matter of compromise between ease of film handling (thicker films being less prone to curl on removal from the substrate: a problem for tacky films and those susceptible to static electricity) and the requirement of a measurable flux, with little uptake of permeant. For the Eudragit® latices, a thickness of approximately 80 → 100 μm was used.

For casting, films (and substrate) were placed on a levelled platform, in a fan-less laboratory oven. Typical drying time and temperature for the Eudragit® films were 24 hrs, at 313 K, unless otherwise stated; the PAMA and PHMA films were cast at the same temperature for 15 hrs. The PBMA films were normally cast for 72 hrs at a temperature of 353 K, although initially other times such as 3 hrs, and other times and temperatures (313 K for 24 hrs) were also tried. During casting, the ovens contained 200 g of silica gel per film, to sorb water vapour and prevent condensation forming on the oven walls.

7.6.3 Monitoring of film drying.

The evaporation of the aqueous phase, from a number of film types, was monitored both visually by means of a custom designed Perspex door to the casting oven, and gravimetrically by positioning the casting substrate on a top pan balance (placed inside the oven). In such cases the temperature and relative humidity of the oven were monitored by means of a thermocouple attached to a Comark[3] electronic thermometer, and an Omega[4] digital thermo-hygrometer, respectively, both with output to a chart recorder. The probes to the latter two instruments were positioned in the oven, just above the surface of the drying latex and within the glass retaining cylinder, *i.e.*, within the evaporative 'flux.'

7.6.4 Preparation of solvent cast films.

Solvent cast films of the homopolymer surfactant-free poly(methacrylate) latices were prepared from freeze-dried polymer solid dissolved in a suitable solvent: typically

---

[1] Dow Corning, Belgium. Supplied by Fisons PLC, FSA Lab. Supplies, Loughborough, UK.

[2] C & P Chemicals and Polymers Groups, ICI Petrochemicals and Plastics Division, Middlesbrough, Cleveland, UK.

[3] Comark Electronics, Littlehampton, Sussex, UK.

[4] Omega Engineering, Stamford, U.S.A.

butan-2-one^{H}, supplied by BDH[1]. The solid polymer was initially dissolved in the solvent to be used to a concentration of 5% W/V. Film casting was achieved by decanting the required volume, to give a usable film thickness (ca 80 → 100 μm), onto a levelled P.T.F.E. substrate. Initial drying was performed at ambient temperatures in a fume cupboard, with the substrate positioned under a plastic shield to reduce the airflow over the film and therefore prevent the solvent evaporating too quickly. Once the film had solidified (after approximately 4 hrs) the film, still on its substrate, was transferred to a vacuum oven, where it was kept under vacuum, at ambient temperature, for approximately 96 hrs to remove any residual solvent.

7.6.5 Method of film removal from the casting substrate.

The method of removal of a film from its substrate was dependant on the type of film. In the case of the Eudragit® latex films, heating the back of the glass substrate over hot water (353 K) for a few minutes was sufficient to allow the film to be peeled off, without stretching. (The films were sufficiently large, at 9.5 cm diameter, to be handled without the necessity of touching the area of the film to be used in the experiment.) Eudragit® *NE* films were on occasion found to be lifted from the substrate with the glass retaining cylinder as it was removed, simply allowing the film be cut away.

In order to remove the surfactant-free films from their substrates, it was necessary to soak the film + substrate in hot water (353 K) and peel the film a small distance at a time, with further wetting as each section was removed. The films were quite prone to stretching if removed too vigorously, and the hot water caused previously released regions of film to re-attach themselves to the substrate.

The solvent cast films were usually easily removed from the PTFE substrate, providing that the film was not too brittle at ambient temperatures.

7.7 Film characterisation.

7.7.1 Determination of film thickness.

Film thickness was measured using a **plane-foot gravity-drop dial gauge**, with a resolution of ±1 μm. Because of the uneven (*'mud-cracked'*) surface of the majority of the films under investigation, the thickness was measured over a number of sites on the film, and an average calculated. Over the full diameter, film thickness varied by up to ca 10% of the total thickness. However, because it was normal to use only the central region of such a film, the variation in thickness was more of the order of ca 3 → 4%.

The quoted film thickness is typically inclusive of that due to the presence of the additive, unless otherwise stated. In solute permeability experiments (see paragraph 7.10) the thickness stated is the unswollen (dry) thickness, and again in the case of the additive present films, the unleached thickness is used. The film thickness, used to calculate the permeability coefficients of the additive-present films, is discussed further in Chapter 10.

---

[1] BDH Chemicals Ltd., Poole, Dorset, UK.

7.7.2 Quantification of film additive leaching.

The amounts of water soluble additive leached as a function of time was typically determined **gravimetrically**. Additive containing films were initially weighed when dry, and then leached for various times in 250 g of (orthophosphate) buffer solution at pH 6 (to imitate the pH of the solute permeability experiments, see paragraph 7.10). Leaching was executed at ambient temperature with the sample placed on an orbital shaker, for a period of up to 96 hrs.

Following the leaching period, films were quickly rinsed with distilled water, and dried until constant weight was achieved. The difference between the initial (additive-present) film weight and final (dry) weight yielding the amount of additive leached.

Films which showed a tendency to adhere to themselves were attached to a piece of wire so that they remained flat during the course of the experiment. The wire was pre-weighed, and its weight accounted for in the calculations.

7.7.3 Determination of film porosity.

Various films were tested for porosity, including additive-free and additive-present films and films leached of their additive, by the technique of **mercury intrusion porosimetry**, using a Carlo-Erba[1] Porosimeter 2000 Series, capable of determining pore-size and pore-volume distributions, in the size range of 3.7 → 7,500 nm radius, by a capacitance system. Mercury^{H} is used as the intrudent due to the property of mercury of being non-wetting for most materials such that it has to be forced into the pores. The cumulative volume intruded is measured as a function of the exerted pressure.

The sample under study is totally immersed in mercury^{H}, in a dilatometer, and the pressure is increased hydraulically. As mercury enters the samples' pores, the mercury level in the dilatometer stem decreases by an equal volume: the change in capacitance through the dilatometer, due to the movement of the mercury down the dilatometer stem, being monitored by electrodes at either end. As the applied pressure (to the mercury in the dilatometer) is increased, the radius of pores that can be filled with mercury is decreased. The minimum pore size is thus a function of the maximum pressure attainable by the instrument which was 1999 bar corresponding to a pore radius of 37.5 Å (or $\approx 2\times10^5$ Pa and 3.75 nm, respectively, in S.I. units).

7.7.3.1 Operating procedure.

A known weight of sample was placed in a dilatometer. Two types of dilatometer were available: one of which whose stem (the *standard* stem) was straight through; and the other of which (the *powder* stem) whose stem outlets entered the dilatometer body perpendicular to the stem. This latter dilatometer was designed for powder samples, and was meant to prevent a powdered sample from rising up the dilatometer stem on top of the incoming flow of mercury, during filling. This powder stem was found to be the most suitable for film samples: allowing mercury to reach both sides of the film and preventing

---

[1] Carlo-Erba, British importer: Fisons PLC, Loughborough, UK.

the film becoming trapped against the glass wall, with mercury against only one film face, as was found to sometimes occur with the standard stem.

Filling the dilatometer with mercury was accomplished using a macropore unit, which evacuated the dilatometer and out-gassed the sample. The dilatometer remained under vacuum whilst being filled with mercury: the vacuum serving to draw mercury from the reservoir and also to prevent entry of any residual gas. In theory, returning the macropore unit to atmospheric pressure allowed the determination of any pore sizes greater than 7,500 nm to be measured, via a change in mercury level (measured on a moving digital scale behind the stem). However, this was not practicable due to unexpectedly large drops in the height of the mercury column. This *overlarge* intruded volume was almost certainly caused by unfilled pockets in the dilatometer – possibly caused by the tacky films either adhering to themselves or to the glass walls of the vessel.

The filled dilatometer was then transferred from the macropore unit to the autoclave of the porosimeter. Pressure was applied to the sample by means of a pressure multiplier system. The autoclave itself was filled with dielectric high pressure oil, which acts to hydraulically transmit the pressure to the mercury inside the dilatometer. As the pressure increased, the level of mercury in the calibrated dilatometer stem decreased causing a change in capacitance that is processed to give a result of accumulated intruded volume on the pressure-pump control unit.

7.7.3.2 Interpretation of results.

Calculated results were initially corrected against a control ('blank' sample) value consisting of the compression obtained for a dilatometer filled with mercury alone (*i.e.*, no polymer sample). (Blanks were run at regular intervals, or whenever the mercury or dilatometer was replaced. At a pressure of 1999 barr {$\approx 2\times10^5$ Pa} the typical mercury compression was 28 → 32 mm^3.) The normalised results were then plotted graphically in the form of x-y graphs of either (i) '*cumulative specific intruded volume of mercury* ($mm^3\ g^{-1}$)' versus '*pore radius* (μm)', or (ii) a differential type graph of '*d{cumulative intruded volume}/ d{ln(pore radius)}*' versus '*ln(pore radius)*'. The former of these plots indicates the presence of a pore distribution by a sharp change of gradient: a narrow pore distribution being indicated by a sudden step as opposed to a gradual change of gradient. The differential curve is the easier of the two curves to interpret: a pore distribution being indicated by a peak whose width is a measure of the size of the distribution. (Also see Appendix A.)

7.7.4 Electron microscopy.

The surfaces, and internal structures, of a number of films were investigated using both S.E.M. and T.E.M.

Film specimens micrographed at C.B.D.E.[1] were cast onto acetate sheets (or placed on acetate sheets) for ease of handling. The acetate sheets were, in the case of the cross-

---

[1] The author is indebted to Judi Parkes at C.B.D.E. for much of this work, which was performed using a Hitachi field emission S.E.M.

sections, scored with a cutter under liquid nitrogen and then fractured (*i.e.*, all S.E.M. cross-sections were fractured under nitrogen). The specimens were then coated with a thin layer of gold to make them conductive.

S.E.M. work was also performed at the Institute of Polymer Technology and Materials Engineering[1]; and T.E.M. at the Centre for Cell and Tissue Research[2] using a freeze fracture technique (normally on the surfactant-free latex films) as described below.

7.7.4.1 Freeze-fracture transmission electron microscopy (F.F.T.E.M.).

This work involved the use of a tensile snap method, rather than the more usual microtome knife, to prepare the polymer sample for examination under the T.E.M. The diluted polymer dispersion or a thin strip of film (1 mm × 3 mm) was inserted, together with a drop of inert mineral oil, into a pair of hollow brass tubes that were held end-to-end by a pair of specially designed forceps such that the film bridged the junction of the tubes. The tubes, held under liquid N_2 (which freezes the oil such that it acts to hold the film in place) and in a spring-loaded specimen cup, were then inserted into sub-cooled N_2 held at its triple point (63 K). Freeze-fracture was then performed using an automatic freeze-fracture unit[3], programmed to fracture the specimens at a temperature of 133 K whilst under a vacuum of 5×10^{-7} Torr. Immediately after fracture, the specimen was shadowed with platinum – evaporated from a carbon crucible at an angle of 45°. The replicas thus formed were then stabilised by coating, from above, with carbon. Upon removal from the apparatus, the required platinum/carbon replica, overlaying the original frozen sample, was removed by soaking in trichloroethylene, which also dissolved the mineral oil. After a further three washes in the trichloroethylene, the samples were mounted on (400 mesh) T.E.M. grids for observation in a JEOL 1200 Ex T.E.M. This technique was advantageous over conventional microtome/T.E.M. in that the fracture *and* replication were performed at liquid N_2 temperature[4] thus preventing thermal distortion of the polymer. Similarly, the platinum/carbon replica allowed the use of high electron beam currents (*i.e.*, high magnifications) that can distort samples of polymer.

7.7.5 Determination of water uptake by films.

Water uptake by the free-films was determined **gravimetrically**. Dried films of known weight were soaked in either orthophosphate buffer (pH 6), or water, for approximately 72 hrs, or until fully swollen, whilst situated in a (shaking) constant temperature bath at 303 K. On removal from the water, the films were blotted dry with filter paper to remove any excess surface water, and then re-weighed. For the additive present films, corrections were often required arising from leaching of the additive. These corrections were made by drying the film and weighing to determine the weight loss of solid

---

[1] Institute of Polymer Technology and Materials Engineering, University of Technology, Loughborough, UK.

[2] Dr. Ashley Wilson at the Centre for Cell and Tissue Research (CCTR), University of York, Heslington, York, UK.

[3] Cryoetch CF-4000, Oxford Instruments.

[4] Samples are often fractured following cooling in liquid nitrogen, but are removed for the fracture to take place. However, all T.E.M. work in this study was performed using this more specialised tensile snap technique.

from the film during the course of the experiment. This value then being accounted for in the calculation of the water uptake.

7.7.6 Determination of permeant-solute uptake/partition coefficients.

The uptake of the solutes, used as permeants (*e.g.*, *4*-nitrophenol, anilines, etc.), by films was determined by allowing a known weight of film to reach equilibrium in a known concentration (and volume) of permeant: the concentration of the permeant being monitored **spectrophotometrically** to determine both whether equilibrium had been reached and also the equilibrium concentration of the permeant. Samples were stored in a shaking constant temperature bath, normally at 303(±2) K, and in the dark until equilibrium was reached. The volume of solute solution used was such that the effect of water uptake, by the film, on the concentration of the solute was negligible. The typical weight loss found in a film, on soaking, (due to loss of endogenous additive, etc. – see results Chapters) was accounted for in the calculations.

Partition coefficients were determined in a similar manner by using a range of permeant concentrations. Comparison of the measured uptake of permeant (in units of g (g.polymer)$^{-1}$) with the equilibrium concentration (in units of g (g.water)$^{-1}$) allowed the determination of the (dimensionless) quantity of permeant partitioned into the film.

7.8 Determination of water vapour permeability coefficients.

Water vapour permeability was measured by fixing a film of known thickness to the top of a sample bottle (28 ml capacity) containing a saturated solution of ammonium sulphate (5 ml). The film was sealed into position by means of a glue prepared by dissolving a sample of the film in organic solvent (usually butan-2-one). Films were normally oriented such that the substrate side of the film was facing the water vapour. The prepared sample (bottle) was then mounted in a desiccator, containing silica gel, which was positioned in a darkened incubator at a temperature of 298 K.

At 298 K, **saturated ammonium sulphate solution**[1] produces a constant relative humidity (*i.e.*, the percentage humidity, at 298 K, within a closed space when an excess of the substance is in contact with a saturated aqueous solution of the solid phase) of 81%, which varies very little with temperature (*e.g.*, ±0.1% over a temperature range of ±5 K[531]). With the sample bottle placed in the desiccator, there was an effective relative humidity difference of 81% between the film faces – which corresponds to a water vapour pressure difference of 1.92 cm Hg.

7.8.1 Calculation of water vapour permeability coefficients.

The water vapour flux, dW/dt (g.hr^{-1}), through a film was measured **gravimetrically**: the sample being removed from the desiccator periodically to ascertain its weight loss as a function of time, from which the flux was determined by means of a least squares regression analysis. The water vapour permeability coefficient, P_w (g hr^{-1} cm^{-1} cm.Hg^{-1}), could then be calculated from the following equation (as derived in Appendix A):

---

[1] Ammonium Sulphate supplied by Fisons PLC, FSA Lab. Supplies, Loughborough, UK.

$$
\begin{aligned}
P_w &= \frac{dW}{dt}\left(\frac{l}{A\Delta p}\right) \\
&= \frac{dW}{dt}\left(\frac{l}{A \times 1.92}\right)
\end{aligned}
\tag{7.5}
$$

where:

l = film thickness (cm);
A = exposed film area (cm^2) ($A = \pi r^2$ where r = radius of exposed area);
1.92 = water vapour pressure difference, across the film (cm.Hg).

A number of control samples were also run for comparison with the experimental samples. These consisted of an open sample bottle, containing only the saturated ammonium sulphate, and a second bottle sealed with a film of aluminium foil. The former of these gave an indication of the rate of weight loss from the sample bottle by evaporation alone, whilst the latter provided an indication of the effectiveness of the polymer-glue seal by virtue of the fact that silver foil should afford an impermeable barrier to the permeant.

7.9 Determination of gas permeability coefficients.

The gas permeability coefficients of various films were measured using a modified British Standard apparatus and method (B.S.2782 [168]). The method utilises a **Daventest**[1], non-overflowing Davenport Apparatus (see **Figure 7.3**) into which the film under test is placed separating two chambers of a pressure vessel. The upper chamber contains the test gas at atmospheric pressure, whilst the lower chamber, of known initial volume, is evacuated such that there is a pressure difference across the film of the order of ca 76 cm.Hg. The rate of gas flow through the film is then measured as a function of time: the pressure increase in the lower chamber, due to the permeating gas, being monitored by means of the mercury manometer.

The apparatus was modified (compared to the B.S. model) by means of a new insert fitted into the lower chamber (see **Figure 7.3**) to reduce the gas flux through the film and therefore allow the measurement of greater fluxes than would otherwise be possible. (A high flux causes the mercury in the manometer to move too quickly to be measured.) Gases used were CO_2 and N_2 ("white spot," oxygen-free grade), both supplied by BOC Ltd[2].

7.9.1 Calculation of the gas permeability coefficients.

The flux of a gas through a film in the Daventest apparatus is given by:

$$Flux = \frac{dV}{dt} = \frac{V_0 + 2ah}{H - h}\frac{dh}{dt} \tag{7.6}$$

as derived in Appendix A. The gas permeability coefficient P_g is then calculated from:

$$P_g = \frac{(Flux \times l)}{(A(H - h))} \times \frac{T}{T'} \tag{7.7}$$

---

[1] Daventest Ltd., Welwyn Garden City, Hertfordshire, UK.
[2] BOC Ltd., Brentford, Middlesex, UK.

where:

Flux = as equation (7.6) ($cm^3\ s^{-1}$);
l = film thickness (cm);
A = exposed film area (cm^2);
$H - h$ = driving pressure (cm.Hg);
T/T' = correction for temperature (dimensionless ratio: 273 (K)/ambient (K)).

Thus, substituting for flux in equation (7.7) gives:

$$P_g = \frac{\left[\frac{(V_0 + 2Ah)}{H - h}\frac{dh}{dt}\right] \times l}{(A(H - h))} \times \frac{T}{T'} \qquad (7.8)$$

The units of gas permeability are therefore: $cm^3.cm.s^{-1}.cm^{-2}.cm\ Hg^{-1}$.

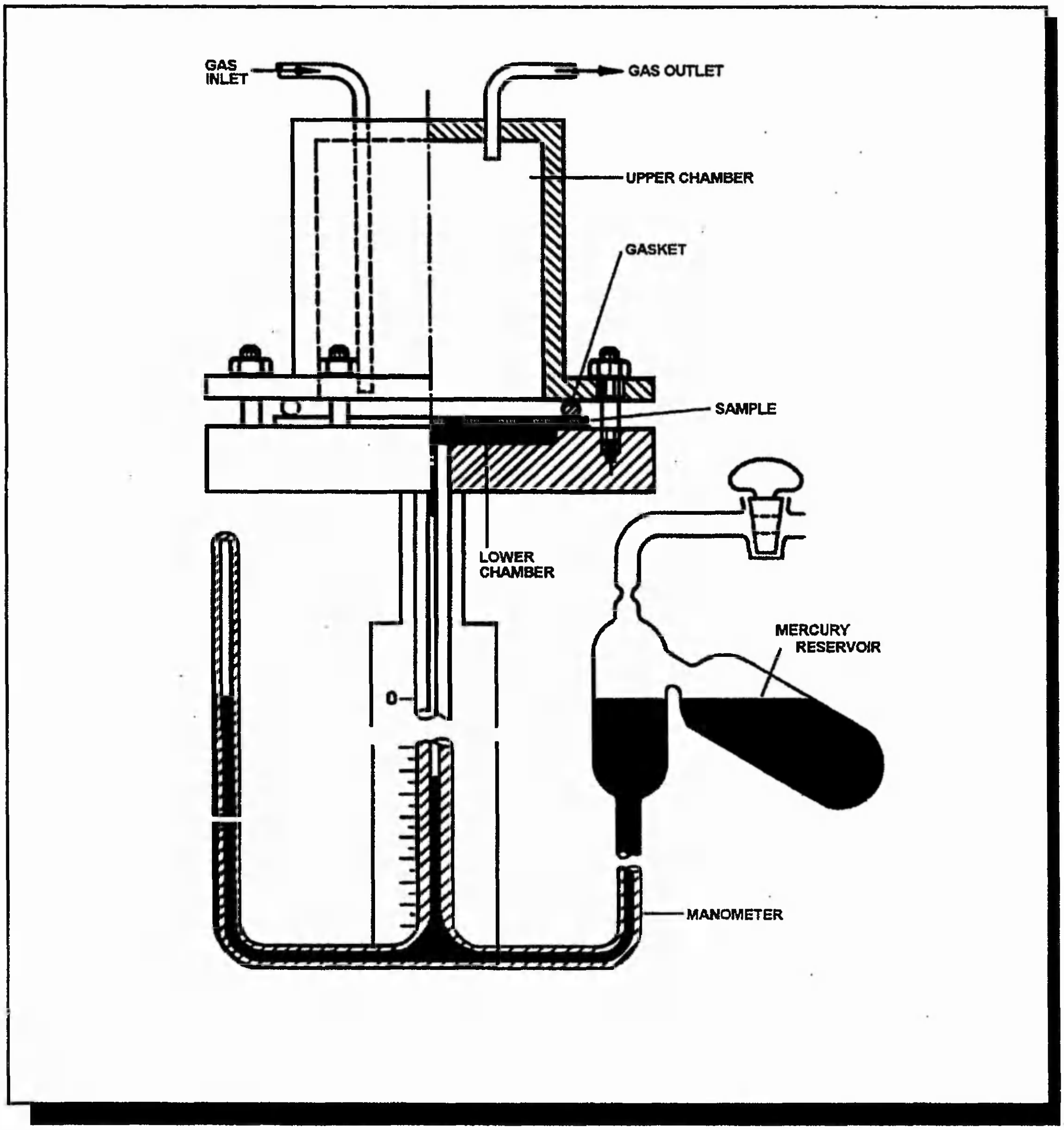

Figure 7.3 Daventest gas permeability apparatus.

7.10 Determination of solute permeability coefficients.

The solute permeabilities of free-films were determined **spectrophotometrically** using a specially designed two chambered **solute permeability cell** in which the film under test acted as the dividing membrane between the two chambers. Films were oriented with the polymer-substrate side facing the donor permeant (as in all permeability experiments, unless stated otherwise). The film was held in position by ground glass flanges and fastened by means of screw-adjustable clamps. At the start of a solute permeation experiment, the permeant solution would be put into one side of the cell, henceforth termed the permeant or **donor compartment**, whilst the second chamber, hereafter termed the **receiver compartment**, was normally filled with orthophosphate buffer solution (pH 6). Each chamber of the cell was filled simultaneously with 65 ml of solution, and was stirred at 100 r.p.m. using glass propeller-type stirrers driven by a common motor and pulley system. Up to five cells could be run at any one time, positioned in constant temperature baths (303 K) for the duration of the experiment. The apparatus is schematised in **Figure 7.4**.

The absorbance and, hence, concentration of permeant passing through the film was monitored using a Philips[1] PU8730 U.V./visible scanning spectrophotometer configured with a PU8737 automatic cell changer (cell programmer); six (80 μl capacity/1 cm pathlength) flowcells; a PU8702 computer interface; and controlled by PU8714 user programming software (version 1.0) on an I.B.M. compatible personal computer[2]. The receiver solution was continuously pumped through all P.T.F.E. tubing (bore 0.6 mm)

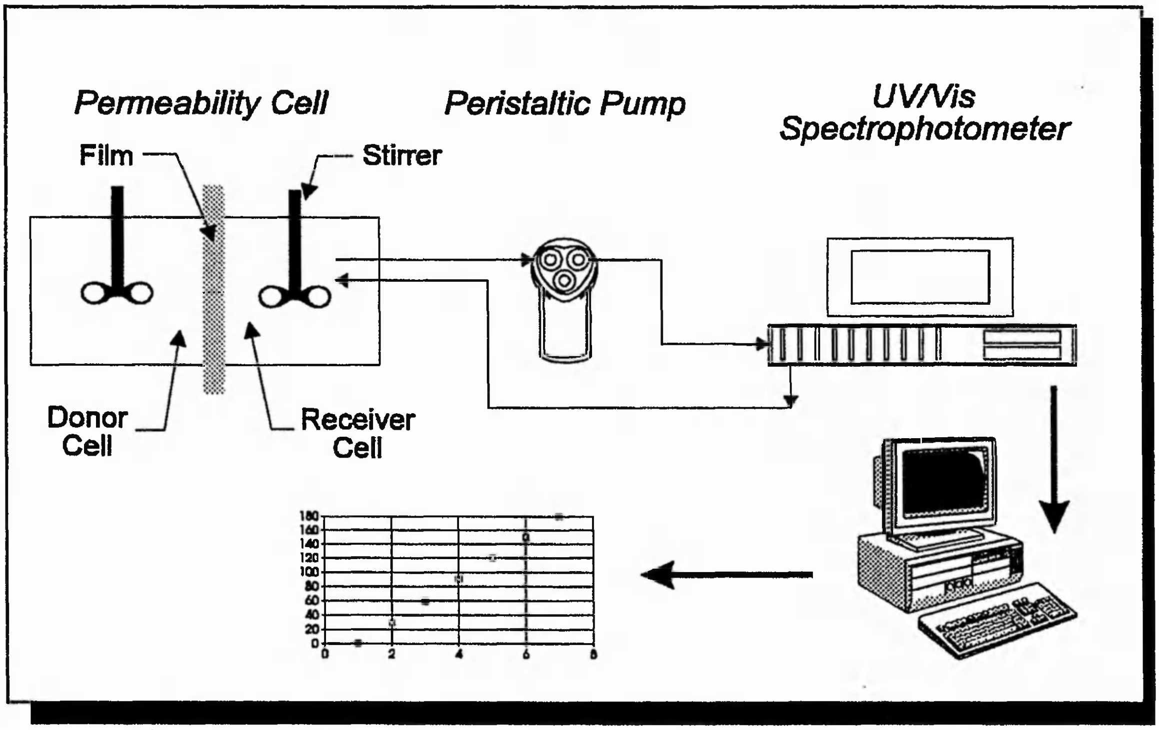

Figure 7.4 Schematic of apparatus for the determination of a solute permeability coefficient.

---

[1] Philips Scientific, Philips Analytical, Cambridge, UK.

[2] Epson AX3: 80386 + 80387 coprocessor, fitted with 4Mb ram, 40Mb hard disk, and running under MS-DOS version 5.

(except for that tubing in contact with the pump rollers, which was PVC collard tubing – supplied by Anachem[1]) to the spectrophotometer by means of an 8-channel peristaltic pump supplied by Gilson[2]. (This pump having been chosen for the high number of rollers in contact with the pump tubing at any one time such that the pulsed peristaltic action was minimised). Pump speed was normally 25 r.p.m. giving a flow rate of ca 300 ml hr^{-1}, and the use of flowcells[3] permitted continuous pumping whilst absorbance readings were taken.

Both permeability cell chambers were filled simultaneously, to avoid undue stress to the films. Absorbance readings were then taken at 15 min intervals (time zero being set as from the first reading, which was taken as soon as all of the permeability cells were filled). Each measurement was referenced (zeroed) against orthophosphate buffer solution, in an identical, but unpumped, flowcell.

Data from the spectrophotometer was downloaded (see paragraph 7.10.1) and stored in an ASCII[4] format file on the computer for analysis by spreadsheet[5]. The data obtained allowed the flux of permeant to be determined: a typical experimental lasting 24 hrs.

7.10.1 Philips User Programming Software.

The spectrophotometer was normally controlled using its own in-built software: computer control utilising the Philips User Programming software normally only being used to control the downloading of data, via a null modem cable, from the spectrophotometer's memory to the computer's hard disk. The spectrophotometer's volatile memory was highly sensitive to mains electrical spikes, and data was frequently lost when this occurred during the running of an experiment. On completion of the data gathering, the contents of the volatile memory could be saved to battery backed-up memory, where it was safe until downloaded to the computer. Usage of the User Programming software, to both download data and control the spectrophotometer is described in Appendix B.

7.10.2 Solute permeants.

4-nitrophenol[6, H] was recrystallised from toluene, and then dissolved in orthophosphate buffer (pH 6) at 0.2 g dm^{-3}. (4-nitrophenol dissociates at low pH, and undergoes a colour change from a green {in its undissociated form} to a clear solution. The buffer is therefore utilised to maintain a constant pH, and therefore colour, when the solution was being monitored spectrophotometrically. At pH 6, 4-nitrophenol exists at approximately 99% in its undissociated form.) Monitoring was performed at a wavelength of 320 nm: the concentration of the 4-nitrophenol then being calculated as part of the spreadsheet analysis with a coefficient pre-determined from a Beer-Lambert type plot.

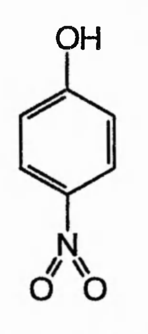

Figure 7.5
4-nitrophenol.

---

[1] Anachem, Luton, Bedfordshire, UK.
[2] Gilson Medical Electronics, supplied by Anachem.
[3] Hellma Flow-Through Compact Cell, Hellma England Ltd. Supplied by Philips.
[4] American Standard Code for Information Interchange.
[5] Microsoft® Excel version 4.0a, running under Microsoft® Windows™ version 3.1.
[6] Fisons PLC, FSA Lab Supplies, Loughborough, UK.

The other permeants used were a range of **anilines**[H] of increasing length of side chain, *i.e.*, aniline[1] (measured at a wavelength, λ, of 280.1 nm), methyl aniline[1] (λ = 28.3 nm), ethyl aniline[1] (λ = 284.3 nm) and propyl aniline[2] (λ = 284.3 nm), (**Figure 7.6**). The absorbance wavelengths at which the concentrations of these permeants were measured were not those of the maximum absorbance, due to the anilines exhibiting very high absorbances at their peak wavelengths – even at low concentrations.

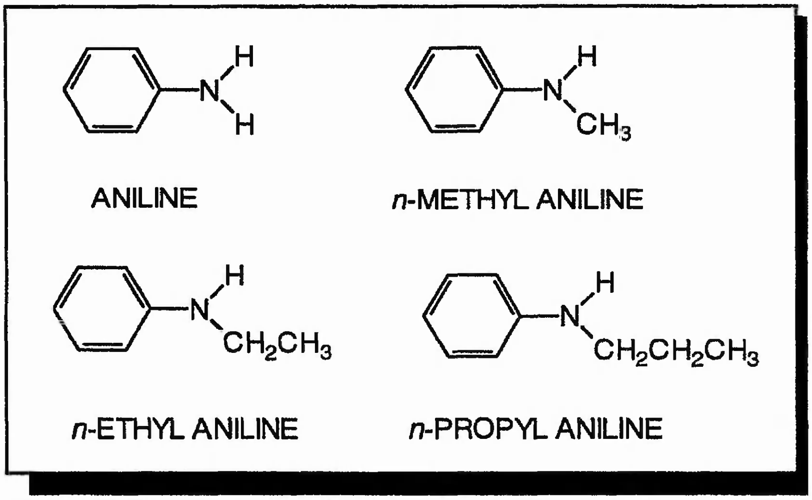

Figure 7.6 Permeant anilines: showing the lengthening alkyl group.

All anilines, with the exception of the propyl aniline, were used at a concentration of 8 mM, (*i.e.*, 0.7450 g dm^{-3}, 0.8573 g dm^{-3}, and 0.9694 g dm^{-3} for aniline, methyl aniline and ethyl aniline, respectively) made up in orthophosphate buffer, pH 6. Propyl aniline, which is less water soluble than the other anilines used, was prepared to a concentration of 2 mM (0.2704 g dm^{-3}) with buffer. The buffer solution was also used as the reference (blank) when measuring the absorbances of all of the anilines.

The anilines were found to absorb onto the PVC tubing passing through the peristaltic pump, leading to a loss of permeant (not a problem for the 4-nitrophenol). Therefore, for these experiments, the permeant flux was monitored by manually sampling the receiver solution, at 30 minute intervals, into 1 cm pathlength, matched quartz (U.V.) cells, in the spectrophotometer.

7.10.3 Calculation of the solute permeability coefficients.

Absorbance data downloaded from the spectrophotometer was converted to concentration data (*i.e.*, permeant concentration in the receiver compartment of the permeability cell) by means of Beer-Lambert coefficients (as determined from the gradient of permeant concentration-absorbance graphs). The solute permeability coefficient, P_S, was then calculated from the following equation (as derived in Appendix A):

$$P_s t = \frac{2.303 l V}{2A} \log_{10}\left[\frac{C_0}{C_0 - 2C_t}\right] \qquad (7.9)$$

---

[1] Fisons PLC, FSA Lab Supplies, Loughborough, UK.

[2] Pfaltz & Bauer Ltd. Supplied by Phase Separations Ltd., Deeside, Clwyd, Wales.

where:
l = film thickness (m);
V = volume of receiver solution (m^3);
A = area of film exposed to permeant solution (m^2);
C_0 = donor permeant concentration (g dm^{-3});
C_t = permeant concentration (g dm^{-3}) in the receiver cell at time, t. (hrs)

A least-squares regression analysis was carried out on the earliest linear region of the plot of $\frac{2.303 l V}{2A}\log_{10}\left[\frac{C_0}{C_0 - 2C_t}\right]$ versus t (*i.e.*, after the cessation of the lag period resulting from the approach to permeant equilibrium within the film) to determine the gradient and, hence, the permeability coefficient.

7.10.4 Electrolyte permeation.

Electrolyte (KCl{0.2 M}) permeation was determined using a conductivity meter[1] with the probe stationed in the receiver chamber of the permeability cell, and chart recorder[2].

7.11 Use of radiolabelled compounds.

The two chambered permeability cell was normally filled with distilled water, to which the labelled permeant was then added in the donor side. Both the donor and receiver chambers were sampled, and measured. This allowed the total amount of the permeant to be tracked, and allowed the uptake by the film to be monitored. In a number of cases, the water in the surrounding water bath was also monitored, providing an indication of whether the permeability cell was prone to lateral leakage around the glass-film interfacial flanges.

7.11.1 Compounds under investigation.

All labelled compounds used were supplied by Amersham International Ltd[3].

7.11.1.1 Tritiated water, THO.

Tritiated water has only one of the water's $^1_1$H atoms replaced by a tritium, $^3_1$T, isotope of hydrogen (hence, THO). The tritium undergoes beta decay giving a stable daughter $^3_2$He nuclide. The beta decay has a maximum energy of 0.0186 MeV, with a mean value of 0.0057 MeV. As with all of the following elements that undergo beta decay, analysis was done by liquid scintillation counting using a Canberra Packard model 2250CA Tri-Carb liquid scintillation counter. Tritium has a half life, $T_{1/2}$, of 12.43 years, and it was therefore unnecessary to account for this over the relatively short duration of these experiments.

The THO, although not a permeant in the usual sense, can be considered as such if it is thought of as a concentration of labelled water in 'normal' (*i.e.*, unlabelled) water. The 'flux' of labelled water through Eudragit® *NE* was investigated when travelling both in the same direction, and against a flux of a more typical solute permeant (4-nitrophenol).

---

[1] Corning 220: supplied by R.W. Jenning, Science House, Nottingham, UK.
[2] Farnell.
[3] Amersham International PLC., Amersham Laboratories, Amersham, Buckinghamshire, UK. Amersham also supply safety and (local) legislative guides.

40 μCi[1] (10.8 μl) of THO was added to the donor side of the permeability cell using a microlitre pipette. (All volumes and, hence, concentrations, used in any calculations were based on the data from sheets provided with each labelled compound, giving information of specific activity, and concentration, etc.) 250 μl samples were taken at known intervals, from both chambers of the cell, and added to Canberra Packard Ultima Gold Scintillation Cocktail (10 ml) for counting. Counting of individual samples was for a period of 10 mins. The recorded counts per minute (c.p.m.) were corrected for counting efficiency (to give an activity in disintegrations per minute {d.p.m.}) using calibration data from a set of Amersham Searle $^{3}_{1}$T quenched standards (see paragraphs 7.11.3.1 → 7.11.3.1.2). Note that (8×10^{-3}% of either chamber was removed by the sampling during the experiment.

Despite the changing 4-nitrophenol concentration (as it permeated) in some of these experiments, the tSIE (transformed Spectral Index of External Standard: a measure of the efficiency of the quench correction) figure remained constant, throughout the course of each experiment indicating that quenching due to the 4-nitrophenol was not a problem.

Concentrations for the different readings were determined by taking the recorded activity (d.p.m.) at any time, *t*, and determining the concentration as a proportion of the known initial activity. This was the simplest method, since not all molecules present were labelled in some of the following compounds. The overall concentration was, however, provided, and the volume, and activity added to the cell were known quantities.

7.11.1.2 ^{14}C labelled sucrose.

Carbon-14 is a beta emitter, with a maximum energy of 0.156 MeV, and a mean energy of 0.045 MeV. The half-life is 5730 years, which is insignificant over the duration of the experiment. The stable daughter nuclide is nitrogen-14.

The labelled sucrose is prepared by extraction from Canna leaves that have been allowed to photosynthesize in the presence of ^{14}C-labelled CO_2 for ca 16 hrs. Not all sucrose molecules are labelled (and not every carbon on each labelled sucrose molecule is ^{14}C), and a proportion of the sample is carrier. To the donor solution was added 5 μCi (25 μl) of the labelled sucrose. The donor solution itself was a solution of unlabelled sucrose, made to the same concentration as the labelled sucrose. Samples of 250 μl were removed for counting.

7.11.1.3 ^{36}Cl labelled sodium chloride.

Chlorine-36 has a $T_{1/2}$ of 3.01×10^{5} years (again insignificant when compared to the experiment duration), and undergoes ß-decay to give a stable daughter nuclide of argon-36. The mean beta energy is 0.25 MeV, and the maximum energy is 0.709 MeV. The Cl^- was added at the concentration provided. 5 μCi (58 μl) was added to the donor chamber of the cell. Efficiency of counting was determined by comparing the count of a sample of known activity, and was accepted as 95%. Samples of 250 μl were removed and measured as in the manner of the THO.

---

[1] 1 μCi = 3.7×10^{4} disintegrations per second = 2.22×10^{6} disintegrations per minute. (1 Bq = 1 d.p.s.)

7.11.1.4 ^{22}Na labelled sodium chloride.

Unlike the previous isotopes, $^{22}_{11}$Na is a gamma emitter and was analysed using a solid scintillation method (Canberra Packard 500 Auto Gamma Counter, with a 3" crystal). The efficiency of counting was estimated (from the measured number of counts per minute compared to the expected number of disintegrations per minute) as being approximately 54% (this was only an estimation from a sample count, ignoring detector geometry, etc.).

As with the labelled Cl^-, 5 μCi (40 μl) was added to the donor chamber of the permeability cell. However, the labelled Na^+ ion concentration was negligible in comparison with that of the labelled Cl^- ion (*i.e.*, ca 10^{-6} M for the Na^+, *cf.* 10^{-4} M for the Cl^-). To allow a comparison of the fluxes, the Na^+ concentration was therefore made up to that of the Cl^- with unlabelled NaCl carrier.

7.11.2 Isotope uptake during permeation experiments.

The uptake of the isotopes by the various films was monitored by investigating the overall loss in activity from the permeability cell (whilst monitoring the cell's surroundings so that the loss was not attributable to leakage). Obviously the total number of measurable disintegrations should remain constant, within the limits of experimental uncertainty (*i.e.*, allowing for the randomness of the decay process): the half-lives of the isotopes leading to negligible decay during the course of a permeation experiment, and the magnitude of the background radiation being negligible in comparison to that being measured.

7.11.3 Liquid scintillation counting.

Liquid scintillation counting is used to measure the decay of beta emitting nuclides. The sample is dissolved in a scintillator and energy from the emitted ß-particles is converted, by means of a fluor, to light photons that are accurately counted by means of a photomultiplier tube in the liquid scintillation counter.

7.11.3.1 Quenching.

Energy transfer from the ß-decay process is not 100% efficient due to energy lost as vibrational/rotational energy. Further losses, more important in the detection process, occur due to inefficiency of the energy transfer in the fluorescence process. These losses are termed quenching, and are due to three main reasons:

- ✗ Chemical quenching: non-aromatic chemicals, especially halogenated compounds, ketones and aldehydes, all cause quenching by interfering with the energy transfer from the radiation to the fluor.
- ✗ Colour quenching: light absorbing compounds reduce the number of photons available to the detector. PPO fluoresces in the blue region (300 → 400 nm) of the spectrum, therefore red compounds demonstrate greater colour quenching than do green or blue compounds.
- ✗ Physical quenching: occurs when (i) photons are absorbed at a surface, or (ii) the radioactive particles are not in intimate contact with the scintillation cocktail due to insufficient solubilisation.

7.11.3.1.1 Photon detection.

Photon detection occurs by means of photomultiplier tubes (PMTs). For each 1 keV of decay energy, between 5 → 7 photons are generated, each of which only has an approximate 33% chance of producing an electron pulse in the detection system, due to quenching effects reducing the photon emission below the detection threshold of the PMT. Counting efficiency may also be reduced if the number of decays is such that the PMT does not have enough time to recover in between consecutive photon strikes (PMT dead time).

The result of the detection process is calibrated in the number of '**counts per minute**.' Due to quenching, this number will normally be less than the actual number of **disintegrations per minute.** The ratio of the number of counts per minute to the number of disintegrations per minute in the solution is the **efficiency** of counting.

7.11.3.1.2 Quench correction.

The effect of quenching is to cause a shift of the beta spectrum, due to the reduced photon yield. This effectively makes the spectrum appear as if the isotope is emitting energy at a reduced level and is worse for isotopes with low beta energies. Quenching effects can be corrected by a number of methods. In the case of this project, samples contained a known initial activity (determined from the specific activity of the supplied sample and the volume used). In a number of cases, the efficiency of counting was simply estimated from a comparison of the observed count to the expected number of disintegrations. (It was in general only necessary to know the relative number of observed counts per minute over the course of a permeation experiment: a knowledge of the true number of disintegrations per minute, however, would be more correct.)

For the tritium counting in this project, the results of a set of tritium quenched standards (Amersham/Searle) were available and, hence, were used. Such standards are calibrated for activity by comparison with the National Bureau of Standards (U.S.A.) tritium solution standard: Standard Reference Material (SRM) N°. 4947, tritiated toluene in toluene. The method of calibration was liquid scintillation channels ratio quench correction using secondary standards proposed from SRM 4947.

The channels ratio method uses the ratio of counts from different channels (energy ranges) of the detector to calibrate for loss of efficiency from a graph of counting efficiency as a function of channels ratio. Because of the shift in the spectrum with increased quenching (the count rate decreases with increasing quenching) the counting efficiency will vary as a function of the channels ratio, and the set of known-quenched standards provides for the calibration graph. Such a calibration is recorded within the instrument (the tSIE), which uses the Quench Indicating Parameter (QIP) of the tSIE to compensate for quenching, and therefore gives an output of the absolute activity of the sample.

Results and Discussion, Chapter 8: Morphology and Permeability of Eudragit® Films.

8.1 Introduction.

In this Chapter, the film formation and morphology of various Eudragit® copolymers are examined together with their solute, gas, and water vapour permeability coefficients. All latices were used as received, but diluted to 5% solids content (from the original 30%), and plasticiser was added where needed (*i.e.*, all except Eudragit® *NE*) prior to film formation.

8.2 Film formation and morphology.

8.2.1 Eudragit® *NE*.

All Eudragit® films were cast at a temperature of 313 K for 24 hrs, in an oven containing fixed weights of desiccant. **Figure 8.1** and **Figure 8.2** plot the conditions within the laboratory oven during casting. It is apparent that the temperature inside the oven was *not* constant. The saw-tooth waveform of the temperature plot is typical of the thermostatic control of an oven, and shows the temperature to vary by ± 1 K around the mean temperature. (The oven was not fan assisted and so, after the initial disturbance due to insertion of the film into it, the air over the film – and therefore over the temperature and relative humidity {R.H.} probes – would be still aside from the convection currents caused by heat rising from the heating elements positioned in the base of the oven.) Although the oven was left permanently at the casting temperature, it is clear that the temperature dropped to just under 303 K when the door was opened. This drop in temperature was countered within an hour after insertion of the film.

The instability of the temperature had an effect on the R.H. which varied by ca ± 6%. The R.H. was measured directly above the latex/film surface, in the evaporative flux, and was not necessarily representative of the entire oven interior, which contained silica gel as a desiccant.

Constant weight and, hence, the attainment of **a fully dried film, was achieved in slightly less than 11 hrs**. This was accompanied by an overall rise in the oven temperature of approximately 1 K, and a corresponding sharp decrease in the R.H. The average **rate of water loss** from the wet latex was equal to 0.027 g min^{-1} (or **3.809×10^{-4} g min^{-1} cm^{-2}**), as determined by the change in the cumulative weight loss (over the steady-state region) as a function of time, and was constant from between 1.5 hrs and 8 hrs (**Figure 8.2**).

The data points of the cumulative weight loss curve can be fitted to an equation of a fifth order polynomial in order to calculate instantaneous film drying rates (see Vanderhoff[507] *et al.*):

$$W = -4.75269\times10^{-13}t^5 + 7.521428\times10^{-10}t^4 - 4.702172\times10^{-7}t^3 + 1.50198\times10^{-4}t^2 + 1.327713\times10^{-3}t + 4.010172\times10^{-2} \tag{8.1}$$

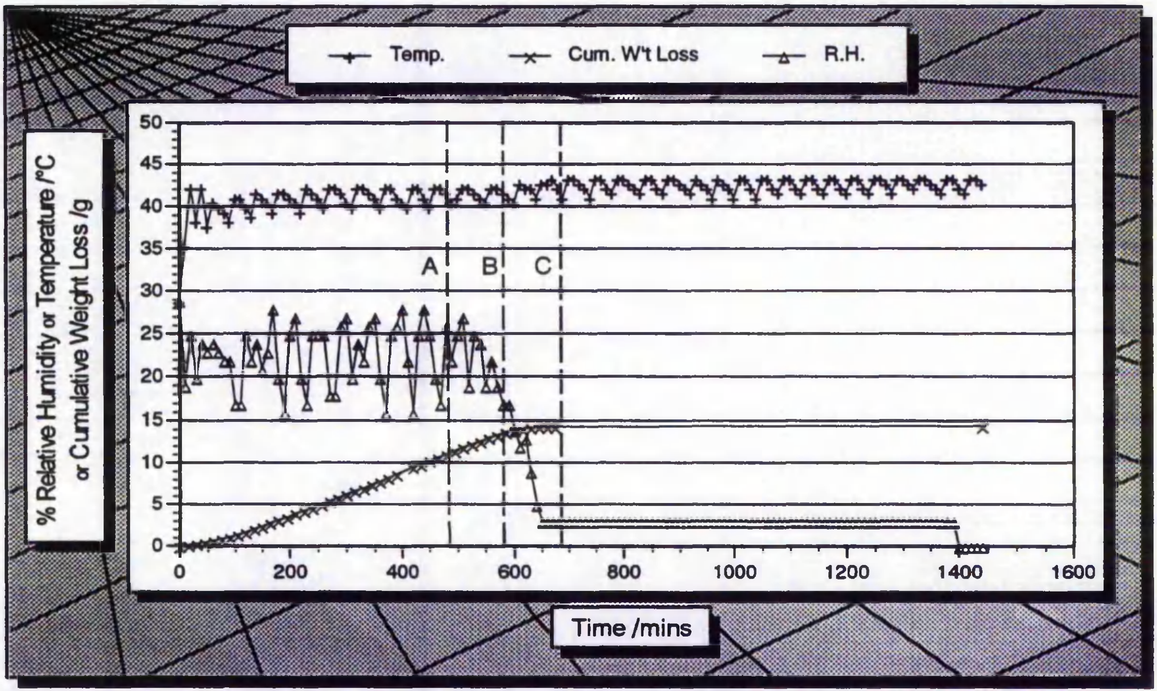

Figure 8.1 Oven conditions during the drying of a Eudragit® *NE* film cast from 5% polymer solids content. A = skin + iridescence (16.5% vol. fraction); B = fully formed skin (50% vol. fraction); C = film totally clear.

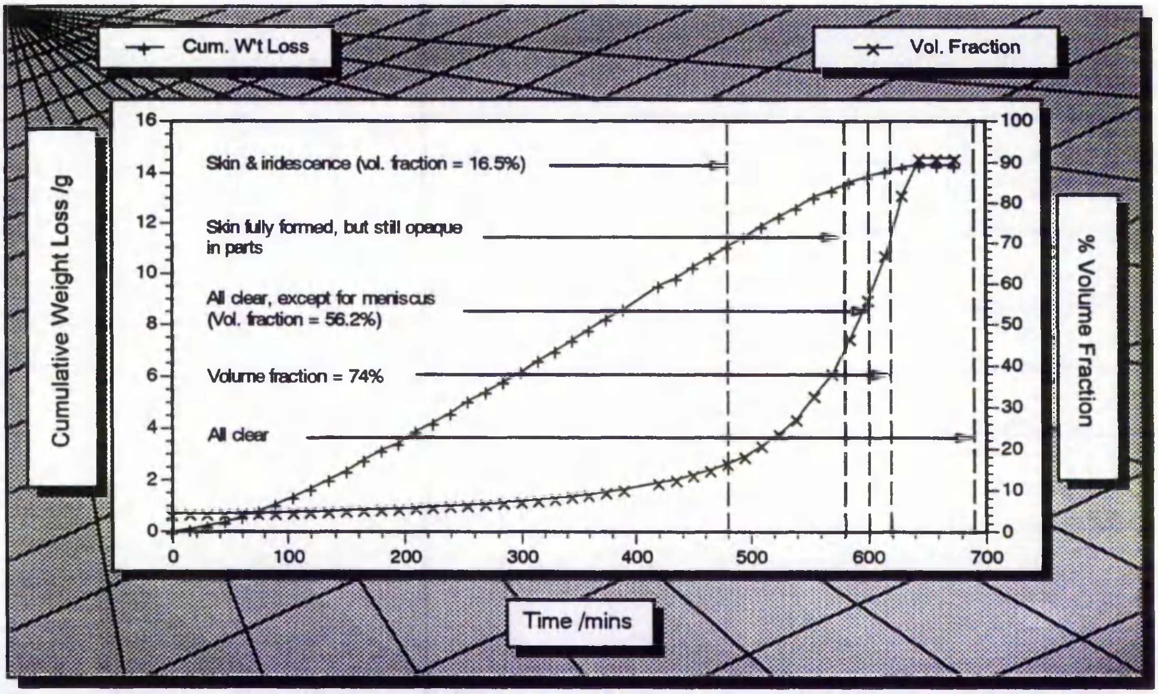

Figure 8.2 Plots of cumulative weight loss, and percentage volume fraction of polymer solids during the casting of a Eudragit® *NE* film.

Correlation between the calculated data from such a function and the experimental data, results in a correlation coefficient, r^2, of 0.99998. The derivative (dW/dt) of the polynomial function allows the instantaneous evaporation rate of the water, during the experiment, to be determined. (Such a derivative actually shows that there was a small increase in the rate of evaporation, over the range of the 'constant rate' region of the cumulative weight loss curve, from 0.025 → 0.027 g min^{-1}.) It can be ascertained, however, that the rate of evaporation began to decrease at a time of 450 min, corresponding to a mean volume fraction, Φ, of 14% (polymer solids). This indicates that there was a fall in the evaporation rate well before the latex particles came into intimate contact. However, due to the non-uniform drying of the film, this value of 14% is an average value for the film as a whole, but locally may be much higher.

At a time of 480 min, **iridescence** was visible on a small region of the latex surface, and it was in this region of iridescence that a **skin** was first observed (Φ = 16.5%). The initial skin was also over a small region of the surface only (not covering the whole film), and it was noted, from observation of subsequent films, that the first sign of skin formation could occur randomly anywhere on the latex surface.

The skin was seen to spread in the form of a front, outwardly, from the site of its first presence, with concentric bands of iridescence of differing colours (**Figure 8.3**). Such iridescence is indicative of crystalline long range order in the latex particle packing, with a particle separation of the order of the wavelength of visible light (400 → 600 nm): the different colours indicating that the bands in the drying front consist of regions of latex of different packing fraction.

The skin was fully formed at 580 min (Φ = 44%), although approximately one sixth of the film area was still white at this time indicating wet latex or 'gel' underneath the skin. By 600 min (Φ = 56%), the film was transparent all over apart from the meniscus at the cylinder wall, which was last to dry – possibly due to it being unrepresentatively thick (surface → substrate) compared to the rest of the film.

The rate of evaporation decreased rapidly after 550 min due to the decreased open wet area, whilst Φ increased at a similar rate. The increase in Φ caused the particles to be fixed in a stationary position, such that in these regions the film was 'gel-like.'

A Φ of 74% (corresponding to the close packing of uniform spheres) occurred at a time of 620 min. This is some 2 hrs after the first signs of iridescence, however, it should again be

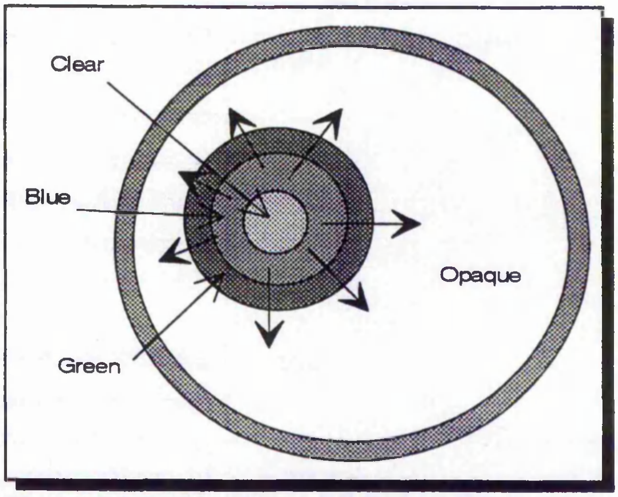

Figure 8.3 Iridescence and film formation at a time of ca 500 min.

noted that the volume fraction is an average figure for the latex/film as a whole. This **non-uniformity of drying** occurred despite the fact that the films were placed on a levelled platform which gave a final film thickness with ⟨ 10% variation across the diameter. Such non-uniform drying is in agreement with the observations of Joanicot [257] *et al.*, Okubo [366] *et al.* and Pramojaney [402] *et al.*, and appears to be related to skin formation and the relief of stresses [391] in the film by slippage of the skin over the wet latex underneath.

Chevalier [95] *et al.*, when observing the drying of core-shell latex particles (poly(acrylic acid) shell, poly(butyl acrylate)-poly(styrene) copolymer core and with a hydrophilic shell of surfactant) noted a coalescence front (as seen in this study for Eudragit® *NE*) for a drying film, which spread from the periphery inwards. Only in the case of the cleaned latex was it claimed that the film dried uniformly. (Note, however, uniform drying was not evident in the drying of the surfactant-free latices, or the dialysed Eudragit® *NE* as utilised as part of this study {see Chapter 9}.) Eudragit® *NE* is reported to contain endogenous surfactant (3.3% [204]), and the drying front described by Chevalier is presumably similar to that observed for Eudragit® *NE*. Vanderhoff observed that as a latex film underwent further gradual coalescence, incompatible surfactant was exuded to the film surface [500]. No such exudation was observed by S.E.M. in this study, but this could be due to either the polymer and surfactant displaying better compatibility, or due to the polymer film undergoing only very slow, if any, further polymer fusion/film densification after casting, or more simply, due to the low level of surfactant not being visible.

In many cases, 'islands' of iridescence/skin were formed on the drying latex which eventually merged and led to the formation of the 'fissured' surface. **Eudragit® *NE* films** were found to **have a textured matt-finished upper surface**. This surface texture normally consisted of one or two relatively large vein-like 'fault' lines ('**mud-cracks**') with the remainder of the surface covered with a much finer level of crazing. Whether the larger mud-cracked effect consisted of fissures or ridges in the film surface was sometimes difficult to ascertain: the cracks, if that is what were present, were very shallow, and too narrow to allow their thickness to be measured with the flatfooted dial gauge. However, films that swelled were typically more opaque in the regions of the mud-cracks, perhaps indicative of a less dense structure, allowing a greater degree of hydration; shining of a light through a film typically gave shadow over the bulk of the film area, whereas the mud-cracks allowed a greater intensity of light to be passed indicating the film was thinner in the region of the crack. It was not apparent, however, whether the film was slightly thicker to one side of the fissure compared to the other: as may occur if the skin from one drying front were able to rise over the skin of a second front at the point of their confrontation.

Chevalier [95] *et al.* noted that the final region of the film to dry appeared hazy, and suggested that this was due to residual surfactant, concentrated at this point. The Eudragit® *NE* films in this study showed no such affect, appearing of uniform transparency.

The rate of film drying was linear (with a correlation coefficient of $r^2 = 0.9997$, ignoring the initial lag and final stages of drying) over much of its range (**Figure 8.4**). This indicates a process controlled by the rate of evaporation. Plotting the cumulative weight loss as a function of the square root of time ($t^{½}$, as depicts Fickian desorption) yields a curve which is linear ($r^2 = 0.9993$), but over a much smaller range of the drying time (ca 260 min, towards the end of drying, compared to ca 400 min {*i.e.*, most of the range} for the curve proportional to t). It is significant that this range occurs towards the end of the drying period: indicating a change in the mechanism of drying from an evaporative process, to a diffusion controlled process. The fact that the point at which the change (of mechanism) occurs cannot be predicted more precisely is again a result of the non-uniform drying, such that the two mechanisms would operate concurrently, with the exception of the final stages of drying (after full skin formation: ≈ 580 min).

The **lower surface** (substrate side) of the films **showed no sign of 'mud-cracking'**, appearing **smooth and glossy**. This would indicate that the upper surface features were a result of skin formation. However, another consideration is the fact that the polymer is in contact with the Pyrex glass substrate. Glass has a higher coefficient of heat conduction than air which will affect the drying at the two surfaces. The implication of this arises when the majority of the water has been removed and the latex is subject to a thermal annealing process: the substrate side being subject to a greater degree of thermal transmittance than the air side, as discussed by Pramojaney[402] *et al.*

Freeze-fracture cross-section T.E.M.s of Eudragit® *NE* films cast under the conditions described above are shown in **Plate 8.1** and **Plate 8.2**. The structure observed in these plates may account (due to its interaction with light) for the matt, grainy, appearance of the films, and possibly results from vestiges of the particles, which have been greatly deformed. However, the structures show poor correlation with the Eudragit® *NE* particle size (*i.e.*, are bigger than expected) and may simply be artifacts of the fracture mechanism. It was thought that the points of fracture were being influenced by the distribution of endogenous surfactant which could cluster and provide areas of weakness within the film.

Despite the visual differences between the upper and lower surfaces of the film, no difference could be seen in S.E.M.s of the upper and lower surfaces. Lehmann[313] noted that Eudragit® *NE* films (M.F.F.T. of less than 283 K) cast at temperatures of 10 → 20 K above their M.F.F.T. showed no sign of particulate structure within a few minutes after drying. The z-average mean P.C.S. **particle diameter of Eudragit® *NE*** was **163.0 nm**, and had a monomodal distribution with a polydispersity value of 0.022. No particles (or the structure seen in the F.F.T.E.M.s) were evident in the S.E.M.s.

8.2.2 Eudragit® *RL*.

The formation of Eudragit® *RL* films loaded with 15% triacetin per gram of *RL* solids, at 313 K oven temperature, were monitored and changes in various parameters are shown in **Figure 8.6** and **Figure 8.7**. Like the Eudragit® *NE*, a fifth order polynomial could be fitted to the cumulative weight loss data (with a correlation coefficient $r^2 = 0.99998$):

$$\begin{aligned} W = {} & -5.811801 \times 10^{-13} t^5 + 9.164145 \times 10^{-10} t^4 - 5.517683 \times 10^{-7} t^3 + \\ & 1.629733 \times 10^{-4} t^2 + 9.371603 \times 10^{-4} t + 1.924172 \times 10^{-2} \end{aligned} \qquad (8.2)$$

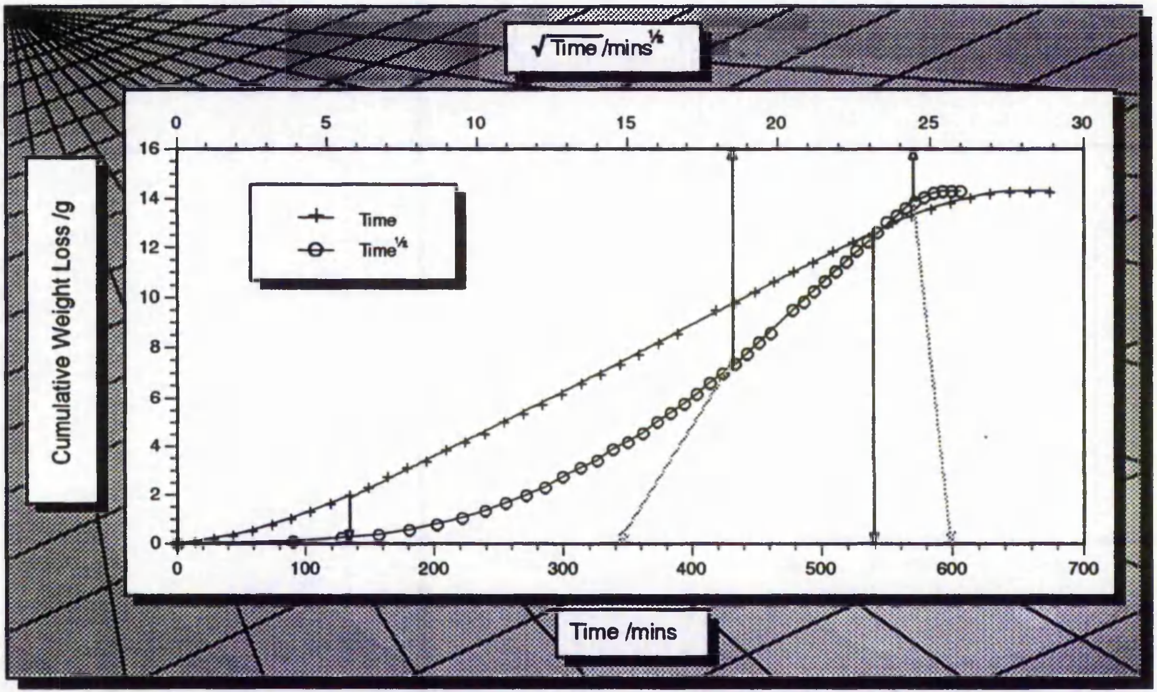

Figure 8.4 Cumulative weight loss during the drying of a Eudragit® *NE* film as both a function of time, and the square root of time.

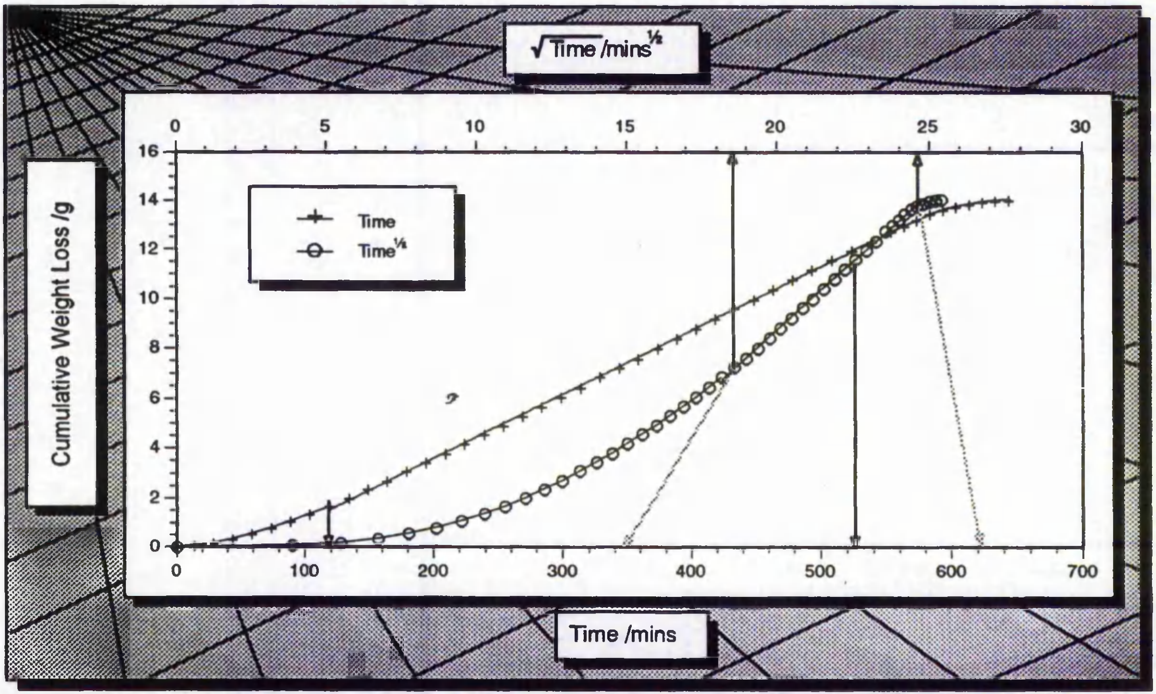

Figure 8.5 Cumulative weight loss during the drying of a Eudragit® *RL* film as both a function of time, and the square root of time.

Plate 8.1 (957363) Freeze-fracture cross-section T.E.M. of Eudragit® *NE* film cast for 24 hrs at 313 K.

Plate 8.2 (957364) Freeze-fracture cross-section T.E.M. of Eudragit® *NE* film cast for 24 hrs at 313 K.

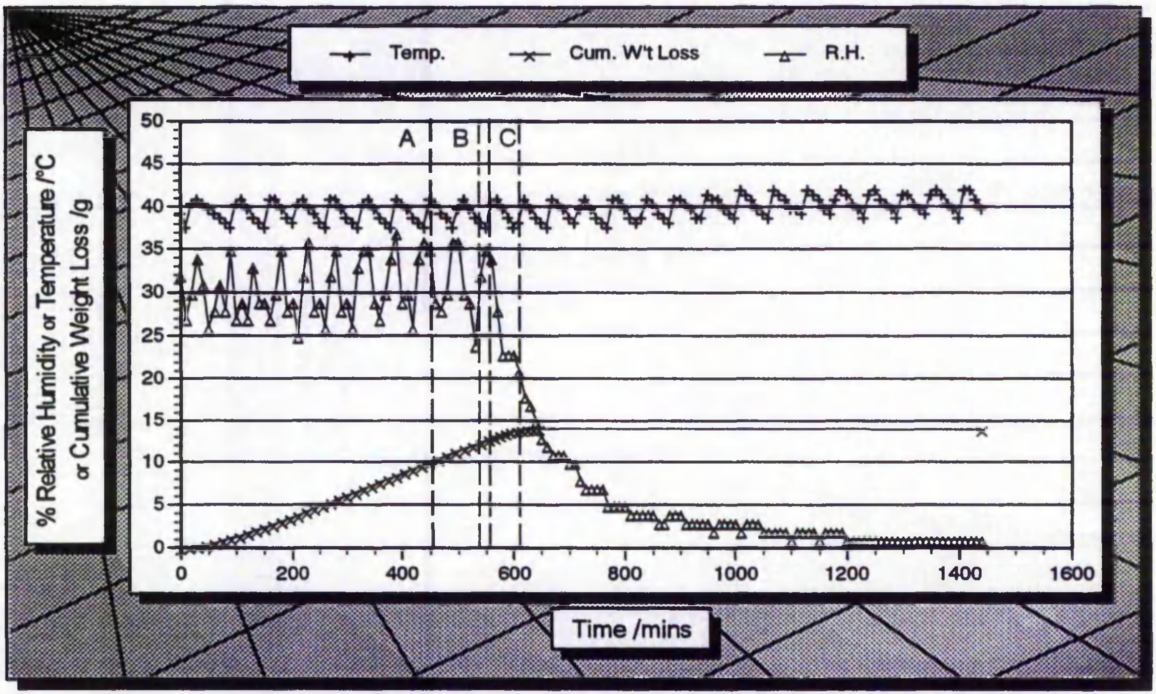

Figure 8.6 Oven conditions during the drying of a Eudragit® *RL* film cast from 5% polymer solids content. A = first sign of a skin; B = hexagonal dimples appeared over front half of film; C = dimples nearly vanished.

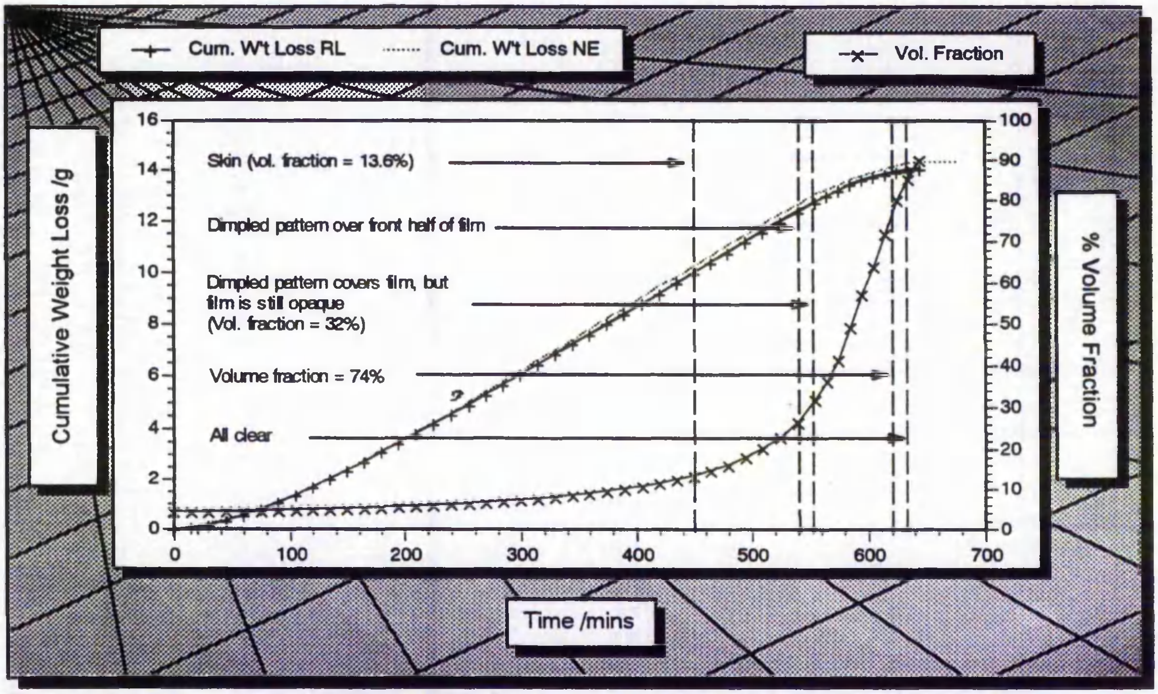

Figure 8.7 Plots of cumulative weight loss, and percentage volume fraction of polymer solids during the casting of a Eudragit® *RL* film.

A plot of dW/dt shows that the rate of evaporation increased slightly, over the 'linear' region, up to a time of 458 min. This was at the approximate time when a **skin** was first seen, and corresponds to a value of Φ (calculated assuming a polymer density of 1.15 g cm^{-3}) of approximately 14%. Isaacs [251] and Pramojaney [402] *et al.* both found quite large increases in the evaporative flux towards the end of film formation (at the end of the constant rate period) which Isaacs attributed to gelation of the latex giving a larger evaporative surface area. No such increase was evident for either Eudragit® *RL* or Eudragit® *NE*. The **average drying rate** of the **Eudragit® *RL*** was 0.026 g min^{-1} (or **3.668×10^{-4} g min^{-1} cm^{-2}**) which is very slightly less than the value for the Eudragit® *NE*. This may either be due to the film being more hydrophilic, and thus holding onto its water (due to hydrogen bonding), or to the higher R.H. of the oven. (A plot of the near identical Eudragit® *NE* data is shown in **Figure 8.7** for comparison.)

A plot of the cumulative drying rate of Eudragit® *RL* as a function of $t^{1/4}$ alongside the plot as a function of time, t, shows that, like Eudragit® *NE*, the curve is linear as a function of t over a much greater range (than that as a function of $t^{1/4}$) (**Figure 8.5** and **Figure 8.4**). It is clear that the bulk of the drying process is an evaporative process rather than a diffusive process.

Eudragit® *RL* films dried in a much more uniform manner, with respect to film surface area, than the Eudragit® *NE* films. The skin, first observed at a time of 455 min, covered approximately one half the film after 540 min and the whole film 10 min later. Whereas the Eudragit® *NE* dried in the form of an advancing front, the Eudragit® *RL* was seen to be still white and opaque underneath this complete skin, with no clear regions to the film. The skin took the form of a pattern of approximately hexagonal shaped 'dimples': white and opaque at the centre, but less opaque towards the edges of the dimple, making them well defined and giving the appearance of a honeycomb. (These dimples were possibly Rayleigh-Bénard convection cells.) At 555 min (Φ = 32%), these features covered the film surface, each being ca 0.5 cm across. This was much greater than the **Eudragit® *RL* latex P.C.S. z-average particle diameter of 177.3 nm**[1]. The rate of evaporation was also slightly less than for the Eudragit® *NE* at an equivalent packing fraction (Φ = 32%).

As drying progressed, the 'dimples' flattened: at 565 min (Φ = 36%) the film appeared much more translucent, being only slightly hazy, and by 605 min (Φ = 64%), the dimples were barely visible. The crystalline cubic close packing fraction (Φ = 74%) occurred at a time of 620 min, and the film appeared completely clear at a time of 635 min.

In a dried Eudragit® *RL* film which had been removed from its substrate, the 'dimples' (which had been observed during casting) were still faintly visible as shallow indentations if the film was held such that the eye was looking flat across the surface (and

---

[1] The P.C.S. z-average particle diameter of Eudragit® *RL* differs to that of Eudragit® *RS* which was 151.9 nm. This difference, and the fact that the latices showed broader size distributions than Eudragit® *NE* was presumably due to their pseudo-latex nature and their method of preparation.

the light was at the correct angle!). Eudragit® *RL* films were otherwise clear (which was presumably a good indication of the plasticiser compatibility with the polymer) and fault free, and slightly tacky (unlike the Eudragit® *NE* which was not tacky). Despite the use of a plasticiser, the films were quite brittle at ambient temperature, and were easily fractured during the course of normal handling. Although brittleness is indicative of a hard (relatively high T_g) polymer, the films showed no sign of residual particulate structure when observed under the resolution of S.E.M., demonstrating that the polymer was sufficiently pliant for particle deformation to occur at the film casting temperature. **Plate 8.3** shows the upper (polymer-air) side of the film, and **Plate 8.4** the fracture cross-section of the film.

8.2.2.1 Fate of triacetin in Eudragit® *RL*.

As previously stated, triacetin was normally added to Eudragit® *RL* at a concentration of 15% per gram of polymer solids. On soaking in water for 12 hrs, the film lost 97.7% of this addition. Soaking for 48 hrs and 96 hrs gave figures of 100%. Monitoring of the leaching of additive from the film spectrophotometrically indicated that most of the triacetin was actually leached out within the first hour of soaking[1]. (Note, Lehmann[313] claims that Eudragit® *RL* contains no emulsifiers or additives apart from ascorbic acid (0.25%) to act as stabiliser.) Rapid leaching of film additives such as plasticiser or surfactant has also been observed by Okor[355], and Donbrow and Freidman[124, 125]. Okor found that 97% of the added triacetin leached from a solvent cast Eudragit® *RL(100)* film within 30 min.

S.E.M.s of Eudragit® *RL* films leached of their plasticiser, and then dried for 24 hrs at 313 K showed no sign of pores resulting from the leaching process, although this is possibly due to the degree of dispersion of the plasticiser and the inability of the S.E.M. to resolve such detail. **Plate 8.5** and **Plate 8.6** show the S.E.M.s of the polymer-air side and the fracture cross-section, respectively, of Eudragit® *RL* films which have been leached of their added triacetin for 96 hrs and then dried at 313 K. The cracks are presumed to be due to the stress imparted by drying the films which would be more brittle following the removal of their plasticiser.

Triacetin itself is non-film forming under the usual casting conditions in the oven, leaving only a very fine residue. Winnik[543] *et al.* comments on the use of plasticiser in latex paints, and the importance of the plasticiser to aid the film formation process, but also that it should be quickly evaporated off (fugitive plasticiser) during film formation such that the final film is not left soft. Such evaporation presumably did not occur with the triacetin (boiling point = 531 K[317]) added to these Eudragit® *RL* films since the final film was malleable (compared to the plasticiser-free film) (and, as stated above, triacetin could be detected when leaching), *i.e.*, the majority of the triacetin was retained by the polymer.

---

[1] Triacetin showed a narrow peak in the UV region (peak at 212 nm; ending at approximately 240 nm with very little tail to higher wavelength). Because this peak was close to the lower limit of the Philips spectrophotometer (and the cutoff due to air absorption), no concentration measurements were made. When the dissolution products of Eudragit® *RL* were scanned this peak was visible, but no others were. (This allowed measurements of the anilines (see paragraph 8.6.7) at wavelengths $\rangle$ 280 nm.)

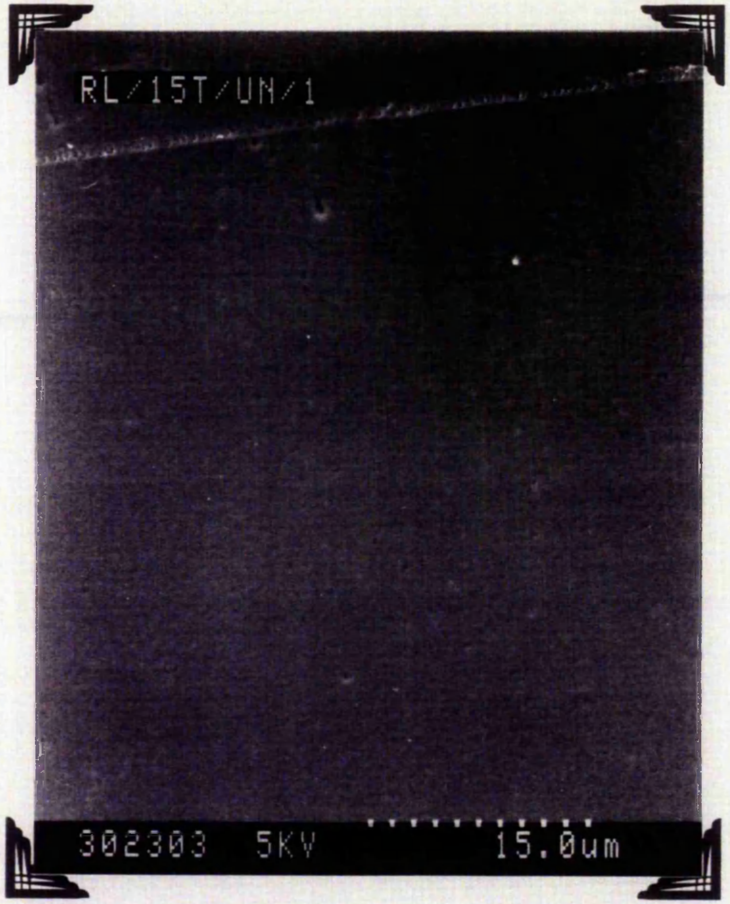

Plate 8.3 (302303) S.E.M. of the upper surface of a Eudragit® *RL* film cast containing 15% triacetin.

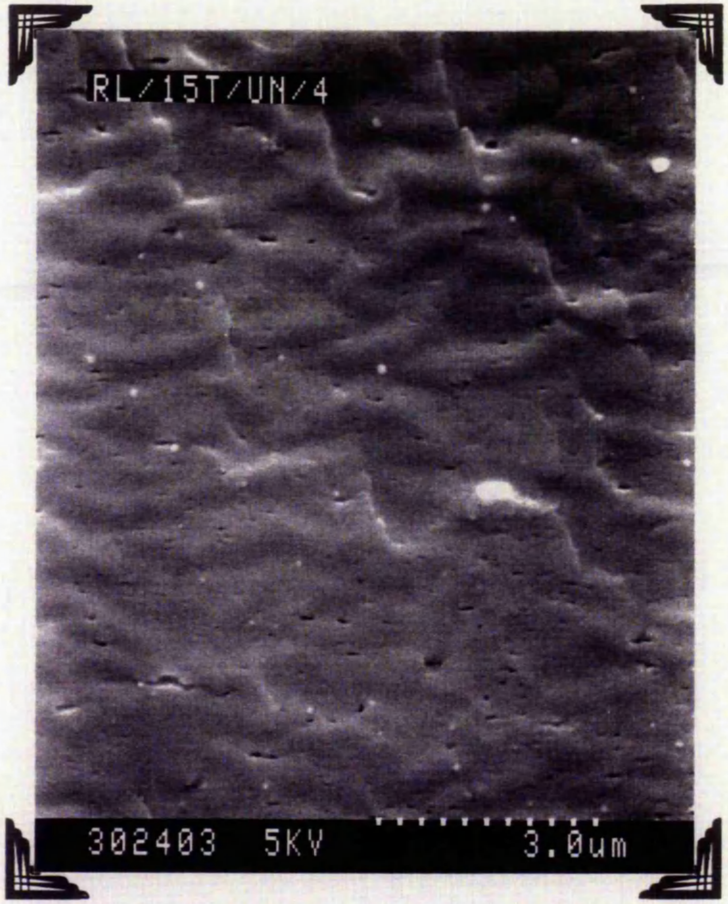

Plate 8.4 (302403) S.E.M. of the centre of the fracture cross-section of a Eudragit® *RL* (+ 15% triacetin) film.

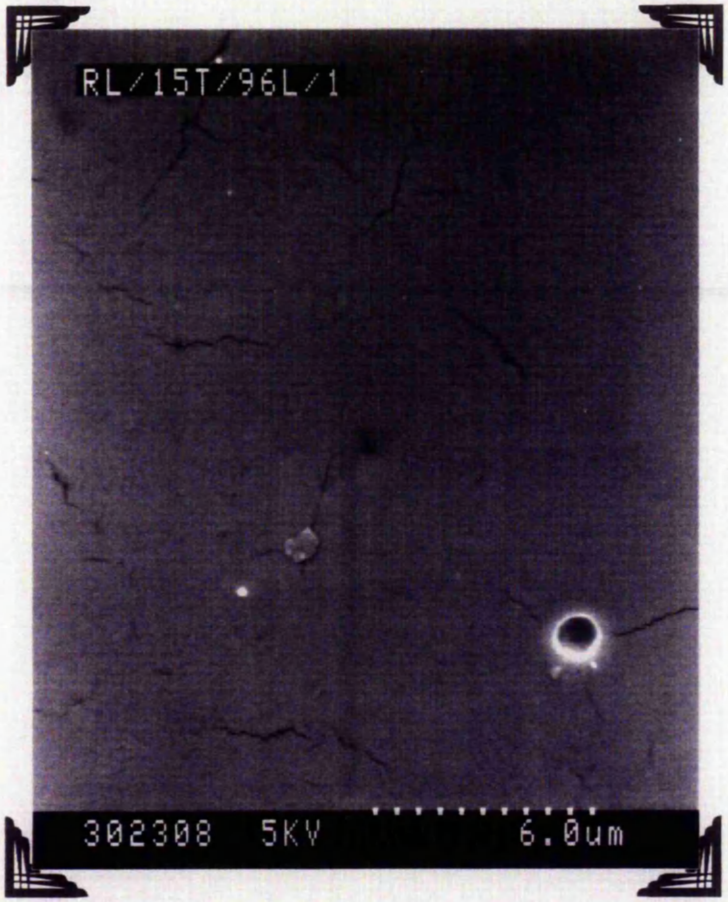

Plate 8.5 (302308) S.E.M. of the top surface of a Eudragit® *RL* film leached of its plasticiser.

Plate 8.6 (303500) S.E.M. of the centre of the fracture cross-section of a Eudragit® *RL* film leached of its plasticiser.

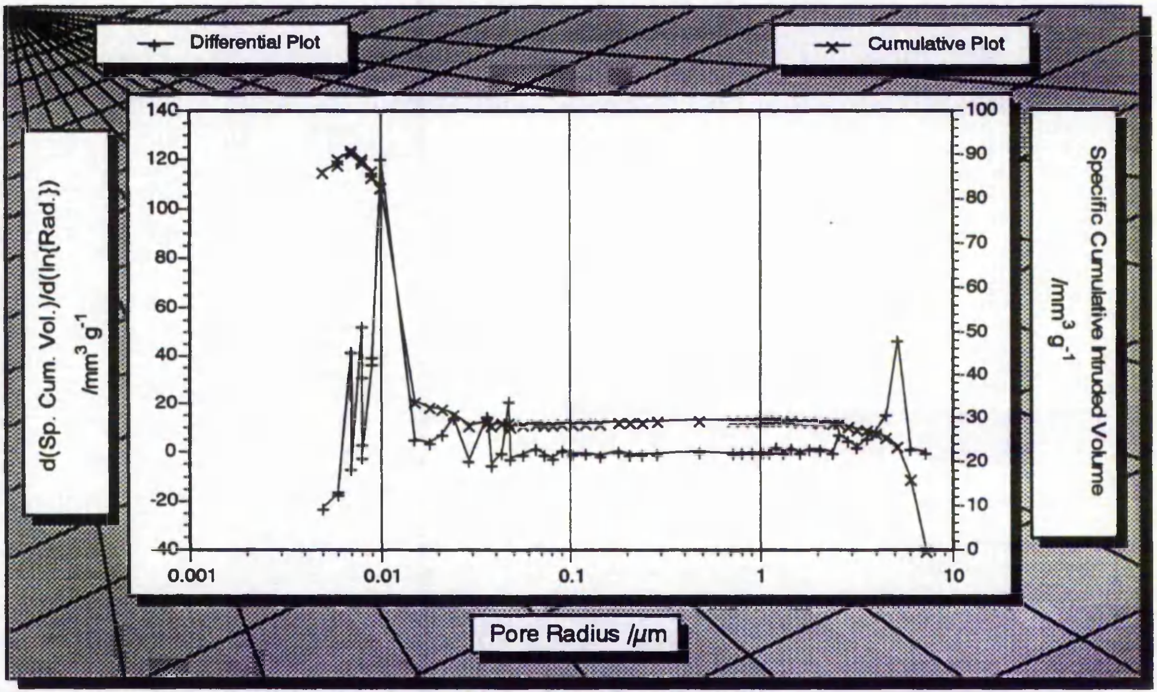

Figure 8.8 Pore distribution of a Eudragit® *NE* film, by mercury porosimetry.

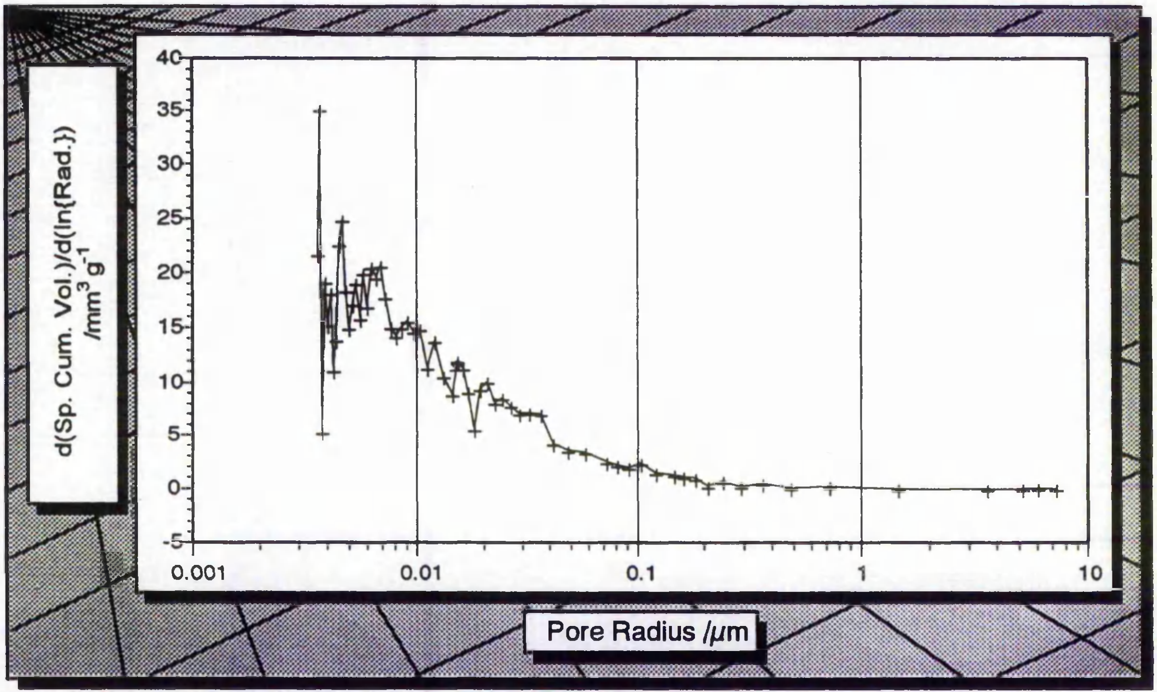

Figure 8.9 Pore distribution of a Eudragit® *RL* film, by mercury porosimetry.

8.3 Mercury porosimetry on Eudragit® films.

An attempt was made to find evidence of a pore structure in Eudragits® *NE*, *RL* and *RS* using the technique of mercury porosimetry[1]. **Figure 8.8** shows the resultant data for the Eudragit® *NE* film, plotted as both a cumulative volume curve, and also as a differential type curve. The former of these two types of curves illustrates a pore (radius) distribution by means of a sudden change of gradient, whilst the latter shows the presence of pores by means of a peak. A small peak was present at between 5 → 6 μm, with more peaks at high pressure (radii $<$0.05 μm). The peak at 5 μm (at relatively low pressure, ≈ 1.4×10^5 N m^{-2}) should result from pores which were evident in the S.E.M. However, none were seen. Possible explanations of this are (i) the fact that the intruded volume is relatively small, implying that the pores, if present, are few in number, or (ii), that the polymer was compressed as the pressure increased. This peak was evident in all samples of Eudragit® *NE* investigated (see Chapter 10). The peaks at the lower end of the size range centre around ca 10 nm and, as such, were beyond the resolution of the S.E.M. (20 nm).

Figure 8.9 shows a differential type plot for mercury porosimetry on Eudragit® *RL*. Very little in the way of any structure is apparent, aside from at the high pressure end of the scale. This is to be expected, from the visual appearance of the Eudragit® *RL* film: being very clear and transparent. A porous film structure tends to appear white and opaque due to differences in refractive index and diffraction of light striking a surface when its structure is smaller than the wavelength of light. The slightly greater cumulative intruded volume found for the Eudragit® *NE* film, and the greater porosity seen in the plot for the Eudragit® *NE* film may account for the fact that the Eudragit® *NE* film is not quite so transparent as the Eudragit® *RL* film.

The results for a Eudragit® *RS* film showed no significant difference to those for the Eudragit® *RL* film.

8.4 The carbon dioxide permeability of Eudragit® films.

The CO_2 permeability coefficients of films prepared from Eudragits® *NE*, *RL* and *L* were measured as a function of film age over the course of a month (**Table 8.1**). The literature on gas permeability displays a large range of varying units making comparisons difficult. Helpfully, Lebovits [307] provides a number of conversion factors[2]. The units given in the table are those from the equation used in the calculation (see Chapter 7), with no simplification, and as used by the Polymer Handbook [398].

---

[1] Note that compression of the mercury is accounted for in the results.

[2] The difference in units arising from the determination of a gas permeability coefficient compared to any other permeability coefficient arises from the fact that in the latter, the same units are generally used to express the concentration in the concentration differential, as are used to express the amount of permeant in the flux (*i.e.*, a concentration gradient is the driving force when calculating, for example, a solute permeability coefficient). However, the flux of a gas is normally based upon a rate of change of volume at fixed pressure, whilst a pressure differential is the driving force. Yasuda [548] details the necessary changes to be made in order that the gas permeability coefficient be expressed with dimensions of L^2/t if deemed necessary.

Table 8.1 Eudragit® film carbon dioxide permeability results (at ambient temperature).

FILM TYPE	AGE	PERMEABILITY COEFFICIENT (±S.D.) /cm^3 cm s^{-1} cm^{-2} cm.Hg^{-1}
NE 30 D	0	$1.99(\pm 0.03)\times 10^{-9}$
	25 hrs	$1.99(\pm 0.04)\times 10^{-9}$
	49 hrs	$2.21(\pm 0.02)\times 10^{-9}$
	73 hrs	2.09×10^{-9}
	6 days	1.92×10^{-9}
	8 d	1.93×10^{-9}
	2 weeks	1.59×10^{-9}
	3 w	1.37×10^{-9}
	1 month	1.31×10^{-9}
RL 30 D (+ TRIACETIN)	0	3.72×10^{-10}
	24 hrs	3.29×10^{-10}
	48 hrs	3.68×10^{-10}
	6 d	2.61×10^{-10}
L 30 D (+ TRIACETIN)	0	2.66×10^{-9}

In relation to its molecular size, CO_2 is normally found to have an anomalously high permeability when compared to other common gases due to its relatively high solubility in acrylate/methacrylate films[242]. The permeability of CO_2 in poly(ethyl acrylate), for example, is higher even than He [242], despite the smaller atomic size of He. Kumins and Roteman [296] quote the Van der Waals' diameter of CO_2 as being 3.23 Å (0.323 nm) (*cf.* 2.65 Å for He [296] and 3.10 Å for N_2[145]), and found that as the gas diameter increased, the minimum free volume required for diffusion increased exponentially in poly(vinyl chloride-poly(vinyl acetate) copolymer. Stannett [463] *et al.* note that the cross-sectional diameter of a molecule, as determined by its ability to pass through a zeolite window, is a good measure of the ability of a gas to move in a restrictive environment. Stanett cites Koros [290] *et al.* for showing the ability of a molecule such as CO_2 to move in restrictive environments (with greater ease than either CH_4, N_2, or Ar, but not He), and suggests this is due to the linearity of the molecule. Koros presumed it was the ability of CO_2 to undergo lengthwise oriented diffusion jumps such that the effective cross-section of the molecule is reduced. (The linearity of N_2 did not provide it with a similar ability, and no explanation for this was forthcoming.) Based on the values evident in **Table 8.1**, the flux of a gas which was slower than CO_2 would be difficult to measure accurately using the Daventest apparatus.

In the case of the Eudragit® *NE* films, the results show that over the course of a month, the CO_2 permeability coefficient decreased (**Figure 8.10**) by 32% compared to the initial value, having first increased by 11%. The initial increase is attributed to relocation and/or exudation of endogenous surfactant (not, however, visible on the film surface presumably because of the low level of addition {*i.e.*, 3.3% [204]}), prior to increased film densification by further gradual coalescence [62, 63]/autohesion [524, 525, 526] (see Chapter 4), leading to the decreased permeability coefficient.

Latex film aging has also been observed by Chainey [91] *et al.* using He gas as a probe. Chainey measured the permeability of films cast from homopolymer latices and solvent cast films of the same latex, and found that the permeability of the latex cast film decreased over a period of 30 days, but never reached the lower value established for the solvent cast film.

Balik [27] *et al.* suggested that the aging phenomena of latex films was due to a residual porosity (with pore sizes less than the wavelength of light and down to a few nanometres). The evidence of the mercury porosimetry experiments performed on these Eudragit® films did indeed indicate that at higher pressures and, hence, smaller pore radii (ca 0.01 μm), there was a likelihood of some structure as seen in the increasing number of peaks in this region (**Figure 8.8** and **Figure 8.9**).

The mercury porosimetry on Eudragit® *NE* had showed some evidence of a pore structure at approximately 5 μm (**Figure 8.8**). It would be expected that if these pores were continuous through the film, then the film would not be able to sustain the vacuum necessary for the gas permeability experimental procedure. The films *were*, however, able to sustain such a vacuum – signifying little evidence of large continuous pores.

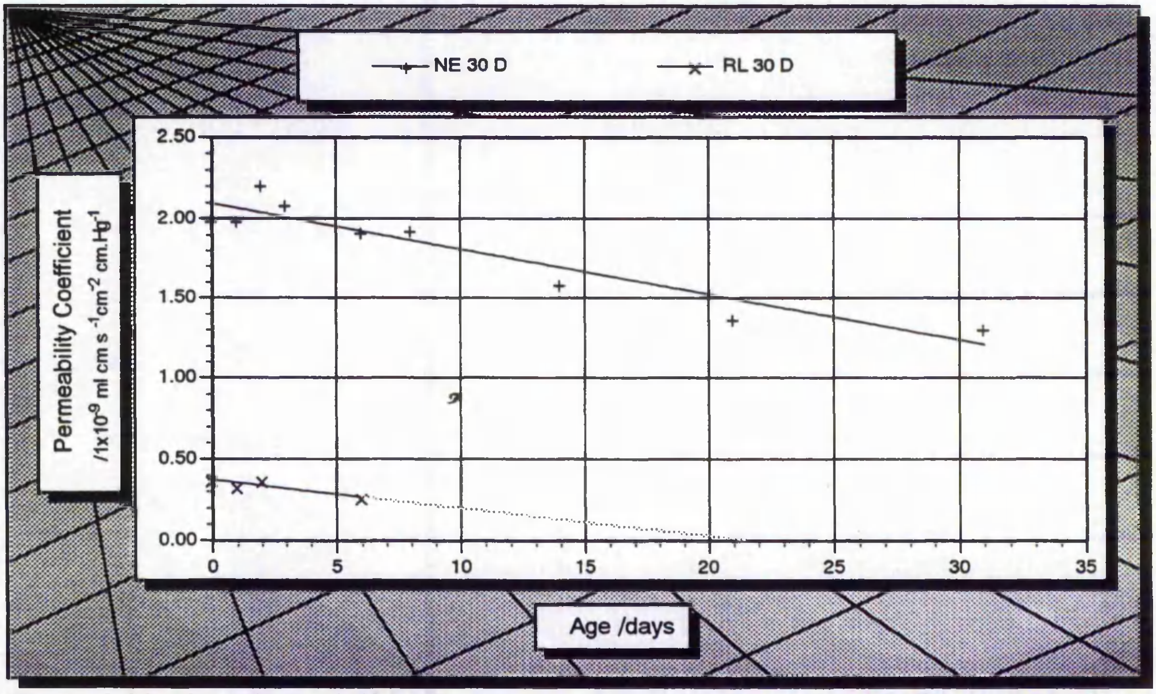

Figure 8.10 The effect of film age on the carbon dioxide permeability coefficients of Eudragits® *NE* and *RL*.

The CO_2 permeability of Eudragit® *RL* is not directly comparable to that of Eudragit® *NE*, since CO_2 would be expected to have a different solubility in each polymer. Additionally, with a T_g of ca 328 K[255, 313] (and this value probably lowered by between 10 → 20 K[313] by the addition of the 15% triacetin plasticiser), the Eudragit® *RL* polymer was in its glassy state at ambient temperature, whereas Eudragit® *NE*, with a T_g of ca 265 K[204], was in its rubbery state at ambient temperature. However, from Arrhenius-type studies, the T_g of a polymer has been found to affect the gas permeability only in certain instances: Yasuda and Hirotsu[549] cite a number of references where the effect of the T_g on gas permeability was examined, leading to one of the following three results: (i) the T_g showing no effect on the gas permeability; (ii) the T_g having an effect with all gases; (iii) the T_g having an effect only on some of the gases under investigation. For a pore-free polymer above its T_g, diffusion of a gas is activated, dependent on the mobility of the polymer chains, and the continual formation (and elimination) of 'holes' to allow passage of the gas, whilst below the T_g, gas diffusion is dependent on the free volume 'fixed' in the polymer (as discussed in Chapter 5). In agreement with this, Kumins and Roteman[295] found that the gases: H_2, He, Ne, O_2, NH_3, CO and CO_2 all gave diffusion coefficients, through poly(vinyl chloride)-poly(vinyl acetate) copolymer, that decreased with increasing Van der Waals' diameter. However, only CO_2 showed any anomalous behaviour (*i.e.*, a discontinuity in the trend of diffusion rate as a function of temperature) at either of the T_g's found for the copolymer, and they attributed this to the size of CO_2 (which is only 0.11 Å bigger than CO) being greater than the free-volume provided by the 'holes' formed for diffusion.

Table 8.1 and **Figure 8.10** show that the plasticised Eudragit® *RL* CO_2 permeability was still decreasing slightly with time. Although the brittle nature of the film made it less able to withstand the stress of continued experimentation after the 6 days of data given in the table, the extrapolated line on the graph does show the decreasing permeability trend.

The CO_2 permeability of Eudragit® *L* (+ 15% triacetin) as given in **Table 8.1** was similar to that of Eudragit® *NE*. This may be expected due to the similarity of the polymer structures in which the main difference arises in the carboxyl groups of Eudragit® *L*. Such groups are more likely to affect the permeability of polar molecules in an aqueous environment rather than the permeability of a gas.

8.5 The water vapour permeability of Eudragit® films.

The water vapour permeability of various Eudragit® films was determined gravimetrically, using a method similar to that used by Banker and Park[30], Patel[385] *et al.* and Roulstone[425] *et al.*, (described in Chapter 7). Roulstone criticised some inadequacies of the method for not reducing film boundary layer effects, and also for the long experimental times involved giving the films time to swell due to sorption of the water vapour. However, the method was described by Roulstone as suitable for providing relative results for the comparison of like films, which did show good reproducibility.

Table 8.2 gives the water vapour permeability coefficient values attained for the various Eudragit® polymer types. As was usual, films were cast at 313 K for 24 hrs. (All films, with the exception of those films cast from Eudragit® *NE*, contained triacetin

Table 8.2 Eudragit® film water vapour permeability coefficients.

FILM† ORIENTATION	**PERMEABILITY COEFFICIENT /1×10^{-6} g hr^{-1} cm^{-1} $cm.Hg^{-1}$**	**S.D. /1×10^{-6} g hr^{-1} cm^{-1} $cm.Hg^{-1}$**
Eudragit® *NE*		
SUBSTRATE	1.65	±0.08
AIR	1.70	±0.05
Eudragit® *RL* (+ TRIACETIN)		
SUBSTRATE	2.65	±0.06
Eudragit® *RS* (+ TRIACETIN)		
SUBSTRATE	2.14	±0.08
Eudragit® *L* (+ TRIACETIN)		
SUBSTRATE	1.39	±0.04

† Orientation refers to the side of the film facing the water vapour, *i.e.*, polymer-substrate or polymer-air side.

{15% $g.polymer^{-1}$}). It is seen that the greater hydrophilicity of Eudragit® *RL*, compared to Eudragit® *RS* (see Chapter 6), endowed it with the higher permeability coefficient. The carboxylated (and, hence, presumably hydrophilic) Eudragit® *L* displayed the lowest value of the three types of polymer under investigation: lower even than Eudragit® *NE*. This is possibly attributable to hydrogen bonding between the weak acid carboxyl groups adding rigidity to the polymer structure and reducing the polymer chain flexibility required for transport. Udeala and Aly [485], similarly found the water vapour transmission of solvent cast Eudragit® *L 100* (measured as an uptake) to be less than that of Eudragit® *RL 100*.

A control experiment consisting of aluminium foil, sealed to the sample bottle with the same 'polymer glue' (*i.e.*, freeze-dried polymer dissolved in organic solvent: usually methyl ethyl ketone) as used to seal the films to their bottles, was found to give no weight loss (*i.e.*, no water vapour flux), indicating that the measured values were entirely due to permeation through the film rather than through the 'glue.'

The experiment was repeated on six identical films as a test of reproducibility. Swelling of the films due to water sorption was not apparent from visual inspection *i.e.*, films remained clear, without turning opaque as do films exposed to liquid water (as opposed to water vapour).

All films examined (with the possible exception of the Eudragit® *L* film) showed a linear water vapour transmission rate with time, up to 200 hrs. In the experiments at 81% R.H. difference, the films did not condense liquid water, and so an activated transport

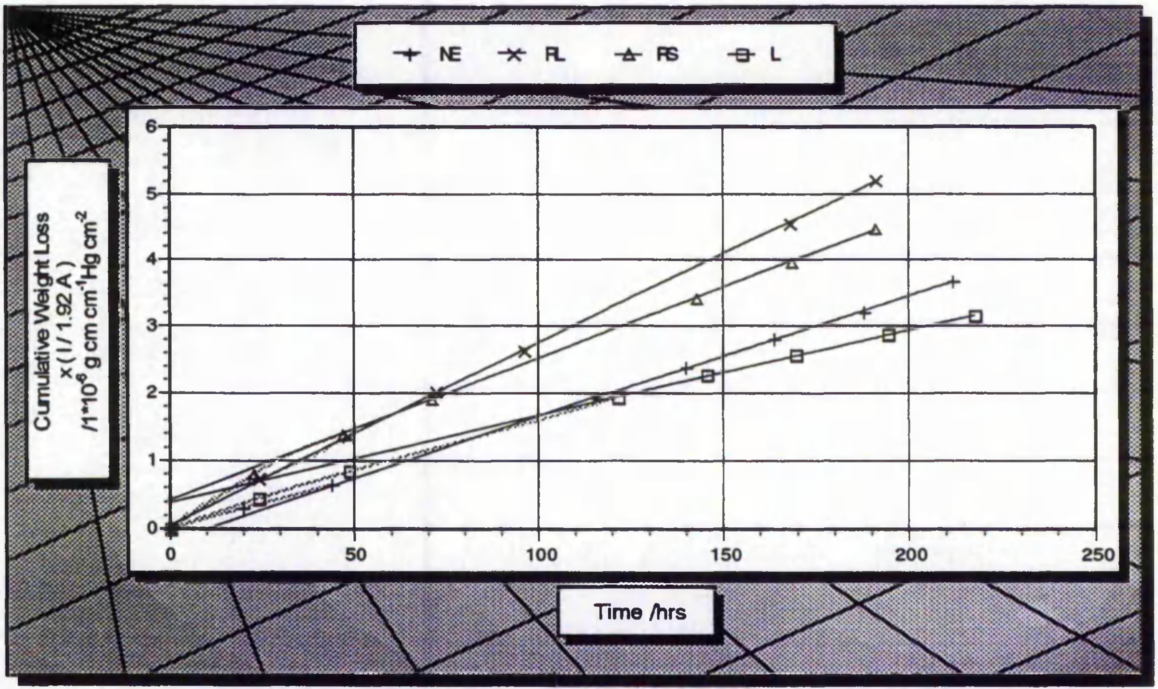

Figure 8.11 Plot for the determination of the Eudragit® water vapour permeability coefficients. (Note: l = film thickness; A = exposed film area; 1.92 = water vapour pressure difference across the film.

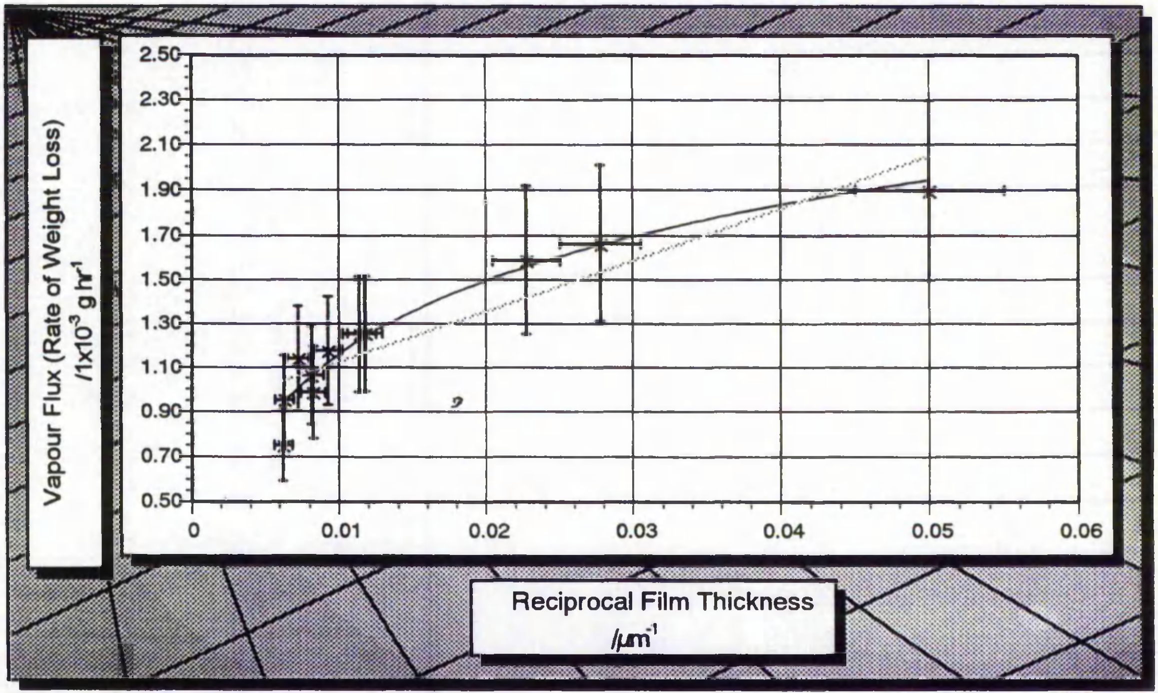

Figure 8.12 Plot of water vapour flux as a function of Eudragit® *NE* film reciprocal thickness.

mechanism is anticipated. The time lags, before the steady state flux was achieved, varied according to polymer (**Figure 8.11**) and were possibly a result of differing degrees of swelling. Eudragit® *NE* showed a positive intercept on the time axis, whereas Eudragits® *RS*, *RL* and *L* showed a negative intercept when the linear region of the line was extrapolated. The linearity of the Eudragit® *RL* plot implies that further gradual coalescence either did not occur, or had no significant affect on the water vapour permeability, over a 200 hr period. Note that those films showing the negative time lags were those films that initially contained the plasticising triacetin. A negative time lag implies a permeant flux that decreases with time, compared to the initial value, possibly indicating that the film structure is changing either as a result of the film swelling to a small extent, or relocation of the plasticiser within the film.

8.5.1 Water vapour permeability and Fick's law.

The derivations of the various permeability coefficient formulae (see Chapter 7 and Appendix A) are from Fick's laws of diffusion[31], and the film permeability can only be described as genuinely Fickian if both laws are obeyed. One component of this is that the permeability coefficient is independent of film thickness. The water vapour permeability of Eudragit® *NE* was measured as a function of film thickness. Adherence to Fick's law is manifest in the linearity of a plot of the vapour flux (shown as the rate of weight loss from the experimental sample bottles, and which is proportional to vapour flux) as a function of film reciprocal-thickness (**Figure 8.12**). Least squares regression analysis on this data provides a correlation coefficient, r^2, of 0.831. It would thus seem reasonable to assume that the water vapour permeation is not Fickian in nature (*i.e.*, with respect to film thickness), and that the flux of water vapour decreased as a function of increasing film thickness. This points to the fact that the method is not particularly valid for producing a definitive permeability coefficient, and is only suitable for simple comparative tests of films.

Linear regression on the water vapour flux as a function of film thickness yields a value of $r^2 = 0.929$, indicating a better correlation than for the vapour flux as a function of reciprocal thickness.

A possible explanation for the non-linearity of the Fickian-type plot arises from the water vapour causing the films to swell. Films were often observed to be bowed inwards – possibly due to an internal vapour concentration gradient causing the lower film face to swell more than the open face. Because the films were restrained in their movement by the 'adhesive' fixing the films to the bottles, there would be a difference in the stresses imparted to a thinner film when compared to a thicker film. Consequently, these stresses may aid or hinder the degree of swelling caused by the water vapour. Udeala and Aly[485] found that water vapour sorption by a number of solvent cast Eudragit® films varied as a function of film thickness. Banker[29] *et al.* also found non-Fickian behaviour for the permeation of water vapour through hydrophilic, substituted cellulosic film: the water vapour permeability coefficient increasing with increasing film thickness (when Fick's laws demand that the permeability coefficient be invariant as a function of film thickness). This he attributed to the existence of Van der Waals' forces and hydrogen bond formation between the water and hydroxyl groups of the polymer and its associated plasticiser. For more hydrophobic films (*e.g.*, PBMA), the permeability coefficient was found to be much more constant.

8.6 The solute permeability of Eudragit® films.

Initial experimental work validated the reproducibility of the solute permeation experimental procedure and the effect, if any, of the various experimental parameters.

8.6.1 *4*-nitrophenol as a solute.

4-nitrophenol was selected as a solute, following earlier studies by Wicks [532] and Roulstone [423], for its solubility in both water and the polymer film, and for its ease of detection in the U.V. spectrum. Pumping *4*-nitrophenol through the measuring spectrophotometer, in the absence of a film, showed it to be stable for the duration of a typical (24 hr) solute permeation experiment. The change in absorbance of a *4*-nitrophenol solution was negligibly small, as shown in **Figure 8.13**. It is seen that in the case of the sample of *4*-nitrophenol monitored together with a control (reference) sample such that it was normalised to a zeroed baseline, the concentration, as a function of time, was relatively flat when compared to the unreferenced line. This therefore overcame the deficiency of the spectrophotometer being a single beam (as opposed to a dual beam) instrument. Because the cells were in a movable carriage, the controlling software was able to store the reference value and automatically deduct it from the sample measurement. (A dual beam instrument would measure the two samples simultaneously.) As stated in Chapter 7, an uncertainty in the film thickness, of up to a 10%, was typically present, and in the majority of films investigated, this would be the major contributory factor to the experimental uncertainty in any permeability coefficient. The exception to this is the solute permeability coefficients of the surfactant-free films (Chapter 9) which were, in some cases, of very low magnitude – the films effectively acting as barriers over the course of a typical 24 hr experiment.

The values of the *4*-nitrophenol permeability coefficients of the Eudragit® films are given in **Table 8.3**. Eudragit® *RL* films had a greater solute permeability coefficient than Eudragit® *RS* films. This was presumably due to the Eudragit® *RL* polymer being more hydrophilic in nature (*i.e.*, in the case of the Eudragit® *RS*, quaternary ammonium groups are present in the ratio of 1:40 neutral ester groups, whilst for Eudragit® *RL*, 5% of the groups are quaternary ammonium groups) such that it was likely to be more hydrated. The rate of diffusion may therefore be enhanced either by i, a polymer plasticisation-type of effect, or ii, by allowing the penetrant to diffuse through water – in which the rate of diffusion would be expected to be greater than when diffusing through polymer.

Samples of Eudragit® *RL* films were investigated for solute permeability after having been leached (48 hrs) of their plasticiser (*i.e.*, for a time greater than the time required for the elution of the maximum amount of 'leachable' plasticiser – refer to paragraph 8.2.2.1). The result of this experiment demonstrated that the **4-nitrophenol permeability coefficient** of a **plasticiser-free Eudragit® *RL*** film was **$2.68(\pm0.18)\times10^{-7}$ m^2 hr^{-1}** with a minimum value of 2.54×10^{-7} m^2 hr^{-1}. The plasticiser thus effectively increases the permeability compared to that of the film leached of its additives (plasticiser plus those persisting from manufacture) by a factor of ca 1.4. However, these results do not indicate the mode by which the permeation is increased: whether either due to the greater mobility of the polymer chains (*i.e.*, true plasticisation), or due to porosity originating in the film as

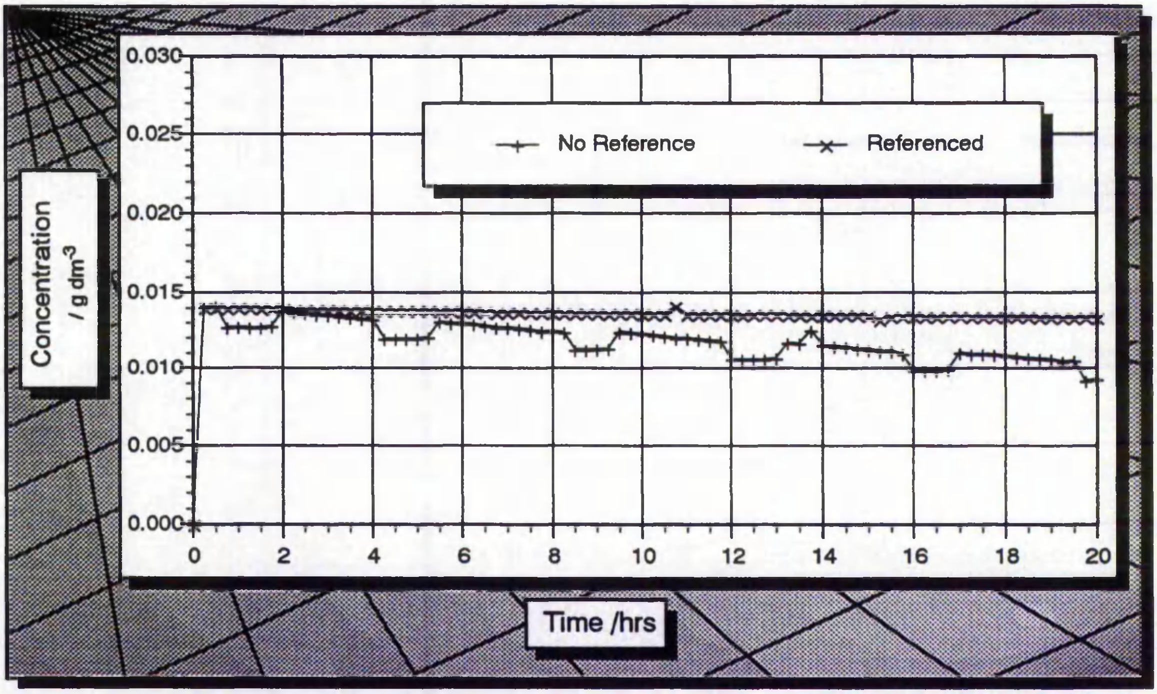

Figure 8.13 Effect of spectrophotometer drift/4-nitrophenol permeant absorption onto pump tubing, on baseline stability.

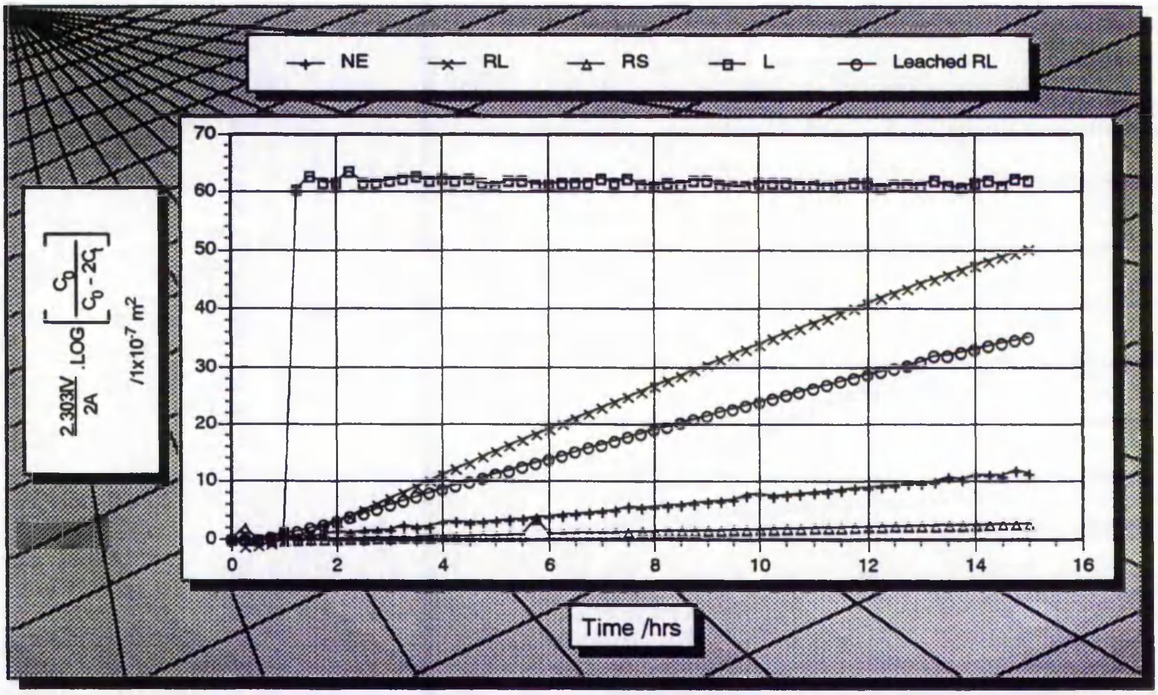

Figure 8.14 Plots for the calculation of the 4-nitrophenol permeability coefficient of Eudragit® films.

Table 8.3 4-nitrophenol permeability coefficients for the various Eudragits® films.

EUDRAGIT® TYPE†	PERMEABILITY COEFFICIENT /m² hr⁻¹	S.D. (%) /m² hr⁻¹	MINIMUM VALUE /m² hr⁻¹
NE	4.00×10^{-8}	0.36×10^{-8} (9)	3.55×10^{-8}
RL	3.81×10^{-7}	0.08×10^{-7} (2)	3.74×10^{-7}
RS	1.53×10^{-8}	0.11×10^{-8} (7)	1.50×10^{-8}
L	FILM DISSOLVED‡		

† All films (except Eudragit® *NE*) contained 15% triacetin.
‡ Note that Eudragit® *L* is soluble, forming polymeric salts, above pH 5.5.

a result of the leaching of the plasticiser in the aqueous environment. This use of the plasticiser was, however, unavoidable in the quest for manageable, free, Eudragit® *RL* films and this was especially the case when additives were included in the film (Chapters 10 & 11) such that the films could not be wetted (leached) before the permeation experiment.

Figure 8.14 shows representative examples of the plots from which the 4-nitrophenol permeability coefficients of the various Eudragits® were calculated. Note that the carboxylated Eudragit® *L* is seen to dissolve, due to polymeric salt formation, after approximately 1 hr – insufficient time to allow a permeability coefficient to be calculated. The plateau value seen is not that for the equilibrium concentration, but is a function of the maximum measurable absorbance of the spectrophotometer – a reading this high would not normally used due to the very low intensity of light transmitted.

8.6.2 Effect of experimental variables on the 4-nitrophenol solute permeability of Eudragit® *NE* films.

Experimental variables that might have affected the calculation of the solute permeability coefficients were investigated in order that the consequences of such change could be accounted for, if necessary.

8.6.2.1 Effect of stirrer speed.

Under normal circumstances, both (permeant donor and receiver) sides of the permeability cell were stirred, at 100 r.p.m., by glass propeller-type stirrers. Stirring ensured good mixing within the cell and avoided static (unmixed) regions. The effects of boundary layers (**Figure 8.15**) 'against' the film must be considered as an inherent part of the system once an equilibrium flux has been achieved, but can be minimised by stirring of the manner used (see Chapter 7). As stated above, stirring was usually executed at 100 r.p.m., but for the purpose of this series of experiments, the stirrer speed was varied, in separate permeability cells (*i.e.*, in separate permeability measurements), from 50 → 250 r.p.m. for both compartments (donor and receiver) at the same time.

It was also possible to vary the speeds of the individual chambers of the cell (donor and receiver), and thus permeability coefficients were also calculated for when either or both sides of the permeability cell were left unstirred. (When only one side of the cell was unstirred, the other side was stirred at the usual 100 r.p.m.) Results are shown for the 4-nitrophenol solute permeability of Eudragit® *NE* as a function of stirrer speed in **Table 8.4**.

The table indicates that the variation of stirrer speed has no significant influence on the effects of boundary layer resistance on permeation in these pumped cells. All values of permeability coefficient fall within the experimental uncertainty, for the typical experimental conditions, of **$4.00(\pm 0.36)\times 10^{-6}$ m^2 hr^{-1}** presumably as a result of mixing being assisted by the efflux from the (pumped) return tube from the spectrophotometer flowcells.

8.6.2.2 Effect of not greasing the flanges on the permeability cell.

When a film was used in the solute permeability cell, increased opacity implied that it swelled, to a lesser or greater extent dependent on the polymer in use. In the case of the Eudragit® *NE*, this swelling simply amounted to the film appearing to turn white and translucent. The Eudragit® *RL*, however, swelled to a much greater extent, and because the film was gripped between the flanges of the two halves of the permeability cell, this swelling caused the film to be distended into one or other of the chambers of cell. Whichever chamber the film moved into appeared to occur at random (both sides of the cell were filled simultaneously so that the process of filling was not a contributory factor. Also, deliberately filling one side of the cell before the other had no effect – presumably due to the film being relatively inflexible and held taut by the flanges of the cell).

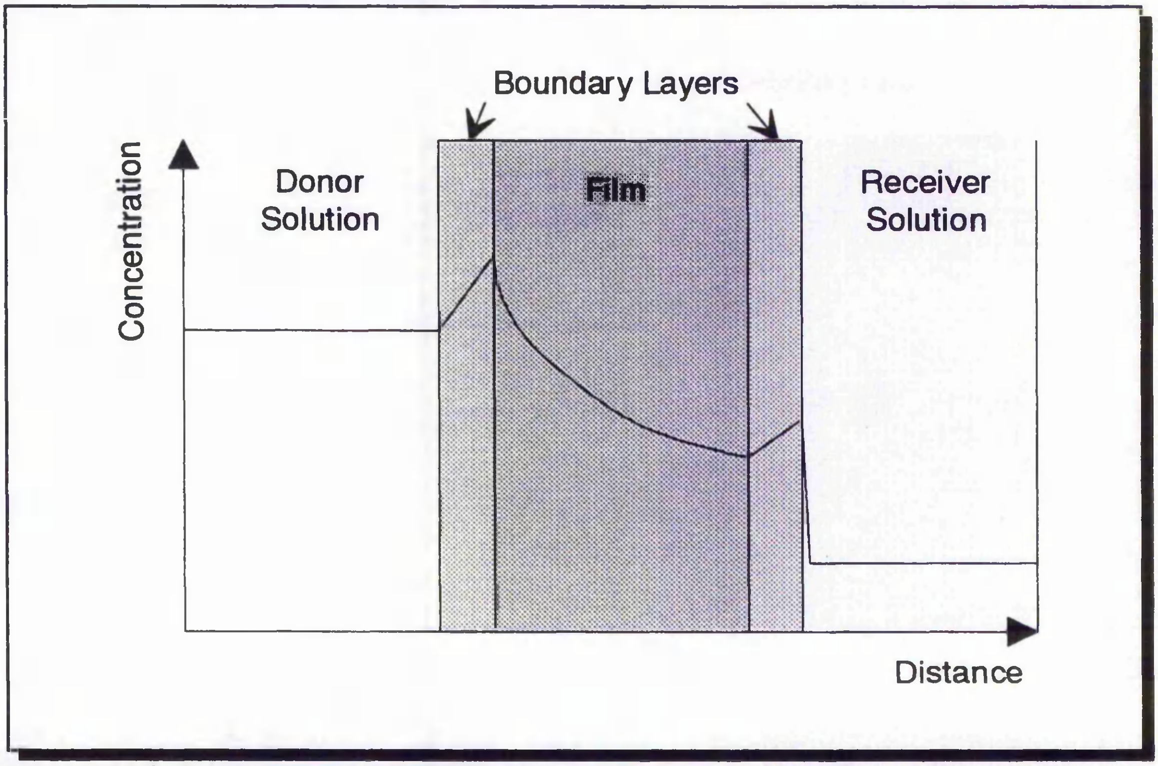

Figure 8.15 Schematic of concentration profile across boundary layers (before the attainment of concentration equilibrium in the film).

Table 8.4 Effect of stirrer speed on 4-nitrophenol solute permeability coefficient of Eudragit® *NE*.

STIRRER SPEED	**PERMEABILITY COEFFICIENT /1×10^{-8} m^2 hr^{-1}**
Both unstirred	4.23(±0.3)
Receiver unstirred	4.02
Donor unstirred	3.85
BOTH COMPARTMENTS STIRRED /r.p.m.	
50	4.39
100	4.00(±0.36)
150	4.28
200	4.07
250	4.35

It was thought that the excessive movement of the Eudragit® *RL* was possibly due to swelling caused by the silicone grease used to seal the film against the flanges of the permeability cell. To test this hypothesis, a number of Eudragit® *RL* films were investigated with the cells ungreased.

The mean **4-nitrophenol permeability coefficient** of the **Eudragit® *RL* films** in the **ungreased permeability cells** was calculated as **3.83(±0.07)$\times10^{-7}$ m^2 hr^{-1}**. This value is almost identical to that for those films in the greased cells. Similarly, the films were seen to swell in the same manner as the greased cells. Thus, it was concluded that the greased flanges did not affect the solute permeability coefficient, meaning that it was possible to continue to use such greased cells, making the practical handling of the permeability cell that much easier.

For films which swelled to an opaque white in water, evidence that the greased flanges provided a watertight seal was the lack of swelling within the area of the flanges. On removal of a film from a cell, it appeared with the open centre section white, surrounded by a transparent disc at the position of the flange, and white again in the region of any film overhanging the cell externally (*i.e.*, in the constant temperature bath). This also provided evidence that very little permeation occurred transversely within the film, outwards from the cell and away from the region under investigation.

8.6.2.3 Effect of variation of the latex percentage solids content.

Aqueous Eudragits® were supplied at concentrations of 30% (W/W) solids dry weight. These were usually diluted to 5% W/W for film casting. However, the effect of variation in the latex solids content, on solute permeability, was investigated.

Table 8.5 Effect of percentage polymer-solids of casting latex on the 4-nitrophenol permeability coefficient.

PERCENTAGE CASTING SOLIDS	PERMEABILITY COEFFICIENT /1x10^{-8} m^2 hr^{-1}
5	4.00
10	3.97
15	4.13
20	4.21
25	4.04
30	4.27

A series of experiments were performed upon **Eudragit® *NE*** in which the casting **percentage solids were varied from 30% to 5% W/W polymer solids**, whilst all films were cast for the usual 24 hrs at 313 K. (The films were cast from differing volumes of latex to give a final film thickness of approximately 100 μm.) **Table 8.5** and **Figure 8.16** present the results of these experiments, and again show that the permeability coefficients were within the experimental uncertainty of those results for the standard casting conditions (24 hrs, 313 K, and 5% polymer solids content), giving a mean result (from the five runs) for the **4-nitrophenol solute permeability coefficient** of **4.12(±0.12)x10^{-8} m^2 hr^{-1}**. (The fact that the lines do not overlay one another results from small variations in the film

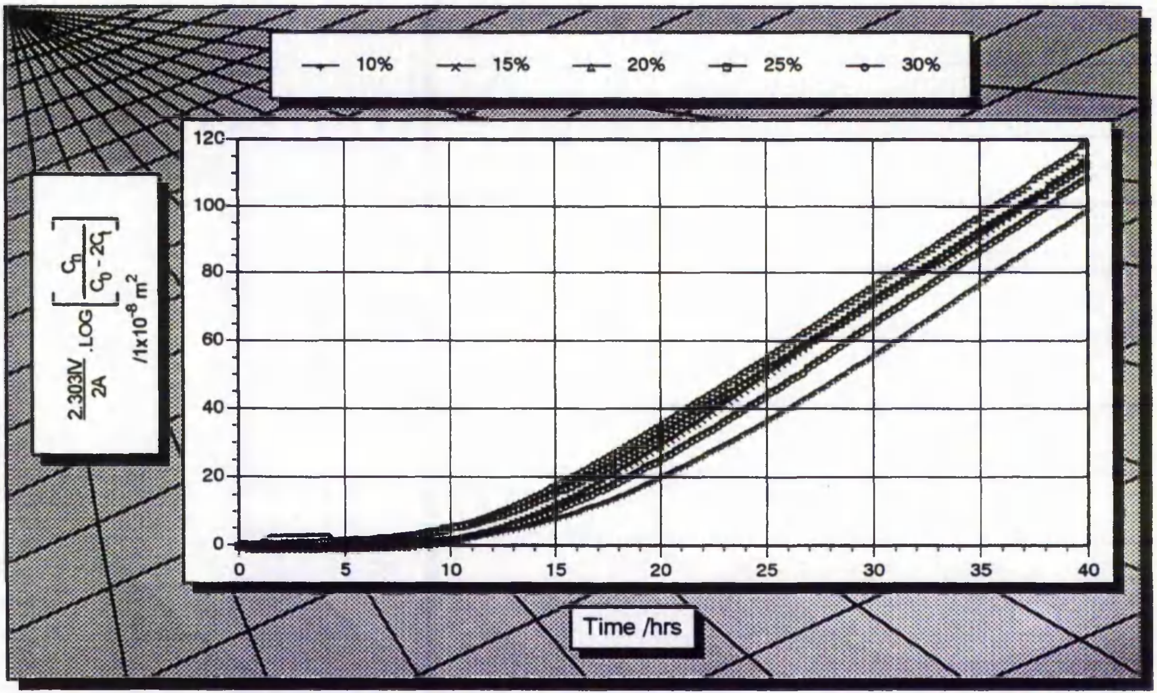

Figure 8.16 Permeability plots for Eudragit® *NE* films cast from latices of differing percentage solids content.

thickness, which results in a variation in the lag time but is accounted for in the calculation of a permeability coefficient.)

Vanderhoff[507] *et al.* among others [105, 451], states that the initial rate of evaporation of water during casting from a latex is identical to the evaporation rate from water on its own (or containing a similar amount of surfactant), *i.e.*, the latex particles themselves have little effect on evaporation, until the final stages of film formation. However, there are factors which might have led to different film morphologies and, hence, permeability coefficients, as a consequence of casting from different percentage solids contents. When casting from a low percentage solids content, as the aqueous phase evaporates during casting, the percentage solids will increase to the equivalent of those higher values that were investigated. The main difference between these five experimental runs was thus the time it took to form dry film and, hence, the time that the film remained in the oven after the water had evaporated. (*I.e.*, a film of high percentage solids will dry faster than a film of low solids {if meant to give films of identical thickness} because of the reduced amount of water present.) Such a film will then be undergoing a thermal annealing process for a greater length of time that could affect the result. Also the time that the latex spent in the wet state could affect the degree of aggregation – especially for latices of marginal stability.

8.6.2.4 Effect of variation of film casting temperature (*i.e.*, film drying rate).

At lower temperatures, water evaporates from a latex more slowly, possibly resulting in a better film [216, 246]. This is countered by the increased hardness of the polymer resulting in increased resistance to particle deformation. Latex cast films are known to increase their degree of coalescence with age, and the gas permeability has been seen [84] to decrease with increasing film age. It was thought that a film cast at a high temperature would undergo this aging process at an enhanced rate (compared to a film cast at lower temperature), due to the increased mobility of the polymer chains and, hence, yield films with lower initial permeability coefficients compared to those films cast at the usual temperature.

The effects of casting temperature on Eudragit® *NE* latex films was investigated using 4-nitrophenol solute permeability measurements on films cast at temperatures in the range 278 K → 343 K (**Table 8.6**). The results show that in the range of 313 → 343 K there is no significant change in the permeability coefficient, with all values lying within the range of experimental uncertainties (all uncertainties are standard deviations calculated from the range of results determined at each temperature).

Films cast at temperatures below 303 K took over a week to form. The film cast at 278 K (in a fridge) appeared 'crystalline' with randomly spaced regions forming a star-like pattern of brittle polymer, that had fractured, presumably due to the stress of contracting (and despite Eudragit® *NE* having a T_g of 265 K [204]). The films cast at either 281 K, ambient temperature, or at 303 K showed no such features, looking similar to all of the other films. The increase in the permeability coefficient of the films cast at the lower temperatures is thus presumably due to increased internal structure (or a greater number of faults) and a lesser degree of coalescence providing a less dense (film density as opposed to relative polymer density) path for the 4-nitrophenol diffusion.

Table 8.6 Eudragit® *NE* 4-nitrophenol solute permeability as a function of film casting temperature.

CASTING TEMPERATURE /(±3) K {° C}	PERMEABILITY COEFFICIENT /1x10^{-8} m^2 hr^{-1}	S.D. /1x10^{-8} m^2 hr^{-1}	MINIMUM VALUE /1x10^{-8} m^2 hr^{-1}
278 {5}	Discontinuous film		
281 {8}	10.1	0.07	10.0
303 {30}	6.08	1.29	4.36
313 {40}	4.00	0.36	3.55
323 {50}	3.48	0.11	3.45
333 {60}	3.70	0.14	3.56
343 {70}	3.66	0.13	3.48

Since there is no change in the 4-nitrophenol permeability coefficient of Eudragit® *NE* at temperatures above 313 K, it can be implied that this thermal treatment (≥ 313 K for 24 hrs) is sufficient to coalesce the films as much as practicable without preparing a film from a polymer melt. Casting in this manner should thus provide a suitable baseline film for further solute permeation experimentation; a film that avoids the pitfalls of having a permeability that is liable to vary to any great extent within a short time.

A film formed from a latex in which it takes longer for the aqueous phase to evaporate may result in a better degree of packing of the latex particles (*i.e.*, fewer faults) since the particles have a greater time to rearrange themselves before they destabilise on coming into close contact. Jaycock and Kayem[254] showed, by using a destabilising dispersant (used to stabilise the pigment in latex paint, but which destabilises the latex), that poly(vinyl acetate) latex film heterogeneity was increased, due to increased flocculation, when compared to a film containing no dispersant. Hoy[246], and Hansen[216], investigated the addition of glycols to latices, which slowed the evaporation rate of water due to hydrogen bonding, allowing the particles sufficient time to re-order during drying, therefore resulting in greater coalescence.

Juhué and Lang[261] present an opposing argument for good particle packing, citing evidence from atomic force microscopy (A.F.M.) on surfactant-free PBMA, cast at 307 K under vacuum, in which a higher surface density of hexagonal clusters (*i.e.*, greater packing order) was seen compared to a film dried under normal pressure and, hence, more slowly. This was explained as resulting from the film cast under vacuum, with a higher rate of evaporation, having a shorter time in which to flocculate before the point of destabilisation was reached. Juhué is in concurrence with Côté[100] *et al.* who, by using light scattering and E.M., also found that an increased casting temperature led to a more homogeneous film (Poly(vinyl acetate), latex-cast at temperatures ranging from 296 K → ⟩ 373 K). Côté stated that the increased kinetic energy and, hence, Brownian motion, of the particles was able to overcome the factors, such as particle-particle repulsion, which might otherwise counter uniform particle packing.

Eudragit® *RL* films cast at 333 K had similar **permeability coefficients ($3.62(\pm0.20)\times10^{-7}$ m^2 hr^{-1})** to those cast at 313 K (*i.e.*, $3.81(\pm0.08)\times10^{-8}$ m^2 hr^{-1}). This would thus seem to imply that Eudragit® *RL* is also 'fully' coalesced at the regular casting temperature of 313 K.

8.6.3 Effect of film age on the 4-nitrophenol solute permeability of Eudragit® *NE*.

Eudragit® *NE* films were aged for one month at ambient temperature, in the dark and in a desiccator (containing silica gel as the desiccant). The mean **4-nitrophenol solute permeability coefficient** of these **1 month old films** was **$5.05(\pm0.18)\times10^{-8}$ m^2 hr^{-1}**, with a minimum value of 4.92×10^{-8} m^2 hr^{-1}. This mean value is thus somewhat higher than expected (*i.e.*, higher, and outside the experimental uncertainty, of the unaged film): the anticipated increase in polymer-chain fusion, due to further gradual coalescence or autohesion, being assumed to decrease the permeant flux. It is possible that the expected increased coalescence has occurred together with exudation of endogenous surfactant yielding a lesser degree of dispersion, therefore allowing easier leaching of this surfactant when the film is hydrated (possibly allowing micropore formation) and, hence, increasing the measured permeability coefficient.

8.6.4 Investigation of a side-dependence to solute permeability.

Some films have demonstrated asymmetric permeability properties, whereby the permeability coefficient of the permeant travelling in one direction is different to the value when travelling in the reverse direction. Such a difference has been attributed to (i) a 'skin' of atypically high density film (by Okubo [366] *et al.* with respect to solvent cast films), or (ii) a porous surface skin caused by latex particle flocculation [2]: both skins being at the air-water interface. Roulstone [427] *et al.*, however, attributed the asymmetry to films having a greater surface area on the air side, finding that 4-nitrophenol permeated the films faster when the donor permeant was against the polymer-substrate side of the surfactant-free PBMA film. This difference in permeability coefficients disappeared over the course of a month, and corresponded to a decrease in the film structure as recorded by T.E.M.

The majority of films probed elsewhere in this thesis, were oriented with the polymer-substrate film surface facing the donor permeant solution, unless otherwise stated.

8.6.4.1 Eudragit® *NE* film side-difference.

The side dependence phenomena for Eudragit® *NE* was negligibly small and within the experimental uncertainty of the method. The 'typical' permeability coefficient for Eudragit® *NE* when the substrate-side was facing the 4-nitrophenol permeant was $4.00(\pm0.36)\times10^{-8}$ m^2 hr^{-1}. This compared with **$4.18(\pm0.24)\times10^{-8}$ m^2 hr^{-1}** when the **air-side** of the film was **facing the 4-nitrophenol**. S.E.M.s and T.E.M.s (**Plate 8.1** and **Plate 8.2**) of Eudragit® *NE* films showed a surface free of 'pinholes' or pores, thus somewhat negating the reasons proposed above for producing a directionally orientated permeability coefficient.

8.6.4.2 Eudragit® *RL* film side-difference.

With the **air-side** of **Eudragit® *RL*** film facing the permeant, the **4-nitrophenol solute permeability coefficient** was **3.88(±0.08)×10^{-7} m^2 hr^{-1}**. This compared with 3.81(±0.08)×10^{-7} m^2 hr^{-1} with the film in the opposite orientation, showing that permeability dependence resulting from film orientation is lost to the experimental uncertainty.

Like the Eudragit® *NE*, the Eudragit® *RL* films (+ triacetin) have been shown to be free of any structural detail when viewed under the S.E.M. (**Plate 8.3** and **Plate 8.4**).

8.6.5 Fickian applicability.

As with the water vapour permeability (paragraph 8.5.1), the expediency of using a Fickian based equation was investigated, looking at the effect of film thickness, and also permeant concentration, on the 4-nitrophenol permeability coefficient.

8.6.5.1 Effect of film thickness on solute permeability coefficient.

Fick's law[31], when applied to membrane permeation, states that the permeability coefficient be independent of film thickness, whilst the flux of permeant should be inversely proportional to film thickness. (See Chapter 5.) The 4-nitrophenol permeability coefficients of Eudragit® *NE* films cast to varying thicknesses (using differing volumes of latex, of 5% polymer solids content) of between 70 μm → 230 μm were investigated. **Figure 8.17** shows a plot of 4-nitrophenol flux versus film reciprocal thickness. (The plot actually shows the rate of change of 4-nitrophenol concentration {as a function of reciprocal thickness} which is proportional to the flux.) Regression analysis on the (least squares) line of best fit yields a value of r^2 = 0.985, indicating that the calculated permeability coefficients are independent of film thickness, in agreement with the Fickian definition. (Note that in **Figure 8.17**, the error bars refer to the typical error in film thickness of 10%, and a typical error in the permeant flux of 14% as found in an experiment for five identical samples.)

The **permeability coefficients**, calculated when the film thickness was varied over approximately 200 μm, give a **mean value of 4.06(±0.3)×10^{-8} m^2 hr^{-1}**. This compares to the previously quoted value of 4.00(±0.36)×10^{-8} m^2 hr^{-1} for a group of experiments prepared to give films of the same thickness.

The Eudragit® *RL* films showed a poorer correlation between flux and reciprocal thickness, than the Eudragit® *NE* films, with a correlation coefficient of r^2 = 0.741. This leads to a correspondingly greater uncertainty in the value of the **mean permeability coefficient** for these results – of **3.44(±1.0)×10^{-7} m^2 hr^{-1}** (*cf.* 3.81(±0.08)×10^{-7} m^2 hr^{-1} for the series of films cast to unvarying thickness {*e.g.*, 100 μm}). This is presumably as a result of the triacetin incorporated into the film. Although it is not known what effect thickness has on the rate of triacetin leaching, it is not unreasonable to assume that the effect of any polymer-permeant-additive interactions will be magnified as film thickness increases.

At the temperature of the solute permeation experiment (303 K), the film will be relatively close to its plasticised T_g of ca 308 K (see Chapter 6). This fact can be influential

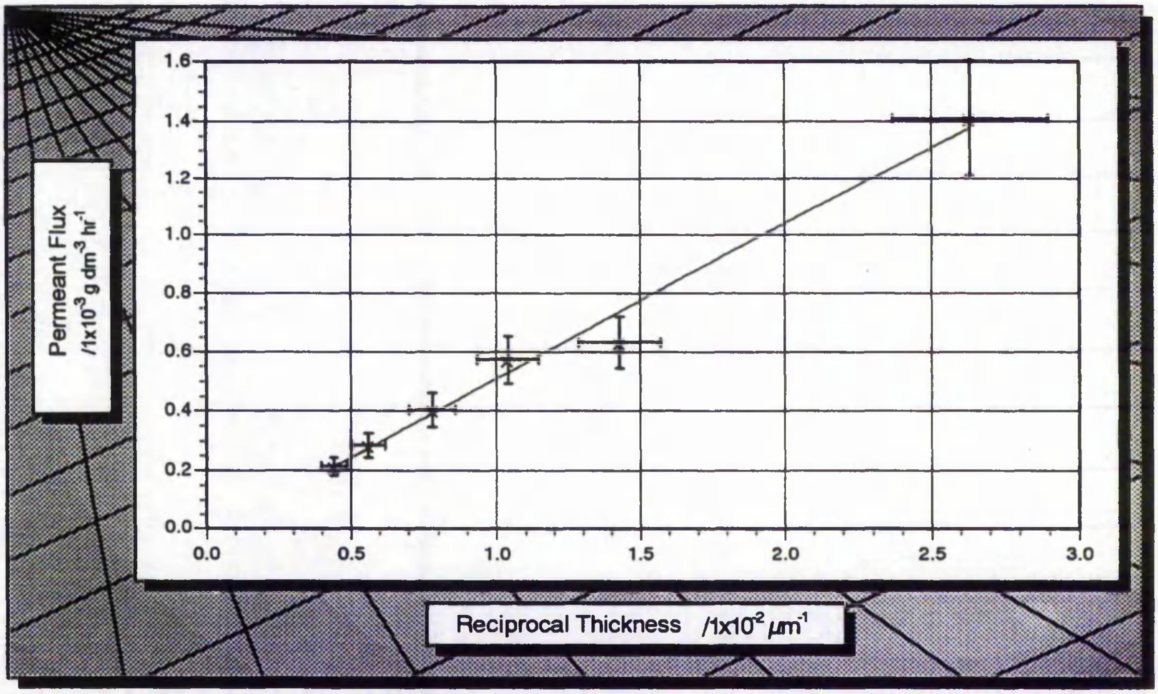

Figure 8.17 Fickian reciprocal thickness plot for the permeation of 4-nitrophenol through Eudragit® *NE* film.

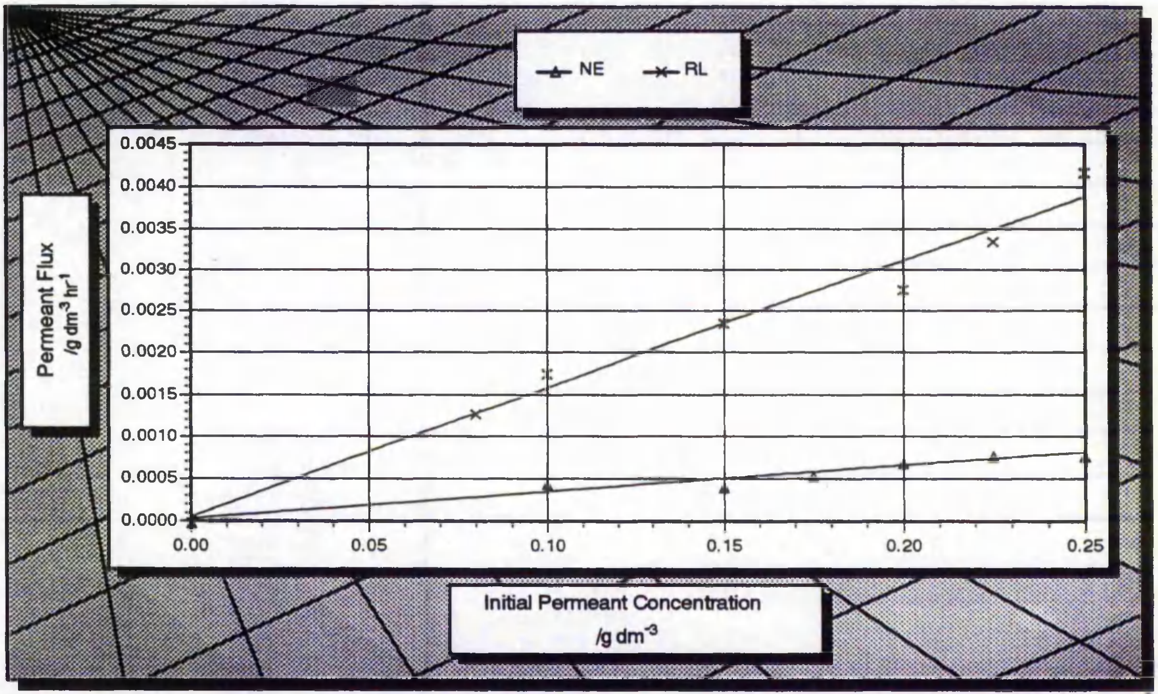

Figure 8.18 The effect of permeant concentration on the permeant flux through Eudragits® *NE* and *RL* films.

on the permeability coefficient in relation to the motion of the polymer chains. Non-Fickian behaviour has been related to the polymer chain relaxation rate[23, 171] (*i.e.*, rate of attainment of equilibrium of time dependent stresses) below the polymer T_g, whereas above the polymer T_g, there exists an equilibrium in such properties and the size distribution of the polymer free-volume and mean cavity volume may affect the Fickian mechanisms of permeant sorption and diffusion[171].

8.6.5.2 Effect of the *4*-nitrophenol permeant concentration on the solute permeability coefficient.

Although Fickian independence of the permeability coefficient with permeant concentration has been observed[166, 186, 446] for various types of polymers, this is not always the case. *E.g.*, Hwang and Tang[249] found anomalous Fickian (concentration) behaviour for the permeation of dissolved oxygen through silicone rubber membranes (which was thought to be an effect of the changing boundary conditions).

The permeability of films was measured using 4-nitrophenol as the permeant, at a range of concentrations (**Table 8.7**). The results for Eudragit® *NE* give a **mean permeability coefficient** of **3.86(±0.3)×10^{-8} m^2 hr^{-1}** when the **permeant concentration was varied between 0.10 g dm^{-3} and 0.25 g dm^{-3}**. This is within the limits of experimental uncertainty of the result for the series of experiments on Eudragit® *NE* using the permeant at the usual initial concentration of 0.2 g dm^{-3}, and is in agreement with Fick's law[31] which states that the permeability coefficient should be independent of the permeant concentration.

Fick's law also states that the flux of permeant is directly proportional to the permeant concentration. **Figure 8.18** shows the relationship between flux and permeant concentration where the regression coefficient, r^2, is 0.944. Deviations from the ideal are generally a result of permeant-polymer interactions. The non-ionic nature of Eudragit® *NE*, make any interactions unlikely to occur.

In the case of Eudragit® *RL* (+ triacetin), the relationship between permeant flux and permeant concentration is slightly better than for Eudragit® *NE* (r^2 = 0.977).

The **mean 4-nitrophenol permeability coefficient through Eudragit® *RL*** was **3.70(±0.14)×10^{-7} m^2 hr^{-1}**, which compares well with the value of 3.81(±0.08)×10^{-7} m^2 hr^{-1} for a series of films where the permeant concentration was at the more typical 0.2 g dm^{-3}. The *4*-nitrophenol, when used at pH 6, is $\rangle$ 99% in its undissociated form (pKa = 7.15), making its interaction with the polymer less likely, despite the anionic nature of Eudragit® *RL* (see Chapter 6) when in an aqueous environment.

8.6.5.2.1 Uptake of *4*-nitrophenol by Eudragits® *NE* and *RL* films.

At the end of a *4*-nitrophenol permeation experiment, both Eudragit® *NE* and *RL* films had swelled with water, making them opaque. The films appeared white, with a green tinge (darkest in Eudragit® *RL*). On drying the films lost their opacity, but the Eudragit® *RL* film in particular remained tainted green due to absorbed *4*-nitrophenol. The uptake of *4*-nitrophenol by Eudragit® *NE* and Eudragit® *RL* (+ 15% triacetin) was measured as a

Table 8.7 Effect of 4-nitrophenol concentration on the Eudragit® film permeability coefficient.

CONCENTRATION OF 4-NITROPHENOL /g dm^{-3}	**PERMEABILITY COEFFICIENT /1×10^{-8} m^2 hr^{-1}**
Eudragit® *NE*	
0.10	3.96
0.15	3.41
0.175	3.57
0.20	4.00
0.225	4.08
0.25	4.16
	MEAN = 3.86(±0.3)×10^{-8} m^2 hr^{-1}
Eudragit® *RL* (+ TRIACETIN)	
0.08	34.8
0.10	38.8
0.15	36.8
0.20	38.1
0.225	37.5
0.25	36.1
	MEAN = 37.0(±1.4)×10^{-8} m^2 hr^{-1}

function of concentration. This allowed the equilibrium 4-nitrophenol polymer-water partition (solubility) coefficient, *S*, to be determined:

$$S = \frac{C_{polymer}}{C_{aqueous}} \tag{8.3}$$

where:

$C_{polymer}$ = equilibrium 4-nitrophenol concentration in polymer (g g^{-1} polymer);
$C_{aqueous}$ = equilibrium 4-nitrophenol concentration in water (g g^{-1} water).

Values of 94.2(±12.7) and 278.6(±21.6) were determined for Eudragit® *NE* and Eudragit® *RL*, respectively (**Figure 8.19**). These values allow for the **weight loss from the film due to leaching of endogenous surfactant and/or added plasticiser based on 0.35% (~11% of the original amount of 3.3%) for Eudragit® *NE*, and 15.5% (104% of original amount added) for Eudragit® *RL***, as determined gravimetrically. (Such weight loss is accounted for in all ensuing uptake/partition calculations {such that uptakes are given in units of grams per gram leached film weight}. The uptake of water by the film was not accounted for, however, but was negligible {⟨0.25%} when compared to the total mass of water as a whole in the experimental sample, such that the change in concentration of the solute solution due to water uptake by the film would also be negligible.)

The 4-nitrophenol partitioned into the Eudragit® *RL* to a greater extent than the Eudragit® *NE*. This is in concurrence with the higher solute permeability coefficient of Eudragit® *RL*. In the case of both Eudragit® *NE* and Eudragit® *RL* polymers, there was a good correlation between the initial solute concentration and the uptake of solute by the polymer (r^2 = 0.981 and 0.987 for Eudragits® *NE* and *RL*, respectively).

8.6.6 The activation energy of 4-nitrophenol solute permeation through Eudragit® *NE* and *RL* films.

Permeability is defined as the product of the solubility coefficient, *S*, and the diffusion coefficient, *D*. Both of the parameters *D* and *S* are known to be temperature activated, and can be expressed in terms of Arrhenius-type equations (Chapter 5). Hence, the activation energy of permeation can also be expressed in a similar manner.

The energy of activation for the permeation of 4-nitrophenol through Eudragit® *NE* was determined by means of an Arrhenius-type plot (**Figure 8.20**). The correlation between the Ln_e[Permeability Coefficient /m^2 s^{-1}] and reciprocal temperature was found to be good, giving a regression coefficient, r^2, of 0.949. The **energy of activation for the permeation of 4-nitrophenol through Eudragit® *NE*** was calculated to be **50.5 kJ mol^{-1}**. (Note that in **Figure 8.20**, the error bars refer to the maximum and minimum values found experimentally.)

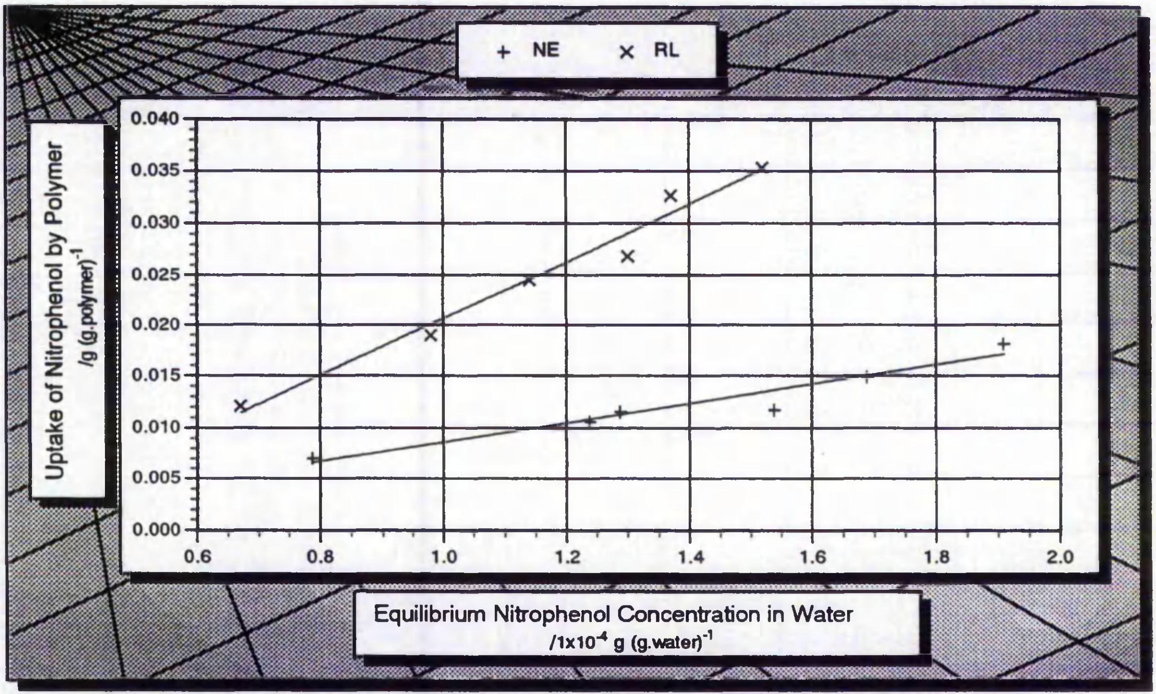

Figure 8.19 Equilibrium 4-nitrophenol uptake graphs for Eudragits® *NE* and *RL*.

Eudragit® *RL* also showed a good correlation between variables for the Arrhenius plot, with a value of 0.987 for the correlation coefficient, r^2. As expected from the higher value found for the 4-nitrophenol solute permeability coefficient for Eudragit® *RL* compared to Eudragit® *NE*, the **activation energy for 4-nitrophenol permeation through Eudragit® *RL* was** lower than that of Eudragit® *NE*, at **40.7 kJ mol^{-1}**.

8.6.7 Anilines as solute permeants.

A series of aqueous solutions of aniline and substituted anilines (diluted in buffer pH 6) of increasing size (aniline, methyl aniline, ethyl aniline and propyl aniline) were used as probes of porosity. Serota[446] *et al.* used a larger group of similarly related molecules (molecular weights from 93 → 123) as permeants through polyethylene, finding that the order of permeability could be correlated to the order of their partition coefficient in a hexane-water solvent system. In a porous membrane system, it would be expected that the solubility of the aniline in the membrane material would become less relevant with increasing pore size and pore number density, as the transport mechanism changed from an activated solution-diffusion mechanism to one in which convective transport through the pores became the predominant transport process.

When the pore size exceeded the molecular size of the penetrant, it would be expected that the calculated 'apparent' permeability coefficients would tend to coincide as permeant molecular size/solubility in the polymer became less pertinent to the transport process. This feature is evident if the permeation of the series of anilines through filter papers is investigated. **Figure 8.21** shows the permeation of the four anilines through a Millipore (Millipore U.K. Ltd., London, UK.) (0.45 μm) filter to have similar apparent permeability coefficients. The four lines shown yield gradients with a standard deviation of 1.1×10^{-7} m^2 hr^{-1} (or 9.7×10^{-8} m^2 hr^{-1} if the line for propyl aniline, which shows a visually different gradient for reasons discussed in the following paragraphs, is ignored). The molecular volume, *V*, (units of cm^3 g.mol^{-1}) of the anilines can be calculated using the atomic contributions as determined by Le Bas[306] (data cited by Wilke and Chang[535]). This yields values of 110.2, 132.4, 154.6, and 176.8, for aniline, methyl, ethyl, and propyl anilines, respectively. From this data, if it is assumed that the anilines are spherical in shape, then their respective molecular radii, *r*, are given by:

$$r = \sqrt[3]{\frac{3V}{4\pi N_A}} \tag{8.4}$$

where N_A = Avagadro's constant = 6.022×10^{23}.
The respective radii of aniline, methyl, ethyl, and propyl anilines can thus be calculated as 3.52 Å, 3.74 Å, 3.94 Å, and 4.12 Å, which gives an indication that the approximate pore diameter for unimpeded aniline transport must be $\rangle$ 8.3 Å.

Table 8.8 gives the permeability coefficients and uptakes of the respective anilines through Eudragit® *NE* and Eudragit® *RL*. The permeability coefficients are higher than for 4-nitrophenol. The propyl aniline is the odd one out, in that, because of its lower aqueous solubility, it was used at a lower concentration: 2 mM as opposed to 8 mM. Hence, although

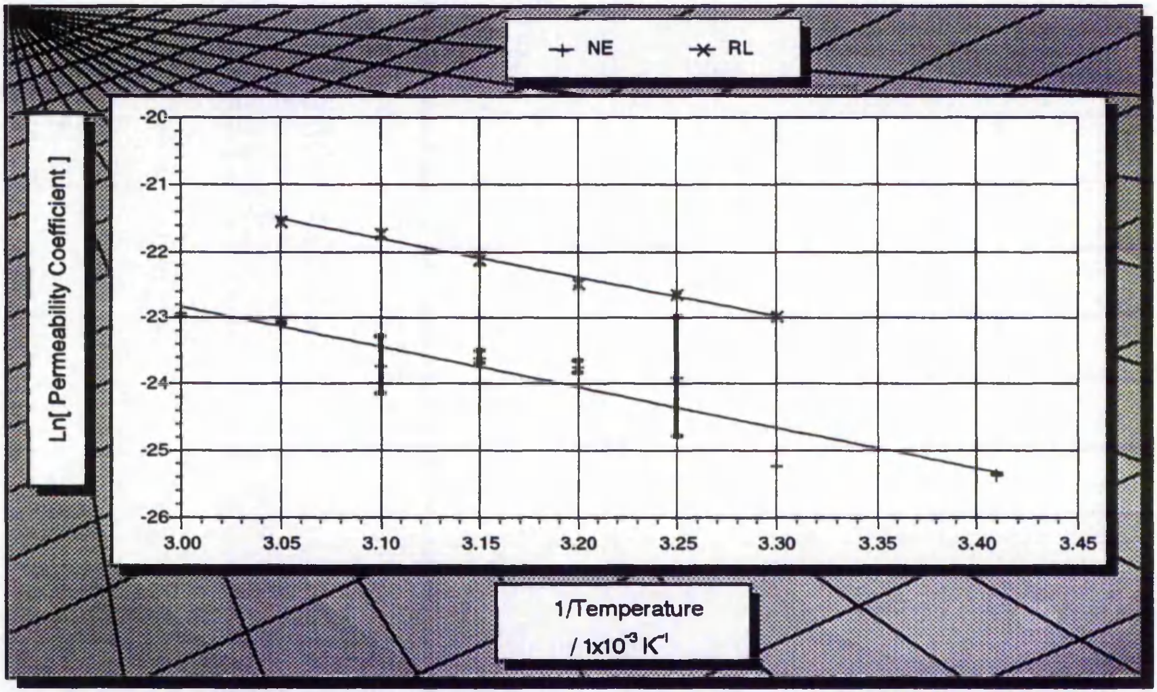

Figure 8.20 Arrhenius-type plots from the permeation of 4-nitrophenol through Eudragits® *NE* and *RL* films.

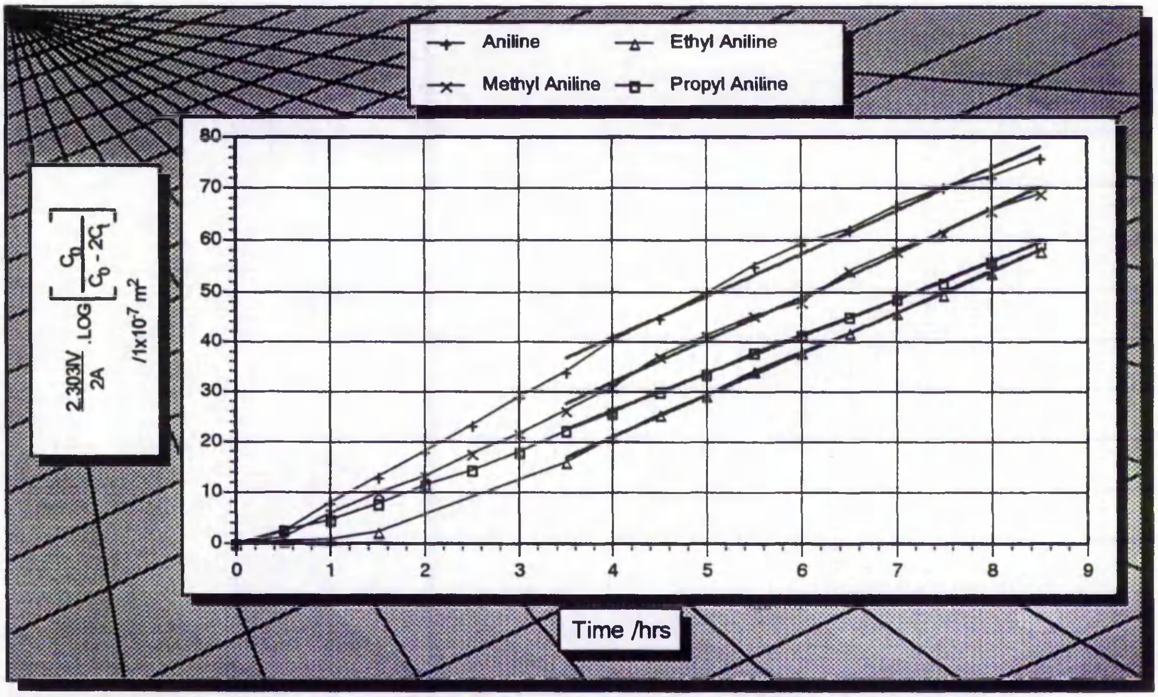

Figure 8.21 The permeation of anilines through Millipore filter papers (0.45 μm).

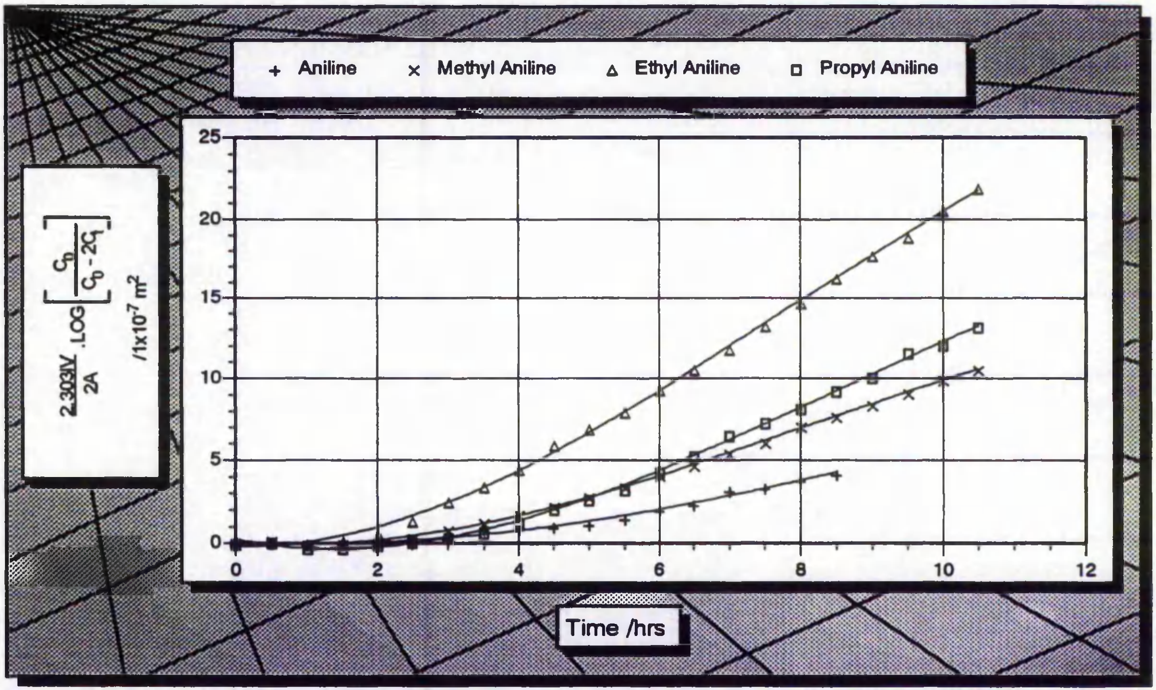

Figure 8.22 Plots for the calculation of the aniline permeability coefficients of Eudragit® *NE* films.

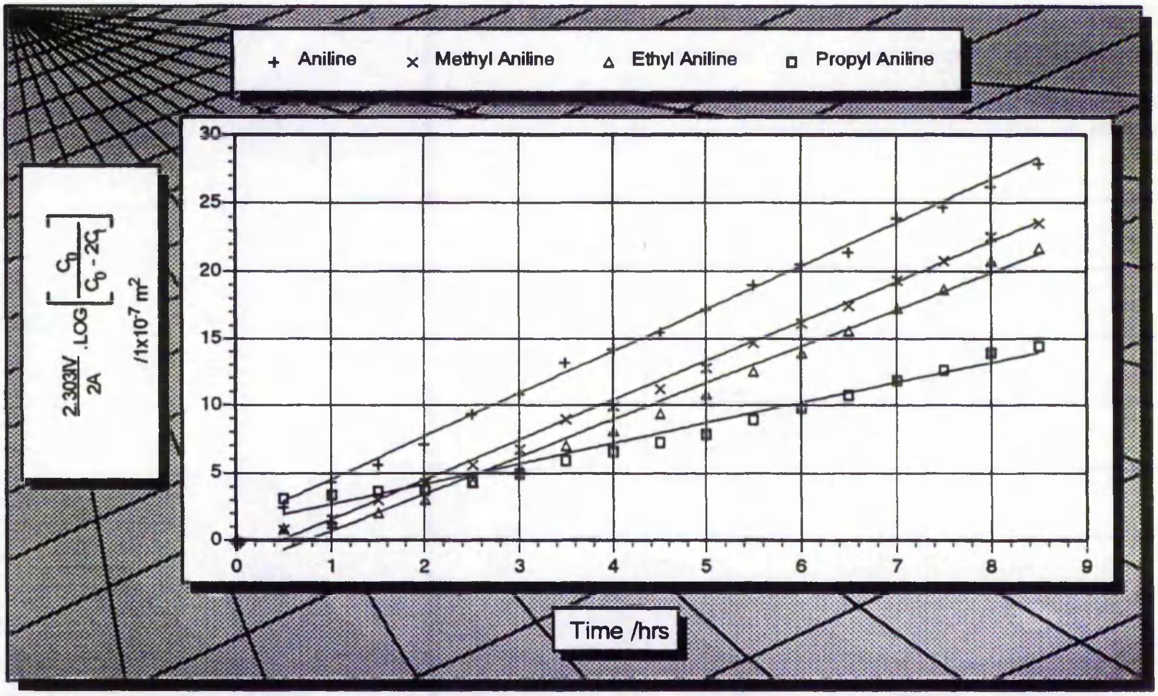

Figure 8.23 Plots for the calculation of the apparent aniline permeability coefficients of Eudragit® *RL* films.

Table 8.8 Aniline permeation and equilibrium uptake by Eudragit® films.

ANILINE	PERMEABILITY COEFFICIENT /1×10^{-7} m^2 hr^{-1}	UPTAKE BY FILM /g (g.film)$^{-1}$	PARTITION COEFFICIENT†
Eudragit® *NE*			
ANILINE	0.91	0.0040	7.67
METHYL ANILINE	1.47	0.0575	60.77
ETHYL ANILINE	2.84	0.1115	123.96
PROPYL ANILINE	1.97	0.0345	138.68
Eudragit® *RL* (+ 15% TRIACETIN)			
ANILINE	3.05	0.0057	7.68
METHYL ANILINE	3.17	0.0381	58.53
ETHYL ANILINE	3.16	0.0671	72.35
PROPYL ANILINE	1.84	0.0247	96.86

† Determined from single uptake value only.

it is possible to compare permeability coefficients for all anilines, it is not possible to directly compare uptake values. The partition coefficients, albeit determined from the uptake at a single concentration, are therefore provided.

During the course of an aniline permeation experiment, the Eudragit® films became swollen and discoloured (brown): the degree of colouration dependent on the aniline. In the case of Eudragit® *NE*, uptakes of the first three anilines increase (**Table 8.8**) with increasing length of alkyl group – and the partition coefficients show this trend to be continued for propyl aniline. This would be expected in that the more hydrophobic the side chain, the more predominantly it would be expected to partition into the hydrophobic polymer, as opposed to the water. (If the amount of an aniline taken up by the film is calculated as a fraction of the initial aniline concentration, then it is found that between ca 0.3% and 8% of the anilines are lost to the Eudragit® *NE* film {*cf.* 0.5 → 6% for Eudragit® *RL*} such that the initial concentration term, C_0, is an overestimate of the true value. This is not accounted for[1] in the permeability coefficient calculation because the result is only intended to investigate porosity. If porosity exists, such that the permeability coefficients are of similar magnitude, the solubility in the film is less significant since the permeant will travel mainly through the pores. However, if porous transport is occurring, the calculated 'permeability coefficient' is not a real permeability coefficient {*i.e.*, not a property of the polymer}, but does give an indication of the relative rate of transport through the film {compared to the non-porous film} and is therefore interpreted as an *apparent* permeability coefficient.)

---

[1] Allowing for propyl aniline uptake (in C_0) increases the permeability coefficient, but insufficiently to obey the trend – indicating that diffusivity in the polymer is also low.

The plots for the calculation of the permeability coefficients of the anilines through Eudragits® *NE* and *RL* are shown in **Figure 8.22** and **Figure 8.23**, respectively. Despite all films being of similar thickness (ca 90 → 100 μm), it is clearly seen that the anilines break through the Eudragit® *RL* without any significant time lag, and much more quickly than in the case of the Eudragit® *NE*, which shows a lag of ca 2 hrs. It is also seen that the gradients of the lines for aniline, methyl aniline and ethyl aniline, when permeating the Eudragit® *RL*, are all approximately equal whereas this is not the case with the Eudragit® *NE*. (The anomalous gradient of the line for the permeation of propyl aniline through Eudragit® *RL* is presumably a function of the degree of solubility and diffusivity in the film. It is also possible that the 'porosity' {see following paragraph} allowing the concordant gradients is insufficient to allow convective transport of the larger propyl aniline molecule.)

Figure 8.24 is a plot of the aniline permeability coefficients as a function of the aniline uptakes, when permeating both Eudragits® *NE* and *RL*. The correlation coefficient, r^2, for each of these lines is 0.946 and 0.717 for Eudragits® *NE* and *RL*, respectively. Despite the fact that only three points are used in calculating these coefficients, it is apparent that there is greater correlation between the aniline permeation through Eudragit® *NE* and the partition of the anilines into the film, than is the case with the Eudragit® *RL* (*i.e.*, in the case of the Eudragit® *RL*, the correlation coefficient implies that permeability is not directly proportional to the solubility). It is suggested that the reason for this is aqueous pathways arising from both the presence of triacetin in the Eudragit® *RL* film, and the polymer functionality. If a network of aqueous pathways is formed due to the leaching of the triacetin, and/or film swelling in the regions of hydrophilicity arising from the polymer's

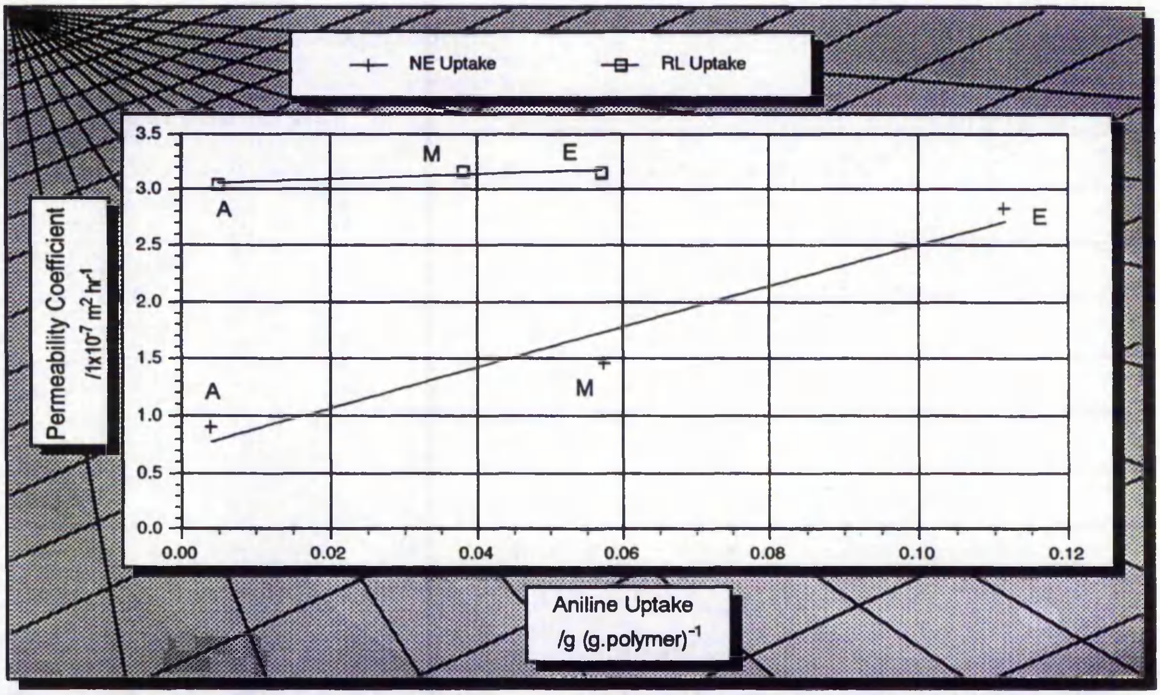

Figure 8.24 Correlation between aniline permeability coefficient and permeant uptake for Eudragit® *NE* and *RL* films. (A = aniline; M = methyl aniline; E = ethyl aniline.)

functional groups, then the mechanism by which the anilines permeate the film will be a combination of both aqueous (convective) diffusion and activated diffusion.

If the swollen aqueous pathways do exist, it would seem reasonable to assume that the rate of diffusion of the anilines through them would be faster than through the polymer. *I.e.*, the aqueous pathways would present a route of lower resistance to permeant transport by virtue of the fact that a liquid undergoes greater thermal motion than a solid. This would hold true even if it were assumed that the pathways were not continuous since the permeant would only need travel through polymer in a region of film which was thinner than the bulk. Evidence for the existence of such aqueous pathways is seen in **Figure 8.23** where there were no lag times for the permeation of the anilines through Eudragit® *RL*, and also from the fact that despite the different solubility coefficients of the anilines, and their different sizes, they all (with the exception of propyl aniline) permeate the film at the same apparent rate. A film undergoing permeation by solution-diffusion should show good correlation between the permeability coefficient and the permeant uptake/solubility – as seen for Eudragit® *NE* (**Figure 8.24**); Eudragit® *RL*, however, demonstrated only poor correlation between the apparent permeability coefficient and permeant solubility.

8.7 Effect of water on Eudragit® films.

Water has the effect of causing both Eudragits® *NE* and *RL* to swell. This was visually apparent in the way that films changed from being transparent to opaque after soaking in water. It was determined (gravimetrically) that the **Eudragit® *NE* and Eudragit® *RL* films showed an equilibrium increase in weight of 0.6213(±0.041) g $(\text{g.film})^{-1}$ and 1.1194(±0.02) g $(\text{g.film})^{-1}$, respectively, due to water uptake at ambient temperature.** (Abdel-Aziz[1] found the water uptake by solvent cast Eudragit® *RL 100* to be 1.4154 g $(\text{g.film})^{-1}$ at 280 K; *cf.* 0.0718 g $(\text{g.film})^{-1}$ for Eudragit® *RS 100*.)

The movement of water through Eudragit® *NE* film was monitored using THO. The permeability coefficient of the water being determined from the concentration of THO in normal (unlabelled) water: $\boldsymbol{P_{THO} = 1.72\times10^{-8}\ \text{m}^2\ \text{hr}^{-1}}$. This figure is also presumably the rate of unlabelled water transport through the swollen film. The graph in **Figure 8.25** shows the change in the number of disintegrations per minute (d.p.m.) as a function of time, in both the donor and receiver sides of the permeability cell, and also the total d.p.m. in the cell. This data was used to calculate the fraction of the known initial concentration of labelled water that had permeated and, hence, the permeability coefficient. The horizontal nature of the total d.p.m. plot (*i.e.*, the uppermost line in **Figure 8.25**) indicates that very little of the labelled water was lost to the film (or glassware). (Note that less than 0.008% was removed from either side of the cell during the removal of samples for analysis. Because of the small amount, it was not replaced.)

From the definition of the permeability coefficient, *P*, of:

$$P = DS \tag{8.5}$$

Where:

D = Diffusion coefficient ($\text{m}^2\ \text{hr}^{-1}$);
S = Solubility or partition coefficient.

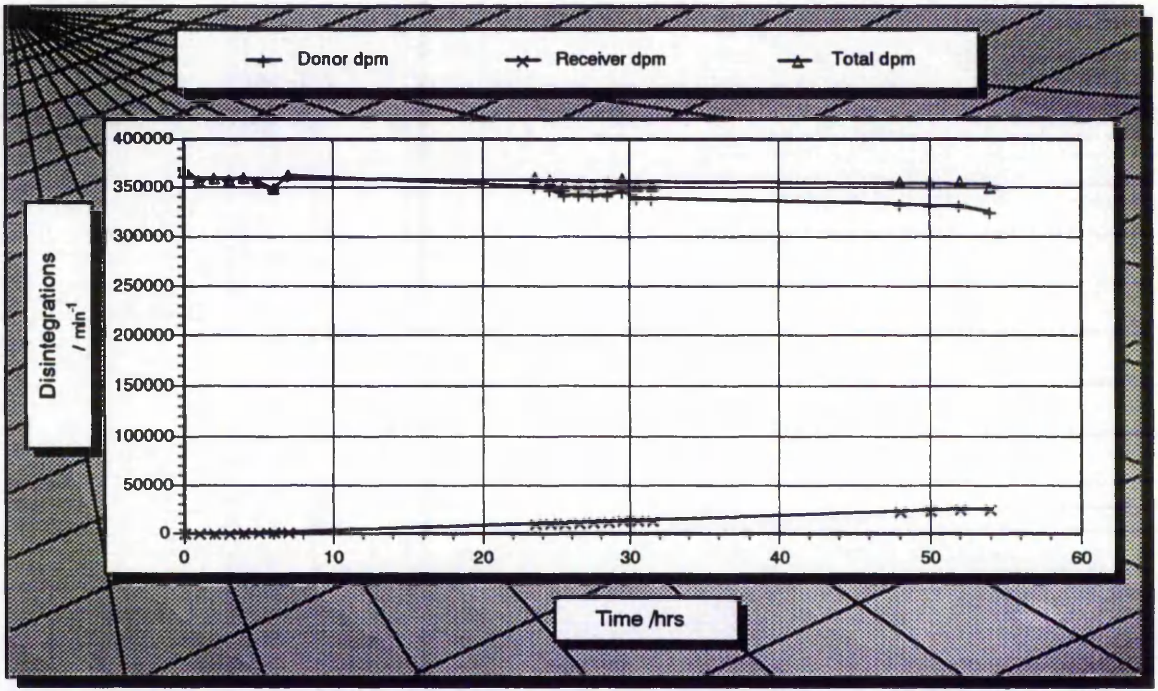

Figure 8.25 Monitoring of the permeation of tritium labelled water through Eudragit® *NE* film.

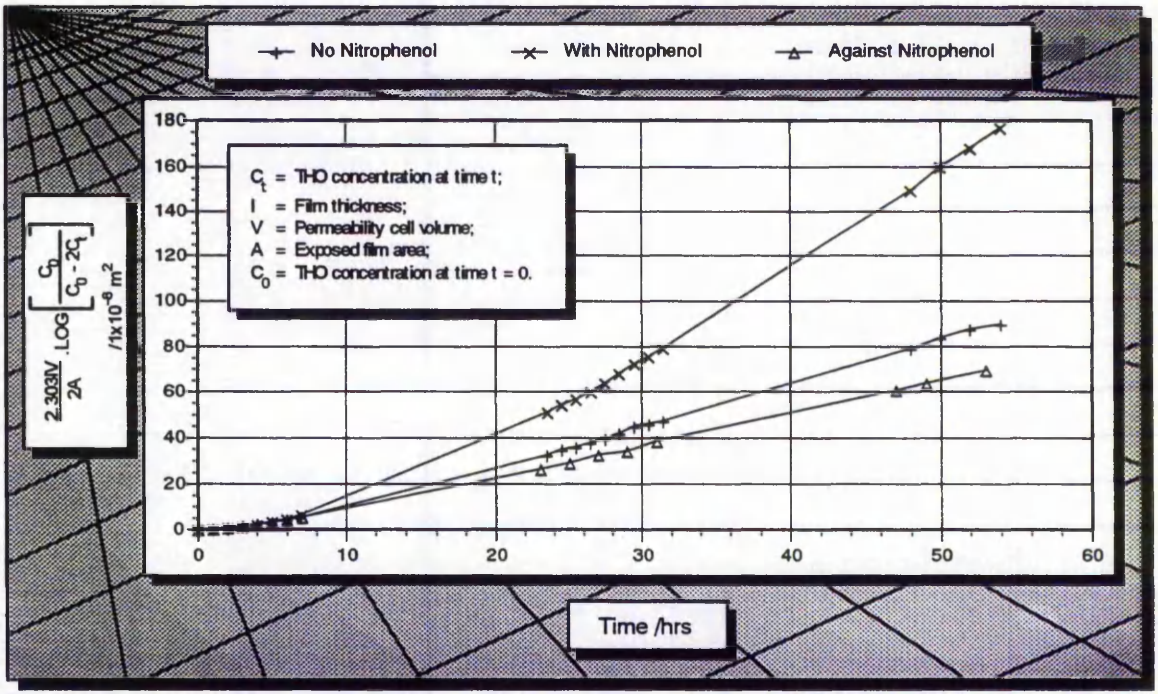

Figure 8.26 Permeation of labelled water (THO) through Eudragit® *NE* films, both with and against a flux of 4-nitrophenol.

Table 8.9 The permeability of THO as a function of 4-nitrophenol permeation through Eudragit® *NE* films.

THO FLUX DESCRIPTION & FILM ORIENTATION†	THO PERMEABILITY COEFFICIENT /1×10^{-8} m^2 hr^{-1}
NO 4-NITROPHENOL – SUBSTRATE SIDE	1.72
WITH 4-NITROPHENOL – SUBSTRATE SIDE	3.52
AGAINST 4-NITROPHENOL – AIR SIDE	1.30

† Orientation refers to the direction of the labelled water (THO) with respect to film casting orientation. (The 4-nitrophenol was always permeating through the film's substrate side.)

Given values of $P = 1.72\times10^{-8}$ m^2 hr^{-1}, and $S = 0.6213$, then the diffusion coefficient of water (at 303 K) can be calculated as $D = 2.77\times10^{-8}$ m^2 hr^{-1} (or 7.70×10^{-8} cm^2 s^{-1}). A diffusion coefficient of 7.70×10^{-8} cm^2 s^{-1} compares with the self-diffusion coefficient of water of 27.5×10^{-5} cm^2 s^{-1} (at 303 K), as extrapolated from data cited by Lakshminarayanaiah[302] in a review of membrane transport. This difference of three orders of magnitude implies that the transport of water was taking place in a highly restrictive environment.

8.7.1 Effect of the flux of 4-nitrophenol on the flux of water.

The flux of tritiated water through Eudragit® *NE* films was measured during the course of a typical experiment to determine the 4-nitrophenol permeability coefficient of a Eudragit® *NE* film (*i.e.*, the experiment giving a 4-nitrophenol permeability coefficient of 4.00×10^{-8} m^2 hr^{-1}): the THO flux being monitored both with and against the 4-nitrophenol flux (in separate experiments). The films were oriented such that the 4-nitrophenol was always passing from substrate side to air side. The permeation of 4-nitrophenol has previously been shown to be independent of film orientation (see paragraph 8.6.4.1), and there was no reason to believe that the permeation of water behaved differently. Any difference in water permeability should thus have been dependent solely on the 4-nitrophenol flux. The comparative results of these experiments are shown in **Figure 8.26**, and the calculated permeability coefficients given in **Table 8.9**. It is seen that when travelling in the same direction as the 4-nitrophenol, the THO had a faster flux than in the absence of 4-nitrophenol. It was thus concluded that the concentration gradient of 4-nitrophenol assisted the 'equilibrium' water diffusion flux in this direction – possibly influenced by association of the 4-nitrophenol and water by hydrogen bonding. Conversely, the flux of water was seen to be inhibited when travelling against the flow of 4-nitrophenol indicating that an osmotic process was not controlling water transport through the film.

8.8 Permeation of electrolyte through Eudragit® films.

The movement of a permeant through a film may be either by solution-diffusion (activated diffusion) or by bulk flow (convective diffusion, or Poiseuille or Knudsen flow if a pressure gradient exists) through pores, or a mixture of both mechanisms. Differentiating between the two mechanisms is difficult if both occur simultaneously, and capillary flow can be independent of permeant size unless the pore diameter is of a similar dimension to that of the permeant. Differentiating between activated and capillary diffusion can be further complicated if the pores do not form an interconnected network. The permeant flux in this case would appear as if for a film of lower density. Rogers and Sternberg[421] comment that if there is cohesive interaction between permeant molecules, then permeant clustering may occur leading to reduced mobility compared to that of the free molecule.

Typically, differentiating between a convective flux and a flux due to solution-diffusion is done by measuring the diffusive flux of a permeant due to a concentration gradient, and then observing the effect of a hydraulic pressure gradient across the film. The presence of a hydraulic pressure increasing the porous permeation rate but not the solution-diffusion process[553]. In this study, the films were found to be too fragile to be able to withstand a pressure sufficiently high to give a change in the measured permeation rate.

An alternative method is to determine whether ions are able to permeate a film. In the absence of a coarse porous network, or an ion exchange mechanism, a film should provide a barrier to ions. Eudragit® *NE*, being non-ionic in nature, should thus be a barrier to the permeation of an aqueous solution of KCl, provided that (i) no pores exist in the film, and (ii) the hydration of the polymer by water does not induce sufficient void space as to provide a contiguous aqueous pathway through which the ions are able to move.

In the case of **Eudragit® *NE***, the permeation of KCl (0.2 M) was investigated by measuring the change in conductivity on the receiver side of the permeability cell, held at a constant temperature of 298 K. **No increase in conductivity** was found, other than that seen in a control sample of distilled water caused by dissolved air (typically 10 μS cm^{-1}, due to dissolution of atmospheric CO_2 – *cf.* an equilibrium concentration of KCl should yield a conductivity of 12.856×10^3 μS cm^{-1}). The lack of a KCl flux is indicative of the fact that pores, if present in Eudragit® *NE*, are smaller than the ionic radius of K^+ or Cl^- ions (hydrodynamic radii[350] = 3.31 Å and 3.32 Å, respectively; *cf.* the respective Van der Waals' radii[145] of 2.30 Å and 1.80 Å). This lack of porosity is in agreement with Göpferich and Lee[204] who investigated the effects of endogenous surfactant in Eudragit® *NE* when the polymer was used in the preparation of a pharmaceutical matrix-type sustained release devices. Matrices prepared from Eudragit® *NE* in which the surfactant had been extracted (by refluxing in water) gave drug (clenbuterol) release rates which were reduced by ca 67%. The higher rate of release by the matrices containing surfactant was ascribed as possibly due to increased hydration of the polymer due to the surfactant, and *not* due to the formation of continuous pores.

The measurement of electrolyte permeation through Eudragit® *RL* (+ 15% triacetin) was complicated due to the dissociation of the quaternary ammonium groups when the film was in aqueous solution (in addition to the complication caused by the leaching of the triacetin). Hence, the permeation of radioactively labelled NaCl was investigated, with the change in permeant on the donor side being monitored by scintillation counting of samples removed from the permeability cell.

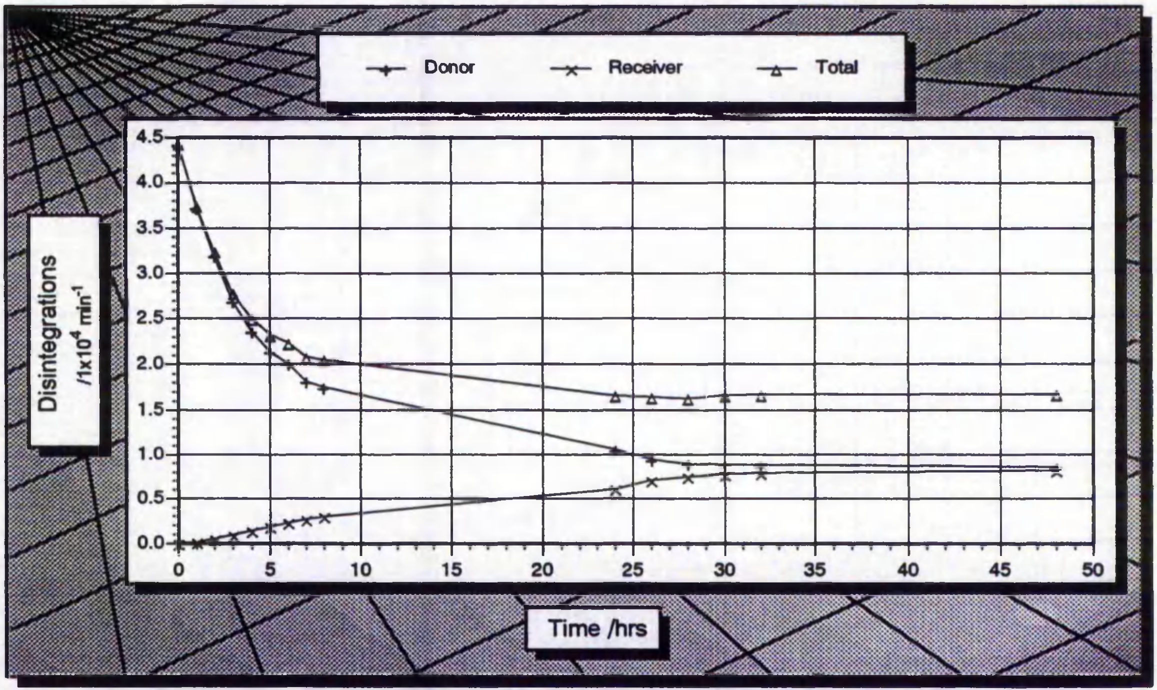

Figure 8.27 The permeation of chlorine-36 labelled NaCl through Eudragit® *RL* film, showing the activity in both compartments of the permeability cell, and the total activity.

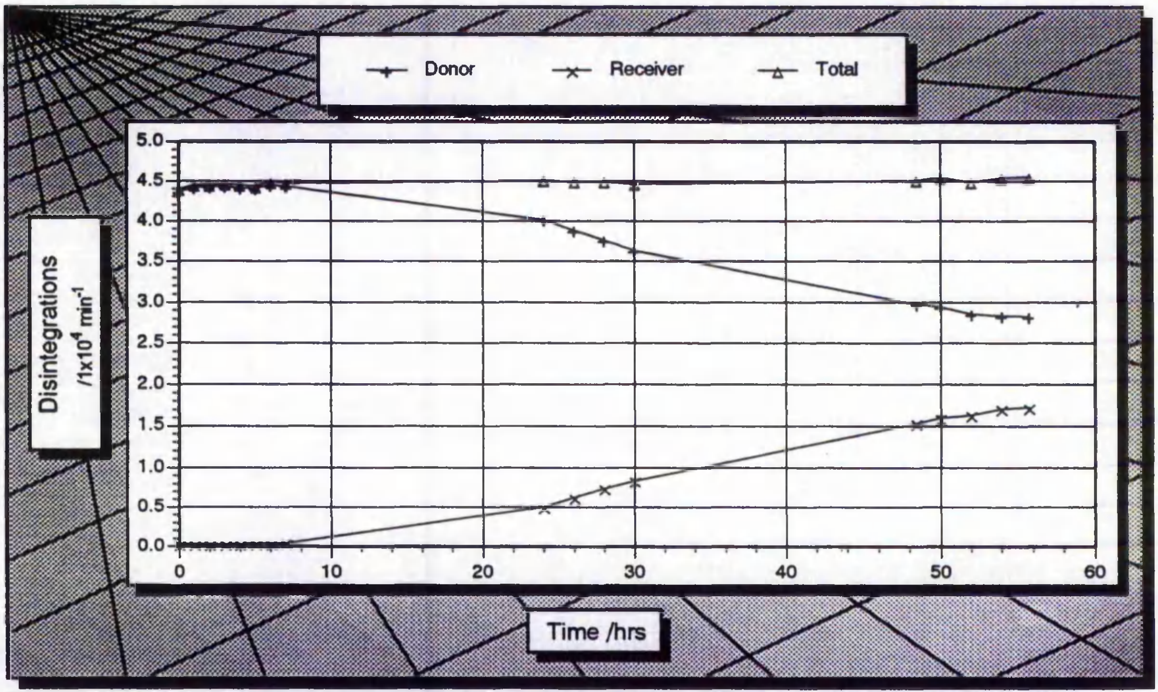

Figure 8.28 The permeation of sodium-22 labelled NaCl through Eudragit® *RL* film.

The flux of $^{36}Cl^-$ (**Figure 8.27**) was seen to reach a plateau (normally indicating equilibrium in the cell), however, before the equilibrium concentration was reached, it was found that 61(±1)% of the total of added labelled chloride 'disappeared.' This was not due to leakage of the permeability cell, and no trace of the $^{36}Cl^-$ was found in the constant temperature bath. It was thus presumably a feature of the film: the labelled chloride either being exchanged for the unlabelled chloride, or the increase in ion concentration causing the film to associate its ions (a mixture of labelled and unlabelled) such that the equilibrium concentration of labelled chloride was no longer available for measurement.

The **permeation of NaCl through Eudragit® *RL***, in which Na^+ was the labelled ion (*i.e.*, $^{22}Na^+$) was also investigated (**Figure 8.28**). No loss in the total Na^+ added was found, and a **permeability coefficient of 1.26×10^{-7} m^2 hr^{-1}** was determined for when the permeant was against the substrate side of the film. With the permeant against the donor side of the film, the permeability coefficient was 1.22×10^{-7} m^2 hr^{-1}. The values are within the ca 10% uncertainty induced by variation in film thickness.

The permeation of Na^+ ions does indicate the presence of pores in Eudragit® *RL* when in solution. Although Cl^- ions may permeate via an ion exchange mechanism with the dissociated ions of the film, Na^+ ions do require a porous network in order to be observed on the receiver side of the film.

The results for the electrolyte permeation experiments therefore provide further evidence that an aqueous network exists in the Eudragit® *RL* films, presumably as a result of both triacetin leaching and polymer hydrophilicity, but not in the Eudragit® *NE* films. The hydrodynamic radii of the Na^+ and Cl^- ions are given as 3.58 Å and 3.32 Å, respectively, by Nightingale[350], giving an indication of the absolute minimum pore size necessary for their permeation, in the absence of other modes of transport.

8.9 Summary and conclusions.

Relative permeability coefficients have been reported for the permeation of various gases, solutes, water vapour and water through a selection of commercial Eudragit® latex-cast films – concentrating mainly on Eudragits® *NE* and *RL*.

Despite visual differences observed during casting, and the greater hydrophilicity of Eudragit® *RL*, compared to Eudragit® *NE*, both films were found to dry in approximately the same time. Neither the dried Eudragit® *RL* or Eudragit® *NE* films were seen, under the S.E.M., to show structure on a particulate level. Mercury porosimetry, and the evidence from CO_2 gas permeability results showed neither film to be particularly porous, although Eudragit® *NE* did exhibit a greater apparent intruded volume by mercury porosimetry: possibly due to compression of the film (the compression of Eudragit® *RL* being inhibited by its functionality).

The CO_2 gas permeability of both Eudragits® *NE* and *RL* decreased with film age indicating that film density was increasing as a function of time – presumably due to increased interdiffusion of the polymer chains. Aging was not evident in the solute permeability results, where presumably it was masked by the effects of polymer swelling.

The difference in appearance of the upper and lower surfaces of the Eudragit® *NE* and *RL* films (with reference to casting), was not reflected in the solute permeability results (*i.e.*, as permeability asymmetry), but was possibly lost within the experimental uncertainty. The water vapour permeability results for Eudragit® *NE* would perhaps show a very minor film asymmetry, but the fact that the permeability coefficient was seen to be dependent on film thickness tends to make these results somewhat less reliable.

Experimental factors that may have affected the solute (4-nitrophenol) permeability results have been shown to have no detrimental affect on the solute permeability of Eudragit® *NE*, and the permeability has been shown to be Fickian with respect to both film thickness and initial permeant concentration. Film casting temperature was likewise seen to have no effect on the solute permeability coefficient, unless the casting temperature approached the polymer T_g.

With regards to Eudragit® *R*, the leaching of the added (15%) triacetin plasticiser was seen to have a significant effect on the solute permeability. Eudragit® *RL* film pre-leached of triacetin showed a lower 4-nitrophenol permeability coefficient than a film containing triacetin, although the greater hydrohilicity of Eudragit® *RL* compared to Eudragit® *RS* was still apparent in the solute permeability results of the triacetin-bearing films.

The plasticiser-free Eudragit® *RL* film gave a 4-nitrophenol permeability coefficient that was approximately seven times greater than that found for Eudragit® *NE* – again assumed to be due to the greater hydrophilicity of the Eudragit® *RL* polymer. Permeant transport through Eudragit® *RL* was found to be Fickian with respect to permeant concentration, but not film thickness. This was ascribed to the greater difficulty of leaching triacetin from the thicker films.

The 4-nitrophenol solute permeability of both Eudragit® *NE* and Eudragit® *RL* film as a function of temperature followed Arrhenius-type behaviour, and the activation energies were determined.

Rogers and Sternberg[421] indicate that the presence of a microporous structure within a film allows the convective transport of a permeant, and that such transport may be independent of the permeant size unless the permeant is of greater than, or a comparable size, to the pore size. The permeability coefficients of a series of anilines of increasing size of side chain were seen to be independent of aniline size in the case of Eudragit® *RL*, but not Eudragit® *NE*. Correlating this with the structureless nature of the films (by S.E.M.), the size-independent permeability rate of Eudragit® *RL* was presumably as a result of the leaching of the triacetin plasticiser, combined with the functionality of the polymer, leading to an aqueous network through which the anilines were able to travel by convective diffusion (rather than solution-diffusion). Evidence for which arises from the independence of the permeability coefficient from the aniline uptake by the films, and the fact that the anilines showed little or no time lag when permeating Eudragit® *RL*.

The permeation of water through Eudragit® *NE* was found to occur in both directions (donor → receiver and receiver → donor, with reference to the direction of the solute permeant), but the rate was dependent on whether the 4-nitrophenol permeant was moving in the same direction or not (*e.g.*, the rate was greater when travelling in the same direction as 4-nitrophenol). In all cases, however, the water and 4-nitrophenol fluxes were of comparable magnitude, and the results showed that osmosis did not contribute to the 4-nitrophenol permeation.

Eudragit® *NE* was seen to be impermeable to ions of K^+ and Cl^-, again indicating that it had no pores of a size greater than the (hydrated) ionic radii (and that no ion exchange mechanism occurred). Eudragit® *RL* (+ triacetin) did allow the passage of Na^+ and Cl^- ions, but determination of the magnitude of the flux, either conductively or using radio-tracer methods, was complicated due to dissociation of ions from the film and ion exchange, respectively. That Na^+ ions were transported across the film indicated that convective pathways of sufficient diameter were present in the film, but these could not be detected by S.E.M. or F.F.T.E.M. in the dried film.

◆

Results and Discussion, Chapter 9: Morphology and Permeability of Surfactant-free Films.

9.1 Introduction.

Films prepared from surfactant-free latices of a number of poly(alkyl methacrylate) polymers have been investigated as part of projects by Chainey[84], and Roulstone[423]. The homopolymer films prepared for use in this study were meant as a continuation of that work, and also to give a comparison with the Eudragit® films investigated as the major part of this study.

The poly(alkyl methacrylates) investigated were prepared by surfactant-free emulsion polymerisation as described in Chapter 7, and included poly(*n*-butyl methacrylate) (PBMA), poly(*n*-amyl methacrylate) (or poly(pentyl methacrylate), PAMA), and poly(*n*-hexyl methacrylate) (PHMA). The monomers are all relatively insoluble in water, and **Table 9.1** gives the monomer solubility as determined by measuring the total organic carbon content of a saturated solution of monomer in water. Latices were of a hydrodynamic **particle size of approximately 650(±50) nm for PHMA and PAMA, and 500(±50) nm for PBMA**, as determined by photon correlation spectroscopy (P.C.S.).

Weight average molecular weights (M_w) were 1,383,000(±144,000) for PBMA[1]; **678,000 for PAMA**; and **350,000 for PHMA**, as measured by G.P.C. It was important that the different batches of a given polymer were of comparable molecular weight since Kaminska[266] has shown (for polystyrene films) that the molecular weight of the polymer can affect the (air) permeability (*e.g.*, film permeability decreased as molecular weight increased).

The PHMA and PAMA polymer particles were found to be too soft to be sized by electron microscopy – the electron beam causing the polymer to flow and therefore distort the particles. Therefore, P.C.S. was used. Roulstone[423] sized PBMA latices by both T.E.M. and P.C.S. finding good correlation between the respective methods. When measuring particles by P.C.S., a latex standard was employed first as a calibration-test of the instrument set-up.

For use in film casting, latices were cleaned by extensive dialysis, but where latex functionality was important, a final stage of microfiltration was included.

9.2 Latex film formation and morphology.

Following Chainey[84] and Roulstone[423], free films prepared from surfactant-free latices were considered as model systems: *i.e.*, systems in which the properties of the films were entirely dependent upon the polymer and its casting conditions.

---

[1] Units: Polystyrene equivalents.

Table 9.1 Monomer solubility in water, at ambient temperature.

MONOMER	% (W/W) MONOMER CONCENTRATION†
BUTYL METHACRYLATE	0.0041
AMYL METHACRYLATE	0.0017
HEXYL METHACRYLATE	0.000723

† Values account for background contamination of water of 0.00017%. Quoted precision (5% RSD.

9.2.1 Casting and morphology of PBMA surfactant-free, free-films.

PBMA has a relatively high $\mathbf{T_g}$, (in relation to ambient temperature) with quoted values [312] in the range of **286 → 308 K** (presumably due to differences of molecular weight). The brittleness at ambient temperature[1] of the free-films, produced in this study, would suggest that the higher end of the quoted T_g range would best describe the polymer used in this study. Zosel and Ley [567] claim a T_g of 302 K, and give a M.F.F.T. of 296 K. Film casting (72 hrs) was performed well above this temperature range (at 353 K).

For comparison with the Eudragit® films of Chapter 8, the oven conditions during the casting of a PBMA film (at 313 K, from a latex at 5% polymer solids content) were monitored, and are shown in **Figure 9.1**. **Figure 9.2** indicates the various visual observations made during the drying process.

Like the Eudragit® *NE* films, the PBMA films were observed to dry in a non-uniform manner, with drying spreading, in the form of a front, from one or more points of nucleation. Drying proceeded in a manner similar to that of the Eudragit® *NE* films. However, the iridescence that had been seen with the Eudragit® *NE* films was very much stronger in the case of the PBMA films, with easily distinguished bands of colour that preceded the formation of a narrow region of skin around the dry, clear area of film. The fact that the iridescence shown by the PBMA films was greater than that of the Eudragit® *NE* suggests the crystalline ordering of the latex particles occurred to a greater extent in the PBMA. This is attributed to the extended range of the double layers of the electrostatically stabilised PBMA particles, compared to the shorter range interactions of the sterically stabilised Eudragit® *NE* latex.

Figure 9.1 shows the changes in weight loss and R.H., for films cast at 313 K. Like the Eudragit® films (of Chapter 8), the temperature above the film increased by 1 K when the film dried. **Figure 9.2** shows that **iridescence** was first observed when the total (average) volume fraction, Φ, was 21%, at a time of 525 min, and that the iridescence was visible across the whole film at a time of 540 min (Φ = 24%). (When casting the Eudragit®

---

[1] The laboratory in which this work was performed usually had a relatively high ambient temperature of approximately 295 K, but could get as high as 302 K in mid summer.

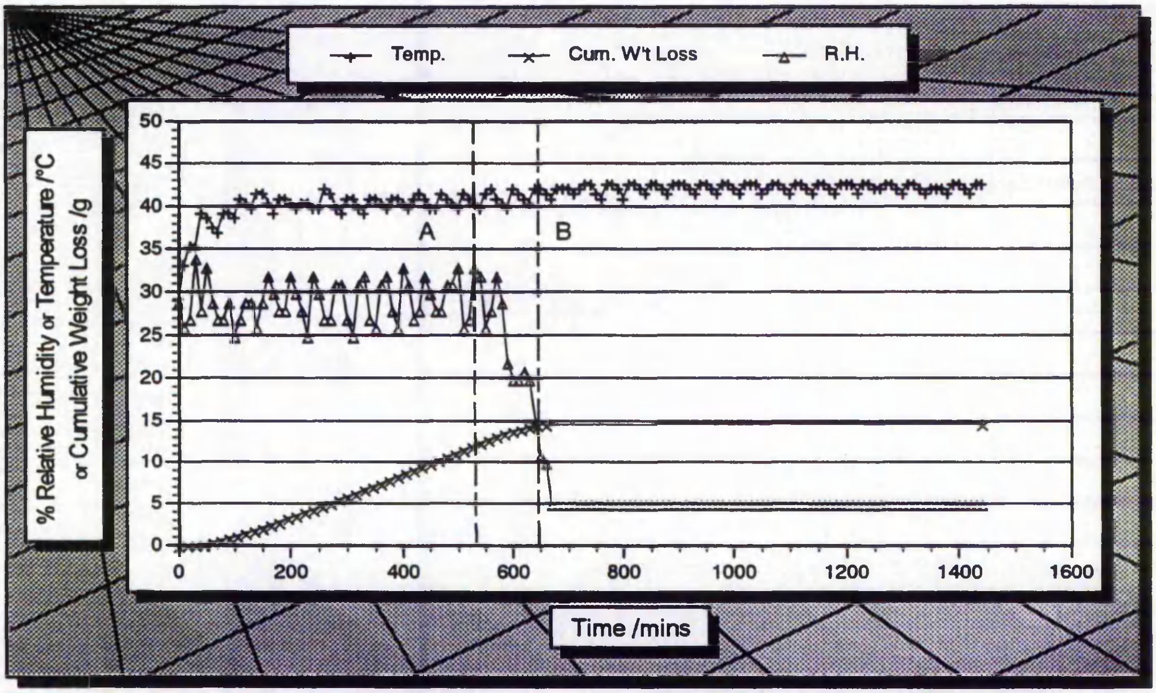

Figure 9.1 Oven conditions during the drying of a PBMA film cast from 5% polymer solids content at 313 K. A = iridescence (21.2% vol. fraction); B = fully formed skin (83% vol. fraction).

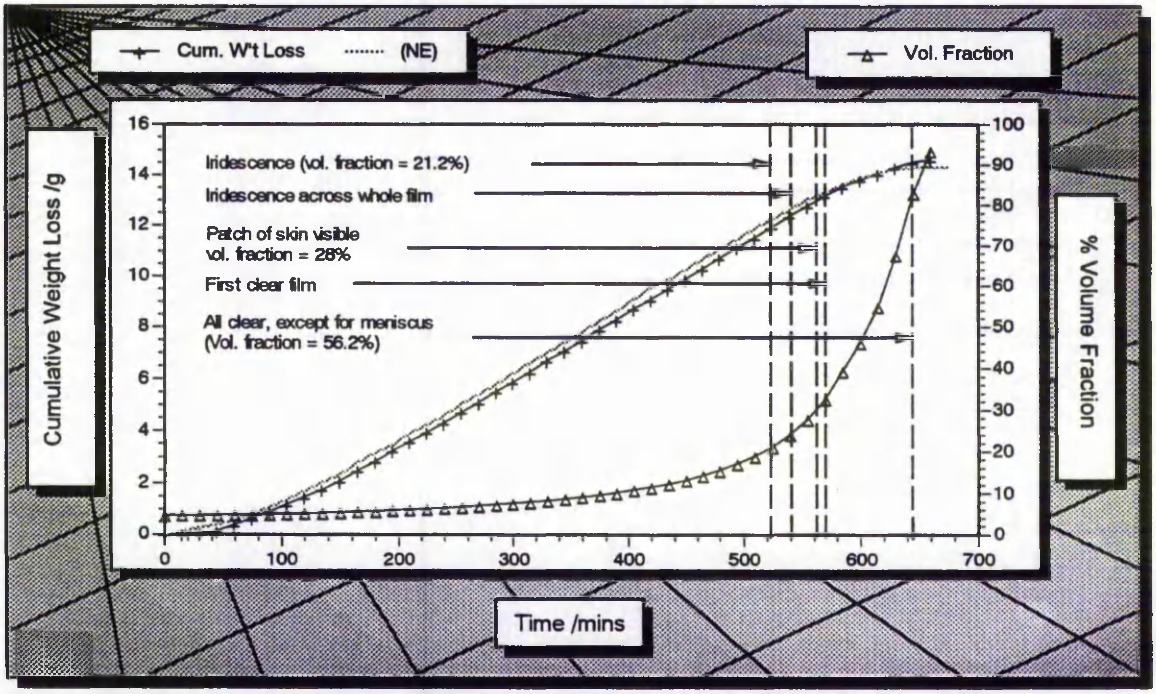

Figure 9.2 Plots of cumulative weight loss, and percentage volume fraction of polymer solids content during the casting of a PBMA film. (Note the comparison with Eudragit® *NE*.)

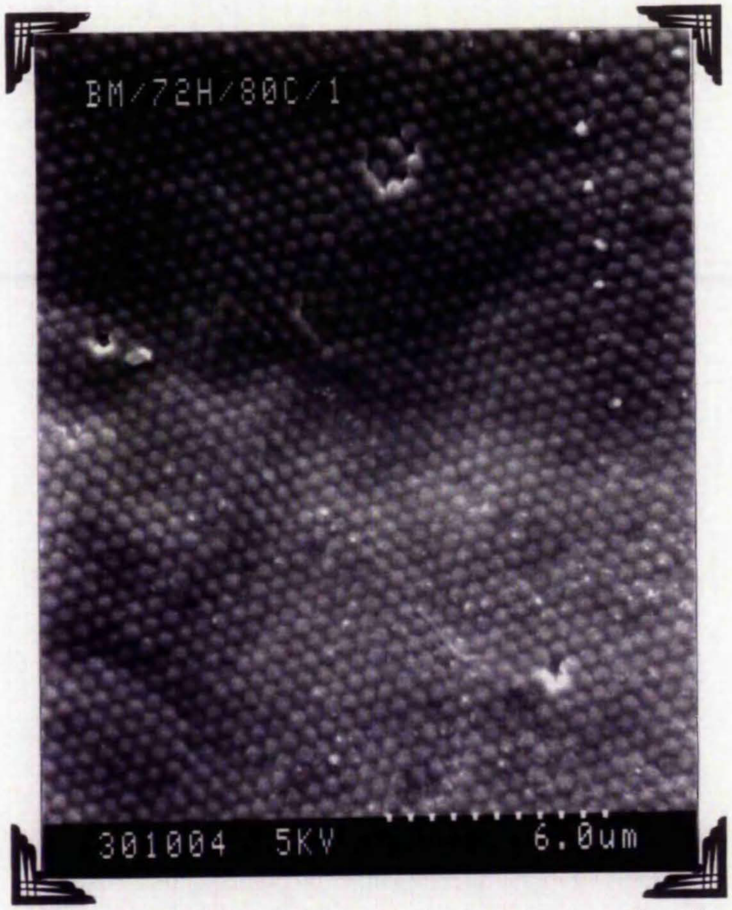

Plate 9.1 (301004) S.E.M. of the upper, air, side of a poly(butyl methacrylate) film cast for 72 hrs at 353 K.

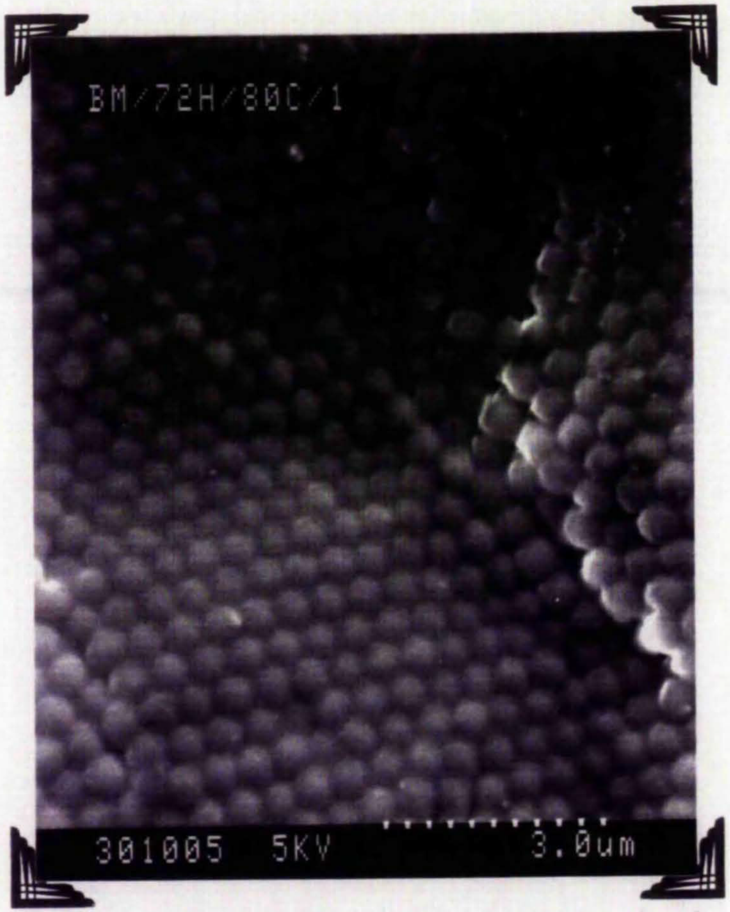

Plate 9.2 (301005) S.E.M. of the upper, air, side of a poly(butyl methacrylate) film cast for 72 hrs at 353 K.

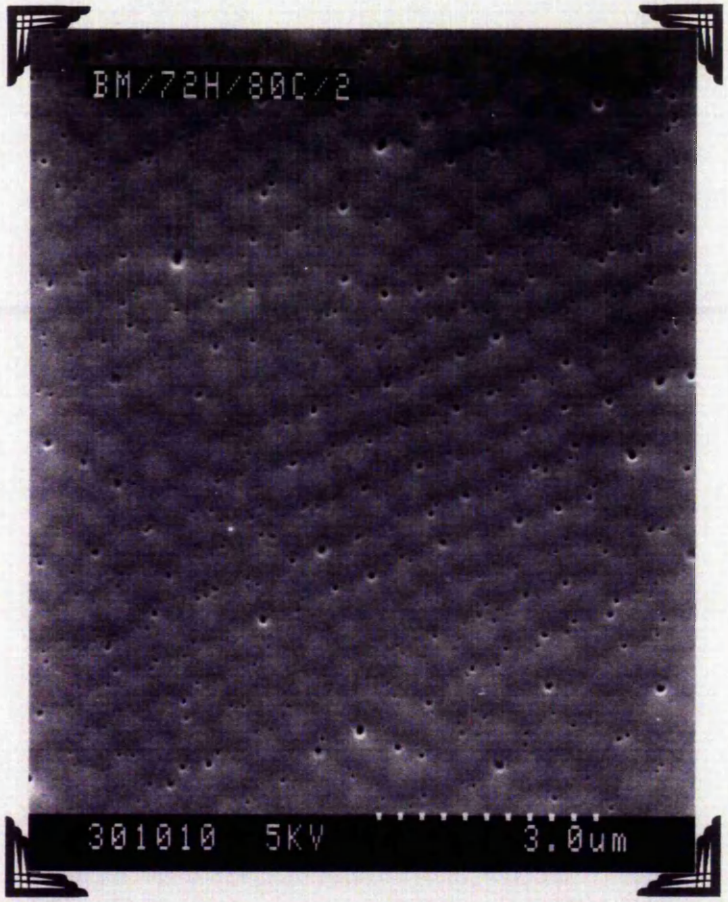

Plate 9.3 (301010) S.E.M. of the lower, substrate, side of a poly(butyl methacrylate) film cast for 72 hrs at 353 K.

Plate 9.4 (893780) T.E.M. of the centre of the fracture cross-section of a poly(butyl methacrylate) film cast for 3 hrs at 353 K.

NE film, iridescence was never seen to cover the whole film.) The first sign of **skin** formation was at Φ = 28% (562 min), at the same position of the original iridescence. This site (of initial skin formation) was henceforth the first position of clear film (Φ = 33%) at a time of 562 min: the clarity spreading to the whole film area (except around the meniscus) in a time of 645 min (Φ = 83%) from the start of the experiment.

Comparing the drying of Eudragit® *NE* to that of PBMA (**Figure 9.2**), it is evident that the steady-state rate of evaporation of the water was the same for both films, and the drying curves are, hence, of a correspondingly similar shape. Some slight difference in the two curves is apparent in the region where the rate of water evaporation starts to decrease: the PBMA appearing to dry much more suddenly than the Eudragit® *NE*. However, both films took the same time to move from the first sign of iridescence to a fully clear film.

The fully dried PBMA film (when removed from the substrate) had a matt finish on the upper surface (polymer-air interface), and a glossy finish on the lower surface (polymer-substrate interface). The upper side of the film also showed 'mud-cracks' (as seen on the Eudragit® *NE*). However, the features seen on the PBMA film surface were fewer in number, but more prominent.

An interesting feature of the freshly prepared dry PBMA film (occurring in the film cast at 313 K, but not that at 353 K) was that when re-soaked in water and then removed to dry in air, the film was observed to undergo diffraction iridescence. This would disappear in a matter of seconds, but could be restored if the film was re-immersed in water. This effect could be reproduced over a period of 2 weeks, after which it stopped. This would thus indicate the presence of structure, at least on the film surface, which would appear to be enhanced to a dimension comparable to the wavelength of visible light when swollen with water (hence, the iridescence being only apparent after soaking). On swelling, the PBMA films did not imbibe sufficient water to turn opaque (in contrast to the Eudragit® films) but remained clear, except in the regions of the 'mud-cracks' (again suggesting that these were areas of weakness within the film). This lack of water uptake was reflected in the speed of drying and loss of iridescence. The total cessation of the iridescence effect after a 2 week period reflects the effects of further gradual coalescence on film densification.

PBMA films, cast for 72 hrs at 353 K, were examined by S.E.M. (**Plate 9.1** to **Plate 9.3**). The upper surface of the film, which appeared to be matt-finished and textured, showed a good example of the close-packing of spheres (particles), albeit with occasional missing particles. The **PBMA particle diameter** is seen to be ca 500 nm and monodisperse, which compares to a size of **530.3 nm** as measured by P.C.S. (the P.C.S. also confirming the latex to be relatively monodisperse when using the multi-angle software {see Chapter 7}). Beneath the holes left by the missing particles, it is possible to see the underlying layers of particles, and it is also evident that no particles are distorted from spherical. The underside of the film (**Plate 9.3**) also shows some structure, but the particles are deformed to some extent – in keeping with the smooth, glossy, appearance of this side of the film. The particle deformation may result from either (i) adhesion of the particles to the glass, or (ii) from compression of the particles against the substrate. The substrate side of the film also shows a number of small holes (**Plate 9.3**), far smaller than the particle size, which were not apparent on the film's upper surface. The results of the solute permeability experiments also implied that these holes did not pass through the entire thickness of the film (see paragraph 9.3.1). The holes possibly result from the fact that the latex contained no surfactant: in addition to assisting in latex stabilisation, a surfactant may aid substrate wetting by reducing the surface tension and, hence, preventing disjoining of the latex when wet, and pinholing of the latex film.

A fracture cross-section S.E.M. (not included) of the PBMA film did not show the particulate structure of the upper and lower surfaces of the film, despite the fact that the missing particles, as seen in the micrograph of the upper surface (**Plate 9.1**), showed some structure in layers close to the surface. This lack of structure was possibly an anomaly of the fracture method causing the polymer to flow (despite the fracture being performed under liquid nitrogen), or the lack of focus in the picture due to the roughness of the fracture surface and low depth of field of the microscope. Also contributory was the fact that the film (**Plate 9.1** to **Plate 9.3**) was aged over three months by the time the micrographs were taken. **Plate 9.4** shows an example of a PBMA (T.E.M.) film fracture cross-section (prepared by the tensile snap method of replication {see Chapter 7}), and confirms the better resolution of T.E.M. and this method (compared to S.E.M.). This film was from a different batch of PBMA latex (prepared to a similar recipe as those films looked at previously), and was cast for only 3 hrs at 353 K. The film was not observed until five days after casting, and although indistinct, the particle boundaries are still visible in the micrograph, albeit grossly deformed from their original spherical shape. T.E.M.s (not presented) of such films cast for 72 hrs showed a similar degree of structure.

The S.E.M.s of the outer surfaces of the films cast for 72 hrs show a structure much closer to that typically seen for non-film-forming polystyrene, than for a film forming latex: presumably, the films are not white and opaque (as are discontinuous polystyrene films with particles of this size order) due to deformation of the particles in the bulk of the film.

9.2.2 Casting and morphology of PHMA and PAMA surfactant-free, free-films.

PHMA has a lower $\mathbf{T_g}$ than PBMA (**263 → 268 K**[399] {*cf.* ≈ 302 K for PBMA}) making it elastic and tacky to touch at ambient temperature. The PBMA films were cast at approximately 50 K above their T_g, and so a temperature of 313 K was chosen as the casting temperature for the PHMA films. Data on film drying are shown in **Figure 9.3** and **Figure 9.4**. Despite the similarities in the shape of the cumulative weight loss plots for PHMA, compared to both Eudragit® *NE* (as shown in **Figure 9.4**) and PBMA, a number of differences were observed. Unlike the surfactant-free PBMA, surfactant-free **PHMA latex showed no observable iridescence**. Within just 7 min from the observation of a wet opaque (white) latex with no iridescence or skin, the front one third of the film was found to be dry and clear: bordered from the wet latex by a thin band of **skin** or flocculated latex. As the front of the skin expanded across the surface of the latex, small 'lagoons' of latex remained wet, trapped in the film and covered with a skin (see schematic in **Figure 9.4**). The opacity of these trapped regions decreased with time, initially to patches of film with a hazy appearance, and finally, to dry, transparent film. These regions were thus the last to dry except for the meniscus of the latex against the retaining cylinder-wall. That iridescence was not observed for PHMA is attributed to the softness of the polymer causing the spheres to deform on initial contact.

The initial regions of film, which dried relatively quickly, showed no sign of 'mud-cracks.' However, the final film did display two or three relatively wide veins that extended a relatively long distance over the film surface. It is believed that these mud-cracks border the final section of the film (as a whole) to dry with those areas of trapped latex that were visible as hazy patches under the skin. (Mud-cracks were still evident in a PHMA film cast at 353 K, indicating that either: i, the polymer was unable to 'flow' and fill the residual void left following the escape of the trapped water; or ii, two or more regions of approaching skin overrode one another, in the manner of tectonic plates, to leave a ridge.)

The cumulative weight loss curve for PHMA can be superimposed almost exactly on to the curve for Eudragit® *NE* (**Figure 9.4**). This again, like the curve for PBMA, indicates that the film drying time was independent of the methacrylate polymer type, and also of any added surfactant. It also shows the film formation rate was independent of latex particle size (*cf.* PHMA ≈ 600 nm, Eudragit® *NE* = 163 nm) – in agreement with Pramojaney[402] *et al.* and Vanderhoff[507] *et al.* (but in contrast to some of the groups earlier work[397]).

Unlike the PBMA films, no evidence of any internal structure was found in PHMA or PAMA films, when cast for 6 hrs at 313 K, and viewed under the T.E.M. (following freeze-fracture at liquid nitrogen temperatures, using the tensile snap method {as described in Chapter 7} and replication within hours of casting). **PAMA** was similar to PHMA, having a similarly low **T_g (263 → 268 K**[399]). **Plate 9.5** and **Plate 9.6** show the freeze-fracture cross-sections of samples of PHMA and PAMA film, respectively. It is of note that there is no evidence of the original particles (P.C.S. diameter ≈ 600 nm), although the films do show a somewhat grainy structure that is most evident for the PAMA. This is in apparent disagreement with Distler and Kanig[121] who argued that latex particles would never achieve complete coalescence due to incompatible polymer chain endgroups on the surface of the particles hindering the mutual interdiffusion of the chains. It is also in contrast to the T.E.M.s of Eudragit® *NE* (Chapter 8, **Plate 8.1** and **Plate 8.2**) which is of comparable T_g and did show some residual structure. It is, however, possible that the boundaries were present as regions of differing film density or hydrophilicity, compared to the bulk of the film, but were indistinguishable by the contrast levels available by T.E.M.

9.2.3 Porosity of PBMA films.

The porosity of a PBMA film, cast for 72 hrs at 353 K was probed using the technique of mercury porosimetry. No definable peaks, indicating the presence of pores, were found (**Figure 9.5**). However, voids and/or compressibility in the film did lead to a small amount of structure below a nominal pore radius of 0.07 μm. This is possibly related to the 'pinholes' as seen in **Plate 9.3**. The low intruded volume of mercury ($\langle$ 43 mm^3 g^{-1} at 1999 bar {1 bar = 10^5 Pa} {*cf.* 800 mm^3 g^{-1} found, for example, in the case of the PBMA film leached of Eudragit® *L*, in Chapter 11}) would seem to suggest that these holes are surface

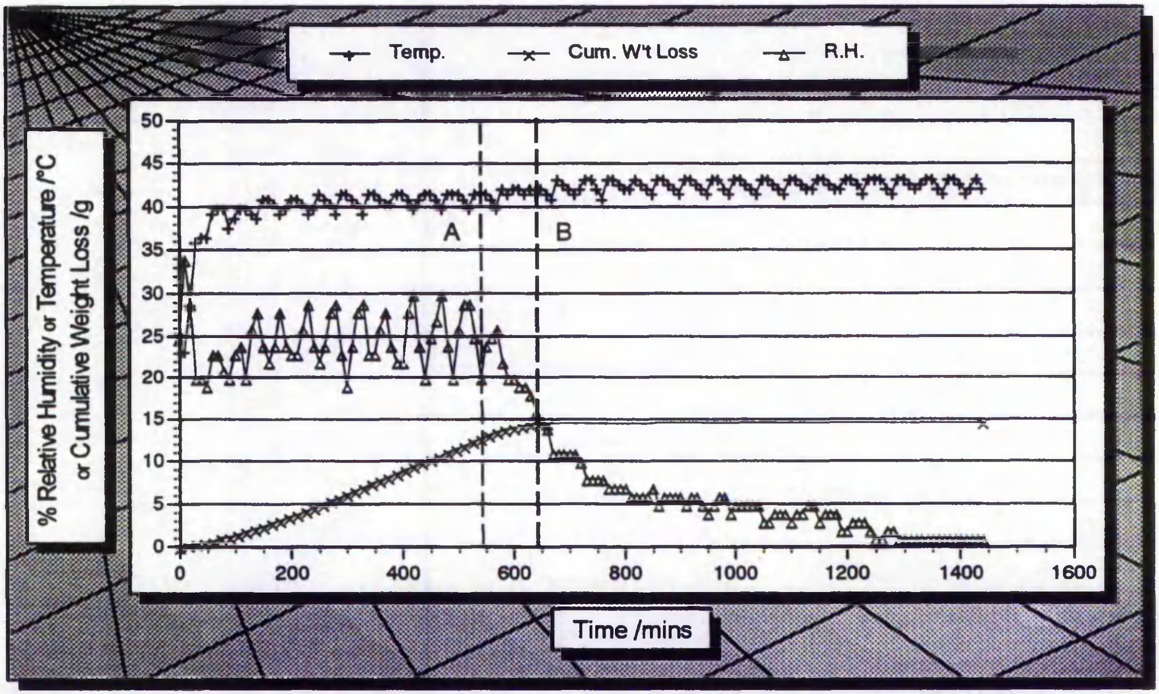

Figure 9.3 Oven conditions during the drying of a PHMA film cast from 5% polymer solids content at 313 K. A = wet latex; B = fully formed skin.

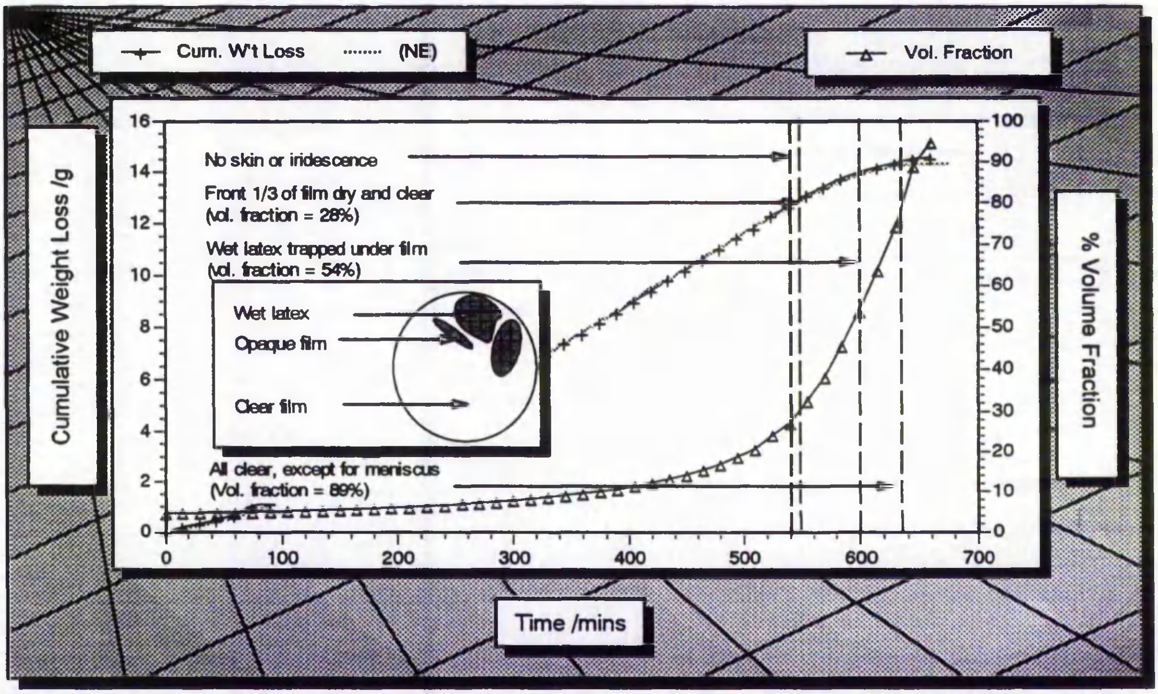

Figure 9.4 Plots of cumulative weight loss, and percentage volume fraction of polymer solids content during the casting of a PHMA film. (Note the comparison with Eudragit® *NE*.)

Plate 9.5 (894065) Freeze-fracture T.E.M. of a poly(hexyl methacrylate) film cast for 6 hrs at 313 K.

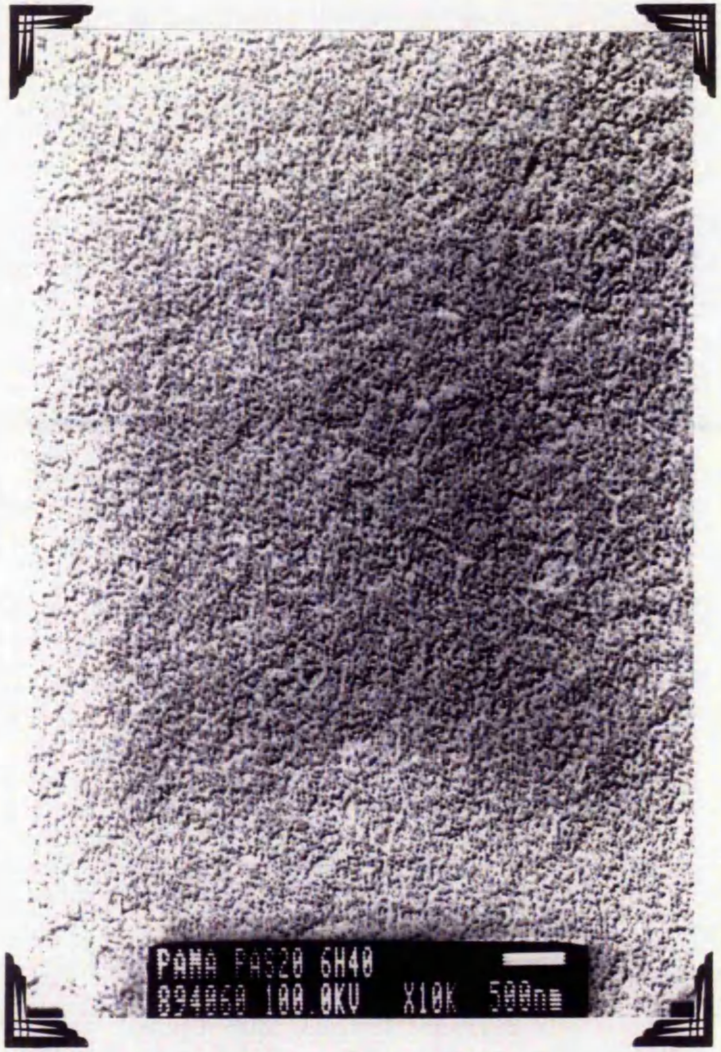

Plate 9.6 (894060) Freeze-fracture cross-section T.E.M. of a poly(amyl methacrylate) film cast for 6 hrs at 313 K.

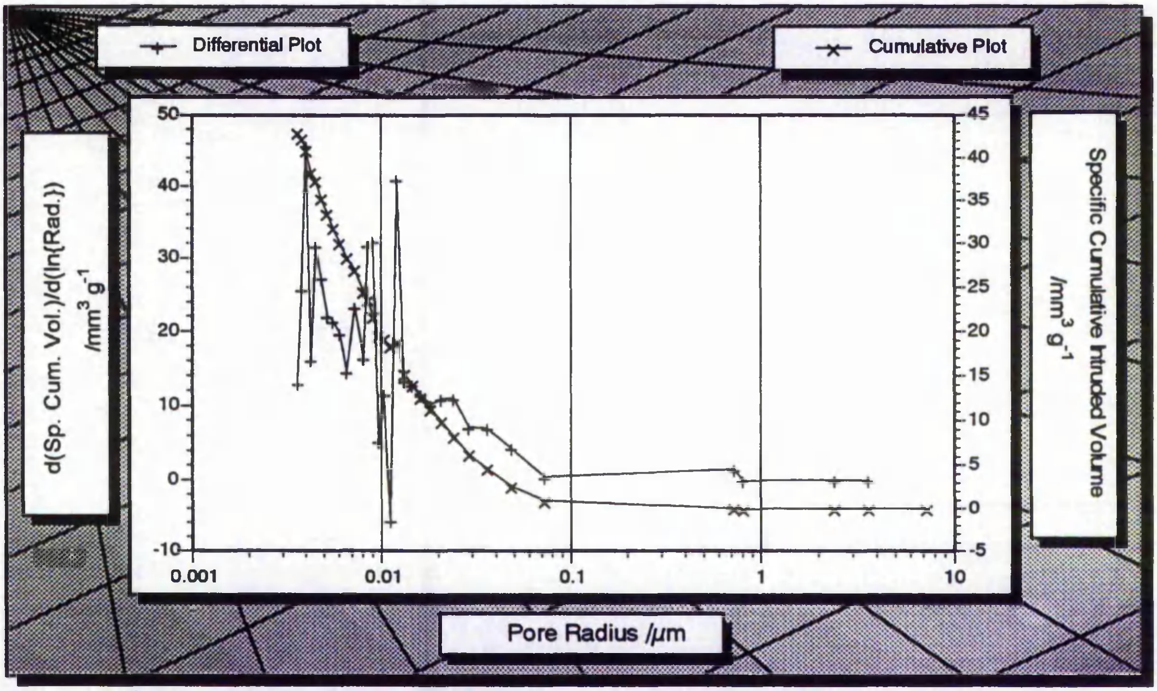

Figure 9.5 Pore distribution in a PBMA film by mercury porosimetry.

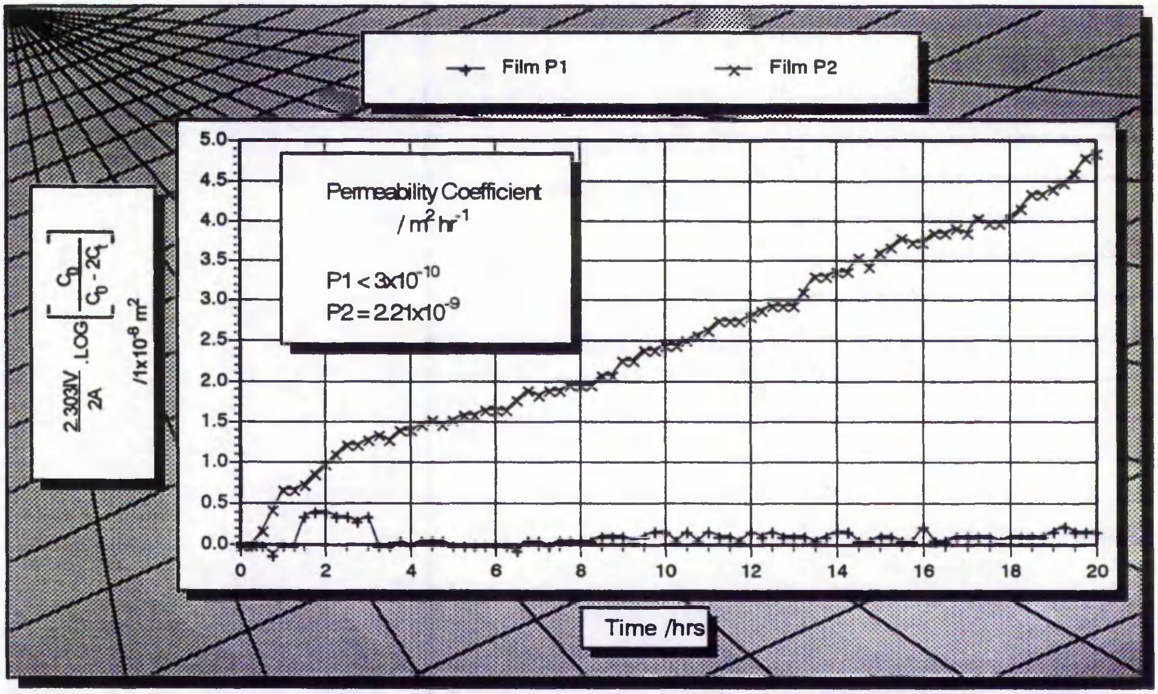

Figure 9.6 Comparison of plots giving the very low 4-nitrophenol permeability coefficients as stated in the body text. Film P1 was cast for 72 hrs, and Film P2 for 3 hrs.

Table 9.2 PBMA film permeability coefficients for *4*-nitrophenol solute, indicating the poor reproducibility, and the effect of the number of films measured on this uncertainty.

NUMBER OF FILMS USED IN CALCULATION	AVERAGE PERMEABILITY COEFFICIENT (±S.D.) /m^2 hr^{-1}	PERCENTAGE UNCERTAINTY
12	$2.35(\pm2.20)\times10^{-9}$	94
6	$7.80(\pm5.27)\times10^{-10}$	68
3	$3.82(\pm1.95)\times10^{-10}$	51

features only and do not protrude far into the film. The intruded volume was similar to that found by Roulstone [423] for solvent cast PBMA. (The negative points on the differential curve are an artifact of the method, occurring (i) when the intruded volume is of similar magnitude to the mercury compression {blank}, or (ii) when the intruded volume takes an inordinate time to equilibrate, for a given pressure increase. The latter may occur if non-cylindrical 'ink well' type pores are present, or if the polymer 'relaxes' after compression.)

9.2.4 Electrolyte permeation.

None of the surfactant-free films allowed the permeation of KCl (initial concentration 0.2 M) as measured by the change in conductivity on the receiver side of the permeability cell: the conductivity only changing by a magnitude similar to that of a control solution of double distilled water stored under similar conditions. This is indicative of the film having no pores of a diameter greater than the hydrated radii of the electrolyte ions (*i.e.*, 3.31 Å and 3.32 Å for K^+ and Cl^-, respectively [350]).

9.3 Solute permeability of surfactant-free films.

9.3.1 PBMA.

Table 9.2 gives the results for the permeability coefficient of *4*-nitrophenol for a number of PBMA films cast for 3 hrs at 353 K. The results varied widely. The poor reproducibility arose despite the fact that the films were inspected visually for pinholes, and rejected if any were found. (Obviously, pinholes as seen in **Plate 9.3** would not be visible to the naked eye.)

Chainey [84] and Roulstone [423] used only the lowest three concordant results. The assumption being that the lowest calculated permeability coefficient must be the correct one, and anything higher was due to a fault in the film.

Reasons for the high failure rates of PBMA films can only speculated upon, but may be attributable to the practical problems involved in casting and handling the films. PBMA has a relatively high T_g, and whilst film casting was performed above the T_g of the polymer, the permeation experiments were performed only just within the upper limit of the range cited in the literature [312] (*i.e.*, 286 → 308 K). The brittleness of the PBMA free-films did suggest that the T_g was above room temperature. S.E.M. evidence showed that the films had an ordered, particulate, structure, in agreement with Roulstone [423]. It is thus possible that the films had similar defects in the particle packing of the latex to those found in true crystals (*e.g.*, dislocations, 'grain' boundaries, vacancies) which could possibly lead to weakness in the structure.

Alternatively, it is possible that the 'mud-cracks' were responsible for weakness in the films. Invariably, when a film split during handling, it was along the lines of a mud-crack, presumably because this was the thinnest area of the film.

A further problem associated with the high T_g of PBMA, was that of removing the films from their casting substrate. The films were brittle and required heating to assist in their removal from the substrate. This was done by soaking in hot water, and required careful control in order to avoid deformation and stretching of the film during removal. This would unavoidably put extra strain on the film which could lead to stress faults.

Variable porosity arising from latex instability was not thought to be a problem. The **PBMA C.C.C.** to a $BaCl_2$ solution was determined as being **20 mM** (±**15%**), which compares favourably to typical values for surfactant-free polystyrene latices [393].

9.3.1.1 PBMA latex films cast for 72 hours.

Because of the high failure rate of PBMA films cast for 3 hrs, casting for a longer period was tested as a means of improving film reproducibility. It was found that the results were much more reproducible if the **PBMA films** remained at **353 K for 72 hrs**. The films produced were found to be virtually total barriers to 4-nitrophenol and gave none of the film failures which were a common feature of the films cast for 3 hrs. Over the period of one week, no visually discernible colour change was apparent in the receiver side of the permeability cell (the presence of 4-nitrophenol normally revealed by the green colouration in the cell). Attempts to spectrophotometrically measure absorbances showed stepwise changes due to their being on the limits of instrument resolution, and gave **4-nitrophenol** fluxes which were unmeasurably low, but estimated to give **permeability coefficients** of the order of **(1×10^{-10} m^2 hr^{-1}**. This is in agreement with the results of Roulstone [423] for films annealed for the same time. These casting conditions were thus employed for the work based on PBMA films in the following Chapters. **Figure 9.6** shows typical curves for PBMA films cast for either 3 hrs or 72 hrs.

PBMA films in water never swelled to the extent whereby they turned opaque (unlike all other films investigated in this study), which suggests that no aqueous pathways existed through the films.

It is thus concluded that the extra hours of heat treatment accelerated the process of further gradual coalescence, giving what could be described as a 'fully coalesced' film, with a correspondingly more reproducible result for solute transport. A **M.E.K. solvent cast PBMA film** gave a 4-nitrophenol solute permeability of similarly low magnitude to the annealed latex cast film suggesting that it offered no worse a degree of polymer chain fusion than the coalescence of the latex cast film. This might be expected for the fundamentally different process of casting from a true solution, where film formation arises from polymer chain entanglement [30] as the solvent evaporates, rather than particle coalescence.

9.3.2 PAMA and PHMA.

If the poor reproducibility of PBMA films cast for 3 hrs at 353 K was due to their relatively high T_g preventing complete coalescence under the casting conditions used (and thereafter hindering further gradual coalescence), then it was proposed that a polymer of lower T_g would help alleviate the problem. PAMA and PHMA, with sub-ambient T_g's (of between 263 → 268 K[312]) were thus chosen for this reason. A casting temperature of 313 K was used such that the films were cast at approximately the same number of degrees above their T_g as were the PBMA films above theirs. However, the reduced casting temperature meant a longer period in the oven in order to evaporate the water, *i.e.*, 15 hrs.

The **PHMA films** were found to be somewhat more difficult to handle than the PBMA films: being **extremely tacky** (and tending to cohere) and very **elastic** in their physical properties. Retention of a static charge, on removal from the substrate, meant that the films were liable to curl and become attached to themselves. PHMA films were found to adhere to the glass casting substrate to a greater degree than the PBMA films – necessitating soaking them in water (but obviously without heating) to assist in their removal. However, the excessive elasticity of the polymer meant that they were easily stretched and warped, from which they did not fully recover. (Refrigerating the films, for removal, did not alleviate the problem.) Similar problems also existed with PAMA films.

The **4-nitrophenol solute permeability coefficient of latex cast PHMA film was $8.20(\pm0.85)\times10^{-9}$ m^2 hr^{-1}**. A **M.E.K. solvent cast PHMA film** gave a lower **4-nitrophenol permeability coefficient** of **$5.48(\pm1.2)\times10^{-9}$ m^2 hr^{-1}**. Latex-cast **PAMA** film had a lower **4-nitrophenol solute permeability coefficient** than PHMA, of **$2.58(\pm0.36)\times10^{-9}$ m^2 hr^{-1}**.

The surfactant-free films investigated thus fitted a trend with the 4-nitrophenol permeability coefficients increasing in the order of polymer hydrophobicity, *i.e.*, PBMA → PAMA → PHMA reflecting the increase in solubility of 4-nitrophenol in the polymer with increasing hydrocarbon side chain length.

9.3.2.1 Effect of film casting temperature on the 4-nitrophenol solute permeability of PHMA.

Eudragit® *NE* (see Chapter 8) films became increasingly brittle as the casting temperature decreased (to below sub-ambient) – eventually becoming discontinuous, with correspondingly anomalous results in the 4-nitrophenol solute permeability coefficient. A number of **PHMA films** were **cast at ambient temperature** for 14 days: the latter 7 of which were under vacuum to assist with water removal. The **4-nitrophenol solute permeability coefficient** of the resultant films was **$8.50(\pm0.5)\times10^{-9}$ m^2 hr^{-1}**. This is within the experimental uncertainty of the permeability coefficients of films cast at 313 K for 15 hrs (*i.e.* $8.20(\pm0.85)\times10^{-9}$ m^2 hr^{-1}), and is presumably due to the low T_g of PHMA (ca 263 K), and the fact that even at ambient temperature, the films were already well above their M.F.F.T. This feature, together with the F.F.T.E.M.s (*e.g.*, **Plate 9.5**) showing a structureless film would seem to indicate that an increase in casting temperature, above 313 K, would be unlikely to have a significant affect on the 4-nitrophenol flux since the temperature increase would be unlikely to affect the film's structure any further.

Table 9.3 The effect of film orientation on the water vapour permeability of latex and solvent cast PHMA films.

FILM ORIENTATION†	PERMEABILITY COEFFICIENT $/1\times10^{-6}$ g hr^{-1} cm^{-1} $cm.Hg^{-1}$	S.D. $/1\times10^{-6}$ g hr^{-1} cm^{-1} $cm.Hg^{-1}$
LATEX CAST PHMA		
SUBSTRATE	1.093	±0.21
AIR	1.084	±0.34
M.E.K. CAST PHMA		
SUBSTRATE	0.382	±0.084
AIR	0.438	±0.074

† Orientation refers to the side of the film facing the water vapour.

9.3.3 Dialysed Eudragit® films.

Upon extensive dialysis, Eudragit® *NE* developed 'liquid opal' colouration (critical iridescence [25]) indicative of the monodispersity of the size distribution. Films cast from dialysed Eudragit® *NE* were visually no different to films cast from the undialysed latex. However, the 4-nitrophenol solute permeability coefficient of a film cast from the dialysed latex was found to be decreased by a factor of 78% compared to a film cast from the undialysed latex. The **4-nitrophenol permeability coefficient of the dialysed Eudragit® *NE* film was 8.84(±0.25)$\times10^{-9}$ m^2 hr^{-1}**, *cf.* 4.00(±0.4)$\times10^{-8}$ m^2 hr^{-1} for the un-dialysed film. The difference in the results for the dialysed and undialysed films presumably due to the additive (endogenous surfactant) that gave the 0.35% weight loss to the undialysed Eudragit® *NE* latex film on soaking in water (see Chapter 8). This would not be present in the dialysed latex film and therefore not leach during the course of the permeation experiment. In experiments using sustained release devices prepared from matrices of Eudragit® *NE*, Göpferich and Lee [204] found the magnitude of the rate of drug release to decrease by approximately two-thirds for a device in which the surfactant was removed, compared to one in which it was present. Göpferich found from D.S.C. evidence that the surfactant formed a separate phase in a surfactant-containing film – presumed due to incompatibility between the surfactant and polymer. Exudation of such incompatible material was not evident on the undialysed films used in this study. However, this may be due to the small amounts involved. The increase in solute flux on additive leaching is discussed further in Chapter 10.

9.4 The water vapour permeability of surfactant-free PHMA films.

Latex film permeabilities lower than their solvent cast equivalents have been reported [323, 425, 427] when water vapour was the permeant. **Table 9.3** gives the water vapour permeability coefficients of PHMA films, as a function of film orientation for both latex and M.E.K. solvent cast films. No side dependence was evident and the latex cast film permeability coefficient is greater than that of the solvent cast film – in direct contrast to Roulstone's [423, 425] findings for PBMA.

Table 9.4 The helium permeability coefficients of PHMA films, at ambient temperature.

FILM AGE /days	PERMEABILITY COEFFICIENT $/1\times10^{-9}$ cm^3 cm s^{-1} cm^{-2} $cm.Hg^{-1}$
0	3.02
2	2.64
18	2.36

9.5 The gas permeability of surfactant-free films.

The gas flux through a latex cast PBMA film was found to be too fast to measure using the Daventest apparatus (see Chapter 7), irrespective of whether the film had been cast for 3 hrs or 72 hrs at 353 K, due to film fracture in the apparatus.

The permeability of PHMA films, cast for 15 hrs at 313 K, was measured using both N_2 and He gases. The **N_2 gas permeability coefficient of PHMA film was $4.31(\pm0.8)\times10^{-10}$ g.p.u.**

Chainey[91] *et al.* investigated the aging of both surfactant-free PBMA latex and solvent cast films using a dynamic measuring technique. Results showed that the He permeability of the latex cast film decreased to a constant level over the course of two weeks. The solvent cast film permeability was invariant over the course of several months, but was always lower than the value found for the latex cast film. The **N_2 permeability of a M.E.K. solvent cast PHMA** film was determined as being **$2.73(\pm0.3)\times10^{-10}$ g.p.u.**: a factor of ca 0.6 less than the value for the latex cast film.

The aging of PHMA film was investigated using He gas as a probe. (The N_2 was exchanged for He in order to increase the gas flux.) Results are given in **Table 9.4**. This shows a slowly decreasing trend in gas permeability coefficient over a period of 18 days. Because of the slow rate of decrease of permeability (possibly due to the film being highly coalesced after casting), it would seem reasonable to assume that the gas permeability of the latex cast PHMA may never reach the value found for the solvent cast film (as was found by Chainey[91] *et al.* for PBMA).

9.6 Summary and conclusions.

The casting rates of the PBMA and PHMA surfactant-free polymer latices have been shown to be little influenced by the polymer type, and the rate was found to be the same as that for the surfactant-present Eudragit® *NE* latex.

Iridescence was more apparent in the case of the hard (by virtue of its high T_g) PBMA surfactant-free latices (compared to the Eudragit® and PHMA latices) as the particle packing density increased. The softer polymer particles presumably deformed more readily such that the ordered 'diffraction grating' effect only existed for a very short period before particle deformation occurred.

All surfactant-free latex films showed the 'mud-cracked' affect: thought to be caused as a consequence of the stresses in the skin which was formed as the latex dried from the top downwards. Even for PHMA formed at 90 K above its T_g, the polymer did not flow sufficiently to heal the surface texture.

The lower T_g PHMA and PAMA latices produced films (at 50 K above their T_g) showing no residual particulate structure when observed by freeze-fracture T.E.M., but the PBMA latex particles at the upper surface of a PBMA film were readily observed by S.E.M. as undeformed spheres, with an occasional missing particle allowing the spheres below the top layer to be seen. The vestiges of spheres were also visible on the substrate side of the film. However, these were deformed by compression against the glass substrate.

Mercury porosimetry showed the PBMA films to be non-porous, indicating that, although little or no deformation was evident in the upper and lower layers of particles, the void-volume symbolising hard close-packed spheres (26%) was not present, showing the particulate structure to be a surface feature only, and not representative of the bulk of the film.

PBMA films cast for 72 hrs at 353 K, rather than 3 hrs, gave much reduced rates of solute flux, but the permeability coefficient was then on the limits of detection with the available apparatus. The 4-nitrophenol solute permeability coefficients of the surfactant-free homopolymer films increased in a manner which reflected their degree of hydrophilicity, *i.e.*, PHMA having a greater 4-nitrophenol permeability coefficient than PAMA, which in turn had a greater permeability coefficient than PBMA. Polymer T_g should also be considered here, however. PBMA, which acted as a barrier to 4-nitrophenol permeation, also had the highest T_g and, hence, the lowest polymer chain mobility. Glassy polymer, with its reduced chain mobility, would be expected to show a reduced permeant flux and, from the range of T_g values quoted in the literature, it is possible that the PBMA polymer *was* in its glassy state during the course of the permeability experiments.

The initial water vapour permeability coefficient of a solvent cast PHMA film was lower than that of a latex cast film, as was the average solute permeability coefficient. The gas permeability coefficient of solvent-cast PHMA film was invariant with film age. The gas permeability coefficient of the latex cast film was higher than that of the solvent cast film, but did decrease with age. Both solvent and latex cast PBMA films were virtually barriers to 4-nitrophenol over the periods investigated.

The solvent cast polymer films always had lower permeability coefficients than the corresponding latex cast films. Despite F.F.T.E.M. showing no evidence of interparticle boundaries for latex cast PHMA film, the gas permeability results following film aging together with the higher flux of the latex cast film (compared to the solvent cast film) suggest that interparticle boundary effects are still important – with film densification in those regions still possible.

The permeation of a solute through a film may potentially be aided or hindered by the presence of particle boundaries depending on whether the rate limiting process is diffusion through the polymer or a sorption-dissolution process. In a film that contains particle boundaries (*i.e.*, regions of lower polymer chain number density), it would be expected that polymer chain mobility would be at a maximum at the boundary, hence, leading to ease of formation of 'holes' through which a permeant can diffuse. Such regions would presumably allow the diffusion of water, as well as permeant, at a higher rate than the bulk polymer. This may then lead to a contiguous aqueous pathway throughout the film, easing permeant diffusion. However, if the pathways are not contiguous, then permeant may be repeatedly forced to dissolve into the polymer, and then back into the water, such that if the sorption/dissolution is rate limiting, then the pathways would hinder diffusion compared to a homogeneous film showing relatively amorphous film properties and where sorption/dissolution need only occur at the film boundaries. The results for the permeation of *4*-nitrophenol through PBMA show that the rate of permeation evidently did decrease with a decrease in the film structure. However, sorption-dissolution need not necessarily be the rate limiting step: as coalescence increases, mutual interdiffusion of polymer chain ends increases and, hence, chain mobility is decreased due to increased film densification in interparticle regions. Hence, the ease of hole formation, necessary for diffusion, is also decreased and it would also be expected that the rate of permeation would decrease. The mutual interdiffusion of the polymer chains may be hindered, however, by the high number of incompatible end groups at the particle-particle interface. These end groups could, however, also serve to increase the hydrophilicity of this region. This is better appreciated in surfactant-present films, where the surfactant would normally reside at the particle interface, increasing the hydrophilicity still further. However, Chevalier[95] *et al.* observed film formation, using neutron scattering and E.M., noting that the surfactant 'shell' around the particle may become either fragmented, fragmented and expelled to the film surface, or retained, as coalescence occurs.

Many of the observations in this Chapter are related to the polymer T_g: the polymer with the sub-ambient T_g showing less structure than the polymer with a relatively high T_g. Although the differences in T_g were accounted for in the respective casting temperatures of the films, to interpret this as being important would imply a linear relationship between the degree of particle coalescence and temperature. Thermal annealing times would therefore seem to be as relevant as temperature, as shown by the fact that less structure was seen in a PBMA film when cast for a longer time. The PHMA, having a sub-ambient T_g, effectively undergoes the same type of thermal annealing at ambient temperature as would PBMA kept permanently in an oven at elevated temperature, and this is evident in that the process of further gradual coalescence is further advanced for PHMA compared to PBMA. Conversely, the PBMA, when held at ambient temperature, would possibly be in its glassy state such that the process of further gradual coalescence, or autohesion, would occur only slowly – if at all.

◆

Results and Discussion, Chapter 10: Sucrose as a Film Additive.

10.1 Introduction.

The aim of the work discussed in this Chapter was to investigate the effects on the permeability of the films of adding a non-ionic, low molecular weight, and extremely water soluble additive in the form of sucrose.

Li and Tu[319] studied the ability of a concentration gradient of a drug (acetominophen) in an ethylcellulose latex film matrix to give a controlled drug release, and found that the addition of increasing amounts of sucrose (in the range 0% → 20% of the weight of the matrix) served to increase the release rate of the drug, without changing the predominantly linear release profile. The leaching of the sucrose was said to lead to the formation of overlapping pores which provided water-filled channels for the diffusion of drug within the matrix, although no evidence of porosity (other than the increased release rate) was presented.

Donbrow and Freidman[125] state a number of different conditions which may result from the addition of a hydrophilic additive into a relatively hydrophobic film, and which may occur individually or in combination. The addition of the additive may result in:

- ✗ a change in the polymer matrix configuration, and the relative proportion of amorphous to crystalline polymer. The film may increase in its degree of hydrophilicity, whilst still resembling a homogeneous film;
- ✗ a continuous hydrated network;
- ✗ void-like porosity;
- ✗ a continuous porous network;
- ✗ increased film transport properties resulting from a permeant showing increased diffusion and/or solubility coefficients in the additive.

At low levels of sucrose addition, **molecular dispersion** in the dried film may be possible, but at high concentrations supersaturation during film formation could result in crystalline regions of sucrose deposition.

It was hoped that investigating the permeation properties of films either containing (leaching), or pre-leached of sucrose would provide some evidence as to the fate of a water soluble film additive, such as might be used in a pharmaceutical-type coating. It might also be noted that the properties of a film containing low levels of sucrose would be analogous to the situation whereby a water soluble drug core is spray-coated with an aqueous latex when the drug may partially dissolve into the coating before it has dried.

10.1.1 Conventions used.

The sucrose was added as an amount per gram of latex solids content (*e.g.*, g (g.*NE*)$^{-1}$). Latices were normally diluted from the supplied 30% W/W solids content in the case of the Eudragits® (or from the percentage solids as measured gravimetrically in the {self-prepared} surfactant-free latices) to 5% solids content for casting. Therefore, sucrose was added with reference to this 5% solids content such that a 1:1 ratio of sucrose to polymer solids content is 1 g of sucrose for every 1 g of polymer (termed 100% (g.*NE*)$^{-1}$). All sucrose loadings are given in terms of a percentage of the initial latex solid content (and not a percentage of the final film weight). (The percentage quoted is therefore not a % W/W. The terminology, for example, % (g.*NE*)$^{-1}$ is used to distinguish between polymer that contains surfactant, and that leached of surfactant which is typically quoted as a % (g.film)$^{-1}$.)

Eudragit® *RL* contained triacetin as a plasticiser (0.15 g g^{-1} ≡ 15% (g.*RL*)$^{-1}$). This was not included in the calculation of the loading of sucrose, and Eudragit® *RL* films described in the text as 'additive-free' *did* contain triacetin unless otherwise stated.

10.2 Observations of sucrose-containing films: film structure and aging.

10.2.1 Eudragit® *NE*.

Eudragit® *NE* films containing low concentrations of sucrose appeared identical to the sucrose-free films. As the loading of sucrose increased, films became progressively more opaque, but never became totally opaque even at the maximum experimental loading of 180%. As the opacity increased, so did the degree of gloss on the film surfaces, which was presumed to be due to the increased sucrose levels. The upper surface of the film (polymer-air interface) was always more tacky than the polymer-substrate interface. Whereas the lower film surface always appeared glossy (like the sucrose-free film), the upper surface, at low levels of sucrose addition, was matt and somewhat grainy in appearance. However, as the content of sucrose increased above 80% (g.*NE*)$^{-1}$, this surface-coarseness also increased to levels where there appeared small, individual, hemispherical 'prominences' that varied in size up to ca 1 mm in diameter.

For films containing $\rangle$ 100% sucrose load, concentric rings of slightly increased opacity were apparent, presumably where sucrose supersaturation occurred in a drying front (and in contrast to the multiple nucleation fronts observed with the sucrose-free films). As the sucrose loading increased, the mud-cracked appearance of the sucrose-free films diminished, to be replaced by the aforementioned blister-like 'protrusions.' At very high sucrose contents ($\rangle$ 150%), the blisters appeared to merge, and the upper film surface appeared shiny and smooth. Such films were, however, still tacky when touched, implying the surface was still composed mainly of polymer.

When sucrose-containing Eudragit® *NE* films were wetted for more than a few minutes, they become opaque (white) as a result of hydration and swelling. Such opacity was different to that caused by the sucrose, and was lost when the film dried. Films that were originally relatively opaque before wetting, dried with greater transparency. However, for those sucrose containing films soaked for only short periods (*e.g.*, $\langle$ 1 hr), small white patches developed on the surface over a period of a few days. These patches did not appear in films soaked for longer than 1 hr.

From observations of films stored for 4 → 5 days at ambient temperature, it was evident that surface protrusions formed on films in which there had previously been none.

In those films which *had* shown such protrusions, their number appeared to increase until they became continuous, forming a complete layer, comparable to that observed in those films containing 〉150% sucrose. Storing the films in the dry atmosphere of a desiccator (containing silica gel as the desiccant) suppressed this phenomena of emerging protrusions, indicating that humidity was necessary in the mechanism of their appearance. *I.e.*, an uptake of water by the film, not sufficiently great so as to result in visible swelling (opacity) of the film, provided the necessary routes for exit (exudation) of the film's additive.

10.2.2 Eudragit® *RL*.

Sucrose-loaded Eudragit® *RL* films looked as near perfect as did the sucrose-free films, at least until the sucrose load was 〉30%. As the loading was further increased, the films appeared to exhibit a slight haze, indicative of little sucrose being exuded to the film surface. The concentric rings observed in the Eudragit® *NE* films at the highest levels of sucrose addition were never apparent in the Eudragit® *RL* films. However, rings of this type were sometimes seen in the wetted film, with these rings appearing to swell and, hence, become slightly more opaque than the rest of the film. Sucrose-containing Eudragit® *RL* films turned opaque on wetting (unlike their sucrose-free counterparts which remained translucent). The wet film was very fragile, and gel-like, and required great care in handling.

The surface exudations, as observed on Eudragit® *NE* film, were never seen on Eudragit® *RL* films suggesting greater compatibility between sucrose and the more hydrophilic Eudragit® *RL* polymer.

10.2.3 Surfactant-free PBMA.

Surfactant-free PBMA became increasingly opaque when loaded with sucrose, in the manner of the Eudragit® *NE* films. PBMA films were very difficult to handle, when additive-free, because of their brittle nature, and this was exacerbated by sucrose addition such that they could not easily be studied.

10.2.4 Microscopic structure.

10.2.4.1 Eudragit® *NE*.

Plate 10.1 to **Plate 10.4** show Eudragit® *NE* films containing 30% sucrose and cast for 24 hrs at 313 K. Whilst **Plate 10.1** appears to show regions on the film's polymer-air interface which are possibly crystals of sucrose embedded into the polymer, **Plate 10.2** shows a different aspect of the same surface, in which such regions are not manifest. This possibly indicates that the aforementioned distribution of sucrose resulting from relief of supersaturation, visible at loads 〉100%, is also present at sucrose levels of 〈100%. Small exudations are evident (**Plate 10.2**) on the film surface: many of which appear to contain a small indentation or pore. Examples of these exudations are shown in greater detail in **Plate 10.3** and **Plate 10.4**. **Plate 10.4** shows the upper surface/freeze-fracture cross-section of the film, and the sizing bar shows the prominence to have a base diameter of ca 50 μm. This is well above the Eudragit® *NE* particle size (of ca 163 nm, by P.C.S.) implying that the prominence was not simply a latex particle expelled at the film surface. **Plate 10.3** shows the prominence to be somewhat spherical in shape, and hence not

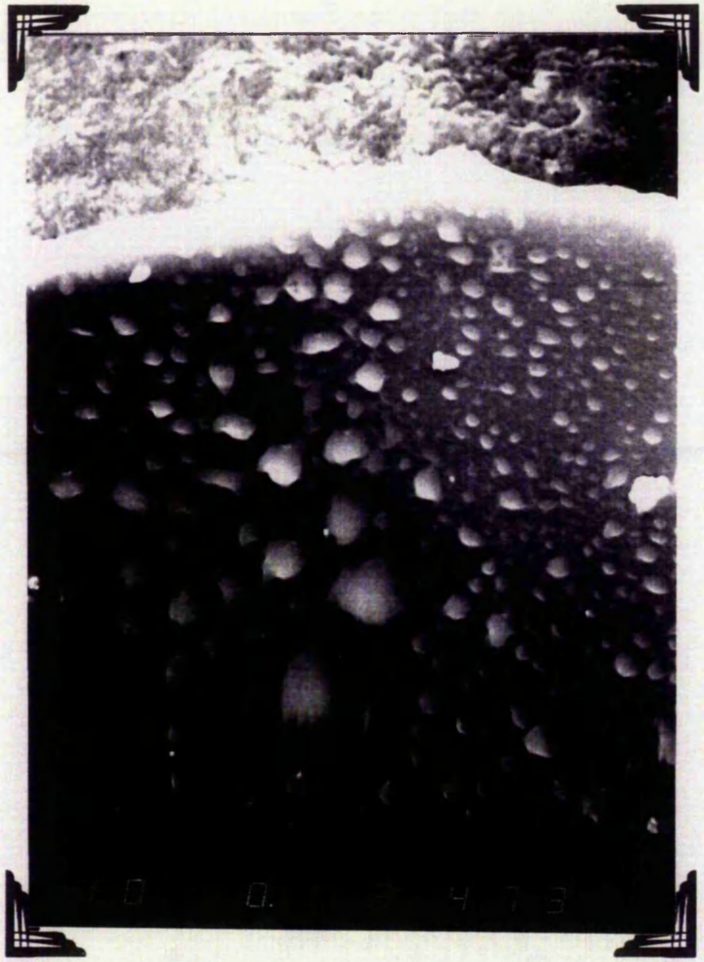

Plate 10.1 (4730) S.E.M. of the upper side (polymer-air interface) of a Eudragit® *NE* film containing 30% sucrose. (Magnification 0.1K.)

Plate 10.2 (4726) S.E.M. of the upper side (polymer-air interface) of a Eudragit® *NE* film containing 30% sucrose. (Magnification 20K.)

Plate 10.3 (4731) S.E.M. of the upper side (polymer-air interface) of a white prominence on the Eudragit® *NE* film surface. (Magnification 2K.)

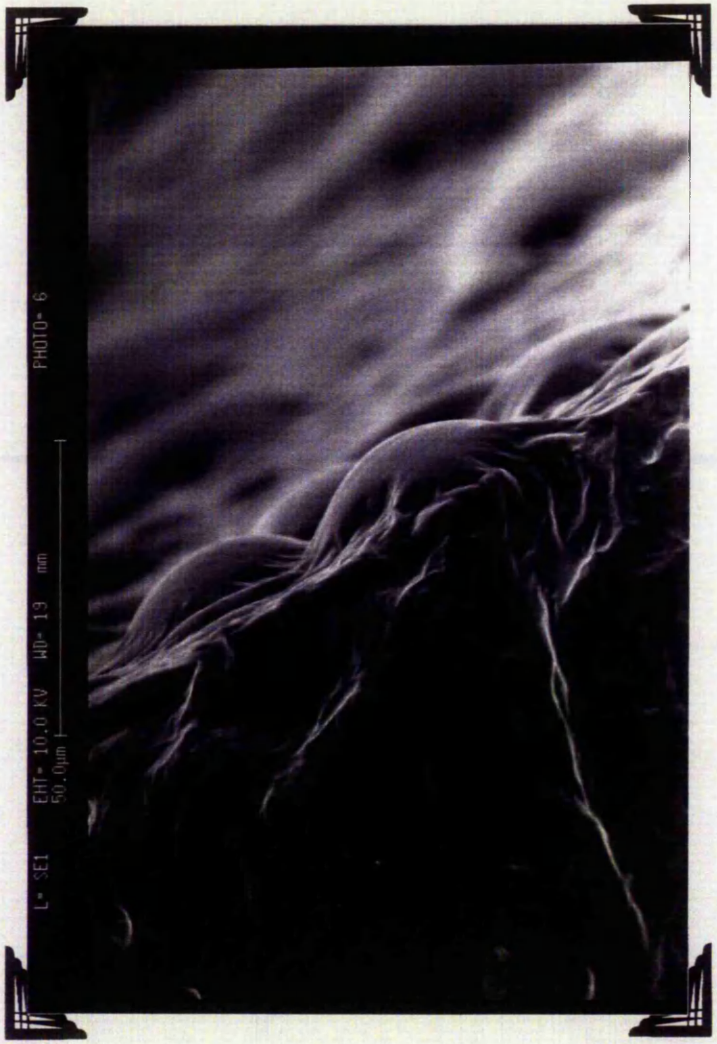

Plate 10.4 (6) S.E.M. of the upper side (polymer-air interface) of a white prominence on the Eudragit® *NE* film surface.

crystalline (as would sucrose embedded in the polymer). Such prominences did not appear on the sucrose-free Eudragit® *NE* film implying that they did not consist of endogenous surfactant. It was concluded that the prominences consisted of polymer which was being pushed upward from beneath by exudations of sucrose (which was incompatible with the polymer), although no artifact existed (as seen by fracture cross-section, **Plate 10.4**) directly beneath the exudation. The non-crystalline nature of the prominences on the sucrose containing films also implied that they consisted of polymer which was capping the sucrose[1] exudations. The 'pore' observed in the top of the exudation provides a possible means of escape for the sucrose when the film is immersed in water.

The lower film face (polymer-substrate side, during casting), albeit containing 28% sucrose as opposed to 30%) appeared featureless (never exhibiting exudations to the extent of the upper face) and slightly grainy, as did the sucrose-free films (see Chapter 8), Any features that might have been present were beyond the resolution of the S.E.M. This suggests that the face consisted predominantly of either polymer or sucrose.

The formation of a skin on the drying latex (as discussed in Chapter 8) suggested that the bulk of the water must evaporate through this skin in order for the film to dry. The possibility therefore exists that the escaping water leaves 'channels' which provide an easier means of passage through the polymer for the exuding sucrose. Such channels could exist in a number of forms, *e.g.*:

✗ pathways of reduced polymer density, resulting from the aforementioned 'pathways of evaporation,' *i.e.*, the last part of the polymer to be completely dried;

✗ pathways of hydrophilicity resulting from the sucrose. Since the sucrose has a greater affinity for the water than the polymer, then it can be envisaged that the channels of rising water form 'columns' of sucrose, concentrated as the escaping water dries (*i.e.*, in terms of a volcano analogy, like a solidified vent);

✗ pathways of reduced polymer density/hydrophilicity resulting from particle-particle interfaces. The interfacial particulate hydrophilicity resulting from the polymer chain endgroups on the particles' surfaces – endgroups which also lead to a reduction in polymer density due to their mutual repulsion.

The existence of channels of hydrophilicity or reduced polymer density would therefore represent both the easiest means of 'escape' for the sucrose when leaching in water, and/or the easiest path for sucrose exudation by the polymer. (Zhao[561] *et al.* and Urban and Evanson[489] demonstrated (using F.T.I.R. spectroscopy) that excess water soluble surfactant could be carried to the polymer-air interface by the flux of evaporating water.)

S.E.M.s were prepared of identical films that had been leached of sucrose (30%), in water for 24 hrs, and then dried, again for 24 hrs, at 313 K. These proved to be featureless. At low magnification, the crystal-like pattern (as seen before leaching in **Plate 10.1**) was

---

[1] Mono & disaccharides are described as crystalline: the spatial molecular structure of sucrose being accurately resolved by crystallographic methods (*i.e.*, neutron scattering[71]).

not present. Higher magnification, revealed that the surface features described for the sucrose-containing films were also absent. The leaching/drying process seemed to remove all of the sucrose (at least to levels below those resolvable by the S.E.M.), whilst the further drying period, at a temperature 48 K above the T_g of the sucrose-free polymer, appeared to allow the film to 'heal' any porosity resulting from the leaching process. (The results from experimentation on the film's solute permeability {see paragraphs 10.6.1.3 and 10.6.1.4} imply that any features resulting from additive leaching would be lost at any drying temperature above the T_g.)

10.2.4.2 PBMA.

Plate 10.5 to **Plate 10.18** show sucrose-containing PBMA films, cast for 72 hrs at 353 K. The S.E.M.s feature a sizing bar to give an indication of the magnification, and are coded as, for example: BM/15S/UN/1. This code gives:

POLYMER TYPE/ADDITIVE LOAD/UNLEACHED or LEACHED/POSITION

where, for example:

15S = 15% sucrose (or 40S = 40% sucrose);
UN = unleached (or 96L = leached for 96 hrs);
1 = upper (polymer-air) film surface. (The key to the numbered positions, in relation to film orientation, are explained in **Figure 10.1**. Numbers 1 and 2 are the upper and lower film faces with respect to casting orientation; 3 → 6 are regions {*e.g.*, upper, centre, lower and full} on the fracture cross-section.)

Plate 10.5 and **Plate 10.6** show the upper surface of a PBMA film containing 15% sucrose. **Plate 10.5** is the lower magnification shot showing an abundance of the white prominences, that were also seen on the S.E.M.s (*i.e.*, **Plate 10.1** to **Plate 10.4**) of sucrose-

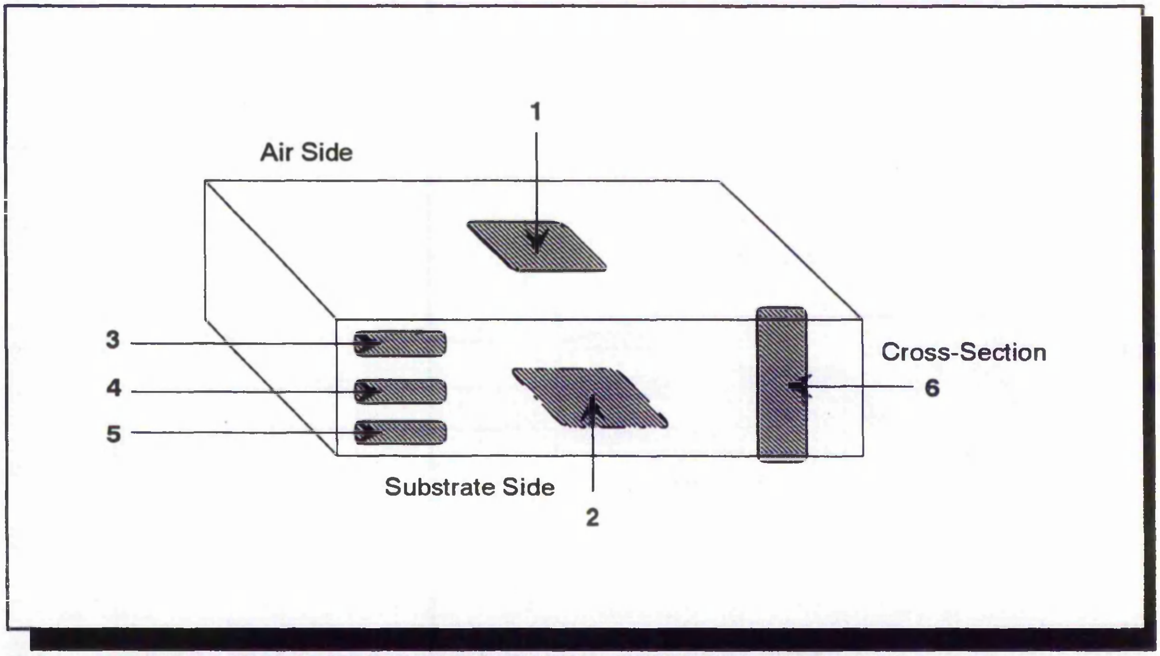

Figure 10.1 Key to S.E.M. position with respect to film orientation.

containing Eudragit® *NE* (albeit at a larger diameter). The higher magnification picture in **Plate 10.6** shows the close packed particles of the PBMA latex, surrounding a prominence. The prominence is approximately ten times smaller than that seen in Eudragit® *NE* (however, these PBMA films *did* contain less additive {15%, *cf.* 30%}). The disruption of the latex particles at this point would tend to suggest that the particles were being pushed aside by the exudation process. Since the PBMA was prepared surfactant-free, these exudations must be of sucrose. Unlike the exudations on the Eudragit® *NE*, those on the PBMA show no central 'pore,' and the exudations seem to sit above the film, rather than spreading over the film, as did those on the Eudragit® *NE* – possibly due to differences in sucrose-polymer compatibility.

The lower side of additive-free PBMA films (see Chapter 9) showed close packed latex particles, compressed from contact with the substrate. The S.E.M.s of the lower side of PBMA films containing 15% sucrose show (**Plate 10.7** and **Plate 10.8**) an accumulation of sucrose – again suggesting that the films dried from the latex-air interface downwards.

Plate 10.7 shows the substrate side of the film at relatively low magnification. Despite there being less sucrose in these films compared to the aforementioned Eudragit® *NE* (+ 28/30% sucrose-loaded) films, exudations of sucrose were present at this interface. High levels of exudation on both sides of the PBMA again suggest that the PBMA is less compatible with the sucrose than was the Eudragit® *NE*.

Plate 10.8 shows the substrate side of the film at high magnification. The close packing of the latex particles, that was observed in the additive-free film (Chapter 9) and on the upper side of this film (around the extrusions) was no longer present. Particles are seen embedded in a second phase (*i.e.*, a phase inversion from sucrose in polymer to polymer in sucrose). Such an accumulation of sucrose, at the base of the film, would occur if the film dried from top to bottom: the latex underneath the skin would contain sucrose at increasingly concentrated levels, due to the sucrose being dissolved in the water. Then, in a manner analogous to which a sucrose solution would leave a residue of sucrose on evaporation of the water, the 'residue' of sucrose in the latex system, dissolved preferentially in the aqueous phase, would be expected to be found mainly at the bottom of the film. As the film dried, the 'channels' via which the water evaporated would become saturated with sucrose (or saturated sucrose solution), limiting the transport of the sucrose to the polymer-air interface. This accumulation of sucrose at the bottom of the film would be aided by the fact that PBMA is a hard polymer, and therefore more likely to force incompatible 'clusters' of sucrose away from the drying regions of film, whereas a softer polymer would be more likely to deform around such clusters.

Like the additive-free PBMA films discussed in Chapter 9, the fracture cross-sections of the PBMA films containing 15% sucrose (cast at 353 K for 72 hrs) show no evidence of the latices particulate nature (**Plate 10.9** and **Plate 10.10** show the face of the cross-section near to the upper and lower surfaces of the film, respectively) – suggesting a high degree of coalescence and particle deformation within the film's interior. There appear to be either exudations of sucrose onto the face of the cross-section, and/or regions of sucrose embedded within the film, and surprisingly (considering the evidence of the S.E.M.s of the upper and lower films faces) they appear to occur in greater number nearer the top surface of the film (coded BM/15S/UN/3).

To the naked eye, films containing 40% sucrose (unleached) appeared uniformly opaque. The S.E.M., however, revealed regions of film which apparently showed a lesser degree of exudation. (*cf.* the upper left and lower right-hand regions of **Plate 10.11**). The region containing exudation is also shown in **Plate 10.12**. In addition to the blister-like exudations, it can be seen that there were regions on the film in which the close packing of the particles becomes disrupted at these higher levels of sucrose addition. **Plate 10.13** shows, in greater detail, the disruption to the latex particle packing density of a region of film surrounding an exudation. Tendrils appear to be drawn from the surrounding particles to the exudation – possibly due to coalescence between these particles and a polymer 'skin' which is being forced upward by the exuding sucrose. If the region surrounding the exudation is less dense to the extent that it is somewhat porous, it may provide a means by which sucrose is leached from the film in an aqueous environment.

A higher magnification view of a region of the film which appears to show fewer exudations is shown in **Plate 10.14.** It is seen that far from there being no sucrose in this region, the latex particles, although close packed, appear to be embedded in sucrose. This would thus seem to imply that at the higher levels of sucrose loading, the sucrose is less uniformly distributed across the surface of the film – possibly as a result of the relief of sucrose supersaturation in the latex drying front.

The substrate side of the film (micrographs not included) showed no obvious sign of the latex particles since the sucrose formed a smooth layer which concealed the particles.

The upper and lower surfaces of the PBMA films leached of 40% sucrose are shown in **Plate 10.15** and **Plate 10.16**, respectively. The upper face of the film appears similar to that of a film leached of 15% sucrose (not included). However, at higher magnification the particles are less distinct, possibly as a result of not all the sucrose being removed, or to a greater degree of particle deformation (due to the presence of non-deformable sucrose between the particles). The lower face of the film (**Plate 10.16**) shows large discontinuities (crevices) which presumably correspond to regions of leached sucrose and possibly lost particles (if particles were embedded in the sucrose).

Plate 10.17 shows the mid-region of the fracture cross-section of an unleached PBMA film loaded with 40% sucrose. Only sucrose is visible, with a few extraneous features that may be due to protruding latex particles. S.E.M.s (not included) showed that such regions existed throughout the full thickness of the film. The films, which typically weighed less than 1 g, of which only 0.4 g would be sucrose, were leached in 250 g of water. It would thus be surprising if the leaching of the sucrose was inhibited to any great extent due to the concentration of sucrose in the water. (The solubility of sucrose {using extrapolated data from reference [273]} in water is approximately 225 g (100 g.water)$^{-1}$, at 303 K.) **Plate 10.18** shows the full-thickness cross-section of the film after leaching for 96 hrs. There appears to be a mixture of porosity and coalesced polymer (or possibly

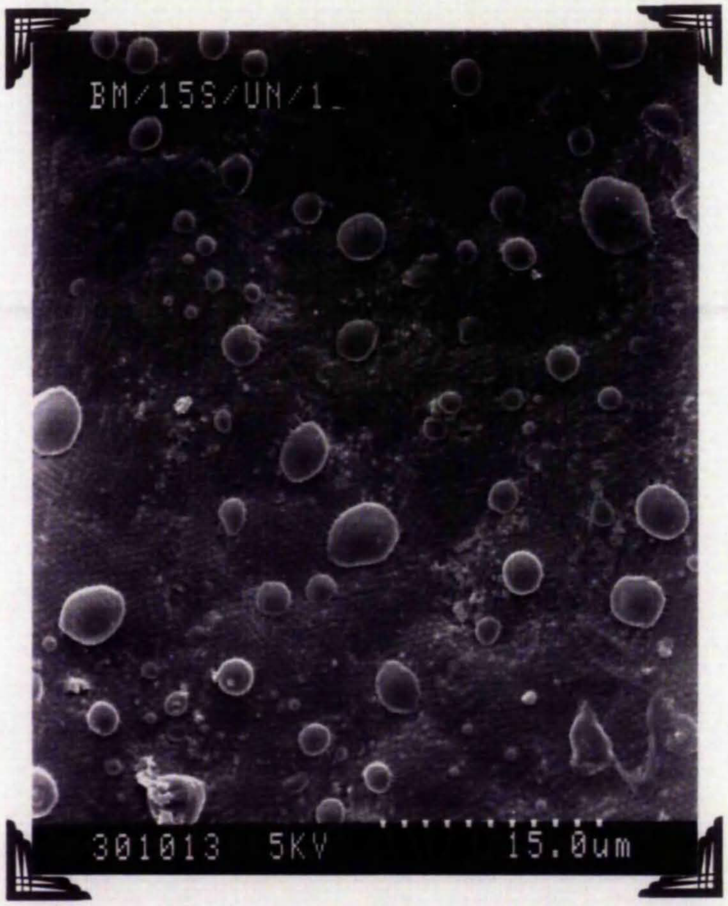

Plate 10.5 (301013) S.E.M. of the upper side (polymer-air interface) of the white prominences on the unleached PBMA (+ 15% sucrose) film surface.

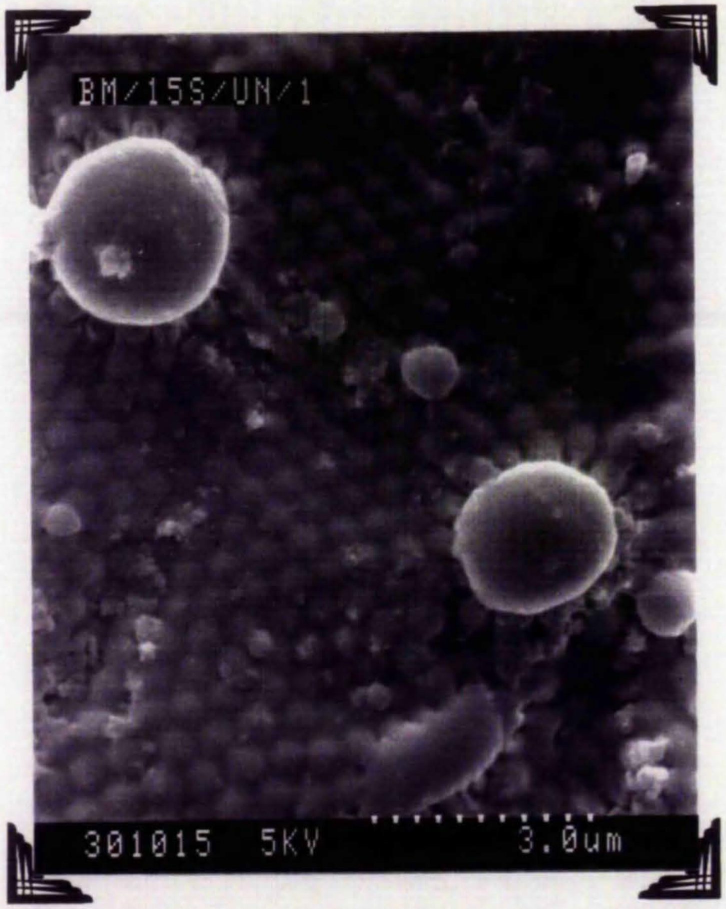

Plate 10.6 (301015) S.E.M. of the upper side (polymer-air interface) of the white prominence on the unleached PBMA (+ 15% sucrose) film surface.

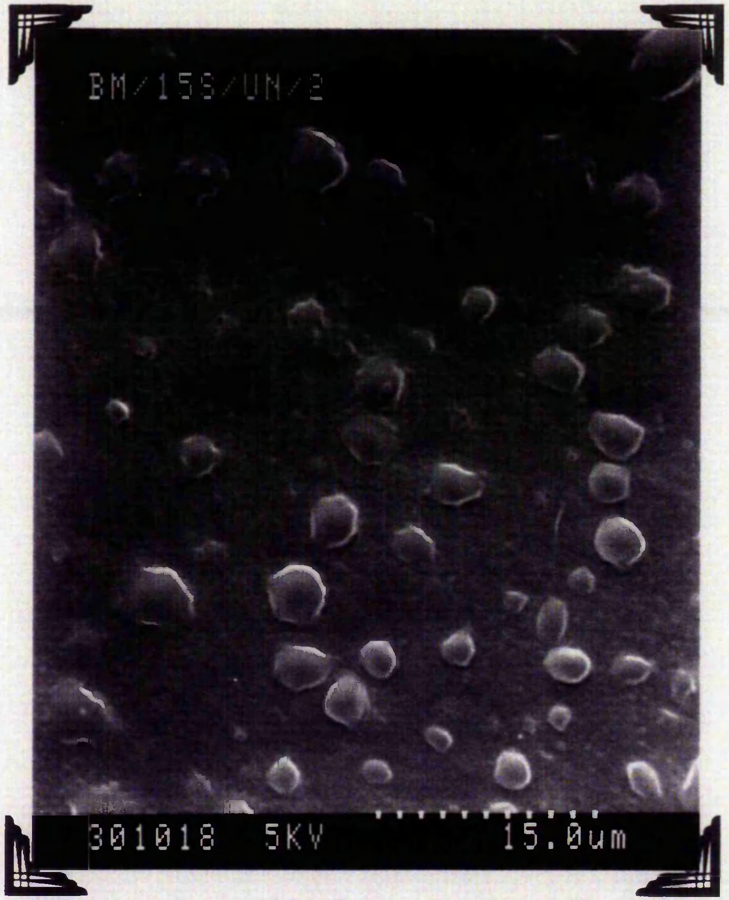

Plate 10.7 (301018) S.E.M. of the lower side (polymer-substrate interface) of the white prominences on the unleached PBMA (+ 15% sucrose) film surface.

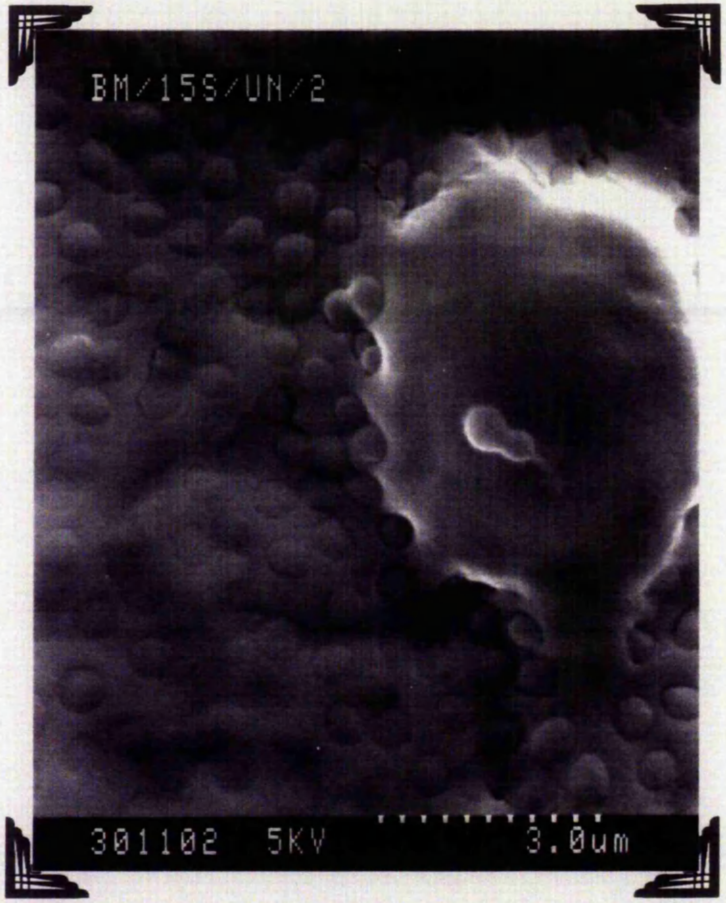

Plate 10.8 (301102) S.E.M. of the lower side (polymer-substrate interface) of the white prominences on the unleached PBMA (+ 15% sucrose) film surface.

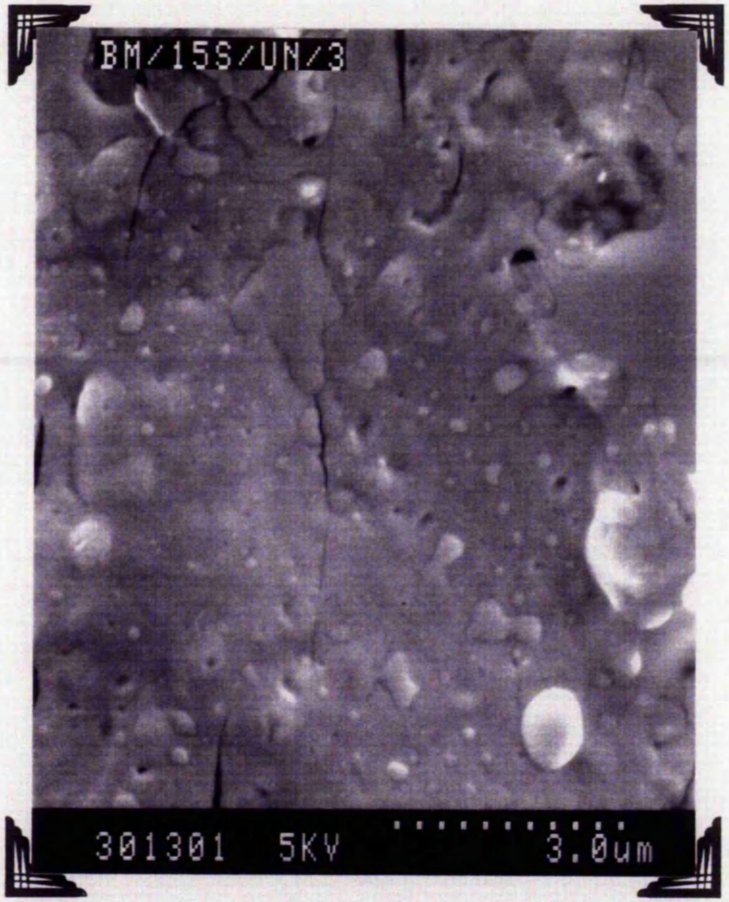

Plate 10.9 (301301) S.E.M. of the near-top fracture cross-section of a PBMA film containing 15% sucrose.

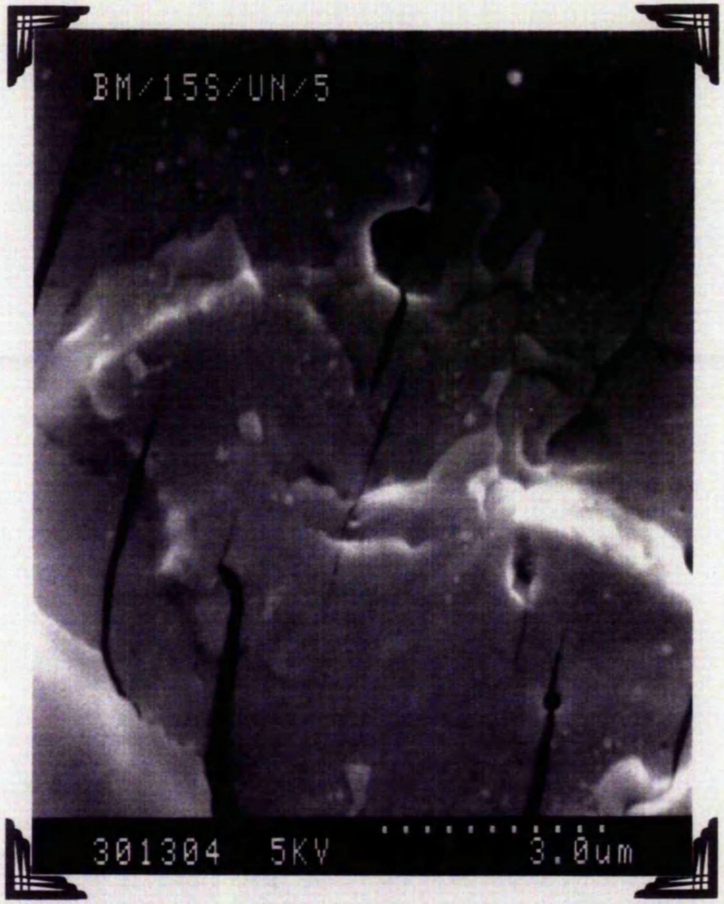

Plate 10.10 (301304) S.E.M. of the near-bottom fracture cross-section of a PBMA film containing 15% sucrose. (It was commented on by the electron microscopist that the cracks in some S.E.M.s were a "preparation artifact" of the conductive coating.)

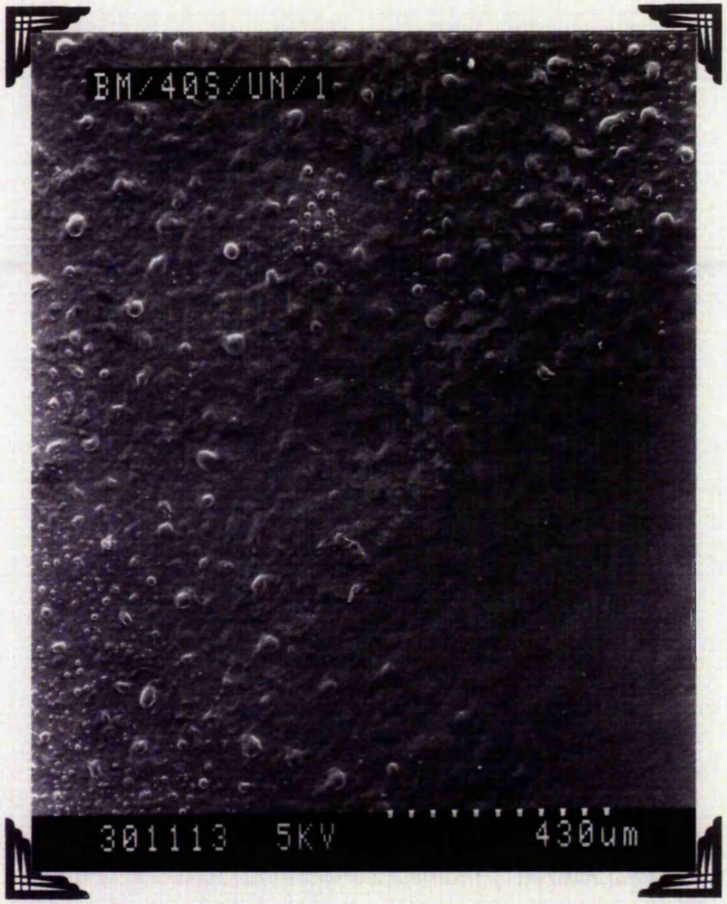

Plate 10.11 (301113) S.E.M. of the upper face of a PBMA film containing 40% sucrose.

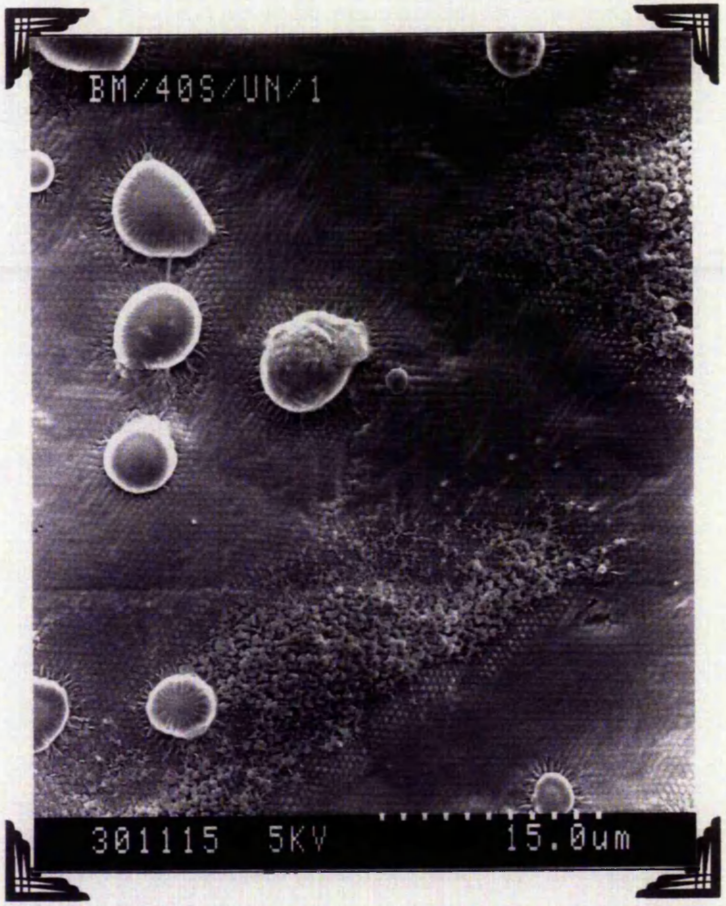

Plate 10.12 (301115) S.E.M. of the upper face of a PBMA film containing 40% sucrose.

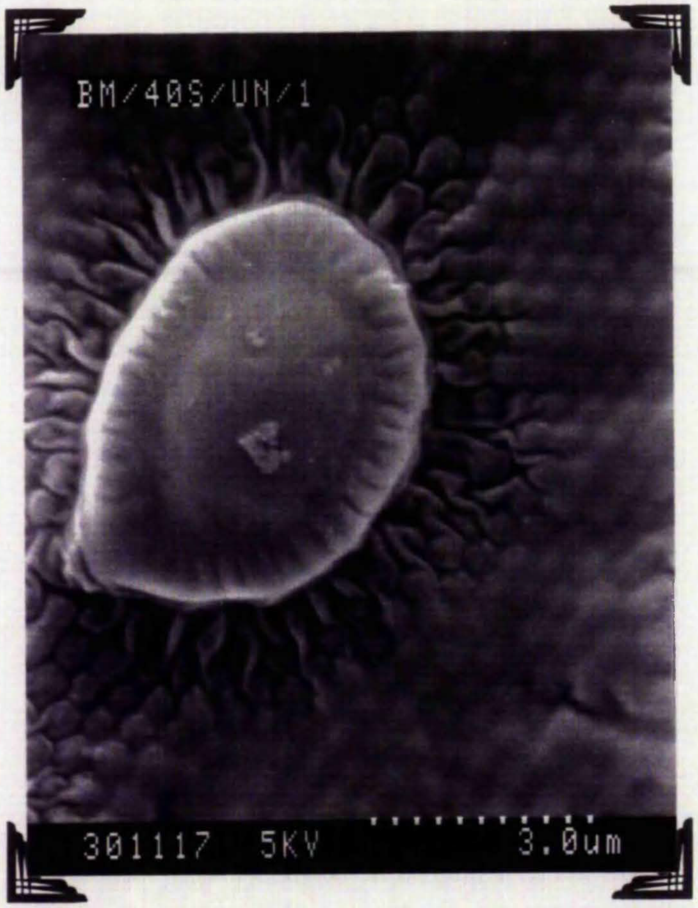

Plate 10.13 (301117) Region of exudation in a PBMA film containing 40% sucrose.

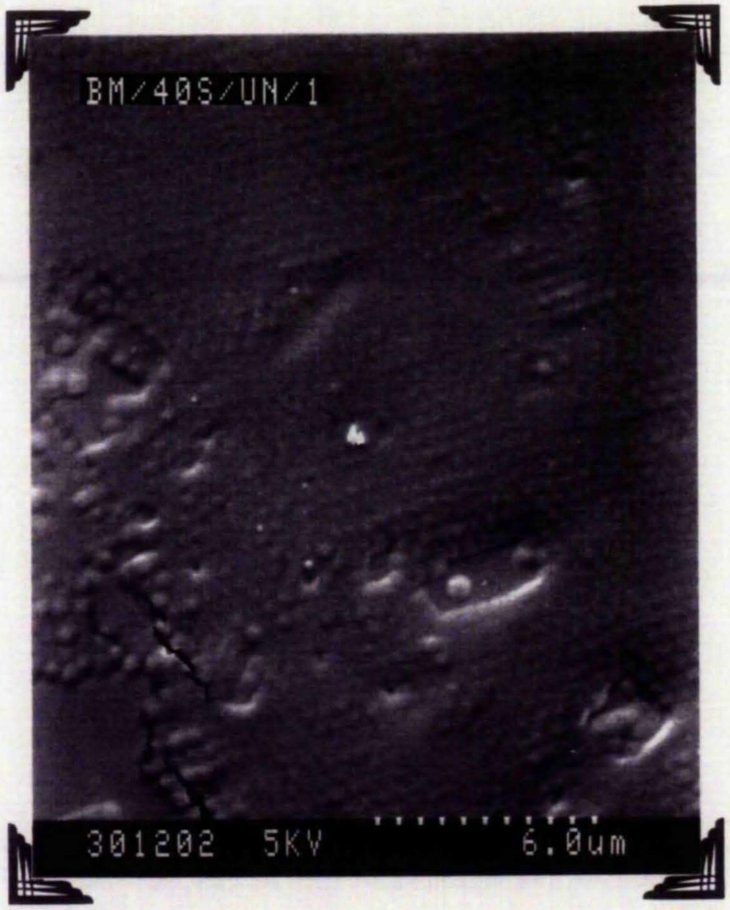

Plate 10.14 (301202) Region of no exudations in a PBMA film containing 40% sucrose.

Plate 10.15 (301210) S.E.M. of the upper face of a PBMA film leached of 40% sucrose.

Plate 10.16 (301215) S.E.M. of the lower face of a PBMA film leached of 40% sucrose.

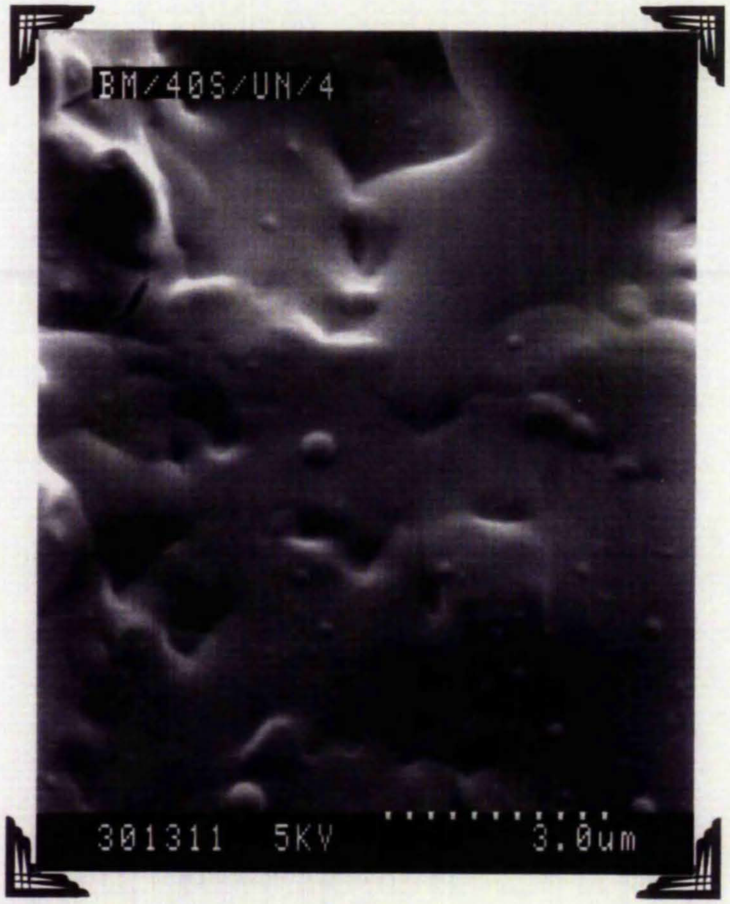

Plate 10.17 (301311) S.E.M. of the fracture cross-section of the unleached PBMA film + 40% sucrose.

Plate 10.18 (301313) S.E.M. of the fracture cross-section of the PBMA film leached of 40% sucrose.

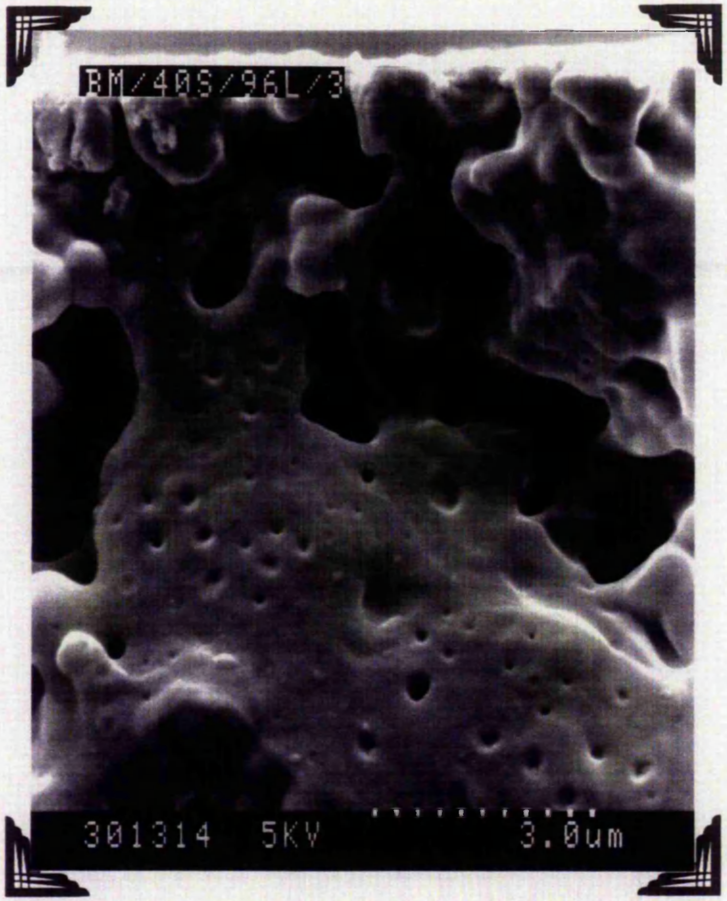

Plate 10.19 (301314) S.E.M. of the top-region of the fracture cross-section of the PBMA film leached of 40% sucrose.

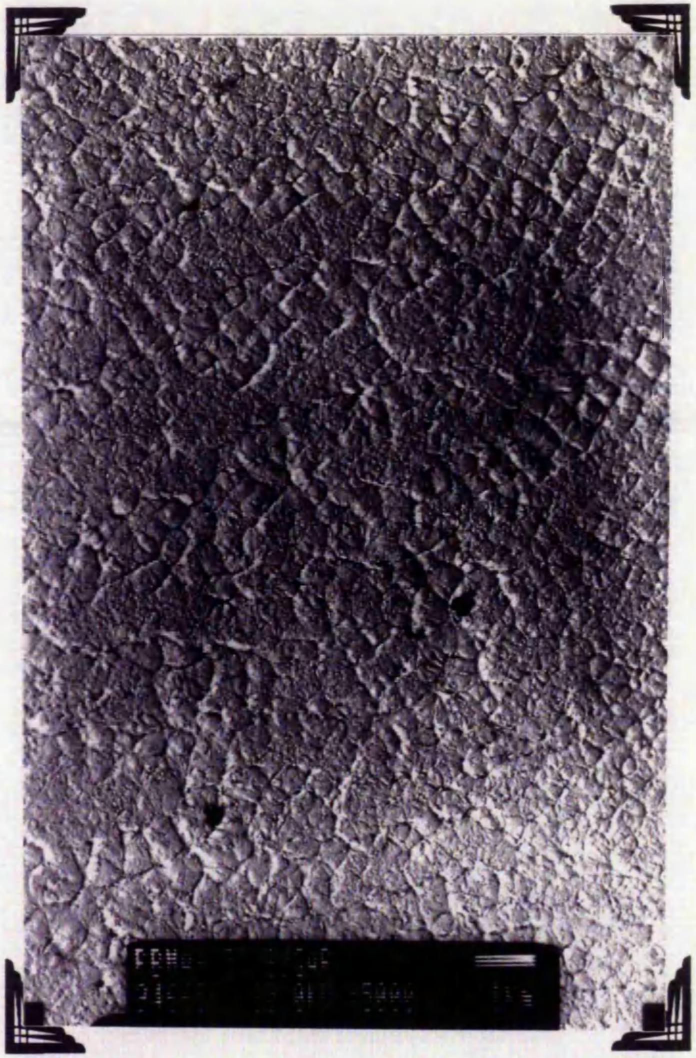

Plate 10.20 (946657) Freeze-fracture cross-section T.E.M. of a PBMA film leached of 5% sucrose.

Plate 10.21 (946658) Freeze-fracture cross-section T.E.M. of a PBMA film leached of 5% sucrose.

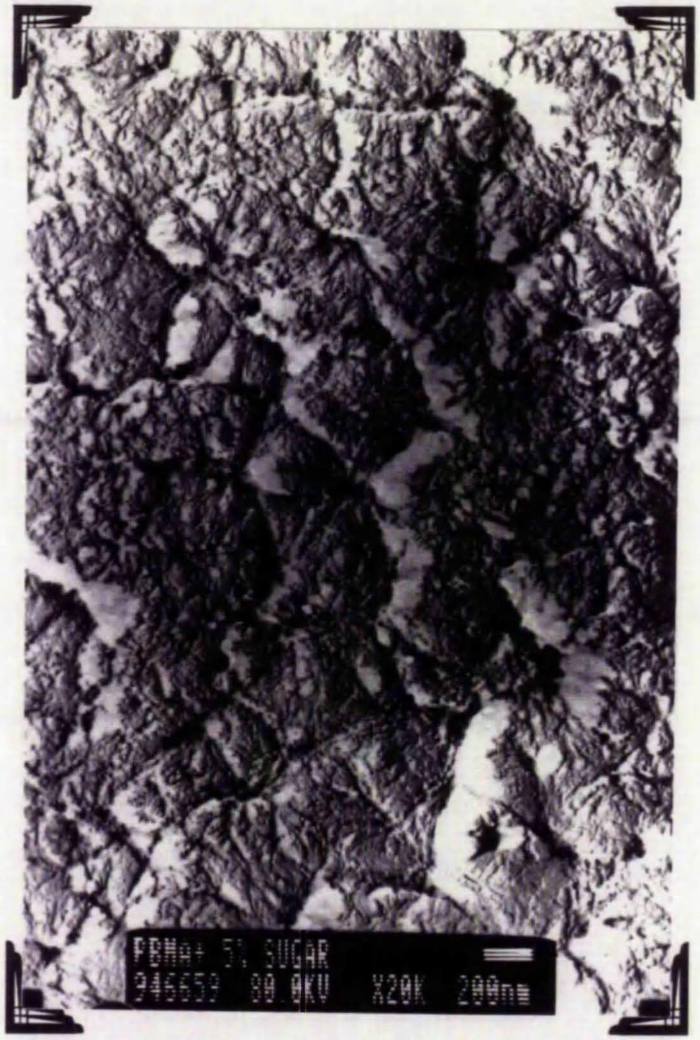

Plate 10.22 (946659) Freeze-fracture cross-section T.E.M. of a PBMA film leached of 5% sucrose.

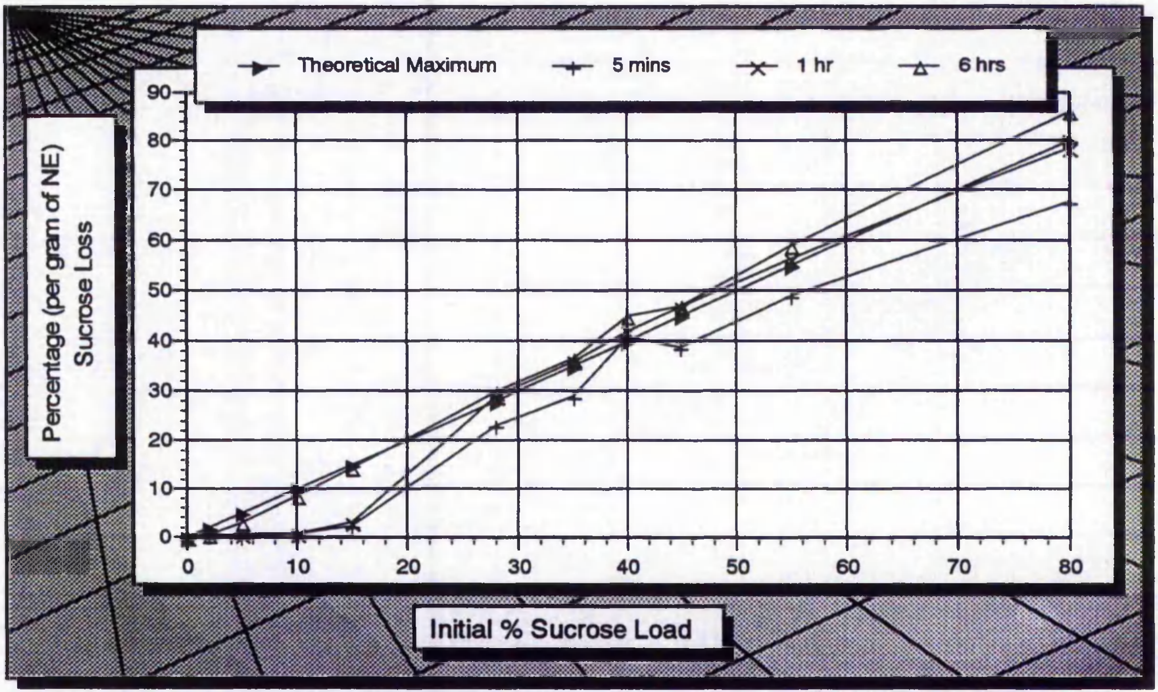

Figure 10.2 Plot of the percentage loading of sucrose (per gram of Eudragit® *NE* film) versus the percentage of sucrose leached (per gram of Eudragit® *NE*) for various leaching times.

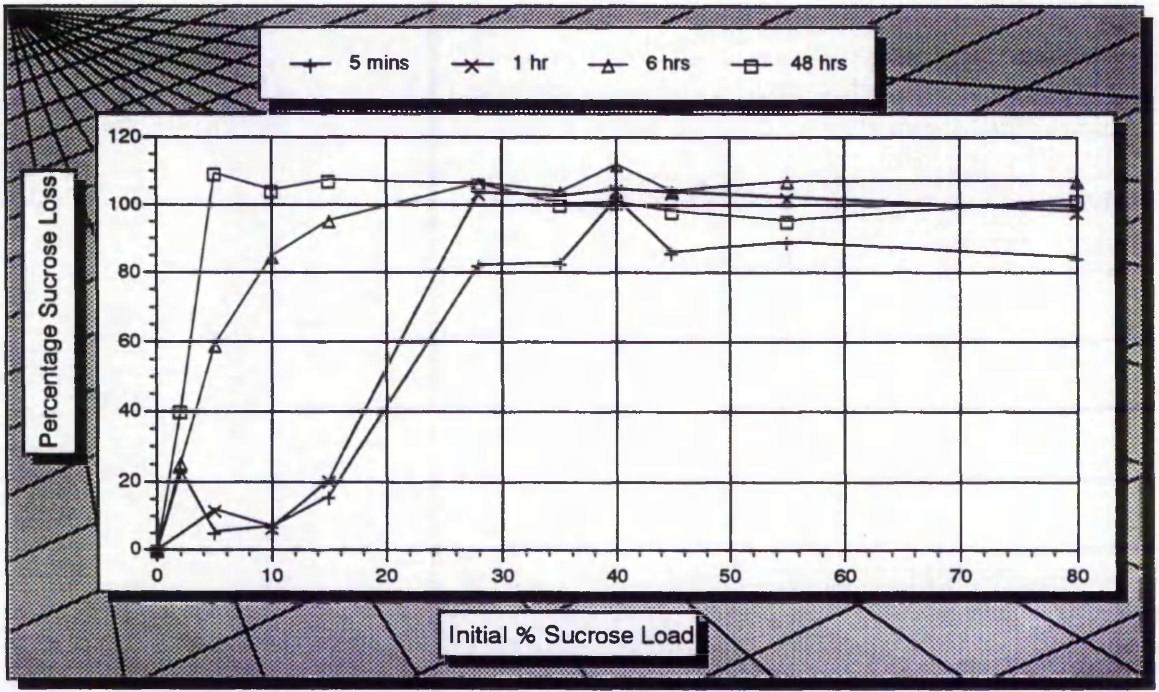

Figure 10.3 Percentage of initial amount of sucrose lost from a Eudragit® *NE* film, after leaching for various times, as a function of initial sucrose content.

residual sucrose). **Plate 10.19** shows the top region of the fracture cross-section shown in **Plate 10.18.** It is apparent that no definite particulate structure exists in this region of the film. However, the degree of porosity surrounding this coalesced region suggests that if the region did consist of sucrose, then it would have been readily leached (after 96 hrs leaching). Other S.E.M.s (not presented) throughout the film's fracture cross-section revealed a similar structure. It is concluded that the smooth-looking regions of film seen in **Plate 10.18** consist of coalesced PBMA rather than sucrose (*cf.* results of leaching sucrose from Eudragit® *NE* {paragraph 10.3.1} in which the sucrose is found to be readily leached in a period of ⟨96 hrs, as used here).

In contrast to the high level of porosity in the 40% loaded films, films loaded with 5% sucrose (**Plate 10.20** → **Plate 10.22**) showed no porosity – even with the enhanced definition of the tensile snap freeze-fracture T.E.M. method of microscopy. At this (5%) load, the PBMA particle boundaries are visible in the fracture cross-section, but are highly deformed. This deformation is greater than that of the 40% level of sucrose addition, whilst the particle boundaries are possibly more visible than in the case of the additive-free film (shown in Chapter 9) cast for 3 hrs. Particle boundaries are conceivably more visible in the sucrose-containing film because the boundaries are where the sucrose is most likely to be found; deformation may occur less at higher sucrose loads because the sucrose is less deformable than the polymer and therefore inhibits particle deformation/coalescence.

10.3 Leaching of sucrose from Eudragit® latex films.

The loss of sucrose from films was measured gravimetrically as a function of the time the film was soaked in water (periods from 5 min → 48 hrs). Films were dried to constant weight before the weight of the leached film was recorded.

10.3.1 Leaching of sucrose from Eudragit® *NE* film.

The rate of loss of sucrose from Eudragit® *NE* films is plotted in **Figure 10.2** and **Figure 10.3**. The loss of sucrose appears, in some instances, to be greater than the load originally added to the films. This is despite the loss of endogenous surfactant[204] being accounted for in the calculation of sucrose loss. (Note that when specific values of weight loss from the sucrose-free film were not measured {after leaching for a certain time}, an average value of 0.35% per gram of Eudragit® *NE* was used.) The experimental values of sucrose loss exceed the theoretical maximum of 100% by up to ca 13%. This may be in part due to experimental uncertainty. However, it was apparent in some S.E.M.s of sucrose-containing films that polymer particles appeared to be dispersed in the sucrose, and uncoalesced. (This was evident in the pictures of the PBMA film, *e.g.*, the underside as seen in **Plate 10.16.**) It would be expected that such latex particles which were dispersed in sucrose, and detached from the bulk of the film, would therefore be lost as the sucrose dissolved and, hence, yield the higher than expected weight loss.

The sucrose leaching data show that above ca 15% addition, there is a sudden increase in the amount of sucrose which can be removed from the film at short leaching times (*i.e.*, ⟨6 hrs). If it is assumed that this increase occurs at a sucrose load hereafter called C_{suc}, then the following points summarise the conclusions drawn from the graphs:

✗ Below C_{suc} and at short leaching times (<6 hrs): sucrose is not easily leached – presumably as a result of the percolating water having insufficient time to penetrate the polymer and reach the dispersed sucrose. This difficulty in leaching sucrose shows that it does not simply reside on the surface of the film.

✗ Below C_{suc} and at long leaching times (>6 hrs): the water penetrates the film to a greater extent and the sucrose is leached more easily.

✗ Below C_{suc}, the dispersed nature of the sucrose yields no significant porosity, but progressive percolation of water, and leaching of sucrose, may yield sufficient void volume to allow increased amounts of sucrose to be leached over the longer periods of leaching – possibly by allowing the water to plasticise the polymer.

✗ Above C_{suc}, there is a marked increase in the amount of sucrose leached from the film at short leaching times. This result is probably a combination of (i) higher levels of sucrose residing at the film's surfaces, from whence it is most easily removed, and (ii) the greater porosity resulting from increased amounts of sucrose progressively leached on the front of the percolating water as it moves towards the film's interior.

The difficulty in removing sucrose which is contained by the polymer matrix (*i.e.*, at low levels of addition, and short leaching times), is an indication of the low diffusivity of sucrose within the polymer (see paragraph 10.4.1). Evidence from monitoring film drying (and S.E.M.s which showed sucrose concentrated at the base of a film) have shown that film formation starts with a skin (of polymer) on the surface of the wet latex – trapping the wet latex, which contains the sucrose, beneath. In order for the film to continue to dry, the bulk water must diffuse through the skin before evaporating. The least dense polymer in the skin will exist between adjacent latex particles, in the regions of coalescence, and it is therefore between particles that the water (containing sucrose) would predominantly diffuse. It is also probable that water (sucrose solution) would become trapped in the voids between close packed latex particles when the particles first came into contact. Assuming that the sucrose would remain preferentially in the aqueous phase of the latex, the evaporation of water from the drying film will therefore tend to concentrate (deposit) sucrose in three places, *i.e.*, (i) in the last region of bulk water (wet latex) at the base of the film (as seen in the micrographs), (ii) in the interstices that existed before deformation of the latex spheres, and (iii) in the channels through which the water, trapped below the skin of the drying film, exited the film. Additionally, sucrose exudation from the dried film would tend to cluster the sucrose, and concentrate it at the film-air interface. This dispersion of sucrose within the film is significant with regard to leaching. In rank order of ease of sucrose leaching from a film immersed in water, sucrose would be most easily lost from a film-water interface, followed by sucrose close to the film surface, followed by sucrose in the bulk of the film.

The actual leaching results therefore show that at low levels of sucrose addition, then the sucrose must be well dispersed in the film. Sucrose in the bulk would only leach if an aqueous channel existed through to the surface of the film, and such hydrophilic channels would exist as a result of point 'iii' in the above paragraph, and also due to sucrose exudation. At higher levels of addition, greater amounts of sucrose are found on the film surface due to both increased levels of exudation and also concentration of the sucrose at the base of the drying film from where it is more easily leached. Additionally, higher concentrations of sucrose within the film lead to aqueous channels which may be larger and/or more frequent such that sucrose within the bulk of the film is also more easily leached.

The leaching of sucrose from Eudragit® *NE* film may be compared with drug release studies using matrix (monolithic) devices. The leaching of the drug propanolol-HCl from such matrix devices cast from aqueous Eudragit® *NE* latex (with the drug dissolved in the aqueous phase) has been shown by Bodmeier and Paeratakul [57] to only give partial release: the release profile showing a plateau before the maximum theoretical value. The release of propanolol-HCl was interpreted using the classification designated by Baker [26], dependent on the volume fraction of drug in the matrix: 0 → 5% V/V = simple monolithic dispersion; 5 → 10% V/V = complex monolithic dispersion; and 15 → 20% V/V = monolithic matrix. Plotting the percentage of drug remaining in the device as a function of load showed that at low loadings, ca 80% of the drug was trapped. This was followed by a plateau at ca 40% drug remaining trapped in the film, at between 50 → 100 mg $(\text{g.polymer})^{-1}$, and another plateau ($\approx$ 20%) at drug loadings $>$ 150 mg $(\text{g.polymer})^{-1}$. These plateaus were said to correspond to the differing classification of matrix device. At low initial drug loadings (where the drug was dissolved in the polymer), release was said to be slow and to be a result of diffusion through the polymer; at intermediate levels of drug load (*i.e.*, the first plateau), when the drug was both dissolved in the polymer and dispersed, release was as a result of diffusion both through the polymer and through liquid filled cavities; whilst at higher loadings, release was via diffusion through water filled pores. The Eudragit® *NE* film was found to be impermeable to the drug, over the time period of the experiment (in contrast to the porous film), and this was said to imply that the additive-free film showed very slow drug partitioning and diffusion, suggesting that the drug was embedded deeply within the matrix at low loading levels as shown by the fact that a large proportion remained trapped within the matrix.

It is presumably an equivalent feature to Bodmeier's plateaus that are found in the results of this study for the amount of sucrose leached as a function of sucrose load: below C_{suc}, sucrose leaching is mainly diffusion controlled, whilst above the level of C_{suc}, increasing film porosity assists the leaching process.

10.3.2 Leaching of sucrose from Eudragit® *RL* film.

The results for the leaching of sucrose from Eudragit® *RL* are given in **Table 10.1**. Eudragit® *RL* was apparently less likely to lose polymer from the film during sucrose leaching (*i.e.*, there are no losses of greater than 100%). After leaching into a sink solution of water for 24 hrs, a mean loss of sucrose of 95.9(±0.8)% of the initial load occurred (after having accounted for the loss of film plasticiser from the Eudragit® *RL* fraction of the film weight) independent of the initial sucrose content. Allowing a further 72 hrs leaching, resulted in no significant further loss of sucrose from the films. Eudragit® *RL* was apparently far more compatible with the sucrose: showing far less exudation/surface sucrose than did Eudragit® *NE*, and none of the films leached the full theoretical amount

Table 10.1 Sucrose loss from Eudragit® *RL* films as a function of leaching time.

SOAK TIME 24 hrs					
% LOAD†	20	40	60	80	100
CORRECTED‡ % LOST	97.12	94.89	95.73	95.94	95.99
SOAK TIME 96 hrs					
% LOAD	20	40	60	80	100
CORRECTED‡ % LOST	94.37	95.91	96.04	97.44	98.79

† Initial percentage load per gram of (triacetin-free) Eudragit® *RL* dried film weight.
‡ Percentage loss of amount of sucrose added to film, corrected for the loss of 104% of the initial load of 15% triacetin (as found for the sucrose-free film) from the Eudragit® *RL* fraction of the film.

---

of sucrose – despite the leaching of triacetin plasticiser which was shown in Chapter 8 to yield aqueous pathways through which the sucrose may also have been leached.

10.4 Permeation of labelled sucrose.

The permeation of sucrose (0.133 g dm^{-3}) through latex films was measured using C-14 labelled sucrose.

10.4.1 Sucrose permeation through sucrose-free and sucrose-loaded Eudragit® *NE* films.

The permeation of sucrose through sucrose-free Eudragit® *NE* films is shown in **Figure 10.4**. This plots the number of disintegrations per minute of carbon-14 in both the donor and receiver sides of the cell (the film was oriented with the polymer-substrate side facing the donor solution), and also the total number of disintegrations. It is immediately apparent that a negligible amount of sucrose permeated the film, over the time span of the experiment (*i.e.*, $\ll$ 1% of the initial activity of ca 47000 d.p.m.). However, the amount of sucrose on the donor side of the cell, and the total amount of sucrose (*i.e.*, number of counts), is seen to decrease (to a much greater extent than the increase on the receiver side). This decrease in the amount of sucrose available for analysis was not due to leakage from the permeation cell, or due to adsorption onto the glass of the cell itself (the latter determined in a separate control experiment without a film present). Similarly, it cannot be attributed to the half-life of carbon-14, which at 5730 years [146] would lead to negligible decay over the experimental period of less than 100 hrs. The significance of this decrease in available sucrose is the implied sorption into the Eudragit® *NE* film, possibly due to swelling of the film with water containing the sucrose, and is ca 3.9% (in a time of 50 hrs) of the initial concentration (0.133 g dm^{-3}).

The permeation of sucrose through sucrose-loaded (40%) Eudragit® *NE* films is shown in **Figure 10.5**. As with the aforementioned sucrose-free film, the permeation of labelled sucrose is seen to be negligible. After 50 hrs, just 0.74% (too little to be visible on the graph) of the available sucrose had permeated the film (*cf.* ≈ 0.25% in the case of the sucrose-additive-free film).

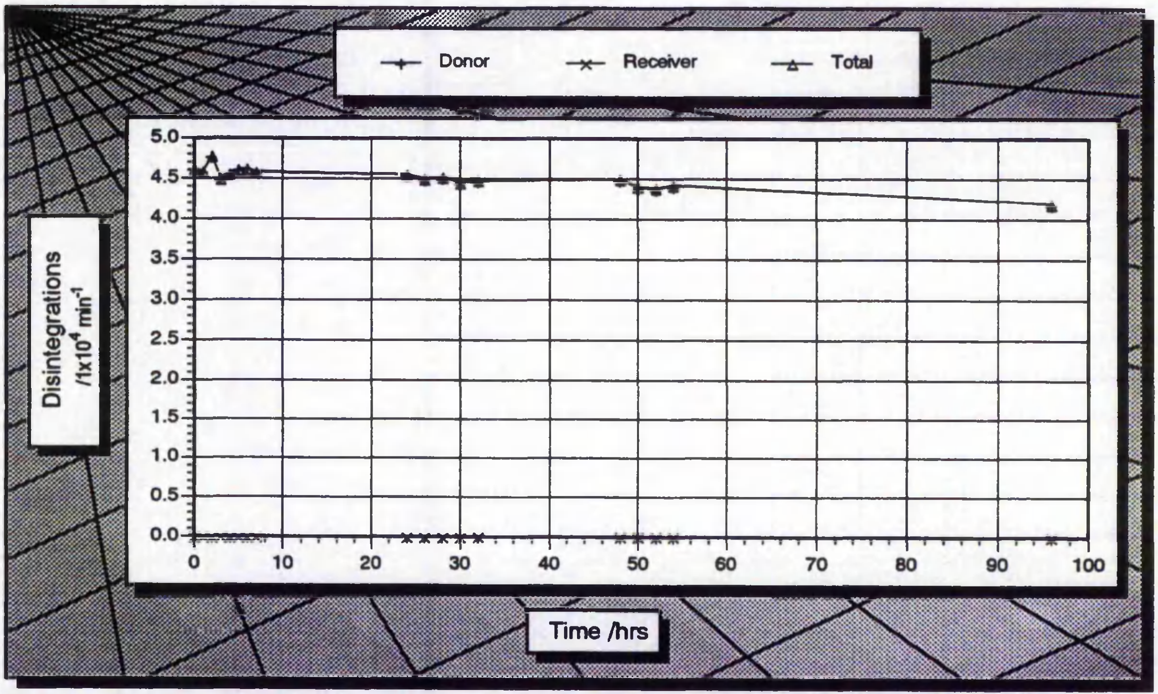

Figure 10.4 The permeation of carbon-14 labelled sucrose through additive-free Eudragit® *NE* film.

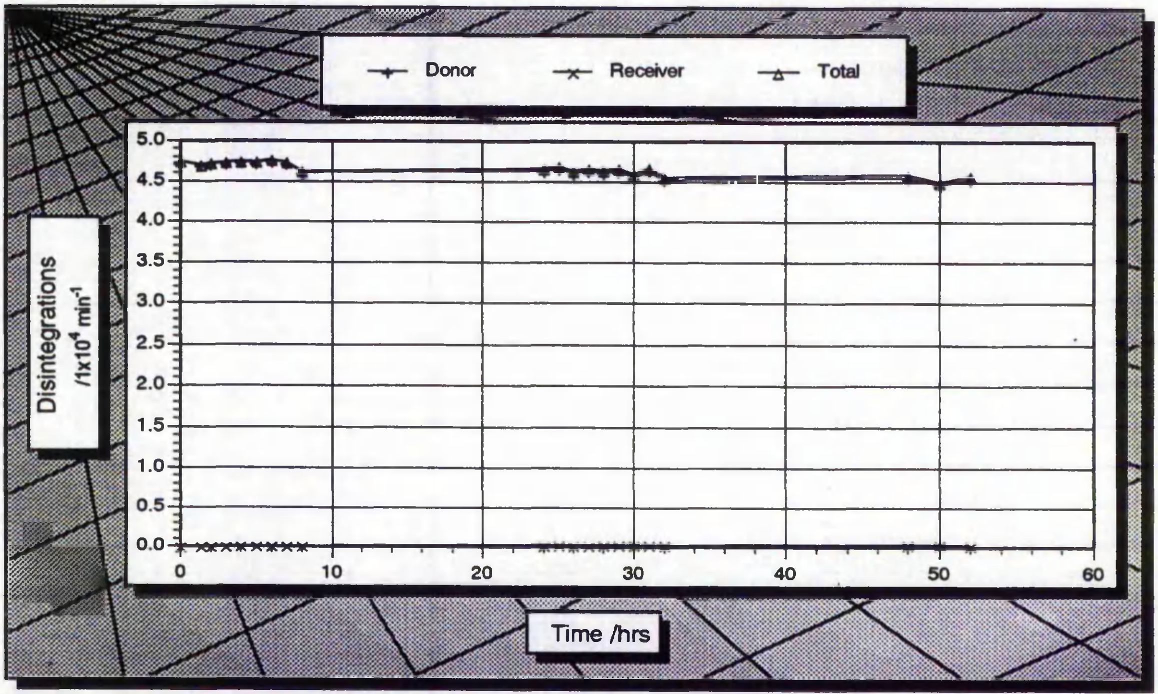

Figure 10.5 The permeation of carbon-14 labelled sucrose through Eudragit® *NE* film loaded with 40% sucrose.

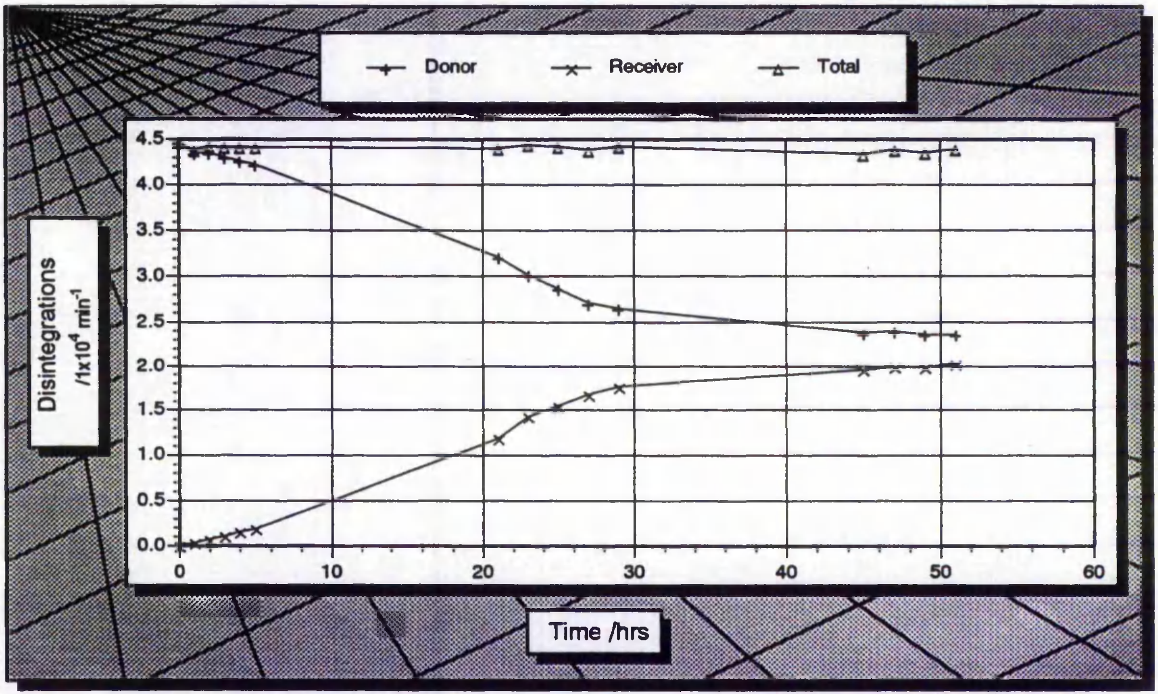

Figure 10.6 The permeation of carbon-14 labelled sucrose through Eudragit® *RL* film.

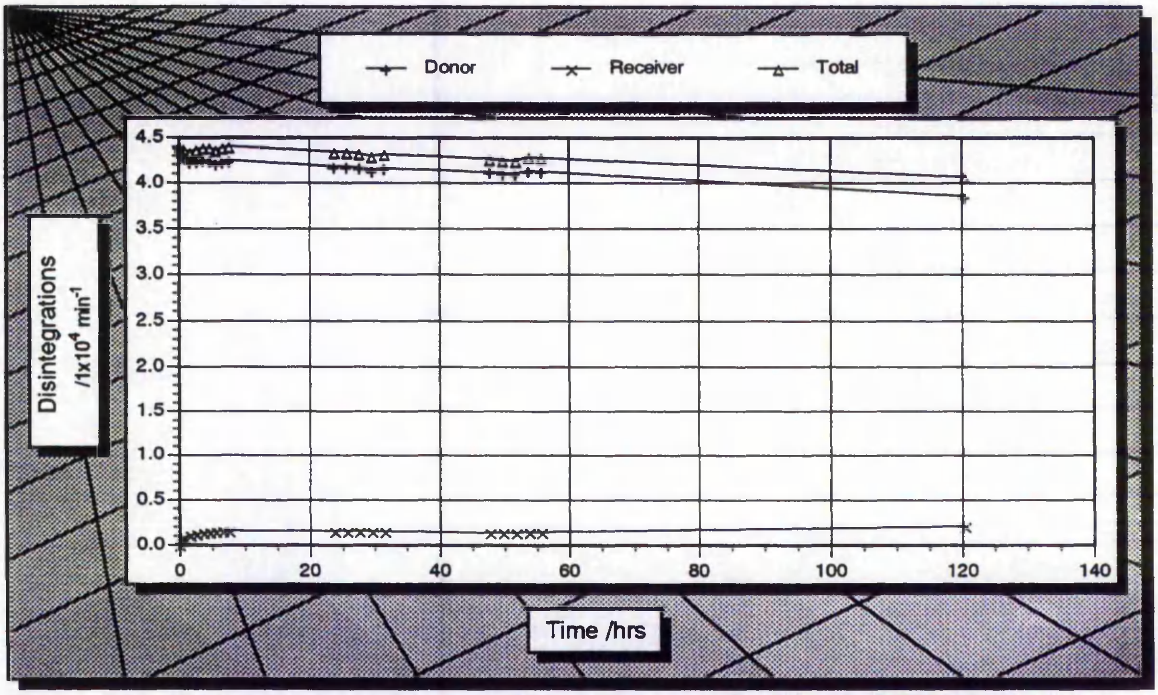

Figure 10.7 The permeation of carbon-14 labelled sucrose through PBMA film.

It was shown previously that a Eudragit® *NE* film with a 40% loading of sucrose would leach the full complement of sucrose in ⟨6 hrs. Despite this presumed opening of the film structure, it was seen that the flux of sucrose from one side of a Eudragit® *NE* film to the other was negligible. It is therefore demonstrated that aqueous channels which allow the sucrose which is contained within the film to be transported to the film surface do exist, but channels that are continuous through the film, and which are of a suitable size to allow the transport of the sucrose without blockage of the channel, do not.

10.4.2 Sucrose permeation through Eudragit® *RL* films.

Figure 10.6 shows the permeation of sucrose through Eudragit® *RL*. Unlike Eudragit® *NE*, it is seen that at ca 50 hrs, the cell was very nearly at equilibrium. The plot of the total number of disintegrations is shown to be almost parallel to the time access, indicating that very little of the permeant sucrose was sorbed by the film (⟨2% of the total in 50 hrs *cf.* ≈ 4% retention of sucrose load in gravimetric leaching results). Assuming that after an initial lag of ca 7 → 8 hrs duration (*i.e.*, longer than the time to leach the plasticiser from the polymer {see Chapter 8}), the flux was relatively linear until such time as there would be a greatly reduced concentration gradient, then the **apparent permeability coefficient for sucrose through Eudragit® *RL*** (+ 15% triacetin) was **4.20×10^{-7} m² hr⁻¹**.

If the leaching of triacetin results in porosity of sufficient size to allow sucrose passage, then the sucrose permeability coefficient may be expected to tend towards the value for the diffusion coefficient of sucrose in water. This can be shown as follows. The flux, *J*, of a permeant is described by Fick's law (see Chapter 5) as:

$$J = \frac{D(C_0 - C_t)}{l} \tag{10.1}$$

where:

D = diffusion coefficient;
l = film thickness;
$C_0 - C_t$ = concentration gradient across the film.

The flux, J, therefore has units of g cm^{-2} s^{-1}. For the experimental situation of a porous film, the total flux, J_T, is described by the sum of the component fluxes, which may consist of a contribution from a flux of permeant through the polymer (J_P) (by solution-diffusion) and from an aqueous component (J_{aq}) (convective diffusion):

$$J_T = J_P + J_{aq} \tag{10.2}$$

Typically, an aqueous flux will be far greater than a flux through polymer due to there being less diffusive resistance. Hence, for a porous film, or a film impermeable to the penetrant (as may be the case for when electrolyte is the permeant or, as in this case, where the results suggest that methacrylate polymers are impermeable to sucrose {over the time frame of the permeation experiment}), the total flux will tend towards the flux through the aqueous system, *i.e.*:

$$J_T \rightarrow J_{aq} \tag{10.3}$$

Experimentally, it is the rate of change of concentration that is determined:

$$\frac{dC}{dt} \tag{10.4}$$

which has units of g cm^{-3} s^{-1}, and is therefore not directly comparable to the flux. The problem may be overcome if both flux and rate of change of concentration are expressed in similar forms, *e.g.*, the rate of change of the number of moles, *n*, of permeant. Thus:

$$\frac{dn}{dt} = \frac{dC}{dt} \times V \tag{10.5}$$

where V = volume of the receiver solution;

and also:

$$\frac{dn}{dt} = J \times A' \tag{10.6}$$

where A' = effective area for diffusion (*i.e.*, area of pore openings).

Therefore:

$$\frac{dC}{dt} \times V = J \times A' \tag{10.7}$$

or, from equation (10.1):

$$D = \frac{dC}{dt} \times \frac{LV}{A'(C_0 - C_t)} \tag{10.8}$$

where L/A' = effective diffusional pathlength per unit pore-opening area.

A similar equation is often used to determine the permeability coefficient, *P*, (Appendix A):

$$P = \frac{dC}{dt} \times \frac{lV}{AC_0} \tag{10.9}$$

It is therefore seen that an experimentally determined permeability coefficient would effectively give a diffusion coefficient if transport occurred predominantly through porosity, and if the effective diffusional path length and pore area are accounted for. In the case of sucrose permeation through Eudragit® *RL*, L/A' is unknown. However, if the measured permeability coefficient is assumed to be a diffusion coefficient, then comparison with the true aqueous diffusion coefficient (assuming no interactions between polymer and permeant) provides a measure of L/A'. Alternatively, the permeability coefficient may be considered as a diffusion coefficient even if the true film thickness and area are used, yielding what is the effective diffusion coefficient (D_{eff}) of the permeant in the polymer:

$$\begin{aligned} D_{eff} &\propto \frac{D_{aq}}{\tau_l} \propto D_{aq} \times \varepsilon \\ &= D_{aq} \times \frac{\varepsilon}{\tau_l} \end{aligned} \tag{10.10}$$

where:

τ_l = tortuosity;

ε = volume fraction of aqueous regions.

The diffusion coefficient for a sucrose solution can be calculated using the equation of Wilke and Chang[535]:

$$D = 7.4 \times 10^{-8} \frac{T(xM)^{0.5}}{\eta V^{0.6}} \tag{10.11}$$

where:

T = temperature = 303 K;
x = correction factor for hydrogen bonding = 2.6, for water[535];
M = solvent molecular weight = 18;
η = viscosity (assumed to be viscosity of water) at 303 K, = 0.7975 cP[1] [531];
V = molar volume, as given by:

$$V = \frac{4}{3}\pi N_A r^3 \tag{10.12}$$

where:

N_A = Avogadro's constant = 6.022×10^{23};
r = sucrose molecular radius (assuming sucrose to be spherical): the values vary in the literature – Colton[98] *et al.* give it as 4.7 Å, whilst Wisniewski and Kim[544] give the square of the radius of sucrose as 27.70 Å.

(V can also be determined using the atomic contributions as given by Le Bas[306]. Both methods give similar values for V.)

Therefore, assuming a sucrose radius of ca 5 Å, then **a diffusion coefficient for sucrose in water, at 303 K, calculates as 0.61×10^{-5} cm^2 s^{-1}** (*i.e.*, 2.20×10^{-6} m^2 hr^{-1}). (This compares to calculated and literature values given by Colton[98] *et al.* as 0.345×10^{-5} cm^2 s^{-1} and 0.697×10^{-5} cm^2 s^{-1} {at 310 K}, respectively, and 0.41×10^{-5} cm^2 s^{-1} as calculated by Wisniewski and Kim[544] at 296 K, again using the method of Wilke and Chang.)

Hence, assuming the experimentally determined permeability coefficient equals an effective diffusion coefficient, then $D_{eff} = 4.20\times10^{-7}$ m^2 hr^{-1}; *cf.* $D_{aq} = 2.20\times10^{-6}$ m^2 hr^{-1}. Therefore $\varepsilon/\tau_l = 0.19$. Also the ratio of the diffusion coefficient in the pore to that in free solution can be related to an assumed spherical pore radius, r_p, and permeant radius, r, by the following equation[411, 544] (attributed by Peppas and Meadows[390] as being a general form of an equation derived by Faxén[152]):

$$\frac{D_{eff}}{D_{aq}} = \left(1 - \frac{r}{r_p}\right)^2 \left[1 - 2.104\frac{r}{r_p} + 2.09\left(\frac{r}{r_p}\right)^3 - 0.95\left(\frac{r}{r_p}\right)^5\right] \tag{10.13}$$

By a process of iteration on a computer, and assuming the radius of sucrose = 5 Å, then the average pore radius is calculated to be 15.76 Å.

10.4.3 Sucrose permeation through surfactant-free PBMA films.

The permeation of labelled sucrose through PBMA film cast for 72 hrs at 353 K is plotted in **Figure 10.7**. The plot is similar to that of Eudragit® *NE*, *i.e.*, a small amount of the sucrose (<5% of the total) is transported through the film, before transport appears to

---

[1] 1cP (centipoise) = 1×10^{-3} kg m^{-1} s^{-1}

Table 10.2 The uptake of water by sucrose-containing Eudragit® *NE* films.

INITIAL SUCROSE LOAD /% (g.*NE*)$^{-1}$	CORRECTED WATER UPTAKE† /% (g.polymer)$^{-1}$
0	62.1
15	87.0
30	68.7
40	73.1
80	85.2

† Corrected for additive loss, *i.e.*, the uptake is the wet film weight as a percentage of the weight of polymer after leaching and drying.

cease. Also like the Eudragit® *NE*, it is apparent from the decrease in the total number of disintegrations counted in the cell, that a certain amount of the labelled sucrose is lost to the film: in a time of 50 hrs, the amount sorbed is approximately 2.8% of the initially added sucrose. Plots of both the total number of disintegrations and the number of disintegrations in the donor side of the permeation cell parallel each other after ca 10 hrs, indicating that the sucrose which is taken up by the film is lost from analysis during the first 10 hrs.

10.5 Uptake of water by sucrose-containing Eudragit® *NE* films.

The uptake of water by sucrose loaded Eudragit® *NE* films is given in **Table 10.2**. The values are corrected for the weight loss due to sucrose (and surfactant) leaching by virtue of the polymer weight being measured after film leaching (for 12 hrs) and drying.

The table indicates no real trend in the uptake of water as a function of sucrose load, other than showing that the uptake is greater than for the sucrose-free film. However, the results are subject to a high cumulative error (≈ 10% for each level of loading) due to the leaching of the sucrose, and also the method whereby excess water was simply blotted off the film's surface. The overall deviation in the results is only slightly greater, at approximately 13%, than the individual uncertainties and, hence, any trend is easily masked. The results for the sucrose loaded films do, however, appear to show an increased water uptake compared to the sucrose-free film, and this could result from the easier access to the film's interior due to the leaching of the sucrose, in combination with increased void-volume within the film. Such an increase in void volume, or capillarity, could itself be an increased cause of uncertainty in the experimental method: the action of blotting the film tending to draw water out of the capillaries or pores. This uncertainty would therefore increase with increasing porosity and, hence, presumably sucrose loading.

In order to overcome the inadequacy of the method, an attempt was made to measure the uptake of water vapour by a film suspended on a microbalance over a saturated solution of ammonium sulphate (*i.e.*, 81% R.H.). However, this method was found to be ineffectual due to the prolonged times required for the films to achieve an equilibrium uptake of water vapour (after two weeks, a film had not started to turn opaque, as would occur in the case of a Eudragit® *NE* film positioned under water in a few hours at most).

10.6 Solute permeation through Eudragit® films either containing, or pre-leached of sucrose.

Eudragit® films were subjected to (i) aqueous 4-nitrophenol and (ii) aqueous aniline permeability studies. The former was used to observe the trend in solute permeability as a function of the loading of sucrose within the film, whilst a series of substituted anilines of increasing side chain size was used to investigate the porosity of the films. The permeation studies investigated the permeability of films either leaching sucrose during the course of the experiment, or having been pre-leached of sucrose.

A complication arising from the leaching of the films (and, in some cases, drying of the leached films {*i.e.*, pre-leached films}) was a change in film thickness – when film thickness is a parameter in the equation for calculating the permeability coefficient. The removal of the sucrose, followed by a period of drying, allowed the film to 'contract' into the void volume left by the liberated sucrose. However, when a free-film was leached, and dried, there was a tendency for the film to curl, making the measurement of the thickness difficult and inaccurate when using the flat-footed dial gauge (see Chapter 7). This was compounded by the fact that the films used in this series of experiments were leached *in situ*, in the permeability cells.

It was therefore decided that the thickness of the film as cast would be used as the common frame of reference when calculating the permeability coefficient. Permeability coefficients are therefore termed ***apparent* permeability coefficients** denoting **the apparent increase in permeability arising from the additive in the film**. This is appropriate if the void volume, resultant from sucrose leaching, is not lost (due to further coalescence of the film), as may occur (see following paragraphs) in an aqueous environment where the sucrose is replaced by water, or when the polymer has a relatively high T_g. Such coalescence can, however, occur if the polymer is of a low T_g and film is leached and then undergoes further drying. Hence, other possible variations in thickness that might be considered include:

✗ an apparent permeability coefficient (hereafter termed $P_{l\,polymer}$) arising from the polymer alone (assuming total sucrose loss). This permeability coefficient is determined using a calculated value of film thickness. (Since the films were cast as discs of known diameter, then the contribution to thickness of a known weight of sucrose {density 1.5805 g cm^{-3} [531]} could be calculated. A calculated thickness is, however, subject to an increased experimental uncertainty if polymer is also being lost – as may occur if latex particles are dispersed in sucrose, as discussed earlier.);

✗ an apparent permeability coefficient (hereafter termed $P_{l+residual\,sucrose}$) calculated using the thickness of polymer + the residual sucrose (determined gravimetrically, after leaching). This is again determined using a calculated film thickness.

10.6.1 Permeation of 4-nitrophenol through Eudragit® *NE* film + sucrose.

Table 10.3 gives the apparent 4-nitrophenol permeability coefficients determined for Eudragit® *NE* films loaded with sucrose to levels up to 180% *i.e.*, a ratio of polymer to sucrose of 1 g : 1.8 g. **Figure 10.8** and **Figure 10.9** show the data graphically.

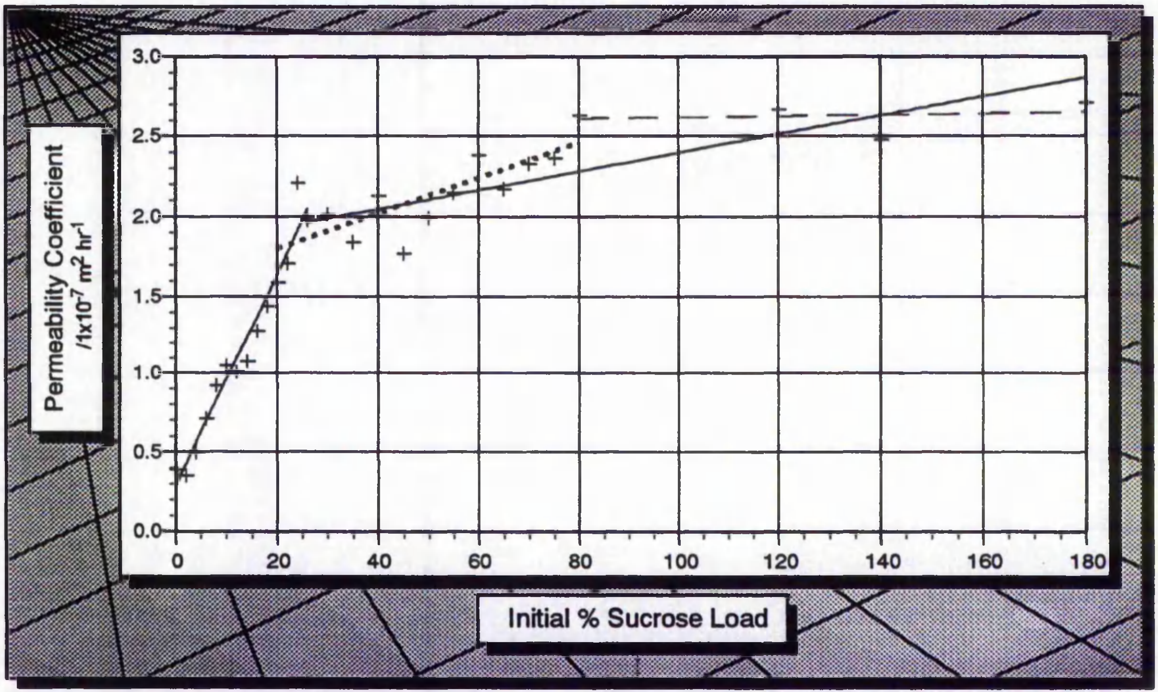

Figure 10.8 The apparent *4*-nitrophenol permeability coefficients for Eudragit® *NE* films, as a function of film (initial) sucrose content.

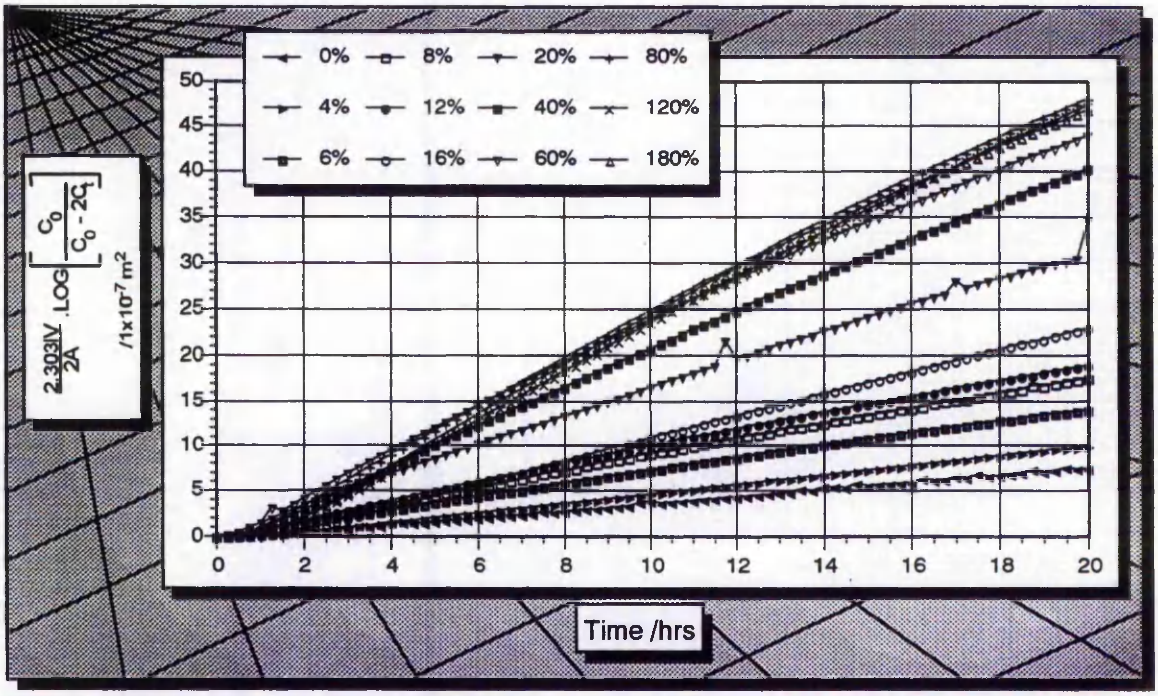

Figure 10.9 Trends in the *4*-nitrophenol permeability coefficients of sucrose loaded Eudragit® *NE* films.

Table 10.3 Apparent permeability coefficients for the transport of 4-nitrophenol through sucrose-loaded Eudragit® *NE* films.

INITIAL SUCROSE LOAD /% (g.*NE*)$^{-1}$	PERMEABILITY COEFFICIENT /1x10^{-7} m^2 hr^{-1}	INITIAL SUCROSE LOAD /% (g.*NE*)$^{-1}$	PERMEABILITY COEFFICIENT /1x10^{-7} m^2 hr^{-1}
0	0.40	35	1.85
2	0.36	40	2.14
4	0.51	45	1.78
6	0.72	50	2.00
8	0.93	55	2.16
10	1.06	60	2.39
12	1.02	65	2.18
14	1.09	70	2.34
16	1.29	75	2.37
18	1.45	80	2.64
20	1.60	100	N/A
22	1.72	120	2.68
24	2.22	140	2.49
26	1.99	160	FILM FAILED
30	2.02	180	2.72

Figure 10.8 shows the trend in the apparent permeability coefficient as a function of the films' initial sucrose content, whilst **Figure 10.9** shows some of the data used to calculate the permeability coefficients. The maximum loading (*i.e.*, 180%) was a result of the film becoming discontinuous. At $\rangle$180% sucrose content, regions of the film consisted predominantly of sucrose, which adhered to the substrate, and split on removal.

From **Figure 10.8** it is evident that the data can be fitted to a number of lines of best fit dependent on the level of sucrose addition. Between the sucrose-free Eudragit® *NE* film and a sucrose loading of just over 20% (g.*NE*)$^{-1}$, the apparent permeability coefficient is seen to increase at a relatively steep gradient that is proportional to the loading of sucrose (correlation coefficient r^2. = 0.959). The line (given by a least squares fit) does not, however, cross the permeability-axis at a value of the sucrose-free film (*i.e.*, 0.4x10^{-7} m^2 hr^{-1}), being described by the equation:

$$P \times 10^7 = 6.763 \times 10^{-2} C_{\% \, sucrose} + 0.289 \qquad (10.14)$$

At $\rangle$20% sucrose addition, the gradient of the line of best fit through the points in **Figure 10.8** is decreased by a factor slightly greater than an order of magnitude, and the (solid) line is described by:

$$P \times 10^{7} = 5.877 \times 10^{-3} C_{\%\,sucrose} + 1.810 \tag{10.15}$$

The points described by this line do, however, show a poorer degree of correlation than those described by equation (10.14), with a correlation coefficient, $r^2 = 0.653$.

As the sucrose loading approaches 180%, it is possible that the permeability coefficient is tending to plateau. The final four points on the graph in **Figure 10.8** could also be fitted to a different line of best fit (as indicated by the dashed line):

$$P \times 10^{7} = 4.03 \times 10^{-4} C_{\%\,sucrose} + 2.58 \tag{10.16}$$

The $C_{\%\,sucrose}$ term of the equation is tending to become less significant as the apparent permeability coefficient inclines towards a limiting value as described by the constant-term of the equation. This is seen in **Figure 10.9** by the tendency of the plots for the higher loadings of sucrose to come closer together, despite the increased span between the different levels of sucrose load. If these final points do indicate that the permeability coefficient has reached a limiting value (the line can not be extended further due to film failure), then the curve described by Equation (10.15) would also change to that indicated by the dotted line. This line is described by:

$$P \times 10^{7} = 1.0999 \times 10^{-2} C_{\%\,sucrose} + 1.258 \tag{10.17}$$

The linear correlation between permeability constant and film additive content (*e.g.*, as described by Equation (10.14)) has been observed by other workers. Donbrow and Freidman[125] investigated the addition of polyethylene glycol to solvent cast ethyl cellulose, also finding a linear relationship. Donbrow gave the coefficient of such an equation (*i.e.*, the factor 6.763×10^{-2} of equation (10.14)) the term "permeability enhancement coefficient, E_p", such that:

$$P_E = E_p C_{PEG} + P_0 \tag{10.18}$$

where:

P_E = enhanced permeability coefficient;
C = additive concentration (% W/W);
P_0 = permeability coefficient of additive-free film.

From the relationship between permeability coefficient and diffusion coefficient:

$$P = DS \tag{10.19}$$

where:

P = permeability coefficient;
D = diffusion coefficient;
S = solubility coefficient;

Donbrow also determined an diffusion enhancement coefficient (E_D) such that:

$$D_E = E_D C_{PEG} + D_0 \tag{10.20}$$

Given the assumption that:

$$D_0 = \frac{P_0}{S} \quad \text{and} \quad E_D = \frac{E_P}{S} \tag{10.21}$$

Donbrow found that values of E_D for a range of permeants of differing solubilities were all of the same order. This therefore implied that the enhancement of the permeability was a function of the drug solubility, *i.e.*, the mechanism of transport was still an activated diffusion process, rather than transport through capillaries. The enhanced permeability was therefore deemed to result from the shortened pathlength through the film – a result of the leached film thickness – since porosity was insufficient to allow the passage of inorganic ions (NaOH). (Although the average polymer thickness may remain the same, closed pores {as opposed to continuous pores} would lead to pathways in which the thickness of polymer, through which a permeant must pass, would be reduced.)

Equations (10.14) and (10.15) or (10.14) and (10.17) can be equated to find the (initial) sucrose loading (range) at which the change in apparent permeability coefficient trend occurs, *e.g.*, using Equations (10.14) and (10.15):

$$\begin{gathered} 6.763\times10^{-2}C_{\%\,sucrose}+0.289=5.877\times10^{-3}C_{\%\,sucrose}+1.810 \\ \therefore C_{\%\,sucrose}=24.6\%\ \left(g.NE\right)^{-1} \end{gathered} \qquad (10.22)$$

Repeating for Equations (10.14) and (10.17) yields a value of 22.8% (g.*NE*)$^{-1}$. Therefore, assuming that beyond a sucrose load of ca 20%, the points shown in **Figure 10.8** form a curve, then this range of ca 23 → 25% correlates with that quantity termed C_{suc}. (Previously discussed in paragraph 10.3.1 for the gravimetrically measured leaching of sucrose from Eudragit® *NE* films as a function of leaching time. *I.e.*, in the region of a film content {before leaching} of 15 → 28%, a change was seen to occur after which it became increasingly easy to remove the sucrose initially added to the film.)

To summarise, it is found that:

✗ high levels of sucrose are leached relatively quickly, and the apparent permeability coefficient tends towards a limiting high;

✗ low levels of sucrose are more difficult to leach (*e.g.*, the 2% load is not leached before the end of the permeability experiment), and the apparent permeability coefficient increases with increasing sucrose load (and, hence, ease of leaching).

It could be speculated that sucrose might fill the 26% void fraction which exists between close packed uniform spheres and that this could be the source of a critical sucrose loading. It should be noted, however, that if $C_{\%\,sucrose}$ occurs at 24.6% (g.*NE*)$^{-1}$ then this corresponds to ca 14% volume fraction (assuming that the density of Eudragit® *NE* polymer = 1.04 [147], and that of sucrose = 1.5805 [531]).

Permeability coefficients have been described as 'apparent' since they are calculated from the film thickness as cast. Permeability coefficients may also be calculated assuming the (calculated) thickness of the polymer alone (*i.e.*, $P_{l\,polymer}$, with the thickness due to the sucrose subtracted from the measured thickness). Results are given in **Table 10.4**. Despite the added uncertainty in the calculated results, it is seen that the increase in apparent permeability coefficient is not simply a result of the film thickness, and the permeability is

Table 10.4 Comparison of apparent 4-nitrophenol permeability coefficients for Eudragit® *NE* films + sucrose, calculated using either the polymer thickness or film thickness.

INITIAL SUCROSE LOAD / % (g.*NE*)$^{-1}$	CALCULATED† $P_{i\,polymer}$ /1×10^{-7} m^2 hr^{-1}	EXPERIMENTAL‡ PERMEABILITY COEFFICIENT /1×10^{-7} m^2 hr^{-1}
2	0.36	0.36
4	0.46	0.51
6	0.58	0.72
8	0.81	0.93
10	0.83	1.06
12	0.79	1.02
14	0.78	1.09
16	1.17	1.29
18	1.15	1.45
20	1.22	1.60

† Assuming a (calculated) thickness of polymer alone.
‡ Assuming the cast film thickness.

still seen to increase linearly ($r^2 = 0.91$) with increasing sucrose content. Although the addition of sucrose to the film results in an increase in film thickness, at 20% addition, the increase in thickness is just ca 10%, whereas the permeability coefficient is increased by greater than an order of magnitude. The implication of the calculated permeability coefficient (for polymer alone) being greater than that of the sucrose-free polymer film is a change in the film density and/or a change in the mechanism of the permeant transport. For a film that remains wet, the leached sucrose would be expected to be replaced by water and, hence, it would seem appropriate to use the original film thickness, as cast, to determine the magnitude of the apparent permeability coefficient.

10.6.1.1 Effect of 4-nitrophenol permeation on the transport of water.

It was found that the permeation of 4-nitrophenol through the sucrose-free film led to a difference in the rate of transport of radioactively-labelled water (THO) (by a factor of 2.71), dependent on whether the water was travelling with or against the 4-nitrophenol flux (see Chapter 8). In a film loaded with 40% sucrose, the apparent THO permeability coefficient increased by greater than an order of magnitude. In contrast to the results for the sucrose-free film, the water moving in a direction opposing the 4-nitrophenol flux showed a higher flux than that moving in the same direction as the 4-nitrophenol. However, the difference between the results was marginal (a factor of only 1.08), and comparable to the rates of 4-nitrophenol permeation. **When moving in the same direction as the 4-nitrophenol, the apparent THO permeability coefficient was 2.10×10^{-7} m^2 hr^{-1}**, whereas **when opposing the 4-nitrophenol direction of transport** (and, atypically, with the THO moving from the air side to the substrate side of the film), **the apparent THO permeability coefficient was 2.26×10^{-7} m^2 hr^{-1}.**

The results for the permeation of THO, in the presence of a flux of 4-nitrophenol are what would be expected if an osmotic potential existed, such that the THO flux would be greatest in the direction of the high concentration of 4-nitrophenol. As stated above, however, the difference in flux (between the two directions) is only 7%, which is typically within the experimental uncertainty of the permeation experiments.

10.6.1.2 Investigation for an asymmetric permeability difference.

Although the sucrose-free Eudragit® *NE* film had shown no sign of an asymmetric permeability coefficient, with reference to the film orientation during film casting, the facial differences observed in sucrose-loaded films implied that an asymmetric permeability may be possible in such films.

For a **Eudragit® *NE* film initially loaded with 25% sucrose** and, hence, on the 'plateau' side of C_{suc}, an **apparent permeability coefficient** of **$2.00(\pm0.06)\times10^{-7}$ m^2 hr^{-1} was measured when the substrate side of the film was oriented to the 4-nitrophenol.** Changing the direction such that the **polymer-air side of the film was oriented to the permeant yielded an apparent permeability coefficient of $2.10(\pm0.12)\times10^{-7}$ m^2 hr^{-1}.**

Therefore it is evident that any difference in permeability arising from the orientation of the film is again, like the sucrose-free film, either not present or lost in the experimental uncertainty of the result.

10.6.1.3 Films leached of sucrose and dried.

The sucrose-containing Eudragit® *NE* films discussed above were leached of their load of sucrose during the course of the permeation experiment. Due to this changing level of sucrose, it was decided to investigate the permeability of the films leached of their sucrose before the start (*i.e.*, pre-leached) of the permeation experiment, for comparison.

The method initially used involved mounting the film into the usual double chambered permeability cell and leaching the sucrose *in situ* (from both faces of the film) into water for a period of 96 hrs. The water into which the sucrose was leached was then removed from the permeability cell and replaced with the permeant/buffer solutions needed for the permeation experiment.

In performing the above procedure, the leached film was left out of aqueous solution (*i.e.*, open to the atmosphere) for ca 15 minutes. This had an affect on the measured permeability coefficient. For example, a film loaded initially with 25% sucrose has previously been shown to have an apparent 4-nitrophenol permeability coefficient of ca 2×10^{-7} m^2 hr^{-1}. Performing the above leaching procedure gave a value of 0.5×10^{-7} m^2 hr^{-1}. *I.e.*, a value only slightly greater than the value for the sucrose-free film – suggesting that the effect of the sucrose leaching was adversely affected by the short period that the film was out of the water. It was therefore decided to investigate the effect on the permeability coefficient of drying the leached film. In contrast, films were also leached of sucrose for an identical period, and their permeability coefficients were determined without the films being allowed to dry (– the results are discussed in paragraph 10.6.1.4).

Table 10.5 The apparent 4-nitrophenol permeability coefficients of Eudragit® *NE* films leached of sucrose, and then either dried or kept wet before the permeability measurement..

INITIAL SUCROSE LOAD /% (g.*NE*)$^{-1}$	DRIED† PERMEABILITY COEFFICIENT /1×10^{-9} m^2 hr^{-1}	DRIED‡ $P_{l\ polymer)}$ /1×10^{-9} m^2 hr^{-1}	ORIGINAL†‡ PERMEABILITY COEFFICIENT /1×10^{-9} m^2 hr^{-1}	WET* PERMEABILITY COEFFICIENT /1×10^{-9} m^2 hr^{-1}
0	8.8‡‡		40	73(±5)
5	2.27	2.22	60††	157
10	1.70	1.68	106	182
25	16.9	13.5	200††	208
30	19.8	16.4	202	163
40	26.7	20.9	214	115

† After leaching (96 hrs) and drying (24 hrs / 313 K); calculated using film thickness as cast.
‡ After leaching and drying as above; determined using calculated polymer thickness.
* After leaching (96 hrs) , but kept wet, calculated using film thickness as cast
†† Estimated from available experimental values.
†‡ Of film leaching sucrose during permeability experiment.
‡‡ Value of dialysed Eudragit® *NE* such that film is used as cast, *i.e.*, no need for leaching and drying.

Films were leached of sucrose for 96 hrs, in water, whilst fixed in the permeability cell, and then dried at 313 K for 24 hrs (*i.e.*, sufficient time for the films to achieve constant weight). Results are shown in **Table 10.5** and **Figure 10.10**. (Note that the legend on the graph indicates the initial loading of sucrose prior to leaching.)

To summarise the terminology, results are given in **Table 10.5** for apparent permeability coefficients assuming a film thickness calculated making one of two assumptions:

Column 2 ‘dried permeability coefficient’ gives an apparent permeability coefficient calculated using a measured film thickness as cast (*i.e.*, the usual method). In the case of a sucrose-free film, the value for dialysed Eudragit® (see Chapter 9) is used – which would presumably be the equivalent of leaching and drying a Eudragit® *NE* film cast from the latex ‘as supplied’ and therefore leached of endogenous surfactant;

Column 3 this dried permeability coefficient ($P_{l\ polymer}$) is calculated assuming that all of the added sucrose is leached, and is thus the permeability coefficient assuming that permeation occurs only through the (calculated) thickness of polymer alone;

Column 4 these results are the apparent permeability coefficients for a film leaching the initial load of sucrose during the course of the experiment (– data supplied for comparison purposes).

From **Figure 10.10** (which shows the results in column 3, *i.e.*, to give $P_{l\ polymer}$) it is seen that results show an increase in permeability above an original sucrose load of 10%: the permeability of a film having been leached of 25% sucrose and dried showing a permeability that is increased by a factor of ca 10 (compared to the film leached of 10% sucrose) – from a value below that of the dialysed polymer, to above it. This division occurs across the sucrose loading referred to previously as C_{suc}. Such a division is apparent in both of the apparent permeability coefficients for the leached and dried films independent of their method of calculation (**Table 10.5**). The trend is shown in **Figure 10.12** using $P_{t\,polymer}$.

It is evident from **Table 10.5** that the apparent permeability coefficient of the leached film may be reduced to a value below that of a film cast from dialysed Eudragit® *NE*, and this is presumably as a result of the additional thermal annealing taking place during the second drying stage, after leaching. The increased permeability of the sucrose-containing (and leaching) films is purely a function of the leaching of the sucrose, and the residual void-volume in the film that remains. The fact that the permeability of the leached films is decreased after as short a time as 15 mins 'drying' indicates the ability of the film to 'heal' this void-volume. Allowing the film to completely dry, to a constant weight, is then seen to completely nullify the effects of the sucrose, and also the effects of the film's endogenous surfactant, up to the point termed C_{suc}; above this point, the permeability is seen to increase despite the sucrose having been completely removed from the film. Hence, it is seen that above a certain level of sucrose loading (C_{suc}), there remains a residual effect on the film's transport properties after leaching the additive, implying that the film is not able to completely 'heal' the porosity or overcome the resultant reduced polymer density that are residual from such high levels of sucrose addition.

10.6.1.4 Films leached of sucrose, but not dried.

In contrast to the films discussed in paragraph 10.6.1.3, films were leached of sucrose in the permeability cells, and 4-nitrophenol permeant was added, in the form of crystals, to the buffer used to leach the sucrose. In this way, the films were kept in an aqueous environment and not allowed to dry at any stage between the sucrose-leaching and the start of the permeability experiment. Results are tabulated in **Table 10.5** – column 5 (for comparison with the dried films), and plotted in **Figure 10.11** and **Figure 10.13**.

The apparent permeability coefficient of the leached film did not decrease in magnitude below the value for the sucrose-free Eudragit® *NE* film, and all values were very much greater than the films that were leached and dried (by greater than an order of magnitude). This implies that the leaching of the additive did lead to the formation of void volume within the film, or porosity – either of which would lead to an increase in flux.

For sucrose loadings below the critical sucrose content (called C_{suc}), the apparent permeability coefficients were all greater than the values for films in which sucrose was leaching during the course of the permeability experiment. The lower levels of sucrose addition had previously been shown to be the most difficult to leach (the 2% load of sucrose taking longer than 20 hrs to leach). Therefore the increased pre-leaching time before the start of permeation presumably accounts for the increased permeability. Above C_{suc}, however, the apparent permeability coefficients appeared to decrease (**Figure 10.13**). This is tentatively ascribed to wet sintering of the polymer after rapid removal of residual sucrose during the protracted period of pre-leaching.

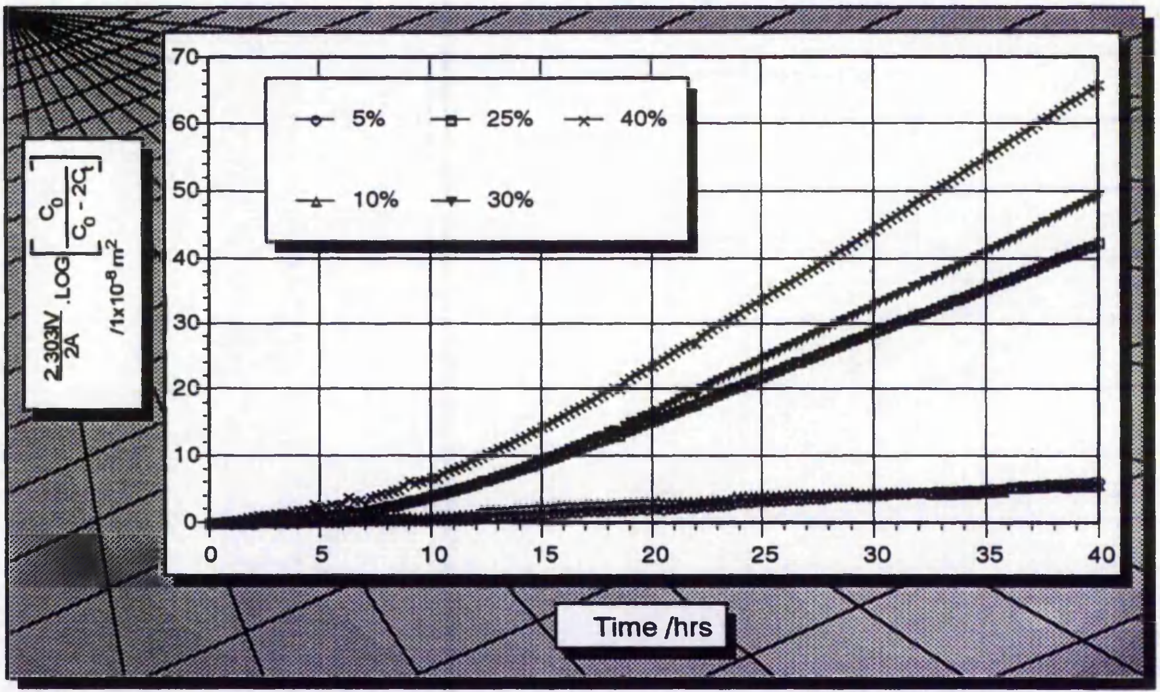

Figure 10.10 The permeation of 4-nitrophenol through Eudragit® *NE* films after being leached of sucrose, and dried.

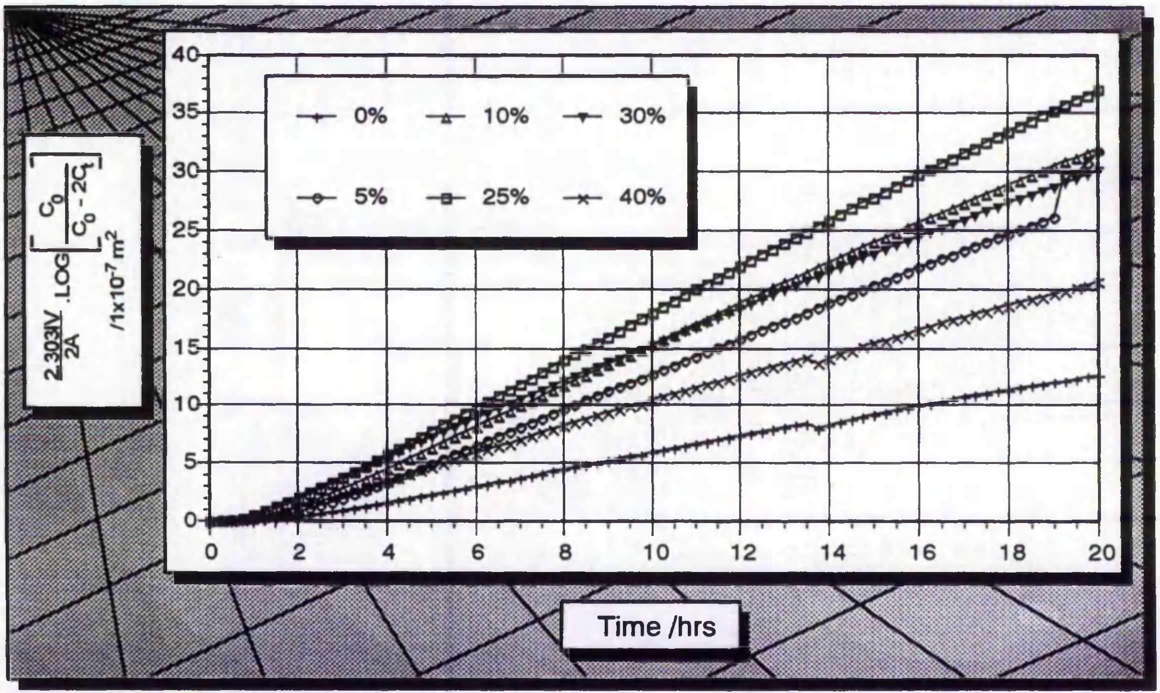

Figure 10.11 The permeation of 4-nitrophenol through Eudragit® *NE* films after being leached of sucrose, and kept wet.

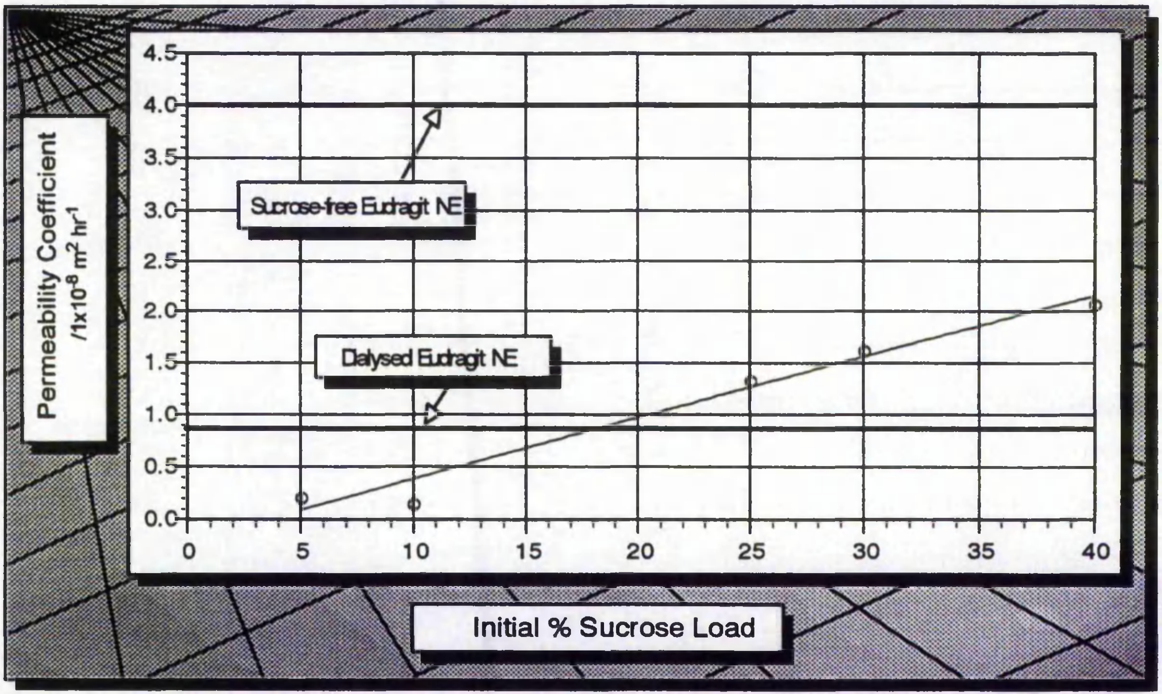

Figure 10.12 Trend in the apparent permeability coefficient ($P_{t\,polymer}$) of Eudragit® *NE* films leached of sucrose, and dried.

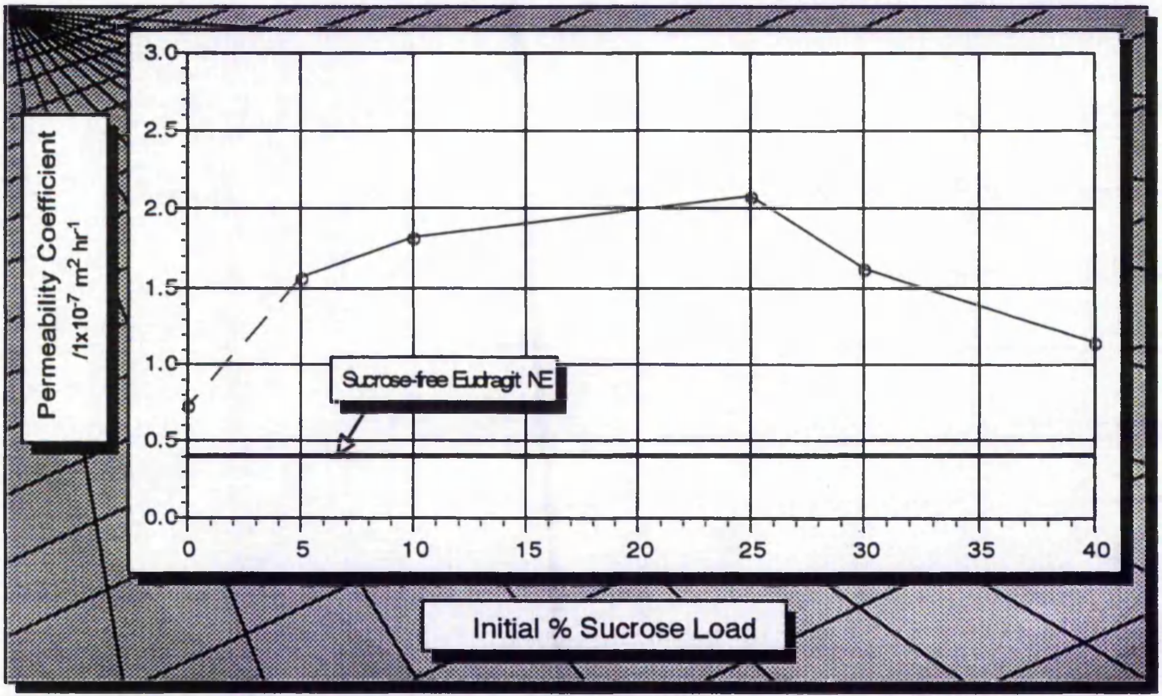

Figure 10.13 Trend in the apparent permeability coefficient of Eudragit® *NE* films leached of sucrose, and kept wet.

10.6.1.5 Arrhenius activation energy for the diffusion of 4-nitrophenol through Eudragit® *NE* films + sucrose.

The activation energy for the permeation of 4-nitrophenol through Eudragit® *NE* films both loaded with 40% sucrose, and leached of 25% sucrose (and dried) were determined. The results are plotted in **Figure 10.14**.

The calculated permeability activation energies, $E_a^{4\text{-}np}$, are found to follow the rank order of the apparent permeability coefficients: *i.e.*, **$E_a^{4\text{-}np}$ = 34.6 kJ mol^{-1} for Eudragit® *NE* containing 40% sucrose; 50.3 kJ mol^{-1} for Eudragit® *NE* leached of 25% sucrose** (calculated from the apparent permeability coefficients determined using their initial film thickness); (and 50.5 kJ mol^{-1} for sucrose-free Eudragit® *NE* {see Chapter 8}) whilst the respective permeability coefficients (at 303 K) are 2.14×10^{-7} m^2 hr^{-1}, 0.169×10^{-7} m^2 hr^{-1} (and 0.4×10^{-7} m^2 hr^{-1}). It is seen that removal of the sucrose from the film increases the activation energy to near that of the sucrose-free film indicating that once the additive is removed, then its effect is negated if the film is allowed to dry.

(Note that if the leached film thickness is used to calculate the apparent permeability coefficient ($P_{l\,polymer}$) for the film leached of 25% sucrose, then the activation energy is increased slightly to 50.9 kJ mole^{-1}.)

10.6.1.6 Effect of film thickness on the 4-nitrophenol permeation through sucrose-containing films.

The Fickian applicability, with respect to film thickness, of sucrose-free Eudragit® *NE* was investigated in Chapter 8 and showed a good correlation between the 4-nitrophenol flux and film reciprocal thickness with a regression coefficient, r^2, of 0.985. (Note: flux is

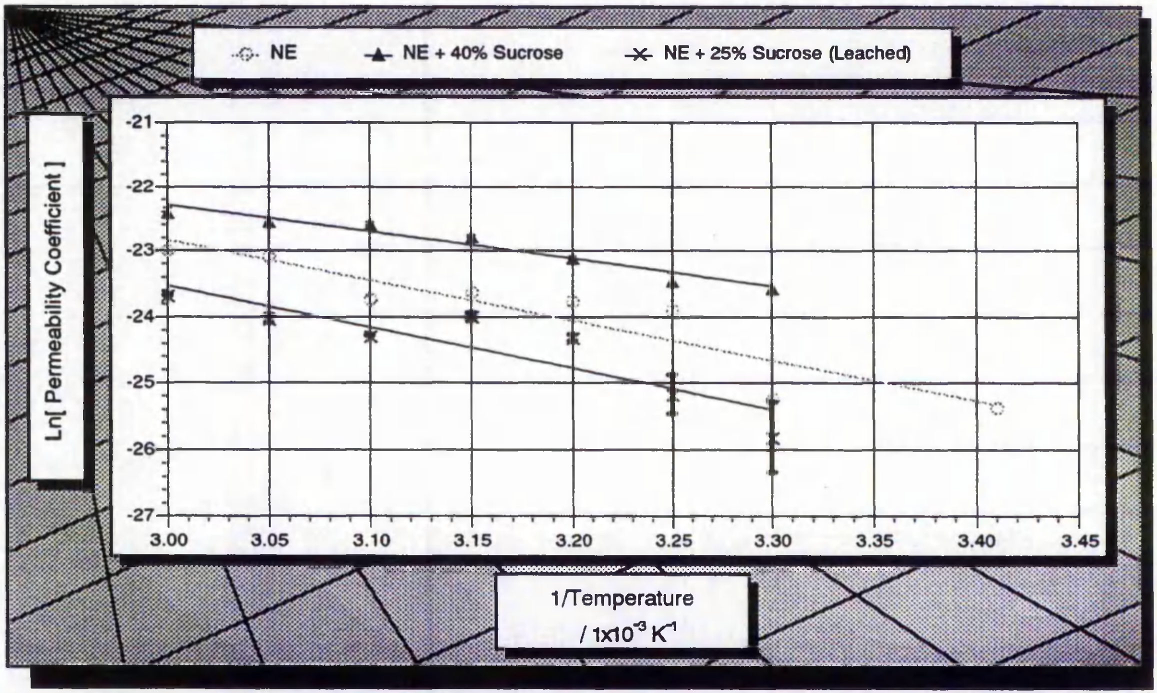

Figure 10.14 Arrhenius-type plots from the permeation of 4-nitrophenol through Eudragit® *NE* films both containing, and leached of sucrose (and sucrose-free for comparison).

proportional to the rate of change of concentration gradient in the permeability cell if the diffusion coefficient is constant, and rate of change of concentration is therefore plotted in the graphs. *I.e.*, in this section the terms 'flux' and 'rate of change of concentration' are used interchangeably.) The 4-nitrophenol permeability was also investigated, both for films either containing or leached of sucrose, as shown in **Figure 10.15** and **Figure 10.16**.

Both a Eudragit® *NE* film containing 40% sucrose, and one whose permeability was determined after leaching 25% sucrose followed by drying for 24 hrs at 313 K, showed good correlation between the permeant flux and film reciprocal thickness with least squares regression analysis giving correlation coefficients, r^2, of 0.955 and 0.988, respectively.

The results therefore suggest that there is little or no interaction between the 4-nitrophenol and the sucrose (or polymer) for the thicknesses of film investigated. Any such interaction would have been apparent as a non-linearity in the aforementioned plots.

10.6.1.7 Uptake of 4-nitrophenol by Eudragit® *NE* films containing sucrose.

The partition coefficient of the 4-nitrophenol permeant was measured for films that were leaching sucrose during the uptake experiment, and also for films that were leached of sucrose and dried (*i.e.*, pre-leached). Uptakes were determined from the spectrophotometric change in permeant absorbance, over a period of typically 96 hrs: *i.e.*, sufficient time for the equilibrium uptake to be established (as shown by no further change in absorbance). After soaking in 4-nitrophenol solution (0.2 g dm^{-3}), sucrose-containing Eudragit® *NE* films were swollen and opaque, with a slight green discolouration indicating some 4-nitrophenol was taken up by the film.

The partition coefficient for the sucrose-free Eudragit® *NE* film (see Chapter 8) was 94.15(±12.74). For a **film pre-leached of 10% sucrose (and dried), a partition coefficient of 98.57(±11.01)** was forthcoming – which is within the standard error of the sucrose-free film. (All sucrose would be expected to be leached from this film, such that the value would be for the polymer alone.) For a **film pre-leached of 40% sucrose, the partition coefficient** (again calculated using the values of leached film weight, *i.e.*, polymer only) was **96.42(±18.0)**. Therefore, as might be expected for films consisting of the same polymer type, the 4-nitrophenol partition coefficients show little variation between the values for the sucrose-free film, and the films pre-leached of their sucrose load. The uptake of 4-nitrophenol (concentration 0.2 g dm^{-3}) by a series of films pre-leached of sucrose at a range of concentrations (between 5%, and 40% was found to be effectively constant at 0.0144(±0.001) g $(g.film)^{-1}$.

Results for films leaching sucrose depended on whether the leached film weight or the initial film weight was used. In the experimental determinations, the sucrose was still present no matter whether it was leached into the 4-nitrophenol solution, or leaching from the film. However, any apparent uptake of 4-nitrophenol by a 10 g dm^{-3} sucrose solution (*i.e.*, much greater than the amount of sucrose that would be leached from a film during the measurement of the uptake) was found to be negligible. The calculated values for the

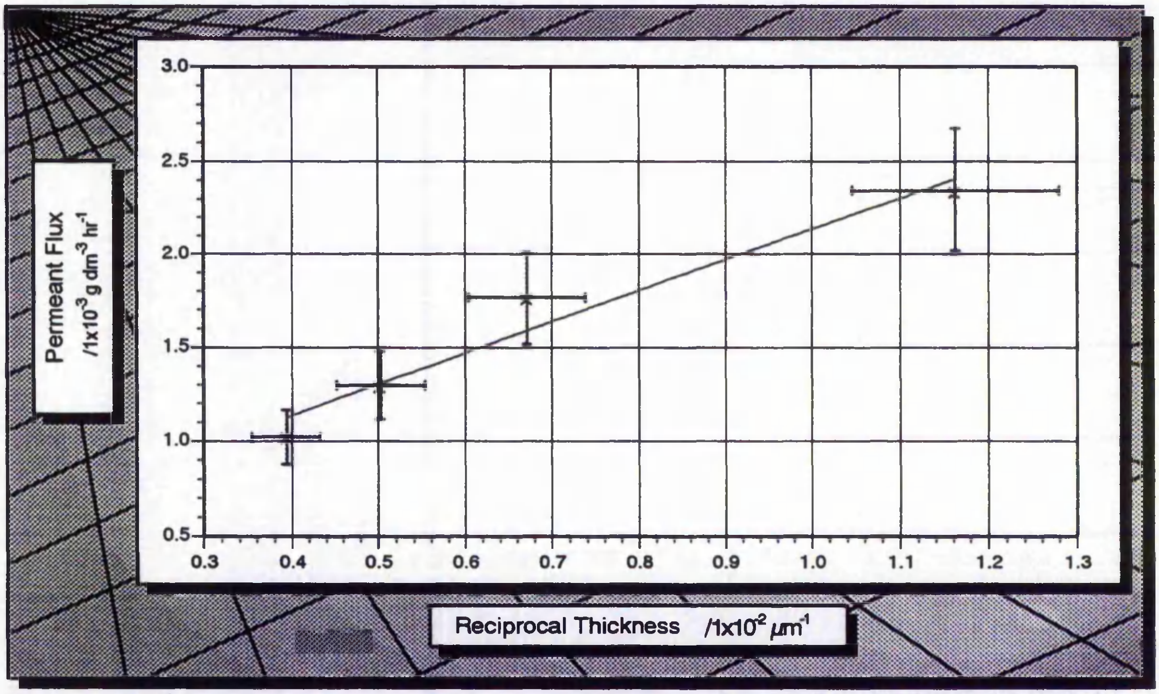

Figure 10.15 Fickian reciprocal thickness (initial film thickness) plot for the permeation of 4-nitrophenol through Eudragit® *NE* film + 40% sucrose.

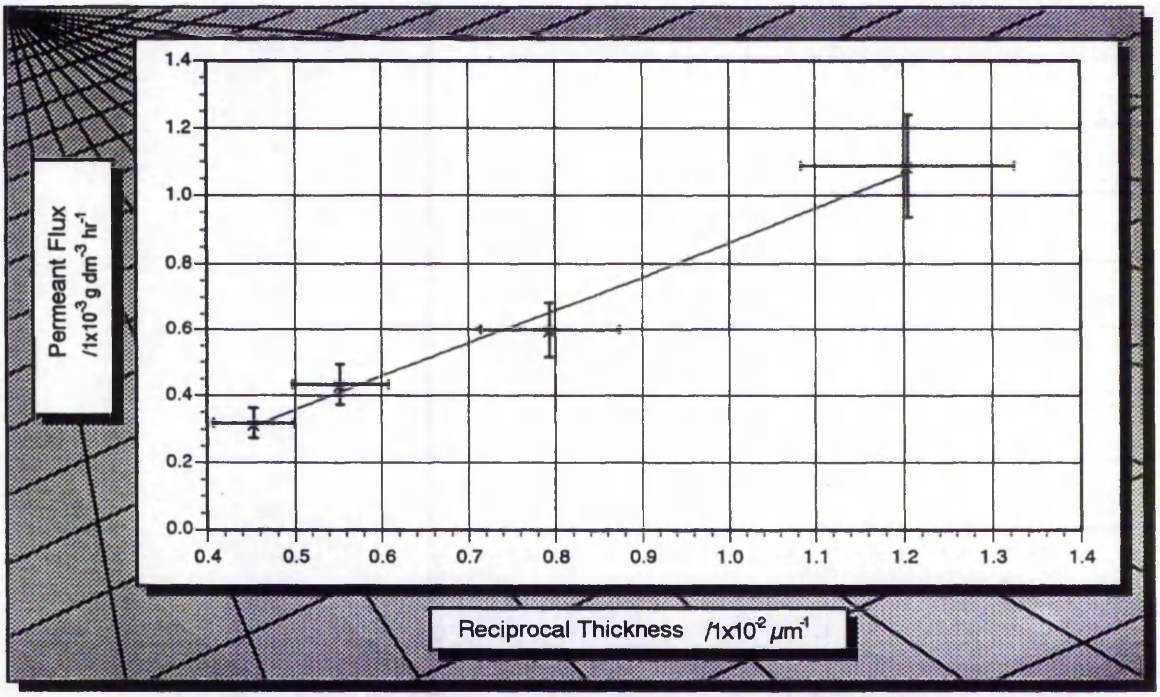

Figure 10.16 Fickian reciprocal thickness (polymer thickness) plot for the permeation of 4-nitrophenol through Eudragit® *NE* film leached of 25% sucrose.

Table 10.6 Apparent permeability coefficients for the transport of 4-nitrophenol through sucrose loaded Eudragit® *RL* films.

INITIAL SUCROSE LOAD /% (g.*RL*)$^{-1}$	**PERMEABILITY COEFFICIENT /1×10^{-7} m^2 hr^{-1}**	**INITIAL SUCROSE LOAD /% (g.*RL*)$^{-1}$**	**PERMEABILITY COEFFICIENT /1×10^{-7} m^2 hr^{-1}**
0	3.81	27	4.65
2	4.00	30	4.85
4	4.00	35	5.08
5	3.48	40	4.93
6	4.04	45	4.84
8	3.85	50	4.69
10	4.11	55	4.79
12	4.32	60	4.91
15	4.47	65	4.54
18	4.59	70	3.85(?)
21	4.51	75	4.67
24	3.10(?)	80	5.20

partition coefficient for the films leaching sucrose were found to be similar to the aforementioned values, *i.e.*, **98.49(±8.64)** and **91.51(±9.21)** for the **films leaching 10% and 40% sucrose**, respectively. These were calculated using the expected leached weight assuming a 10.5% (g.*NE*)$^{-1}$ and 29.8% (g.*NE*)$^{-1}$ weight loss from the respective films (as found during the gravimetric results when monitoring sucrose leaching). The uptake of 4-nitrophenol (0.2 g dm^{-3}) by a series of films leaching sucrose (at a range of concentrations between 5% and 40%) was found to be effectively constant at 0.0148 g (g.film)$^{-1}$ (±18%).

It is therefore evident that the presence (or absence) of sucrose did little to enhance, or change, the uptake of 4-nitrophenol by the Eudragit® *NE* polymer.

10.6.2 Permeation of 4-nitrophenol through sucrose-loaded Eudragit® *RL* film.

The apparent 4-nitrophenol permeability coefficient of Eudragit® *RL* film was 3.81×10^{-7} m^2 hr^{-1} (Chapter 8). The permeability of such films (plasticised with 15% triacetin) was investigated with various loadings of sucrose. Results are tabulated in **Table 10.6** and plotted in **Figure 10.17**. Like the similar plot for Eudragit® *NE* (in **Figure 10.8**), the apparent 4-nitrophenol permeability coefficients of sucrose-containing Eudragit® *RL* can be fitted to two linear equations. Up to a sucrose loading of 25% → 30%, the apparent permeability coefficient increases with increasing sucrose load according to:

$$P \times 10^7 = 3.738 \times 10^{-2} C_{\%\,sucrose} + 3.753 \tag{10.23}$$

showing reasonably good correlation with a value of $r^2 = 0.853$. Above a film sucrose content of 30%, the apparent permeability coefficient tends to plateau at approximately 4.79×10^{-7} m^2 hr^{-1}, with the best fit line described by the equation:

$$P \times 10^7 = 7.22 \times 10^{-4} C_{\% sucrose} + 4.790 \tag{10.24}$$

The experimental uncertainty, however, yields only poor correlation. Sucrose loadings greater than 80% → 100% in Eudragit® *RL* films led to the film splitting on removal from the casting substrate.

The point of interception of the lines described by equations (10.23) and (10.24) is the value previously termed the critical loading concentration (C_{suc}), of:

$$C_{\% sucrose} = 28.29\% \left(g.RL\right)^{-1} \equiv C^{RL}_{suc} \tag{10.25}$$

which is the concentration above which the increasing addition of sucrose to the film effectively has a negligible effect on the permeability coefficient, until the film disintegrates.

Comparing the results for Eudragit® *RL* and Eudragit® *NE* films is complicated by the differences in permeability of the sucrose-free films and, in the case of the Eudragit® *RL*, by the added plasticiser which was shown (Chapter 8) to increase the permeability coefficient of the film by a factor of approximately 1.4. Such differences are, however, accounted for by the constants in equations (10.23) and (10.14), such that the gradients of the lines described by these equations are generally resultant of the added sucrose. It is therefore seen that the increase in permeability in Eudragit® *NE*, due to the sucrose addition is approximately a factor of 1.8 times that seen Eudragit® *RL*. *I.e.*, the sucrose is

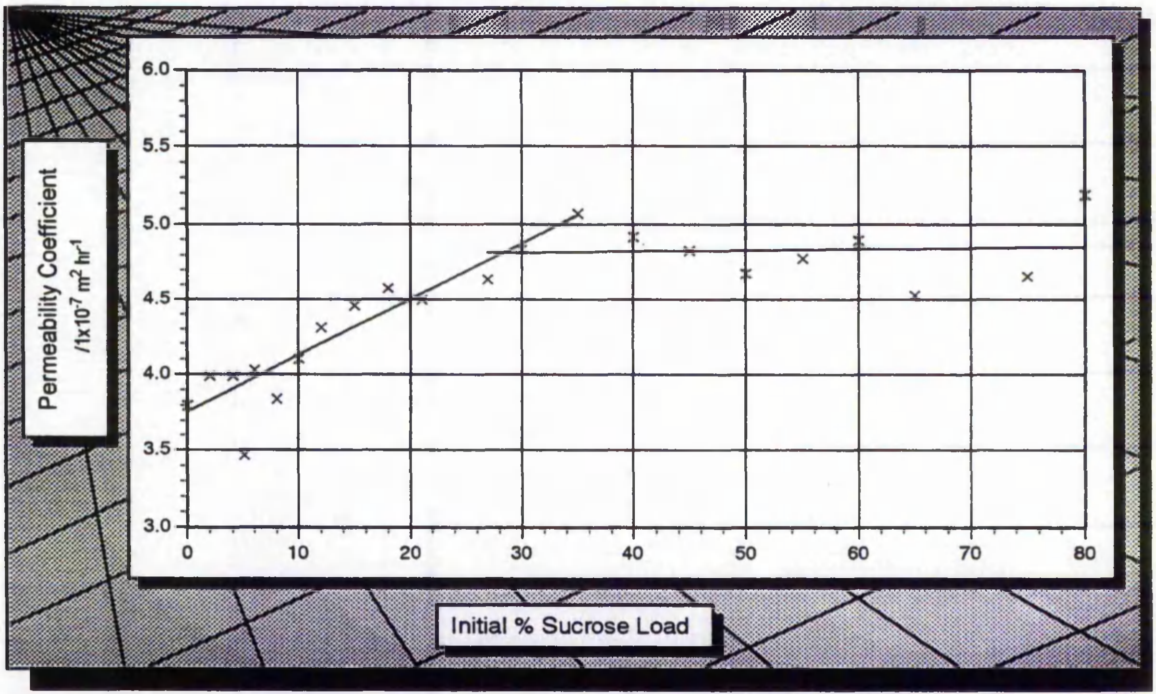

Figure 10.17 The 4-nitrophenol permeation coefficients for Eudragit® *RL* as a function of film (initial) sucrose content.

more effective in increasing the aqueous-solute transport properties of the more hydrophobic film, with the lower initial permeability. However, the final ('plateau') apparent permeability coefficients of the two types of film show the opposite trend, with the value for Eudragit® *RL* (of 4.79×10^{-7} m^2 hr^{-1}) being a factor of approximately 1.8 times higher than that of Eudragit® *NE* (at 2.58×10^{-7} m^2 hr^{-1}).

The differences in the plateau values are a result of the combination of additive (sucrose and triacetin) leaching, film hydrophilicity, and also possibly the differences in film T_g: the film with the higher T_g (*i.e.*, Eudragit® *RL*) requiring greater energy to 'heal' the porosity resulting from the leaching of the sucrose and triacetin.

10.6.3 Permeation (and uptake) of anilines through Eudragit® films.

A series of substituted anilines of increasing alkyl side-chain length were used as a probe of porosity, on the premise that a porous film would allow the differently sized anilines to permeate the film at approximately the same rate (if the pores were larger than the molecular size of all of the anilines), whereas a non-porous film would not due to the differing solubilities of the anilines in the polymer. It was shown in Chapter 8 that the anilines permeated through the Eudragit® *RL* films with near identical apparent permeability coefficients. This was considered to be the result of both the polymer hydrophilicity and the leaching of the triacetin plasticiser, leading to the formation of aqueous pathways. The anilines, however, permeated Eudragit® *NE* films at different rates. In anticipation of analogous behaviour to Eudragit® *RL* – assuming that sucrose leaching results in porosity – the permeation of the substituted anilines through Eudragit® *NE* films leaching a load of 40% sucrose were therefore investigated.

Permeability coefficient data are presented in **Table 10.7**, along with the uptake of the anilines by the films (measured film weights are corrected for the loss of weight of sucrose as determined gravimetrically in paragraph 10.3.1: the sucrose showing no uptake of anilines). The aniline permeations are also plotted in **Figure 10.18**.

It is evident that the permeability coefficients of all anilines were a factor of approximately two greater for the film leaching sucrose, compared to the sucrose-free film. Similarly, the pre-leached films show apparent permeability coefficients ($P_{i\,polymer}$) that were closer to those values of the sucrose-free films.

Despite the inferred porosity resulting from the leaching of sucrose, the anilines obviously did not permeate the Eudragit® *NE* films at similar rates. This implies that the sucrose leaching did not yield continuous pores of suitable size, and that a solution-diffusion mechanism was still the dominant transport process. (From Chapter 8, the radii of the anilines were 3.52, 3.74, 3.94 and 4.12 Å for aniline, methyl aniline, ethyl aniline and propyl aniline, respectively.)

The uptakes of the various anilines, by the sucrose-leaching films, follow the same rank order as the uptakes by the sucrose-free films, and the comments applied to the sucrose-free films (Chapter 8) apply equally here. However, whilst the magnitudes of the uptakes varied between the sucrose-free film and the sucrose-containing films by factors

Table 10.7 Apparent aniline permeability coefficients and equilibrium uptake by Eudragit® *NE* films either containing or having contained 40% loadings of sucrose.

ANILINE TYPE	PERMEABILITY COEFFICIENT /1×10^{-7} m^2 hr^{-1}	ANILINE UPTAKE /g $(g.film)^{-1}$
ADDITIVE FREE Eudragit® *NE*		
ANILINE	0.91	0.0040
METHYL ANILINE	1.47	0.0575
ETHYL ANILINE	2.84	0.1115
PROPYL ANILINE	1.97	0.0345
Eudragit® *NE* + 40% SUCROSE, LEACHING		
ANILINE	2.01	0.0237†
METHYL ANILINE	3.45	0.0681†
ETHYL ANILINE	5.94	0.1414†
PROPYL ANILINE	3.92	0.0426†
Eudragit® *NE* PRE-LEACHED OF 40% SUCROSE.		
ANILINE TYPE	**$P_{l\ polymer}$ /1×10^{-7} m^2 hr^{-1}**	**PERMEABILITY COEFFICIENT /1×10^{-7} m^2 hr^{-1}**
ANILINE	0.893‡	1.14
METHYL ANILINE	1.70‡	2.11
ETHYL ANILINE	2.40‡	3.01
PROPYL ANILINE	1.55‡	1.94

† Corrected for loss of sucrose from polymer.
‡ Calculated using (calculated) leached film thickness, assuming 100% sucrose loss.

of 1.18, 1.27, and 1.23 for the methyl aniline, ethyl aniline, and propyl aniline, respectively, the factor for unsubstituted aniline is 5.93. The increased uptake by sucrose-containing (leaching) Eudragit® *NE* films, imply that the sucrose aided the access of the anilines into the polymer. The uptake of aniline seems disproportionate because the permeability coefficient of the sucrose leaching film (when compared to the sucrose-free film) does not increase to the same extent. However, if the leaching sucrose is leaving sites onto which the anilines may sorb, then more aniline molecules would sorb than, for example, propyl aniline molecules since the radii of the anilines indicate that the cross-sectional area of aniline is ca 73% that of propyl aniline.

10.7 Permeation of electrolyte (KCl) through sucrose-containing Eudragit® *NE* films.

The transport of KCl through sucrose-containing Eudragit® *NE* films was investigated conductometrically. Electrolyte, like the anilines, acts as a probe to film

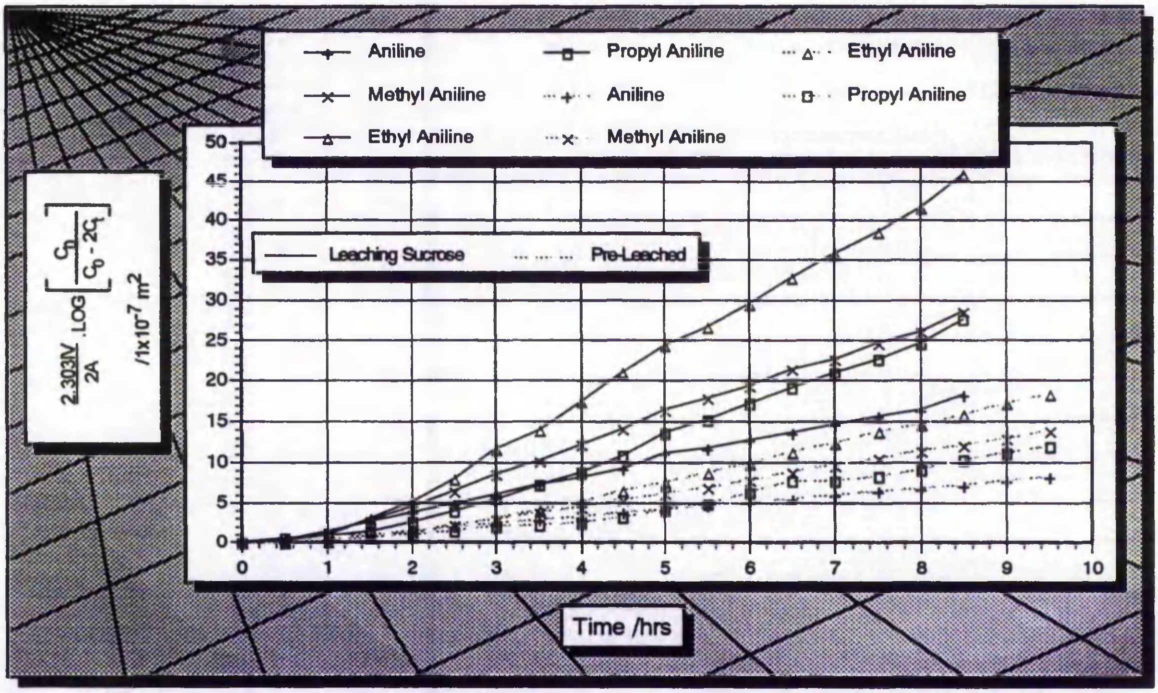

Figure 10.18 Plot for the calculation of aniline permeability through sucrose loaded (40%) and leached Eudragit® *NE* film.

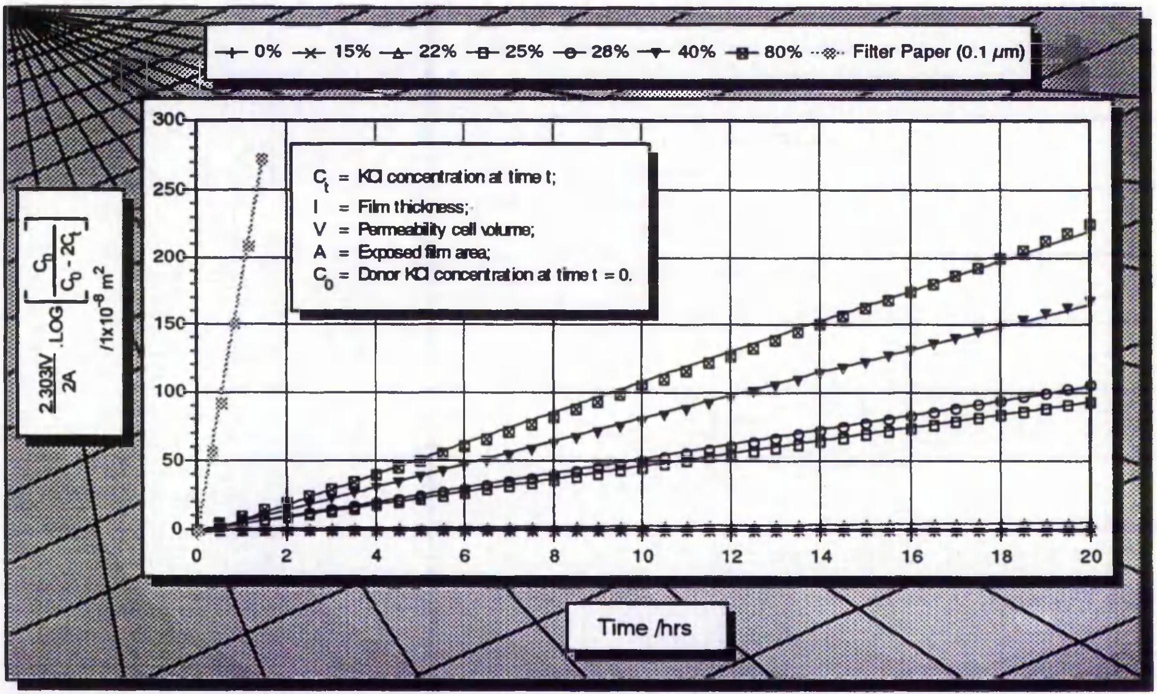

Figure 10.19 Permeation of potassium chloride through Eudragit® *NE* film loaded with various levels of sucrose (+ a Millipore filter paper, for rate comparison).

Table 10.8 Apparent permeability coefficients for the permeation of potassium chloride through sucrose-leaching Eudragit® *NE* films.

INITIAL SUCROSE LOAD /% (g.*NE*)$^{-1}$	PERMEABILITY COEFFICIENT / m^2 hr^{-1}
0	6.07×10^{-11}
15	9.13×10^{-11}
22	2.78×10^{-9}
25	4.68×10^{-8}
28	5.28×10^{-8}
40	8.38×10^{-8}
80	11.2×10^{-8}

porosity. In the absence of pores, or an ion exchange mechanism, electrolyte would not be expected to permeate a polymer film (and this was indeed apparent in Chapter 8, for the additive-free Eudragit® *NE* film).

The apparent permeability coefficients derived for the transport of KCl through Eudragit® *NE* containing an increasing load of sucrose are shown in **Table 10.8** and **Figure 10.19**. Over the KCl concentration range used, the conductivity was found to vary linearly as a function of concentration (using data from the Handbook of Chemistry and Physics [531]) and therefore experimental data could be converted directly into a permeability.

Evident from **Figure 10.19** is the change in film transport properties that occurs in the region of a sucrose-loading of 22 → 25% (g.*NE*)$^{-1}$, – *i.e.*, C_{suc}. Below C_{suc} very little KCl was transported across the film. Above 25%, however, the apparent permeability coefficient increased by greater than an order of magnitude, compared to a sucrose-content of 22%. Despite this large increase in KCl flux, the receiver cell permeant concentration was still less than ca 26% that of the equilibrium concentration after 20 hrs. (Under the same conditions, a 0.1 μm pore size Millipore filter reaches equilibrium in a little over 12 hrs.)

Permeability results for those permeants which were soluble in the film (*e.g.*, 4-nitrophenol) have tended to imply that the film transport properties were near a maximum (rate) at C_{suc}. However, the KCl transport results imply that it was only after a sucrose loading of C_{suc} that the film started to develop any side-to-side (continuous) aqueous pathways. The differences possibly result from the differences in molecular size. Sucrose is reported to have diameter of approximately 5 Å [98, 544] whereas the hydrated Cl^- ion radius is given as 3.32 Å [350], whilst the smaller K^+ ion is given as 3.31 Å [350]. Despite the slightly larger size of the sucrose molecule, however, it has been seen that it can be completely leached from the film, although the leaching was found to be considerably easier (quicker) at the higher sucrose loadings – at loadings higher than C_{suc}, the sucrose being completely leached in less 1 hr. If sucrose leaching leads to free-volume or void space, then it is at best of a dimension only marginally greater than the molecular dimensions of the electrolyte (and presumably less than that of sucrose which was found not to permeate through the Eudragit® *NE* film), and also highly tortuous.

KCl, being insoluble in Eudragit® *NE* polymer, is presumed to transport in the presence of leachable additive by a diffusive (convective) mechanism in aqueous pathways such that the apparent permeability coefficient equals the effective diffusion coefficient, D_{eff} (*cf.* p-10:27-). The aqueous diffusion coefficient (D_{aq}) of K^+ can be calculated as 4.61×10^{-6} m^2 hr^{-1} using equations (10.12) and (10.11) (from p-10:27-) for the molecular volume and diffusion coefficient, respectively. D_{eff}/D_{aq} can therefore be calculated and used to determine the relevant average pore radii, r_p, from equation (10.13). A plot of D_{eff}/D_{aq} versus r_p can be used to determine the value of r_p for a given value of D_{eff}/D_{aq}, and a plot of D_{eff}/D_{aq} (or r_p) versus the percentage of sucrose load in the film shows the effective increase in porosity as the sucrose is added (**Figure 10.20**, and **Figure 10.21**).

At 25% sucrose load, the pore radius is 4.96 Å (**Figure 10.20**) (*cf.* the radius of K^+_{aq} of 3.31 Å[350]). However, above 25% (*i.e.*, C_{suc}, whereafter the KCl flux started to increase indicating increasing film porosity) the pore radius remains virtually constant; rising to 5.82 Å at 80% sucrose load (**Figure 10.21**). It is apparent that the addition of sucrose to the film leads to the formation of continuous aqueous pathways (of a size suitable for KCl transport) in only a small range of addition (20 → 30%). Above 30%, and despite the increasing KCl permeability, there is little further pore enlargement: the increase in KCl permeability possibly resulting from increased pore number density, or reduced tortuosity.

For a **Eudragit® *NE* film pre-leached of 25% sucrose, the apparent KCl permeability coefficient** was reduced from 4.68×10^{-8} m^2 hr^{-1} for the film still leaching its additive load, to a negligible $\mathbf{7.59\times10^{-11}}$ $\mathbf{m^2}$ $\mathbf{hr^{-1}}$, again implying that much of the film's porosity is removed by the drying process.

10.7.1 Osmosis.

Since the sucrose-free Eudragit® *NE* film is impermeable to electrolyte (*cf.* a film loaded with sucrose above C_{suc}), it is possible that at the intermediate levels of sucrose addition the film is effectively acting as a semi-permeable membrane: allowing the diffusion of water but not electrolyte. Under such circumstances, it is possible that an osmotic potential exists which may affect the measured value of the solute permeability coefficients.

The solute permeability cell was open to the atmosphere such that the effect of osmosis would be an increase in the level of the aqueous phase on the side of the film containing the salt solution. No such variation in the levels of the solutions in either side of the chamber was ever noted. Hence, any potential osmotic pressure, which would be apparent as a hydrostatic pressure head, was presumably insignificant (*i.e.*, $\langle$ 5 mm water).

10.8 Porosity of sucrose-containing Eudragit® films.

The porosity of a Eudragit® *NE* film after having been leached of 30% sucrose (and dried) was investigated by the technique of mercury porosimetry. The resultant data is

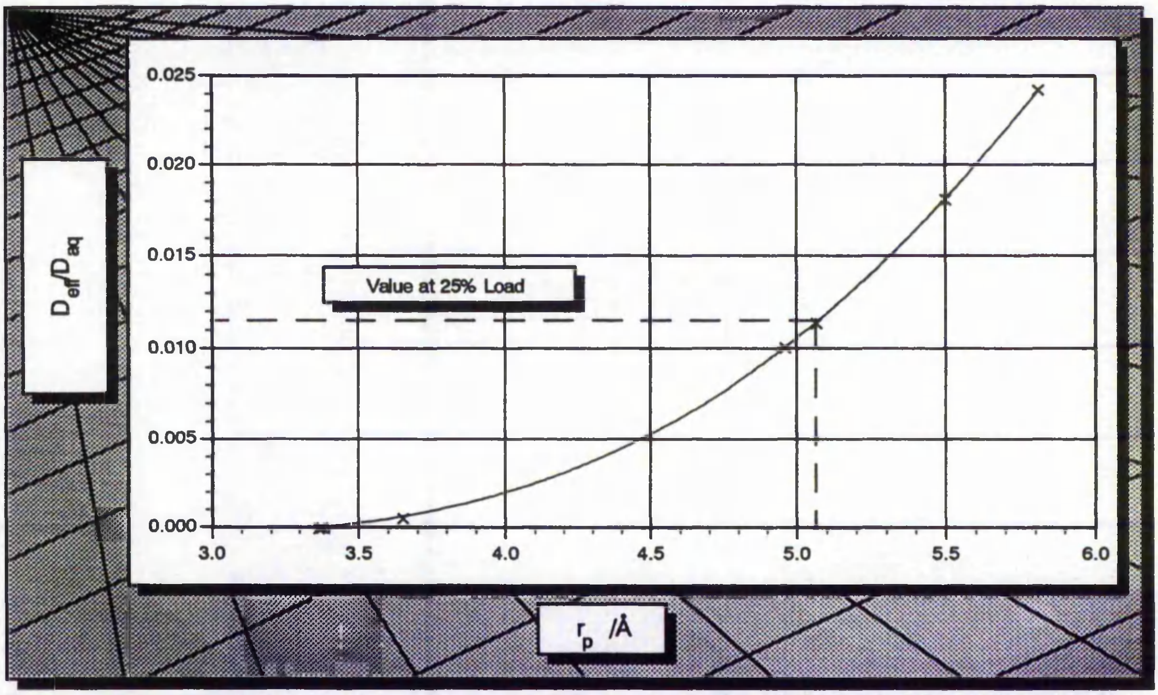

Figure 10.20 Effective potassium chloride diffusion coefficient as a function of pore radius.

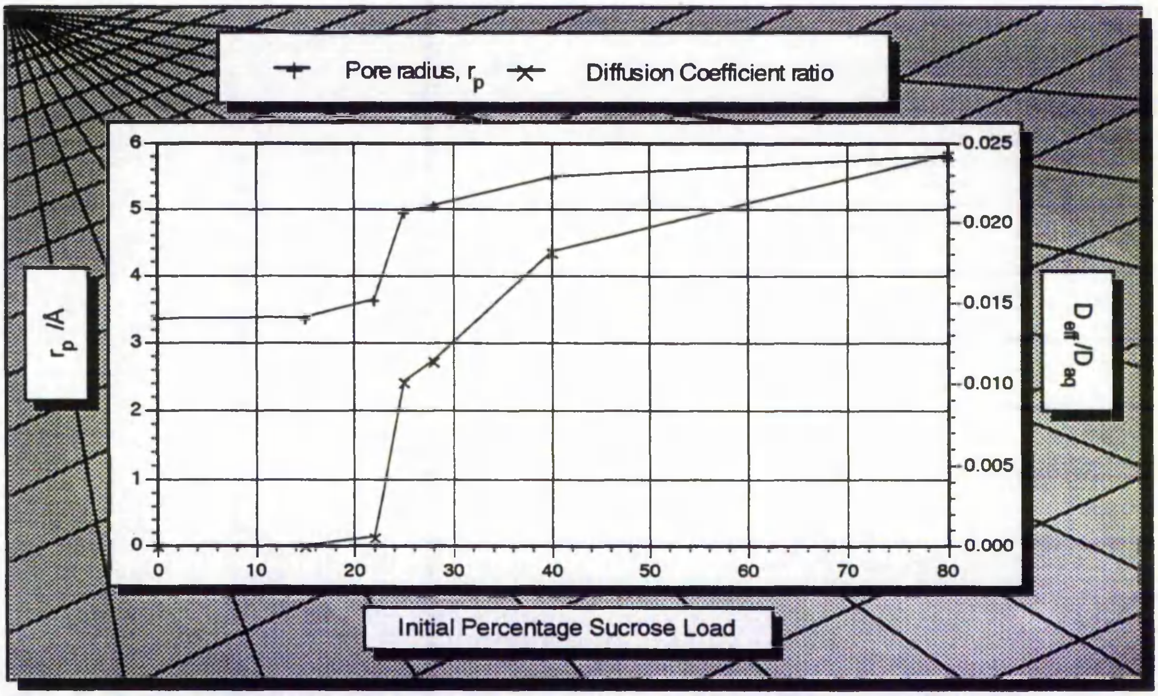

Figure 10.21 Relationship between potassium chloride diffusion coefficient, and film porosity, as a function of sucrose load.

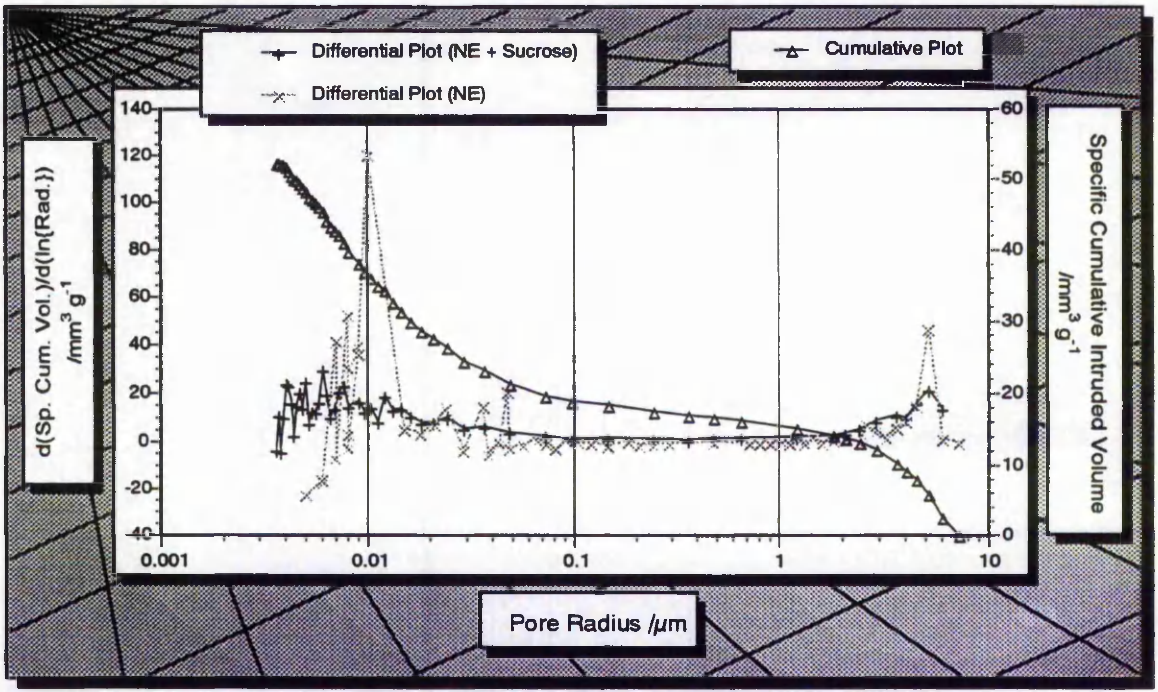

Figure 10.22 Pore distribution in a Eudragit® *NE* film leached of 30% sucrose.

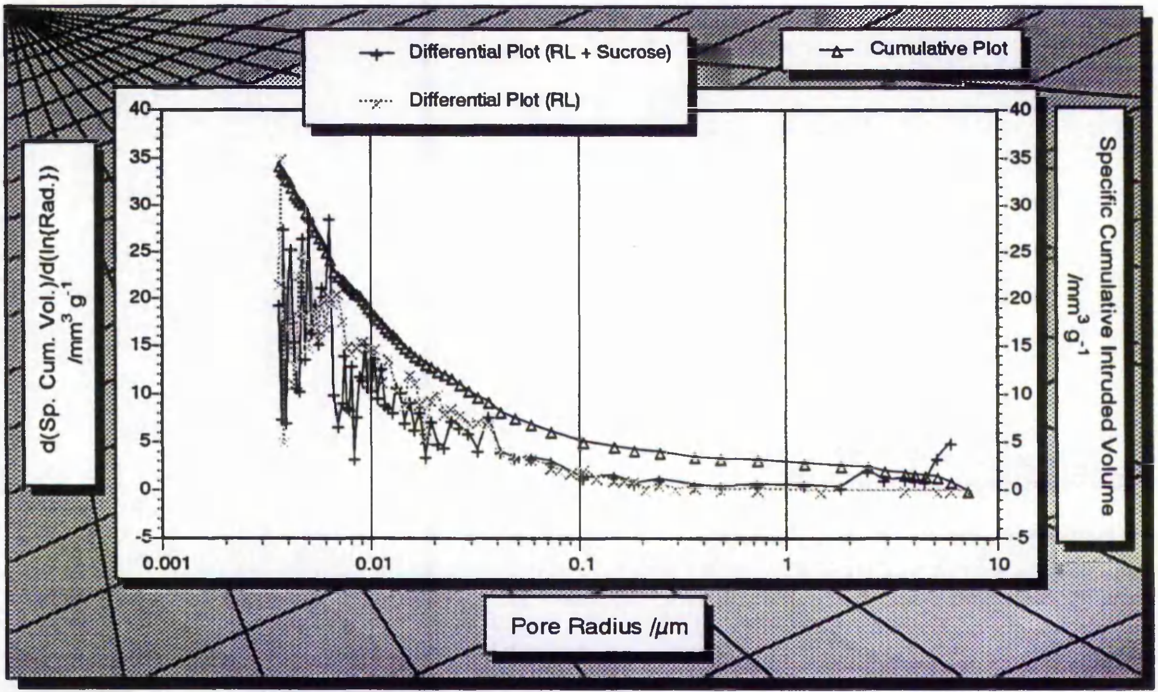

Figure 10.23 Pore distribution in a Eudragit® *RL* film leached of 24% sucrose (and plasticiser).

plotted in **Figure 10.22**. Similar data for a Eudragit® *RL* film leached of 24% sucrose (in addition to its usual 15% plasticiser content) is plotted in **Figure 10.23**.

The difference between the results for the sucrose-leached and the sucrose-free Eudragit® *NE* film is readily apparent, with the differential plot showing smaller peaks, around a pore size of 0.01 μm for the unleached films. This presumably results from the secondary annealing stage given to the leached film, *i.e.*, the drying after the leaching of the sucrose. This result therefore confirms the 4-nitrophenol permeability results for pre-leached and dried films which showed lower permeabilities than films that were either leaching sucrose, or leached and kept wet.

The data for the sucrose-leached Eudragit® *RL* film shows little difference to that of the sucrose-free Eudragit® *RL* film (still containing it's plasticiser), which is also shown in the graph. The overall cumulative intruded volume (at 1999 bar) was found to decrease very slightly from 37 mm^3 g^{-1} to 34 mm^3 g^{-1}. However, this appears to be insignificant, and shows the film is unable to sustain a porous network after drying at 313 K, despite a T_g of 328 K[313] (note that the added plasticiser would be leached with the sucrose {see Chapter 8}). Of the added 24% sucrose, it may be assumed that just over 95% would be leached, (based on the gravimetric leaching results - see paragraph 10.3.2). Of that remaining trapped within the film, its crystalline nature would presumably result in a reduced compressibility of the polymer, and it is possibly this feature which is reflected in the difference in the porosimetry results for the leached film compared to the sucrose-free film.

In summary, the sucrose has little effect on the porosity of a film that has been leached and dried, indicating that the large increase observed in solute permeability results is predominantly a consequence of the effects of the aqueous environment.

10.9 Water vapour permeation through sucrose-containing and sucrose-leached Eudragit® films.

The water vapour permeabilities of sucrose-free Eudragit® *NE* films (see Chapter 8) were thickness dependent (*i.e.*, non-Fickian with respect to film thickness). Similarly, Eudragit® *NE* films (50 → 200 μm) loaded with 40% sucrose showed a high degree of scatter in a plot of water vapour flux[1] as a function of film reciprocal thickness. Least squares best fit lines did, however, show slightly greater correlation between permeant flux and reciprocal thickness ($r^2 \approx 0.90$) – as expected for Fickian-type data – rather than permeant flux as a function of thickness ($r^2 \approx 0.80$).

Films loaded with varying amounts of sucrose showed increased apparent water vapour permeability coefficients compared to the sucrose-free film, but trends in the permeability as a function of sucrose load were difficult to interpret as a result of the relatively high levels of experimental uncertainty. The permeability trend possibly decreases with increasing content of sucrose in the films, and this is apparent for the leached and

---

[1] The flux was assumed to be proportional to the rate of change of weight. (See Chapter 7 for experimental method.)

Table 10.9 Apparent water vapour permeability coefficients for sucrose-loaded (and leached) Eudragit® *NE* films.

INITIAL SUCROSE LOAD /% (g.*NE*)$^{-1}$	**MEAN PERMEABILITY COEFFICIENT** /1x10^{-6} g hr^{-1} cm^{-1} cm.Hg^{-1}	**S.D.** /1x10^{-6} g hr^{-1} cm^{-1} cm.Hg^{-1}
	Eudragit® *NE* + SUCROSE	
0	1.65	±0.08
2	2.14	±0.28
10	1.88	±0.33
15	2.02	±0.12
22	1.94	±0.10
30	1.51	±0.13
	Eudragit® *NE* PRE-LEACHED OF SUCROSE	
	($P_{I\ polymer}$)	
2	2.28	±0.16
10	2.19	±0.20
15	2.12	±0.199
22	2.13	±0.19
30	1.92	±0.11

unleached films (**Table 10.9**). It is therefore surprising that the sucrose-containing films show an increased apparent permeability coefficient when compared to the sucrose-free Eudragit® *NE* film. Similarly, those films leached of sucrose demonstrate permeability coefficients that are higher than the sucrose-free film. The sucrose therefore appears to increase the permeability coefficient at low levels of addition, but then decreases it at higher levels of addition – possibly due to the crystalline sucrose itself being less permeable than the polymer, and the sucrose inhibiting the polymer chain motion such that the polymer becomes less permeable.

At high levels of sucrose addition (>22%) the water vapour flux (for those films containing the additive) tended to decrease slightly over the course of the experiment (250 hrs), and this was thought to be due to migration of the sucrose from the film's interior to the surface, where it became visible as white blister-like patches. For films loaded with 40% sucrose, the initial permeability coefficient of a 50 μm thick film, averaged over a time between 0 & 70 hrs, was a factor of 1.46 greater than the that averaged over a time between 170 & 240 hrs from the start of the experiment. For a 200 μm thick film, the permeability coefficient differed by a factor 1.99 when comparing values over the same periods. Again this could result from the increased quantity of sucrose in the thicker film which would amplify the effects of any water vapour-sucrose interaction. The aforementioned correlation coefficients remained relatively unchanged, independent of over which period the flux versus reciprocal thickness (or thickness) relationship was investigated.

10.10 The permeation of carbon dioxide gas through sucrose containing Eudragit® *NE* films.

The apparent CO_2 permeability coefficient of Eudragit® *NE* film containing 25% sucrose was found to be decreased compared to that found for the sucrose-free film: $P = 1.59\times10^{-9}$ g.p.u.[1] (*cf.* 1.99×10^{-9} g.p.u. when sucrose-free). This decrease in permeability coefficient is presumably a result of the impervious nature of the crystalline regions of sucrose within the film leading to the CO_2 having to take a more tortuous path.

The Higuchi equation predicts [167] the effect of regularly dispersed spherical filler particles upon the permeability coefficient:

$$P_{eff} = \frac{2P_1^2(1-\phi_2)+P_1P_2(1-2\phi_2)-GP_1\left(\frac{P_2-P_1}{2P_1+P_2}\right)^2(2P_1+P_2)(1-\phi_2)}{P_1(2+\phi_2)+P_2(1-\phi_2)-G\left(\frac{P_2-P_1}{2P_1+P_2}\right)^2(2P_1+P_2)(1-\phi_2)} \qquad (10.26)$$

where:

P_{eff} = effective steady state permeability coefficient;
P_1 & P_2 = permeability coefficients of constituent polymers (*i.e.*, Eudragit® *NE* and sucrose, respectively);
ϕ_2 = volume fraction of dispersed (*i.e.*, sucrose) phase;
G = constant based on dielectric constant data for powders and suspensions: typical value quoted as 0.8, but possibly as low as 0.4.

Assuming that sucrose is spherical and regularly dispersed, and if the CO_2 permeability coefficient of sucrose is assumed to be 0 g.p.u., then the above equation is reduced to:

$$P_{eff} = \frac{2P_1^2(1-\phi_2)-GP_1\left(\frac{-1}{2}\right)^2(2P_1)(1-\phi_2)}{P_1(2+\phi_2)-G\left(\frac{-1}{2}\right)^2(2P_1)(1-\phi_2)} \qquad (10.27)$$

Hence, if $P_1 = 1.99\times10^{-9}$ g.p.u., and knowing the weight fraction of sucrose (0.25) such that the volume fraction ϕ_2 can be calculated thus:

$$\phi_2 = \frac{25/1.5805}{\left(25/1.5805 + 100/1.04\right)} \qquad (10.28)$$

where:

1.5805 = density of sucrose (g cm^{-3}) [531];
1.04 = density of Eudragit® *NE* (g cm^{-3}) [147];

yielding a value of $\phi_2 = 0.14$ (*i.e.*, $1 - \phi_2 = 0.86$), then P_{eff} calculates to be 1.52×10^{-9} g.p.u. There is, therefore, good agreement (±5%) between the Higuchi theory and the experimental result.

---

[1] g.p.u. = gas permeability coefficient units = cm^3 cm s^{-1} cm^{-2} cm.Hg^{-1}.

Table 10.10 Apparent permeability coefficients for the transport of *4*-nitrophenol through sucrose loaded PBMA films.

INITIAL SUCROSE LOAD /% (g.PBMA)$^{-1}$	PERMEABILITY COEFFICIENT /1×10^{-7} m^2 hr^{-1}
0	≈ 0.001
5	0.15
20	2.36
40	6.68

10.11 Surfactant-free films.

Because of the handling difficulties of high T_g polymers, it was necessary to soak the PBMA films before they could be removed from the casting substrate. The results presented are therefore for films pre-leached of their additive, and dried, at ambient temperature for 24 hrs. The film thickness used to calculate the permeability coefficients is that of the leached and dried film. However, the S.E.M.s of PBMA leached of its additive (*e.g.*, **Plate 10.15** to **Plate 10.19**) show an open porous structure (*i.e.*, indicating less 'healing' following leaching) such that the leached film thickness, would be expected to be similar to that of the initial thickness.

10.11.1 Permeation of *4*-nitrophenol through PBMA films pre-leached of sucrose.

Because of the difficulty in preparing films of usable size, very few solute permeability results were obtained.

In Chapter 9, it was found that the additive-free PBMA film, when cast for 72 hrs at 353 K, presented a barrier that was virtually impermeable to *4*-nitrophenol, giving a permeability coefficient of ca 1×10^{-10} m^2 hr^{-1}. Consistent with the degree of porosity seen in the S.E.M.s (**Plate 10.15** to **Plate 10.19**), the apparent permeability coefficients of sucrose-containing films were found to increase by nearly three orders of magnitude, with a load of as little as 5% sucrose per gram of polymer. The results (given in **Table 10.10**), although few in number (and as single results, with an unknown degree of uncertainty), do show an increasing trend in apparent permeability coefficient, with increasing sucrose load, indicating the effectiveness of the sucrose in providing what must be (when considering the impermeable nature of the additive-free film {and, hence, PBMA polymer}) continuous pathways through which the permeant travels: presumably in an aqueous environment.

10.11.2 Porosity of PBMA films leached of sucrose.

The porosity of PBMA films pre-leached of both 5% and 40% sucrose was investigated by mercury porosimetry. A plot of the resultant pore distribution is seen in **Figure 10.24**. (Note that the graph's legend indicates the initial sucrose content of the film before leaching.) Compared to the additive-free PBMA film, there is little difference in the pore distribution of the 5% sucrose-leached film, to account for the large increase in *4*-nitrophenol permeability.

The 40% sucrose-leached film shows a massive increase in porosity. Whereas the additive-free film had shown a specific cumulative intruded (mercury) volume of 43 mm^3 g^{-1}, the film leached of 40% sucrose yielded a value of 188 mm^3 g^{-1}. For comparison, the 5% sucrose-leached film was only slightly greater than the additive-free film at 46 mm^3 g^{-1}.

It is seen that the peaks present in the additive-free film, at less than 0.01 μm pore radius are increased in size in the 40% sucrose-leached film. There is then a small gap in the pore distribution before a cluster of peaks starting from just under 0.1 μm up to 1 μm. These peaks are close to the latex particle radius, and are possibly indicative of some displacement in the particle packing.

10.12 Summary and conclusions.

Sucrose is an extremely water soluble additive, which showed no tendency to partition into a non-ionic acrylate/methacrylate polymer (*i.e.*, labelled sucrose would not permeate Eudragit® *NE*).

During latex film formation, the sucrose did, however, become trapped in the film during the evaporation of water upon drying. A number of possibilities exist for the distribution of the sucrose additive within the films: (i) molecularly dispersed; (ii) dispersed in the latex particulate voids (*i.e.*, dispersed in the ca 26% void volume between spheres: volume that would be present, at least until particle deformation started to occur upon casting); (iii) channelled into the 'faults' in the particle packing; (iv) on the film's surfaces, etc. Observation of film drying indicated that a polymer skin was formed initially during film casting: sucrose was therefore presumably incorporated into channels by which the evaporative flux of water exited this thickening polymer skin.

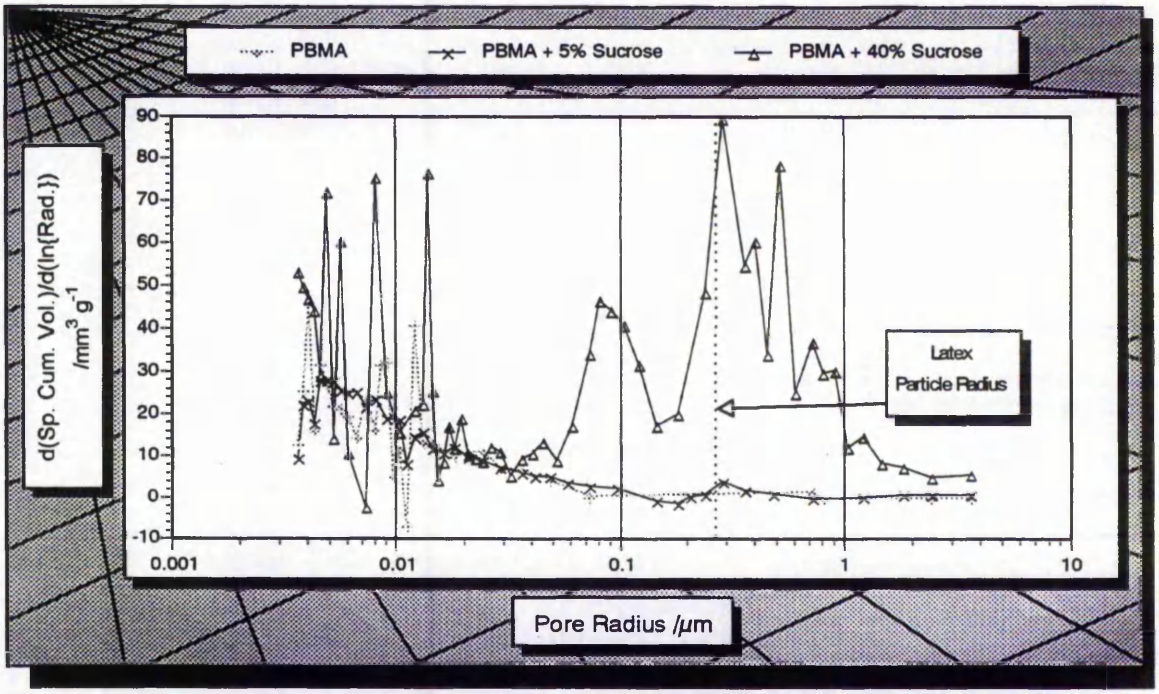

Figure 10.24 Pore distributions in surfactant-free PBMA films leached of sucrose.

The incompatibility of the sucrose with Eudragit *NE* was indicated by exudations of the additive to the film surfaces, when the film was in a humid environment, and the resultant opacity of the sucrose containing films.

In order for sucrose to be removed by leaching, on further exposure to bulk water, hydrophilic/porous pathways to the film surface would be required. The rate of leaching was faster at higher levels of sucrose addition reflecting a more extensive (*i.e.*, higher number density, wider and/or longer) network of aqueous channels.

A connective pathway from one side of the film to the other would not be essential for sucrose leaching which could take place towards either film surface (and therefore both chambers of the permeability cell).

Exudations of sucrose appeared (by the S.E.M.s) to be covered by a layer of polymer, and this was confirmed by the films being tacky to touch (as was Eudragit® *NE*, but not sucrose). Because the polymer was impermeable to sucrose, this implied that the sucrose was exiting the films via the disruptions to particle packing (which were observed, for example, on PBMA films – *i.e.*, films in which particle packing could be observed).

The exudation of incompatible material from films has been noted by a number of workers, most notably Bradford [62, 63] *et al*. Exudation of sucrose from the films investigated in this study would obviously affect their permeability properties. A movement of the sucrose to the surface of the film would reduce the quantity of leachable sucrose in its interior – lessening the possibility of pore formation upon leaching (assuming closure of the polymer behind the exudation). Such a migration to the film surface may have opposing effects on the transport properties of the film dependent on whether the penetrant is gaseous or in aqueous solution. For either type of permeant, the tortuosity of the diffusional path would be reduced, as would any restriction to polymer chain segmental motion caused by the sucrose, and also impermeable regions of the film would be reduced in number. However, a concentrated layer of sucrose at the film surface may yield a continuous, impermeable barrier to a (dry) gas. For an aqueous permeant, such a layer of sucrose would dissolve far more quickly, than sucrose dispersed in the polymer, due to the ease of access for the water, and would thus have no net influence on film permeability.

The consequences of the existence of hydrophilic channels in a normal permeation experiment would be (i) greater freedom for polymer chain segmental motion (plasticisation), and/or (ii) that these were the 'preferred' pathways of greater flux – even for permeants with a marked tendency to partition into the polymer phase, since diffusion in water is so much faster than in polymer. Using the equation of Wilke and Chang (equation (10.11)), an aqueous diffusion coefficient is typically of the order of 1×10^{-5} cm^2 s^{-1} – *e.g.*, the *4*-nitrophenol aqueous diffusion coefficient is 9.11×10^{-6} cm^2 s^{-1} (calculated given a flat {*i.e.*, absorbed} area of 52.5 Å^2, which was assumed to be circular such that a radius could be calculated; a smaller "end-on" area was also given as 25 Å^2 [332, 443, 444]). The *4*-nitrophenol permeability coefficient of sucrose-free Eudragit® *NE* was 4×10^{-8} m^2 hr^{-1} ($\approx 1\times10^{-7}$ cm^2 s^{-1}), implying a diffusion coefficient in the polymer (given that $P = DS$ {see Chapter 5}) of approximately 1×10^{-9} cm^2 s^{-1}, assuming a solubility (partition) coefficient of 94.2 (see Chapter 8).

It is evident, however, at least up to a critical loading of sucrose (C_{suc}) that in order to utilise these pathways to reach the other side of the film, then the permeant must also be capable of solution-diffusion transport in the polymer phase. Below the level of C_{suc}, the aqueous pathways are 'blind alleys' to both sucrose (as a permeant) and KCl. However, *4*-nitrophenol, which is able to partition into the polymer as well as diffuse in an aqueous environment, showed a linearly increasing flux – at least up to the point C_{suc}. Rogers [421] notes that the presence of non-interconnected microvoids will generally increase the rate of permeant transport, as found here, but cohesive forces between permeant molecules may lead to clustering which may negate the increased chain mobility resulting from the voids, therefore reducing the transport properties.

The presence of a continuous network of interconnected voids would allow convective flow [421, 550] in addition to the normal solution-diffusion type (activated) transport. A hydraulic permeability could not be determined for the films that were thought to be porous since they had insufficient strength to maintain their integrity under a pressure gradient sufficient to give a suitable increase in flux. However, at sucrose loadings $> C_{suc}$, connective aqueous pathways which were continuous from side-to-side of the film were shown to exist, since KCl flux became evident – but only to a limited extent. The apparent *4*-nitrophenol permeability coefficient increased much less dramatically above C_{suc}, when it appeared that further sucrose addition resulted in much greater levels of exudation and sucrose residing at the film surfaces.

The pathways created by sucrose leaching, even above a loading of C_{suc} are, at least at their narrowest point, only of molecular dimensions, since convective diffusion of the range of substituted anilines predominantly through aqueous pores was not possible. Surprisingly, the transport of sucrose across films leaching sucrose at a level $> C_{suc}$ was also not possible. The addition of sucrose at loadings $> C_{suc}$ did yield a KCl flux that increased slightly with increasing load, and the film did eventually disintegrate (at a load $>$ 180%) implying that small quantities of sucrose were still being distributed to the film interior and not just on the film surface. Since the average pore radius did not increase greatly, and the *4*-nitrophenol permeability coefficient started to plateau on the high side of C_{suc}, then these high loadings of sucrose presumably reduced tortuosity and increased the number density of the aqueous pathways rather than increased pore size to any great extent.

These results for Eudragit® *NE* film contrasted with those for Eudragit® *RL* which did permit the aforementioned sucrose transport – even when sucrose-free. Eudragit® *RL* films showed increased compatibility with sucrose addition by a lesser degree of opacity and a reduced tendency to exude sucrose. The dispersion of sucrose in the films is comparable to, for example, the dispersion of a drug in a polymer in a monolithic device. Bodmeir and Paeratakul [57] quote Baker [26] for the classification of such devices as either monolithic dispersions or monolithic solutions. A transparent film containing a monolithic solution (*i.e.*, solution on a macroscopic level) generally appears clear, whereas a dispersion appears opaque. The addition of sucrose to films of Eudragit® *RL* appears to bridge this distinction as the load increases. In the case of Eudragit® *NE* film, the bridge (film opacity) occurs at a much lower level of addition (*i.e.*, the film becomes progressively more opaque from the lowest levels of addition), but this may be due to clustering of the sucrose on exudation.

The ability of Eudragit® *RL* film to transport sucrose in solution was most likely due to the increased polymer functionality (rather than compatibility, and compared to Eudragit® *NE*) combined with the leaching of triacetin plasticiser: both of which could (and presumably did) lead to the presence of hydrophilic pathways.

Whether porous pathways created in non-ionic polymer films by sucrose addition and leaching can be maintained when the film was later dried depended, as in the original film formation, on the drying temperature relative to the T_g of the polymer. *E.g.*, leaching high levels of sucrose from PBMA film was found to leave large pores both on the surface and internally. However, this greater porosity in PBMA, as revealed by both mercury porosimetry and the large enhancement in the rate of *4*-nitrophenol permeation, may also result from less compatibility between the polymer and additive, *i.e.*, if sucrose and polymer compatibility can lead to increased film hydrophilicity (as in Eudragit® *RL*), then incompatibility of sucrose with the polymer, as in PBMA, can also lead to porosity due to the increased exudation and clustering of the additive.

Sucrose can be used, up to a critical loading (C_{suc}), to enhance solute transport in a controlled manner, whilst its addition is likely to reduce gas phase permeation, but marginally increase water vapour flux: the latter factors having possible implications for controlled release product storage.

◆

Results and Discussion, Chapter 11: Film Additives Other Than Sucrose.

11.1 Introduction.

The previous Chapter discussed a film additive, sucrose, that was expected to be molecularly dispersed, and easily leached from the film in an aqueous environment, as a method of increasing the permeability of latex films. This Chapter considers the effects of other film additives.

Hydroxypropyl methylcellulose (HPMC {Celacol HPM450 BP[1]}) is a (cold) water soluble[2] non-ionic cellulose ester, with a degree of polymerisation of 250 [392], implying a molecular weight of 58,500. When in contact with small amounts of water, the polymer swells and forms a gel. The polymer is widely used pharmaceutically, and also by the food industry. The hydrophilic nature of the polymer means that it is widely utilised in the preparation of hydrogels. For the purpose of this project, the HPMC was used to give the poly(methacrylate) latices a greater degree of 'swellability' when in an aqueous environment: to encourage the formation of aqueous pathways for the transport of aqueous solutes.

Eudragit® *L 30 D* is an example of a water soluble polymer latex, forming polymeric salts at pH > 5.5. It is typically used for enteric pharmaceutical coatings or matrixes. For the purpose of this study, it was used as a 'large' (130 μm Ø) soluble additive in the films: as a means to provide latex particulate sized pores, as opposed to molecular sized pores which were shown in the previous Chapter to be readily healed on allowing the film to dry.

A number of other additives, as described in the text, and means of increasing film permeability were also looked at briefly.

11.2 Hydroxypropyl methylcellulose as a film additive.

HPMC was added to Eudragit® *NE* films as a percentage per gram of Eudragit® *NE* solids content. The lower solubility of the HPMC (as a result of the HPMC gelling in aqueous solution), compared to sucrose, together with the difficulty of dissolving it in water led to a much lower maximum level of addition.

11.2.1 Appearance and structure of Eudragit® *NE* films containing HPMC.

Of all the types of film investigated during the course of this project, Eudragit® *NE* films containing HPMC were the most easily handled (presumably due to the influence of the higher T_g HPMC[3] on the T_g of the film). Agitation of HPMC as a highly viscous solution needed to be avoided or air bubbles were prone to become trapped and retained in the dried film. The Eudragit® *NE* + HPMC films were easily removed from the casting substrate.

---

[1] 450 refers to the viscosity (mP s^{-1}) of a 1% solution.

[2] Solubility is described [392] as 'limitless,' but limited by solution viscosity.

[3] Okhamafe and York [353] measured the T_g of an HPMC as approximately 429 K (dependent on film age and storage conditions).

In appearance, the films showed a matt texture, having lost the glossiness and some of the transparency of the HPMC-free film. The films also lost their tackiness, without gaining any rigidity, but did seem to acquire a static charge. At low levels of HPMC addition (⟨12%), the films showed a very fine pattern of 'mud-cracks.' As the level of addition increased, the mud-cracking decreased, or was masked by increased graininess of the film.

On soaking in water, Eudragit® *NE* films containing HPMC swelled, but not uniformly, and turned uniformly opaque. Swellings were in the form of blisters which were swollen with (presumably) HPMC solution. Such blisters could occur, for example, (i) as a result of poor HPMC distribution in the film, as might occur due to relief of HPMC saturation in the drying latex, or (ii) due to isolated hydrated HPMC trapped in the film with no access to the film surfaces, such that an osmotic potential could be created between the trapped HPMC and the sink solution outside the film. The pre-leached and dried films were of similar appearance to the additive-present films presumably indicating some retention of the additive (see paragraph 11.2.2).

The exudations observed on Eudragit® *NE* films when sucrose was used as an additive were never seen when HPMC was present as the film additive. This indicates either a greater degree of compatibility between the two polymers, or that the rate of exudation was insufficient (due to the higher molecular weight of the HPMC) to allow visible amounts of HPMC to appear on the film surface.

11.2.2 Leaching of HPMC from Eudragit® *NE* films.

Results for the loss of HPMC from Eudragit® *NE* films on leaching in water are shown in **Figure 11.1** and **Figure 11.2**. It is apparent that the full load of HPMC was not leached, and that, in general, the amount of HPMC leached varied almost in direct proportion to the film content. The vast majority of HPMC that is leached from the film does so in the first hour but, as with the sucrose additive, the lower loading of HPMC (0.06 g g^{-1} of Eudragit® polymer) has greater difficulty leaching than the higher loadings. Again, this is presumably a result of progressive porosity, resultant from leaching, aiding the leaching of HPMC embedded deeper within the film.

The inability to leach the full initial load of HPMC is ascribed to the swelling of the film. The ability of the film to accommodate blisters of water is an indication that the film would also contain any HPMC that is dissolved in that water. This fact, combined with the viscosity of HPMC solution, would together explain the incomplete leaching of HPMC following a period of immersing the film into water, and drying.

Typically, desorption from a polymer would initially be expected to be diffusion controlled and directly proportional to the square root of time, $t^{1/2}$[234, 235] (until the concentration of desorbant decreased to give an exponential decrease in the rate of desorption). Dissolution controlled leaching is, however, directly proportional to t[439, 440]. The dependence of the HPMC desorption from Eudragit® *NE* as a function of the square root of time ($t^{1/2}$) and as a function of time was determined, with neither relationship showing particularly good correlation. This was presumably due to the leaching of the additive

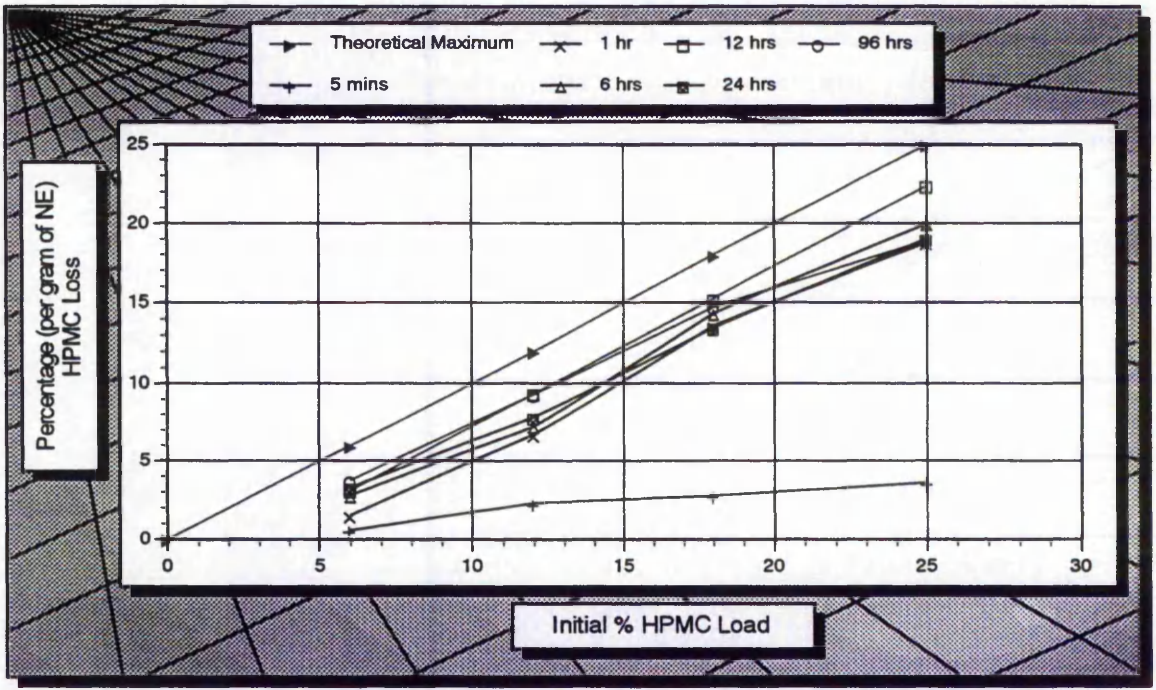

Figure 11.1 Plot of the percentage of HPMC leached (per gram of Eudragit® *NE*) versus the percentage of HPMC loaded (per gram of Eudragit® *NE*) for various leaching times.

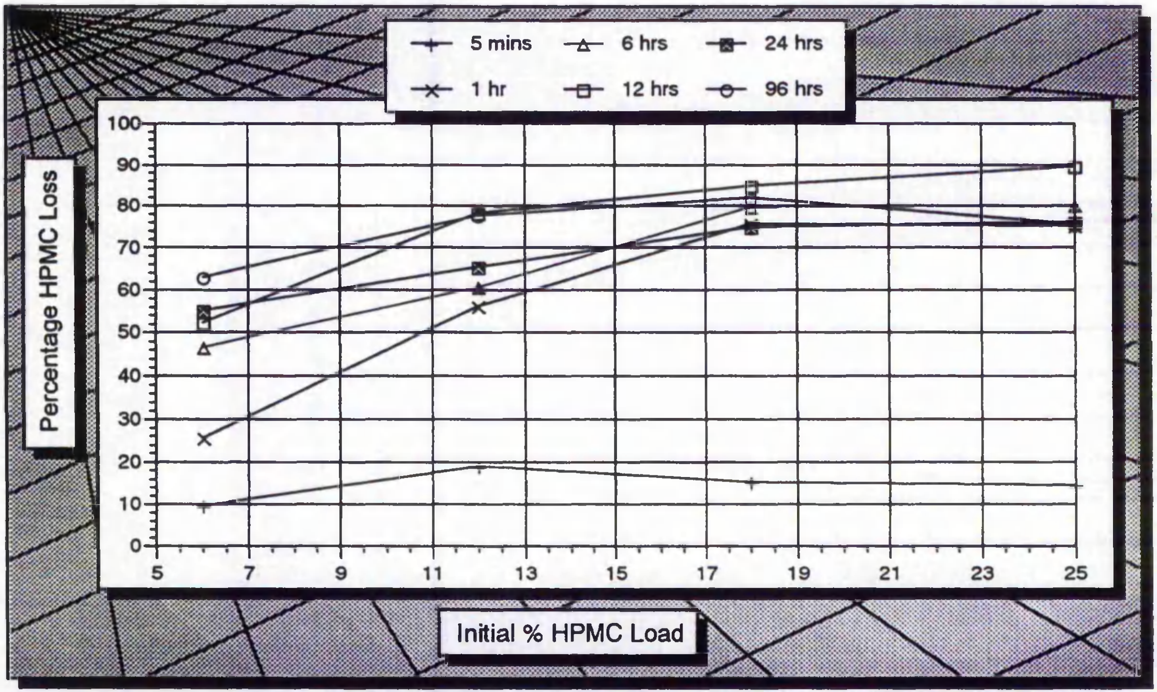

Figure 11.2 Percentage of the initial amount of HPMC lost from a Eudragit® *NE* film, after leaching for various times, as a function of initial HPMC content (per gram of Eudragit® *NE*).

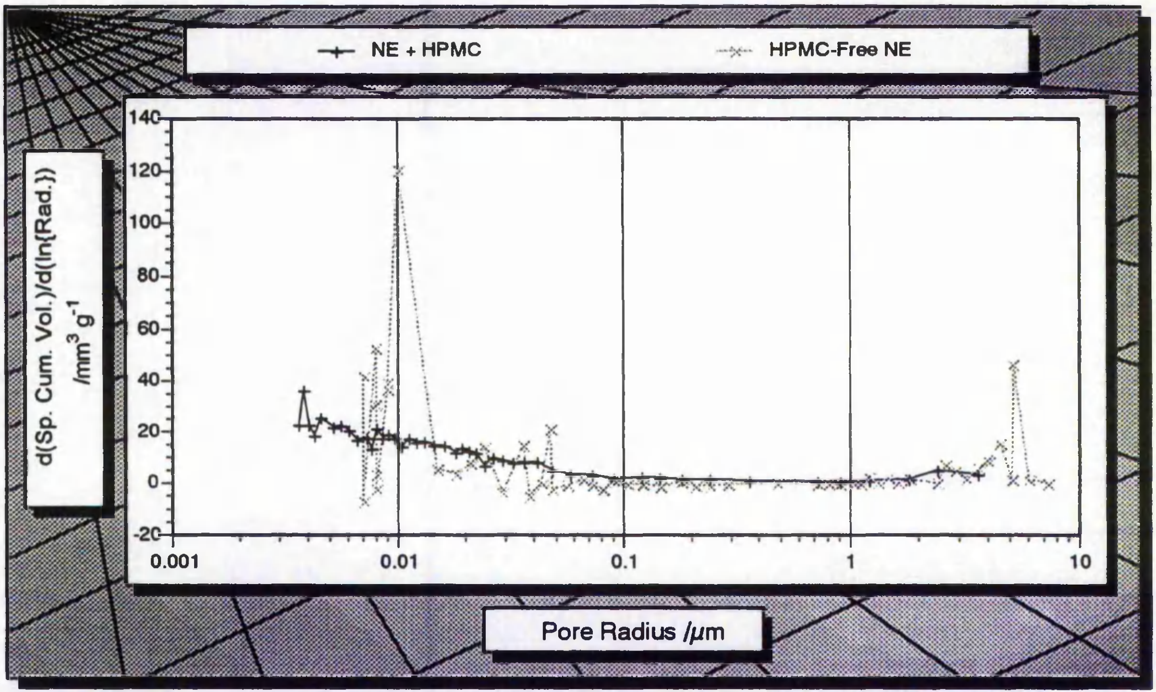

Figure 11.3 Pore radius distribution in a Eudragit® *NE* film leached of HPMC (25% per gram of polymer).

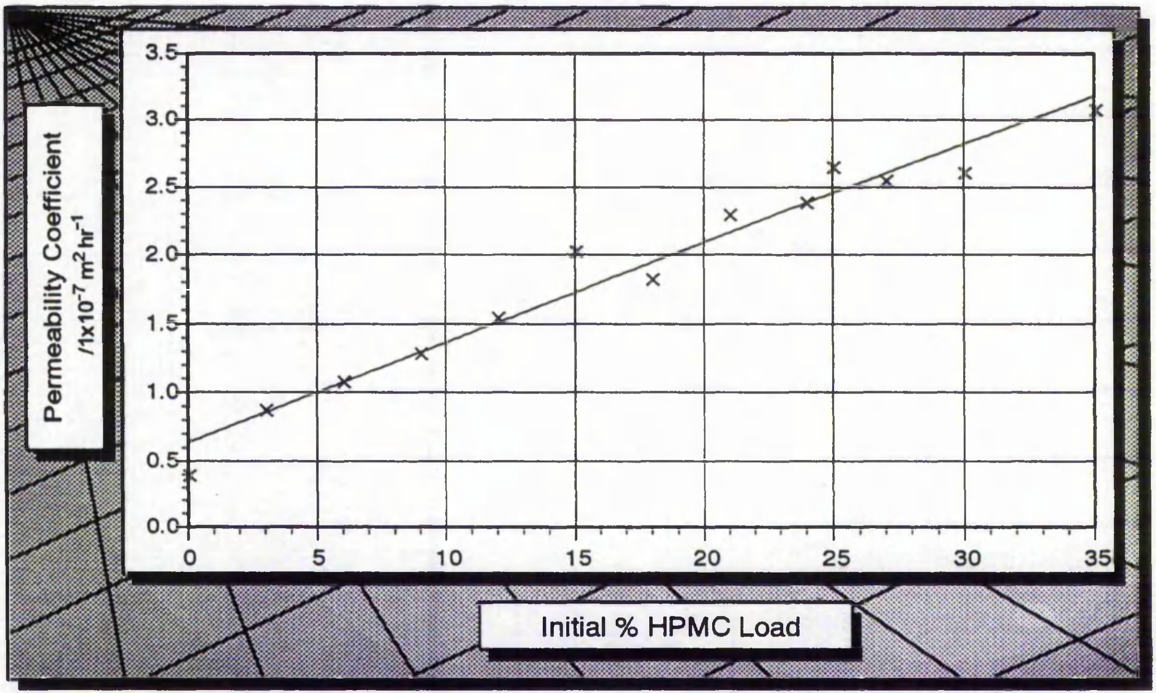

Figure 11.4 The apparent 4-nitrophenol permeability coefficients for Eudragit® *NE* films as a function of (initial) HPMC content.

leading to a change in the release mechanism: desorption by diffusion through the polymer changing to diffusion through pores. The mechanism would also appear to be changed as a result of depletion of the additive leading to an exponentially decaying release rate overall.

11.2.2.1 Pore distribution of Eudragit® *NE* films leached of HPMC.

The pore size distribution of a Eudragit® *NE* film leached of HPMC (96 hrs) and dried at 313 K (24 hrs), was determined using the technique of mercury porosimetry. Results are shown in **Figure 11.3**, together with the results for the HPMC-free film for comparison.

Like the Eudragit® *NE* films leached of sucrose, there is no evidence of the HPMC leaching process leading to a porous network in the Eudragit® *NE* polymer, and also like the sucrose leached film, the HPMC leached film appears to show less porosity (or possibly less compressible free-volume) than the HPMC-free film. From the HPMC leaching results, however, it would be expected that a fraction of the HPMC still resides within the film. The ability of the soft Eudragit® *NE* polymer to heal following leaching (as seen previously following sucrose leaching {Chapter 10}) is again seen to preclude lasting pore formation.

11.2.3 Solute permeability of Eudragit® *NE* films loaded with HPMC.

Solute permeability results have only been investigated for the film in the process of leaching its content of HPMC additive, and values of the apparent permeability coefficients have been calculated using the film thickness as cast.

11.2.3.1 The 4-nitrophenol permeability of Eudragit® *NE* + HPMC loaded films.

The effects on the permeability of a film due to the presence of HPMC may arise in a number of ways:

- ✗ dry, clustered HPMC (*i.e.*, a predominantly amorphous polymer) could be permeable to a solute to a greater or lesser extent, than the Eudragit® methacrylate-acrylate copolymer;
- ✗ trapped HPMC, which was observed to swell in an aqueous environment, could lead to aqueous pathways, through which the permeant may be expected to flow (diffuse) at a faster rate than through the polymer itself, due to reduced polymer density or plasticisation – allowing the polymer chains greater freedom of movement;
- ✗ aqueous leaching of the HPMC may lead to porosity of sufficient size to allow a convective solute permeant flux.

The apparent permeability coefficients for the transport of 4-nitrophenol through Eudragit® *NE* films loaded with different amounts of HPMC are tabulated in **Table 11.1**, and shown graphically in **Figure 11.4**. Again, like the effect of sucrose on film permeability, it is seen that there is an initial increase in apparent permeability coefficient that is in direct proportion (correlation coefficient, $r^2 = 0.96$) to the amount of HPMC added to the film, *i.e.*:

$$P \times 10^7 = 7.261 \times 10^{-2} C_{\% HPMC} + 0.638 \qquad (11.1)$$

The 'permeability enhancement coefficient' of 7.261×10^{-2} is only slightly greater than that calculated for sucrose (6.763×10^{-2}). The line of best fit for the HPMC results is, however,

Table 11.1 Apparent 4-nitrophenol permeability coefficients for Eudragit® *NE* films containing HPMC.

HPMC LOAD % (g.*NE*)$^{-1}$	APPARENT PERMEABILITY COEFFICIENT /1×10^{-7} m^2 hr^{-1}
0	0.400
3	0.877
6	1.08
9	1.29
12	1.55
15	2.03
18	1.83
21	2.30
24	2.39
25	2.65(±0.50)†
27	2.55
30	2.61
35	3.08

† Mean value ± s.d.

linear over a greater range of addition (than sucrose), appearing to fit the data up to a film content of 35%. However, the HPMC solubility (restricted by viscosity) limits the amount of HPMC in the latex such that at higher levels of addition, the latex possibly contains a less than expected load due to gelation of the HPMC (as opposed to dispersion in the latex).

The linear trend in permeability coefficient is apparent despite the aforementioned non-uniform swelling of the film. If the blister-like swellings were sufficiently accommodating to withhold their water/HPMC solution then the average thickness of polymer through which the penetrant diffuses, in the region of a swelling but independent of any aqueous pathways which result from HPMC leaching to a surface, must be approximately constant. Therefore whilst aqueous pathways would contribute to permeability enhancement, blister-like swellings would not (and apparently do not) enhance or reduce permeant diffusion to any great extent. In the region of a swelling the permeant is effectively travelling through parallel films which, despite the corresponding change in boundary conditions, do not greatly affect the standard deviations of the results for films loaded with identical quantities of HPMC.

HPMC had the greater effect (when compared to sucrose) on the apparent 4-nitrophenol permeability coefficient at loadings $\rangle$ 15 → 20% where the apparent permeability coefficient was of higher magnitude (*e.g.*, $\rangle \sim 2.6\times10^{-7}$ m^2 hr^{-1} at ca 25% HPMC; *cf.* $\approx 2.0\times10^{-7}$ m^2 hr^{-1} at ca 26% sucrose).

Table 11.2 Apparent 4-nitrophenol permeability coefficients for Eudragit® *NE* films leached of 25% HPMC (+ side difference phenomena).

FILM† ORIENTATION	$P_{l+residual\ HPMC}$‡ /1x10^{-7} m^2 hr^{-1}	P /1x10^{-7} m^2 hr^{-1}	$P_{l\ polymer}$‡ /1x10^{-7} m^2 hr^{-1}
SUBSTRATE	2.15(±0.004)	2.61(±0.007)	2.04(±0.003)
AIR	2.15(±0.007)	2.64(±0.014)	2.00(±0.006)

† Side of film (with reference to film casting) facing donor permeant.
‡ Determined using an estimated film thickness.

11.2.3.1.1 Eudragit® *NE* films leached of HPMC (& the effect of side difference).

The permeation of 4-nitrophenol through a Eudragit® *NE* film pre-leached (24 hrs) of 25% HPMC was investigated. To calculate an apparent permeability coefficient for the pre-leached film, the thickness of the polymer + residual HPMC should be used (*i.e.*, termed $P_{l+residual\ HPMC}$), to give a true comparison. However, because the amount of trapped HPMC was difficult to ascertain accurately (the results showed a decrease in the amount leached over extended {96 hr} leaching times {**Figure 11.1** and **Figure 11.2**}), then the permeability coefficient was difficult to determine. Values are therefore quoted for (i) $P_{l+residual\ HPMC}$ assuming 20% of the original HPMC[1] remained unleached in the film, together with (ii) the apparent permeability coefficients calculated from the initial film thickness (*P*), and (iii) the permeability coefficient calculated from the thickness of polymer alone ($P_{l\ polymer}$). The range between these sets of results presumably providing an estimate of the uncertainty in the quoted values. The orientation of the leached film, with respect to the donor permeant solution, was also investigated for evidence of a side-difference in permeability. Results are given in **Table 11.2**.

The data shows that the pre-leached and dried films did not exhibit a side dependence phenomena with respect to the 4-nitrophenol permeability. The apparent permeability coefficient results are, however, unexpectedly high since the $P_{l+residual\ HPMC}$ value is of the same magnitude as that found for a film leaching an initial load of ca 20% HPMC. Based on the gravimetric HPMC leaching results of **Figure 11.2**, the pre-leached film would be expected to retain some residual HPMC – which can presumably act to enhance the permeability of a film following a prior period of leaching and drying. However, only 20% → 25% residue of the original load is expected (implying a permeability coefficient comparable to an initial load of ca 6%): the anomaly presumably due to the non-uniform film swelling.

11.2.3.1.2 Arrhenius activation energy for 4-nitrophenol permeation.

The effect of temperature on the permeation of 4-nitrophenol through Eudragit® *NE* films loaded with 25% HPMC was investigated, and the results are shown in **Figure 11.5** in the form of an Arrhenius-type plot. The **activation energy**, as determined from the gradient of the line of best fit, was **10.67 kJ mol^{-1}** (which compares to 50.5 kJ mol^{-1} for the additive-free film, and 34.6 kJ mol^{-1} for a film containing 40% sucrose).

---

[1] Thickness of HPMC calculated (using method employed to calculate sucrose thickness in Chapter 10) assuming a HPMC density [392] of ca 1.3 g cm^{-3}.

Table 11.3 Variation in apparent 4-nitrophenol permeability coefficient of Eudragit® *NE* + HPMC (25%) loaded films, as a function of initial film thickness.

FILM THICKNESS /μm	APPARENT PERMEABILITY COEFFICIENT /1×10^{-7} m^2 hr^{-1}
65	2.68
95	2.31
124	2.35
149	2.29
180	2.00
MEAN APPARENT PERMEABILITY COEFFICIENT = 2.33(±0.24)	

11.2.3.1.3 The effect of initial film thickness on the 4-nitrophenol permeation through HPMC containing films.

The flux of 4-nitrophenol through Eudragit® *NE* films containing HPMC at a concentration of 25% per gram of polymer was found to be Fickian, with respect to film reciprocal thickness over the range of 69 μm → 180 μm, but there is less correlation between the permeant flux and film reciprocal thickness ($r^2 = 0.914$) than was shown for the HPMC-free film ($r^2 = 0.985$). The results are shown in **Figure 11.6** (the error bars indicating the typical 10% uncertainty in film thickness).

The mean value for the apparent 4-nitrophenol permeability coefficients was $2.33(\pm0.24)\times10^{-7}$ m^2 hr^{-1}. However, there were signs of a trend of decreasing apparent permeability coefficient with film thickness (**Table 11.3**). Assuming a porous or hydrated network was formed through the film due to either dissolution or swelling of the HPMC, then it is likely that the network contained a viscous solution of HPMC (*i.e.*, the gravimetric leaching results indicate the presence of residual HPMC in the leached films). When compared to a solely aqueous network, the viscosity of the HPMC solution would restrict the rate of diffusion of the 4-nitrophenol. This effect would be amplified in a thicker film since it would be slower to leach HPMC due to its viscosity impeding its own dissolution.

11.2.3.2 The permeation of anilines through Eudragit® *NE* + HPMC loaded films.

The permeation of the series of anilines of increasing side chain length through Eudragit® *NE* + HPMC is shown graphically in **Figure 11.7**, with the apparent permeability coefficients given in **Table 11.4**, together with the uptake of the anilines by the polymers. The apparent permeability coefficients were all greater than those of the HPMC-free film.

The apparent permeability coefficients are of the same order of magnitude as those for permeation through sucrose loaded Eudragit® *NE* films (Chapter 10). However, the individual results, for permeation through the HPMC loaded films vary – with some anilines showing a higher permeability, and some a lower permeability, than the comparable result for the sucrose loaded films. By comparing the mean and standard deviation of the results

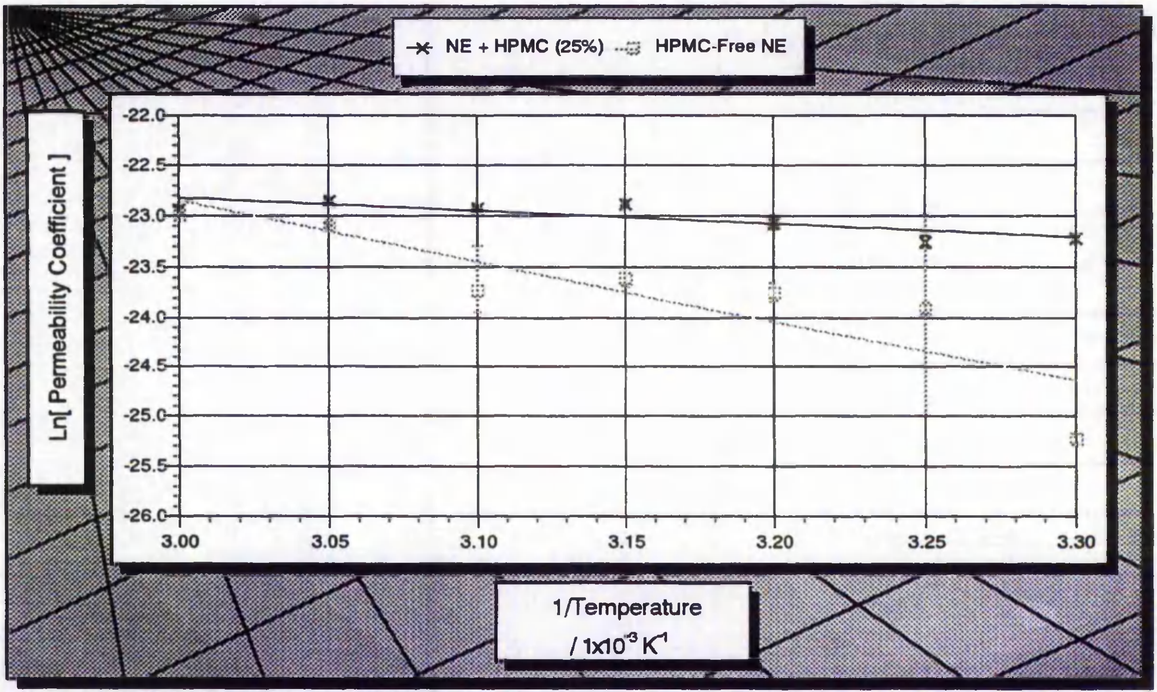

Figure 11.5 Arrhenius-type plots from the permeation of 4-nitrophenol through Eudragit® *NE* film containing 25% HPMC (and, for comparison, additive-free).

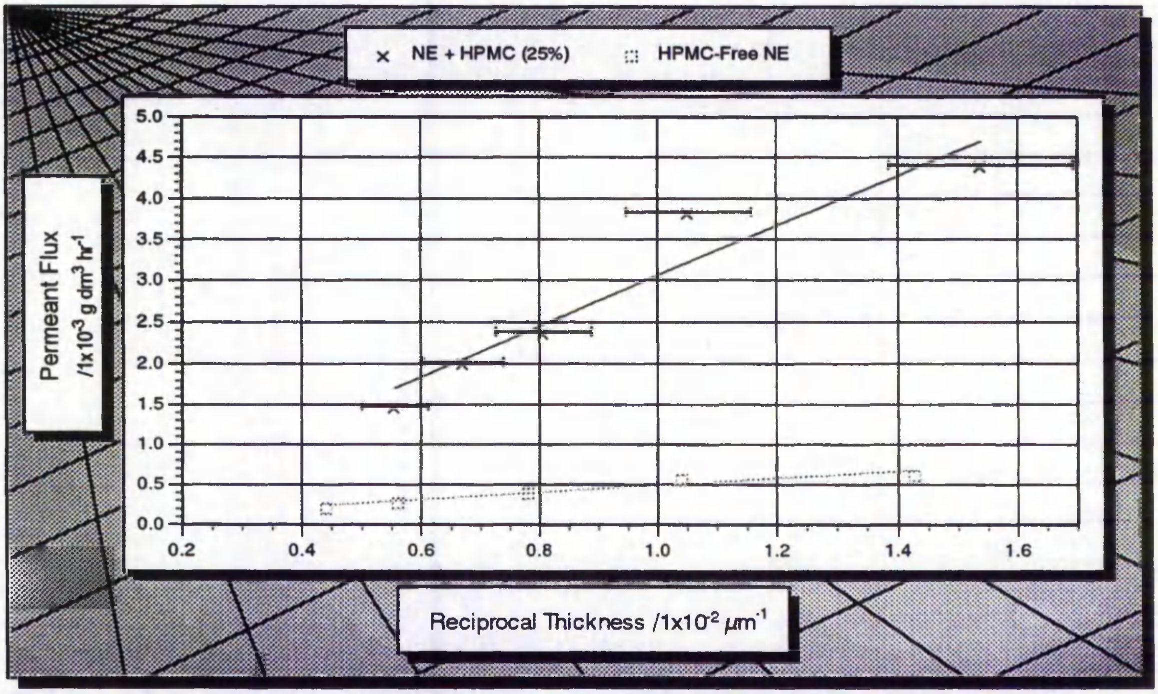

Figure 11.6 Fickian reciprocal thickness (initial film thickness) plot for the permeation of 4-nitrophenol through Eudragit® *NE* film + HPMC (25%).

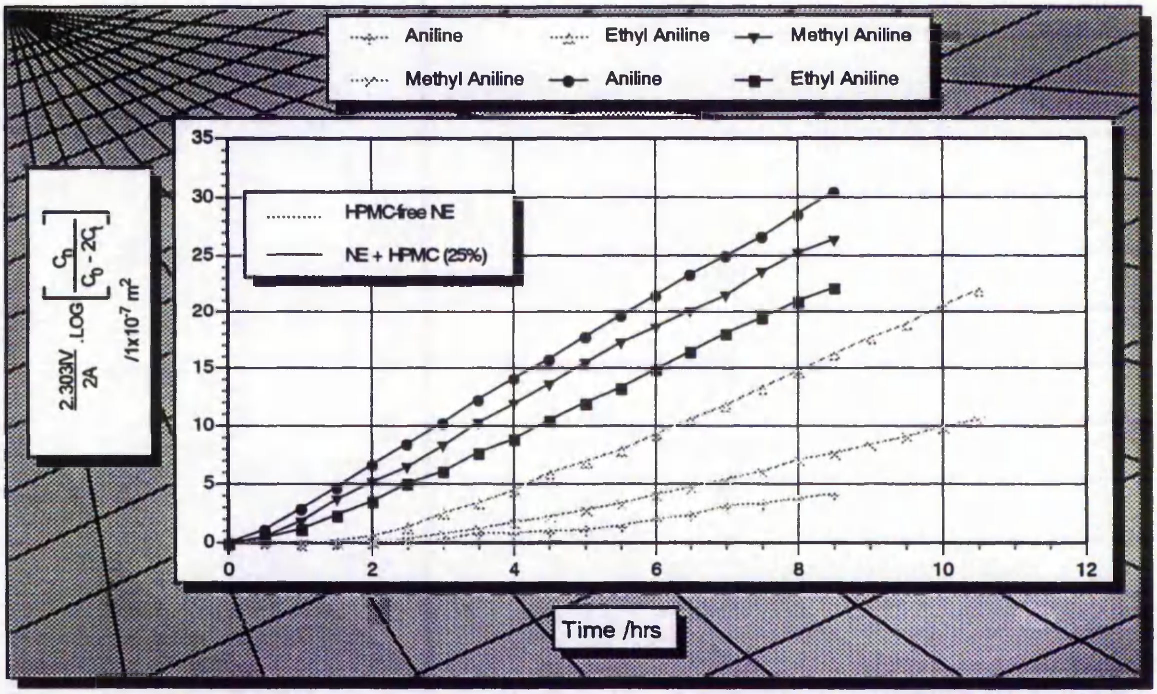

Figure 11.7 Plot for the calculation of aniline permeability through HPMC loaded (25%) Eudragit® *NE* films.

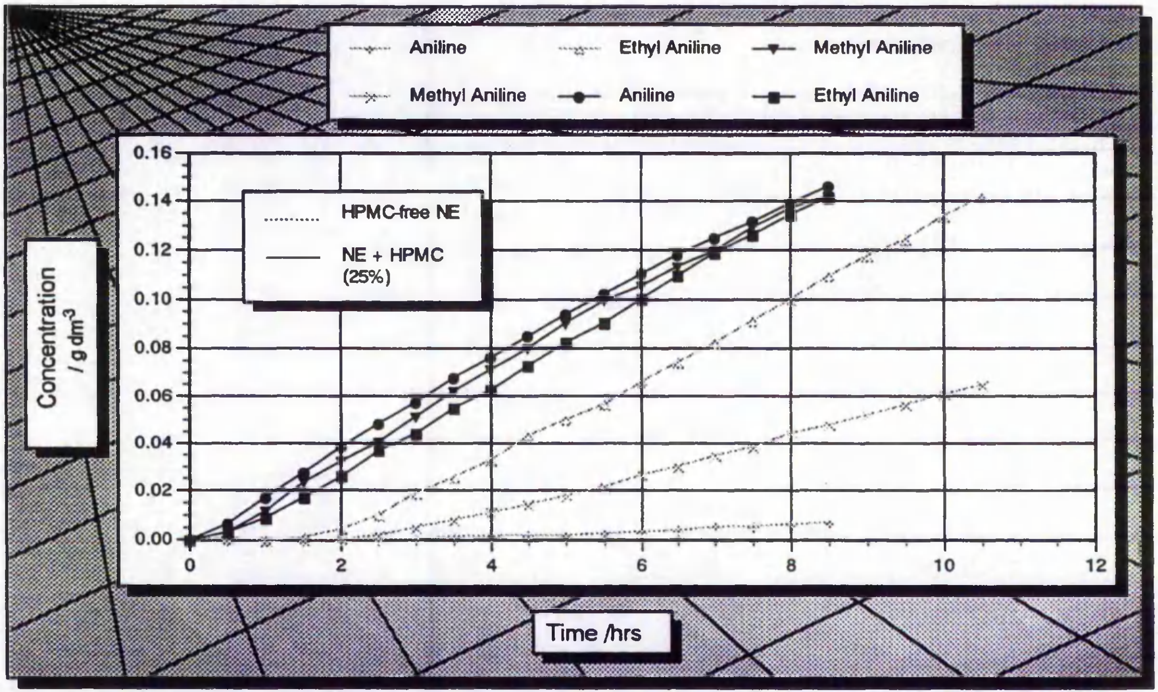

Figure 11.8 Increase in aniline concentration on the receiver side of Eudragit® *NE* films loaded with HPMC (25%).

Table 11.4 Apparent aniline permeability coefficients and equilibrium uptakes by Eudragit® *NE* films leaching HPMC.

ANILINE TYPE	APPARENT PERMEABILITY COEFFICIENT† /1x10^{-7} m^2 hr^{-1}	ANILINE UPTAKE‡ /g (g.film)$^{-1}$
ANILINE	3.66	0.0867
METHYL ANILINE	3.33	0.3526
ETHYL ANILINE	2.92	0.4773

† Films initially loaded with 25% HPMC.
‡ Uptakes calculated using initial (cast) film weight and therefore account for uptake by both the Eudragit® *NE* and HPMC. However, the initial load of HPMC was constant (20%) and the result is only used to show each aniline a exhibits different solubility.

for the permeation of aniline, methyl aniline, and ethyl aniline, then the sucrose loaded film exhibits a higher deviation ($3.80(\pm1.99)\times10^{-7}$ m^2 hr^{-1}) than does the HPMC loaded film ($3.30(\pm0.37)\times10^{-7}$ m^2 hr^{-1}). *I.e.*, the permeation of the three anilines through the HPMC loaded film is closer to that expected for a porous film, in which the molecular size and penetrant solubility (in the polymer) has less effect.

The similarity in the transport rates of the anilines through films of similar thickness is also apparent from the plot of the increase in permeant concentration measured on the receiver sides of the permeability cells during the permeation experiments (**Figure 11.8**). The comparable fluxes are indicative of their independence of aniline solubility (given that the solubility of the anilines does vary, as seen in **Table 11.4**) in the Eudragit® *NE* films. This feature of almost identical rates of change of concentration gradient was not apparent for the HPMC-free films (also shown on **Figure 11.8**), and was not evident for the films leaching sucrose (40%).

The values of the apparent 4-nitrophenol permeability coefficient may be used as a predictor of the occurrence of aniline transport by a convective diffusion mechanism. At 25% HPMC addition where coincident aniline transport rates do occur, the 4-nitrophenol permeability coefficient of Eudragit® *NE* was found to be ca 2.6×10^{-7} m^2 hr^{-1} (**Table 11.1**). This is of comparable magnitude to the 4-nitrophenol permeability coefficient of a Eudragit® *NE* film loaded with 80% sucrose. However, a 40% sucrose loaded Eudragit® *NE* film gave a 4-nitrophenol permeability coefficient of ca 2.1×10^{-7} m^2 hr^{-1}, and such films did not exhibit convective aniline transport. It therefore might be expected that the anilines would not permeate an HPMC loaded film by a convective mechanism when the 4-nitrophenol permeability coefficient was $<2.1\times10^{-7}$ m^2 hr^{-1}. Hence, (from the data in **Table 11.1**) a Eudragit® *NE* film containing $\leq$ 20% HPMC would be expected to transport the anilines by a (predominantly) solution-diffusion mechanism, as opposed to a convective mechanism.

11.2.4 Water vapour permeability of Eudragit® *NE* + HPMC loaded films.

The apparent water vapour permeability coefficients of Eudragit® *NE* films containing 25% HPMC were of similar magnitude to those observed for the sucrose containing films – being slightly greater than the results for the HPMC-free films. This might be expected [29]

Table 11.5 Apparent water vapour permeability coefficients for Eudragit® *NE* films, either containing or leached of HPMC (25%).

FILM ORIENTATION	PERMEABILITY COEFFICIENT /1×10^{-6} g hr^{-1} cm^{-1} $cm.Hg^{-1}$	S.D. /1×10^{-6} g hr^{-1} cm^{-1} $cm.Hg^{-1}$
UNLEACHED		
SUBSTRATE	2.03	±0.16
PRE-LEACHED		
SUBSTRATE	1.85†	±0.05
AIR	1.97†	±0.11

† $P_{l+residual\ HPMC}$ as determined using experimentally measured film thickness.

due to the increased polar nature which resulted from the cellulosic polymer. Results are given in **Table 11.5**, for both unleached and leached films. The effects of any difference in permeability coefficient resulting from the differing sides of the films (*i.e.*, substrate or air side with reference to casting) is lost in the experimental uncertainty.

11.2.5 Carbon dioxide permeability of Eudragit® *NE* + HPMC loaded films.

The **apparent CO_2 permeability coefficient of Eudragit® *NE* films containing 25% HPMC was determined as 1.37×10^{-9} g.p.u[1].** This is lower than the values for the HPMC-free film, and is indicative of a reduced diffusivity/solubility of CO_2 in the HPMC-loaded film, compared to the Eudragit® *NE* polymer alone. It is, however, more surprising that the value is lower than that found for the sucrose-containing film. The result appearing to indicate that the tortuosity in the path through the sucrose-containing film (assuming that the sucrose forms impermeable clusters) provides less hinderance than the HPMC. The higher molecular weight HPMC could, however, require a greater cooperative polymer chain segmental motion (than the smaller sucrose molecule which presents a simple barrier) in the surrounding Eudragit® polymer (and HPMC) to provide a diffusional path.

11.3 Eudragit® *L 30 D* as a film additive.

Eudragit® *L* differed from the other film additives investigated in that it is itself a latex (see Chapter 6) and is of comparable particle size to the latex from which the additive-free film is formed (*i.e.*, 130.7 nm for Eudragit® *L*; *cf.* 163.0 nm for Eudragit® *NE*, by P.C.S.).

Because the Eudragit® *L* is not in solution when the film is formed (*i.e.*, the pH is below 5.5), mixing (see Chapter 7) of the two latices (both at 5% solids content) causes a significant dilution of the Eudragit® *NE* (although the total polymer solids content remains at 5%). For example, whilst casting a film from a fixed volume of latex prepared from a 1:1 mix of Eudragits® *NE* and *L* should yield a film of comparable thickness to a film prepared from either of the two types of latex used individually, the thickness of Eudragits® *NE* would be ca 50% of that for a film cast using one of the other additives utilised in this study.

---

[1] g.p.u. = gas permeability coefficient units = cm^3 cm s^{-1} cm^{-2} $cm.Hg^{-1}$.

11.3.1 Film structure.

11.3.1.1 Structure of Eudragit® *NE* films, either containing or leached of Eudragit® *L*.

Mixed Eudragit® *NE* and *L* films were transparent, and more brittle than the Eudragit® *L*-free Eudragit® *NE* films due to the high T_g of the Eudragit® *L*[1] which was used (in the mixed polymer film) plasticiser-free. The brittleness of the film therefore increased with increasing proportion of Eudragit® *L*: the film eventually fracturing under the stress due to contraction (combined with adhesion to the casting substrate) on drying at the highest levels of addition (> 180%).

Plate 11.1 to **Plate 11.4** show the upper and lower faces, and the fracture cross-sections[2], of mixed Eudragit® *NE*-Eudragit® *L* (1:1 ratio, *i.e.*, 100% Eudragit® *L* per gram of Eudragit® *NE*) films. There was no particulate (crystalline-like) close-packed structure present in the films after coalescence. (NB. The code on **Plate 11.2** proclaims the plate to depict an upper film surface. However, the code represents the orientation by which the film was presented to the micrographer, who then aligned the film, to that described in the Plate's label, before the micrograph was taken. It is, in fact, the polymer-substrate side of the film.) Both the upper and lower faces of the film were similar, although small 'pin-holes' were evident in the lower polymer-substrate face. It is presumed that the pattern on the film surface is evidence of hard Eudragit® *L* polymer particles randomly distributed in a well-coalesced matrix of the softer Eudragit® *NE* polymer.

The fracture cross-sections (**Plate 11.3** and **Plate 11.4**) show unstructured particle packing (*i.e.*, no hexagonal close packed particles), again showing what appear to be pinholes. It is possible that the structure is simply a result of the hard particles being embedded in the soft polymer (typically hard polymer particles would show a hexagonal close packed crystal-like structure): their packing being disrupted by the ability of the softer polymer to 'flow' between them (albeit insufficiently to fill the pinholes); or is possibly a result of the incompatibility between the two polymer types (*i.e.*, stability would have been reduced by the change in pH necessary to mix the two polymers {see Chapter 7}, such that the latices would be more easily coagulated as the water evaporated during casting and the particles were brought into closer contact).

Carboxylated Eudragit® *L* dissolves in neutral to alkaline conditions (at pH > 5.5), forming polymeric salts. Eudragit® *NE* is non-ionic and, hence, pH independent with respect to its dissolution (and transport) properties [147]. It is therefore possible to dissolve the Eudragit® *L* polymer out of the mixed polymer film, using a solution of suitable pH.

Eudragit® *NE* was found to gel and dissolve in toluene (dissolution is slow due to the high molecular weight), whereas Eudragit® *L* showed little or no tendency to dissolve in toluene, and remained unchanged in appearance. A Eudragit® *NE* film soaked in toluene remained relatively intact, but deformed quite markedly and dissolved sufficiently for it to become detached from the casting substrate.

---

[1] T_g of Eudragit® *L* = 303 K [313]; T_g of Eudragit® *NE* = 265 K [204].
[2] All fractures were performed under liquid nitrogen.

Plate 11.1 (203210) S.E.M. of the upper side (polymer-air interface) of a Eudragit® *NE* + Eudragit® *L* (1:1) film.

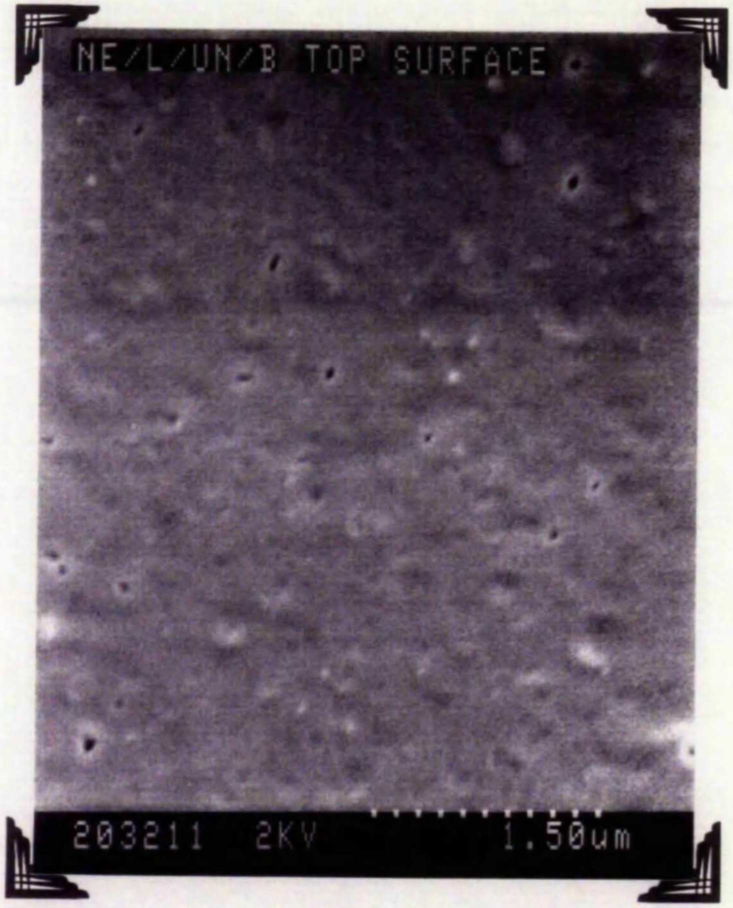

Plate 11.2 (203211) S.E.M. of the lower side (polymer-substrate interface) of a Eudragit® *NE* + Eudragit® *L* (1:1) film.

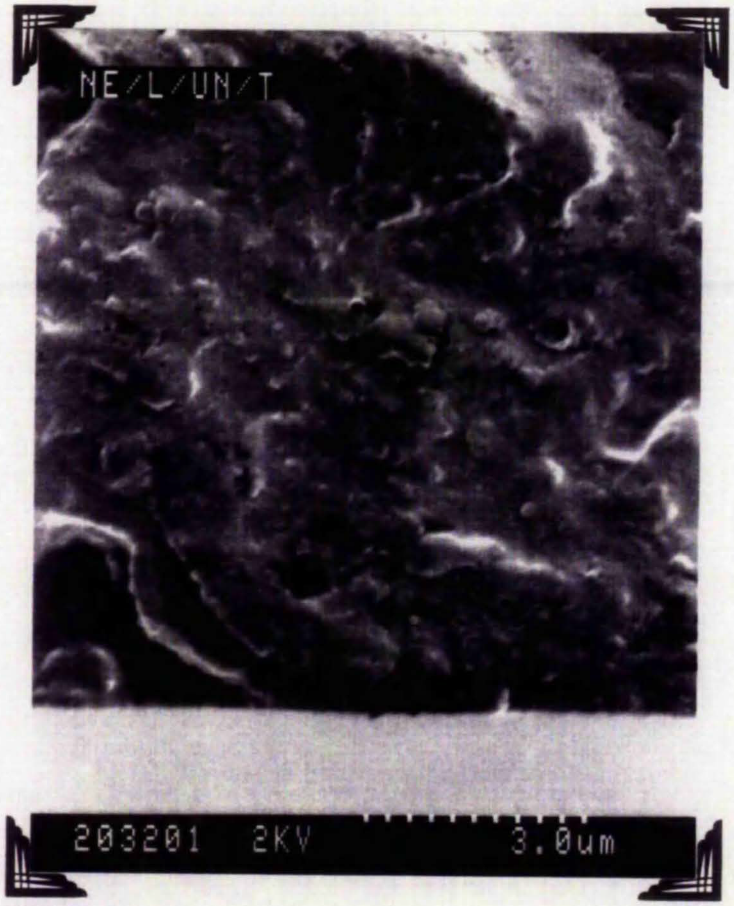

Plate 11.3 (203201) S.E.M. of the fracture cross-section of a 1:1 *NE* + *L* film.

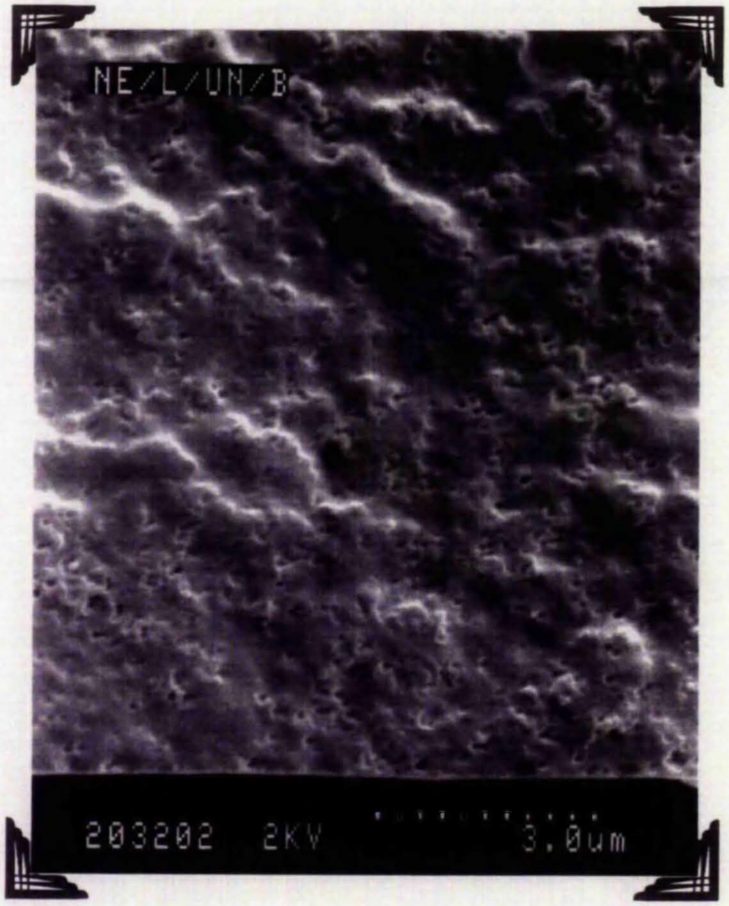

Plate 11.4 (203202) S.E.M. of the fracture cross-section of a 1:1 *NE* + *L* film.

Plate 11.5 (202917) S.E.M. of the upper side (polymer-air interface) of a Eudragit® *NE* + *L* (1:1) film leached in buffer.

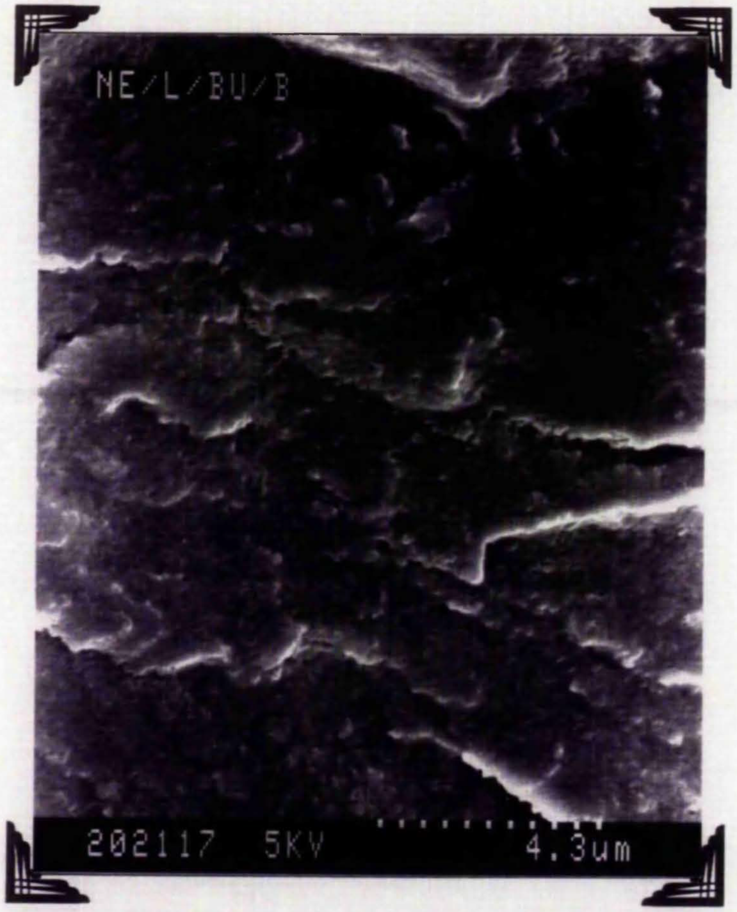

Plate 11.6 (202117) S.E.M. of the fracture cross-section of a Eudragit® *NE* + *L* (1:1) film leached in buffer.

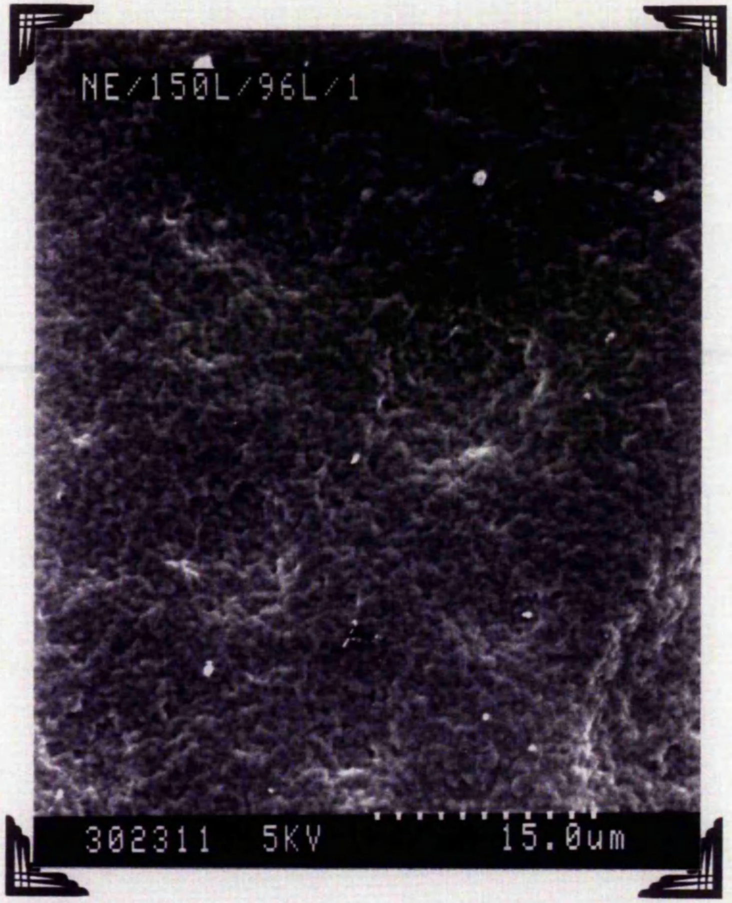

Plate 11.7 (302311) S.E.M. of the upper side (polymer-air interface) of a Eudragit® *NE* + *L* (2:3 or 150%) film leached in buffer.

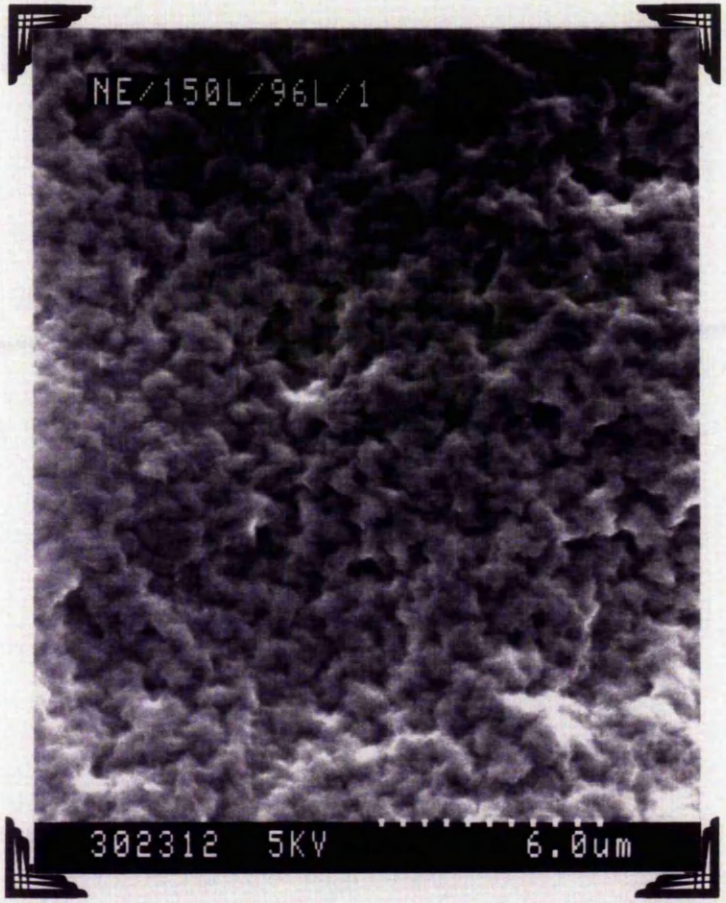

Plate 11.8 (302312) S.E.M. of the upper side (polymer-air interface) of a Eudragit® *NE* + *L* (2:3) film leached in buffer.

Plate 11.9 (302313) S.E.M. of the upper side (polymer-air interface) of a Eudragit® *NE* + *L* (2:3) film leached in buffer.

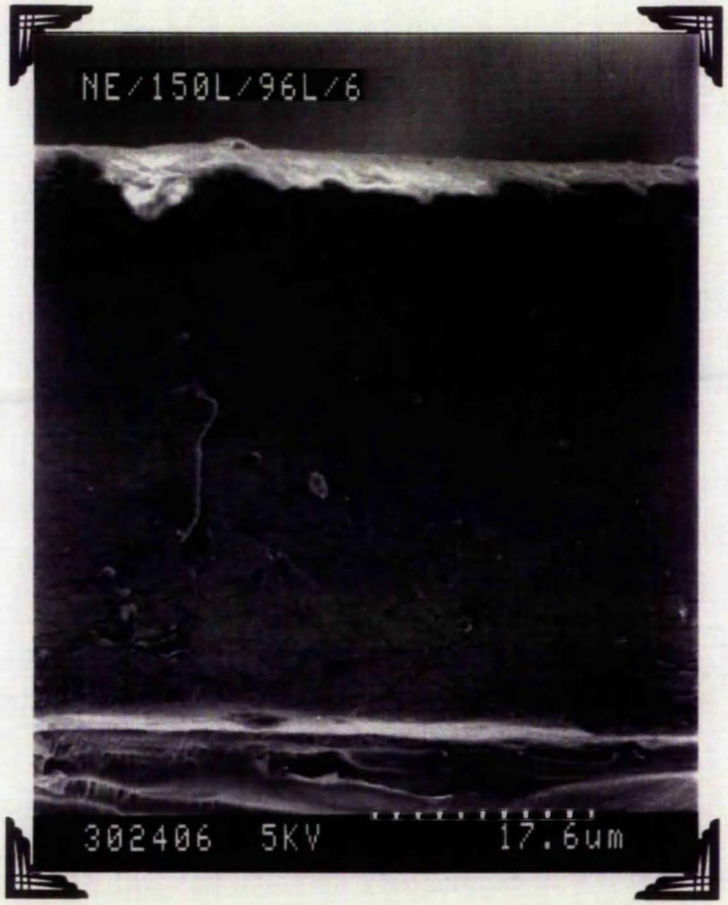

Plate 11.10 (302406) S.E.M. of the fracture cross-section of a Eudragit® *NE* + *L* (2:3) film leached in buffer.

Plate 11.11 (302410) S.E.M. of the near-upper surface fracture cross-section of a Eudragit® *NE + L* (2:3) film leached in buffer.

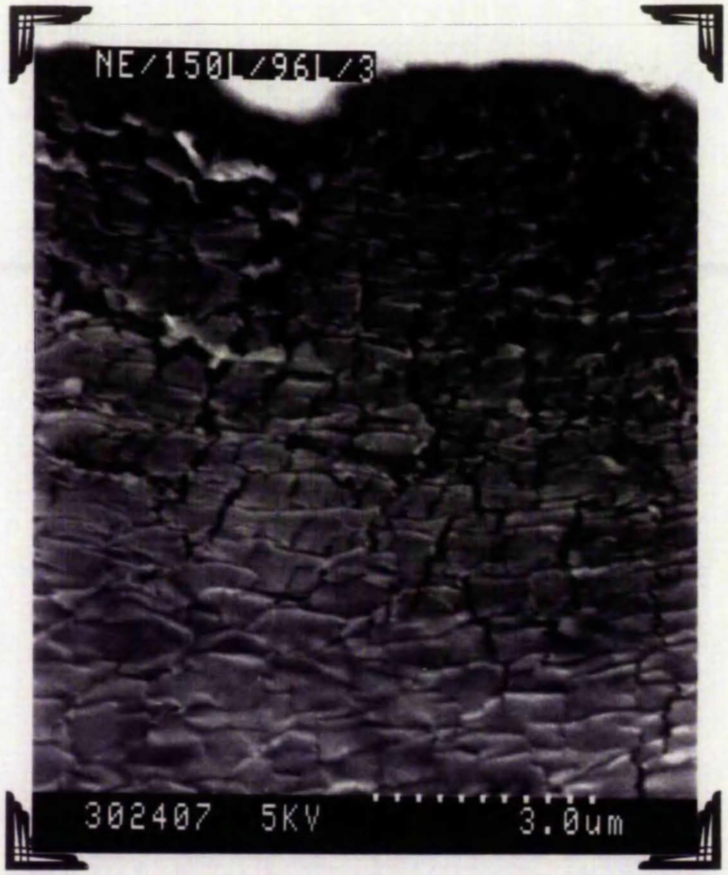

Plate 11.12 (302407) S.E.M. of the near-upper surface fracture cross-section of a Eudragit® *NE + L* (2:3) film leached in buffer.

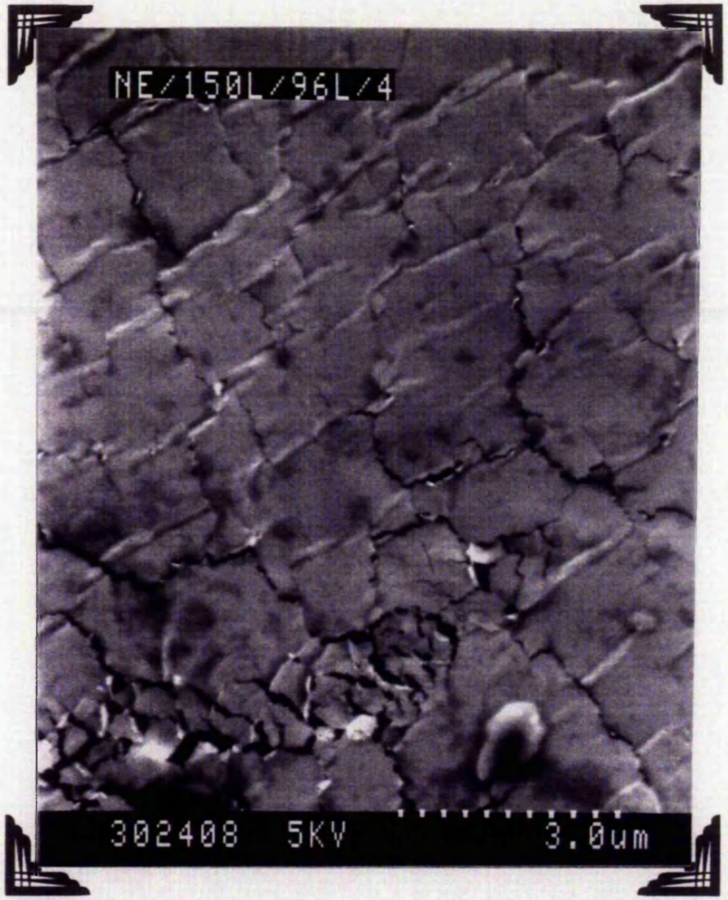

Plate 11.13 (302408) S.E.M. of the near-centre section fracture cross-section of a Eudragit® *NE* + *L* (2:3) film leached in buffer.

Plate 11.14 (302409) S.E.M. of the near-lower surface fracture cross-section of a Eudragit® *NE* + *L* (2:3) film leached in buffer.

The ability to leach either type of polymer, with their differing T_g's (which span ambient temperature) permits the effect of polymer T_g and leaching (porosity) to be observed

11.3.1.1.1 Films leached in buffer.

On soaking a mixed polymer film (1:1 ratio of Eudragit® *NE* : *L* polymers) in buffer (pH 6), the film swelled and appeared white and opaque (as did the Eudragit® *L*-free Eudragit® *NE* film). On drying, the film returned to being transparent, and remained flexible in the manner of a low T_g polymer.

Whilst the film was wet, it was sometimes possible to peel the film into two layers and this was initially ascribed to stratification of the two polymer types. However, such stratification was not apparent in the S.E.M.s of the leached or unleached films. **Plate 11.5** shows the polymer-air surface of a Eudragit® *NE*/Eudragit® *L* film (1:1 polymer ratio) leached in buffer for 96 hrs. Comparison with the plate of the equivalent unleached film (**Plate 11.1**) reveals little visual difference. The same is not true, however, for the fracture cross-section: *e.g.*, **Plate 11.6** (*cf.* **Plate 11.3** and **Plate 11.4**), where the leached film appears to have a less grainy appearance – possibly due to loss of the harder particles.

Possible reasons for the lack of difference in surface features may include the inability of the buffer to fully leach the Eudragit® *L* (note that the surface pattern previously ascribed to being due to the presence of hard Eudragit® *L* particles is still present), or the ability of the soft Eudragit® *NE* polymer to 'heal' the particulate sized holes that would result from the leaching of the Eudragit® *L*. However, the former reason is unlikely, based on gravimetric evidence (paragraph 11.3.2), and film healing due to polymer flow would presumably remove all surface features. Further evidence of Eudragit® *NE* film structure was, however, forthcoming from leached films prepared from a mixture of 2 parts Eudragit® *NE* to 3 parts Eudragit® *L* (*i.e.*, 150% Eudragit® *L* per gram of Eudragit® *NE*).

Plate 11.7 to **Plate 11.9** show the upper film surfaces of a buffer leached film at a range of increasing magnifications. These films show the effect of leaching to a far greater extent than the films prepared from the polymers mixed to a 1:1 ratio. Knowing that the buffer leaches only the Eudragit® *L*, it is interesting to see that the film, after leaching, shows the vestiges of the latex particles, albeit deformed from their original spherical shape. This is a feature not previously seen either in the additive-free or leached ex-sucrose-containing Eudragit® *NE* films. The implication of this structure is that the Eudragit® *L* was well dispersed within the Eudragit® *NE*, and that the harder Eudragit® *L* polymer limits the extent to which deformation of the Eudragit® *NE* latex particles can occur.

The fracture cross-section of the Eudragit® *NE* + Eudragit® *L* (2:3) polymer film does not, however, show such particulate detail (**Plate 11.10** to **Plate 11.14**). Different regions of the cross-section showed different structure, with part of the film appearing greatly cracked, whereas other regions were virtually featureless. **Plate 11.11** and **Plate 11.12** both show regions of the cross-section close to the upper surface (polymer-air interface) of the film, and are obviously quite different. This effect (*i.e.*, variation in structure) was also observed in the centre of the cross-section, and also in the cross-section near the bottom surface of the film (although only the cracked regions are shown here: **Plate 11.13** and **Plate 11.14** show the centre and bottom, respectively). The cracked regions of film may be purely an artefact of the fracturing technique, but it is also possible that they were regions of residual concentrations of the hard Eudragit® *L* (re: the rifts which occur in PBMA + Eudragit® *L* loaded films discussed in paragraph 11.3.1.2), which could not withstand the stresses of drying after leaching.

A further detail to note (that is apparent in **Plate 11.10**) is the film thickness. The film, as cast would be expected to be approximately 100(±10) μm thick, and yet the plate shows a film that is only approximately 40 → 45 μm thick. This is evidence that a fraction of the film (*i.e.*, approximately 60 → 65%) is lost (compatible with a possible loss of 60% for a film prepared from Eudragit® *NE* + 150% Eudragit® *L* (*i.e.*, 2:3)). This presumably illustrates the loss of structure from the interior of the film: the soft Eudragit® *NE* polymer having 'collapsed' in on itself, and coalesced ('healed').

11.3.1.1.2 Films leached in toluene.

Mixed Eudragit® *NE* and Eudragit® *L* (1:1 ratio) films remained transparent when soaked in toluene, unlike those films soaked in buffer. However, on drying the films rapidly turned white and opaque (⟨ 1 min), and remained opaque even after 96 hrs under vacuum at a temperature of 313 K: indicating that the film was not simply swollen with toluene. The opacity differed from that of a wet film (which was more translucent than opaque), being a more brilliant white, and having a smooth matt finish as opposed to a glossy wet-look finish which allowed some light transmittance.

Addition of a drop of buffer (pH 4 → 6) made the film transparent (after drying). Films soaked for a further 96 hrs in buffer (pH 6), after having been leached in toluene did not disintegrate, however, implying that sufficient Eudragit® *NE* remained to give the film a degree of structural integrity.

The opaque films leached in toluene were very brittle and became transparent on soaking in water. Re-soaking the film in toluene failed to redeem the dry opacity. Assuming that the aforementioned residual Eudragit® *NE* partially dissolved in the toluene, perhaps giving a gel, it would film form on drying in the manner of a solvent cast film, possibly coating the Eudragit® *L* particles, and preventing these dissolving in buffer (or at least preventing the escape of the dissolved *L* such that the particles were, in effect, 'reformed' on drying).

Fracture cross-sections of a film leached in toluene are shown in **Plate 11.15** and **Plate 11.16**. (NB. The 'B' and 'T' in the film code are irrelevant in the case of the cross-sections.) **Plate 11.17** and **Plate 11.18** show higher magnification shots of the film in **Plate 11.16** whereas **Plate 11.19** and **Plate 11.20** show that in **Plate 11.15**. It was previously shown for the buffer leached film, that the film thickness was less than expected, attributed to contraction of the Eudragit® *NE* polymer, following leaching, during drying. **Plate 11.15** shows a film which is presumably predominantly Eudragit® *L*, and which is approximately 98 μm thick, *i.e.*, close to the expected thickness as cast. This would therefore seem to uphold the idea that a hard polymer is better able to sustain a porous structure, compared to a soft polymer.

Plate 11.17 to **Plate 11.20**, which are of the film interior, reveal a highly porous structure. Pores are also visible on the film surface and, hence, the possibility that they form a continuous network of cross-connected channels through the film must be considered. **Plate 11.21** and **Plate 11.22** show the polymer-air interface at two different magnifications. The Eudragit® *NE* latex particles were 163 nm (P.C.S. z-average size), with low polydispersity (see Chapter 8). However, there are a number of reasons for the range of pore sizes seen in the film: *e.g.*, i, the degree of particle deformation; ii, the full diameter of the particles not necessarily being visible at the surface; iii, 'healing' of the polymer; iv, more than one particle lost. The pores visible in **Plate 11.22** are ca 83 nm for what appear to be holes resultant from single particles, which is less than the Eudragit® *NE* particle size. It is evident from the shape of the pores, however, that in some cases, multiple nearest neighbour particles have been leached.

Plate 11.23 and **Plate 11.24** show the lower face of the 1:1 ratio Eudragit® *NE* + Eudragit® *L* film which has been leached in toluene. The lower face appears very similar to the upper face (**Plate 11.21** and **Plate 11.22**), as may be expected if the two latices are homogeneously mixed.

11.3.1.2 Structure of PBMA films, either containing or leached of Eudragit® *L*.

Eudragit® *NE* mixed with Eudragit® *L* provided an example of a mixture of a soft polymer and a hard polymer, and showed their ability or inability to retain porosity after leaching one or other of the polymer types. Mixing Eudragit® *L* into PBMA, with its T_g of approximately 303 K[567], is therefore an example of mixing two hard polymers.

Plate 11.25 to **Plate 11.32** show a film of 1:1 ratio PBMA + Eudragit® *L* (*i.e.*, 100% Eudragit® *L* per gram of PBMA) leached of Eudragit® *L* in buffer pH 6 for 96 hrs, and dried. Micrographs of increasing magnification of the upper film surface are shown in **Plate 11.25** to **Plate 11.28**. It is immediately obvious that the film structure differs to that of the Eudragit® *NE* and Eudragit® *L* film. Whereas the latter tended to show porosity due to individually leached particles, the porosity in the PBMA and Eudragit® *L* appears to be in the form of large rifts, which separate islands of layered, close packed PBMA particles. Looking inside the rifts, the degree of porosity appears similar to that seen in the cross-sections of the Eudragit® *NE* + Eudragit® *L* films, with sufficient number of (PBMA) latex particles bridging the rifts to give the film some structural integrity.

Plate 11.29 shows the leached film in cross-section, whilst the upper, centre, and lower regions of this cross-section are shown at higher magnification in **Plate 11.30**, **Plate 11.31**, and **Plate 11.32**, respectively. These films were leached whilst still attached to the glass casting substrate, due to their very brittle nature. However, the three regions of the cross-section appear to show a uniform degree of Eudragit® *L* having been leached. Nowhere in the film's interior were there regions showing the close packed particle structure found on the film's surface, implying that the surface is covered by a non-continuous skin.

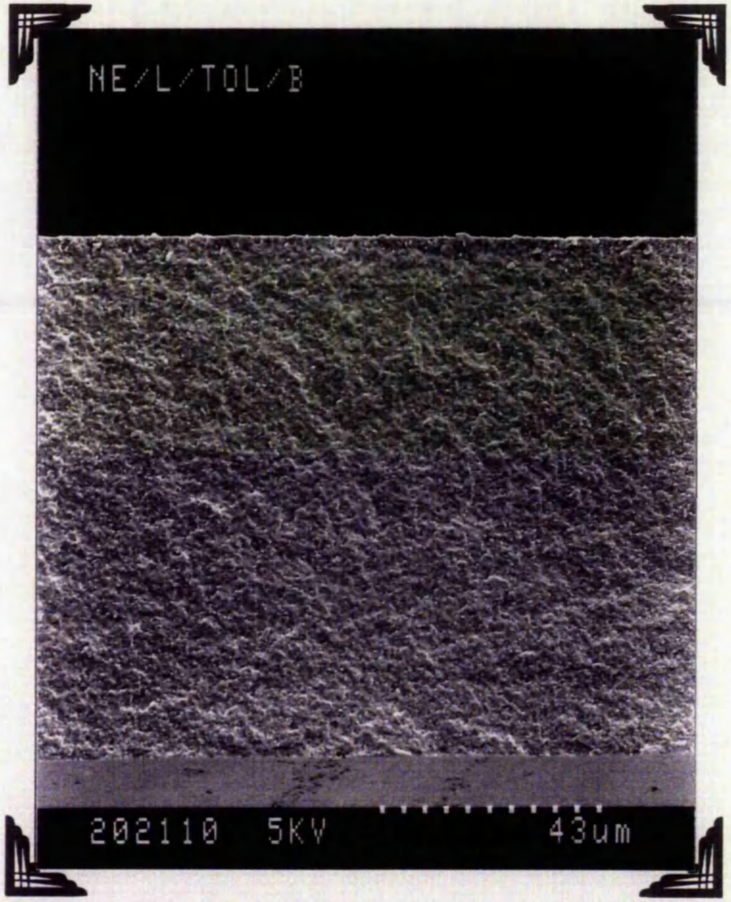

Plate 11.15 (202110) S.E.M. of the full thickness fracture cross-section of a Eudragit® *NE* + *L* (1:1) film leached in toluene.

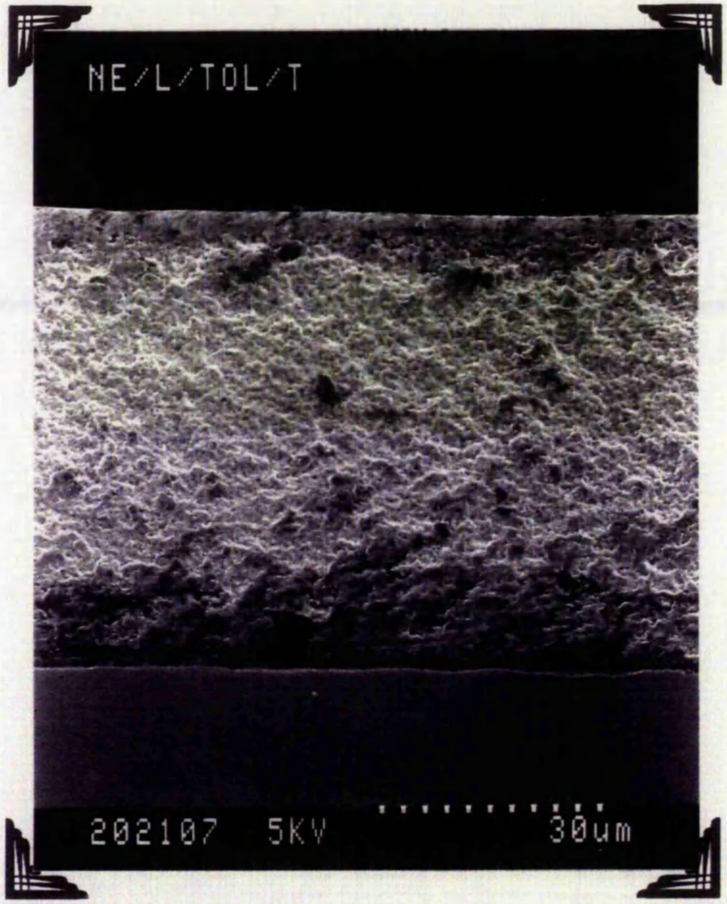

Plate 11.16 (202107) S.E.M. of the full thickness fracture cross-section of a Eudragit® *NE* + *L* (1:1) film leached in toluene.

Plate 11.17 (202108) S.E.M. of the fracture cross-section of a Eudragit® *NE* + *L* (1:1) film leached in toluene.

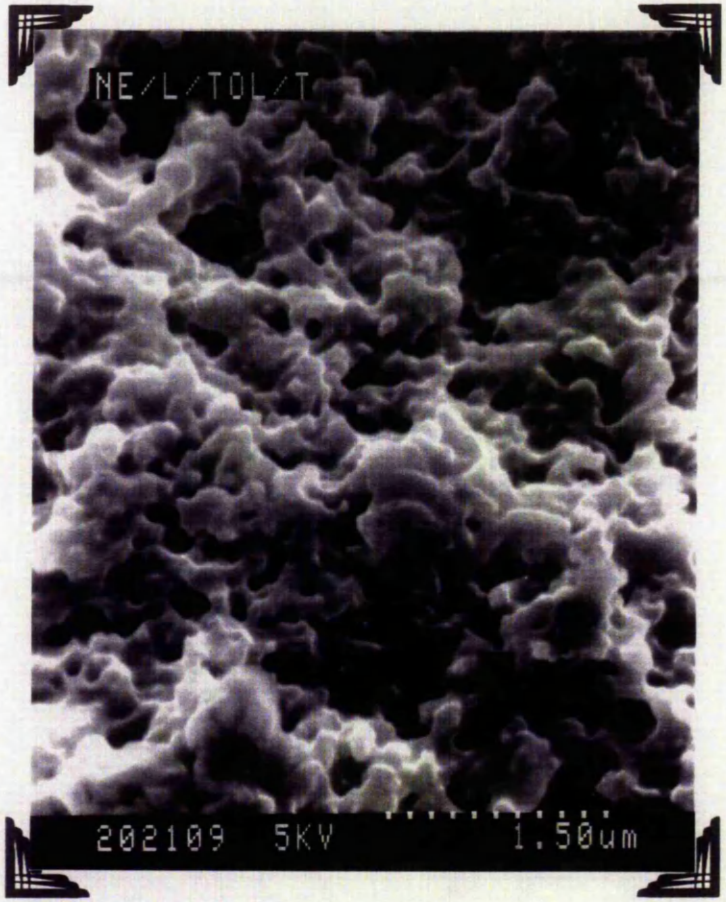

Plate 11.18 (202109) S.E.M. of the fracture cross-section of a Eudragit® *NE* + *L* (1:1) film leached in toluene.

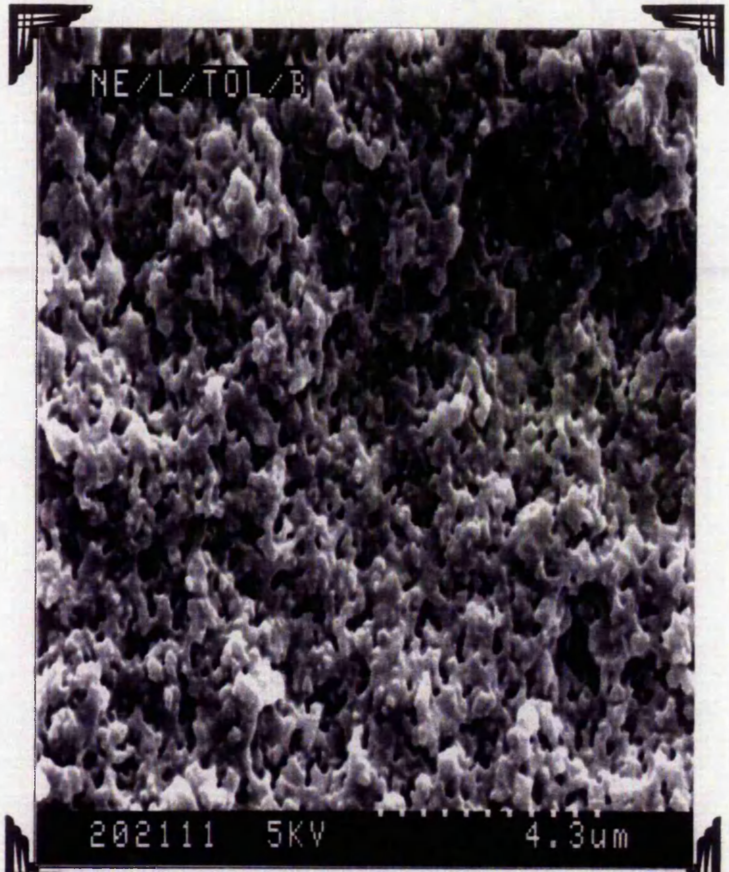

Plate 11.19 (202111) S.E.M. of the fracture cross-section of a Eudragit® *NE* + *L* (1:1) film leached in toluene.

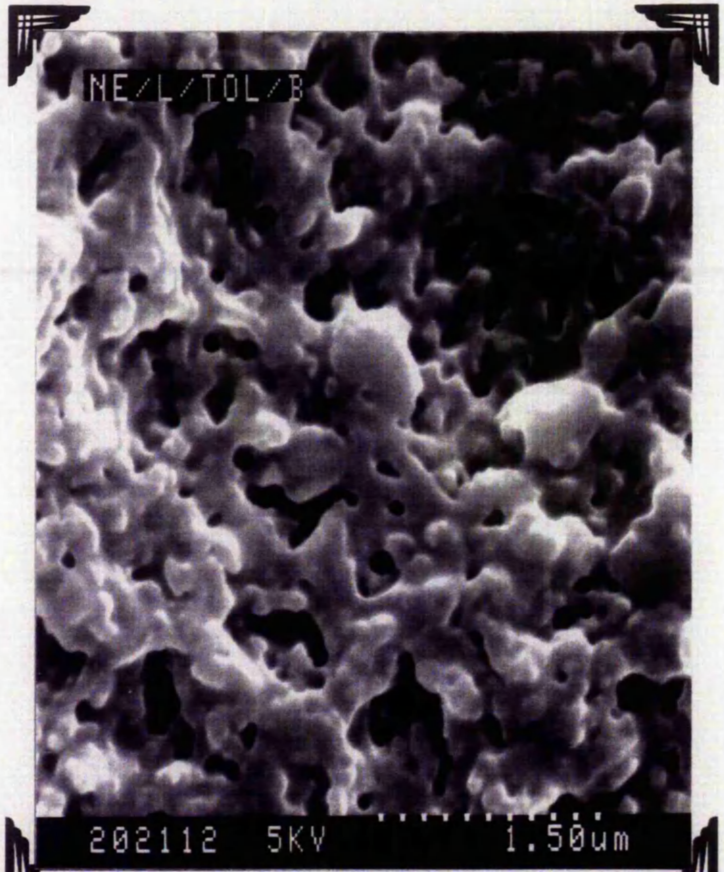

Plate 11.20 (202112) S.E.M. of the fracture cross-section of a Eudragit® *NE* + *L* (1:1) film leached in toluene.

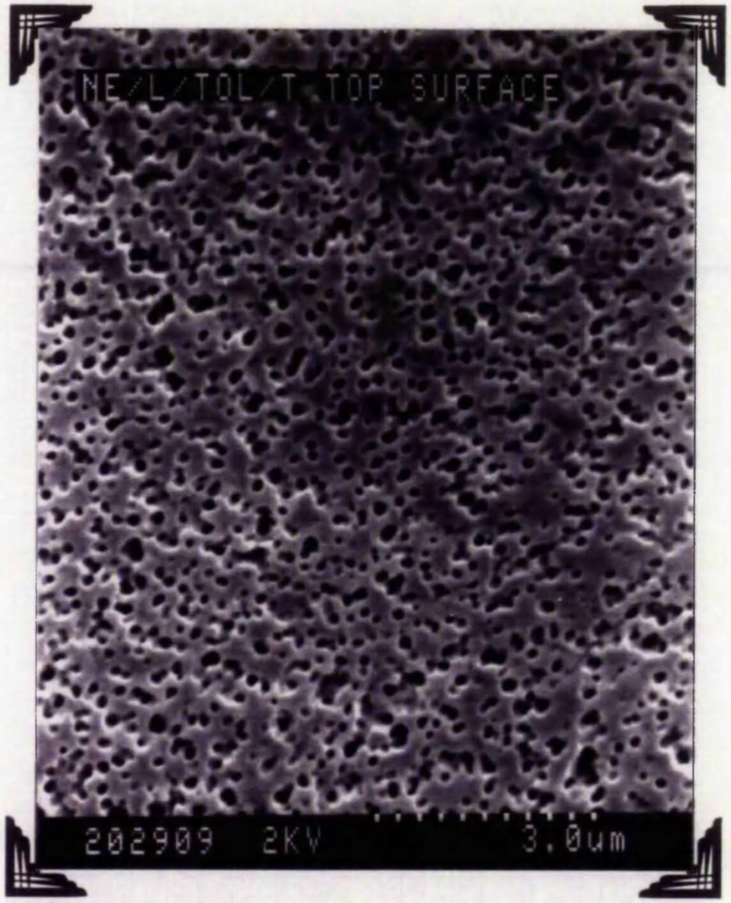

Plate 11.21 (202909) S.E.M. of the top surface (polymer-air interface) of a Eudragit® *NE* + *L* (1:1) film leached in toluene.

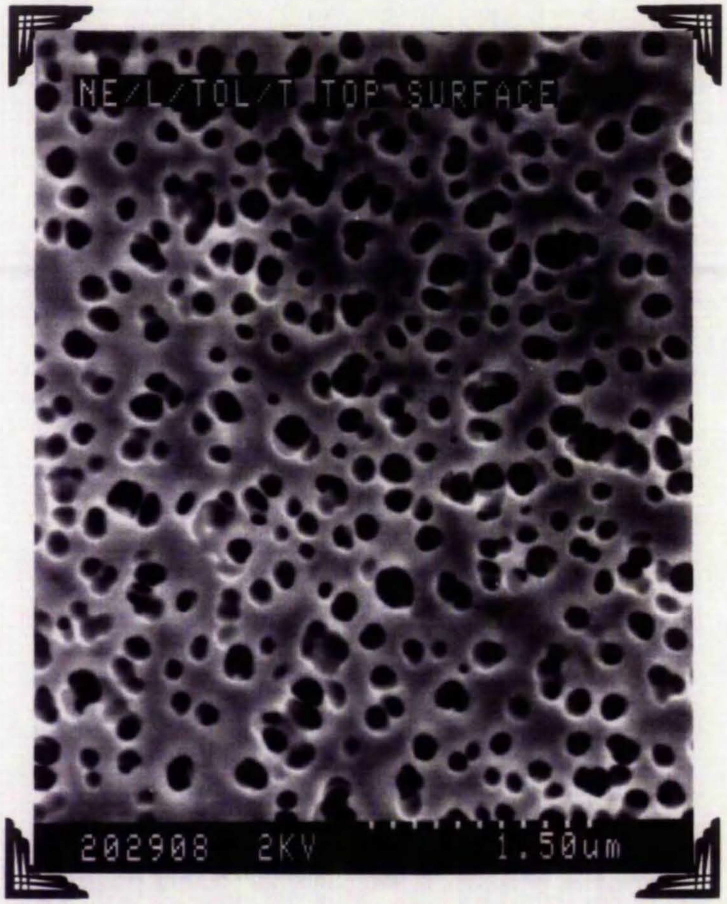

Plate 11.22 (202908) S.E.M. of the top surface (polymer-air interface) of a Eudragit® *NE* + *L* (1:1) film leached in toluene.

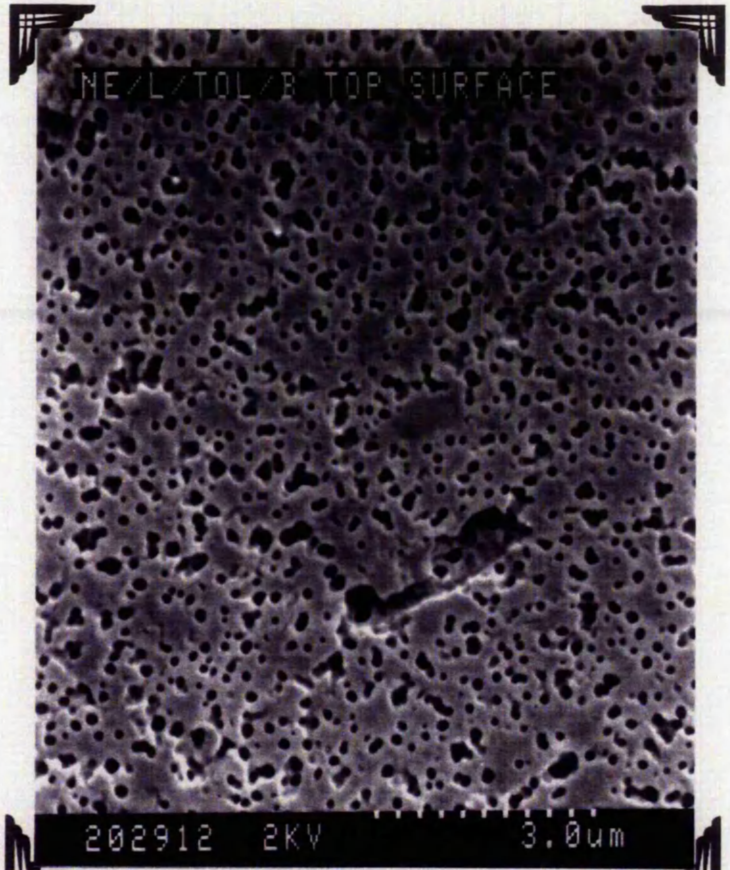

Plate 11.23 (202912) S.E.M. of the bottom surface (polymer-substrate interface) of a Eudragit® *NE* + *L* (1:1) film leached in toluene.

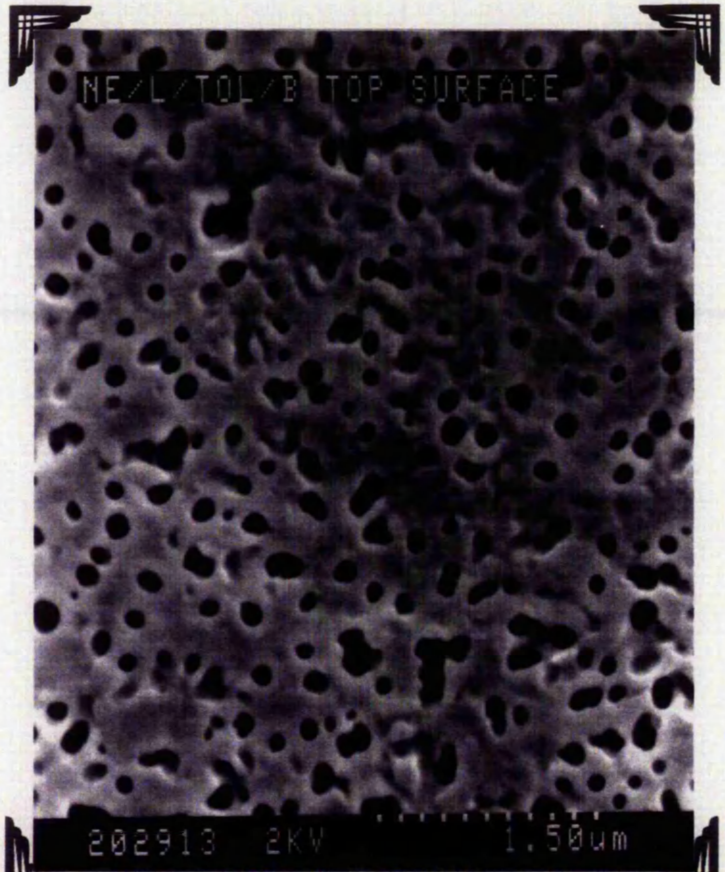

Plate 11.24 (202913) S.E.M. of the bottom surface (polymer-substrate interface) of a Eudragit® *NE* + *L* (1:1) film leached in toluene.

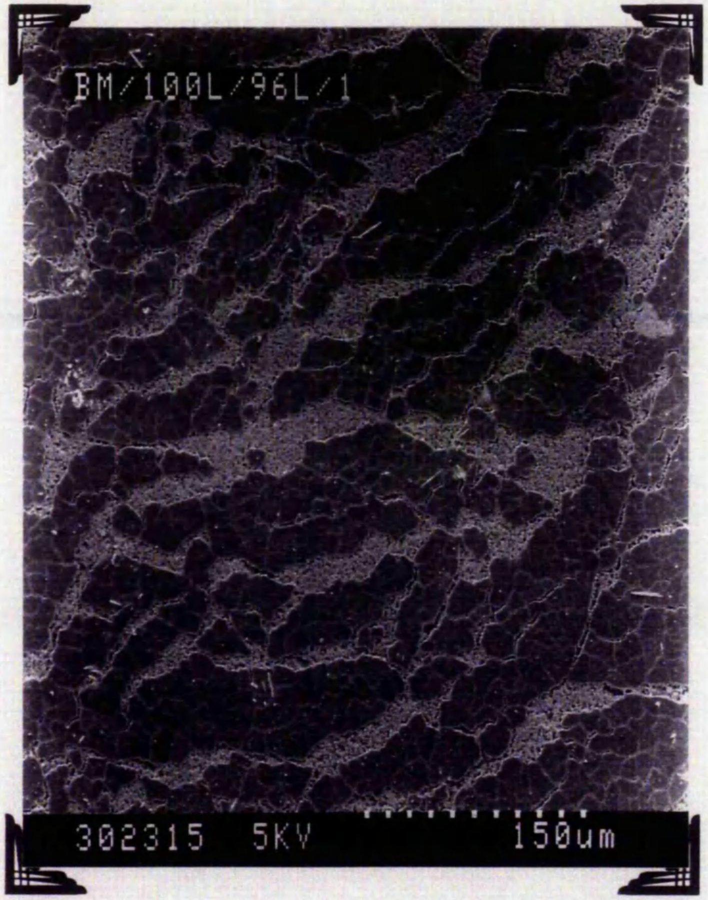

Plate 11.25 (302315) S.E.M. of the top surface (polymer-air interface) of a PBMA + Eudragit® *L* (1:1) film leached in buffer.

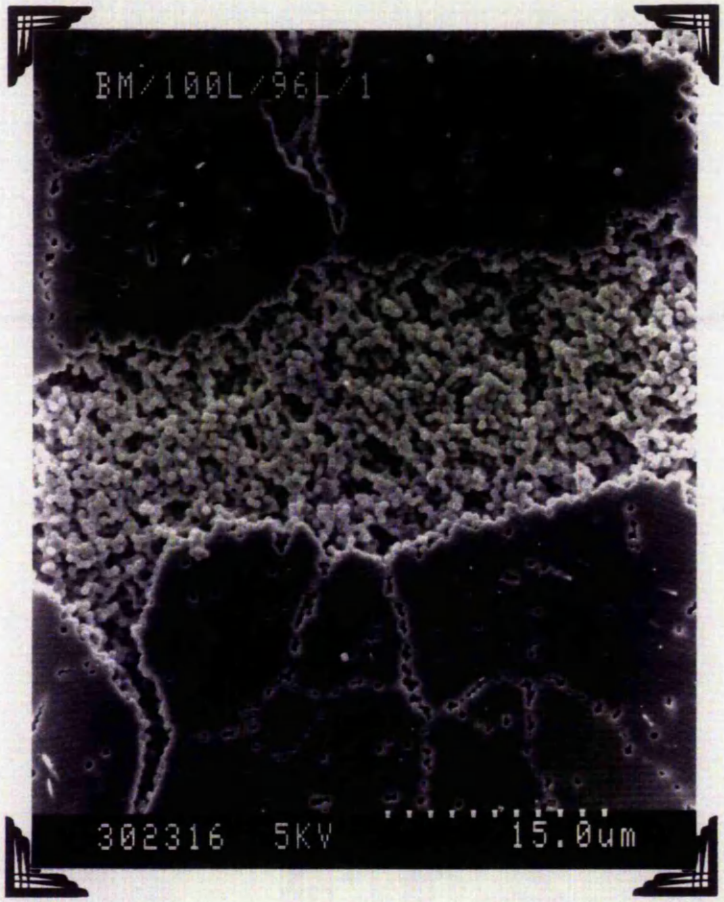

Plate 11.26 (302316) S.E.M. of the top surface (polymer-air interface) of a PBMA + Eudragit® *L* (1:1) film leached in buffer.

Plate 11.27 (302317) S.E.M. of the top surface (polymer-air interface) of a PBMA + Eudragit® *L* (1:1) film leached in buffer.

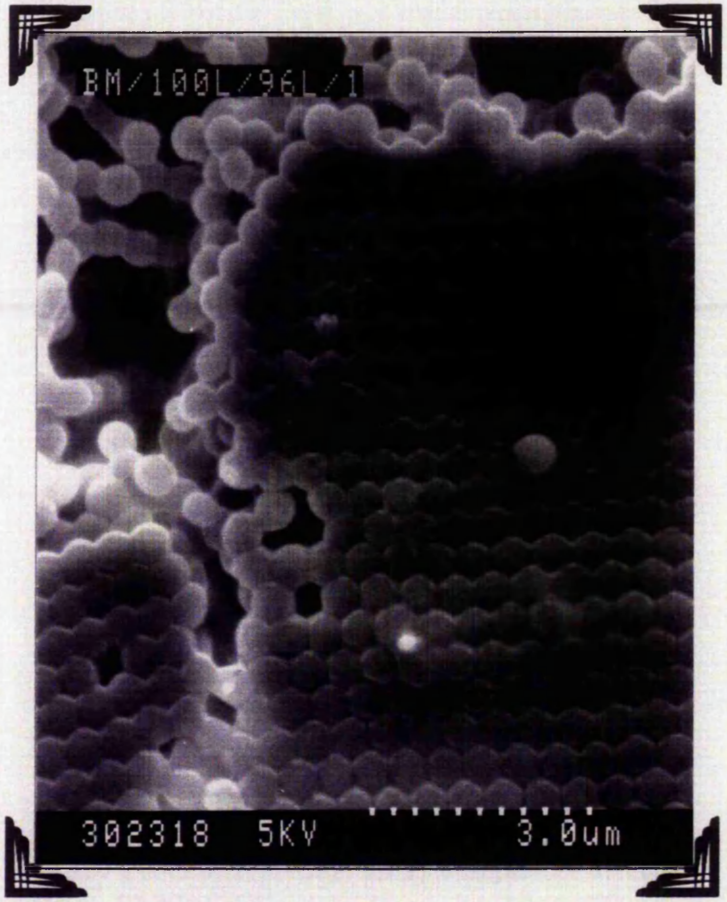

Plate 11.28 (302318) S.E.M. of the top surface (polymer-air interface) of a PBMA + Eudragit® *L* (1:1) film leached in buffer.

Plate 11.29 (302413) S.E.M. of the full fracture cross-section of a PBMA + Eudragit® *L* (1:1) film leached in buffer.

Plate 11.30 (302414) S.E.M. of the near-top fracture cross-section of a PBMA + Eudragit® *L* (1:1) film leached in buffer.

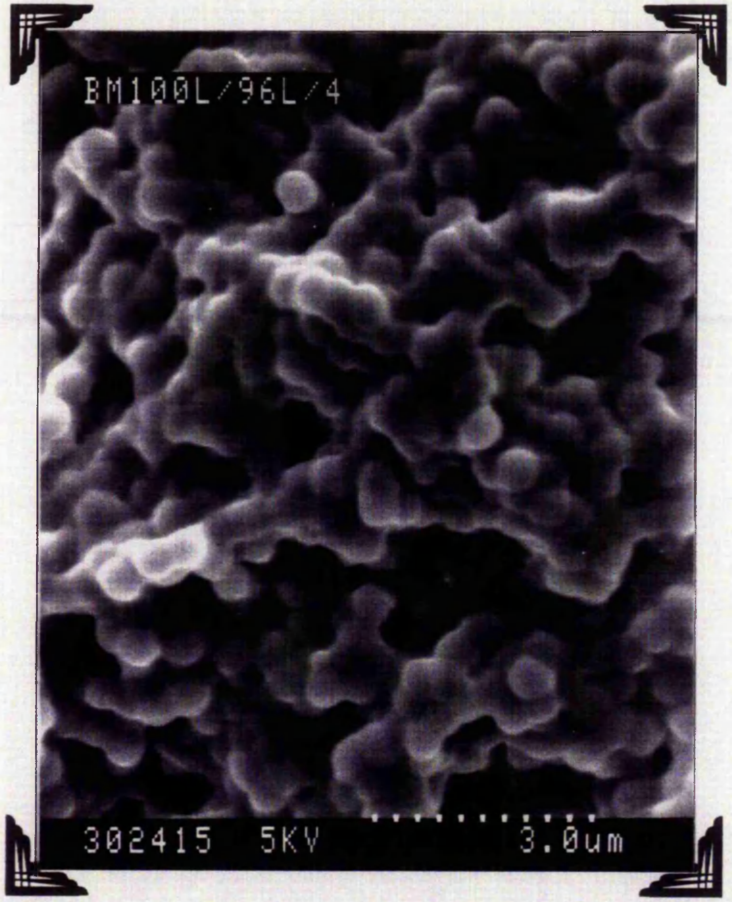

Plate 11.31 (302415) S.E.M. of the centre-section fracture cross-section of a PBMA + Eudragit® *L* (1:1) film leached in buffer.

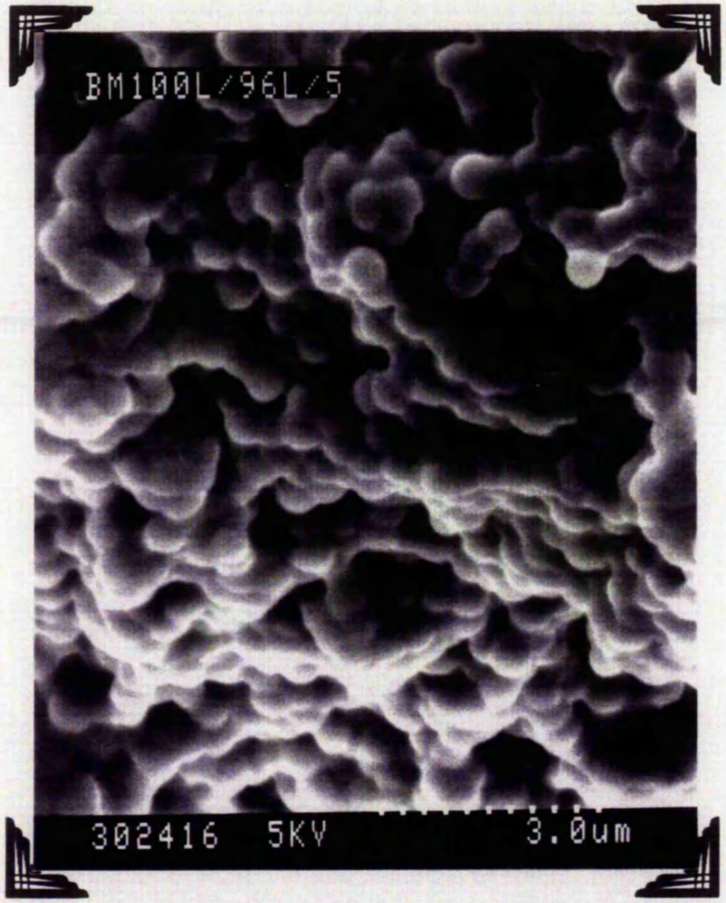

Plate 11.32 (302416) S.E.M. of the near-bottom fracture cross-section of a PBMA + Eudragit® *L* (1:1) film leached in buffer.

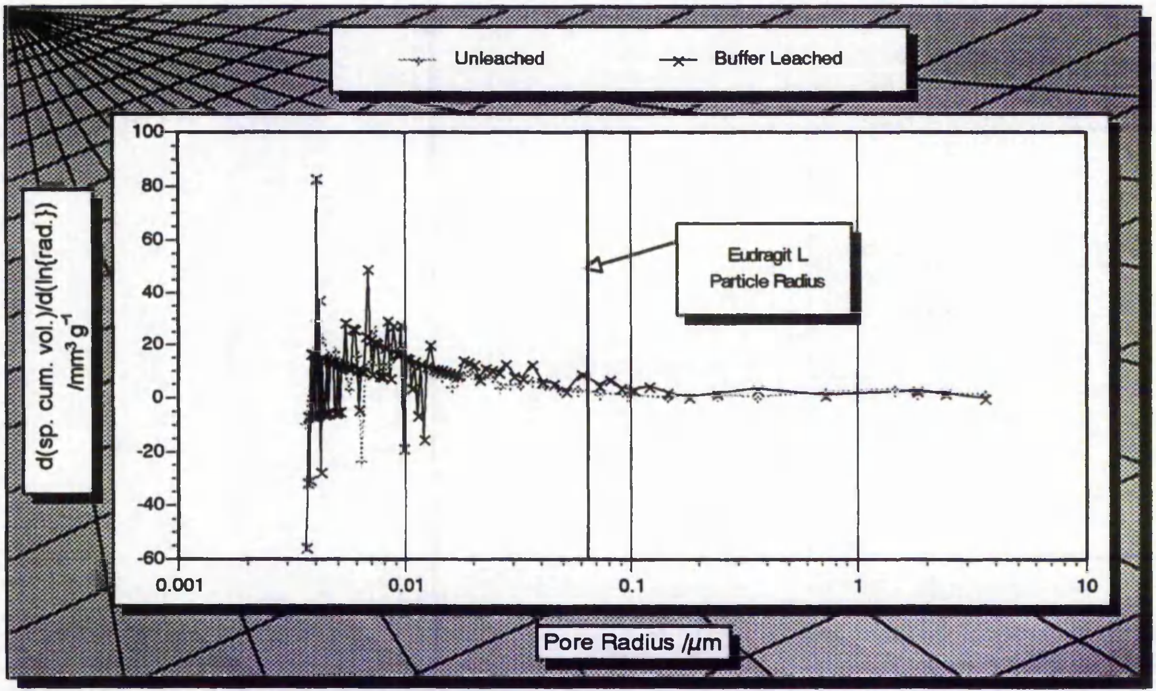

Figure 11.9 Pore distribution of a Eudragit® *NE* + *L* (1:1) film leached of Eudragit® *L* in buffer pH 6.

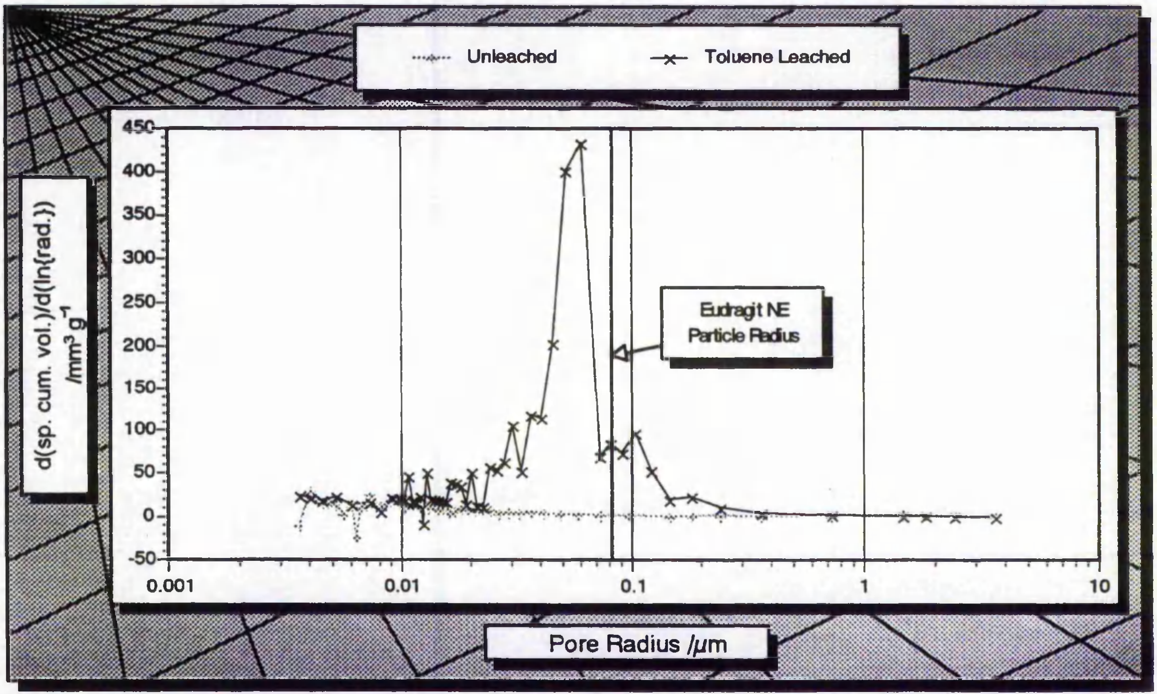

Figure 11.10 Pore distribution of a Eudragit® *NE* + *L* (1:1) film leached of Eudragit® *NE* in toluene.

The degree of porosity within the fracture cross-section appears to be less than that found for the Eudragit® *NE* + Eudragit® *L* film, and it is not obvious that the pores are continuous through the film's structure. However, the larger particle size of the PBMA latex (*i.e.*, approximately 500 nm, *cf.* 163 nm for Eudragit® *L*) may give the illusion of the porosity being of a lesser extent.

The films were extremely brittle, and it was not possible to remove them from the substrate in pieces of sufficient size to examine their permeability properties.

11.3.1.3 Pore size distribution of films prepared using Eudragit® *L* as an additive.

11.3.1.3.1 Eudragit® *NE* + *L* films.

Mercury porosimetry was used to investigate the pore distribution of mixed Eudragit® *NE* and Eudragit® *L* films (1:1 ratio of polymers), and also films (1:1 initial ratio) leached of either Eudragit® *L* in buffer, or Eudragit® *NE* in toluene (**Figure 11.9** and **Figure 11.10**, respectively).

As expected, the film leached of Eudragit® *L* (to leave the softer Eudragit® *NE*) showed little evidence of porosity – comparable with the unleached film. For the situation in which the soft polymer was leached to leave the hard polymer, a large pore distribution was found, centred about a pore radius of 0.05 → 0.06 μm (**Figure 11.10**), which is slightly below the particle radius of the leached particles.

11.3.1.3.2 PBMA + Eudragit® *L* films.

The pore radius distribution in a PBMA film leached of Eudragit® *L* (1:1) was also investigated using mercury porosimetry to probe film structure. (**Figure 11.11**). Pore

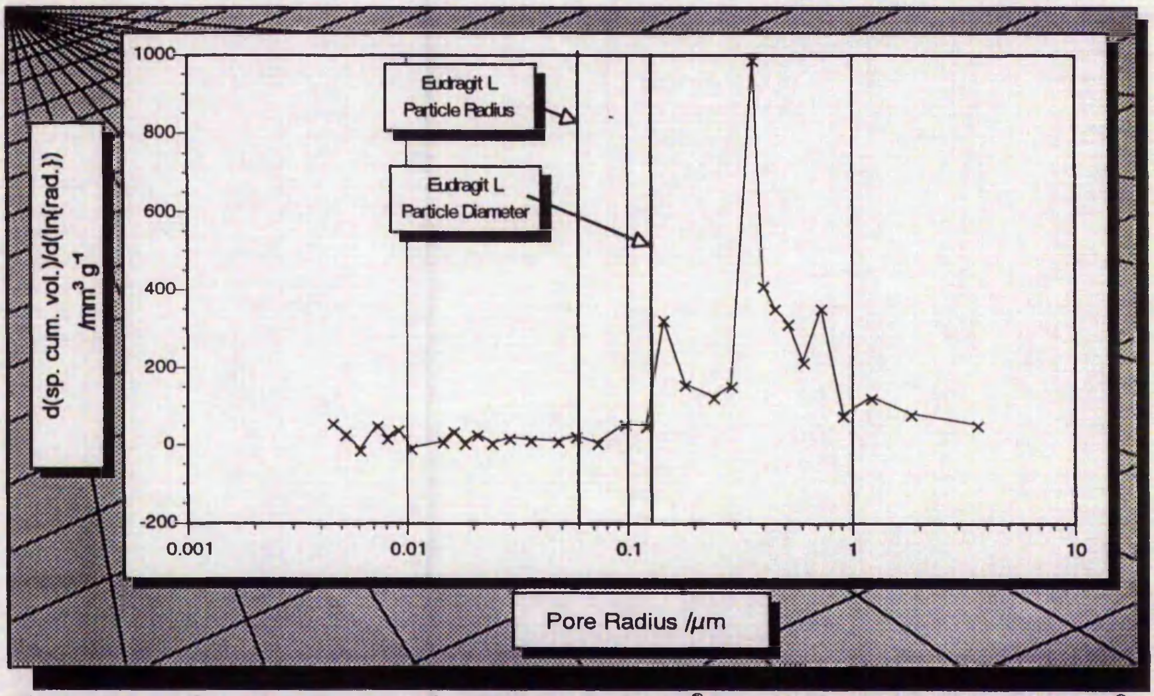

Figure 11.11 Pore distribution of a PBMA + Eudragit® *L* (1:1) film leached of Eudragit® *L* in buffer pH 6.

distributions are seen to occur at ca 0.16 μm, 0.35 μm, and 0.7 μm – showing some correlation with the Eudragit® *L* particle radius of ca 0.065 μm (with factors of ca 2.5, 5.4, and 10.8, respectively).

The specific cumulative intruded volume of the PBMA film leached of Eudragit® *L* was much greater than that seen for the Eudragit® *NE*/Eudragit® *L* films: the latter when leached of Eudragit® *NE* yielding a value of 334 mm^3 g^{-1}, at 1999 bar, which compares to a figure of over 800 mm^3 g^{-1} for the PBMA film leached of Eudragit® *L*.

11.3.2 Leaching of Eudragit® *L* from Eudragit® *NE* films.

The amount of Eudragit® *L* leached (into buffer pH 6) from mixed Eudragit® *NE* + Eudragit® *L* films, of various loads, was determined as a function of leaching time (**Figure 11.12** to **Figure 11.14**).

Compared to the molecularly dispersed additives, in which leaching from the film will be dependent on the time for the sink solution to reach the additive, and the time for it to diffuse out through the polymer (or aqueous pathways), the leaching of Eudragit® *L* will additionally depend on the time for the relatively large, high molecular weight, Eudragit® *L* particles to dissolve. This presumably accounts for the fact that at a time of 6 hrs after beginning leaching, less than 100% of the initial load of Eudragit® *L* has been removed from the film (despite the ability to leach 100% if given sufficient time, *e.g.*, 12 hrs), *cf.* for the dispersed additives the maximum leachable quantity is removed within ca 1 hr of the film being inserted into the sink solution.

Whereas at short leach times (*e.g.*, 5 mins → 1 hr), the amount of Eudragit® *L* leached appeared relatively constant (independent of initial load – see **Figure 11.13**), at a time of 6 hrs, the amount of Eudragit® *L* leached from the Eudragit® *NE* decreased as a function of initial load. This would seem to imply that at a time of 6 hrs, the leaching was less dependent on the dissolving of the polymer particles and, hence, more dependent on the ability of the dissolved Eudragit® *L* polymeric salts to diffuse out of the film. At a time of 12 hrs, the majority of the Eudragit® *L* was lost from the film.

Plots of the leaching process as both a function of time and the square root of time (**Figure 11.14** and **Figure 11.15**, respectively) represent dissolution and diffusion controlled release, respectively. Whilst the plot for diffusion controlled release ($t^{1/2}$) is the more linear of the two, it is apparent that neither plot fully depicts the release profile in the expected linear manner. It is seen that there is a 'step' (*e.g.*, ┌┘) in the results (centred at ca 6 hrs), which increases in size with increasing load of Eudragit® *L*. This is presumably a result of the aforementioned combination of the time taken to dissolve the particulate Eudragit® *L* latex before leaching can occur, and its slow diffusivity if uniformly distributed within the film. At high loadings of Eudragit® *L*, where the 'step' is most pronounced, the Eudragit® *L* will be most abundant and will therefore require increased dissolution/diffusion times. Neither plot being linear would also result from the Eudragit® *L* occurring both on the surface of the film and in its interior such that leaching is a combination of both a dissolution (for the surface located Eudragit® *L*) and diffusion controlled mechanism.

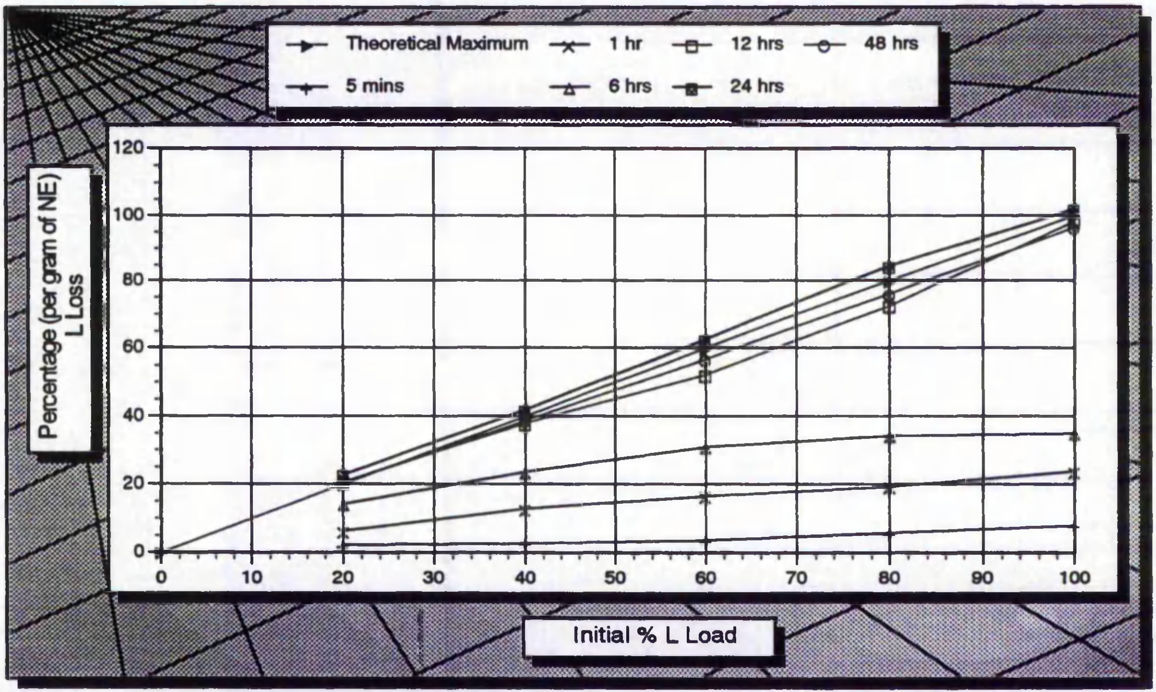

Figure 11.12 Percentage of Eudragit® *L* leached (per gram of Eudragit® *NE*) versus the percentage of Eudragit® *L* loaded (per gram of *NE*) for various leaching times.

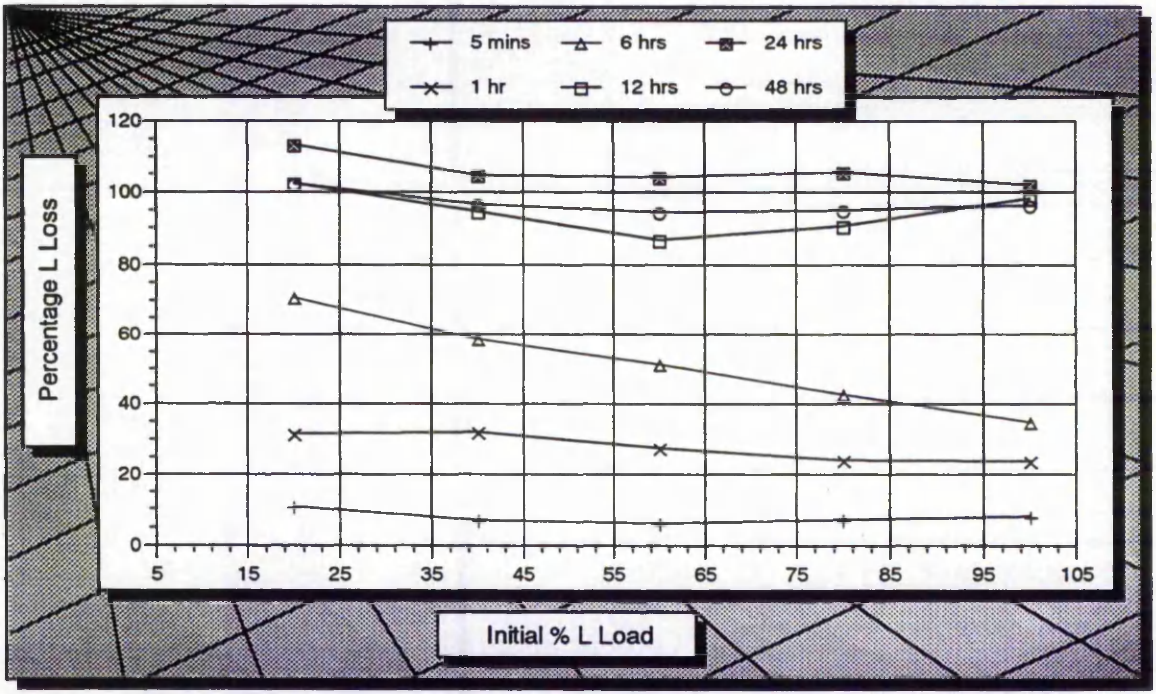

Figure 11.13 Percentage of the initial load of Eudragit® *L* leached from a Eudragit® *NE* film as a function of the initial Eudragit® *L* content (per gram of *NE*).

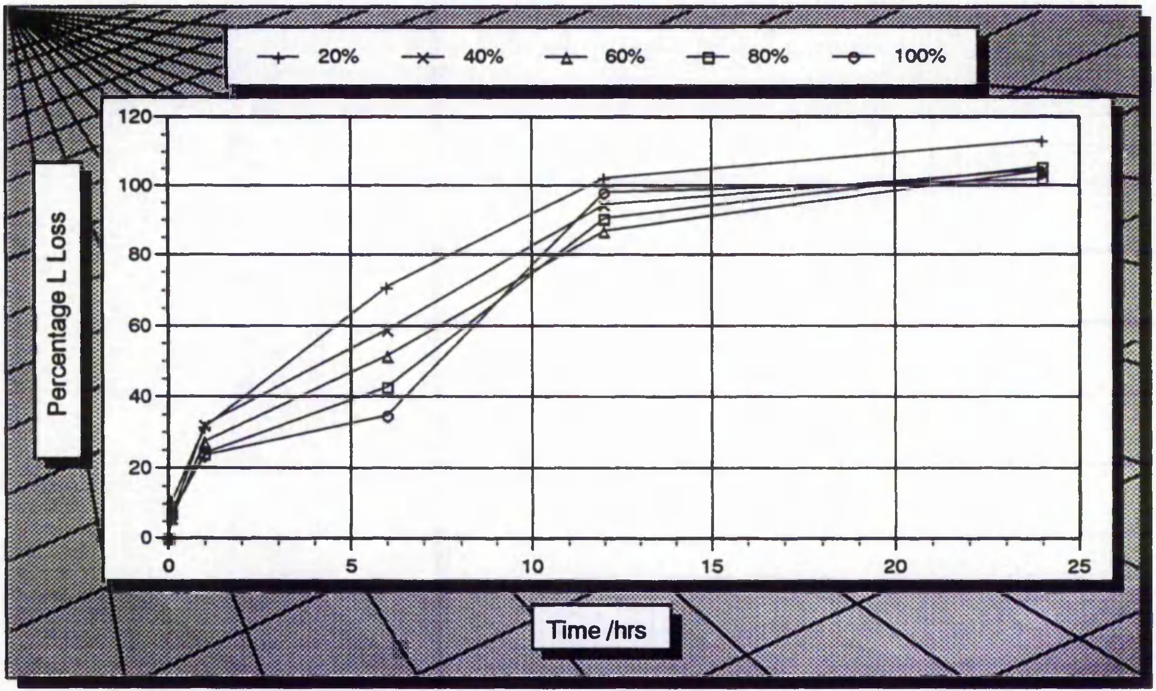

Figure 11.14 Plots of Eudragit® *L* leaching from Eudragit® *NE* films as a function of time.

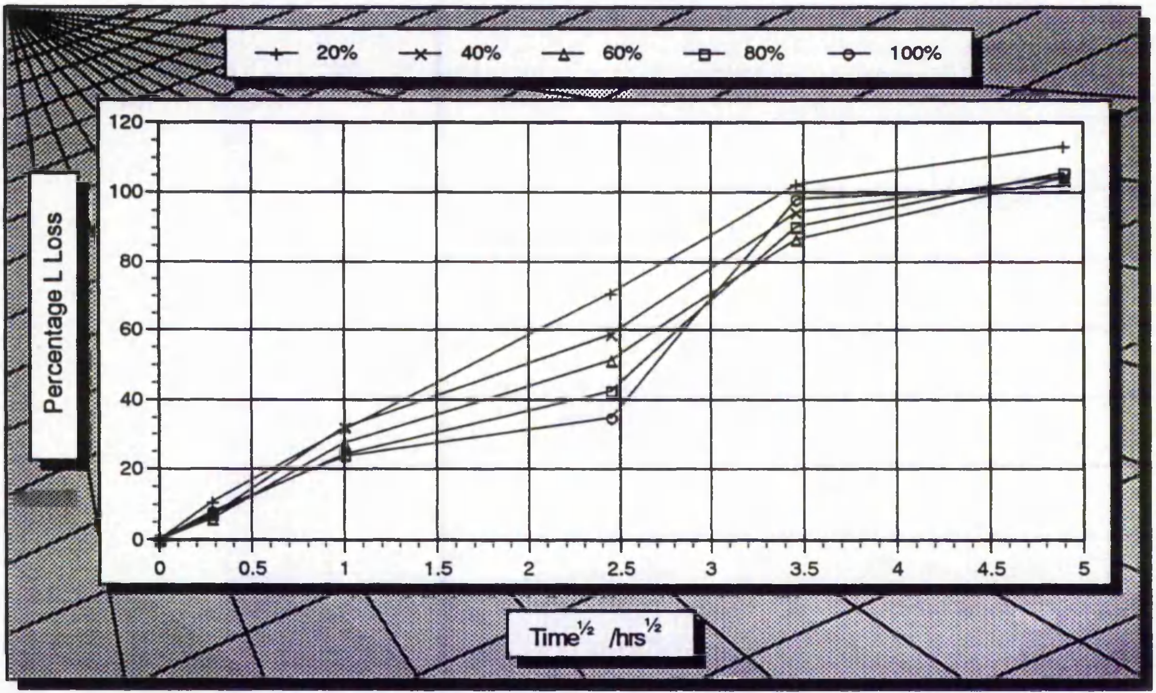

Figure 11.15 Plots of Eudragit® *L* leaching from Eudragit® *NE* films as a function of the square root of time.

11.3.3 Solute permeability.

11.3.3.1 The *4*-nitrophenol permeability of Eudragit® *NE* + *L* loaded films.

The apparent *4*-nitrophenol permeability coefficients of Eudragit® *NE* loaded with various levels of Eudragit® *L* (in buffer pH 6 and, hence, leaching the Eudragit® *L*) are given in **Table 11.6**, and **Figure 11.16**. The apparent permeability coefficient initially increases linearly with increasing load of Eudragit® *L*, but a break occurs in the line of best fit between a Eudragit® *L* loading of 0.2 → 0.3 g g^{-1} of Eudragit® *NE*. The initial increase in apparent permeability coefficient is described by:

$$P \times 10^7 = 9.106 \times 10^{-2} C_{\%L} + 0.278 \qquad r^2 = 0.910 \qquad (11.2)$$

whilst at higher Eudragit® *L* film content, the line is described by:

$$P \times 10^7 = 1.967 \times 10^{-2} C_{\%L} + 2.023 \qquad r^2 = 0.871 \qquad (11.3)$$

The **intersection of the two lines occurs at a Eudragit® *L* loading of 24.44% (g.*NE*)$^{-1}$**, (which compared to a value of 24.6% for the sucrose loaded film). At a Eudragit® *L* loading of 180% (per gram of Eudragit® *NE*), the film was found to disintegrate as the Eudragit® *L* was leached.

11.3.3.1.1 Investigation of film permeability asymmetry.

It is possible that the differences between the non-ionic Eudragit® *NE* and anionic Eudragit® *L* could lead to differing degrees of instability for each latex during film casting (evaporation of the water). This could lead to stratification of the polymer types, and consequently, a permeability that was dependent on film orientation. The differences in

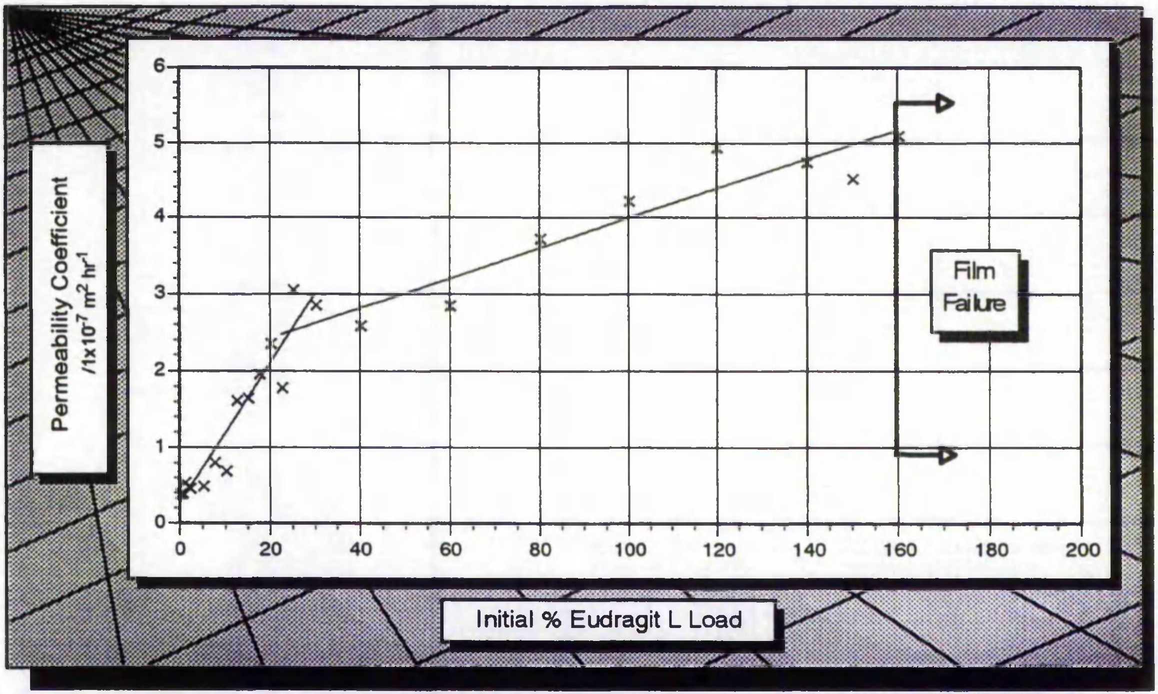

Figure 11.16 The apparent *4*-nitrophenol permeability coefficients for Eudragit® *NE*, as a function of Eudragit® *L* content (% per gram of Eudragit® *NE*).

Table 11.6 Apparent 4-nitrophenol permeability coefficients for Eudragit® *NE* films containing Eudragit® *L*.

Eudragit® *L* LOAD /% (g.*NE*)$^{-1}$	**APPARENT PERMEABILITY COEFFICIENT /1x10^{-8} m^2 hr^{-1}**
0	4.00
0.5	4.17
1	5.51(±0.43)
2	4.71
5	5.10
7.5	8.22
10	7.04(±0.50)
12.5	16.3
15	36.6
17.5	19.7
20	23.7(±2.05)
22.5	18.0
25	30.7
30	28.7
40	26.0
60	28.6
80	37.3
100	42.3(±0.09)
120	49.5(±0.6)
140	47.5
150	45.3
160	51.1
⟩180	FILM FAILS

permeabilities are shown in **Figure 11.17** and **Figure 11.18** (for two repeat runs of each orientation), and the permeability coefficient data is given in **Table 11.7**.

The results show a small difference between the mean values for each orientation, outside of the uncertainty as given by the standard deviation in the experimental results, but within the 10% uncertainty in film thickness (to which the permeability coefficient is directly proportional). It is apparent that no significant asymmetric permeability difference existed in the Eudragit® *NE* + *L* (1:1 ratio) films.

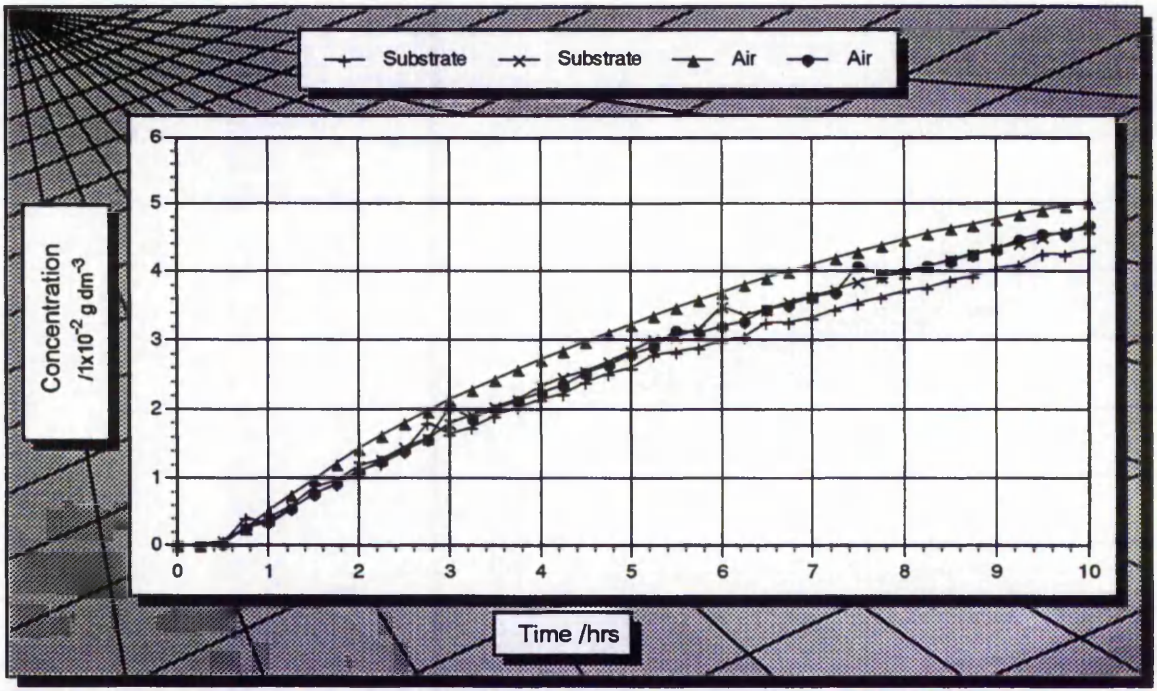

Figure 11.17 Increase in the concentration of 4-nitrophenol on the receiver side of Eudragit® *NE* + *L* (1:1) films of differing orientation to the donor permeant solution.

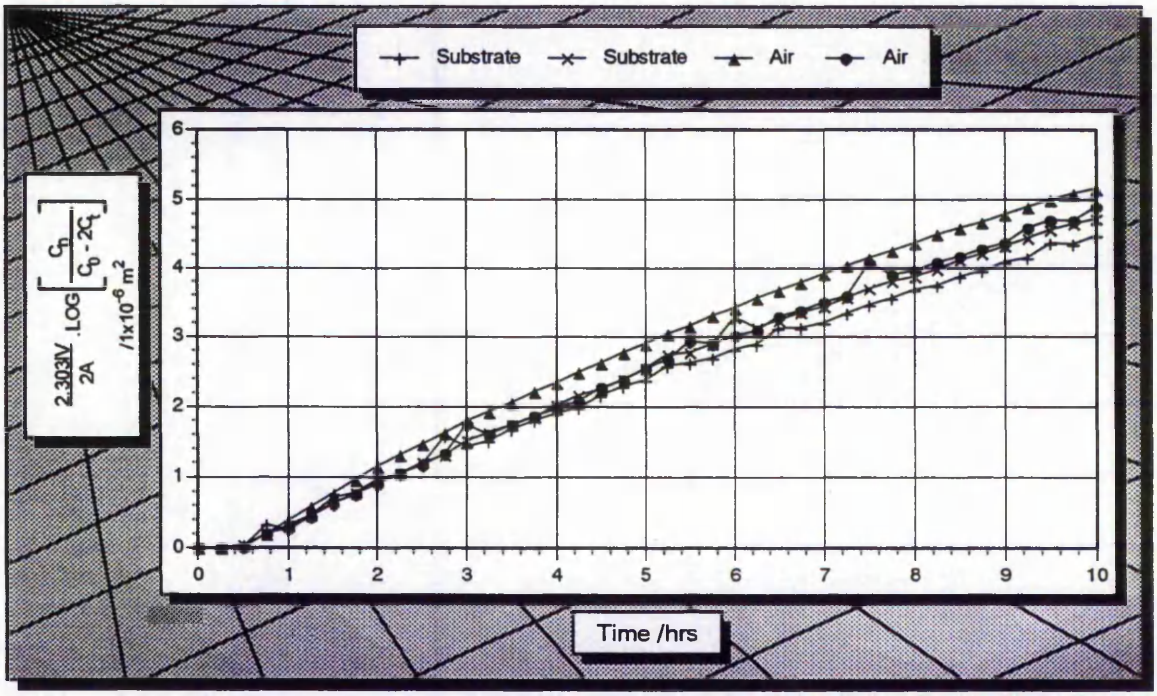

Figure 11.18 Plot to determine the apparent 4-nitrophenol permeability coefficients of Eudragit® *NE* + *L* (1:1) films of differing orientation to the donor permeant solution.

Table 11.7 Variation in Eudragit® *NE* + *L* (1:1 ratio) apparent *4*-nitrophenol permeability coefficients with film orientation.

FILM ORIENTATION†	APPARENT PERMEABILITY COEFFICIENT /1x10^{-7} m^2 hr^{-1}	S.D. /1x10^{-7} m^2 hr^{-1}
SUBSTRATE	4.23	0.092
AIR	4.60	0.042

† Film side facing permeant donor solution.

11.3.3.1.2 Arrhenius activation energy for *4*-nitrophenol permeation.

The **activation energy for the permeation of 4-nitrophenol through a 1:1 ratio Eudragit® *NE* + Eudragit® *L* film** was determined from the Arrhenius-type plot shown in **Figure 11.19** as **18.24 kJ mol^{-1}**. This value is higher than that found for the (25%) HPMC loaded film but lower than that of the (40%) sucrose loaded film and also the additive-free Eudragit® *NE* film (*cf.* 10.67, 34.6, and 50.5 kJ mol^{-1}, respectively).

It would be expected that the pore size distribution resulting from the leaching of particulate Eudragit® *L* would be greater than that from leaching molecular HPMC. The route of a permeant through the Eudragit® *NE* film leached of Eudragit® *L* would therefore be of less resistance and, hence, yield a lower permeation activation energy. However, the (presumed) dispersed nature of the HPMC, whilst yielding smaller pores, may produce a higher pore density, and weight for weight provide for a greater possibility of a contiguous pore network: *e.g.*, if a single particle of Eudragit® *L* were to be 'dispersed' in a Eudragit®

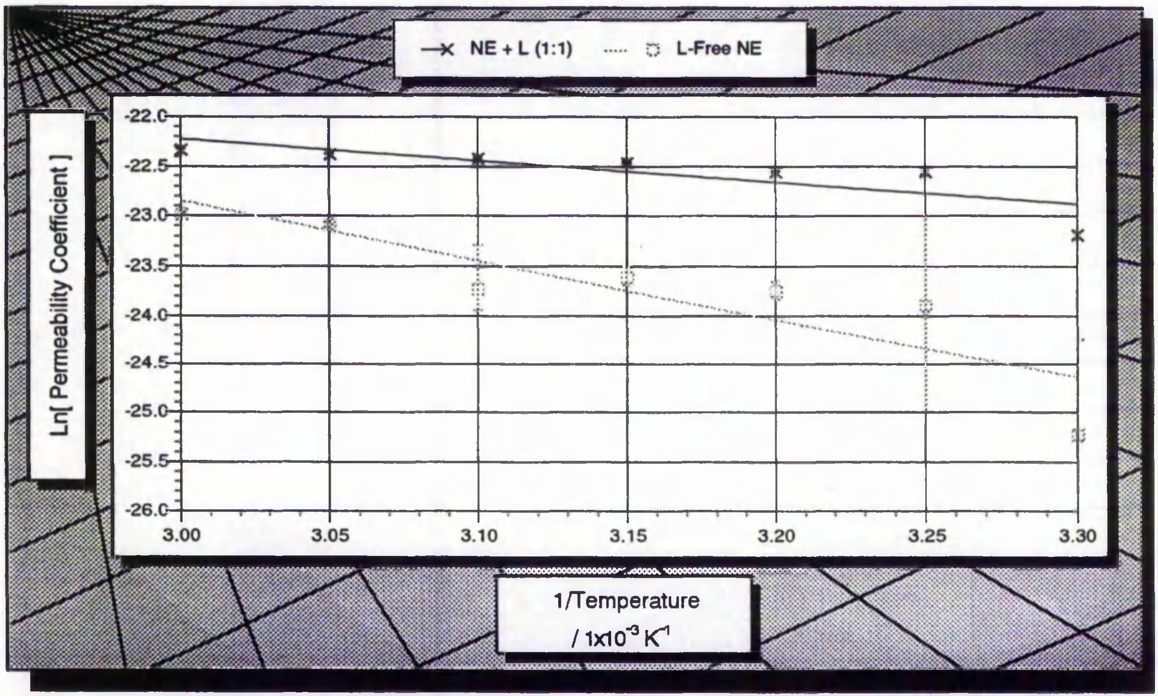

Figure 11.19 Arrhenius-type plot for the permeation of *4*-nitrophenol through Eudragit® *NE* + *L* (1:1 ratio) film.

NE film, whilst an equivalent weight of HPMC were to be dispersed in a second film, then a penetrant molecule would have a higher probability of hitting the HPMC (or a molecule of HPMC) than the Eudragit® *L* latex particle. In addition, the HPMC was observed to hydrate the film to a greater extent. This swelling can be considered as forcing apart the Eudragit® *NE* polymer chains – allowing increased chain mobility (*i.e.*, plasticisation) and, hence, ease of diffusion of the permeant.

11.3.3.1.3 Effect of film thickness on the 4-nitrophenol permeation through Eudragit® *NE* films containing Eudragit® *L*.

The permeation of 4-nitrophenol through 1:1 ratio Eudragit® *NE* + *L* films was found to be Fickian with respect to film thickness (**Figure 11.20**) where $r^2 = 0.947$. **Figure 11.21** shows the increasing lag times with increasing film thickness. The rate of change of concentration was assumed proportional to the flux (which is defined as the product of the rate of change of concentration and the permeant diffusion coefficient) and it is this rate of change of concentration which is actually plotted, and termed 'flux', in **Figure 11.20**: the flux being determined over approximately the first hour after the lag period.

It is not surprising that the flux was Fickian, since the film consisted mainly of Eudragit® *NE* due to the leaching of its Eudragit® *L* load. However, not all Eudragit® *L* would be expected to be leached in the first 10 hrs (see **Figure 11.12** and **Figure 11.13**). The Eudragit® *L*-free Eudragit® *NE* film was found to show Fickian permeation properties, with respect to film thickness, and this film consisting mainly of Eudragit® *NE* would be expected to show similar properties. If the film were to be highly porous, it would be expected that the much greater flux of 4-nitrophenol through the aqueously filled pores would mask the activated transport through the polymer. This would presumably lead to the flux being independent of film thickness. The fact that the flux *did* decrease as a function of film thickness implies that the complete leaching of the Eudragit® *L* had not occurred sufficiently (at the experimental time at which the flux was measured) for the formation of continuous, connecting pores through the full thickness of the film.

11.3.3.1.4 Eudragit® *NE* + *L* films leached in toluene.

As shown in the micrographs (**Plate 11.15 → Plate 11.24**), a Eudragit® *NE* + *L* film leached in toluene was porous. However, the leached film did not disintegrate when soaked in buffer pH 6 – implying sufficient residual Eudragit® *NE* existed to provide structural integrity and/or to protect the Eudragit® *L* by either preventing access by the buffer, or containing the Eudragit® *L* within a shell of solvent cast Eudragit® *NE* such that if it did dissolve, it remained constrained to film form again on drying.

Despite the evidence of porosity, the apparent 4-nitrophenol permeability coefficients were lower than those of the buffer leached film. This was presumably a result of the loss of the pore structure when soaked in buffer (pH 6) during the permeability experiment (*i.e.*, it was stated previously that the white opacity of the toluene-leached film was permanently lost after re-soaking in buffer: indicative of a loss of porosity). The **toluene-leached Eudragit® *NE* + *L* (1:1 ratio) film** gave a mean **apparent permeability coefficient** of $\boldsymbol{P_{l+residual\,NE} = 2.35(\pm 0.72)\times 10^{-7}\ \mathrm{m^2\ hr^{-1}}}$ (*cf.* $4.00\times 10^{-8}\ \mathrm{m^2\ hr^{-1}}$ for Eudragit® *NE* film).

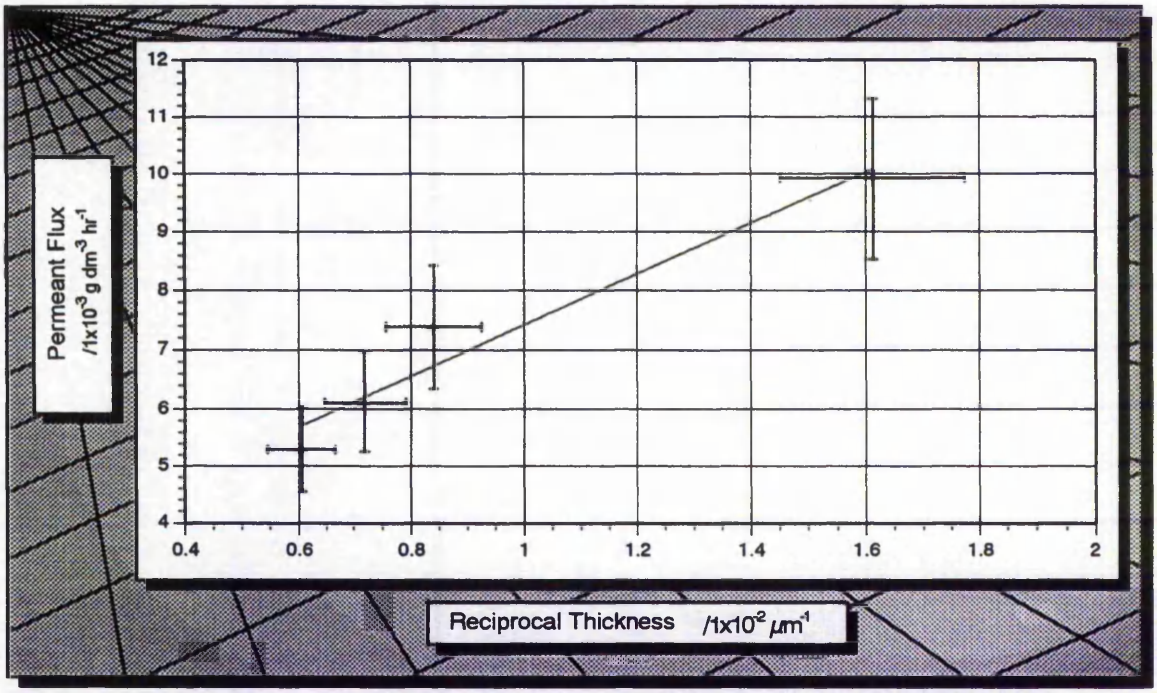

Figure 11.20 Fickian reciprocal thickness (initial film thickness) plot for the permeation of 4-nitrophenol through Eudragit® *NE* + *L* (1:1 ratio) films.

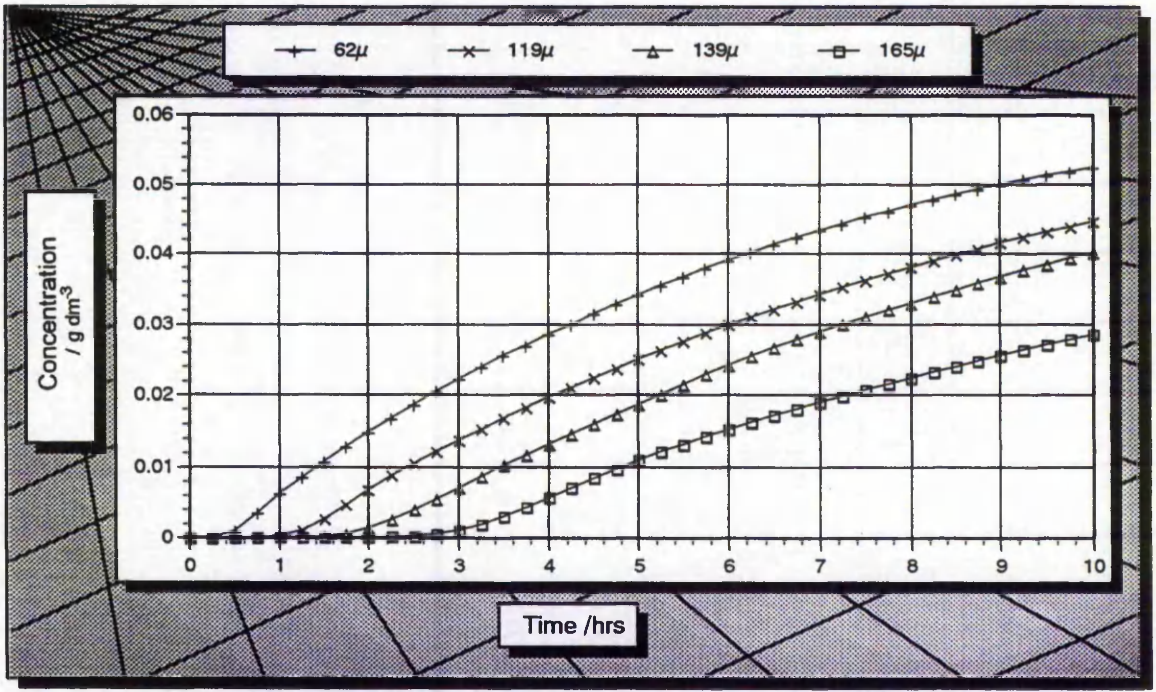

Figure 11.21 Receiver cell 4-nitrophenol concentration for Eudragit® *NE* + *L* (1:1) films of various film thickness.

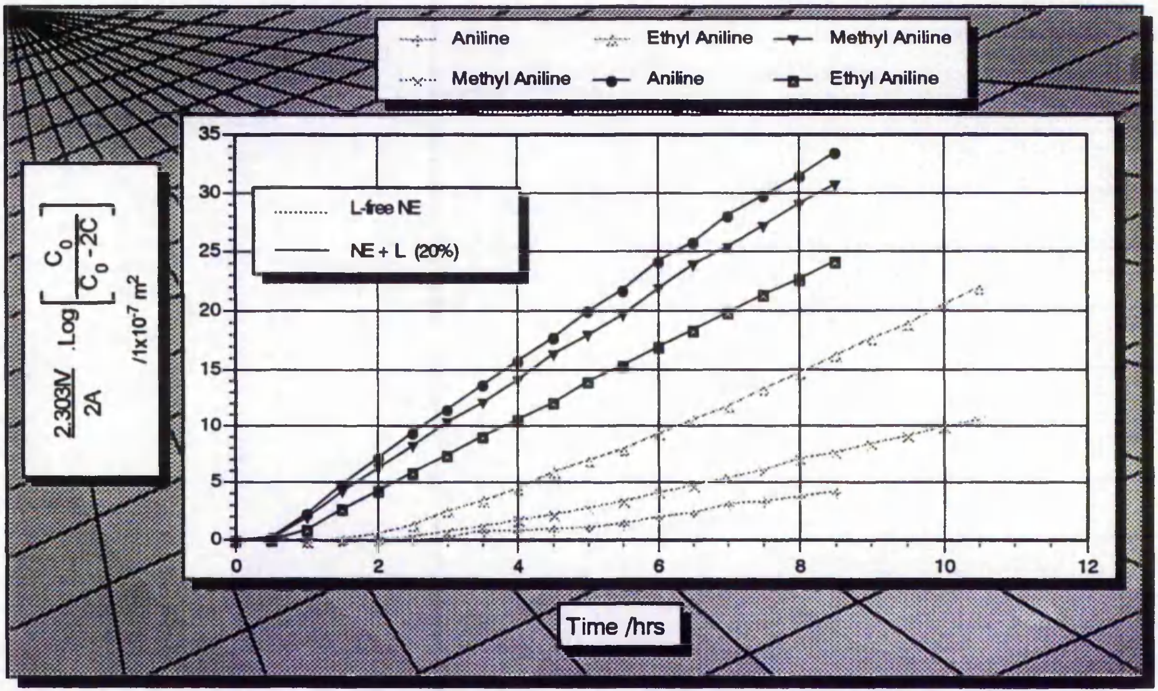

Figure 11.22 Plot to determine the aniline permeability of Eudragit® *NE* + *L* (20%) films.

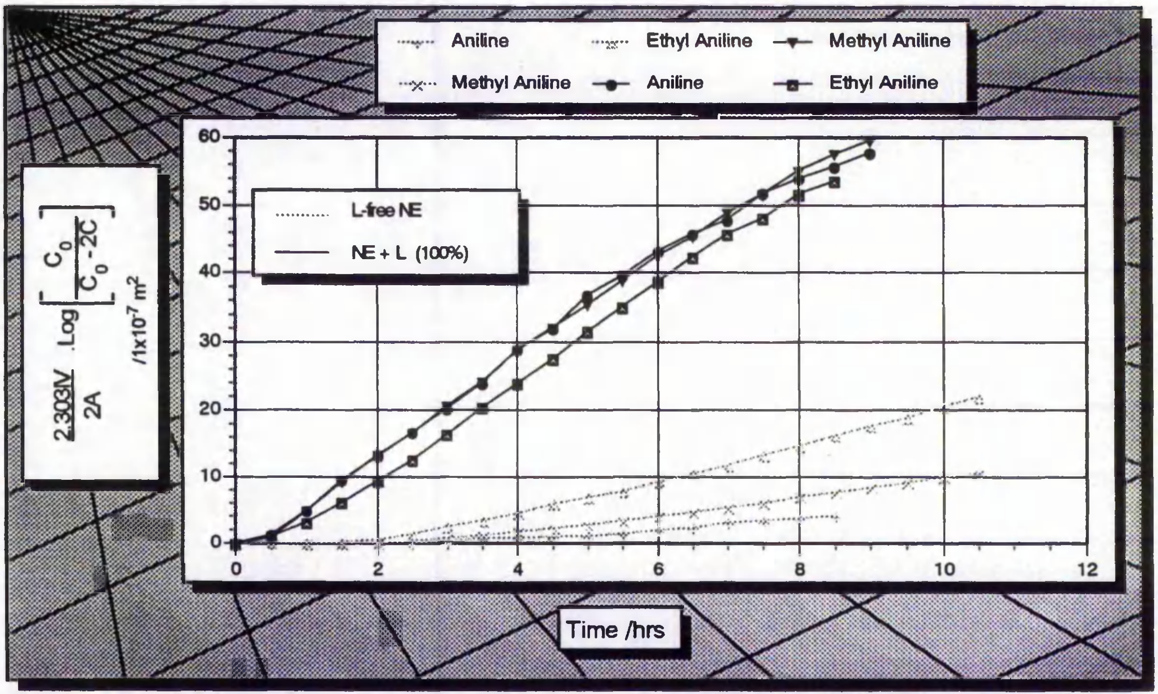

Figure 11.23 Plot to determine the aniline permeability of Eudragit® *NE* + *L* (100%) films.

Table 11.8 Apparent aniline permeability coefficients for Eudragit® *NE* + *L* films.

ANILINE	APPARENT PERMEABILITY COEFFICIENT $/1\times10^{-7}$ m^2 hr^{-1}	ANILINE UPTAKE† /g $(g.film)^{-1}$
0% *L* LOAD (*i.e.*, Eudragit *NE*)		
ANILINE	0.91	0.0040
METHYL ANILINE	1.47	0.0575
ETHYL ANILINE	2.84	0.1115
20% *L* LOAD		
ANILINE	4.20	0.019
METHYL ANILINE	3.89	0.060
ETHYL ANILINE	3.19	0.133
100% *L* LOAD		
ANILINE	7.67	0.010
METHYL ANILINE	7.37	0.033
ETHYL ANILINE	7.40	0.076

† Both the polymer and the polymer-additive are liable to show affinity for the anilines.

11.3.3.2 The permeation of anilines through Eudragit® *NE* + Eudragit® *L* films.

The permeation of a range of anilines through Eudragit® *NE* + *L* films was investigated at two different loadings of Eudragit® *L* (100% and 20% per gram of Eudragit® *NE* solids content); as used previously to examine the effect of the degree of porosity on the permeation of similar molecules of different size (**Table 11.8**, **Figure 11.22** and **Figure 11.23**). It is evident that the higher additive load (*i.e.*, 100%) yields apparent permeability coefficients that are both greater in magnitude and whose magnitude is more coincident, despite the differing solubilities of each individual aniline for the film. This implies that the activated transport mechanism is less relevant for the higher loading, due to increased permeation through pores or channels resultant from the additive leaching.

Eudragit® *NE* films containing 20% of Eudragit® *L* absorbed greater amounts of the anilines than films containing 100% of Eudragit® *L* (**Table 11.8**), indicating that Eudragit® *NE* apparently had a greater affinity for the anilines than Eudragit® *L*, when in mixed films. This, in turn, implies that a (hypothetical) film containing both Eudragit® *NE* and unleached Eudragit® *L* should show a lower apparent permeability coefficient, if transport occurs via a solution-diffusion type mechanism, than should the additive-free Eudragit® *NE* film. *I.e.*:

$$P = DS \tag{11.4}$$

For the films discussed here, however, the reduction in solution-diffusion type transport, resulting from residual Eudragit® *L* still unleached from the film at the time that the permeability measurements were made, is presumably countered by the increased porosity

Table 11.9 Apparent water vapour permeability coefficients of Eudragit® *NE* + *L* films.

EUDRAGIT® *L* LOAD /% (g.*NE*)$^{-1}$	MEAN (±S.D.) PERMEABILITY COEFFICIENT /1x10^{-6} g hr^{-1} cm^{-1} cm.Hg^{-1}
0	1.65 (±0.08)
20	1.24 (±0.22)
40	1.36 (±0.23)
60	1.19 (±0.23)
80	1.14 (±0.09)
100	1.16 (±0.19)
L (+ 15% TRIACETIN) (NO *NE*)	1.39 (±0.04)

due to latex-size particulate leaching (as opposed to molecular leaching): the magnitude of the increase in the rate of diffusion in an aqueous environment presumably being far greater than the decrease in the rate of diffusion caused by an increase in the tortuosity in the path of the diffusant due to the Eudragit® *L*.

Comparing the results (**Table 11.8**) of the mixed Eudragit® *NE* + *L* films to those of the Eudragit® *L*-free Eudragit® *NE* films shows apparently anomalous uptake results if it is assumed that Eudragit® *NE* has a greater affinity for the anilines than Eudragit® *L* (as was suggested above). However, the leaching of small amounts of Eudragit® *L* may open the Eudragit® *NE* structure sufficiently for it to show an increased uptake when compared to the Eudragit® *L*-free film. Since the Eudragit® *NE* film loaded with 100% Eudragit® *L* consists of only 50% Eudragit® *NE* then there is less Eudragit® *NE* to take up the anilines.

11.3.4 Water vapour permeability of Eudragit® *NE* + Eudragit® *L* films.

In Chapter 8, it was shown that the water vapour permeability coefficient of a Eudragit® *NE* film was higher than that of Eudragit® *L*. Therefore as may be expected, the apparent water vapour permeability coefficients of Eudragit® *NE* films loaded with various levels of Eudragit® *L* are also lower than that of the Eudragit® *L*-free Eudragit® *NE* film. The mixed films actually yield permeability coefficients that are also lower than the Eudragit® *L* film. However, 'additive-free' Eudragit® *L* films were plasticised with triacetin (15% (g.*L*)$^{-1}$) which presumably accounts for the higher value. Results are given in **Table 11.9**. Despite the relatively high levels of experimental uncertainty, the decreasing trend in permeability coefficient with increasing Eudragit® *L* load is apparent in the results (**Figure 11.24**).

11.3.5 Carbon dioxide permeability of Eudragit® *NE* + Eudragit® *L* films.

The CO_2 permeability coefficients of mixed Eudragit® *NE* + *L* (1:1) films were determined as described in Chapter 7 for (i) the film as cast, (ii) films leached of Eudragit® *L* in buffer, and (iii) films leached of Eudragit® *NE* in toluene for 24 hrs (**Figure 11.25**). (The leached film thickness was used to calculate the permeability coefficients $\{P_{l+residual\ polymer}\}$ of the leached films whilst the initial film thickness was used for the unleached film.)

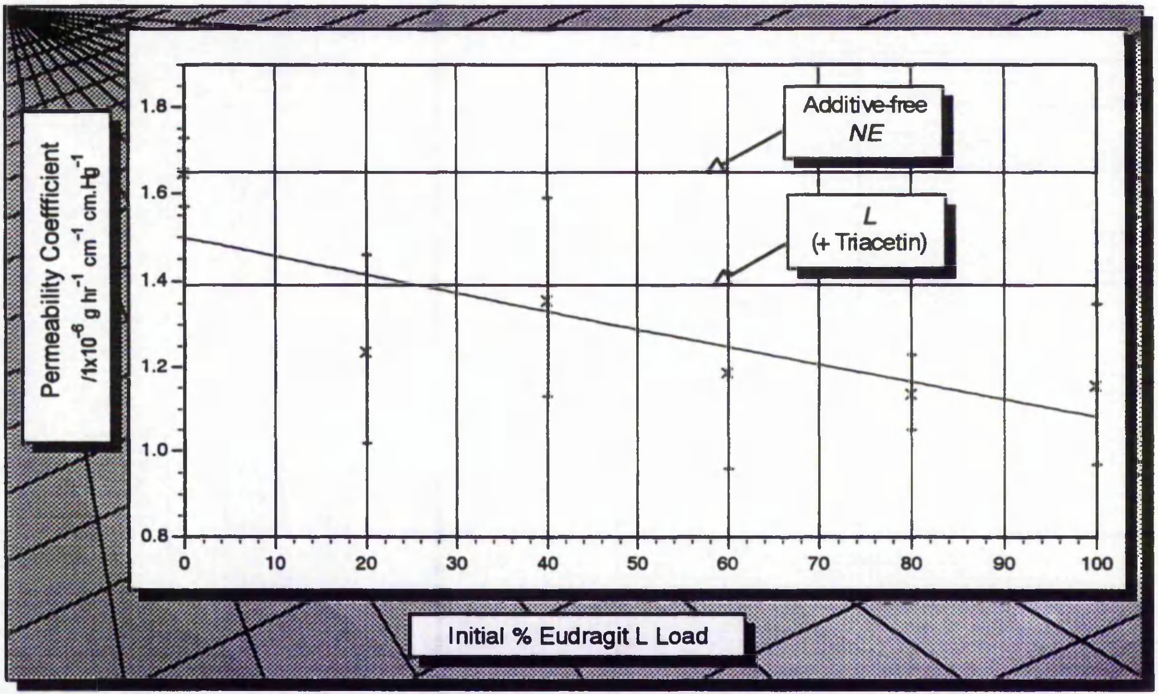

Figure 11.24 Water vapour permeability coefficients of Eudragit® *NE* + *L* films as a function of percentage Eudragit® *L* loading per gram of Eudragit® *NE*.

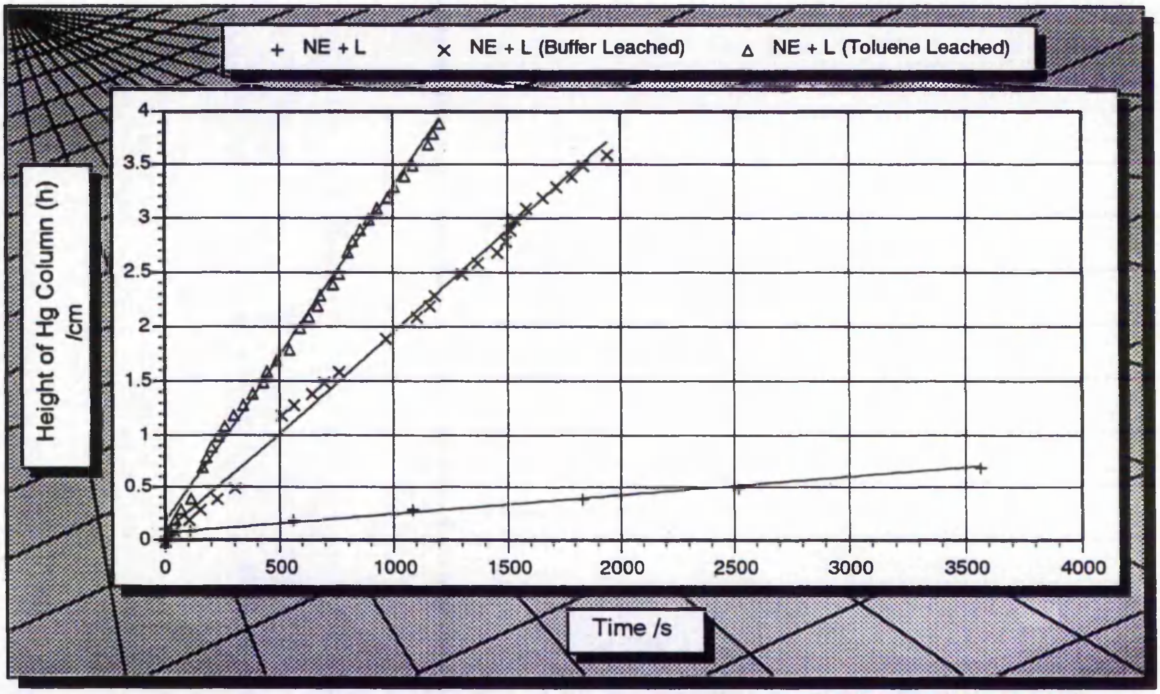

Figure 11.25 Graph to determine the carbon dioxide flux (*i.e.*, dh/dt {see Appendix A}) through Eudragit® *NE* + *L* (1:1 initial polymer ratio) films.

Table 11.10 Apparent carbon dioxide permeability coefficients for Eudragit® *NE* + *L* films.

FILM STATUS	APPARENT PERMEABILITY COEFFICIENT, / cm^3 cm s^{-1} cm^{-2} cm.Hg^{-1}
UNLEACHED	3.71×10^{-10}
LEACHED IN BUFFER	3.36×10^{-9}
LEACHED IN TOLUENE	5.47×10^{-9}

Although the leached films showed higher fluxes and, hence, permeability coefficients (**Table 11.10**), than films containing both types of polymer, all fluxes *were* measurable on an apparatus in which porosity typically leads to fluxes which are too great to measure (*i.e.*, assuming that it is possible to initially attain the necessary vacuum, the height change of the mercury column occurs in seconds, as opposed to minutes). This implies that no pores exist which are continuous through the full thickness of the film (despite the porosity observed in the S.E.M.s). *I.e.*, sufficient polymer remains to act as a barrier in the film – so that at some point it is necessary for the CO_2 to dissolve into the polymer, thereby slowing the rate of diffusion (and allowing the gas permeability apparatus to retain a vacuum for sufficient time for the measurement to be taken).

11.4 Other Additives.

11.4.1 Eudragit® *NE* film + triacetin (plasticiser).

Triacetin was used to plasticise the two Eudragit® polymers investigated (*e.g.*, additive-free Eudragit® *L*, and Eudragit® *RL*/*RS* and *RL* + additives) whose T_g's were higher than ambient temperature. Although Eudragit® *NE* does not require plasticising, a sample of such films was tested with triacetin added at various levels in order to investigate its effect.

Whilst the addition of triacetin (15%) to Eudragit® *RL* film was found to increase the apparent permeability coefficient (see Chapter 8), the same was not true when the triacetin was added to the Eudragit® *NE*: the apparent permeability coefficient decreased passing through an apparent minimum at 2% addition (**Table 11.11**). (Above 10% the film was too tacky to be of use.) The results are not unexpected in that other workers [e.g., 199] have found plasticisers to initially decrease film transport properties, when the plasticiser aids film coalescence during casting, after which increasing the amount of (water soluble) plasticiser allows leaching and, hence, increases permeant transport rates.

11.4.2 Sodium chloride as a film additive.

The micrographs of the upper and lower surfaces of PBMA films shown in the previous Chapters have demonstrated the close packed nature of the latex particles prior to film formation. Such packing is presumably present in all films investigated (assuming surfactant-free PBMA is one of the least stable latices used), but is not observed by the techniques used due to film formation making the particle boundaries more diffuse. In an attempt to increase film porosity by removing the packing ability of the latices, films were cast from latices containing sodium chloride to destabilise the particles such that

Table 11.11 The effect of added plasticiser on the apparent *4*-nitrophenol permeability coefficient of Eudragit® *NE*.

TRIACETIN CONTENT /% (g.*NE*)$^{-1}$	APPARENT PERMEABILITY COEFFICIENT /1×10^{-8} m^2 hr^{-1}
0	4.00
1	3.07
2	2.74
5	3.10
10	3.12

coagulation occurred before the particles were arranged in close packed formation. Not only have destabilised latices been shown to exhibit increased sponge-like porosity[366], due to the poorer particle packing, but also to show an increased water uptake[458] (compared to stabilised latices of the same polymer).

11.4.2.1 Dialysed Eudragit® *NE* films loaded with NaCl.

Films cast from dialysed Eudragit® *NE* loaded with low levels of NaCl (⟨2%) looked identical to additive-free Eudragit® *NE* films: the lower levels of addition showing no obvious sign of gross particle destabilisation. As the level of addition was increased (⟩2%), the film became progressively more opaque, and showed typically crystalline 'flower-like' patterns on the film surface. S.E.M.s of (dialysed) Eudragit® *NE* films loaded with 10% NaCl are shown in **Plate 11.33** to **Plate 11.36**.

Plate 11.33 is a low magnification micrograph of the upper film surface, showing the crystalline patterns. Such patterns were, as might be expected, not evident on the additive-free dialysed Eudragit® *NE* latex film, which appeared featureless. Crystals are in evidence through the whole of the fracture cross-section (**Plate 11.35**). The white dots seen in **Plate 11.34** and **Plate 11.36** show distinctly crystalline edges, which contrast with the hemispherical prominences seen in the sucrose loaded films. The polymer itself appears no different to any other Eudragit® *NE* film, showing the particles to be well coalesced around the NaCl. The discrete crystals of NaCl additive are not well dispersed within the film, showing that it has little compatibility with the polymer.

The apparent *4*-nitrophenol permeability coefficients of Eudragit® *NE* films loaded with various levels of NaCl are given in **Table 11.12**.

Results are not easily interpreted due to the fact that any increase in permeability may arise from: i, the film being cast from a latex that is destabilised (or which will become unstable as the NaCl concentration increases as the water evaporates during film casting); or ii, the leaching of the NaCl leading to increased film porosity (in the manner of the sucrose additive used in Chapter 10). It is evident, however, that although the

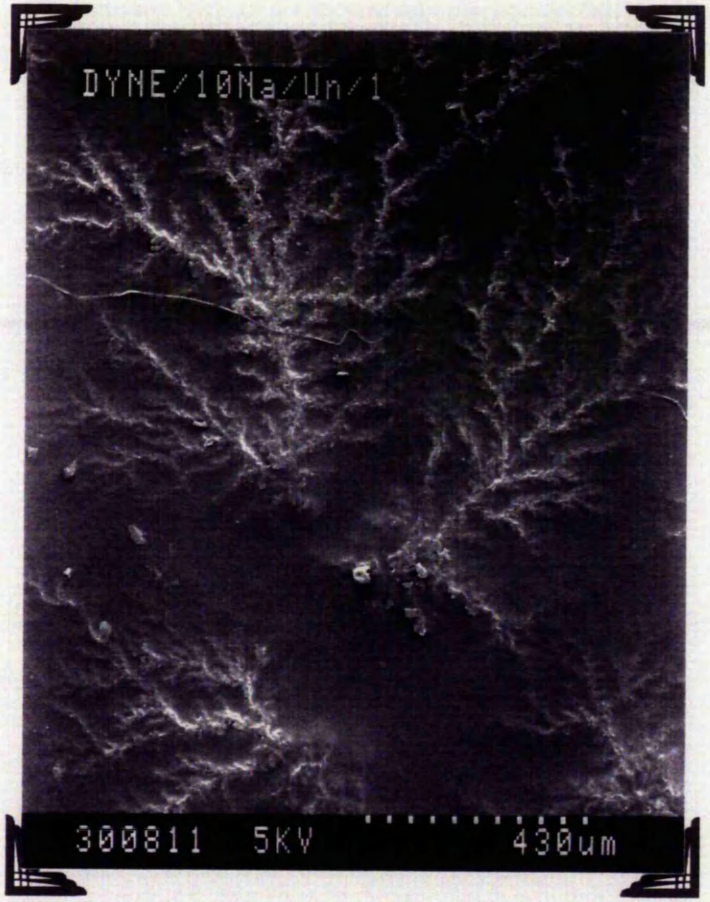

Plate 11.33 (300811) S.E.M. of the top surface (polymer-air interface) of a dialysed Eudragit® *NE* film loaded with sodium chloride (10%).

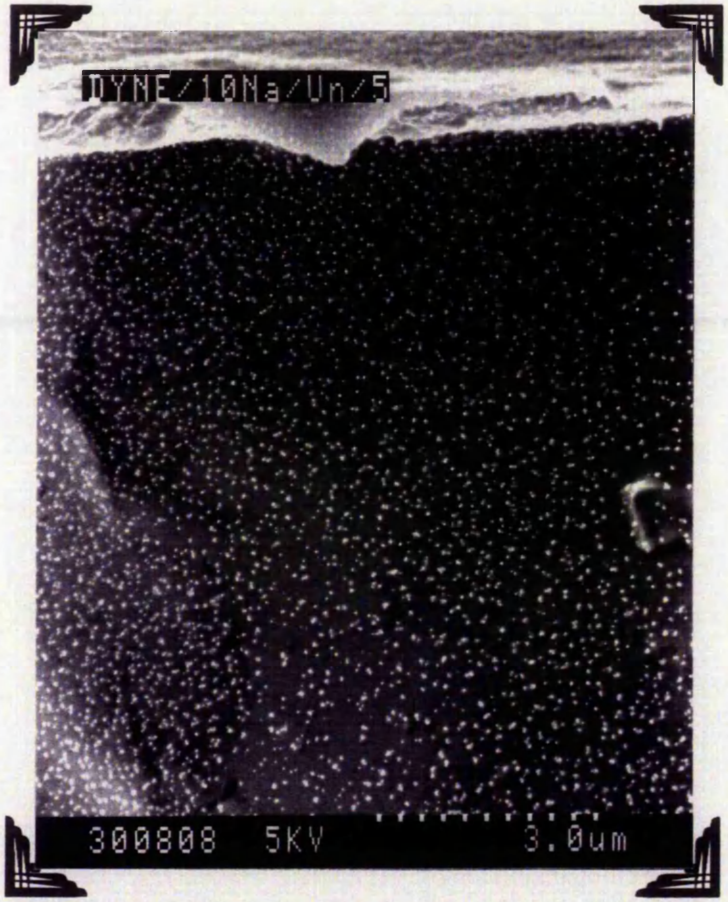

Plate 11.34 (300808) S.E.M. of the near-bottom fracture cross-section of a dialysed Eudragit® *NE* film loaded with sodium chloride (10%).

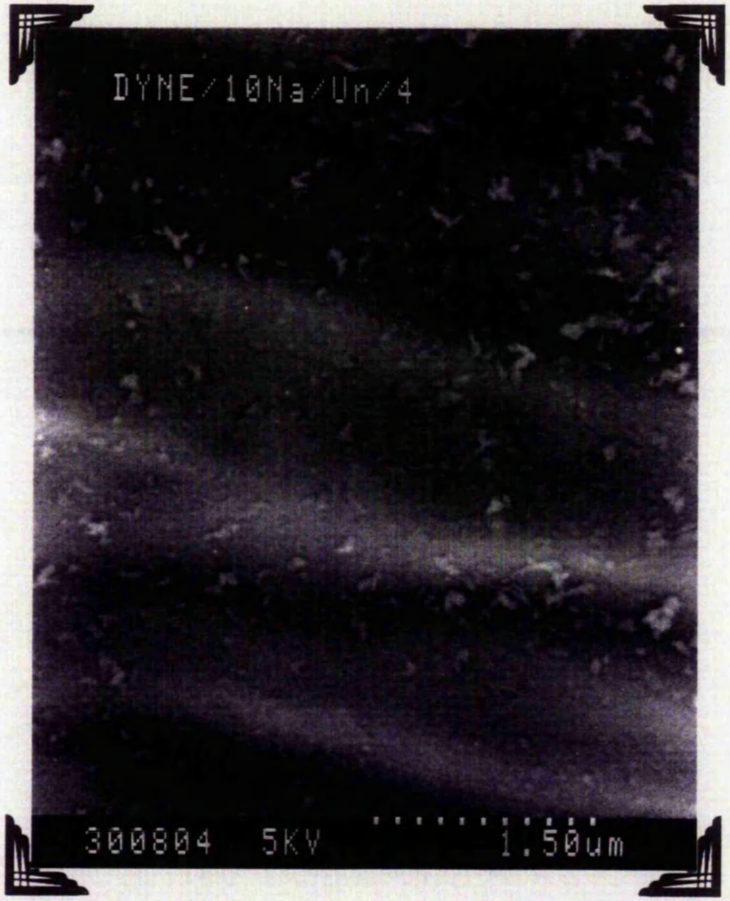

Plate 11.35 (300804) S.E.M. of the centre-section fracture cross-section of a dialysed Eudragit® *NE* film loaded with sodium chloride (10%).

Plate 11.36 (300806) S.E.M. of the near-top fracture cross-section of a dialysed Eudragit® *NE* film loaded with sodium chloride (10%).

Table 11.12 Apparent 4-nitrophenol permeability coefficients of films cast from dialysed Eudragit® *NE* latex + sodium chloride.

NaCl LOAD /% (g.*NE*)$^{-1}$	APPARENT PERMEABILITY COEFFICIENT /1x10^{-7} m^2 hr^{-1}
0	0.0884
0.25	1.01
0.5	1.22
1	1.32
2	1.27
5	1.10
10	1.13
20	1.17

4-nitrophenol permeability coefficient was greatly increased (compared to the additive-free dialysed latex film, which was itself less permeable than the undialysed latex film), there was no trend of increasing permeability with increasing level of additive addition. It is presumed that the scatter in the data is a result of the poorer level of particle packing, due to latex instability, and hence inferior film quality.

11.5 Summary and conclusions.

The transport properties of the Eudragit® *NE* films loaded with HPMC were generally similar to those of the sucrose loaded films: the differences being mainly ascribed to non-uniform blister-like swellings, and the inability to leach the full load of HPMC additive. The trapped HPMC possibly imbibing water to swell the film due to an osmotic potential being formed between the HPMC and the external aqueous phase. The HPMC could be entrapped in the film due to its high molecular weight, causing it to be slow to diffuse through the polymer, and because of its high viscosity when in aqueous solution.

If it is assumed that the HPMC is concentrated into channels by the film drying process (like those channels described for the sucrose loaded Eudragit® *NE*), then on leaching it would be expected that these channels would swell (due to the HPMC) to an extent greater than the bulk of the film. In doing so, however, the high viscosity of concentrated HPMC solutions may lead to the leaching process itself being much slower than, for example, sucrose under similar conditions – again leading to trapped HPMC over the time frame of the permeability experiments.

Like the sucrose containing Eudragit® *NE* films, films leached of HPMC and dried showed no sign of residual porosity.

The 4-nitrophenol solute permeability of the HPMC loaded Eudragit® *NE* films showed an 'enhancement coefficient' that was greater than for similar films loaded with sucrose. At the highest levels of HPMC addition, the magnitude of the apparent permeability coefficient was greater than that for the highest loadings of sucrose (even though the highest HPMC load was less than the highest sucrose load), and despite the higher viscosity of the aqueous HPMC-containing channels (compared to similar sucrose-containing channels) through which the 4-nitrophenol is proposed to travel due to the channels providing an easier path than the polymer. The higher viscosity presumably lowers the aqueous 4-nitrophenol permeability, but this reduction is perhaps compensated for by the film being able to retain a greater fraction of the HPMC (than sucrose) due to (i) the aforementioned higher HPMC solution viscosity and (ii) possibly because of better compatibility between Eudragit® *NE* and HPMC than between Eudragit® *NE* and sucrose. The ability to retain HPMC implies better hydration during the course of a permeation experiment, since there is a reduced probability of wet sintering occurring after the additive is leached. However, the non-uniform swelling of the HPMC loaded films impaired the reproducibility of the permeability results and led to higher levels of uncertainty in both permeability results and gravimetric leaching results – a problem exacerbated in the pre-leached films due to the variable nature of the amounts of residual HPMC, which was possibly clustered in the regions of the film that showed the blister-like swellings.

As may be expected from the high permeability results, the activation energy of permeability for the HPMC loaded films was lower, being approximately one fifth of that of the additive-free films, and one third of that of the sucrose loaded films.

The high degree of aqueous porosity of HPMC loaded Eudragit® *NE* films was apparent in the permeability results of the anilines with increasing side chain length and, hence, hydrophobicity. The film initially loaded with 25% HPMC yielding approximately similar apparent permeability coefficients, independent of aniline solubility in the film: this being indicative of a transport mechanism through a porous network, and independent of the need for the aniline to dissolve into the polymer.

Film transport properties were decreased if the HPMC loaded film was not wetted, indicating that, for example, a gaseous permeant finds the path through the film to be relatively more tortuous than in the case of the additive-free film; presumably as a result of the higher T_g of the HPMC decreasing polymer chain segmental motion compared to the HPMC-free Eudragit® *NE* film. Even water vapour, which might be expected to hydrate the HPMC and, hence, the film, showed little change in apparent permeability coefficient compared to the additive-free film.

Films prepared from a Eudragit® *NE* + Eudragit® *L* mixture of latices consisted of both a soft polymer and a hard polymer. Structural observations were interpreted based on these facts, and the ideal case in which a soft polymer would appear well coalesced and featureless, whereas a hard polymer would be expected to show spherical close packing, of the type typically used to describe simple metal atom structures, and possibly yield a friable film.

The unleached polymer appeared to show a matrix of coalesced Eudragit® *NE* with what were presumed to be hard Eudragit® *L* particles randomly distributed in the Eudragit® *NE* matrix: the Eudragit® *L* showing no ordered particle packing.

Films soaked in buffer (pH 6) swelled such that they appeared opaque when wet. However, they dried transparent – indicating that little or no porosity was conferred on the dry film after leaching the Eudragit® *L*. This lack of structure indicated the ability of the Eudragit® *NE* to 'heal' latex particle-sized 'holes.' It was also possible, however, that Eudragit® *L*, confined by the bulk of the Eudragit® *NE* matrix, could remain trapped (even when dissolved by the buffer) if the path by which the buffer percolates into the film shows insufficient void-volume for the removal of the Eudragit® *L* when in its salt form: the Eudragit® *L* forming a solvent-cast 'particle' on film drying.

The distribution of the Eudragit® *NE* and *L* was apparent from the S.E.M.s of the Eudragit® *NE* films leached of high loadings of Eudragit® *L*, where it was possible to see deformed Eudragit® *NE* 'particles.' The presence of such interlinked particles giving the leached film its strength and also showing the reduced extent of the deformation that was possible for particles constrained by the well-distributed Eudragit® *L* particles.

Eudragit® *NE* + *L* films having been leached of *NE* in toluene dried white, indicating a high degree of residual porosity: resulting from the hard Eudragit® *L* particles being unable to coalesce and fill the space. This was also apparent in the film thickness of the leached films: the film leached of Eudragit® *NE* appearing far closer to the thickness of the film as cast, whereas the film leached of Eudragit® *L* contracted to account for the filling of the volume fraction left by the leached polymer.

All S.E.M.s of Eudragit® *NE* + *L* films leached of Eudragit® *NE* showed a high degree of porosity, both on the film surface and also within the bulk of the film. It was found that the opacity and, hence, porosity in the toluene leached films could be removed by short exposure of the film to buffer: the buffer presumably dissolving the Eudragit® *L* sufficiently to allow it to flow, and become 'solvent-cast' in the pores on drying.

It was shown that a film leached of Eudragit® *L could* lead to pore formation by preparing and leaching a film consisting of two hard polymers, *i.e.*, PBMA + Eudragit® *L*.

The porosity of both Eudragit® *NE* + *L* films leached of Eudragit® *NE*, and PBMA + Eudragit® *L* films leached of Eudragit® *L* was readily apparent in the results of the mercury intrusion porosimetry experiments. Both types of film showed pore distributions centred about a single main pore radius. However, this did not correlate to the leached latex particle size (presumably as a result of film coalescence, after leaching, and the leaching of particle multiplets leading to a distribution of pore sizes).

The leaching of Eudragit® *L* from mixed Eudragit® *NE* + *L* films appeared to indicate that the majority of the Eudragit® *L* could be leached (possibly 95 → 100% of the initial load). However, leaching times were far longer than for the other additives investigated:

presumably as a result of the time required to dissolve a particulate system as opposed to a molecular system, but also as a result of the high degree of dispersion of the two polymers constituting the film, implying that the dissolved Eudragit® *L* would have to travel through a porous network in order to exit the Eudragit® *NE* matrix (a network whose slow formation would inhibit its development). As such, the time required for maximum leaching was typically greater than the time for the typical permeation experiment to reach concentration equilibrium in the permeability cell. (The leaching of Eudragit® *NE* with toluene yielded a film that remained intact when also inserted into buffer. This was attributed to the Eudragit® *NE* gelling to a certain extent such that there was sufficient residual Eudragit® *NE* {possibly solvent-cast} to give the film some structural integrity when the Eudragit® *L* was also leached. The solvent cast Eudragit® *NE* possibly acting to contain the Eudragit® *L* and, hence, prevent its leaching.)

The results for the leaching of Eudragit® *L* differed from those of the other additives investigated in that the amount leached at any time was inversely proportional to the initial load. *I.e.*, the higher the film content of Eudragit® *L*, the more difficult it was to leach; whereas the higher the sucrose (or HPMC) content, the more easily it was leached. Again this is presumably as a result of the difficulty of accessing, and hence dissolving, the Eudragit® *L* embedded deep within the bulk of the film, and the time then required to dissolve once access had been achieved. Particulate dispersion (as opposed to molecular dispersion) is less likely to lead to the formation of contiguous pathways by virtue of the decreased level of dispersion that would be exhibited by similar (weight) loadings of the additives.

Despite the evidence of the S.E.M.s for dry films, it might be assumed (as was shown for the sucrose leached films) that the buffer leached Eudragit® *NE* + *L* films, when kept wet, do exhibit a level of porosity similar to that seen in the films leached of Eudragit® *NE*. The loss of porosity on drying being solely a result of the coalescence of the soft polymer.

Solute permeability results for the Eudragit® *NE* + *L* films were similar to those of the other additives, showing an initial linear increase in the apparent *4*-nitrophenol permeability coefficient, before tending to plateau at approximately 25% Eudragit® *L* load. The highest apparent permeability coefficients were higher than those observed for the sucrose loaded Eudragit® *NE* films, but comparable with the HPMC loaded films.

The activation energy of *4*-nitrophenol solute permeation for the film leaching Eudragit® *L* was low, but not quite so low as that for the HPMC additive. This probably arose due to the particulate Eudragit® *L* being less well dispersed, on a weight for weight basis, in the Eudragit® *NE* than the HPMC, therefore reducing the probability, and hence, number, of continuous pathways.

The permeation of the series of anilines through the Eudragit® *L* leached Eudragit® *NE* + *L* films implied that the transport was still dependent on the aniline solubility to a greater extent than for similar levels of HPMC addition: only at a loading of 1:1 did the apparent permeability coefficients tend to a similar value. This presumably reflects not the difference in the size of the pores resulting from the leaching of either HPMC or Eudragit® *L*, but more likely the fact that the pores resulting from the Eudragit® *L* leaching are less likely to be continuous through the film thickness (and therefore necessitating that the anilines do dissolve into the polymer at some point during transport, whereas the HPMC pores do not). The lack of non-continuous porosity was confirmed by the very low gas permeability coefficients observed.

Note that if the apparent 4-nitrophenol and aniline permeability coefficients are compared, it is seen that the 4-nitrophenol permeability coefficient is ca 4.2×10^{-7} m^2 hr^{-1} when the aniline permeability is predominantly via a convective transport mechanism – as in the case of Eudragit® *NE* loaded with 100% Eudragit® *L*. At a Eudragit® *L* load of 20%, where the aniline permeability showed a greater degree of dependence on the aniline solubility, the apparent 4-nitrophenol permeability coefficient was ca 2.4×10^{-7} m^2 hr^{-1}. When the film was loaded with HPMC (25%), the anilines again showed some degree of variance in their respective permeabilities, and the 4-nitrophenol permeability coefficient at this (25%) load was 2.7×10^{-7} m^2 hr^{-1}. Hence, comparing these 4-nitrophenol permeability coefficients for the respective additives (Eudragit® *L* and HPMC) it might be expected that the anilines would *not* show solubility-independent transport in the HPMC (25%) loaded film (*i.e.*, not until the HPMC additive load yields a 4-nitrophenol permeability coefficient of the order ca 4.2×10^{-7} m^2 hr^{-1}). Hence, it is also not surprising that the aniline permeability of the sucrose loaded (40%) film investigated in Chapter 10 did not show solubility-independent transport. From the 4-nitrophenol permeability results of the sucrose loaded film (**Table 10.3**), it might be expected that convective transport would begin to dominate the transport mechanism above a sucrose load of ca 80%.

The addition of plasticiser to Eudragit® *NE* appeared to enhance the degree of coalescence, initially reducing the apparent solute permeability, but making the film excessively tacky.

Addition of sodium chloride to dialysed Eudragit® *NE* in an attempt to destabilise the latex led to a film giving relatively high, but unpredictable, apparent 4-nitrophenol permeability coefficients. Although the destabilisation was not evident by the resolution of the S.E.M.s of the films, the lack of reproducibility in the results presumably does result from the poorer quality of the film. The micrographs did show the presence of the NaCl, which was in evidence on the film surface and in the film interior. Leaching of these crystals would also account for the increased permeability compared to the additive-free film.

◆

Results and Discussion, Chapter 12: Functionalised Latex Films.

12.1 Introduction.

Latex particle surfaces can be functionalised to produce a variety of covalently bound chemical groups or biochemical moieties [28, 395]. When the particles are used in the form of a dispersion, post reaction recovery by destabilisation leads to loss of valuable latex. If the same latices could be used when cast as a film, or as an additive in a film, whilst retaining their activity, then re-utilisation would be possible. The ease of access to the functional groups is then of prime importance. Although Distler and Kanig [121] identified hydrophilic material located at interparticle boundaries in films, freeze-fracture cross-sections of films usually occur across the diameter of the particles, rather than between layers, suggesting added strength at the particle boundaries prompted by hydrogen bonding of functional groups.

Although not a film additive in the same context as the aforementioned additives, acrylic acid was used as a polymerisation additive in a **shot growth type** [e.g., 89] **reaction.** A PBMA latex was polymerised with a shot of acrylic acid (AA) added during the final stages of the polymerisation in an attempt to increase the hydrophilicity of the particles' surfaces, and hence, the hydrophilicity of the interparticle boundaries in a coalesced film. Increasing the density of the charged network in the film, it was hoped, would increase the permeation rate of the film.

If a permeant is normally transported through the film by a solution-diffusion type activated mechanism (which is therefore dependent on a degree of hydrophobicity of the permeant to yield some compatibility between polymer and permeant), it is possible that increasing the hydrophilicity of the film may inhibit transport by reducing the tendency of the permeant to dissolve into the polymer. It is thus necessary to increase the level of charge to a such a degree that the film is likely to swell greatly with water, allowing the permeant to travel through that water (where it would have a higher diffusion coefficient than in the polymer) without being inhibited by the necessity of having to wait for the relatively slow polymer chain motion to open a diffusion-hole. *I.e.* at the very least, it is necessary for the water to plasticise the film.

12.2 Preparation of functionalised latex particles.

Vijayendran [521] determined from studies of copolymerisation reactions that the concentration of various acrylic acids, of differing degrees of hydrophilicity, either in the aqueous phase of the reaction, on the particle surface, or buried within the particle was essentially dependent on the solubility of the acid in the monomer (styrene). The most insoluble acid was found mainly in the water; the most soluble in the particle; whilst AA with its limited solubility in styrene was found mainly on the particle surface. Sakota and Okaya [433] used a "shot-growth" technique to get a high load (⟩80%) incorporation of carboxyl groups onto a latex particle surface on addition at 95% conversion. In order to make use of this technique, it was necessary to first study the kinetics of PBMA polymerisation in order to identify the correct time for a "shot" addition.

The kinetics and mechanism of surfactant-free emulsion polymerisation has been little studied [93, 229] when compared to the emulsifier present systems used commercially and where the qualitative theory of Harkins [221] and the quantitative theories of Smith and Ewart [457] are well established. Agreement with such theory is reduced as the aqueous solubility of a monomer increases. However, for monomers having a similar aqueous solubility to that of styrene, it may be anticipated that the kinetics and mechanism might be similar.

Total organic carbon analysis showed that BMA solubility was 0.0041% W/W (*cf.* styrene 0.0031% W/W). Despite this similarity, it is apparent from conversion-time curves for the two monomers that there are considerable differences.

For styrene, the conversion-time (*C*-*t*) data [196] (see **Figure 12.1**) was in accord with Smith-Ewart case III core-shell polymerisation or the surface phase polymerisation of Wessling and Harrison [530], which predicts $C^{2/3}$ versus t to be linear. Molecular weight data [229] showed bimodal peaks which implied a reaction proceeding at two loci, presumed to be the core and the shell of the particles, as a result of a monomer concentration gradient within the particles [93] consisting of a monomer starved core, relative to the shell through which monomer must diffuse to gain access to the core.

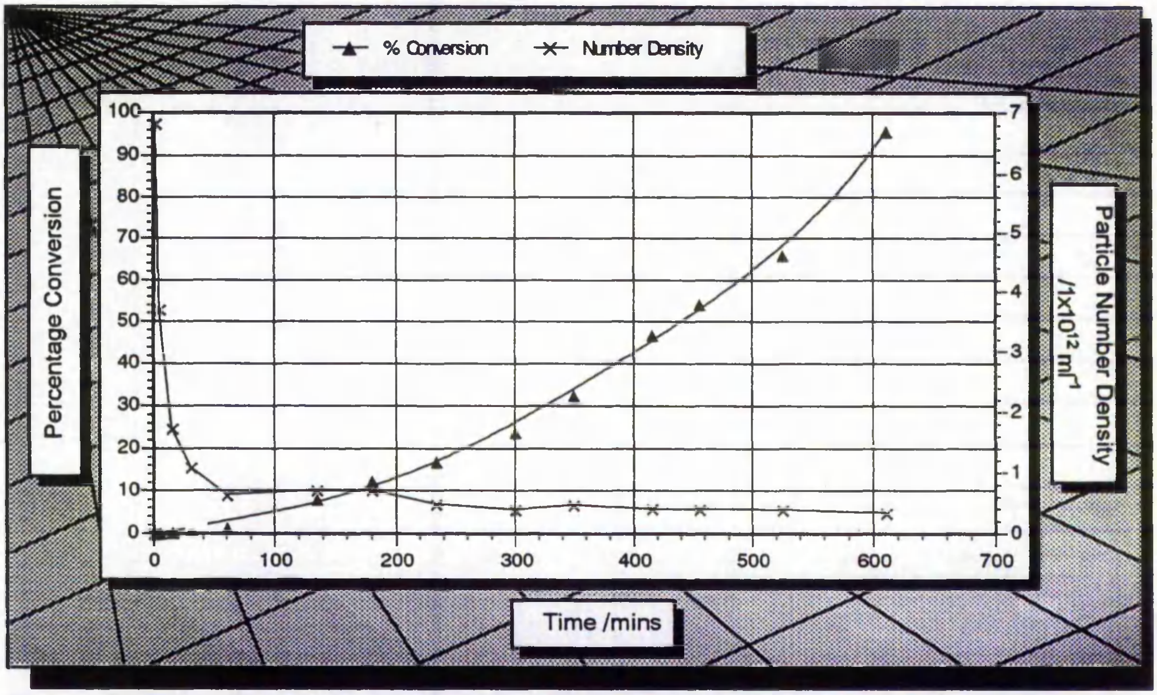

Figure 12.1 Plot of percentage conversion of monomer to polymer and latex particle number density during the course of a styrene polymerisation [196].

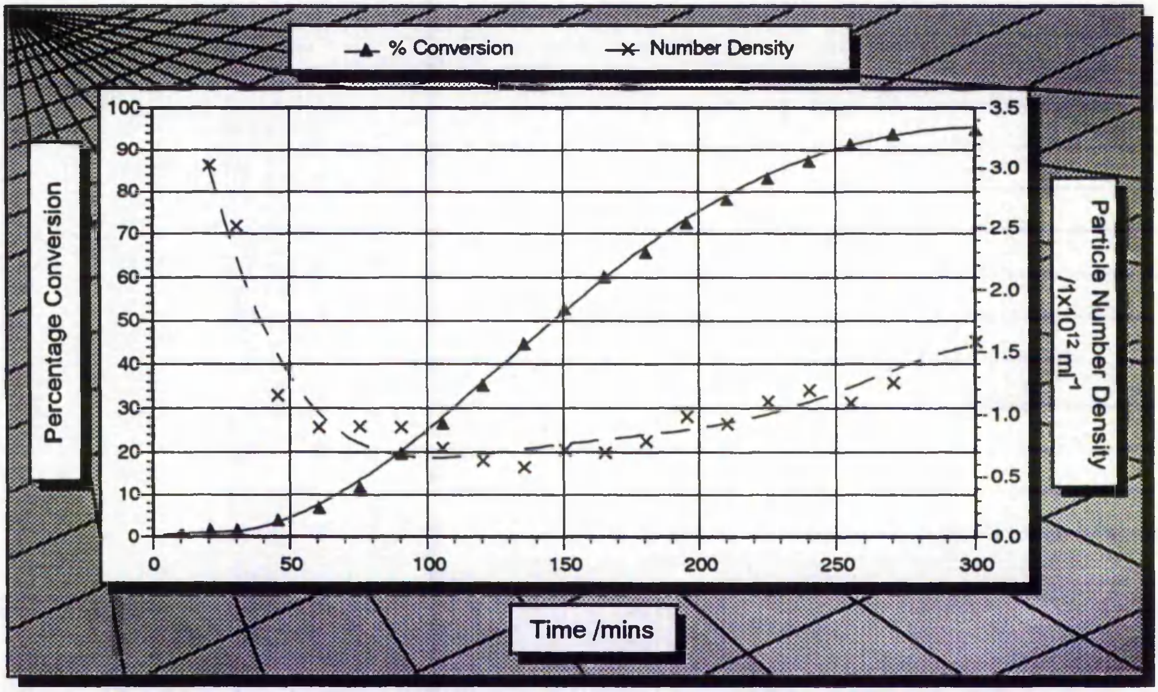

Figure 12.2 Plot of percentage conversion of monomer to polymer and latex particle number density during the course of a butyl methacrylate polymerisation.

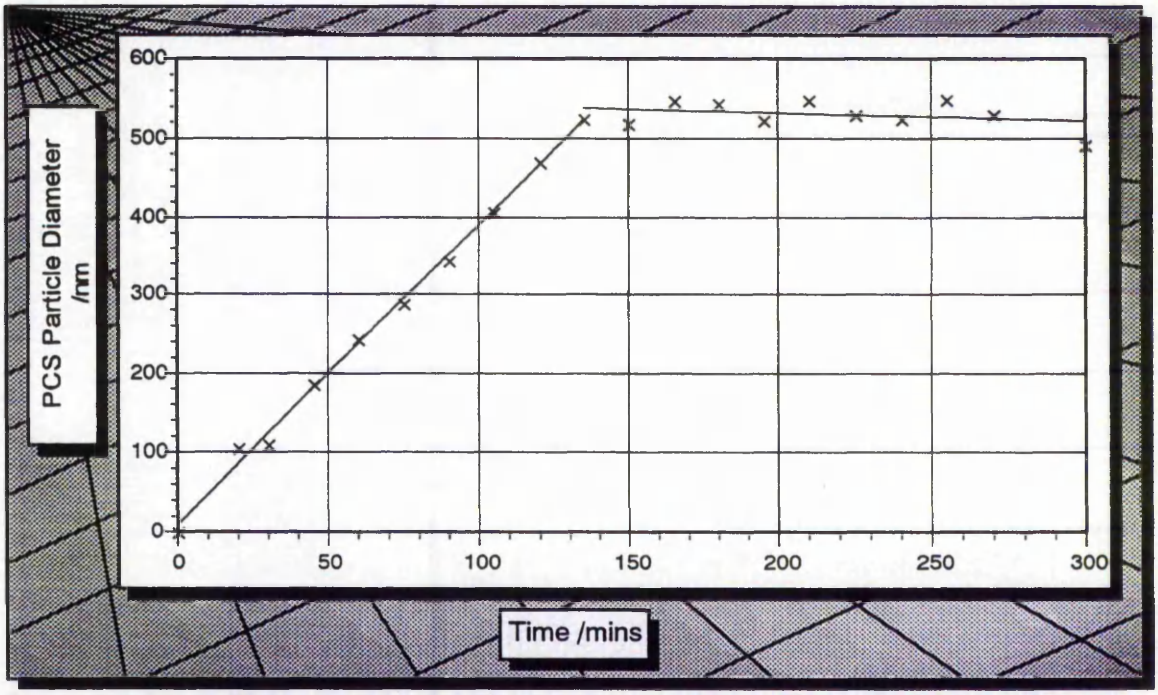

Figure 12.3 Plot of latex particle size (by photon correlation spectroscopy) during the course of a butyl methacrylate polymerisation.

In this work, it can be seen (**Figure 12.2**) that for BMA, the familiar pattern of limited coagulation of nuclei with growth at constant number density occurs, but that the conversion-time data in interval II is linear in contrast to the $C^{2/3}$ dependence observed for styrene[1].

With respect to the data for the BMA reaction, it is seen in **Figure 12.3** that, unlike styrene, the PBMA particle size increased linearly up to the maximum size. Similarly, after the initial lag period, the percentage conversion curve was also linear, during the mid-part of the reaction, once the particle number density had reached a minimum – the number density decreasing to a relatively constant level after approximately 40 mins (after approximately 5% conversion). The conversion versus time curve therefore suggests Smith-Ewart case II kinetics.

It is noticeable from the kinetic graphs that the particle size reaches a maximum at a time of ca 130 minutes from reaction initiation. However, this corresponds to only 44.91% conversion of monomer to polymer. Despite the continuation of the constant rate of conversion after this point in time, it is assumed that at this conversion, all remaining monomer exists in the polymer particles. The reaction recipe contained 45 g monomer initially, implying that at 44.91% conversion, the remaining monomer = 24.79 g. Assuming that 1 g of monomer converts to 1 g of polymer, then when the particles cease to grow, there exists 24.79 g of BMA monomer in 20.21 g of PBMA polymer (*i.e.*, 1.2266 g BMA : 1 g PBMA). Since the molecular weight of BMA = 142, and PBMA has a density[399] of 1.055 g cm^{-3}, then the solubility of the monomer in the polymer = 9.12 moles dm^{-3} (*cf.* styrene solubility = 5 moles dm^{-3}).

Knowing the rate of reaction (R_p) from the gradient of the linear region of the conversion curve, the average number of radicals per particle ($\bar{n}$) during interval two can be calculated from:

$$\frac{d\left(\frac{\%\,conv.}{100}\times N_M\right)}{dt} = R_p = \frac{k_p N_p [M]\bar{n}}{N_A} \tag{12.4}$$

where:

N_M = initial number of moles of monomer;
k_p = propagation rate constant (mol^{-1} dm^3 s^{-1});
N_A = Avagadro's constant (mole^{-1});
N_P = particle number density (dm^{-3});
M = concentration of monomer in polymer particles (mole dm^{-3}).

---

[1] Note that Smith-Ewart kinetics predict the following relationships:

Smith-Ewart Case II: $C \propto t \qquad r^3 \propto t \qquad R_p \propto r^0 \qquad (12.1)$

Smith-Ewart Case III: $C^{2/3} \propto t \qquad r^2 \propto t \qquad R_p \propto r^1 \qquad (12.2)$
(Core-Shell model)

Smith-Ewart Case III: $C^{1/2} \propto t \qquad r^{3/2} \propto t \qquad R_p \propto r^{3/2} \qquad (12.3)$

for conversion (C), particle radius (r), and rate of polymerisation (R_p) as a function of reaction time (t).

The propagation rate constant at the reaction temperature of 323 K can be determined from an Arrhenius-type equation, given that $k_p = 369 \text{ mol}^{-1} \text{ dm}^3 \text{ s}^{-1}$ at 303 K [76] and the activation energy of the reaction = $20.4 \times 10^3 \text{ J mol}^{-1}$ [326].

Therefore given that the rate of reaction = $6.48 \times 10^{-5} \text{ mol dm}^{-3} \text{ s}^{-1}$ and $k_p = 609 \text{ mol}^{-1} \text{ dm}^3 \text{ s}^{-1}$, then:

$$6.48 \times 10^{-5} = \left(\frac{609}{6.02 \times 10^{23}}\right) \times \left(7.2 \times 10^{14}\right) \times (9.12) \times \bar{n}$$

$$\bar{n} = 9.8 \text{ particle}^{-1} \tag{12.5}$$

i.e., the average number of radicals per particle, $\bar{n} \approx 10$ rather than the 0.5 required by Smith-Ewart II kinetics. The high value of $\bar{n}$ and the greater solubility of monomer in polymer tend to suggest a reaction in the bulk of the particle, and the unimodal molecular weight [423] suggests that in contrast to styrene, a single locus, *i.e.*, bulk (most probably) or surface phase are involved.

Disanayaka [120] *et al.* has contrasted the type of freeze-fracture pattern observed for polystyrene – *i.e.*, a developed structure with radial lines from the centre to the surface: said to be characteristic of a core-shell mechanism of growth – with the regularly organised globules observed in methyl methacrylate emulsion polymer generated by homogeneous nucleation [163]. The evidence of the tensile-snap freeze-fracture T.E.M. of PBMA shows the radial pattern shown by styrene – and believed to be indicative of a core-shell mechanism (see **Plate 12.1**).

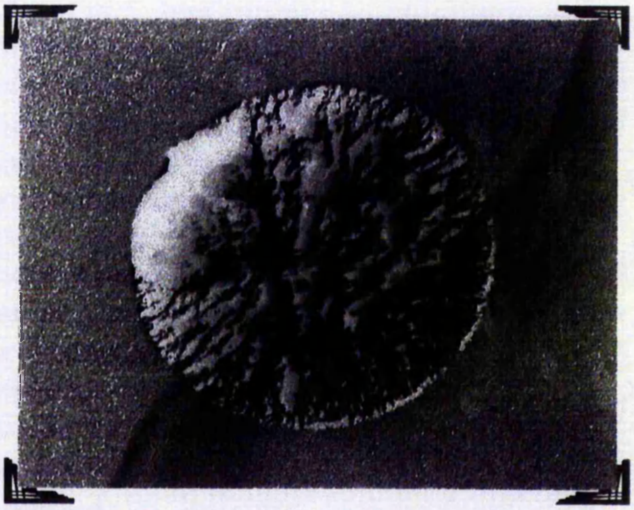

Plate 12.1 Freeze-fracture T.E.M. of a PBMA latex particle.

Although clearly different from styrene kinetics, a firm conclusion as to the mechanism of the soap-free BMA polymerisation is thus difficult and not further developed in this work where the main aim was to establish the time for 'shot' addition.

The recipe for the shot growth BMA-AA polymerisation was described in Chapter 7. It was intended that the shot of AA was to be added when the BMA had achieved 90% conversion to the polymer. From the results for the percentage conversion (of monomer to polymer) and (PCS, z-average) particle size taken from the reaction monitoring (shown in **Figure 12.2** and **Figure 12.3**, respectively), it was estimated that the shot should be added at a time of 245 mins. (Reaction reproducibility is of obvious importance, and it was found that storage of the monomer, following distillation to remove the inhibitor, was detrimental to this objective, even when the monomer was refrigerated to prevent thermal polymerisation.) Measurement of a sample taken moments before the addition of the shot (243 mins), showed the actual conversion at this time, for the reaction to which the shot was added, was 84%. After completion of the reaction, the latex was steam stripped to remove any residual monomer, and then cleaned by microfiltration (including an acid washing stage to convert the carboxyl groups to the acid form).

12.3 End group titrations.

Figure 12.4[1] shows an end point for carboxyl groups (when titrated against sodium hydroxide) of 186 μl for 20 ml carboxylated PBMA latex (hereafter coded K54), equivalent to 42 μmol g^{-1}). K54 latex film prepared from 5 ml of latex cast for 72 hrs at 353 K shows no accessible carboxyl groups within the film or even on the film surface. K54 latex film loaded with 40% sucrose (cast for 72 hrs at 353 K, and leached for 96 hrs in water) shows a carboxyl end point at 27 μl or 58% of the end point to be expected for 5 ml of latex. This result therefore correlates with the permeation studies in Chapter 10 in which it was shown that sucrose opens hydrophilic pathways for ions to enter the film.

12.4 Solute permeability of functionalised PBMA latex films.

PBMA latex film was found (Chapter 9) to effectively act as a barrier to the *4*-nitrophenol permeant over the time frame of a typical permeability experiment. The acrylic acid functionalised PBMA latex film provided no measurable improvement in *4*-nitrophenol flux: the film again presenting a barrier over a period of 72 hrs.

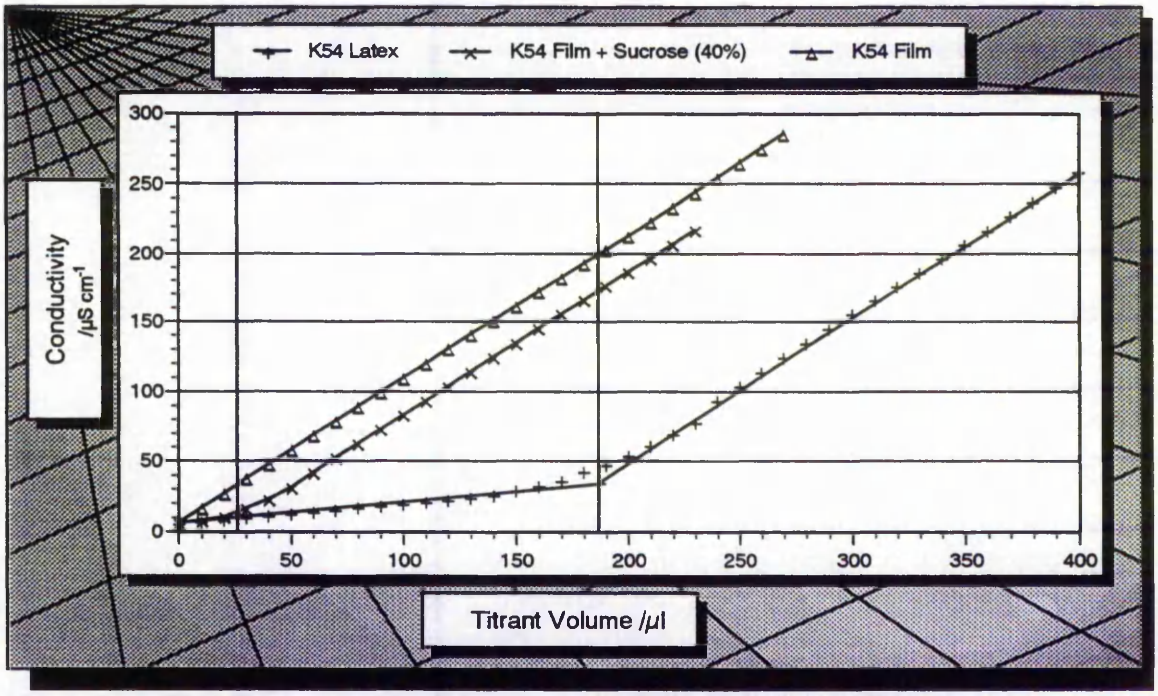

Figure 12.4 End-group analysis of carboxylated PBMA latices and film.

---

[1] The author acknowledges M. Ashmore for performing the titrations as part of an undergraduate project. The figure depicts data reconstructed onto the same set of axes (differing NaOH concentrations having been used originally to increase sensitivity).

12.5 Summary and conclusions.

It has been shown that the polymerisation kinetics of BMA monomer differ from those of styrene despite the similar aqueous solubilities of the two monomers.

These preliminary findings using the AA-shot PBMA, which could not be pursued further due to contractual time limitations, suggest that water soluble, leachable additive could be used to make latex films suitable for use as reactive substrates for, *e.g.*, catalytic reactions where expensively synthesised latex would be reusable.

◆

Conclusions, Chapter 13: Final Summary and Conclusions.

13.1 Summary of results.

13.1.1 Film appearance and structure.

13.1.1.1 Film casting.

Because the majority of the latex drying processes involve evaporation from what is effectively bulk water, the drying curves to the various latices were virtually identical (when cast under the same conditions) in shape, and independent of polymer hydrophilicity (*e.g.*, the drying curve for Eudragit® *RL* could be overlaid on that of Eudragit® *NE*, and similarly for PBMA).

Films were observed to dry non-uniformly across their surface area, and also from the top downwards, with a 'skin' forming initially. The prospect of the polymer hydrophilicity affecting the final stages of drying (where water must diffuse through polymer) was not evident in the results – possibly as a result of the non-uniformity of drying across the film's surface area, such that only average latex particle packing fractions could be determined for the latex/film as a whole.

13.1.1.2 Additive-free films.

All of the films used were transparent to varying degrees – Eudragit® *RL* showing the highest clarity. Other films were somewhat hazy, but with sufficient transparency to allow a blurred image of an object when viewed through the film. Again with the exception of Eudragit® *RL*, all films showed a textured polymer-air side, with either graininess or a vein-like network of 'mudcracks.' Such mudcracks were most visible in the surfactant-free films. The mudcracks were believed to be a result of the stresses of drying, and the presence of plasticiser in some of the Eudragit® films may have alleviated the feature. (Note that Eudragit® *L* tended to crack, on drying, without the plasticiser.) Eudragit® *RL* was particularly featureless, showing no sign of mudcracking. All latex cast films appeared smooth, and hence presumably more dense, at the polymer-substrate interface

Under the S.E.M., Eudragit® *NE* and *RL* films showed no signs of residual latex particle structure, either on the surface or internally. The enhanced resolution of T.E.M., combined with the tensile snap method of film fracture, also failed to reveal any structure in the low T_g PAMA and PHMA films. PBMA films tended to show latex particles on both film surfaces (albeit compressed at the polymer-substrate interface), despite a casting temperature well in excess of the polymer T_g, but no interparticle structure was evident internally by S.E.M., and was negligible by F.F.T.E.M.

13.1.1.3 In the presence of additives.

The presence of sucrose in the films tended to increase the level of film opacity (which increased with increasing load). Eudragit® *NE* films containing HPMC had a matt appearance, and reduced tackiness. Eudragit® *L* did not change the visual appearance of the Eudragit® *NE* films to which it was added.

NaCl was added to dialysed Eudragit® *NE* to destabilise the latex, and disrupt particle packing during film formation, as a method of producing a porous film. Visually, such a film appeared identical to the additive-free film at low levels ($\langle$2%) of NaCl addition. As the level of NaCl increased, so did the film opacity. This was possibly due to both the presence of the NaCl, combined with poorer particle packing: the presence of the NaCl also being visible as crystalline formations on the film surface. S.E.M. fracture cross-sections showed crystalline NaCl indicating that the additive was not entirely molecularly dispersed.

Porosity was only evident in films when leached of additive *and* when the polymer had a T_g above ambient. PBMA leached of either Eudragit® *L*, or sucrose, showed porosity (both via S.E.M. and mercury porosimetry). This was also the case when Eudragit® *L* was leached of Eudragit® *NE*. However, when a soft polymer was leached of additive, no porosity was observed (*e.g.*, Eudragit® *NE* leached of either sucrose or Eudragit® *L*).

13.1.2 Additive dissolution.

Dissolution of an additive from the films was dependent on the additive load, its level of dispersion (*i.e.*, molecular or particulate), and the molecular weight/size of the additive. Low levels of additive were generally more difficult to leach than high levels. This was a result of the low levels being better dispersed within the films, with no easy pathways for their exit, or the entrance of the dissolution medium. At high levels of addition, such pathways would be created by the dissolution of that additive closest to the film-air interface. It was found that HPMC could not be fully leached, even at long dissolution times – presumably due to its high viscosity (which would be accentuated in the aqueous environment of the limited porosity resulting from the HPMC leaching).

The leaching of Eudragit® *L* from Eudragit® *NE*. films was complicated by the necessity to dissolve the comparatively large particles.

13.1.3 4-nitrophenol permeability.

13.1.3.1 Additive-free films.

All films, except PBMA, were found to be permeable to 4-nitrophenol. PBMA was found to show no measurable 4-nitrophenol flux over the experimental time period.

The 4-nitrophenol permeability coefficients of the three surfactant-free polymer films increased with increasing hydrophobicity of the polymer, *i.e.*, PHMA $\rangle$ PAMA $\rangle$ PBMA. This reflected the expected trend in solubility for a hydrophobic permeant in increasingly hydrophobic polymers. In the case of PBMA, it was found that the scatter of the results was decreased by increased thermal annealing: the un-annealed film showing a large experimental uncertainty with results spread over an order of magnitude. Given this fact and that the more hydrophobic PAMA/PHMA polymers showed higher permeability coefficients, it would appear that the increased permeability of some of the un-annealed PBMA films was a result of faults in the film structure or particle packing.

Of the three Eudragit® polymers, the permeability coefficient increased in the order *RS* $\langle$ *NE* $\langle$ *RL*. Eudragit® *RL* was expected to exhibit a higher permeability than Eudragit®

RS as a result of its increased hydrophilicity and, hence, the increased probability of the permeant being able to move through an aqueous environment – with the associated decreased restriction to its movement.

The hydrophilicity of the Eudragit® *R* polymer films was enhanced by the addition of plasticiser: the permeability coefficient of Eudragit® *RL* film leached of plasticiser being lower than the unleached film. Similarly, the hydrophilicity of Eudragit® *NE* was increased by the presence of endogenous surfactant: a dialysed film showing a reduced permeability compared to the undialysed film which contained leachable surfactant.

The results for the Eudragit® polymers suggested that the permeability coefficient was dependent on the hydrophobicity of the polymer, in agreement with the results for surfactant-free films. However, if water swelled the film (*e.g.*, due to the presence of hydrophilic polymer, surfactant or plasticiser) then the increased diffusion coefficient possible in an aqueous environment led to a film with supplemented transport properties, even if no true porosity (*i.e.*, porosity of sufficient size to allow unimpeded permeant passage, as opposed to transient porosity) existed.

13.1.3.2 In the presence of additives.

The *4*-nitrophenol permeability coefficient showed an initial linear increase when sucrose was used as the additive leaching during the course of the permeation experiment. Beyond ca 25% addition, the permeability showed a much shallower rate of increase – up to 180%, at which point the film failed structurally. (The reason for the loss of linearity was better defined by the use of electrolyte and the aniline permeants.)

The ability of a soft polymer to retain porosity after leaching a water soluble additive, and drying, was investigated using Eudragit® *NE* leached of sucrose. When a level of sucrose addition (which had yielded a relatively large increase in *4*-nitrophenol permeability coefficient when the sucrose was leaching during permeation) was leached and dried prior to the permeation experiment, the enhancement of permeability was found to be lost. In contrast, leaching the film but not allowing it to dry allowed the enhanced permeability to be substantially retained. This thus gives an impression as to the ability of the low T_g polymer to 'heal' itself, upon drying. The same impression is provided by S.E.M. evidence which showed Eudragit® *NE* leached of sucrose to be pore-free, whilst PBMA leached of sucrose was porous.

Eudragit® *NE* films containing HPMC gave an initial linear increase in permeability coefficient up to higher levels of addition than did sucrose, and to a permeability coefficient of higher magnitude. This greater efficiency resulted from the increased difficulty in leaching the HPMC – attributed to the ability of the HPMC-loaded Eudragit® *NE* films to imbibe water, with the formation of a viscous gel.

A two stage increase in permeability was seen when Eudragit® *L* was used as a leachable additive. Like HPMC, however, the level of enhancement was greater than that resulting from sucrose, as shown by their respective permeation activation energies.

13.1.4 Aniline permeability.

13.1.4.1 Additive-free films.

Eudragit® *RL* films displayed a transport mechanism in which permeation occurred through either aqueous channels or pores as opposed to a solution-diffusion mechanism. Despite the different solubility coefficients, of the series of anilines, the permeability coefficients tended to coincide: presumably as a result of both the leaching of the triacetin plasticiser and the hydrophilicity of the functionalised polymer. None of the surfactant-free latex films displayed convective transport. Despite the presence of the surfactant in Eudragit® *NE*, it too showed solubility dependent aniline permeability coefficients. The magnitude of the permeability coefficient and aniline uptake (for ethyl aniline, methyl aniline, and aniline) by Eudragit® *NE* showed the same rank trend as their hexane-water partition coefficients as determined by Serota[446] *et al.*

13.1.4.2 In the presence of additives.

Eudragit® *NE* films containing Eudragit® *L* exhibited convective transport at high levels of addition. The value of the 4-nitrophenol permeability coefficient for the Eudragit® *L* load at which convective aniline transport occurred in a mixed Eudragit® *NE* + *L* film could possibly be used to predict whether coincidental aniline transport rates would occur in other film-additive combinations. Therefore, based on the values of their 4-nitrophenol permeability coefficients, convective transport is anticipated at only the highest levels of HPMC addition (to Eudragit® *NE*), whilst in the case of the sucrose additive, the solution-diffusion mechanism would appear to operate up to levels of addition of ca 80%.

13.1.5 Electrolyte permeability.

13.1.5.1 Additive-free films.

Whilst Eudragit® *NE* films were impermeable to electrolyte (*i.e.*, they were non-porous, insoluble in water, and provided little or no opportunity for ion exchange), Eudragit® *RL* films were found to be permeable.

13.1.5.2 In the presence of additives.

Eudragit® *NE* films loaded with sucrose above ca 25% (*i.e.*, above the limit of the linear trend in 4-nitrophenol permeability coefficient) showed an electrolyte flux of increasing magnitude. Analysis of the permeability coefficient (which was assumed to be equal to the diffusion coefficient in such situations) showed the porosity to be only of slightly greater radius than that of the permeating electrolyte: a feature that is in accord with the very slow rate of attainment of equilibrium in the permeability cell (compared to when the membrane dividing the cell was a filter paper) – but giving further support for a porous transport mechanism.

13.1.6 Sucrose permeability.

Eudragit® *NE* films were impermeable to sucrose, both when additive-free and when loaded with sucrose as a film additive. This result implies that the porosity which was necessary in order to leach sucrose additive trapped within the film is not necessarily continuous through the film to allow permeation. The slow leaching of low levels of sucrose additive imply that the sucrose was not simply on the surface of the film. The ability to leach such low levels of sucrose points to the fact that it was trapped in channels within the film that do have access to the film surface.

Considering the high levels of porosity observed in some of the leached hard polymer films (*e.g.*, PBMA leached of sucrose or Eudragit® *L*), and assuming that this same level of porosity occurs in soft polymer films (at least until the films are dried), it is quite surprising that continuous porosity does not exist. It is, however, possible that a certain degree of 'healing' (sintering) occurs when the films are wet: sufficient to impede the transport of sucrose, once the sucrose additive has been leached.

Additive-free Eudragit® *RL* films did allow the transport of sucrose – due to the leaching of triacetin and/or greater polymer hydrophilicity. The 'pores' formed had a radius approximately three times that of the sucrose molecular radius.

13.1.7 Gas and water vapour permeability.

None of the additives, when present in the films, increased the rate of CO_2 permeation. Permeability coefficients were often decreased when compared to the additive-free films, and this was due to either the additive being less permeable than the polymer, or the polymer chain motion being hindered.

Despite a number of the additives increasing the hydrophilicity of the film, exposure of the film to water vapour never led to swelling (whitening) to the extent shown when exposed to liquid water. None of the additives yielded a large increase in the water vapour permeability coefficient.

13.1.8 Increased polymer hydrophilicity.

Whilst Eudragit® *NE* films showed higher 4-nitrophenol permeability coefficients than the corresponding dialysed films, this was probably due to their containing leachable surfactant (which was not present in the dialysed films). The same is typically true of films showing increased transport rates at levels of surfactant addition above surface coverage found by other workers [e.g., 74]. Increasing the hydrophilicity of PBMA films by using an acrylic acid coating on a PBMA latex showed that the increased hydrophilicity was not necessarily readily accessible. The addition of a leachable additive (*i.e.*, sucrose) increased the accessibility of the carboxyl groups, which might make such a film capable of catalytic activity.

13.2 Final conclusions.

The transport properties of a polymer latex film have been found to be enhanced, in a systematic manner in solute permeation experiments by the addition of water soluble hydrophilic additives.

13.2.1 The influence of the physical properties of the polymer.

The polymer T_g is of great importance and the properties of a polymer film depend on the storage temperature and/or the environment in which the film is utilised.

- ✘ Soft polymer[1] particles (*e.g.*, Eudragit® *NE*) coalesced, on film formation, to a degree whereby they appeared featureless (on a particulate scale) under the F.F.T.E.M. Hard polymer (*e.g.*, PBMA) particles, however, still showed evidence of vestigial latex particles at the film surfaces.
- ✘ A film prepared from a hard polymer latex showed a greater level of iridescence when casting, when compared to a film cast from a soft polymer.
- ✘ A hard polymer latex film leached of its additive retained a degree of porosity on drying (*e.g.*, PBMA leached of sucrose or Eudragit® *L*, or Eudragit® *L* leached of Eudragit® *NE*). A soft polymer film leached of its additive was found to return to the construction of the additive-free film (*e.g.*, Eudragit® *NE* leached of its additives).

The ability to prepare a porous film (especially a free-film, as opposed to a coating) has a number of contradictory requirements. To retain the porosity (following additive leaching) required to increase film permeability dictates the use of a hard polymer. Such a polymer is, however, least suitable for film forming – at worst forming a powder. If the polymer does coalesce into a film, then the film is likely to show extended aging properties, such as increasing densification of particle boundaries and further gradual coalescence. Such characteristics lead to greater unpredictability in the properties of coatings prepared from such polymers, when compared to coatings prepared from soft polymers in which aging is minimised due to the particle coalescence being further advanced (*i.e.*, Eudragit® *NE* was found to show little change in solute permeability properties after accelerated aging by high temperature annealing).

The higher mobility of soft polymer chains is therefore most likely to produce a well coalesced film due to their motion providing sufficient chain fusion during the casting period to yield a film in which any further chain interdiffusion is no different from that of a film cast from a melt or (good) solvent; *i.e.*, the further gradual motion of the chains need not necessarily be thought of as coalescence, as it is less likely to influence the properties of the film, and is simply the random motion of the polymer chains constituting the film as a whole. The same cannot be said for a hard polymer, in which the further gradual coalescence is increasing the structural strength of the film, leading to a lessening of the particulate structure.

---

[1] Soft or hard polymer refer to the T_g of the polymer being either below or above ambient temperature, respectively.

The effects of film aging in a hard polymer could be removed by longer casting times, and higher casting temperatures. This was true for surfactant-free PBMA, where an increase in the casting time from 3 hrs to 72 hrs led to a film whose permeability properties were vastly superior (in terms of reproducibility) and which showed much less particulate structure compared to films observed (under the F.F.T.E.M.) in previous work [423].

13.2.2 The influence of water.

A permeant which is soluble in a polymer will diffuse through it due to the random cooperative molecular motions of the polymer chains, *i.e.*, independent of the presence of water. Typically, a hydrophobic penetrant is most likely to dissolve into a hydrophobic polymer. As a result of its method of formation (*i.e.*, free-radical emulsion polymerisation) a polymer latex is likely to have a certain degree of hydrophilicity due to the presence of surfactant. In the case of a surfactant-free emulsion polymerisation, there will be charged polymer chain end groups on the particle surfaces. Such hydrophilicity is likely to increase the permeability of a film by allowing water into the film providing a path of less diffusive resistance (*e.g.*, the 4-nitrophenol permeability of Eudragit® *RL* is greater than Eudragit® *RS*). Efentakis [137] *et al.* concluded, however, that the role of surfactant in drug dissolution from a hydrophobic polymer matrix was to increase the release rate of the drug due to leaching and, hence, pore formation, rather than its ability to increase the "wettability" (as determined from contact angle measurements and calculations of spreading coefficients) of the matrix. This would appear, however, to be related to the amount of additive or coalescing aid, etc.: increased coalescence reducing the rate of transport of water, and aqueous solutes, unless leaching of the additive leads to porosity. This may therefore be dependent on the location of the additive. For example, if the additive (*e.g.*, surfactant) is 'permanently' bound to the latex particle surfaces in the film, or if heat treatment has effectively 'sealed-in' the additive, then this un-extractable additive may imbibe water by an osmotic process [458]. The imbibition will be limited, however, due to the increasing hydrostatic pressure in the water-swollen regions due to the resistance of the polymer to deformation. Swelling of HPMC loaded Eudragit® *NE* films was possibly enhanced by an osmotic process. Although the HPMC would not be grafted to the polymer, a similar effect may result due to the difficulty of leaching the viscous gel.

The presence of water may have a number of effects on the transport properties of a polymer latex film. Not only would it allow the permeation of penetrants which are insoluble in the polymer alone, but it may also act to plasticise the polymer, albeit localised in the hydrophilic regions of the film (possibly at the particle boundaries). Plasticisation would presumably increase the rate of transport of both hydrophobic *and* hydrophilic permeants. At the lowest levels of addition of molecular additives such as sucrose or HPMC, leaching does not result in porosity of a size suitable to allow unimpeded permeant transport. The enhancement of permeability may therefore be considered to result from the greater void space within the films yielding a greater degree of polymer chain motion due to a loosening of the film structure.

Permeation through the films used in these studies may be interpreted as (i) pure solution-diffusion type (activated) transport, (ii) permeant transport through hydrophilic and/or plasticised pathways, and (iii) (unimpeded) transport through pores – in which the pore diameter is greater than the permeant size, and which pass from side-to-side of the film. Each of these may occur singularly, or together. Note that items (ii) and (iii) differ in that for the latter case, the pores might be considered to be in permanent fixed positions and of fixed size, whereas in the former case plasticisation channels will be transient and dependent on the cooperative motion of the polymer chains – albeit to a lesser degree than case (i) where permeant transport will depend on the probability of the penetrant to secure a (diffusive) hole of suitable size. The change from transport type (ii) to (iii) being gradual, dependent on the initial load of leachable additive.

4-nitrophenol does not readily permeate through the surfactant-free PBMA film, but does permeate in the presence of various additives. Similarly, the increased 4-nitrophenol permeability coefficient of surfactant-present Eudragit® *NE* latex films when compared to dialysed Eudragit® *NE* films is purely an enhancement due to the presence of surfactant. If, however, an additive fails to increase the gas permeability of a film, it must be assumed that the additive itself does not plasticise the polymer. An increase in the permeability coefficient of an aqueous solute is, therefore, predominantly dependent on the additive allowing a greater amount of water into the film.

13.2.3 The influence of the film additives.

The distribution of the various additives has been ascribed to the manner in which the films dry from top to bottom. Distribution of a water soluble additive can occur in a number of ways. Assuming that the additive is, before casting, uniformly distributed totally in the aqueous phase:

- ✗ the additive can become trapped in the interstices between the coalescing particles (the inability of additives such as sucrose to permeate the film tends to imply that the additive will only be found around or between particles as opposed to between polymer chains);
- ✗ if initially dilute, the additive may be preferentially concentrated in the aqueous phase leading to an increasing concentration gradient towards the base of the film. The evaporation of water from the base of the film through the skin may, however, carry the additive towards the film surface, to be deposited in the film if the concentration of additive in the evaporation channel is at saturation: leading to a concentration gradient which decreases towards the upper film surface;
- ✗ the rapid attainment of a saturated solution of the additive may result in a high concentration of additive at the base of the film, but will also lead to a high concentration in the interior of the film due to the additive having no option but to precipitate as increasing amounts of water are evaporated during film drying.

Each of the above premises tends to imply that although the additive may show a concentration gradient towards one film surface or the other, additive would be expected throughout the film. Further distribution may occur as a result of incompatibility of the polymer and the additive leading to:

- ✗ clustering in the interior of the film;
- ✗ expulsion at the film surfaces;

as a result of interfacial tension favouring polymer-polymer cohesion over that of polymer-additive. S.E.M.s of leached hard polymer films tended to show uniform porosity across the thickness of the film, rather than at just one face, confirming that the additives within the film were generally well distributed. Accumulation of additive at the film surfaces (*e.g.*, sucrose on Eudragit® *NE*) is wasteful since it does nothing to enhance permeability. Being quickly dissolved, it would do little to inhibit solute permeation.

The addition of the particulate Eudragit® *L* to a Eudragit® *NE* film, for example, differs in that its distribution is more dependent on its abundance and degree of mixing, when compared to a molecular additive. Since the Eudragit® *L* additive and the film-forming Eudragit® *NE* latex are of similar particle size, then with an equal mixture of the two latices, and sufficient initial mixing, it is reasonable to assume that a uniform distribution can be achieved. This may, however, be prejudiced during film casting by the differing stabilities of the latices, and the fact that the differing surface functionality may lead to variation in the proximity of approach of nearest neighbour particles dependent on latex type, *e.g.*, Eudragit® *NE* versus Eudragit® *NE*; Eudragit® *NE* versus Eudragit® *L*; or Eudragit® *L* versus Eudragit® *L*. As with the other additives, however, porosity due to the leaching of Eudragit® *L* appeared uniform across the full film thickness, when observed under the S.E.M., showing no evidence of a stratified film.

All of the leachable film additives investigated tended to yield a trend in the plot of apparent permeability coefficient (as a function of additive load) which initially increased linearly, with load, before tending to plateau. The break in this curve tended to occur at the point where the film transport mechanism changed from being predominantly via a solution-diffusion mechanism to one where convective transport occurred (as evinced by electrolyte passage through a film that was previously a barrier).

The measured apparent permeability coefficient would be expected to be a function of all types of transport: *i.e.*, it is a function of the measured increase in permeant on the receiver side of the film, and the respective fluxes are additive [167], *i.e.*:

$$\frac{dC}{dt} \propto J_1 + J_2 + \cdots\cdots + J_n \tag{13.1}$$

where:

J = respective fluxes of each various mode of transport;
C = receiver concentration.

From this it would be expected that the measured apparent permeability coefficient might increase with increasing load of additive, up to the point where a convective flux occurs, after which the apparent permeability coefficient would increase to a greater extent due to the higher diffusion coefficients found in water (when compared to polymer). There was no sudden increase in flux (despite permeant transport being faster in an aqueous environment compared to in the polymer) due to the fact that convective transport is not a sudden occurrence in the film. Considering the effect of the increasing loadings of additive at a point where a hypothetical single continuous pore is about to form: the leaching of the additive at this point effectively decreases the thickness of the film at this point. (*I.e.*, a closed pore exists in which convective transport occurs through a fraction of the average film thickness.) This decrease in thickness is a uniform and linear process such that if the break-point occurs at, for example, 25%, then at a loading up to 24.99* there is still present the thinnest of films such that convective transport cannot yet occur through the full thickness, *i.e.*, transport may be by solution-diffusion through i, the polymer (*e.g.*, J_1) and ii, interparticle boundaries (*e.g.*, J_2), with convective flux (*e.g.*, J_3) gradually increasing from an additive load of 25% upwards.

When the additive is clustered within the film, then the non-continuous pores formed are likely to be narrow-necked 'inkwell' type voids.

That an additive such as sucrose can be completely leached from a film, albeit slowly at low loadings, suggests that the pores have access to one of the film surfaces. The fact that the labelled sucrose (permeant) is, however, unable to permeate from one side of the film to the other, at additive loadings below 25%, suggests that the pores are not continuous through the full thickness of the film. Where the additive is well dispersed throughout the film, but is present in insufficient amounts to lead to coarse channels on leaching, then the access of water to the clusters will be through only narrow hydrophilic pathways – which explains the slow kinetics of leaching.

It is the increase in the number and size of the hydrophilic pathways, from interparticle boundary plasticisation up to macroscopic pores, which leads to the systematic increase in permeability coefficient with increase in additive loading.

With reference to the modes of transport through a latex film, and equation (13.1), the flux through an additive-free film would be either solely due to permeant transport in solution in the polymer, if possible (or otherwise transport via hydrophilic pathways resultant from latex particle's surface hydrophilicity and adsorbed surfactant and its hydration), then:

$$\frac{dC}{dt} \propto J_{polymer} \tag{13.2}$$

The diffusion coefficient is, at this time, the diffusion coefficient of the polymer film.

The additive, at low loadings, is well dispersed in hydrophilic channels which result from its initial dispersion during casting, and its carriage to the surface during film drying. Leaching of this dispersed additive, and its replacement by water yields a higher flux due to the widening of the channels/pathways through the polymer. The transport of the permeant is still impeded by the polymer, and no continuous, wide, pores exist. Due to the ease of permeant transport through these routes, $J_{polymer}$ tends to be negligible, with respect to total film transport, and is replaced by $J_{plasticisation}$. This flux increases with increasing content of additive in the film and, hence, the measured diffusion coefficient also increases.

Once continuous porosity exists, allowing unimpeded film transport (albeit by a tortuous route), then:

$$\frac{dC}{dt} \propto J_{plasticisation} + J_{porosity} \tag{13.3}$$

It is believed that this is the rate of change of concentration observed in the receiver permeability cell after the initial linear increase in permeability coefficient. The diffusion coefficient associated with $J_{porosity}$, is that of the permeant in water (as opposed to polymer), and is therefore effectively a constant for the conditions of the experiment.

It would be expected that $J_{plasticisation}$ would tend to $J_{porosity}$, as the additive load increased. However, it is believed that the porosity does not increase to such an extent before the film falls apart, and therefore there is always a highly tortuous path that must be taken. (Hence, the low electrolyte fluxes observed.)

The three main additives investigated each had their own advantages, with respect to their ability to increase film permeability. Sucrose is a relatively small molecule which dissolves quickly. This allows it to be well dispersed and readily leached from the film. HPMC does not dissolve in water quite so readily, and forms a relatively viscous solution on dissolution. This viscosity would tend to impede the diffusion rate of a permeant in the HPMC solution. In mitigation, however, the viscosity also means that the additive is not readily removed from the film such that there is less of a tendency for the film to heal, even after drying: the residual HPMC allows the possibility to repeat the process of permeation whilst leaching (albeit as if starting from a lower level of additive). In addition to the leaching of the additive leading to porosity (or simply a decrease in localised film thickness), the high degree of swelling shown by HPMC would tend to imply that even if the additive were not to leach, it would have a plasticising effect on the film as a consequence of water imbibition.

Eudragit® *L* is possibly the least effective of the additives. The gain which might result from its large size (and, hence, large pore size) is in reality lost due to the time it takes for such a large body to dissolve, and due to the decreased ability to disperse a given weight of additive when compared to a molecular additive. Despite this, however, a break in the *4*-nitrophenol apparent permeability curve, as a function of Eudragit® *L* load, was still in evidence, and the activation energy of *4*-nitrophenol permeation was nearer to that shown by the HPMC additive than that of the additive-free Eudragit® *NE* film.

Each of the additives investigated can effectively be used to increase film permeability. **Low levels of addition of an additive** tend to allow control of permeation via a solution-diffusion mechanism of film transport due initially to **increased access of water into the film** (and possible plasticisation of the film by the water), **and a decrease in effective film thickness. Higher levels of additive load lead to convective film transport**, allowing the permeation of electrolyte and yielding transport that, to a greater extent, is independent of permeant solubility in the polymer (*i.e.*, below this level of addition, transport is perm-selective dependent on the solubility of the permeant in the polymer), but shows little effective increase in permeability, presumably due to the fact that there is a high degree of tortuosity in the porous network, and also due to the narrowness of the pore diameter. Increasing the level of additive still further was found to lead to an increase in the electrolyte transport through the film, implying either an increase in the pore number density, or a widening of the existing pore diameter. Whilst such an increase allowed somewhat greater electrolyte transport, the effect on the other permeants was minimal compared to the initial increase in permeability. This was presumably a result of the limiting amount of additive which could be contained by the film such that despite the increasing porous network, the tortuosity of that network becomes a limiting factor, and no significant increase in film transport is seen before the additive loading is such that film fails structurally.

13.3 Future work.

Although the additives investigated in this study have been shown to increase the aqueous solute transport properties of the films investigated, none of the films have shown the ideal desirable properties required of a polymer for such investigations (*i.e.*, easily characterised transport properties brought about by good additive dispersion, ease of handling, etc.) Obviously, however, the idealism of the properties are dependent on the application of the film. With regard to a study of permeability, and the desire to find a means for aqueous solute-independent transport, requirements have been found to be contradictory:

✗ A latex that is a good film former is typically tacky, and not easily handled.

✗ A latex that is not tacky, and which is of sufficiently high T_g to yield permanent porosity following leaching and drying is typically not a good film former.

Eudragit® *NE* solved some of these problems, but was too soft to retain porosity, and contained leachable surfactant which complicated the characterisation of its transport properties. None of the readily available methacrylate monomers polymerises to yield a polymer of suitable T_g. Therefore, for future study, the **preparation of an idealised surfactant-free copolymer** whose T_g is between that of the 'too soft' Eudragit® *NE* and 'too hard' PBMA may be worthwhile.

Film stratification would be of value to the decorative/protective coatings industry, where a cheaper polymer could be used to give bulk thickness to a better quality (*i.e.*, appearance or performance) skin. However, stratification of a film is not easily achieved. A proposed method for stratification (based on the fact that water soluble additives have been found to accumulate to some extent, during casting, at the final site of bulk water – *i.e.* the base of the film) arises from the ability of the Eudragit® *L* latex to form a salt at a set pH. A film cast from a mixture of non-salt forming latex (*e.g.*, Eudragit® *NE*) and Eudragit® *L* in which the pH is adjusted such that the Eudragit® *L* is in its salt form would presumably yield a film in which the skin is formed initially, from the Eudragit® *NE*, whilst the Eudragit® *L* becomes increasingly concentrated beneath. Further evaporation of the aqueous phase would eventually lead to the precipitation of the Eudragit® *L* which would effectively yield a solvent (water) cast base to the film. The final film would therefore show an increasing concentration gradient of Eudragit® *NE* towards the polymer-air interface, with an increasing concentration gradient of Eudragit® *L* towards the polymer-substrate interface.

An alternative method may be to cast a film from latices of differing densities. Polymers typically used for latices are unlikely to show sufficient density variation to yield stratification with depth of aqueous phase. However, a number of methods have been reported by which (multi-)hollow latex spheres may be produced [271, 361, 363]. A mixed latex consisting of solid and hollow spheres would presumably yield a film in which the solid spheres constitute the base, and the hollow spheres the polymer-air interface. (Hollow latex spheres have been prepared with the purpose of being able to float [271]: a feature which further increases the probability of stratification.)

The carboxylated shot-growth latex was prepared with the intention of increasing the degree of hydrophilicity in the latex particle boundaries of a film, with the hope that this would lead to hydrophilic channels or pathways through which a penetrant may travel. The acidic nature of such pathways provides for the possibility of a chemical reaction occurring with the penetrant as it moves through the film: *e.g.*, an acid **catalysed reaction.** Such a reaction could presumably be the acid catalysed inversion of sucrose: *i.e.*, sucrose on the donor side of the film to yield invert sucrose on the receiver side. The films used in this study (with the possible exception of Eudragit® *L* which would, in any case, disintegrate if not crosslinked) lacked the necessary degree of acidity, and would obviously need to be made sufficiently porous to allow the permeation of sucrose. (Sucrose was not able to permeate the additive-free films. This implies that when sucrose does permeate a film leached of an additive to yield sufficient porosity, then the sucrose travels between particles rather than through the packed polymer chains which constitute a particle. The carboxylation of the full polymer chain as opposed to just the latex particle surfaces is therefore unnecessary.)

Finally, many of the additives and polymers considered might be suitable for use as pharmaceutical coatings. Many of the intricacies associated with free-films would be alleviated (albeit, perhaps, at the expense of an entirely new set of problems) by investigating the film + additive combinations when sprayed onto drug cores. Such a project should be feasible for a pharmacist with ready access to a supply of drug cores, and bench-sized coating apparatus.

◆

Chapter 14: References.

1 Abdel-Aziz S.A.M., Studies in Permeability in Polymeric Films., PhD Thesis, University of Strathclyde, (1976).

2 Abdel-Aziz S.A.M., Anderson W., Armstrong P.A.M., *Surface Difference and Solute Permeability in Films of Certain Acrylic-Methacrylic Ester Polymers.*, J. Appl. Polym. Sci., 19, p1181-1192, (1975).

3 Abdel-Aziz S.A.M., Anderson W., *The influence of casting solvent composition on structure and permeability of acrylic-methacrylic ester copolymer films.*, J. Pharm. Pharmac., 28, p801-805, (1976).

4 Adamson A.W., In Physical Chemistry of Surfaces., Second Edition, Ch. 10, *Wetting, Flotation, and Detergency.*, p473-503, Wiley Interscience, N.York, (1967).

5 Aerdts A.M., Theelen S.J.C., Smit T.M.C., German A.L., *Grafting of Styrene and Methyl Methacrylate onto Polybutadiene in Semi-Continuous Emulsion Processes and Determination of Copolymer Microstructure.*, Polymer, 35 (8), p1648-1653, (1994).

6 Ahmed S.M., El-Aasser M.S., Pauli G.H., Poehlein G.W., Vanderhoff J.W., *Cleaning Latexes for Surface Characterization by Serum Replacement.*, J. Colloid & Interface Sci., 73 (2), p388-405, (1980).

7 Aithal U.S., Aminabhavi T.M., *Molecular Transport of some Industrial Solvents Through a Polyurethane Membrane.*, J. Appl. Polymer Sci., 42, p2837-2844, (1991).

8 Allain C., Ausserre D., Rondelez F., *Direct Optical Observation of Interfacial Depletion Layers in Polymer Solutions.*, Phys. Rev. Lett., 49 (23), p1694-1697, (1982).

9 Almog Y., Reich S., Levy M., *Monodisperse Polymeric Spheres in the Micron Size Range by a Single Step Process.*, Br. Polym. J., p131-136, (Dec. 1982).

10 Alper J., *Research News Item: Rising Chemical "Stars" Could Play Many Roles.*, Science, 251, p1562-1564, (March, 1991).

11 Anderson J.L., Quinn J.A., *Restricted Transport in Small Pores. A Model for Steric Exclusion and Hindered Particle Motion.*, Biophys. J., 14, p130-150, (1974).

12 Andrianov K.A., Yakushkina S.Ye., Goniava L.N., Polymer Sci. USSR, 8, p2398, (1966).

13 Anwari F., Carlozzo B.J., Chokshi K., Chosa M., DiLorenzo M., Heble M., Knauss C.J., McCarthy J., Rozick P., Slifko P.M., Stipkovich W., Weaver J.C., Wolfe M., *Changes in Hiding During Latex Film Formation: Part II. Particle Size and Pigment Packing Effects.*, J. Coatings Technol., 63 (802), p35-46, (1991).

14 *Aquacoat Aqueous Polymeric Dispersion. The Revolutionary Aqueous Coating System.*, FMC Manual, FMC Corporation, Philadelphia, U.S.A.

15 Armstrong R.D., Wright J.D., *Impedance Studies of Poly(ethyl methacrylate) Coatings Formed Upon Tin-Free Steel.*, Corrosion Sci., 33 (10), p1529-1539, (1992).

16 Arshady R., *Microspheres and Microcapsules: A Survey of Manufacturing Techniques. Part 1: Suspension and Crosslinking.*, Polym. Eng. Sci., 29 (24), p1746-1758, (1989).

17 Arshady R., *Microspheres and Microcapsules: A Survey of Manufacturing Techniques. 2: Coacervation.*, Polym. Eng. Sci., 30 (15), p905-914, (1990).

18 Arshady R., *Microspheres and Microcapsules: A Survey of Manufacturing Techniques. 3: Solvent Evaporation.*, Polym. Eng. Sci., 30 (15), p915-924, (1990).

19 Arshady R., *Review. Preparation of Polymer Nano- and Microspheres by Vinyl Polymerisation Techniques.*, J. Microencapsulation, 5 (2), p101-114, (1988).

20 Arshady R., Ledwith A., *Suspension Polymerisation and its Application to the Preparation of Polymer Supports.*, Reactive Polymers, 1, p159-174, (1983).

21 Asbeck W.K., Van Loo M., *Critical Pigment Volume Relationships.*, Ind. Eng. Chem., 41, p1470-1475, (1949).

22 Asbeck W.K., *Dispersion and Agglomeration: Effects on Coatings Performance.*. J. Coatings Technol., 49 (635), p59-70, (1977).

23 Astarita G., Nicolais L., *Physics and Mathematics of Heat and Mass Transfer in Polymers.*, Pure & Appl. Chem., 55 (5), p727-736, (1983).

24 Aten W.C., Wassenburg T.C., *Influence of the Surfactant Distribution on the Water Resistance of Clear Latex Films.*, Plastics and Rubber Proc. & App., 3 (2), p99-104, (1983).

25 Bagchi P., Gray B.V., Birnbaum S.M., Poly(vinyl toluene) Model Latices., in Polymer Colloids II., Ed. R.M. Fitch, Pub. Plenum Press, p225-264, (1980).

26 Baker R., in Controlled Release of Biologically Active Agents., Pub. John Wiley & Sons, N.Y., p39-83, (1987).

27 Balik C.M., Said M.A., Hare T.M., *Residual Porosity in Polymeric Latex Films.*, J. Appl. Polym. Sci., 38, p557-569, (1989).

28 Bangs L.B. Uniform Latex Particles., Pub. Metachem Diagnostics, (1984).

29 Banker G.S., Gore A.Y., Swarbrick J., *Water Vapour Transmission Properties of Free Polymer Films.*, J. Pharm. Pharmacol., 18, p457-466, (1966).

30 Banker G.S., Park G.E., *New Water-Based Colloidal Dispersions.*, Pharm. Technol., 5 (4), p55-61, (1982).

31 Barrer R.M., Diffusion and Permeation in Heterogeneous Media., Ch. 6, in Diffusion in Polymers, Eds. Crank J., Park G.S., p165-217, Pub. Academic Press, (1968).

32 Barrer R.M., in Diffusion In and Through Solids., Pub. Cambridge University Press, (1941).

33 Barrer R.M., *Molecular Sieve Action of Solids.*, London Chem. Soc. Quarterly Reviews, Vol. III (4), p293-320, (1949).

34 Barrer R.M., *Permeation, Diffusion, and Solution of Gases in Organic Polymers.*, Trans. Farad. Soc., 35, p628, (1939).

35 Barrer R.M., Barries J.A., Slater J. *Sorption and Diffusion in Ethyl Cellulose. Part III. Comparison Between Ethyl Cellulose and Rubber.*, J.Polym. Sci., 27, p177-197, (1958).

36 Bassett D.R., in Science and Technology of Polymer Colloids., Eds. G.W. Poehlein, R.H. Ottewill, J.W. Goodwin, N.A.T.O. ASI Series, 1, p220, Pub. Martinus Nijhoff, (1983).

37 Bauche F., J. Chem. Phys., 21, p1850, (1953).

38 BDH Hazard Data Sheets, Product Code 5705315.

39 Benita S., Donbrow M., *Dissolution Rate Control of the Release Kinetics of Water-Soluble Compounds From Ethyl Cellulose Film-Type Microcapsules.*, Int. J. Pharm., 12 , p251-264, (1982).

40 Benson S.W., North A.M., J. Am. Chem. Soc., 81, p1339, (1959).

41 Berrie A.H., Pigments and Their Use in Polymers., Ch. 2 in The Chemist in Industry 1. Fine Chemicals for Polymers., E.S. Stern (Ed.), Clarendon Press, Oxford, p22-41, (1973).

42 Berthalot C.L. Eassai de Statique Chimique., Paris, France, (1803).

43 Bevington J.C., Melville H.W., Taylor R.P., *The Termination Reaction in Radical Polymerization. Polymerizations of Methyl Methacrylate and Styrene at 25° C.*, J. Polym. Sci., 12, p449-459, (1954).

44 Bevington J.C., Melville H.W., Taylor R.P., *The Termination Reaction in Radical Polymerizations. II. Polymerizations of Styrene at 60° C and of Methyl Methacrylate at 0 and 60° C, and the Copolymerization of these Monomers at 60° C.*, J. Polym. Sci., 14, p463-476, (1954).

45 Bierwagon G.P., *CPVC Calculations.*, J. Paint Technol., 44 (574), p45-55, (1972).

46 Bierwagon G.P., *Critical Pigment Volume Concentration (CPVC) as a Transition Point in the Properties of Coatings.*, J. Coatings Technol., 64 (806), p71-75, (1992).

47 Bierwagon G.P., *Film Formation and Mudcracking in Latex Coatings.*, J. Coatings Technol., 51 (658), p117-126, (1979).

48 Billmeyer jr. F.W., Textbook of Polymer Science., 2nd Ed., Pub. John Wiley & Son, New York, (1971).

49 Bindschaedler C., Gurney R., Doelker E., *Influence of Emulsifiers on Film Formation from Cellulose Acetate Latexes. Experimental Study of Phase Separation Phenomena due to Sodium Dodecyl Sulphate.*, J. Appl. Polym. Sci., 34, p2631-2647, (1987).

50 Bindschaedler C., Gurney R., Doelker E., *Theoretical Concepts Regarding the Formation of Films from Aqueous Microdispersions and Application to Coating.*, Labo-Pharma Probl. Tech. 31/331, p389-394, (1983). {French Translation.}

51 Blandin H.P., David J.C., Vergnaud J.M., Illien J.P., Malizewicz M., *Modelling the Drying Process of Coatings with Various Layers.*, J. Coatings Tech. 59 (746), p27-32, (1987).

52 Blackley D.C., Emulsion Polymerisation – Theory and Practice., Appl. Sci. Pub. Ltd., London, (1975).

53 Blume I., Smit E., Wesling M., Smolders C.A., *Diffusion Through Rubbery and Glassy Polymer Membranes.*, Makromol. Chem., Macromol. Symp., 45, p237-257, (1991).

54 Bo P., Stannett V., *On the Salt Rejection of Non-Ionic Polymeric Membranes.*, Desalination, 18, p113-135, (1976).

55 Bodmeier R., Paeratakul O., *Drug Release From Laminated Polymeric Films Prepared From Aqueous Latexes.*, J. Pharm. Sci., 79 (1), p32-36, (1990).

56 Bodmeier R., Paeratakul O., *Drug Release From Polymeric Films and Laminates Prepared From Aqueous Latexes.*, Congress Int. Technol. Pahrm., 2, p61-68, (1989).

57 Bodmeier R., Paeratakul O., *Evaluation of Drug-Containing Polymer Films Prepared from Aqueous Latexes.*, Pharmaceutical Research, 6(8), p725-730, (1989).

58 Bohrer M.P., *Diffusional Boundary Layer Resistance to Membrane Transport.*, Ind. Eng. Chem. Fundam., 22, p72-78, (1983).

59 Bondy C., Coleman M.M., *Film Formation and Film Properties Obtained with Acrylic, Styrene/Acrylic & Vinyl Acetate/Veova Copolymer Emulsions.*, J. Oil & Colour Chemists' Assoc., 53, p555-577, (1970).

60 Bovey F.A., Kolthoff I.M., *Mechanism of Emulsion Polymerisation IV: Kinetics of Polymerisation of Styrene and Water Solutions.*, J. Polym. Sci., 5 (4), p487-504, (1950).

61 Brace R., M.Sc. Thesis, University of Bristol, (1970).

62 Bradford E.B., Vanderhoff J.W., J. Macromol. Chem., 1, p335, (1966).

63 Bradford E.B., Vanderhoff J.W., *Additional Studies of Morphological Changes in Latex Films.*, J. Macromol. Sci. Phy., B6, p671-694, (1972).

64 Bradford E.B., Vanderhoff J.W., *The Morphology of Synthetic Latexes.*, J. Polym. Sci., Part C, (3), p41-64.

65 Bradford E.B., Vanderhoff J.W., *The Particle Diameter Determination of Film-Forming Latexes by Electron Microscopy.*, J.Colloid Sci , 14, p543-561, (1959).

66 Bradford E.B., Vanderhoff J.W., *The Particle Diameter Determination of Film-Forming Latexes by Electron Microscopy of their Deformed Particles.*, J.Colloid Sci., 17, p668-687, (1962).

67 Briggs D., Seah M.P., (Eds) Practical Surface Analysis (by Auger and X-ray Photoelectron Spectroscopy)., J. Wiley, Chichester, (1983).

68 British Standard BS 2782 (ISO 2556-1974), part 8, method 821A, *Determination of the Gas Transmission Rate of Films and Thin Sheets Under Atmospheric Pressure (Manometric Method)*, British Standards Institute, (1979).

69 Brown G.L., *Formation of Films from Polymer Dispersions.*, J. Polym. Sci., 22, p423-434, (1956).

70 Brown W.E., J. Appl. Phys., 18, p273, (1947).

71 Brown G.M., Levy H.A., Acta Cryst., B29, p793, (1973).

72 Brodnyan J.G., Konen T., *Experimental Study of the Mechanism of Film Formation.*, J. Appl. Polym. Sci., 8, p687-697, (1964).

73 Brydson J.A., Plastics Materials., 3rd Ed. Pub. Newnes-Butterworths, London, England, (1975).

74 Buckton G., Efentakis M., Al-Hmoud H., Rajan Z., *The Influence of Surfactants on Drug Release from Acrylic Matrices.*, Int. J. Pharm., 74 Part 2-3, p169-174, (1991).

75 Burchard W., *New Aspects of Polymer Characterization by Dynamic Light Scattering.*, CHIMIA, 39 (1), p10-18, (1985).

76 Burnett G.M., Evans P., Melville H.W., J. Chem. Soc., Faraday Trans., 49, p1096, (1953).

77 Cansell F., Henry F., Pichot C., *Study of Polymer Latex by Dielectric Measurements in the Microwave Domain: Influence of Latex Characteristics.*, J. Appl. Polym. Sci., 41, p547-563, (1990).

78 Cao T., Xu Y., Wang Y., Chen X., Zheng A., *Effects of Monomer Feed Methods in Emulsion Polymerizations and Hydrophilicity of Monomers on Morphology of Latex Particles and their Minimum Film Formation Temperatures.*, Polym. Int., 32, p153-158, (1993).

79 Carlo-Erba Instruction Manual, Montedisson Group, Farmitalia Carlo-Erba.

80 Carothers W.H., *An Introduction to the General Theory of Condensation Polymers.*, J. Am. Chem. Soc., 51, p2548-2559, (1929).

81 Chafi N., Montheard J.P., Vergnaud J.M., *Dosage Form with Drug Attached to Polymer (Polyanhydride) Dispersed in a Eudragit Matrix: Preparation and Release of Drug in Gastric Liquid.*, Int. J. Pharm., 45 Part 3, p229-236, (1988).

82 Chafi N., Kolli M., Vergnaud J.M., Montheard J.P., *Amines Release From Schiff Bases Polymers and Diffusion from Dosage Forms with Eudragit RL in Acidic Medium.*, J. Appl. Polym. Sci., 43 (10), p1837-1847, (1991).

83 Chafi N., Montheard J.P., Vergnaud J.M., *Release of 2-Aminothiazole From Polymeric Carriers.*, Int. J. Pharm., 67 Part 3, p265-274, (1992).

84 Chainey M., Permeation Through Polymer Latex Films, CNAA PhD Thesis, Trent Polytechnic, (1984).

85 Chainey M., Transport Phenomena in Polymer Films., Ch. 11, in Handbook of Polymer Science and Technology., Vol. 4, Ed. Cherimisinoff, p499-540, (1989).

86 Chainey M., Hearn J., Wilkinson M.C., Br. Polym. J., p132-136, (1981).

87 Chainey M., Hearn J., Wilkinson M.C., *Interference from Atmospheric Carbon Dioxide in Latex Titrations.*, J. Colloid and Interface Sci., 117 (2), p477-484, (1987).

88 Chainey M., Wilkinson M.C., Hearn J., *Permeability of Heterogeneous Films Cast From Core-Shell Polymer Latices.*, Makromol. Chem. Suppl., 10/11, p435-446, (1985).

89 Chainey M., Wilkinson M.C., Hearn J., *Preparation of Overcoated Polymer Latices by a "Shot-Growth" Technique.*, Ind. Eng. Prod. Res. Dev., N°. 2, American Chem. Soc., 21 (2), p171-176, (1982).

90 Chainey M., Wilkinson M.C., Hearn J., *Preparation of Polymer Latex Films by a Flash Casting Technique.*, J. Appl. Polym. Sci., 30, p4273-4285, (1985).

91 Chainey M., Wilkinson M.C., Hearn J., *Permeation Through Homopolymer Latex Films*, J. Polym. Sci., Polym. Chem. Ed., 23, p2947-2972, (1985).

92 Chan A.H., Koros W.J., Paul D.R., *Analysis of Hydrocarbon Gas Sorption and Transport in Ethyl Cellulose using Dual Sorption/Partial Immobilisation Models.*, J. Membrane Sci., 3, p117-130, (1978).

93 Chang H.S., Chen S.A., *Kinetics and Mechanism of Emulsifier-free Emulsion Polymerisation. 11. Styrene/Water Soluble Comonomer (Sodium Methallyl Sulfonate) System.*, J. Polym. Sci., Part A, Polym. Chem., 26, p1207-1229, (1988).

94 Chang H.S., Chen S.A., *Particle Growth Mechanism of Large Particle Emulsifier-Free Polymerisation of Styrene.*, Makromol. Chem. Rapid Commune, 8 (6), p297-304, (1987).

95 Chevalier Y., Pichot C., Graillat C., Joanicot M., Wong K., Maquet J., Lindner P., Cabane B., *Film Formation with Latex Particles.*, Colloid and Polym. Sci., 270 part 8, p806-821, (1992).

96 Cho I., Lee K-W., *Morphology of Latex Particles Formed by Poly(Methyl Methacrylate)-Seeded Emulsion Polymerization of Styrene.*, J. Appl. Polym. Sci., 30, p1903-1926, (1985).

97 Chung-Li Y., Goodwin J.W., Ottewill R.H., *Studies on the Preparation and Characterisation of Monodisperse Polystyrene Latices IV. The Preparation of Latex Particles with a Size Greater Than 1 μm.*, Progr. Colloid and Polym. Sci., 60, p163-175, (1976).

98 Colton C.K., Smith K.A., Merrill E.W., Farrell P.C., *Permeability Studies with Cellulosic Membranes.*, J. Biomed. Mater. Res., 5, p459-488, (1971).

99 Comyn J. (Ed.) Polymer Permeability., Pub. Elsevier, (1985).

100 Côté jr. W.A., Day A.C., Wilkes G.W., Marchessault R.H., *Particle Packing in Latex Films.*, J. Colloid and Interface Sci., 27 (1), p32-37, (1968).

101 Cox R.A., Creasey J.M., Wilkinson M.C., *Anomalies in Particle Shape During Seeded Growth of Polystyrene Latices.*, Nature, 252 (5483), p468-469, (1974).

102 Cox R.A., Wilkinson M.C., Creasey J.M., Goodall A.R., Hearn J., *Study of the Anomalous Particles Formed During the Surfactant-Free Emulsion Polymerization of Styrene.*, J. Polym. Sci., Polym. Chem. Ed., 15, p2311-2319, (1977).

103 Crank J., The Mathematics of Diffusion., 2nd Ed., Oxford University Press, (1975).

104 Crank J., Park G.S. (Eds.), Diffusion in Polymers, Academic Press, (1968).

105 Croll S.G., *Drying of Latex Paint.*, J. Coatings Tech., 58 (734), p41-49, (1986).

106 Croll S.G., *Heat and Mass Transfer in Latex Paints During Drying.*, J. Coatings Tech., 59 (751), p81-92, (1987).

107 Culotta E., Koshland jr. D.E., *Buckyballs: Wide Open Playing Field For Chemists.*, Science, 254, p1706-1709, (December, 1991).

108 Davidson J.A., Collins E.A., *Latex Particle Size Analysis. II. A Method of Improving Electron Micrographs of Latex.*, J. Colloid And Interface Sci., 29 (3), p 456-459, (1969).

109 Davis S.S., Illum L., *Polymeric Microspheres as Drug Carriers.*, Biomaterials, 9 (1), p111-115, (1988).

110 Daynes H.A., *The Process of Diffusion Through a Rubber Membrane.*, Proc. Royal Soc. (London), Ser. A, 97, p286, (1939).

111 Debye P., J. Phys. Chem. 51, p18, (1947).

112 de Gennes P.G., J. Chem. Phys., 55, p572, (1971).

113 de Gennes P.G., *Polymers at an Interface; A Simplified View.*, Adv. Colloid and Interface Sci., 27, p189-209, (1987).

114 Derjaguin B.V., Landau L., Acta Physichim., URSS, 14, p633, (1941).

115 deV Naylor T., in Comprehensive Polymer Science, Vol. 2, Polymer Properties, Ch. 20, Allen & Bebbington Eds, Pergamen Press.

116 Devon M.J., Gardon J.L., Roberts G., Rudin A., *Effects of Core-Shell Latex Morphology on Film Forming Behaviour.*, J. Appl. Polym. Sci., 39, p2119-2128, (1990).

117 Deźelić N., Petres J.J., Deźelić Gj., *Preparation of Monodisperse Polystyrene Latices.*, Kolloid-Z. u. Z. Polymere, 242, p1142-1150, (1970).

118 Dillon R.E., Matheson L.A., Bradford E.B., *Sintering of Synthetic Latex Particles.* J. Colloid Sci., 6, p108-117, (1951).

119 Dinsmore R.P., U.S. Patent No. 1 732 795, (1927).

120 Disanayaka B., Zhao C-L., Winnik M.A., *Polymer Colloid Morphology Studied by Freeze-Fracture electron Microscopy.*, Langmuir, 6 (1), p162-168, (1990).

121 Distler D., Kanig G., *Fine Structures of Polymers from an Aqueous Dispersion.*, Colloid and Polymer Sci., 256, p1052-1060, (1978). {C.B.D.E. translation.}

122 Distler D., Kanig G., *Morphology of (Meth-)Acrylic Latex Films.*, Org. Coat. Plast. Chem., 43, p606-610, (1980).

123 Dobler F., Pith T., Lambla M., Holl Y., *Coalescence Mechanism of Polymer Colloids II. Coalescence with Evaporation of Water.*, J. Colloid and Interface Sci., 152, p1, (1992).

124 Donbrow M., Friedman M., *Permeability of Films of Ethyl Cellulose and PEG to Caffeine.* J. Pharm. Pharmac., 26, p148-150, (1974).

125 Donbrow M., Friedman M., *Enhancement of Permeability of Ethyl Cellulose Films for Drug Penetration.*, J. Pharm. Pharmac., 27, p633-646, (1975).

126 Donbrow M., Friedman M., *Timed Release from Polymeric Films Containing Drugs and Kinetics of Drug Release.*, J. Pharm. Sci., 64 (1), p76-80, (1975).

127 Douglas S.J., Davis S.S., Illum L., *Nanoparticles in Drug Delivery.*, CRC Critical Review Ther. Drug Carr. Syst., 3 (3), p233-261, (1987).

128 Douglas J.A., Sefton M.V., *The Permeability of Eudragit RL and HEMA-MMA Microcapsules to Glucose and Insulin.*, Biotech. & Bioeng., 36 Part 7, p653-664, (1990).

129 Drezal S.S., Kozlov L.V., Eliseeva V.I., *Some Special Features of the Formation of Emulsifier-Free Latexes.*, Probl. Sin. Issled Svoistv Pererab Lateksov(?), p178-183. {C.D.E. Translation.}

130 Duncan R., Kopacek J., *Soluble Synthetic Polymers as Potential Drug Carriers.*, Adv. Polymer Sci., 57, p51-101, (1984).

131 Dunn A.S., *Problems of Emulsion Polymerisation.*, J. Oil & Colour Chem. Assoc., 2(?), p50-54 + 65, (1991).

132 Durbin P.D., PhD Thesis, Lehigh University, Microfilm No. 8108193.

133 Durbin D.P., El-Aasser M.S., Vanderhoff J.W., Ind. Eng. Chem. Prod. Res. Dev., 23, p569, (1984).

134 Eckersley S.T., Rudin A., *The Effect of Plasticisation and pH on Film Formation of Acrylic Latexes.*, J. Appl. Polym. Sci., 48, p1369-1381, (1993).

135 Eckersley S.T., Rudin A., *Mechanism of Film Formation from Polymer Latexes.*, J. Coatings Technol., 62 (780), p89-100, (1990).

136 Edelhauser H.A., J. Polym. Sci., Part C, 27, p291, (1969).

137 Efentakis M., Al-Hmoud H., Buckton G., Rajan Z., *The Influence of Surfactants on Drug Release from a Hydrophobic Matrix.*, Int. J. Pharm., 70 Part 1-2, p153-158, (1991).

138 Egusa S., Makuuchi K., *Characterization of Carboxylated Latices Prepared by Radiation-Initiated Emulsion Polymerization. Comparison with Chemically Prepared Latices.*, J. Colloid and Interface Sci., 79 (2), p350-364, (1981).

139 Einstein A., <u>Investigations on the Theory of the Brownian Movement.</u>, Ed R. Furth, Dover Publications, NY, (1956).

140 El-Aasser M.S., Iqbal S., Vanderhoff J.W., Colloid and Interface Sci., Vol. V, Academic Press N.Y., p381, (1976).

141 Elbing E., McCarthy S., Snowden S., Coller B.A.W., Wilson I.R., *Aqueous Latex Polymerisation of Acrylonitrile.*, J. Chem. Soc., Faraday Trans. 1, 82, p943-952, (1986).

142 Elias G. -G., Bührer H.G., In <u>Polymer Handbook.</u>, 2nd Ed., Ch IV, Eds Brandrup J., & Immergut E.H., p157, (1975).

143 Eliseeva V.I., Ivanchev S.S., Kuchanov S.I., Lebedev A.V., *Emulsion Polymerisation and its Applications in Industry*., (NY Consultants Bureau, 1981), Russian Title (1976). {Ref. As Cited by Guthrie [211].}

144 Ellgood B., *Recent Advances in Vinylidene Chloride Copolymers for Surface Coatings*. J. Oil & Colour Chem. Assoc., 68, p164-169, (1985).

145 Ellis H. (Ed.) *Shape,Size, and Structure of Atoms and Molecules*., Ch. 4, in *Revised Nuffield Advanced Science Book of Data*., Pub. Longman Group Ltd., (1986).

146 Ellis H. (Ed.) *Atomic and Nuclear Properties*., Ch. 2, in *Revised Nuffield Advanced Science Book of Data*., Pub. Longman Group Ltd., (1986).

147 *Eudragit* (product brochure), Röhm Pharma GMBH, Weiterstad. A loose leaf folder containing various prospectuses and data sheets on the various Eudragit product. Available from: Dumas U.K. Ltd., Tunbridge Wells, Kent, TN2 5TT.

148 Everett D.H., Gültepe M.E., Wilkinson M.C., *Problems Associated with the Surface Characterisation of Polystyrene Latices*., J. Colloid and Interface Sci., 71 (2), p336-349, (1979).

149 Eyring H., J. Chem. Phys., 4, p283, (1936).

150 Fales J.L., Springer T.E., Vanderborgh N.E., Stroeve P., *Effect of Polymer Morphology on Proton Transport Through Ionomeric Polymers*., Proc. Electrochem. Soc., 86, (8), p203-218, (1986).

151 Farrell P.C., Babb E.L., *Cellulosic Membrane Permeability*, J. Biomed. Mater. Res., 7, p276-300 (1973).

152 Faxén H., Ark. Mat. Astron. Fys., 17 (27), p1, (1923).

153 Feeney P.J., Napper D.H., Gilbert R.G., *Surfactant-Free Emulsion Polymerizations: Predictions of the Coagulative Nucleation Theory*., Macromolecules, 20, p2922-2930, (1987).

154 Fessi H., Marty J-P., Puisieux F., Carstensen J.T., *Square Root of Time Dependence of Matrix Formulations with Low Drug Content*., J. Pharm. Sci., 71 (7), p749-752, (1982).

155 Fick A., Poggendortts Ann., 94, p59, (1855).

156 Fick A., Ann. Physik, Leipzig, 170, p59, (1855).

157 Fischer E.K., Harkins W.D., J. Chem. Phys., 36, p98, (1932).

158 Fisher L.W., Melpolder S.M., O' Reilly J.M., Ramakrishnan V., Wignall G.D., *Neutron Scattering from Interfacially Polymerized Core-Shell Latexes*., J. Colloid and Interface Sci., 123 (1), p24-35, (1988).

159 Fitch R.M., *Colloids*., in *Encycl. Polym. Sci. Eng*., 3, p727-746, (1985).

160 Fitch R.M., *The Control of Particle Size and Size Distribution in Latexes and Emulsions*., Proc. Water-Borne Higher-Solids Coatings Symposium, 8 part 2, p25-43, (1981).

161 Fitch R.M., *The Homogeneous Nucleation of Polymer Colloids.*, Brit. Polym. J., 5 (6), p467-483, (1973).

162 Fitch R.M., McCarvill W.T., *Surface Chemistry of Polystyrene Colloids Prepared by Mixed Initiator/ Surfactant Systems.*, J. Colloid Sci., 66(1), p20-25, (1978).

163 Fitch R.M., Tsai C.H., *Homogeneous Nucleation of Polymer Colloids, IV.: The Role of Soluble Oligomeric Radicals.*, in Polumer Colloids, R.M. Fitch (Ed.), Plenum, N. York, p73, (1971).

164 Fites A.L., Banker G.S., Smolen V.F., *Controlled Drug Release Through Polymeric Films.*, J. Pharm. Sci., 59, (5), p610-613, (1970).

165 Floyd F.L., Holsworth R.M., *C.P.V.C. as Point of Phase Inversion in Latex Paints.*, Polym. Sci. Eng., 63, p180-185, (1990).

166 Flynn G.L., Roseman T.J., *Membrane Diffusion II: Influence of Physical Adsorption on Molecular Flux through Heterogeneous Dimethylpolystyrene Barriers.*, J. Pharm. Sci., 60 (12), p1788-1796, (1971).

167 Flynn G.L., Yalkowsky S.H., Roseman T.J., *Mass Transport Phenomena and Models: Theoretical Concepts.*, J. Pharm. Sci., 63 (4), p479-510, (1974).

168 Ford N.C., Langley K.H., *The Minilab Called Photon Correlation Spectroscopy.*, Optical Spectra, p40-42, (Sept., 1979).

169 Fox T.G., Loshaek S., *Influence of Molecular Weight and Degree of Crosslinking on the Specific Volume and Glass Temperature of Polymers.*, J. Polym. Sci., 15, p371-390, (1955).

170 Frenkel J., J. Phys. (U.S.S.R.), 9, p385, (1943).

171 Frisch H.L., *Diffusion of Penetrants in Polymers.*, J. Polymer Sci., Part C (10), p11-15, (1965).

172 Frisch H.L., *Gas Permeation Through Membranes due to Simultaneous Diffusion and Convection.*, J. Phys. Chem., 60, p1177-1181, (1956).

173 Frisch H.L., *Mechanisms for Fickian Diffusion of Penetrants in Polymers.*, J. Polym. Sci., Polymer Letters, B3, p13-16, (1965).

174 Fujii Y., Iatani H., Kigoshi S., *Morphological Structures of the Membranes Prepared from Polymer Solutions.*, Polym. J., 24 (8), p737-755, (1992).

175 Fujita H., *Diffusion in Polymer-Diluent Systems*, Adv. Polym. Sci., 3, p1-47, (1961).

176 Fujita H., Fortschr. Hochpolym.-Forsch.-Bd., 3, S.1, (1961).

177 Funke W., Zorll U., *New Aspects of Lacquer Films with Heterogeneous Structure.*, Defazet, 29 (4), p146-153, (1975). {C.B.D.E. Translation.}

178 Gardner C., Drug Targeting: Potentials and Limitations., in Topics in Pharmaceutical Science., Eds. D.D. Breimer, Speiser P., p291-303, (1983).

179 Gardon J.L., *Emulsion Polymerisation ??*, J. Polym. Sci., Part A1, 6, p623, (1968).

180 Gardon J.L., *Emulsion Polymerisation II: Review of Experimental Data in the Context of the Revised Smith-Ewart Theory.*, J. Polym. Sci., Part A1, 6, p643-664, (1968).

181 Gardon J.L., *Emulsion Polymerisation III: Theoretical Prediction of the Effects of Slow Termination Rate Within Particles.*, J. Polym. Sci., Part A1, 6, p665-685, (1968).

182 Gardon J.L., *Emulsion Polymerisation IV: Experimental Verification of the Theory Based on Slow Termination Rate Within Latex Particles.*, J. Polym. Sci., Part A1, 6, p687-710, (1968).

183 Gardon J.L., *Emulsion Polymerisation. V. Lowest Theoretical Limits of the Ratio* k_r/k_p. J. Polym. Sci., Part A1, 6, p2853-2857, (1968).

184 Gardon J.L., *Emulsion Polymerisation. VII. Effects of Instantaneous Chain Termination During the Interval of Particle Nucleation.* J. Polym. Sci., Part A1, 9, p2763-2773, (1971).

185 Gardon J.L., *Evidence For and Against Concentration Gradients in Polymerizing Latex Particles.*, J. Polym. Sci., Polym. Chem. Ed., 11, p241-251, (1973).

186 Garret E.R., Chemburkar P.B., *Evaluation, Control, and Prediction of Drug Diffusion Through Polymeric Membranes II. Diffusion of Aminophenones Through Silastic Membranes: A Test of the pH-Partition Hypothesis.*, J. Pharm. Sci., 57, p949-959, (1968).

187 Ghebre-Sellassie I., Gordon R.H., Middleton D.L., Nesbitt R.U., Fawzi M.B., *A Unique Application and Characterization of Eudragit E 30 D Film Coatings in Sustained Release Coatings.*, Int. J. Pharm., 31, p43-54, (1986).

188 Ghebre-Sellassie I., Gordon R.H., Nesbitt R.U., Fawzi M.B., *Evaluation of Acrylic-Based Modified-Release Film Coatings.*, Int. J. Pharm., 37 (3), p211-218, (1987).

189 Ghosh P., Chadha S.C., Mukherjee A.R., Palit S.R., *Endgroup Studies in Persulfate-Initiated Vinyl Polymer by Dye Techniques. Part 1. Initiation by Persulfate Alone.*, J. Polym. Sci., Part A, 2, p4433-4440, (1964).

190 Ghosh P., Chadha S.C., Palit S.R., *Endgroups Studies in Persulfate-Initiated Vinyl Polymer by Dye Techniques. Part II. Initiation by Redox Persulfate Systems.*, J. Polym. Sci., Part A, 2, p4441-4451, (1964).

191 Ghosh P., Mukherjee A.R., Palit S.R., *Incorporation of Hydroxyl Endgroups in Vinyl Polymer. Part I. Initiation by Hydrogen Peroxide Systems.*, J. Polym. Sci., Part A, 2, p2807-2815, (1961).

192 Ghosh P., Mukherjee A.R., Palit S.R., *Incorporation of Hydroxyl Endgroups in Vinyl Polymer. Part II. Aqueous Polymerization of Methyl Methacrylate Initiated by Salts or Complexes of some Metals in their Higher Oxidation States.*, J. Polym. Sci., Part A, 2, p2817-2826, (1964).

193 Gilbert R.G., Napper D.H., *Theoretical Analysis of Rates of Emulsion Polymerisation.*, J. Chem. Soc. Faraday Trans. 1, 70 p391-399, (1974).

194 Goodall A.R., Surface Characterisation and Kinetic Studies on Polystyrene Latices., PhD Thesis, Trent Polytechnic, (1976).

195 Goodall A.R., Hearn J., Wilkinson M.C., *Problems Associated with the Surface Characterisation of Polystyrene Latices.*, J. Polym. Sci., Polym. Chem. Ed., p1019-1037, (1979).

196 Goodall A.R., Wilkinson M.C., & Hearn J., Characterisation of Particles During Growth in Emulsifier-Free Emulsion Polymerisation of Styrene., in Polymer Colloids II, Ed. R.M. Fitch, Plenum Pub. Corp., p629-650, (1980).

197 Goodall A.R., Wilkinson M.C., Hearn J., *Formation of Anomalous Particles during the Emulsifier-Free Polymerization of Styrene.*, J. Colloid and Interface Sci., 53 (2), p327-331, (1975).

198 Goodall A.R., Wilkinson M.C., Hearn J., Cote P, *The Influence of Benzaldehyde and Benzoic Acid on the Surface Characteristics of Polystyrene Latices.*, Br. Polym. J., 10, p205-208, (1978).

199 Goodhart F., Harris M.R., Murphy K.S., Nesbitt R.U., *An Evaluation of Aqueous Film-Forming Dispersions for Controlled Release.*, Pharm. Technol., 8 (4), p64-71, (1984).

200 Goodwin J.W., Hearn J., Ho C.C., Ottewill R.H., *Preparation and Characterisation of Polymer Latices in the Absence of Surface Active Groups.*, Br. Polym. J., 5, p347-362, (1973).

201 Goodwin J.W., Hearn J., Ho C.C., Ottewill R.H., *Studies on the Preparation and Characterisation of Monodisperse Polystyrene Latices.*, Colloid and Polym. Sci., 252, p464-471, (1974).

202 Goodwin J.W., Ottewill R.H., Pelton R., Vianello G., Yates D.E., *Control of Particle Size in the Formation of Polymer Latices.*, Br. Polym. J., 10, p173-180, (1978).

203 Goossens J.W.S., Zembrod A., *Characterisation of the Surface of Polymer Latices by Photon Correlation Spectroscopy.*, J. Dispersion Sci. Technol., 2 (2 & 3), p255-266, (1981).

204 Göpferich A., Lee G., *The Influence of Endogenous Surfactant on the Structures and Drug-Release Properties of Eudragit NE 30 D Matrices.*, J. Controlled Release, 18, p133-144, (1992).

205 Gould R.F., In Contact Angle, Wettability and Adhesion. Advances in Chemistry, Series 43, A.C.S., (1964).

206 Grancio M.R., Williams D.J., *The Morphology of the Monomer-Polymer Particle in Styrene Emulsion Polymerisation.*, J. Polym. Sci., Part A-1, 8, p2617-2629, (1970).

207 Gregoriadis G., *Targeting of Drugs.*, Nature, 265 (3), p407-411, (1977).

208 Gregoriadis G., Poste G. (Eds.), Targeting of drugs, anatomical and Physical Considerations., Plenum Press, New York, (1988).

209 Gregoriadis G., Senior J., Poste G. (Eds.), Targeting of Drugs with Synthetic Systems., NATO-ASI Series, (N°. 113), Plenum Press, New York, (1986).

210 Guo J-H., Robertson R.E., Amidon G.L., *Influence of Physical Aging on Mechanical Properties of Polymer Free Films: The Prediction of Long Term Aging Effects on the Water Permeability and Dissolution Rate of Polymer Film-Coated Tablets.*, Pharm. Res., 8 (12), p1500-1504, (1991).

211 Guthrie W.H., New Free Radical Initiators. PhD Thesis, Lehigh University.

212 Hahn K., Ley G., Schuller H., Oberthür R., *On Particle Coalescence in Latex Films.*, Colloid and Polym. Sci., 264, p1092-1096, (1986).

213 Hahn K., Ley G., Oberthür R., *Colloid Science: on Particle Coalescence in Latex Films* (II)., J. Colloid Polym. Sci., 266(7), p631-639, (1988).

214 Hamilton C.J., Murphy S.M., Atherton N.D., Tighe B.J., *Synthetic Hydrogels: 5. The Permeability of Poly(2-Hydroxyethyl Methacrylate) to Cations– An Overview of Solute-Water Interactions and Transport Processes.* Polymer, 29, p1879-1886, (1988).

215 Hansen F.K., Is There Life Beyond Micelles?, ACS Symp. Series, Ch. 2, 492, p12-27, (1992).

216 Hansen C.M., *The Air Drying of Latex Coatings.*, Ind. Eng. Chem., Prod. Res. Dev., 13 (2), p150-152, (1974).

217 Hansen F.K., Ugelstad J., *A Theory for Homogeneous Nucleation.*, J. Polym. Sci., Polym. Chem .Ed., 16, p1953-1979, (1978).

218 Hansen F.K., Ugelstad J., *Particle Nucleation in Emulsion Polymerisation II. Nucleation in Emulsifier-Free Systems Investigated by Seeded Polymerisation.*, J. Polym. Sci., Polym. Chem .Ed., 17, p3033-3045, (1979).

219 Hansen F.K., Ugelstad J., *Particle Nucleation in Emulsion Polymerization. III. Nucleation in Systems with Anionic Emulsifier Investigated by Seeded and Unseeded Polymerization.*, J. Polym. Sci., Polym. Chem .Ed., 17, p3047-3067, (1979).

220 Hansen F.K., Ugelstad J., *Particle Nucleation in Emulsion Polymerisation IV. Nucleation in Monomer Droplets.*, J. Polym. Sci., Polym. Chem .Ed., 17, p3069-3078, (1979).

221 Harkins W.D., *A General Theory of the Mechanism of Emulsion Polymerisation.*, J. Am. Chem. Soc., 69, p1428-1444, (1947).

222 Harkins W.D., *General Theory of Mechanism of Emulsion Polymerisation. II.*, J. Polym. Sci., 5 (2), p217-251, (1950).

223 Haward R.N., *Polymerization in a System of Discrete Particles.*, J. Polym. Sci., 4, p273-287, (1949).

224 Hawkett B.S., Napper D.H., Gilbert R.G., *Emulsion Polymerisation Kinetics. General Solutions for Smith-Ewart Cases I and II.*, J. Chem. Soc. Faraday Trans. I, 71, p2288-2295, (1975).

225 Hawkett B.S., Napper D.H., Gilbert R.G., *General Solution to the Smith-Ewart Equations for Emulsion Polymerisation Kinetics.*, J. Chem. Soc., 4, p690-698, (1977).

226 Hearn J., Studies on Polymer Latices., PhD Thesis, University of Bristol, (1971).

227 Hearn J., Ottewill R.H., Shaw J.N., *Characterisation of Latex Particles Produced by Emulsion Polymerisation.*, Br. Polym. J., 2, p116-120, (1970).

228 Hearn J.,Wilkinson M.C., Goodall A.R., *Polymer Latices as Model Colloids.*, Adv. Colloid & Interface Sci. 14, (2 & 3), p173-236, (1981).

229 Hearn J., Wilkinson M.C., Goodall A.R., Chainey M., *Kinetics of the Surfactant-Free Emulsion Polymerization of Styrene:- The Post Nucleation Stage.*, J. Polym. Sci., 23 p1869-1883, (1985).

230 Hearn J., Wilkinson M.C., Goodall A.R., Cope P., The Effect of Reaction Bu-Products, Surface Groups Lability and Microbial Activity on the Surface Characteristics of Polymer Latices., in Polymer Colloids II., Ed. R.M. Fitch, Plenum Pub. Corp., p379-403, (1980).

231 Hemenway C.P., Latimer J.J., Young J.E., Tappei, 68 (5), p102, (1985).

232 Hiemenz P.C., in Principles of Colloid and Surface Chemistry., Marcell Dekker Inc., ISBN 0-8247-6573-7, (1977).

233 Higuchi W.I., *A New Relationship for the Dielectric Properties of Two Phase Systems.*, J. Polym. Chem., 62, p649-653, (1958).

234 Higuchi T., J. Pharm. Sci., 50, p874, (1961).

235 Higuchi T., *Mechanism of Sustained Action Medication: Theoretical Analysis of Rate of Release of Solid Drugs Dispersed in Solid Matrices.*, J. Pharm. Sci., 52, p1145-1149, (1963).

236 Hixson A.W., Crowell J.H., *Dependence of Reaction Velocity upon Surface and Agitation. I – Theoretical Consideration.*, Ind. Eng. Chem., 23, p923-931, (1931).

237 Hofmann F., Delbruk K., German Patent No. 250 690, (1909).

238 Hofmann F., Delbruk K., German Patent No. 254 672, (1912).

239 Hofmann F., Delbruk K., German Patent No. 255 129, (1912).

240 Hogan J.E., *Aqueous Versus Organic Solvent Coating.*, Int. J. Pharm. Tech. & Prod. Manuf., 3 (1), p17-20, (1982).

241 Hohenstein W.P., Mark H., J. Polym. Sci., 1, 127, p549, (1946).

242 Holdsworth A.K., Hourston D.J., *Gas Permeability Studies of Latex Interpenetrating Polymer Network Films.*, Polym. Mat. Sci., p128-129, (1991).

243 Holsworth R.M., *Application of Thermal Methods of Analysis to Organic Coatings and Related Materials.*, J. Paint Technol., 41 (530), p167-178, (1969).

244 Hook J.W., Harren R.E., in Organic Coatings Technology., G.D. Parfitt and A.V. Patsis (Eds), Pub. Marcell Dekker, N.Y., p299, (1984).

245 Hoy K.L., *Effect of Reaction Pathway on Emulsion Polymer Structure.*, J. Coat. Technol., 51 (651), p27-41, (1979).

246 Hoy K.L., *Estimating the Effectiveness of Latex Coalescing Aids.*, J. Paint Technol., 45 (579), p51-56, (1973).

247 Hwa J.C.H., *Mechanism of Film Formation from Latices. Phenomenon of Flocculation.*, J. Polym. Sci., Part A, 2, p785-796, (1964).

248 Hwang S-T., Kammermeyer K., *Permeability as a Phenomenological Coefficient.*, p1-29, Unknown ref. Possibly from a book with the title or chapter title of *Separation and Purification.*

249 Hwang S-T., Tang T.E.S., Kammermeyer K., *Transport of Dissolved Oxygen Through Silicone Rubber Membrane.*, J. Macromol. Sci. Phys., B5 (1), p1-10, (1971).

250 Iley W.J., *Effect of Particle Size and Porosity on Particle Film Coatings.*, Powder Technol., 65 Part 1-3, p441-445, (1991).

251 Isaacs P.K., *Influence of Emulsifiers on Film Formation from Latexes.*, J.Macromol. Chem., 1 (1), p163-185, (1966).

252 *I.U.P.A.C. Manual of Symbols & Terminology*, Appendix 2, Part 1, *Colloid & Surface Chemistry.*, Pure and Applied Chem., 31, p578, (1972).

253 Jayasuriya R.M., El-Aasser M.S., Vanderhoff J.W., Yue H.J., *Characterization of Surface Endgroups in Polystyrene Latexes.*, J. Polym. Sci., Polym. Chem. Ed., 23, p2819-2832, (1985).

254 Jaycock M.J., Kayem G.J., *Stability and Flocculation in a Latex Paint. Part 2: Flocculation in the Drying Paint Film.*, J. Oil & Colour Chem. Assoc., 1, p11-17, (1983).

255 Jenquin M.R., Sarabia R.E., Liebowitz S.M., McGinity J.W., *Relationship of Film Properties to Drug Release from Monolithic Films Containing Adjuvants.*, J. Pharm. Sci., 81 (10), p983-989 (1992).

256 Jensen D.P., Morgan L.W., *Particle Size as it Relates to the Minimum Film Formation Temperature of Latices.*, J. Appl. Polymer Sci., 42, p2845-2849, (1991).

257 Joanicot M., Wong K., Maquet J., Chevalier Y., Pichot C., Graillet C., Lindner P., Rios L., Cabane B., *Ordering of Latex Particles During Film Formation.*, Prog. in Colloid & Polym. Sci., 81, p175-183, (1990).

258 Joanicot M., Wong K., Richard J., Maquet J., Cabane B., *Ripening of Cellular Latex Films.*, Macromolecules, 26 (12), p3168-3175, (1993).

259 Johnson K.L., Kendall K., Roberts A.D., *Surface Energy and the Contact of Elastic Solids.*, Proc. R. Soc. Lond. A., 324, p301-313, (1971).

260 Josefowitz D., Mark H., India Rubber World, 106. p33, 1932.

261 Juhué D., Lang J., *Effect of Surfactant Postadded to Latex Dispersion on Film Formation: a Study by Atomic Force Microscopy.*, Langmuir, 9, p792-796, (1993).

262 Juhué D., Lang J., *Latex Film Formation in the Presence of Organic Solvents.*, Macromolecules, 27, p695-701, (1994).

263 Juhué D., Lang J., *Latex Film Surface Morphology Studied by Atomic Force Microscopy: Effect of a Non-Ionic Surfactant Postadded to Latex Dispersion.*, Colloids & Surfaces A: Physico. Chem. Eng. Aspects, 87, p177-185, (1994).

264 Kala H., Dittgen M., Moldenhauer H., Zessin G., *On the Pharmaceutical Technology of Film Coating.*, Pharmazie, 34 (11), (1979). {C.B.D.E. Translation.}

265 Kamel A.A., El-Aasser M.S., Vanderhoff J.W., *The Preparation and Surface Characterisation of an Ideal Model Colloid.*, J. Disp. Sci. Technol., 2 (2-3), p183-214, (1981).

266 Kaminska A., *The Effect of Various Factors on the Gas Permeability of Polymeric Films.*, Polimery (Warsaw), 25 (2), p47-48, (1980). {C.B.D.E. translation.}

267 Kan C.S., *Latex Film Formation: Determination of Deforming Forces During Coalescence.*, Advanced Coating Fundamentals, TAPPI Notes, p101-107, (1993).

268 Kanig G., Neff H., *Contrast Method for the Electron Microscope Examination of Polymer Films Containing Acidic and Ester Groups.*, Colloid & Polym. Sci., 253, p29, (1975). (C.B.D.E. Translation.}

269 Kast H., *Aspects of Film Formation with Emulsion Copolymers.*, Makromol. Chem., Suppl. 10/11, p447-461, (1985).

270 Kato K., Kondo H., Morita A., Esumi K., Meguro K., *Synthesis of Polystyrene Latex with Amphoteric Surfactant and its Characterization.*, Colloid. Polym. Sci., 264 (9), p737-742, (1986).

271 Kawashima Y., Niwa T., Takeuchi H., Hino T., Itoh Y., *Hollow Microspheres for use as a Floating Controlled Drug Delivery System in the Stomach.*, J. Pharm. Sci., 81 (2), p135-140, (1992).

272 Kawashima Y., Niwa T., Takeuchi H., Hino T., Ito[1] Y., *Control of Prolonged Drug Release and Compression Properties of Ibuprofen Microsponges with Acrylic Polymer, Eudragit RS, by Changing Their Intraparticle Porosity.*, Chem. Pharm. Bull., 40 (1), p196-201, (1992).

273 Kaye G.W.C., Laby T.H., Tables of Phusical and Chemical Constants., 13th Ed., Pub. Longman, (1971).

274 Kellaway I.W., Najib N.M., *Adsorption of Hydrophilic Polymers at the Polystyrene-Water Interface.*, Int. J. of Pharm., 6, p285-294, (1980).

275 Kendall K., Padget J.C., *Latex Coalescence.*, Int. J. Adhesion and Adhesives, 2, p149-154, (1982).

276 Kesting R.E., Membrane Polumers., Ch. 4, in Sunthetic Polumeric Membranes:- A Structural Perspective. 2nd Ed., p106-179, (1985).

277 Kesting R.E., Membrane Function., Ch 8, in Sunthetic Polumeric Membranes:- A Structural Perspective. 2nd Ed., p227-270, (1985).

278 Keusch P., Price J., Williams D., J. Macromol. Sci., 7, p623, (1973).

279 Keusch P., Williams D., J. Polym. Sci., 11, p193, (1973).

280 Keusch P., Graff R.A., Williams D., *Polymer Segment Density Distributions in Saturated Polystyrene Latex Systems.*, J. Polym. Sci., Macromolecules, 7 (3), p304-310, (1974).

---

[1] Note that the name Ito is spelt differently on each of the Kawashima papers.

281 Killmann E., Sapuntzjis P., Maier H., *Dynamic Light Scattering for Characterization of Latices.*, Makromol. Chem., Macromol. Symp., 61, p42-58, (1992).

282 Kim J.H., Sulfonated Polusturene Model Colloids: Preparation, Characterization and Application as a Heterogeneous Catalust., PhD Thesis, Lehigh University, (1956), Microfilm 8705030.

283 Kim J.H., Chainey M., El-Aasser M.S., Vanderhoff J.W., *Preparation of Highly Sulfonated Polystyrene Model Colloids.*, J. Polym. Sci., Part A, 27, p3187-3199, (1989).

284 Kim S.W., Cardinal J.R., Wisniewski S., Zentner G.M., Solute Permeation Through Hudrogel Membranes. Hudrophilic vs Hudrophobic Solutes., Chapter 20 in Unknown Book, possibly called Water in Polymers, Pub. Am. Chem. Soc., p347-359, (1980).

285 Kim K.D., Sperling L.H., Klein A., *Characterisation of Film Formation from Direct Mini-Emulsified Polystyrene Latex Particles via SANS.*, Macromolecules, 26 Part 17, p4624-4631, (1993).

286 Kim H-B., Wang Y., Winnik M.A., *Synthesis, Structure and Film-Forming Properties of Poly(butyl Methacrylate)-Poly(Methacrylic Acid) Core-Shell Latex.*, Polymer, 35 (8), p1779-1786, (1994).

287 Kim H-B., Winnik M.A., *Effects of Surface Acid Groups Neutralisation on Interdiffusion Rates in Latex Films.*, Macromolecules, 27, p1007-1012, (1994).

288 Kim Y.H., Wool R.P., *A Theory of Healing at a Polymer-Polymer Interface*, Macromolecules, 16, p1115-1120, (1983).

289 Kolthoff I.M., Miller I.K., *The Chemistry of Persulfate. I. The Kinetics and Mechanism of the Decomposition of the Persulfate Ion in Aqueous Media.*, J. Am. Chem. Soc., 73, p3055-3059, (1951).

290 Koros W.J., Chan A.H. Paul D.R., *Sorption and Transport of Various Gases in Polycarbonate.*, J. Membrane Sci., 2, p165-190, (1977).

291 Kowalski A., Vogel M., Blankenship R.M., European Patent 22,633, (1981).

292 Kowalski A., Vogel M., Blankenship R.M., U.S. Patent 4,427,836, (1984).

293 Kumins C.A., *Transport Through Polymer Membranes.*, J. Polym. Sci., Part C (10), p1-9, (1965).

294 Kumins C.A., Kwei T.K., Free Volume and Other Theories., Ch. 4, in Diffusion in Polumers., Eds. J. Crank & G.S. Park, Pub. Academic Press, p107-140, (1968).

295 Kumins C.A., Roteman J., *Diffusion of Gases and Vapours Through Polyvinyl Chloride-Polyvinyl Acetate Copolymer Films I. Glass Transition Effect.*, J. Polym. Sci., 55, p683-698, (1961).

296 Kumins C.A., Roteman J., *Diffusion of Gases and Vapours Through Polyvinyl Chloride-Polyvinyl Acetate Copolymer Films II. The Effect of Polymer Segment Mobility.*, J. Polym. Sci., 55, p699-711, (1961).

297 Kurja J., Nolte R.J.M., Maxwell I.A., German A.L., *Free Radical Polymerization of Styrene in Dioctadecyldimethylammonium Bromide Vesicles.*, Polymer, 34 (10), p2045-2049, (1993).

298 Kwei T.K., Arnheim W.M., *The Diffusion of Gases Through Filled Polymers.*, J. Polym. Sci., Part C (10), p103-109, (1965).

299 Labib M.E., Robertson A.A., *Application of a Diafiltration Technique in Latex Studies.*, J. Colloid and Interface Sci., 67 (3), p543-547, (1978).

300 Labib M.E., Robertson A.A., *The Conductometric Titration of Latices.*, J. Colloid and Interface Sci., 77 (1), p151-161, (1980).

301 Laghoueg N., Paulet J.L., Taverdet J.L., Vergnaud J.M., *Oral Polymer-Drug Devices with a Core and an Erodible Shell for Constant Drug Delivery.*, Int. J. Pharm., 50, p133-139, (1989).

302 Lakshminarayanaiah N., *Transport Phenomena in Artificial Membranes.*, Chem. Rev., 65 (5), p491-565, (1965).

303 Lammas G., Report on work in Postgrad. Sch. of Pharmacy, Bradford University, under Dr. P. York, (1989).

304 Lamprecht J., *New Criterion for Film Formation in Aqueous Dispersions of Polymers.*, Colloid & Polym. Sci., 258(8), p960-967, (1980). {C.B.D.E. translation by B.C.H. Warren.}

305 Lange J., Hergeth W.D., Wartewig S., *Infra-Red Spectroscopy of Polymeric Core-Shell Latexes.*, Acta Polymerica 39(a), p479-481, (1988).

306 Le Bas G., in The Molecular Volume of Liquid Chemical Compounds., Longmans, London & New York, (1915).

307 Lebovits A., *Permeability of Polymers to Gases, Vapours and Liquids.*, Modern Plastics, p139-211, (1966).

308 Lee D.I., Ishikawa T., J. Polym. Sci., Polym. Chem. Ed., 21, p143, (1983).

309 Lee S., Rudin A., Control of Core-Shell Latex Morphology., Ch. 15, ACS Symp. Series, 492, p234-254, (1992).

310 Lee S., Rudin A., *Synthesis of Core-Shell Latexes by Redox Initiation at Ambient Temperatures.*, J. Polym. Sci., Polym. Chem. Ed., 30, p2211-2216, (1992).

311 Lee S., Rudin A., *The Mechanism of Core-Shell Inversion in Two-Stage Latexes.*, J. Appl. Polym. Sci., Part A, Polym. Chem. 30, p865-871, (1992).

312 Lee W.A., Ruthorford R.A., in Polymer Handbook 2nd Ed., Eds Brandrup J., & Immergut E.H., *The Glass Transition Temperatures of Polymers.*, pIII-139-III-192, (1975).

313 Lehmann K.O.R., *Chemistry and Application Properties of Polymethacrylate Coating Systems.*, In Drugs and Pharmaceutical Sciences, 36, Aqueous Polymeric Coatings for Pharmaceutical Dosage Forms., Ed. J.W. McGinity, Pub. Marcell Dekker, New York, Ch. 4, p153-246, (1989).

314 Lehmann K., *The Application and Processing of Acrylic Coatings in the Form of Aqueous Dispersions Compared with Organic Solutions.*, Acta Pharm. Fenn, 91, p225-238, (1982).

315 Lehmann K.O.R., Bössler H.M., Dreher D.K., *Controlled Drug Release From Small Particles Encapsulated with Acrylic Resin.*, Niol. Macromol. Monogr., 5, Polym. Delivery Systems., p111-119, (1979).

316 Lehmann K. Von., Drehar D., *The Use of Aqueous Synthetic Dispersions in the Film-Coating of Drugs.*, Pharm. Ind., 34 (12), p894-899, (1972). {C.B.D.E. Translation.}

317 Lenga R.E., Ed., Safety. The Sigma-Aldrich Library of Chemical Safety Data., Ed. II, Vol. 1 & 2, Sigma-Aldrich Corporation, (1988).

318 Li L.C., Peck G.E., *Water Based Silicone Elastomer Controlled Release Tablet Film Coating III – Drug Release Mechanisms.*, Drug Dev. & Ind. Pharm., 15 (12), p1943-1968, (1989).

319 Li L.C., Tu Y-H., *Latex Film Matrix Systems with a Concentration Gradient for Controlled Drug Delivery.*, Drug Dev. & Ind. Pharm., 17 (15), p2041-2054, (1991).

320 Linné M.A., Klein A., Miller G.A., Sperling L.H., Wignall G.D., *Film Formation from Latex: Hindered Initial Interdiffusion of Constrained Polystyrene Chains Characterised by Small Angle Neutron Scattering.*, J. Macromol. Sci. Phys., b27, (2 & 3), p217-231, (1988).

321 Linné M.A., Klein A., Sperling L.H., J. Macromol. Sci. Phys., b27, (2 & 3), p181, (1988).

322 Lissant K.J., *The Geometry of High-Internal-Phase-Ratio Emulsions.*, J. Colloid and Interface Sci., 22, p462-468, (1966).

323 List P.H., Kassis G., *Permeability of Various Tablet Coatings to Water Vapour and Oxygen.*, Acta Pharmaceutica Technologica, 28 (1), p21 (1982). {C.B.D.E. translation.}

324 List P.H., Laun G., *Relationship Between Solvent Residues and the Permeability of Eudragit L Films.*, Pharm. Ind., 42 (4), p399-401, (1980).

325 Lonsdale H.K., *Review: The Growth of Membrane Technology.*, J. Memb. Sci., 10, p81-181, (1982).

326 Lora S., Palmo G., Busulini L., Castilletti B., Eur. Polym. J., 10, p1223, (1974).

327 Luck W.A., Ch. 3, in Water in Polymers., Ed. S.P. Rowland, ACS Symp. Ser. 127, Am. Chem. Soc., (1980).

328 Luther M., Henck C., German Patent No. 558 890, (1927).

329 Madras S., McIntosh R.L., Mason S.G., *A Preliminary Study of the Permeability of Cellophane to Liquids.*, Can. J. Res., 278, p764-779, (1949).

330 Malvern Instruments Ltd., (Spring Lane, Malvern, Worcs. UK), Short Course Guide, Three Day Training Course, (1991).

331 Maron S.H., Elder M.E., Ulevitch I.N., J. Colloid Sci., 9, p89, (1954).

332 Marsh H., Campbell H.G., *The Characterisation of Microporous Carbons by Adsorption from Liquid and Vapour Phases.*, Carbon, 19, p489-498, (1971).

333 Mason G., *Formation of Films from Polymer Latices: A Theoretical Treatment.*, Brit. Polym. J., 5, p101-108, (1973).

334 McBain J.W., Trans. Faraday Soc., 9, p99, (1913).

335 McCarvill W.T., Fitch R.M., *The Preparation and Surface Chemistry of Polystyrene Colloids Stabilized by Sulphonate Surface Groups.*, J. Colloid and Interface Sci., 64 (3), p403-411, (1978).

336 Meares P., J. Am. Chem. Soc., 76, p3415, (1954).

337 Membrane Permeability to Nonelectrolytes: Discontinuous Systems. Ch. 10, in Nonequilibrium Thermodynamics in Biophysics., p113-132, Reference otherwise unknown.

338 Michaels A.S., Parker jr. R.B., *Sorption and Flow of Gases in Polyethylene.*, J. Polym. Sci., 41, p53-71, (1959).

339 Michaels A.S., Vieth W.R., Barrie J.A., *Diffusion of Gases in Polyethylene Terephthalate.*, J. Appl. Phys., 34 (1), p13-20, (1963).

340 Minghong W., Weiping S., Zueteh M., *Synthesis of Polyacrylate Core-Shell Structure Latex by Radiation Techniques.*, Radiat. Phys. Chem., 42 (1-3), p171-174, (1993).

341 Moore W.J., *Basic Physical Chemistry.*, Pub. Prentice/Hall International, (1983).

342 Most C.F., *Some Filler Effects on Diffusion in Silicone Rubber.*, J. Appl. Polym. Sci., 14, p1019-1024, (1970).

343 Muhammad N.A., Boisvert W., Harris M.R., Weiss J., *Modifying the Release Properties of Eudragit L30D.*, Drug Dev. & Ind. Pharm., 17 (18), p2497-2509, (1991).

344 Mukerjee P., *The Nature of the Association Equilibria and Hydrophobic Bonding in Aqueous Solutions of Association Colloids.*, Adv. Colloid and Interface Sci., 1, p241-275, (1967).

345 Myers R.R., Schultz R.K., *Acrylic Latex Film Formation in the Critical Temperature Range.* J. Appl. Polym. Sci., 8, p755-764, (1964).

346 Nakagami H., Keshikawa T., Matsumura M., Tsukamoto H., *Application of Aqueous Suspensions and Latex Dispersions of Water-Insoluble Polymers for Tablet and Granule Coating.*, Chem. Pharm. Bull., 39 (7), p1837-1842, (1991).

347 Napper D.H., *Conformation of Macromolecules. A Physical Chemistry Experiment.*, J. Chem. Ed., 46, p305-307, (1969).

348 Napper D.H., Gilbert R.G., *Emulsion Polymerization: The Mechanisms of Latex Particle Formation and Growth.*, in *An Introduction to Polymer Colloids.*, Eds F. Candau, R.H. Ottewill, Pub. Kluwer Academic Publishers, p159-185, (1990).

349 Nicholson J.W., Wasson E.A., *Film Spreading and Film Formation by Waterborne Coatings.*, In *Surface Coatings*. Ch. 2, Vol. 3, p91-123, (1990).

350 Nightingale Jr. E.R., *Phenomenological Theory of Ion Solvation. Effective Radii of Hydrated Ions.*, J. Phys. Chem., 63, p1381-1387, (1959).

351 Noyes A., Whitney W., J. Am. Chem. Soc., 19, p930, (1897).

352 Okamura S., Motoyama T., *Emulsion Polymerisation of Vinyl Acetate.*, J. Polym. Sci., 58, p221-227, (1962).

353 Okhamafe A.O., York P., *The Glass Transition in some Pigmented Polymer Systems Used for Tablet Coating.*, J. Macromol. Sci.-Phys., B23 (4-6), p373-382, (1985).

354 Okor R.S., *Effect of Polymer Cation Content on Certain Film Properties.*, J. Pharm. Pharmacol., 34, p83-86, (1982).

355 Okor R.S., *Influence of Hydrophilic Character of Plasticizer and Polymer on Certain Film Properties.*, Int. J. Pharm., 11 (1), p1-9, (1982).

356 Okor R.S., Study of Certain Factors Which Influence Solute Permeability of Polymer Films., PhD Thesis, University of Strathclyde, (1980).

357 Okor R.S., Anderson W., *An Effect of Permeability Asymmetry in Single and Layered Films.*, J. Pharm. Pharmacol., Suppl. Brit. Pharm. Conf. 1978, 30, p4P, (1979).

358 Okor R.S., Anderson W., *Permeability Asymmetry in Composite Films of an Acrylate-Methacrylate Copolymer.*, J. Pharm. Pharmacol., Suppl. Brit. Pharm. Conf. 1978, 30, p6P, (1979).

359 Okor R.S., Anderson W., *Variation of Polymer Film Composition and Solute Permeability.*, J. Pharm. Pharmacol., Suppl Brit. Pharm. Conf. 1979, 31, p78P, (1980).

360 Okubo M., He Y., *Preparation of Asymmetric Film by Blending Two Kinds of Polymer Emulsions Having Greatly Different Storage Stabilities.*, J. Appl. Polym. Sci., 42 (8), p2205-2208, (1991).

361 Okubo M., Ichikawa K., Fujimura M., Fujimura M., *Production of Multi-Hollow Polymer Microspheres by Stepwise Alkali/Acid Method II. Alkali Treatment Process.* Colloid Polym. Sci., 269, p1257-1262, (1991).

362 Okubo M., Ichikawa K., Fujimura M., ACS Symposium Series , 492, p282, (1992).

363 Okubo M., Kanaida K., Matsumoto T., J. Appl. Polym. Sci., 33 (5), p1511, (1987).

364 Okubo M., Katsuta Y., Matsumoto T., *Studies on Suspension and Emulsion: Peculiar Morphology of Composite Polymer Particles Produced by Seeded Emulsion Polymerisation.*, J. Polym. Sci., Polym. Letters Ed., 20, p45-51, (1982).

365 Okubo M., Nakagawa T., *Formation of Multihollow Structures in Crosslinked Composite Polymer Particles.*, Colloid Polym. Sci., 272, p530-535, (1994).

366 Okubo M., Takeya T., Tsutsumi Y., Kadooka T., Matsumoto T., *Asymmetric Porous Emulsion Film.*, J. Polymer Sci., Polymer Chem. Ed., 19, p1-8, (1981).

367 Oppenheim R.C., *Solid Colloidal Drug Delivery Systems: Nanoparticles.*, Int. J. Pharm., 8, p217-234, (1981).

368 O' Toole J.T., *Kinetics of Emulsion Polymerization.*, J. Appl. Polym. Sci., 9, p1291-1297, (1965).

369 Ottewill R.H., Colloidal Properties of Latex Particles., in An Introduction to Polymer Colloids., Eds. F. Candau and R.H. Ottewill, p129-157, (1990).

370 Ottewill R.H., Satgurunathan R., *Nonionic Latices in Aqueous Media Part 1. Preparation and Characterization of Polystyrene Latices.*, Colloid and Polym. Sci., 265, p845-853, (1987).

371 Ottewill R.H., Satgurunathan R., Waite F.A., Westby M.J., *Non-Ionic Polystyrene Latices in Aqueous Media.*, Br. Polym. J., 19, p435-440, (1987).

372 Ottewill R.H., Shaw J.N., *Electrophoretic Studies on Polystyrene Latices.*, J. Electroanal. Chem., 37, p133-142, (1972).

373 Ottewill R.H., Shaw J.N., *Studies on the preparation and Characterisation of Monodisperse Polystyrene Latices. I. Preparation.*, Kolloide, 215 (2), p161-166, (1966).

374 Overbeek J. Th.G., *Monodisperse Colloidal Systems, Fascinating and Useful.*, Adv. Colloid & Interface Sci., 15, p251-277, (1982).

375 Padget J.C., Moreland P.J., *Use of AC Impedance in the Study of Anticorrosive Properties of Chlorine Containing Vinyl Acrylic Latex Polymers.*, J. Coat. Technol., 55, p39-51, (1983).

376 Palit S.R., Makromol. Chem., 36, p89, (1959).

377 Palit S.R., Makromol. Chem., 38, p96, (1960).

378 Palit S.R., Chem Ind. p1531, (1960).

379 Palit S.R., Ghosh P., Microchem. Tech. Symp. Ser., 2, p663, (1961).

380 Palit S.R., Guha T., Das R., Konar R.S., Aqueous Polymerisation., in Encyclopedia of Polymer Science and Technology., Eds H.F. Mark, N.G. Gaylord, N.M. Bikales, Vol. 2, Pub. Interscience NY, (1965).

381 Palit S.R., Mukherjee B.N., Konar R.S., *Formation of Carboxyl Endgroups in Polymers and their Detection by the Dye Partition Test.*, J. Polym. Sci., 1, p45-52, (1961).

382 Pappenheimer J.R., Physiol. Rev., 33, p387, (1953).

383 Pappenheimer J.R., Renkin E.M., Borrero L.M., Am. J. Physiol., 167, p13, (1951).

384 Park G.S., *An Experimental Study of the Influence of Various Factors on the Time Dependent Nature of Diffusion in Polymers.*, J. Polym. Sci., 11 (2), p97-115, (1953).

385 Patel M., Patel J.M., Lemberger A.P., *Water Vapour Permeability of Selected Cellulose Ester Films.*, J. Pharm. Sci., 53 (3), p286-290, (1964).

386 Paul D.R., *Effect of Immobilizing Adsorption on the Diffusion Time Lag.*, J. Polym. Sci., Part A-2, 7, p1811-1818, (1969).

387 Paul D.R., Kemp D.R., *The Diffusion Time Lag in Polymer Membranes Containing Adsorptive Fillers.*, J. Polym. Sci., Polym. Symp., 41, p79-93, (1973).

388 Pedley D.G., Skelly P.J., Tighe B.J., *Hydrogels in Biomedical Applications.*, Br. Polym. J., 12, p99-110, (1980).

389 Pelton R., Chemical Reactions at the Latex-Solution Interface., in Scientific Methods for the Study of Polymer Colloids and their Applications., Eds F. Candau, R.H. Ottewill, Pub. Kluwer Academic Publishers, p493-516, (1990).

390 Peppas N.A., Meadows D.L., *Macromolecular Structure and Solute Diffusion in Membranes: An Overview of Recent Theories.*, J. Memb. Sci., 16, p361-377, (1983).

391 Perera D.Y., *Internal Stress and Film Formation in Emulsion Paints.*, J. Oil & Colour Chem. Assoc., 11, p275-281, (1985).

392 Personal Communication, re-HPMC: Courtaulds Chemicals, Spondon, Derby, DE2 7BP, UK.

393 Personal Communication: J. Hearn, Nottingham Trent University, Nottingham, England.

394 Peterson C.M., *Permeability Studies on Heterogeneous Polymer Films.*, J. Appl. Polym. Sci., 12, p2619-2667, (1968).

395 Pichot C., *Recent Developments in the Functionalization of Latex Particles.*, Makromol. Chem., Macromol. Symp. 35/36, p327-347, (1990).

396 Pochan D., *Morphology of Films Dried From Latexes Containing Water-Soluble Polymers: Dielectric Relaxation-Phenomena.*, Water-Borne & Higher-Solids Coatings Symposium, No. 14, p155-166, (1987).

397 Poehlein G.W., Vanderhoff J.W., Witmeyer R. *Drying of Latex Films.*, J., Polymer Preprints, 16 (1), p268-273, (1975).

398 Polymer Handbook., 2nd Ed., Ch. IV, Eds Brandrup J., & Immergut E.H., p157, (1975).

399 Polysciences (U.K.) Ltd., Moulton Park, Northampton, England. *Private communication.*

400 Poznansky M.J., Juliano R.L., *Biological Approaches to the Controlled Delivery of Drugs: a Critical Review.*, 36 (4), p277-236, (1984).

401 Pradip, Fuerstenau D.W., The Effect of Polymer Adsorption on Wettability of Coal., in Process Technology Proceedings, N° 4. Flocculation in Biotechnology and Separation Systems., Ed Y.A. Attia, Pub. Elsevier, p95-106, (1989).

402 Pramojaney N., Poehlein G.W., Vanderhoff J.W., *A Mathematical Model for the Drying of Latex Films.*, Drying '80, 2, p93-100, (1980).

403 Priest W.J., *Particle Growth in the Aqueous Polymerization of Vinyl Acetate.*, J. Phys. Chem., 56, p1077-1082, (1952).

404 Pusch W., Walch A., *Membrane Structure and its Correlation with Membrane Permeability.*, J. Memb. Sci., 10, p325-360, (1982).

405 Pusch W., Walch A., *Synthetic Membrane: State of the Art.*, Desalination, 35, p5-20, (1980).

406 Pusey P.N., Tough R.J.A., *Dynamic Light Scattering, a Probe of Brownian Particle Dynamics.*, Adv. Colloid & Interface Sci., 16, p143-159, (1982).

407 Randle K.J., *Statistical Optics and its Application to Colloid Science.*, Chem. Ind., 19, p74-81, (1980).

408 Ratner B.D., Hoffman A.S., Synthetic Hydrogels for Biomedical Applications., Ch. 1, in Hydrogels for Medical and Related Applications., ACS Symp. Ser., 31, p1-35, (1976).

409 Rasenberg C.J.F.M., Huisman H.F., *Measurement of the Critical Pigment Volume Concentration by Means of Mercury Porosimetry.*, Prog. in Org. Coat., 13, p223-235, (1985).

410 Rembaum A., Yen S.P.S., Molday R.S., *Synthesis and Reactions of Hydrophilic Functional Microspheres for Immunological Studies.*, J. Macromol. Sci.–Chem., A13 (5), p603-632, (1979).

411 Renkin E.M., *Filtration, Diffusion, and Molecular Sieving Through Porous Cellulose Membranes.*, J. Gen. Physiol., 38, p225-243, (1954).

412 Richard J., Maquet J., *Dynamic Micromechanical Investigations into Particle/ Particle Interfaces in Latex Films.* Polymer, 33 (19), p4164-4173, (1992).

413 Richard J., Mignaud C., Wong K., *Water Vapour Permeability, Diffusion and Solubility in Latex Films.*, Polym. Int., 30, p431-439, (1993).

414 Richmond P., Lal M., *A Theoretical Treatment of Entropic Repulsions by Polymers.*, Chem. Phys. Lett., 24 (4), p594-596, (1974).

415 Riddle E.H., In Monomeric Acrylic Esters. Analytical Methods., Pub. Rheinhold, Ch. 7, p203-221, (1954).

416 Roe C.P., *Surface Chemistry Aspects of Emulsion Polymerisation.*, Ind. Eng. Chem., 60 (9), p20-33, (1968).

417 Rogers C.E., Permeation of Gases and Vapours in Polymers., Ch. 2, in Polymer Permeability., Ed. J. Comyn, p11-73, Pub. Elsevier, (1985).

418 Rogers C.E., *Polymer Membranes in New Energy Technologies.*, Polym. Mater. Basic Res., p112-124, (1978).

419 Rogers C.E., *Transport Through Polymer Membranes with a Gradient of Inhomogeneity.*. J. Polym. Sci., Part C (10), p93-102, (1965).

420 Rogers C.E., Meyer J.A., Stannett V., Szwarc M., Some Factors Affecting the Permeability Constant., in Permeability of Plastic Films and Paper to Gases and Vapours., Part II, Authors Stannett V., Szwarc M., Bhargava R.L., Meyer J.A., Myers A.W., Rogers C.E., p12-27, Pub. Technical Assoc. Pulp & Paper Ind., (1962).

421 Rogers C.E., Sternberg S., *Transport Through Permselective Membranes.*, J. Macromol. Sci., B5 (1), p189-206, (1971).

422 Röhm Pharma Provisional Information Sheet, *Miscibility of Eudragit L 30 D with Eudragit NE 30 D. 1. Stabilization by pH Adjustment Where Eudragit L 30 D is Present in Equal Proportion or Predominates. & 3.Stabilisation by pH Adjustment and the Addition of an Emulsifier Where Eudragit NE 30 D Predominates.*, Supplied by Dumas U.K. Ltd., Tunbridge Wells, Kent, England.

423 Roulstone B.J., Permeation Through Polymer Latex Films., CNAA Phd Thesis, Trent Polytechnic, (1989).

424 Roulstone B.J., Wilkinson M.C., Hearn J., Wilson A.J., *Studies on Polymer Latex Films: I. A Study of Latex Film Morphology.*, Polym. Int., 24, p87-94, (1991).

425 Roulstone B.J., Wilkinson M.C., Hearn J., *Studies on Polymer Latex Films: II. Effect of Surfactants on the Water Vapour Permeability of Polymer Latex films* Polym. Int., 27, p43-50, (1992).

426 Roulstone B.J., Wilkinson M.C., Hearn J., *Studies on Polymer Latex Films: III. Permeability of Latex Films to Aqueous Organic Solutes.*, Polym. Int. 27, p51-55, (1992).

427 Roulstone B.J., Wilkinson M.C., Hearn J., *Studies on Polymer Latex Films: IV. Comparison of the Permeability of Latex and Solvent-Cast Films.*, Polym. Int., 27, p305-308, (1992).

428 Russell G.T., Napper D.H., Gilbert R.G., *Termination in Free-Radical Polymerizing Systems at High Conversion.*, Macromolecules, 21, p2133-2140, (1988).

429 Ryan K., *The Post-Grafting of Polymers to Colloidal Particles.*, Chem. Ind., p359-364, (June 1988).

430 Sakai Y., Tanzawa H., *Poly(methyl Methacrylate) Membranes.*, J. Appl. Polym. Sci., 22, p1805-1815, (1978).

431 Sakota K., Okaya T., *Method for the Determination of Surface Basic Groups in Cationic Polystyrene Latices.*, J. Appl. Polym. Sci., 21, p1009-1016, (1977).

432 Sakota K., Okaya T., *Polymerisation Behaviour and Distribution of Carboxyl Groups in Preparation of Soap-Free Carboxylated Polystyrene Latexes.*, J. Appl. Polym. Sci., 21, p1035-1043, (1977).

433 Sakota K., Okaya T., *Preparation and Characterisation of Carboxylated Isoprene/Styrene Copolymer Latexes*, J. Appl. Polym. Sci., 20, p1735-1744, (1976).

434 Samuelov Y., Donbrow M., Friedman M., *Sustained Release of Drugs from Ethylcellulose-Polyethylene Glycol Films and Kinetics of Drug Release.*, J. Pharm. Sci., 68 (3), p325-329, (1979).

435 Sanli O., Aras L., *Measurement of Transport Properties of Poly(methyl methacrylate-* co-methacrylic acid) Ion-Containing Membranes., Br. Polym. J., 22, p155-159, (1990).

436 Scholsky K.M., Fitch R.M., *Controlled Release of Pendant Bioactive Materials From Acrylic Polymer Colloids.*, J. Controlled Release, 3, p87-108, (1986).

437 Scholsky K.M., Fitch R.M., *Examination of Small Polystyrene Latex Particles Using a Negative Staining Technique.*, J. Colloid and Interface Sci., 104 (2), p 592-595, (1985).

438 Schultz G.V., Z. Phys. Chem., 8, p290, (1956).

439 Sciarra J.J., Gidwani R.N., *The Release of Various Ingredients from Aerosols Containing Selected Film-Forming Agents.*, J. Soc. Cosmet. Chem., 21, p667-681, (1970).

440 Sciarra J.J., Gidwani R.N., *Evaluation of Selected Physical Constants of Polymeric Films and Proposed Kinetics of Drug Release.*, J. Pharm. Sci., 61 (5), p754-761, (1972).

441 Scranton A.B., Mikos A.G., Scranton L.C., Peppas N.A., *The Physical Mechanism for the Production of Hydrophilic Polymer Microparticles from Aqueous Suspensions.*, J. Appl. Polym. Sci., 40, Part 5-6, p997-1004, (1990).

442 Senf H-J., Wollmann H., Cyranka U., *Occurrence of Negative Time Lags in Permeability Studies of Solutes Through Polyethylene.*, J. Pharm. Sci., 62 (12), p2059, (1973).

443 Seidl J., Krška F., Makromol. Chem., 28, p87, (1973).

444 Seidl J., Krška F., Chem. Prum., 25 (11), p597, (1975).

445 Seiner J.A., *Microvoids as Pigments. A Review.*, Ind. Eng. Chem. Prod. Res. Dev., 17, p302-317, (1978).

446 Serota D.G., Meyer M.C., Autian J., *The Effects of Structure on the Permeability of Substituted Anilines from Aqueous Solutions Through Polythene.*, J. Pharm. Sci., Drug Cosmet. Ind., 107 (3), p416-419, (1970).

447 Shaffer O.L., Dimonie V.L., El-Aasser M.S., *A Polymer Thin-Film Technique to Study the Micromorphology of Core-Shell Latexes.*, J. Polym. Sci., Part A, 25, p2595-2603, (1987).

448 Shaffer O.L., El-Aasser M.S.D., Vanderhoff J.W., *TEM Analysis of Core-Shell Latex Morphology.*, Proc. Annual Meeting E.M. Soc. America, 45, p502-503, (1987).

449 Shaw D.J., Electrophoresis., Academic Press, London, (1969).

450 Shaw J.N., *The Characterisation of Monodisperse Polystyrene Latices.*, J. Polym. Sci., Part C, 27, p237-251, (1969).

451 Sheetz D.P., *Formation of Films by Drying of Latex*, J. Appl. Polym. Sci., 9, p3759-3773, (1965).

452 Shenkel J.H., Kitchener J.A., Nature, 182, p131, (1958).

453 Sielicki M., Focht D.D., Martin J.P., *Microbial Transformations of Styrene and* [^{14}C] *Styrene in Soil and Enrichment Cultures.*, Appl. and Env. Microbiol. 35 (1), p124-128, (1978).

454 Silberberg A., The Hydrogel-Water Interface., Ch. 15, in Hydrogels for Medical and Related Applications., ACS Symp. Ser., 31, p198-205, (1976).

455 Singh P., Desai S.J., Simonelli A.P., Higuchi W.I., *Role of Wetting on the Rate of Drug Release from Inert Matrices.*, J. Pharm. Sci., 57 (2), p217-226, (1968).

456 Smith W.V., *The Kinetics of Styrene Emulsion Polymerisation.*, J. Am. Chem. Soc., 70, p3695-3702, (1948).

457 Smith W.V., Ewart R.H., *Kinetics of Emulsion Polymerisation.*, J. Chem. Phys., 16 (6), p592-599, (1948).

458 Šňupárek jr. J., Bidman A., Hanuš J., Hájková B., *Water Absorption in Acrylic Latex Films.*, J. Appl. Polym. Sci., 28, p1421-1428, (1983).

459 Sperling L.H., Klein A., Yoo J.N., Kim K.D., Mohammadi N., *The Utilization of SANS to Solve Polymer Latex Structural Problems: Basic Science and Engineering.*, Polym. Adv. Technol., 1 (3-4), p263-273, (1990).

460 Sperry P.R., Snyder B.S., O'Dowd M.L.m Lesko P.M., *Role of Water in Particle Deformation and Compaction in Latex Particle Film Formation.*, Langmuir, 10, p2619-2628, (1994).

461 Spitael J., Kinget R., *Influence of Solvent Composition upon Film-Coating.*, Pharm. Acta Helv., 55 (6), p157-160, (1980).

462 Spitael J., Kinget R., *Preparation and Evaluation of Free-Films: Influence of Method of Preparation and Solvent Composition Upon Permeability.*, Pharm. Acta Helv., 52 (3), p47-50, (1977).

463 Stannett V.T., Koros W.J., Paul D.R., Lonsdale H.K., Baker R.W., *Recent Advances in Membrane Science and Technology.*, Adv. Polym. Sci., 32, p69-121, (1979).

464 Stannett V., Williams J.L., *The Permeability of Poly(Ethyl Methacrylate) to Gases and Water Vapour.*, J. Polym. Sci., C (10), p45-59, (1965).

465 Staverman A.J. Rec. Trav. Chim., 70, p344, (1951).

466 Stock R.S., Ray W.H., *Interpretation of Photon Correlation Spectroscopy Data: a Comparison of Analysis Methods.*, J. Polymer Sci., 23, p1292-1447, (1985).

467 Stockmayer W.H., J. Polym. Sci., 24, p314, (1957).

468 Stone-Masui J.H., Stone W.E., Characterisation of Polysturene Latices by Photoelectron and Infra-Red Spectroscopy., in Polymer Colloids II., Ed. R.M. Fitch, Plenum Pub. Corp., p331-360, (1980).

469 Stone-Masui J., Watillon A., J. Colloid and Interface Sci., 52 (3), p479 (1975).

470 Strawbridge K.B., Hallet F.R., *Polydisperse Mie Theory Applied to Hollow Latex Spheres: An Integrated Light Scattering Study.*, Canadian J. Phys., 70 (6), p401-406, (1992).

471 Sullivan D.A., *Water and Solvent Evaporation from Latex and Latex Paint Films.*, J. Paint Technol., 47 (610), p60-67, (1975)

472 Sumitomo H., Hashimoto K., *Polyamides as Barrier Materials.*, Adv. Polym. Symp., 64, p63-91, (1985).

473 Sundberg D., Casassa P., Pontazopoulos J., Muscato M.R., Kronberg B., Berg J., J. Appl. Polym. Sci., 41, p1425, (1990).

474 Talen H.W., Hover P.F., *On Film Formation by Emulsion Paints and some Properties of these Films.*, Deutsche Farben Z, 13, p50-55, (1959). {C.B.D.E. translation.}

475 Tamai H., Niino K., Suzawa T., *Surface Characterisation of Styrene/Sodium Styrenesulfonate Copolymer Latex Particles.*, J. Colloid and Interface Sci., 131 (1), p1-7, (1989).

476 Taubes G., *The Disputed Birth of Buckyballs.*, Science, 253, p1476-1479. (1991).

477 Thakar N.S., Othmer D.F., Ind. Eng. Chem.,45, p589, (1953).

478 Thau G., Bloch R., Kedem O., *Water Transport in Porous and Non-Porous Membranes.*, Desalination, 1, p129-138, (1966).

479 Theeuwes F., *Elementary Osmotic Pump.*, J. Pharm. Sci., 64 (12), p1987-1991, (1975).

480 Theodoor J., Overbeek G., *Strong and Weak Points in the Interpretation of Colloid Stability.*, Adv Colloid and Interface Sci., 16, p17-30, (1982).

481 Tice T.R., Gilley R.M., *Preparation of Injectable Controlled-Release Microcapsules by a Solvent Evaporation Process.*, J. Controlled Release, 2, p343-352, (1985).

482 Tomlinson E., Davis S.S., (Eds), Site Specific Drug Delivery., Wiley, Chichester, (1986).

483 Trommsdorff E., Kohle H., Lagally P., Makromol. Chem., 1, p169, (1948).

484 Twigt F., Piet P., German A.L., *Preparation and Co-Catalytic Properties of Functionalized Latices.*, Eur. Polym. J., 27 (9), p939-945, (1991).

485 Udeala O.K., Aly S.A.S., *Degradation Kinetics of Thiamine Hydrochloride in Directly Compressed Tablets III. Water Vapour Transmission Through Free and Applied Eudragit Films.*, Drug Dev. Ind. Pharm., 15 (11), p1797-1825, (1989).

486 Ugelstad J., Hansen F.K., *Kinetics and Mechanism of Emulsion Polymerisation.*, Rubber Chem. Technol., 49 (3), p536-609, (1976).

487 Ugelstad J., Mørk P.C., Aasen J.O., J. Polym. Sci., Part A-1, 5, p2281, (1967).

488 Upson D.A., *Reactive Functional Latex Polymers.*, J. Polym. Sci., Polym. Symp. 72, p45-54, (1985).

489 Urban M.W., Evanson K.W., *Factors Governing Surfactant Assembly at the Latex Film Interfaces: An FT-I.R. Spectroscopic Study.*, Polym. Comm., 31 p279-282, (1990).

490 Van Amerongen G.J., J. Polym. Sci., 2, p381, (1947).

491 Vandegaer J.E., *Latex Growth.*, J. Appl. Polym. Sci., 9, p2929-2938, (1965).

492 van den Hul H.J., Vanderhoff J.W., *Desorption of Emulsifiers from Polystyrene Latexes.*, Proceedings Vth Int. Congress on Surface Active Substances, Section B, p319-330, (1968).

493 van den Hul H.J., Vanderhoff J.W., *Well-Characterised Monodisperse Latexes.*, J. Colloid and Interface Sci., 28 (2), p336-337, (1968).

494 van den Hul H.J., Vanderhoff J.W., *The Characterization of Latex Particle Surfaces by Ion Exchange and Conductometric Titration.*, J. Electroanal. Chem., 37, p161, (1972).

495 Van Der Hoff B.M.E., Emulsion Polymerisation., Ch. 7, in Solvent Properties of Surfactant Solutions., by Kozo Shineda, Pub. Dekker, New York, p285-340, (1967).

496 Van Der Hoff B.M.E., *Kinetics of Emulsion Polymerisation.*, Advances in Chem. Series, 34, p6-31, (1962).

497 Van Der Hoff B.M.E., *On the Mechanism of Emulsion Polymerization of Styrene. II. Polymerizations in Soap Solutions Below and Above the Critical Micelle Concentration and some Remarks on the Kinetics of Emulsion Polymerisation.*, J. Polym. Sci., 44, p241-259, (1960).

498 Vanderhoff J.W., Characterisation of Latexes by Ion Exchange and Conductometric Titration. in Characterization of Metal & Polymer Surfaces., Vol. 2, Polymer Surfaces., Ed. L-H Lee, Academic Press, p365-395, (1977).

499 Vanderhoff J.W., *"Core-Shell" Morphology in Emulsion Polymerisation.*, Proc. Water-Borne and High-Solids Coating Symposium, University of Southern Mississippi, (1976).

500 Vanderhoff J.W., *Mechanism of Film Formation of Latices.*, Br. Polym. J., 2, p161-172, (1970).

501 Vanderhoff J.W., *Mechanism of Latex Film Formation.*, Paint and Varnish Prod., p25-37, (Dec., 1970).

502 Vanderhoff J.W., The Mechanism of Emulsion Polymerization. Ch. 1, in Vinyl Polymerization., Part II, Ed. G.E. Ham, Pub. Marcell Dekker, New York, p1-138, (1969).

503 Vanderhoff J.W., *Well Characterised Monodisperse Polystyrene Latexes as Model Colloids.*, Pure and Appl. Chem., 51, p1263-1273, (1980).

504 Vanderhoff J.W., Bradford E.B., Carrington W.K., *Transport of Water Through Latex Films*, J. Polym. Sci., Polym. Symp., 41, p155-174, (1973).

505 Vanderhoff J.W., Park J.M., El-Aasser M.S., ACS Symposium Series, 492, p272, (1992).

506 Vanderhoff J.W., Park J.M., El-Aasser M.S., *Preparation of soft hydrophilic Polymer Core/Hard Hydrophobic Polymer Shell Particles for Microvoid Coatings by Seeded Emulsion Polymerisation.*, Polym. Mater. Sci. Eng., 64, p345-346, (1991).

507 Vanderhoff J.W., Poehlein G.W., Pramojaney N., Yenwo G.M., *Latex Drying Rates on Solid and Porous Substrates.*, Synth. Conf. Proc. Vol. ?, p253-261, (1980).

508 Vanderhoff J.W., Tarkowski H.L., Jenkins M.C., Bradford E.B., *Theoretical Consideration of the Interfacial Forces Involved in the Coalescence of Latex Particles.*, J. Macromol. Chem., 1 (2), p361-397, (1966).

509 Vanderhoff J.W., Van Den Hul H.J., Tausk R.J.M., Overbeek J. Th. G., The Preparation of Monodisperse Latexes with Well-Characterized Surfaces.. in Clean Surfaces., Ed. G. Goldfinger, Pub. Marcell Dekker Inc., N.Y., p15-44, (1970).

510 Vanderhoff J.W., Vitkuske J.F., Bradford E.B., Alfrey jr. T., *Some Factors Involved in the Preparation of Uniform Size Latexes.*, J. Polym. Sci., 20, p225-231, (1956).

511 Vandezande G.A., Rudin A., *Novel Composite Latex Particles for Use in Coatings.*, J. Coatings Tech. 66 (828), p99-108, (1994).

512 Van Tent A., te Nijenhuis K., in Proceedings, XVIIth International Conference in Organic Coatings Science and Technology., Luzern, Switzerland, p317, (1991).

513 Van Tent A., te Nijenhuis K., *Turbidity Study of the Process of Film Formation of Polymer Particles in Drying Thin Films of Acrylic Latices.*, J. Colloid and Interface Sci., 150 (1), p97-114, (1992).

514 Van Tent A., te Nijenhuis K., *Turbidity Study of the Process of Film Formation of Thin Films of Aqueous Acrylic Dispersions.*, Prog. Org. Coat., 20, p459-470, (1992).

515 Vanzo E., Marchessault R.H., Stannett V., *Particle Size Determination of Film Forming Latices by Electron Microscopy.*, J. Colloid Sci., 19, p578-583, (1964).

516 Verwey E.J.W., Overbeek J.Th.G., in Theory of the Stability of Lyophobic Colloids., Pub. Elsevier, (1948).

517 Vezin W.R.,Florence A.T., *Diffusive Desorption of Small Solute Molecules from Amorphous Polymers, PMMA, PVA, PACA.*, European Polym. J., 17, p93-99, (1981).

518 Vickerman J.C., Secondary Ion Mass Spectroscopy., in Methods of Surface Analysis., Ed. J.M. Walls, Cambridge University Press, p169-215, (1989).

519 Vieth W.R., Howell J.M., Hsieh J.H., *Dual Sorption Theory.*, J. Membrane Sci., 1, p177-220, (1976).

520 Vieth W.R., Sladek K.J., *A Model for Diffusion in a Glassy Polymer.*, J. Colloid Sci., 20, p1014-1033, (1965).

521 Vijayendran B.R., *Effect of Carboxylic Monomers on Acid Distribution in Carboxylated Polystyrene Latices.*, J. Appl. Polym. Sci., 23, p893-901, (1979).

522 Vijayendran B.R., Bone T., *Effects of Surfactants on Film Formation of Poly (Vinyl Acetate) and Poly (Vinyl Acetate-Butyl Acrylate) Latexes.*, J. Dispersion Sci. Technol., 3 (1), p81-97, (1982).

523 Vijayendran B.R., Bone T., Gajria C., In Some Studies on Vinyl Acrylic Latex–Surfactant Interactions., Emulsion Polym. Vinyl Acetate Pap. Symp. J., Meeting 1980, Ed. El-Aasser, p253-283, (1980).

524 Voyutskii S.S., *Amendment to the Papers by Bradford, Brown, and Co-workers: "Concerning Mechanisms of Film Formation from High Polymer Dispersions."*, J. Polym. Sci., 32 (125), p528-530, (1958).

525 Voyutskii S.S., Autohesion & Adhesion of High Polymers, Polymer Reviews, 4, Wiley Intersci., N. York, (1963).

526 Voyutskii S.S., Vakula V.L., *Effects of Self-Diffusion and Inter-Diffusion in Polymer Systems.*, Rubber Chem. Technol., 37, p1153-1177, (1964).

527 Wang Y., Kats A., Juhué D., Winnik M.A., *Freeze-Fracture Studies of Latex Films Formed in the Absence and Presence of Surfactant.*, Langmuir, 8, p1435-1442, (1992).

528 Wang Y., Winnik M.A., *Effect of Coalescing Aid on Polymer Diffusion in Latex Films.*, Macromolecules, 23 (21), p4731-4732, (1990).

529 Wang Y., Winnik M.A., *Polymer Diffusion Across Interfaces in Latex Films.*, J. Phys. Chem., 97, p2507-2515, (1993).

530 Wessling R.A., Harrison I.R., J. Polym. Sci., Part A1, 9, p3471-3489, (1971).

531 West R.C., (ed.), In *C.R.C. Handbook of Chemistry and Physics, 62nd Edition.*, C.R.C. Press Inc., (1981-1982).

532 Wicks S.R., *Competitive Sorption Studies with Nylon 6 and Active Carbon.*, PhD Thesis, University of Bath, (1982).

533 Wiersema P.H., PhD Thesis, University of Utrecht, (1964).

534 Wiersema P.H., Loeb A., Overbeek J. Th. G., J. Colloid and Interface Sci., 22, p78, (1966).

535 Wilke C.R., Chang P., *Correlation of Diffusion Coefficients in Dilute Solutions.*, A.I.Ch. E. J., 1, p264-270, (1955).

536 Wilkinson M.C., Hearn J., Cope P., Chainey M.C., *A Microfiltration Technique for Cleaning Polymer Latices.*, Br. Polym. J., 13, p82-89, (1981).

537 Wilkinson M.C., Hearn J., Cope P., Goodall A.R., *Comments on the Purification of Polymer Latices by the Dialysis Technique.*, J. Colloid & Interface Sci., 77 (2), p566-570, (1980).

538 Wilkinson M.C., Sherwood R., Hearn J., Goodall A.R., *The Influence of Residual Styrene Monomer, Benzaldehyde, and Microbial Activity on the Surface Properties of Polystyrene Latices.*, Br. Polym. J., 11 (1), p1-6, (1979).

539 Wilkinson M.C., *Cleaning of Polymer Latexes.* Review – To Be Published.

540 Williams D.J., *The Morphology of Polystyrene Latex Particles.*, J. Elasto-plastics, 3, p187-200, (1971).

541 Williams D.J., *Latex Particle Morphology during Polymerization and at Saturation Equilibrium.*, J. Polym. Sci., 12, p2123-2132, (1974).

542 Wilson E.A., Miller J.R., Rowe E.H., J. Phys. and Colloid Chem., 53, p357, (1949).

543 Winnik M.A., Wang Y., Haley F., *Latex Film Formation at the Molecular Level: The Effect of Coalescing Aids on Polymer Diffusion.*, J. Coatings Technol., 64 (811), p51-61, (1992).

544 Wisniewski S., Kim S.W., *Permeation of water-soluble solutes through poly(2-hydroxyethyl methacrylate) crosslinked with ethylene glycol dimethacrylate.*, J. Memb. Sci., 6, p299-308, (1980).

545 Wood D.A., *Polymeric Materials used in Drug Delivery Systems.*, p71-123.

546 Yang S.I., Klein A., Sperling L.H., J. Polym. Sci., Polym. Phys. Ed., 27, p1649, (1990).

547 Yaseen M., Raju V.S.N., *A Critical Analysis of Various Methods for Preparation of Free Films of Organic Coatings.*, Prog. in Org. Coatings, 10, p125-155, (1982).

548 Yasuda H., *Units of Gas Permeability Constants.*, J. Appl. Polym. Sci., 19 (9), p2529-2536, (1975).

549 Yasuda H., Hirotsu T., *The Effect of Glass Transition on Gas Permeabilities.*, J. Appl. Polym. Sci., 21, p105-112, (1977).

550 Yasuda H., Lamaze C.E., *Permselectivity of Solutes in Homogeneous Water-Swollen Polymer Membranes.*, J. Macromol. Sci.-Phys., B5 (1), p111-134, (1971).

551 Yasuda H., Lamaze C.E., *Transfer of Gas To Dissolved Oxygen in Water Via Porous and Nonporous Polymer Membranes.*, J. Appl. Polym. Sci., 16, p595-601, (1972).

552 Yasuda H., Lamaze C.E., Ikenberry L.D., *Permeability of Solutes Through Hydrated Polymer Membranes., Part 1. Diffusion of Sodium Chloride.*, Makromol. Chem., 118 (2858), p19-35, (1968).

553 Yasuda H., Lamaze C.E., Peterlin A., *Diffusive and Hydraulic Permeabilities of Water in Water-Swollen Polymer Membranes.*, J. Polymer Sci., Part A-2, 9, p1117-1131, (1971).

554 Yates D.E., Ottewill R.H., Goodwin J.W., *Purification of Polymer Latices.*, J. Colloid and Interface Sci., 62 (2), p356-358, (1977).

555 Yoo J.N., Sperling L.H., Glinka C.J., Klein A., *Characterization of Film Formation from Polystyrene Latex Particles via SANS. 1. Moderate Molecular Weight.*, Macromolecules, 23, p3962-3967, (1990).

556 Yoo J.N., Sperling L.H., Glinka C.J., Klein A., *Characterization of Film Formation from Polystyrene Latex Particles via SANS. 1. High Molecular Weight.*, Macromolecules, 24, p2868-2876, (1991).

557 Yuk S.H., Cho S.H., Lee H.B., *Electric Current-Sensitive Drug Delivery Systems Using Sodium Alginate/Polyacrylic Acid Composites.*, Pharm. Res., 9 (7), p955-957, (1992).

558 Zentner G.M., Cardinal J.R., Feijen J., Song S-Z., *Progestin Permeation Through Polymer Membranes IV: Mechanism of Steroid Permeation and Functional Group Contributions to Diffusion Through Hydrogel Films.*, J. Pharm. Sci., 68 (8), p970-975, (1979).

559 Zentner G.M., Rork G.S., Himmelstein K.J., *Osmotic Flow Through Controlled Porosity Films: An Approach to Delivery of Water Soluble Compounds.*, J. Controlled Release, 2, p217-229, (1985).

560 Zhao C.L., Dobler F., Pith T., Holl Y., Lambla M., *Surface Composition of Coalesced Acrylic Latex Films Studied by XPS and SIMS.*, J. Colloid and Interface Sci., 128 (2), p437-449, (1989).

561 Zhao C.L., Holl Y., Pith T., Lambla M., *Colloid Science: FTIR-ATR Spectroscopic Determination of Distribution of Surfactants in Latex Films.*, Colloid & Polym. Sci., 265 (9), p823-829, (1987).

562 Zhao C.L., Holl Y., Pith T., Lambla M., *Surface Analysis and Adhesion Properties of Coalesced Latex Films.*, Brit. Polymer J., 21, p155-160, (1989).

563 Ziegel K.D., *Gas Transport in Segmented Block Copolymers.*, J. Macromol. Sci.-Phys., B5 (1), p11-22, (1971).

564 Ziegel K.D., Frensdorff H.K., Blair D.E., J. Polym. Sci., A-2 (7), p809, (1969).

565 Zimm B.H., J. Chem. Phys., 16, p1093, (1948).

566 Zimmt W.S., J. Appl. Polym. Sci., 1, p323, (1959).

567 Zosel A., Ley G., *Film Formation of Latices with Crosslinked Particles.*, Polym. Bull., 27, p459-464, (1992).

◆

Appendix A:
Derivation of Formulae used in Analysis of Experimental Data.

A1. Analysis of mercury porosimetry results.

A non-wetting liquid cannot spontaneously enter a capillary (pore) which has a wetting angle of ⟩ 90° due to the surface tension (capillary depression). The pressure required to cause intrusion is a function of pore radius. Assuming cylindrical pores, the pore radius, *r*, is thus given by the **Washburn equation**[4, 79] for capillary wetting:

$$r = \frac{2\gamma \cos\theta}{P} \tag{A.1}$$

where:

γ = surface tension (N m^{-1});
θ = contact angle (degrees); &
P = exerted pressure (Pa).

For a capillary of circular cross-section, the surface tension of the liquid is exerted over the contact area, over a length equal to the pore circumference. The surface tension force acts perpendicularly to the plane of the surface of contact, and is given by:

$$Force = 2\pi r\gamma \tag{A.2}$$

The force tending to push the liquid out of the capillary is given by:

$$Force_{(cap^y)} = 2\pi r\gamma \cos\theta \tag{A.3}$$

Acting against this is the externally applied pressure, which acts over the area within the contact circumference and is given by:

$$Force_{(app.press.)} = \pi r^2 P \tag{A.4}$$

At equilibrium, these two forces are equal such that:

$$2\pi r\gamma \cos\theta = \pi r^2 P \tag{A.5}$$

This simplifies to give the Washburn equation.

Assuming that the surface tension of mercury γ = 480 mN m^{-1} and that the contact angle is 141.3°, it is found that:

$$r \approx \frac{7500}{P} \tag{A.6}$$

where:

r = pore radius (nm); &
P = applied pressure (Pa).

Note that the contact angle of 141.3° as quoted by Carlo-Erba[79] is an average value determined from a "large number of different samples" giving values in the range

125° → 152°, and is dependent upon the nature of the sample. Similarly, surface tension is also a variable, with temperature, from 484.2 → 472 mN m^{-1} as the temperature changes from 298 → 323 K.

The method makes a number of assumptions, *e.g.*, that the pores are cylindrical and that the pore shape is constant throughout the pore size range. For irregularly shaped pores, the ratio between the pore cross-section (related to pressure exerted) and the pore circumference (related to surface tension) is not proportional to the radius, and depending on the pore shape will tend to give a lower than expected result for the pore radius from equation (A.6). In practice, problems can also arise if the pore opening is narrower than the pore volume. This leads to a false initial reading of pressure and volume such that after the pressure has been set to a particular required value, it may drop slightly, with time, as the 'inside' of the pore is filled. This problem is minimised by allowing the pressure reading to stabilise before the intruded volume is read from the display.

A2. Derivation of the water vapour permeability coefficient equation.

A permeability coefficient is a measure of the ease of permeant transport through a film. The flux per unit area is generally described by the product of a permeability coefficient and the driving force, where the driving force is a concentration gradient or a pressure differential. The method for determining the water vapour permeability coefficient assumes that the flux of water vapour is under steady state conditions, and that the amount of water vapour within the film is negligible. From Fick's first law, the amount of water vapour (g hr^{-1}), dW/dt passing through the film of unit area is given by the flux, J:

$$J = \frac{dW}{dt} = -D\left(\frac{dC}{dx}\right) \tag{A.7}$$

Integrating:

$$J\int_{x_1}^{x_2} dx = -D\int_{C_1}^{C_2} dC = D\int_{C_2}^{C_1} dC \tag{A.8}$$

If C_0 & C_t are the concentrations at time $t = 0$ and $t = t$, respectively, and if the thickness of the film l is given by $x_2 - x_1$, then:

$$J = D\left[\frac{C_0 - C_t}{x_2 - x_1}\right] = \frac{D}{l}(C_0 - C_t) \tag{A.9}$$

If S is the solubility of the water vapour within the film, and p the pressure of the water vapour, then from substitution of Henry's Law, *i.e.*:

$$C = Sp \tag{A.10}$$

we get:

$$J = \frac{D}{l}(C_0 - C_t) = \frac{DS}{l}(p_0 - p_t) = \frac{DS\Delta p}{l} \tag{A.11}$$

But, $DS = P_w$, the water vapour permeability coefficient. Hence, by re-arrangement, for a film of area A, the water vapour permeability coefficient is given by the following:

$$P_w = \frac{dW}{dt}\left(\frac{l}{A\Delta p}\right) \tag{A.12}$$

A3. Derivation of the gas flux equation as required by the Daventest apparatus.

At any time, t, the gas pressure is given by:

$$Pressure = \rho g h \tag{A.13}$$

where:

ρ = density of mercury (g cm^{-3});
g = gravitational force (cm s^{-2}); &
h = height of mercury column with respect to the initial height (cm).

If the volume of the lower chamber (see **Figure 7.3**) of the apparatus is given by equation (A.14):

$$Volume = V_0 + ah \tag{A.14}$$

where:

V_0 = total volume beneath film (to the top of the mercury column) (cm^{-3});
a = cross sectional area of manometer capillary (cm^{-2});

Substitution of equations (A.13) and (A.14) into the ideal gas equation (A.15):

$$PV = nRT \tag{A.15}$$

thus gives:

$$PV = \rho g h\left(V_0 + ah\right) = nRT \tag{A.16}$$

$$PV = \rho g\left(V_0 h + ah^2\right) = nRT \tag{A.17}$$

The gas flux is thus then given by:

$$Flux = \frac{dn}{dt} = \frac{1}{RT}\left[\frac{d(PV)}{dt}\right] = \frac{\rho g}{RT}\left[V_0\frac{dh}{dt} + 2ah\frac{dh}{dt}\right] \tag{A.18}$$

The driving pressure, $\rho g H - h$ during the course of the experiment is essentially constant at approximately 1 atm, where H is the height of a column of mercury at atmospheric pressure[1]. This implies:

$$\frac{dn}{dt} = \frac{P}{RT}\frac{dV}{dt} = \frac{\rho g(H - h)}{RT}\frac{dV}{dt} \tag{A.19}$$

---

[1] The variable 'h' can have dimensions of either length or pressure dependent on context. When used as in Equation (A.16), it takes dimensions of length (cm), but when used in the form (H - h), it acts as a correction factor to a pressure and therefore has units cm.Hg.

And therefore:

$$\frac{dn}{dt} = \frac{\rho g(H-h)}{RT}\frac{dV}{dt} = \frac{\rho g}{RT}\left[V_0 + 2ah\right]\frac{dh}{dt} \tag{A.20}$$

implying:

$$Flux = \frac{dV}{dt} = \frac{V_0 + 2ah}{H-h}\frac{dh}{dt} \tag{A.21}$$

It should be noted that in practice, the h term is constantly changing. The term dh/dt is therefore determined from the linear region of the gradient of a graph of the change in height of the mercury column as a function of time. The term $V_0 + 2ah$, which is effectively the volume of the chamber below the film + the volume of the capillary to the top of the mercury column, is similarly changing as a function of time but is taken to be a constant with the value of h being taken as that seen at the midpoint of the experiment (*i.e.*, when h is the mid-value of the change in height of the mercury column).

A4. Derivation of the solute permeability coefficient equation.

Determination of the solute permeability coefficient is usually achieved by means of a **Barrer** type plot, as described in Chapter 5. This is a graph of concentration of permeant as a function of time. For Fickian diffusion, such a plot is linear after the initial lag period, during which time the film is becoming saturated with permeant. In Chapter 5, the equation of the Barrer plot was given from a solution to Fick's second law as:

$$M = \frac{DC_1 t}{l} - \frac{C_1 l}{6} \tag{A.22}$$

where:

M = mass of diffusant per unit area transported through the film;
D = diffusion coefficient;
l = film thickness, *i.e.*, $x = 0 \rightarrow l$;
C_1 = concentration in the polymer at $x = 0$.

The steady-state gradient is therefore given by:

$$\frac{dM}{dt} = \frac{DC_1}{l} = \frac{DSC_0}{l} \tag{A.23}$$

if the donor permeant solution concentration, C_0, is given by:

$$C_1 = SC_0 \tag{A.24}$$

Also, M can be converted to a concentration (*i.e.*, on the receiver side of the film) by the inclusion of the volume, V, of the receiver solution. Hence, if the permeability coefficient is given by:

$$P = DS \tag{A.25}$$

Then the gradient of the linear region of a Barrer plot (dC/dt) will thus give the permeant flux. The solute permeability coefficient, P_s, (m^2 hr^{-1}) can then be determined from:

$$P_s = \frac{dC}{dt}\left[\frac{l \times V}{A \times C_0}\right] \tag{A.26}$$

where:

dC/dt = permeant flux (g dm^{-3} hr^{-1});
l = film thickness (m);
V = volume of receiver solution (m^3);
A = area of film exposed to permeant solution (m^2); &
C_0 = initial permeant (donor) concentration (g dm^{-3}).

This method of derivation of the permeability coefficient makes a number of assumptions:

- ✗ that the donor permeant concentration remains constant during the course of the experiment;
- ✗ that the film does not swell such that its thickness changes during the experiment.

The answer provided by this method is thus necessarily a compromise: the donor concentration obviously does change as solute permeates the film, and for hydrophilic films, water uptake does cause the film to swell. Also, permeants are typically soluble in the film such that solute is effectively lost from the experiment.

For the purpose of determining the solute permeability coefficient, Roulstone [423] minimised the former of these two assumptions by determining the solute flux from the point when the change in concentration was less than 1% of that from the initial donor concentration. However, during the course of this study, it was realised that this method leads to other problems:

- ✗ for films of a relatively high flux, it is possible that a concentration change of greater than 1% can occur before the end of the lag period such that it is not the true steady-state linear flux that is measured;
- ✗ for films of a relatively low flux, it is difficult to determine the end of the lag period, such that the slope of a plot of concentration with time may appear linear from time zero.

It may possibly have been better for Roulstone to have used a saturated solution of permeant, in the donor side of the permeability cell, with the concentration maintained by having an excess of permeant solid present.

A number of researchers such as Sakai and Tanzawa [430] and Sanli and Aras [435] have used an equation based upon the integrated form of Fick's first law. The derivation of an equation of a similar form is given by Flynn [167] *et al.* The equation is based on the assumptions that there exists a steady state system in which the membrane is saturated with the permeant and that the concentration gradients at the film-liquid interfaces instantaneously adjust such that there is a continuum without any step in concentration. The method sums the solutions to the two cases of diffusion: into the membrane from the external donor, and from the membrane into the external receiver phase. The relative amount of permeant (as opposed to concentration) in the film is assumed to be negligible.

Assuming that the concentration gradient within the film is linear, then the concentration gradient at a time, t, across a film thickness $x = l$ is given by:

$$-\frac{dC}{dx} = \frac{C_1 - C_2}{l} \qquad \text{(A.27)}$$

Where C_1 and C_2 are the interfacial concentrations in the film, on the donor and receiver sides, respectively.

These are related to the donor and receiver solution concentrations by their partition or solubility coefficients, S.

From Fick's first law, the flux, J, per unit area at time, t, is given by:

$$J = \frac{dM}{dt} = -D\frac{dC}{dx} = D\left(\frac{C_1 - C_2}{l}\right) \qquad \text{(A.28)}$$

Where M is the total amount of material in the donor phase at time, t.

At time, t, the permeant solution concentration on the donor side of the film, assuming a negligible amount of permeant in the film, is given by:

$$C_0 = \frac{M_D - M}{V_D} \qquad \text{(A.29)}$$

where V_D is the donor volume, subscript 0 implies at a time when $t = 0$, and subscript D implies the donor phase.

The corresponding concentration in the receiver side is given by:

$$C_t = \frac{M_R + M}{V_R} \qquad \text{(A.30)}$$

Substituting into equation (A.28):

$$\frac{dM}{dt} = \frac{dS}{l}\left(\frac{M_D - M}{V_D} - \frac{M_R + M}{V_R}\right) \qquad \text{(A.31)}$$

Therefore:

$$\frac{dM}{dt} = \frac{DS}{l}\left(\frac{V_R(M_D - M) - V_D(M_R + M)}{V_D V_R}\right) \qquad \text{(A.32)}$$

$$\frac{dM}{dt} = \frac{DS}{l}\left(\frac{V_R M_D - M(V_R + V_D) - V_D M_R}{V_D V_R}\right) \qquad \text{(A.33)}$$

And so:

$$\frac{dM}{dt} = \left(\frac{DS}{l}\right)\left(\frac{V_D + V_R}{V_D V_R}\right)\left(\frac{V_R M_D - V_D M_R}{V_D + V_R} - M\right) \qquad \text{(A.34)}$$

Let:

$$\beta = \frac{V_R M_D - V_D M_R}{V_R + V_D} \qquad \text{(A.35)}$$

Then, integrating equation (A.34):

$$\int_0^M \frac{dM}{\beta - M} = \left(\frac{DS}{l}\right)\left(\frac{V_D + V_R}{V_D V_R}\right)t \qquad \text{(A.36)}$$

which gives:

$$-\ln[\beta - M]_0^M = \left(\frac{DS}{l}\right)\left(\frac{V_D + V_R}{V_D V_R}\right)t \qquad \text{(A.37)}$$

$$-\ln[\beta - M] - Ln[\beta - 0] = \left(\frac{DS}{l}\right)\left(\frac{V_D + V_R}{V_D V_R}\right)t \qquad \text{(A.38)}$$

$$-\ln\left[\frac{\beta - M}{\beta}\right] = \left(\frac{DS}{l}\right)\left(\frac{V_D + V_R}{V_D V_R}\right)t \qquad \text{(A.39)}$$

Substituting for β:

$$-\ln\left[\frac{\dfrac{V_R M_D - V_D M_R}{V_R + V_D} - M}{\dfrac{V_R M_D - V_D M_R}{V_R + V_D}}\right] = \left(\frac{DS}{l}\right)\left(\frac{V_D + V_R}{V_D V_R}\right)t \qquad \text{(A.40)}$$

Which simplifies to:

$$-\ln\left[\frac{V_R M_D - V_D M_R - M(V_R + V_D)}{V_R M_D - V_D M_R}\right] = \left(\frac{DS}{l}\right)\left(\frac{V_D + V_R}{V_D V_R}\right)t \qquad \text{(A.41)}$$

In our permeability cell, the donor volume = receiver volume: *i.e.*, $V_D = V_R = V$. Also, at $t = 0$, $M_R = 0$. Therefore:

$$-\ln\left[\frac{VM_D - 0 - 2MV}{VM_D - 0}\right] = \frac{DS}{l}\left(\frac{2V}{V^2}\right)t \qquad \text{(A.42)}$$

$$-\ln\left[\frac{VM_D - 2MV}{VM_D}\right] = \left(\frac{2DS}{lV}\right)t \qquad \text{(A.43)}$$

$$-\ln\left[\frac{2V(M_D - M) - VM_D}{VM_D}\right] = \left(\frac{2DS}{lV}\right)t \qquad \text{(A.44)}$$

Dividing the top and bottom of the log. function by V^2:

$$-\ln\left[\frac{\frac{2V(M_D - M)}{V^2} - \frac{VM_D}{V^2}}{\frac{VM_D}{V^2}}\right] = \frac{2DSt}{lV} \qquad \text{(A.45)}$$

Therefore:

$$\frac{2DSt}{lV} = -\ln\left[\frac{\frac{2(M_D - M)}{V} - \frac{M_D}{V}}{\frac{M_D}{V}}\right] \qquad \text{(A.46)}$$

At time $t = 0$, M_D/V = initial donor concentration = C_0.
At time $t = t$, $(M_D - M)/V$ = instantaneous donor concentration = C_t.
Therefore:

$$\frac{2DSt}{lV} = -\ln\left[\frac{2C_t - C_0}{C_0}\right] = 2.303\log_{10}\left[\frac{C_0}{2C_t - C_0}\right] \qquad \text{(A.47)}$$

But the permeability coefficient, $P = DS$, hence, from substituting for DS, and re-arranging:

$$P_S t = \frac{2.303lV}{2A}\log\left[\frac{C_0}{2C_t - C_0}\right] \qquad \text{(A.48)}$$

Experimentally, we observe the system with respect to the increase in concentration on the receiver side of the permeability cell, as opposed to the decrease in concentration on the donor side, such that:

$$P_S t = \frac{2.303lV}{2A}\log_{10}\left[\frac{C_0}{C_0 - 2C_t}\right] \qquad \text{(A.49)}$$

◆

Appendix B: Philips User Programming Software.

The Philips User Programming Software when used to retrieve data, required a batch file (named with a '*.CTL*' extension, *e.g.*, *GETDATA.CTL*) of commands. A generic example of such a batch file is as follows:

```
! OPEN [hard disk]:[path]\filename.dat                                      ..1
! FORMAT [number of cells, including any reference cells]                   ..2
GET ALL ABS                                                                 ..3
! CLOSE                                                                     ..4
! DOS                                                                       ..5
```

Line 1 opens a data file on the stated drive, in the subdirectory at the end of the stated path in a file called 'filename.dat', *e.g.*, ! OPEN C:\DATA\NEWDATA.DAT.

Line 2 formats the number of columns into which the data will be placed, in the data file. This would normally correspond to the number of flowcells in use *e.g.*, ! FORMAT 6.

Line 3 is the command to download the data (all) as absorbances.

Lines 4 & 5 then close the data file, and exit the Philips software, returning the user to the DOS command prompt.

Each time the above file was used, it was necessary to change the name of the data file (*e.g.*, filename.dat in the above example) to prevent it overwriting the previously saved file, and also to set the number of cells used in order that the correct number of columns was formatted.

Version 1.0 of the Philips software was found to be incompatible with the HIMEM.SYS/EMM386.SYS extended memory drivers (necessary to run the spreadsheet) of Microsoft's® Disk Operating System (MS-DOS®) version 5.0, resulting in the computer crashing. This could be overcome by removing these commands from the computer's configuration files before running the Philips software, and then replacing them afterwards.

The following program would control the spectrophotometer from the start to the finish of an experiment. The *wait* statements pause the program (requiring a key-press on the computer to restart) allowing operations, such as the filling of the permeability cells, to be carried out. They are not strictly necessary, but give an indication on the computer screen of the program's progress.

```
! WAIT SETTING UP CELL PROGRAMMER                                           ..1

CELL ON NORMAL CYCLES 500 TIME 15.0                                         ..2

CSTEP TO3                                                                   ..3
CE2 ON SAMPLE                                                               ..4
CE3 ON REFERENCE                                                            ..5
CE4 ON SAMPLE
CE5 ON SAMPLE
```

```
CE6 ON SAMPLE
CE7 ON SAMPLE
CE8 OFF
CE1 OFF                                                          ..11

! WAIT STRIKING DEUTERIUM LAMP                                   ..12
DEUTERIUM ON

! WAIT SETTING METHOD                                            ..14
FIXED AT 320 ABS LSMOOTH INTEGRATION 0.01 CYCLE                  ..15
        TIME 0.02 HIGH 3 LOW -0.3                           ..15 cont.
ZERO
CSTEP TO2                                                        ..17
! WAIT READY TO RUN                                              ..18
RUN
SAVE DATA                                                        ..20

! OPEN [hard disk]:[path]\filename.dat                           ..21
! FORMAT [number of cells, including any reference cells]
GET ALL ABS
! CLOSE
! DOS                                                            ..25
```

Line 2 sets up the cell programmer to take 500 readings at 15 minute intervals.

Line 3 moves cell 3, the reference cell, into the light beam, ready for setting a zero.

Lines 4 → 11 set up the flowcells as being either off, samples, or references. Cell 3 was always used as the control. Cell 2 contained a blanking-plate: it was to here the cell programmer went between the readings (for the 15 min. break) to protect the detector from being permanently exposed, and also so that no solution was permanently in the light beam.

Line 13 turns on the deuterium lamp. (This was normally left on permanently due to the fact the spectrophotometer was in use full time, and to save having to allow for the 20 minute warm-up period.)

Line 15 sets the method: setting the wavelength to 320 nm; to take absorbance readings (as opposed to percentage transmittance); with low smoothing (this is not applicable in this example, but allows 'noise' in a signal during a long integration time to be smoothed); to take an absorbance reading for a duration of 0.01 seconds on each cell during each pass; the cycle time option is not applicable in this example, but allows cycling of the reading of the individual cells during a single pass of the cell transporter: *i.e.*, the group of cells could be made to made to move into the measuring position 500 hundred times (using line 2) with each cell being measured a set number of times whilst in the beam (line 15); and finally, line 15 sets values for the high and low absorbances. (The values shown are the minimum and maximum seen on the spectrophotometer display screen. However, the computer data recorded absorbances up to approximately 6 absorbance units, despite the fact that this is, practically speaking, meaningless.)

Line 17 sets a zero value: again not necessary if a reference sample is used.

Line 18 steps the cell programmer to the blanked off cell.

Line 19 starts the method

Line 20 stores the contents of the volatile memory, after the 500 cycles. Only after this point is the data safe.

Lines 21 → 25 are as in the previous program, and save the data to the computer.

The data file on the computer disk is stored in an ASCII format. This is readable by most spreadsheet programs, but the data is in such a form that it cannot yet be used. Each (15 minute) cycle will be transferred onto a row of the spreadsheet program, however, only one column will be used (assuming the spreadsheet emulates graph-paper). In order to use the data, it is necessary for each number to occupy a single cell. *i.e.*, four cells measured every 15 minutes for 2 hrs would require a grid of four columns by nine rows (to include time = 0). The ASCII data can be converted to this format using the 'parse' function built into most spreadsheets.

Spero Meliora

(I hope for better things)

The
Nottingham
Trent
University

Libraries &
Learning
Resources

The Boots Library: 0115 848 6343
Clifton Campus Library: 0115 848 6612
Brackenhurst Library: 01636 817049